

بِسْمِ اللَّهِ الرَّحْمَنِ الرَّحِيمِ  
الْحَمْدُ لِلَّهِ الَّذِي  
أَنْزَلَ هَذِهِ السُّورَةَ  
وَجَعَلَ فِيهَا آيَاتٍ  
بَيِّنَاتٍ لِقَوْمٍ يَعْلَمُونَ

# Peristalsis subject to Entropy Generation



By

**Sadaf Nawaz**

**Department of Mathematics  
Quaid-i-Azam University  
Islamabad, Pakistan  
2021**

# Peristalsis subject to Entropy Generation



By

**Sadaf Nawaz**

Supervised By

**Prof. Dr. Tasawar Hayat**

**Department of Mathematics**

**Quaid-i-Azam University**

**Islamabad, Pakistan**

**2021**

# Peristalsis subject to Entropy Generation



By  
**Sadaf Nawaz**

A THESIS SUBMITTED IN THE PARTIAL FULFILLMENT OF THE REQUIREMENT  
FOR THE DEGREE OF  
**DOCTOR OF PHILOSOPHY**  
IN  
**MATHEMATICS**

Supervised By  
**Prof. Dr. Tasawar Hayat**  
**Department of Mathematics**  
**Quaid-i-Azam University**  
**Islamabad, Pakistan**  
**2021**

## **Author's Declaration**

I **Sadaf Nawaz** hereby state that my PhD thesis titled **Peristalsis subject to Entropy Generation** is my own work and has not been submitted previously by me for taking any degree from the Quaid-I-Azam University Islamabad, Pakistan or anywhere else in the country/world.

At any time if my statement is found to be incorrect even after my graduate the university has the right to withdraw my PhD degree.

Name of Student: **Sadaf Nawaz**

Date: **26-05-2021**

## Plagiarism Undertaking

I solemnly declare that research work presented in the thesis titled "Peristalsis subject to Entropy Generation" is solely my research work with no significant contribution from any other person. Small contribution/help wherever taken has been duly acknowledged and that complete thesis has been written by me.

I understand the zero tolerance policy of the HEC and Quaid-I-Azam University towards plagiarism. Therefore, I as an Author of the above titled thesis declare that no portion of my thesis has been plagiarized and any material used as reference is properly referred/cited.

I undertake that if I am found guilty of any formal plagiarism in the above titled thesis even afterward of PhD degree, the University reserves the rights to withdraw/revoke my PhD degree and that HEC and the University has the right to publish my name on the HEC/University Website on which names of students are placed who submitted plagiarized thesis.

Student/Author Signature: \_\_\_\_\_



Name: Sadaf Nawaz

# Peristalsis subject to Entropy Generation

By

**Sadaf Nawaz**

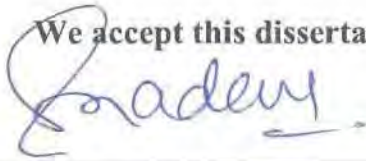
CERTIFICATE

A THESIS SUBMITTED IN THE PARTIAL FULFILLMENT OF THE  
REQUIREMENTS FOR THE DEGREE OF THE

**DOCTOR OF PHILOSOPHY IN MATHEMATICS**

We accept this dissertation as conforming to the required standard

1.



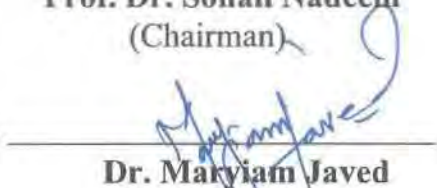
**Prof. Dr. Sohail Nadeem**  
(Chairman)

2.



**Prof. Dr. Tasawar Hayat**  
(Supervisor)

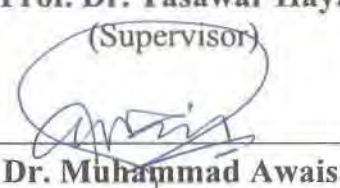
3.



**Dr. Maryyam Javed**  
Associate Professor

Department of Applied Mathematics & Statistics  
Institute of Space Technology (IST),  
(External Examiner)

4.



**Dr. Muhammad Awais**  
Assistant Professor

Department of Mathematics, COMSATS,  
University Islamabad, Attock Campus  
(External Examiner)

**Department of Mathematics**  
**Quaid-I-Azam University**  
**Islamabad, Pakistan**  
**2021**

## Certificate of Approval

This is to certify that the research work presented in this thesis entitled **Peristalsis subject to Entropy Generation** was conducted by Ms. **Sadaf Nawaz** under the kind supervision of **Prof. Dr. Tasawar Hayat**. No part of this thesis has been submitted anywhere else for any other degree. This thesis is submitted to the Department of Mathematics, Quaid-I-Azam University, Islamabad in partial fulfillment of the requirements for the degree of Doctor of Philosophy in field of Mathematics from Department of Mathematics, Quaid-I-Azam University Islamabad, Pakistan.

Student Name: **Sadaf Nawaz**

Signature: 

External committee:

a) **External Examiner 1:**

Name: **Dr. Maryiam Javed**

Designation: Associate Professor

Office Address: Department of Applied Mathematics & Statistics, Institute of Space Technology (IST), Islamabad.

Signature: 

b) **External Examiner 2:**

Name: **Dr. Muhammad Awais**

Designation: Assistant Professor

Office Address: Department of Mathematics, COMSATS, University Islamabad, Attock Campus.

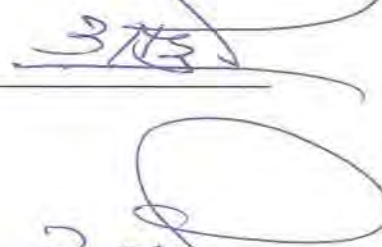
Signature: 

c) **Internal Examiner**

Name: **Dr. Tasawar Hayat**

Designation: Professor

Office Address: Department of Mathematics, QAU Islamabad.

Signature: 

**Supervisor Name:**

**Prof. Dr. Tasawar Hayat**

Signature: 

**Name of Dean/HOD:**

**Prof. Dr. Sohail Nadeem**

Signature: 



*DEDICATED TO  
MY PARENTS  
AND  
SUPERVISOR*

## *Acknowledgement*

*In the name of ALLAH the most beneficent and the most merciful. First and foremost, all praises and thanks to Allah Almighty for His blessings, courage and the strength He gave me in completing this thesis. HE who gave me the ability, knowledge, opportunity and help me all the times i needed, without His will i cannot write a single word. I also expressed my devotion to our beloved Prophet Hazrat Muhammad ﷺ for His guidance through teaching of motivation, patience, humanity and immense knowledge. He declared it as religious obligation for every Muslims to seek and acquire knowledge.*

*I also expressed my gratitude to my respected supervisor Prof. Dr. Tasawar Hayat for his guidance, encouragement, inexhaustible inspiration and valuable suggestions. His valuable suggestions and constructive remarks really helped me in research work. I am grateful to him for his supervision.*

*I wish to express my heartiest gratitude to my family especially my mother Mehmooda Bibi and my father Muhammad Nawaz, who support me financially as well as morally. I have no words to say thanks to my mother who always supported me a lot, built my confidence and pray for me every time. My mother has a great part in my studies, without her continuous support and encouragement it would not possible for me to acquire the higher education and fulfill my dreams. Thanks Mom for understanding and supporting me. Thank you for giving me strength to chase my dreams. May Allah give my parent the long healthy life (Ameen). I am also thankful to my sisters Ifat Nawaz and Kanwal Nawaz, who were always there when I need a friend to share my thoughts and to release my stress. Thanks Ifat Api for moral support. Special*

*thanks to Kanwal for listening and supporting me through her stress releasing company. Also Special thanks to brother in law Ghulam Mujtaba for their support, care and encouragement. I am also grateful to my brother Faisal Nawaz for helping me at every stage. How can I forget to thank my little niece Uruwa Mujtaba and nephew Muhammad Moiz (Jugnu) for their love and care. Thanks my family for their love, support and encouragement, without them the journey would not be possible.*

*I would also like to acknowledge my all teachers who taught me since from my childhood as everyone polished me at different stages and make me able to reach at this stage. I also expressed my gratitude to post graduate professors. I would like to thank Prof. Dr. Sohail Nadeem, Chairman of Mathematics Department for their valuable remarks.*

*I am very grateful to all my lab fellows who were there in my PhD session. Thanks everyone for their help and support.*

*I would also like to thank all the office staff of Mathematics department for their administrative supports. Thanks everyone for treating very nicely and humbly in all administrative matters.*

*In the end I am thankful to everyone who directly and indirectly helped me during this journey.*

*Sadaf Nawaz*

*26-05-2021*

## Preface

*Peristalsis is an important activity that is involved extensively in real life situations. Physiological situations greatly witnessed the existence of this phenomenon. Chyme movement in stomach, bile movement, spermatic transportation, ovum movement, urine transport in bladder etc. are few activities found in this regard. This inherent property is responsible for transportation of materials from one part to others. Due to its novel involvement in physiology it is found convenient to build the clinical devices based on this principle. This is found advantageous in the way of diagnosis and cure of certain diseases. This results in vast majorities of new innovations in the fields of biomedical sciences. Many medical devices like heart lung machine (used in open heart surgery supplies the oxygenated blood to aorta that deliver it to rest body part), dialysis machine (through which blood is filter and toxin and solutes are removed from blood), endoscope (used as diagnosis purposes) etc. work under peristalsis. Many pumping devices like roller pumps, finger and hose pumps etc. are also mentioned in this direction. Human physiology systems are found very complex, spontaneous and irreversible. During these complex processes, energy conversion has always been witnessed, which also results in loss of energy in many physiological situations. All these processes cause change in thermodynamics of the system. This may also leads to disorderliness of the system. For stable system it is very essential to study the system and found the factors for these disorderliness and obtain the ways to optimize these. This system's disorderliness is referred as entropy. Mathematical modeling is found very beneficial to study these analyses and to get an estimate about the factor to increase entropy. Some measures are determined to control these. Mathematical modeling also results in reduction of the experimental expenses and time. In this way firstly data is analyzed theoretically through*

*mathematical model then on the basis of estimate the experiments and further testing techniques are adopted. Here second law of thermodynamics is adopted for entropy analysis. During fluid flow analysis the fluid friction, chemical reactions, thermal irreversibility via magnetic field or radiation, diffusion irreversibility etc. are some factors that may lead to change in entropy. Hence in this thesis different factor are checked for entropy generation in field of peristalsis. Different types of materials with nanofluid features are examined. Effect of different embedded parameters on entropy are observed and analyzed physically. This thesis is structured as follow:*

*Chapter one includes the basic knowledge and literature about the concepts used in this direction. This contains the detailed analysis of peristalsis, non-Newtonian fluids, nanofluids, magnetohydrodynamics (MHD) and current, chemical reaction, porous medium, slip conditions, compliant walls, mixed convection, heat and mass transfer and entropy. This chapter also covers the basic laws for the analysis including mass, momentum, energy and concentration conservation laws.*

*Chapter two contains the mixed convective flow due to peristalsis. Silver water nanofluid has been evaluated in this study. Hall effect and radiation are also studied. Slip conditions are employed at the channel walls. Comparison is set for different shapes of nanomaterial including bricks, cylinders and platelets. Entropy analysis is attempted for different shaped nanoparticles. Technique of perturbation is adopted for solution of system. Effect of sundry parameters on Bejan number and trapping is also accounted. Contents of this chapter are published in *Journal of Molecular Liquids*, 248 (2017) 447-458.*

*Chapter three covers the magneto-nanoparticles in water based nanoliquids. Mixed convection and viscous dissipation are also considered. Second order slip conditions*

are accounted at the boundary. Entropy generation and Bejan number are evaluated. Streamlines are also part of the study. Analysis is based on the comparison between Maxwell and Hamilton Crosser models. The content of this chapter is accepted and in press in *Scientia Iranica*, 27 (2020) 3434-3446.

Chapter four aims to cover the concept of hybrid nanofluid. Study is analyzed for titanium oxides and copper nanoparticles with water as base fluid. Secondary velocity is also studied in view of rotating frame. Hall effect and porous medium are present. Convective boundary conditions are accounted. Non-uniform heat source/sink and radiation are also present. Maxwell-Garnett's model also help to investigate the thermal conductivity for hybrid nanofluid. Entropy generation is also examined. *NdSolve* of *Mathematica* is adopted as solution methodology. The contents of this chapter are published in *Journal of Thermal Analysis and Calorimetry*, 143 (2021) 1231-1249.

Chapter five reports the investigation on entropy in a channel with inclined magnetic field. Williamson nanofluid is utilized here. Buongiorno model with Brownian motion and thermophoresis effects is utilized. Compliant wall of channel are considered. Further slip effects at boundary are investigated. Entropy analysis contains the thermal, Joule, fluid friction and diffusion irreversibilities. Contents of this chapter are reported in *Physica Scripta*, 94 (2019) 10.1088/1402-4896/ab3467.

Chapter six addresses the peristaltic phenomenon in curved configuration. Williamson fluid with well-known Soret and Dufour effects are incorporated. MHD characteristics are examined by applying it in radial direction. Curvilinear coordinates are chosen to model the problem. Flexible wall characteristics are

*incorporated in terms of elastance, rigidity and stiffness. Partial slip is accounted. Considered flow analysis is solved via perturbation. Wessienberg number is adopted to prepare the zeroth and first order approximations. Steamlines are also plotted to investigate the bolus size. Results of this chapter are published in Computer Methods and Programs in Biomedicine, 180 (2019) 105013.*

*Chapter seven communicates the peristalsis for Sisko nanofluid. This chapter further highlights the effects of nonlinear thermal radiation and Joule heating. Slip conditions are also employed. Entropy generation is investigated for viscous dissipation, nonlinear thermal radiation and diffusion and Joule heating irreversibilities. NDSolve is employed as solution technique which gave the convergent results in less computation time. Results are also validated by comparison. This chapter is published in Journal of Thermal Analysis and Calorimetry, 139 (2020) 2129–2143.*

*Chapter eight investigates the study of endoscope impact on peristalsis in present of porous medium. Sisko fluid is utilized for shear thinning effects. Modified Darcy law is incorporated for reporting the porous medium effects. Entropy is accounted for different pertinent parameters. Convective conditions are accounted here. The findings of this analysis are reported in Physica A, 536 (2019) 120846.*

*Chapter nine provide attention on entropy generation for Rabinowitsch nanofluid. A comparative study based on viscous, shear thickening and shear thinning fluid is reported. Chemical reaction is studied. A non-uniform heat source/sink parameter is involved in the energy equation with viscous dissipation and Brownian motion and thermophoresis effects. Slip is also considered on the boundary. Velocity, temperature, concentration, entropy and heat transfer coefficient are examined for*

comparison. The results of this research is published in *Applied nanoscience*, 10 (2020) 4177–4190.

Chapter ten covers the entropy analysis for homogeneous-heterogeneous reaction. Prandtl nanofluid is utilized in peristalsis. Magnetic field is applied in the perpendicular direction to flow. Joule heating is also considered. Buongiorno model is utilized. Second law of thermodynamics is employed to study entropy generation. Graphs are plotted for velocity, temperature, homogeneous-heterogeneous reaction and heat transfer coefficient and entropy. The findings of this chapter are reported in *European Journal Physical Plus*, 135 (2020) 296.

Chapter eleven investigates the entropy in view of variable thermal conductivity. Third grade fluid for peristalsis is adopted. MHD and Joule heating are considered. Compliant characteristics of channel walls are outlined. Graphs are plotted numerically via *NDSolve* of *Mathematica*. Mixed convection is involved in this study. Results are examined graphically. Trapping is also examined via streamlines. This study is published in *European Journal Physical Plus*, 135 (2020) 421.



## NOMEN CLATURE

$\pm\eta$	Channel walls
$d$	Half width of channel
$t$	Time
$a$	Wave amplitude
$c$	Wave speed
$\lambda$	Wavelength
$B_0$	Strength of applied magnetic field
$g$	Gravitational acceleration
$T_0, T_1, T_m$	Walls temperature and mean temperature
$C_0, C_1, C_m$	Walls concentration and mean concentration
$u, v, w$	Velocity field
$\sigma_{eff}, \sigma_p, \sigma_f$	Electric conductivity of nanofluid, nanoparticles and base fluid respectively
$\mu_{eff}, \mu_f$	Viscosity of nanofluid and base fluid
$\rho_{eff}, \rho_f, \rho_p$	Density of nanofluid, base fluid and nanoparticles respectively
$K_{eff}, K_f, K_p$	Thermal conductivity of nanofluid, base fluid and nanoparticles respectively

$n^*$	Nanoparticle shape factor
$\sigma^*$	Stephan-Boltzman constant
<b>J, E, F</b>	Current density, electric field, Lorentz force
$e, n_e$	Electron charge, number density of free electrons
<b>T, C</b>	Temperature, Concentration
$(\rho C_p)_{\text{eff}}, (\rho C_p)_f, (\rho C_p)_p$	Heat capacity of nanofluid, base fluid and nanoparticles
$(\rho\beta_T)_{\text{eff}}, (\rho\beta_T)_f, (\rho\beta_T)_p$	Effective thermal expansion of nanofluid, base fluid and nanoparticles
$p$	Pressure
$\xi_1, \xi_4$	First and second order velocity slip parameters respectively
$\xi_2, \xi_5$	First and second order thermal slip parameters respectively
$\xi_3$	Concentration slip parameter
$q_r$	Radiative heat flux
$k^*$	Mean absorption coefficient
$\varphi^*$	Volume fraction of nanoparticles
$m$	Hall parameter

Re	Reynolds number
Pr	Prandtl number
Ec	Eckert number
Br	Brinkman number
Gr	Grashof number
Rd	Radiation parameter
M	Hartman number
$\Psi$	Stream function
$\theta$	Dimensionless temperature
$\varphi$	Dimensionless concentration
$N_s$	Entropy generation
Be	Bejan number
$E_1, E_2, E_3$	Compliant wall parameters
$\Omega$	Angular frequency
$\rho_{hnf}$	Density of hybrid nanofluid
$\sigma_{hnf}$	Electric conductivity of hybrid nanofluid
$\mu_{hnf}$	Viscosity of hybrid nanofluid
$\kappa_{hnf}$	Thermal conductivity of hybrid nanofluid
$(\rho C_p)_{hnf}$	Effective heat capacity of hybrid nanofluid

$Q_0$	Heat generation or absorption coefficient
$B_1, B_2$	Heat transfer coefficients at the wall
$k_1$	Porosity parameter
$T'$	Taylor number
$S$	Heat source or sink parameter
$Bi_1, Bi_2$	Biot numbers
$\chi$	Inclination angle for magnetic field
$\tau$	Capacity ratio
$\alpha^*$	Thermal diffusivity
$D_B$	Brownian motion coefficient
$D_T$	Thermophoretic diffusion coefficient
$A_1$	First Rivlin Erickson tensor
$We$	Weissenberg number
$\varepsilon$	Amplitude ratio
$\delta$	Wave number
$Sc$	Schmidt number
$Nb, Nt$	Brownian motion parameter, thermophoresis parameter
$R$	Dimensional parameter

$L, L_1, L_2$	Diffusion coefficient parameter, Diffusion coefficient parameters for case of homogeneous and heterogeneous reactions
$\Lambda$	Temperature difference parameter
$\zeta$	Concentration difference parameter
$D$	Coefficient of molecular diffusion
$K_T$	Thermal diffusion ratio
$C_s$	Concentration susceptibility
$k$	Curvature parameter
$S_r$	Soret number
$D_u$	Dufour number
$\beta_1$	Sisko fluid parameter
$Da$	Darcy number
$\gamma_1$	Chemical reaction parameter
$k_c, k_s$	Rate constants
$C_1^*, C_2^*$	Concentrations of species
$H, K$	Strength of heterogeneous and homogeneous reactions respectively
$\alpha_1$	Prandtl fluid parameter

$\beta$	Fluid parameter
$A_2$	Second Rivlin-Ericksen
$\zeta$	Variable thermal conductivity parameter

# Contents

<b>1</b>	<b>Fundamental concepts and literature survey</b>	<b>6</b>
1.1	Background . . . . .	6
1.2	Basic laws and fundamental equations . . . . .	18
1.2.1	Mass conservative law . . . . .	18
1.2.2	Momentum conservative law . . . . .	19
1.2.3	Energy conservative law . . . . .	19
1.2.4	Concentration law . . . . .	21
1.2.5	Compliant walls . . . . .	21
<b>2</b>	<b>Entropy generation in peristalsis with different shapes of nanomaterial</b>	<b>23</b>
2.1	Introduction . . . . .	23
2.2	Flow configuration . . . . .	24
2.2.1	Entropy generation and viscous dissipation . . . . .	28
2.3	Solution methodology . . . . .	29
2.3.1	Zeroth order systems and solutions . . . . .	29
2.3.2	First order systems and solutions . . . . .	30
2.4	Discussion . . . . .	31
2.5	Conclusions . . . . .	45
<b>3</b>	<b>Investigation of entropy generation in peristalsis of magneto-nanofluid with second order slip conditions</b>	<b>46</b>
3.1	Introduction . . . . .	46
3.2	Flow Configuration . . . . .	46

3.2.1	Entropy generation and viscous dissipation . . . . .	50
3.3	Solution methodology . . . . .	51
3.3.1	Zeroth order systems and solutions . . . . .	51
3.3.2	First order systems and solutions . . . . .	51
3.4	Discussion . . . . .	52
3.4.1	Analysis of velocity . . . . .	52
3.4.2	Analysis of temperature . . . . .	55
3.4.3	Analysis of entropy generation and Bejan number . . . . .	58
3.4.4	Streamlines . . . . .	61
3.5	Conclusions . . . . .	67
<b>4</b>	<b>Modeling and analysis of peristalsis of hybrid nanofluid with entropy generation</b>	<b>68</b>
4.1	Introduction . . . . .	68
4.2	Problem modeling . . . . .	69
4.2.1	Entropy generation . . . . .	73
4.3	Analysis . . . . .	74
4.3.1	Velocity . . . . .	74
4.3.2	Temperature . . . . .	79
4.3.3	Entropy generation analysis . . . . .	84
4.3.4	Heat transfer rate . . . . .	86
4.3.5	Streamlines . . . . .	91
4.4	Conclusions . . . . .	95
<b>5</b>	<b>Entropy generation in peristaltic flow of Williamson nanofluid</b>	<b>96</b>
5.1	Introduction . . . . .	96
5.2	Formulation . . . . .	96
5.2.1	Determination of Entropy generation . . . . .	102
5.3	Analysis . . . . .	103
5.3.1	Velocity . . . . .	103
5.3.2	Temperature . . . . .	105



5.3.3	Concentration . . . . .	107
5.3.4	Heat transfer coefficient . . . . .	109
5.3.5	Entropy generation . . . . .	110
5.3.6	Validation of problem . . . . .	111
5.4	Conclusions . . . . .	112
<b>6</b>	<b>Effects of radial magnetic field and entropy on peristalsis of Williamson fluid in curved channel</b>	<b>113</b>
6.1	Introduction . . . . .	113
6.2	Modeling . . . . .	114
6.3	Solution methodology . . . . .	120
6.3.1	Zeroth order solutions . . . . .	121
6.3.2	First order solutions . . . . .	122
6.3.3	Entropy analysis . . . . .	124
6.4	Analysis . . . . .	124
6.4.1	Validation of the Problem . . . . .	137
6.5	Conclusions . . . . .	138
<b>7</b>	<b>Numerical study for peristalsis of Sisko nanomaterials with entropy genera- tion</b>	<b>139</b>
7.1	Introduction . . . . .	139
7.2	Problem formulation . . . . .	140
7.2.1	Expression for entropy generation . . . . .	145
7.3	Analysis . . . . .	146
7.3.1	Velocity . . . . .	146
7.3.2	Temperature . . . . .	148
7.3.3	Nanoparticle concentration . . . . .	152
7.3.4	Entropy generation analysis . . . . .	154
7.3.5	Heat transfer coefficient . . . . .	158
7.3.6	Trapping . . . . .	160
7.3.7	Validation of problem . . . . .	164

7.4	Conclusions . . . . .	164
<b>8</b>	<b>Entropy generation and endoscopic effects on peristalsis with modified Darcy's law</b>	<b>166</b>
8.1	Introduction . . . . .	166
8.2	Modeling . . . . .	167
8.2.1	Entropy generation . . . . .	172
8.3	Solution methodology . . . . .	172
8.4	Analysis . . . . .	173
8.5	Conclusions . . . . .	182
<b>9</b>	<b>Entropy optimization for peristalsis of Rabinowitsch nanomaterial</b>	<b>183</b>
9.1	Introduction . . . . .	183
9.2	Problem formulation . . . . .	184
9.2.1	Solution of the problem . . . . .	188
9.2.2	Expression for entropy generation . . . . .	188
9.3	Analysis . . . . .	189
9.3.1	Velocity . . . . .	189
9.3.2	Temperature . . . . .	191
9.3.3	Concentration field . . . . .	195
9.3.4	Entropy generation analysis . . . . .	198
9.3.5	Heat transfer coefficient . . . . .	200
9.4	Conclusions . . . . .	202
<b>10</b>	<b>Entropy analysis in peristalsis with homogeneous-heterogeneous reaction</b>	<b>203</b>
10.1	Introduction . . . . .	203
10.2	Problem formulation . . . . .	203
10.2.1	Entropy generation . . . . .	209
10.3	Analysis . . . . .	210
10.3.1	Validation of problem: . . . . .	223
10.4	Conclusions . . . . .	223

<b>11 Entropy analysis for the peristaltic flow of third grade fluid with variable thermal conductivity</b>	<b>225</b>
11.1 Introduction . . . . .	225
11.2 Modeling . . . . .	225
11.2.1 Entropy generation . . . . .	230
11.3 Analysis . . . . .	230
11.3.1 Velocity . . . . .	230
11.3.2 Temperature . . . . .	233
11.3.3 Entropy analysis . . . . .	236
11.3.4 Heat transfer coefficient . . . . .	238
11.3.5 Trapping . . . . .	240
11.4 Conclusions . . . . .	242

# Chapter 1

## Fundamental concepts and literature survey

Here our aim is to provide the background about some relevant concepts utilized in the subsequent chapters. This includes the concepts of peristalsis, entropy, nanofluid and some basic law and equations related to fluid flow.

### 1.1 Background

The word peristalsis is originated from the Greek word “peristaltikos” which means “clasp and compressing”. This type of motility is responsible for transportation among different parts of body. In this mechanism the material is propelled through the progressive waves consisting of contraction and expansion (as first presented by Bayliss and Starling [1]) and this helps in movement of the material. These waves may be short or long in length. It is based on the involuntary characteristic of the smooth muscles that are involved in peristalsis. Hence this mechanism cannot be controlled by someone by choice but smooth muscles works when they are stimulated to do so. This motility is very useful in digestion and some other situations witnessed in physiology.

In living beings this activity is found in transport of food particle through esophagus, chyme movement in stomach, urine transport from kidney, movements involved in the small and large intestines, vasomotion of blood vessels, bile movement in duct, spermatic movement, ovum

movement in fallopian tube etc. This activity is initiated in the human beings when any food stuff is chewed and swallowed through the esophagus. At this stage the peristaltic wave start from the upper position of tube and propagate along the complete length and transfer this food to stomach and here epiglottis also helps to route this bolus into esophagus instead of entering this into windpipe. This is also termed as esophageal peristalsis. Afterwards this chewed food stuff is churns through peristalsis and mix it with gastric juices. The gastric juices help to dissolve this food through chemical and mechanical actions. At last after few hours this food becomes the chyme which is the semi-solid like mixture. Then through peristalsis this material is forced to small intestine where nutrients are absorbed through intestinal walls into blood streams. At last final absorption took place in large intestine when peristalsis carried this material to large intestine where waste material also eliminated through it.

Reverse peristalsis also occurs in cub- chewing animals including cows, sheep, camels etc. where chewed material is brought back to mouth for chewing again. In human beings the reverse peristalsis does not occur normally. This happens under certain circumstance like food poisoning that caused disturbance in stomach and activate the emetic centre of brain that results in immediate vomiting.

Beside the contribution of peristalsis in living organisms, this activity is involved in many industrial, engineering and biomedical applications. At industrial level this activity is adopted for the transportation of toxic liquid, sanitary fluid transport etc. It is also employed in the transportation of nuclear waste material. It is also used in pumping phenomenon like roller pumps, finger and hose pumps etc. Moreover these pumps are utilized in mining and metallurgy, food and beverage, biopharmaceutical etc. Heart lung machine, dialysis machine and endoscopy also involve peristalsis.

Due to such applicability of the topic in the field of physiology, medical devices, industrial applications persuaded the mathematicians, physicists and engineers to investigate more in this arena. The myogenic theory of peristalsis goes back to Engelmann [2] who investigated this activity in ureter. He concluded that there is no ganglias in the muscular layer but few at the end of the ureter. Afterward some initial attempts were endeavored by Lapidés [3] and Boyarsky [4]. They studied the physiology of human ureter. The significance behind any mathematical modeling of physiological fluid flows is to get a better understanding for the

specific flow that is being modeled. As the peristaltic flow is evident in mostly physiological situations so the precise mathematical analysis may help to study the flow in human body. Latham [5] did the pioneer work on peristalsis. He considered the viscous fluid for study of peristalsis in ureter. He compared the experimental results with theoretical research. These are found in good comparison. After him Shapiro et al. [6] did the study for peristalsis in two-dimensional channel. They examined the series of waves in inertia free flow by adopting the long wavelength and small Reynolds number approach. Theoretical results are also validated experimentally for axisymmetric and plane configurations. Burns and Parkes [7] analyzed the peristalsis in view of lubrication approach. They obtained the series solution. Their model was best suited for creeping flow as they have neglected the inertial terms from Navier-Stokes equations. Barton and Raynor [8] accounted the peristaltic activity in tubes for the study of movement of chyme to small intestine. Fung and Yih [9] and Hanin [10] also analyzed peristalsis. Peristaltic activity in circular shape cylindrical tubes is investigated by Yin and Fung [11], Li [12] and Chow [13]. They have considered the viscous fluid. Li [12] gave a comparison for axisymmetric and two-dimensional channel by obtaining a series solution. Chow [13] also analyzed the axisymmetric flow by series solution. Here the flow is induced by Hagen-Poiseuille flow. Meginniss [14] discussed the peristalsis in a roller pump tube in presence of low Reynolds number. Lykoudis and Roos [15] studied the peristaltic flow in ureter. They have utilized the lubrication approximation. Zien and Ostrach [16] also applied the lubrication theory to their problem by considering viscous, two-dimensional and incompressible fluid. At zero mean volume flow rate inertial effects in Navier-Stokes equations has been studied. They declared that their model is appropriate for the case of ureter. Results for peristalsis in view of experimental and theoretical sense are also validated by Yin [17], Eckstein [18], Weinberg [19] and Yin and Fung [20]. Weinberg [19] mentioned that his results are in good comparison with ureteral analysis. Weinberg et al. [21] studied the impacts on ureter by imposing different waves. Jaffrin and Shapiro [22, 23] investigated the pumping and reflux in peristalsis. Lew et al. [24] investigated flow in the small intestine. Circular cylindrical axisymmetric tube has been taken for the analysis. They obtained two series form solution. One for the case of peristalsis compression without net fluid transport and other when peristalsis generated deprived of net pressure gradient. Lew and Fung [25] collaborated for work on peristalsis in

valve vessels for small Reynolds number. Fung [26] examined the peristaltic wave in ureter by evaluating the muscles action. He considered the tissues elasticity as exponential type. Hill modified equations were utilized for muscles. Flow was considered axisymmetric having the small wavelength. Peristalsis in a tube by utilizing the finite-element technique is examined by Tong and Vawter [27]. Jaffrin [28] examined the peristaltic transport in inertial system. He accounted the streamline curvature effects. His investigation can be applied to roller pumps and alimentary canal. Peristaltic activity by using the Frobenius techniques in two-dimensional geometry is examined by Mitra and Parasad [29]. Negrin et al. [30], Manton [31], Gupta and Seshadri [32] and Liron [33] also put forward their attempts. In this regard, Brown and Hung [34] also executed the study on experimental and computational bases. In another study [35] they have solved the Navier stokes equations numerically in curvilinear coordinates. Kaimal [36] and Bestman [37] dealt with this activity by utilizing long wavelength strategy. Rath [38] planned the study for lobe shape tube. Results for pressure flow and velocity are calculated and compared. Some other studies from literature can be referred through studies [39-50].

Until now, we have given the attention to discuss the literature on the peristalsis of viscous fluid. However in real life problems, all the fluids do not exhibit the viscous fluid characteristics (direct and linear relationship between shear stress and deformation rate). Mostly natural phenomenon witnessed the involvement of non-Newtonian fluids. As peristalsis is found extensively in human body, where we observed that the chewable food, blood, chyme etc. all lie in the category of non-Newtonian fluids. Besides these, different oils, ketchup, lubricants, shampoo, toothpaste, honey, custard, muds, paints, polymer solutions, industrial materials etc. all behave as non-Newtonian fluids. All the non-Newtonian fluids depend on their rheological properties. Hence these cannot be mathematically modelled through single constitutive relation. Different models has been presented ([51, 52]) and utilized by the researchers depending on the fluid characteristics. Raju and Devanathan [53] provided their first attempt for power law fluid. This fluid model describes the pseudoplastic, dilatant and Newtonian fluid for changing the values of power law index. They treat the blood as pseudoplastic fluid during the flow in axisymmetric tube. Becker [54] gave a detailed description of different non-Newtonian fluids. He also examined different types of flow problems. Deiber and Schowalter [55] investigated the peristalsis of viscoelastic material in a tube. They also accounted the porous medium. Viscoelastic materials

are also employed by Bohme and Friedrich [56] in planar channel. They investigated the inertia free fluid subject to lubrication approach. Approximate solutions are obtained up to second order of approximation for amplitude ratio. Pressure discharge and pumping efficiency were the focus of their study. Micropolar fluid is also attended by Devi and Devanathan [57]. Pressure gradient and micro-rotation is examined. Srivastava and Srivastava [58] look for the peristalsis of Casson fluid. They considered blood as two-layer suspension of Casson fluid and peripheral layer of plasma. Results were compared with studies for without peripheral layer. Investigation for second order fluid flow in a tube is due to Siddiqui and Schwarz [59]. They deduced their results for the special case of axisymmetric Newtonian fluid. Misra and Pandey [60, 61] talked about the non-Newtonian fluids by utilizing the power law fluid model as food bolus in one of their studies for esophagus. Mernone et al. [62] attended the Casson fluid model and calculated the perturbation solutions. Herschel-Bulkley model has been explored by Vajravelu et al. [63]. Trapping and pressure rise were also investigated. Hayat and Ali [64, 65] scrutinized the third grade and power law models for peristalsis. Horoun [66, 67] designed the analysis for third and fourth grade fluids by taking the asymmetric and inclined asymmetric geometries respectively. Reddy et al. [68] examined the power law model for asymmetric peristalsis. They considered the waves traveling with different amplitudes for asymmetry in geometry. Hayat et al. employed different fluid models (Burger [69], micropolar [70], Carreau [71]) for peristalsis by moderating different flow assumptions. Wang et al. [72] attended Sisko model. This predicts the shear thinning and shear thickening effects for different values of power law index. Mekheimer and Elmaboud [73] carried out the study for couple stress fluid. They modelled the study in an annulus. Frictional forces, pressure rise and trapping were focused. They emphasized on the application of endoscope. Hariharana et al. [74] presented an investigation for Burger and power law models in a tube. They employed the different wave forms including square, trapezoidal, multi sinusoidal and sinusoidal. They utilized the Fourier series in their analyses. Path lines were also drawn to investigate the reflux. Muthu et al. [75] discussed micropolar model for fluid in a tube. Hayat et al. [76, 77] continued to extend the literature by attaining the attempts for Maxwell and Johnson-Segalman models. Tripathi et al. [78] focused on viscoelastic materials by employing the fractional Maxwell technique. Hayat et al. [79] studied the third grade fluid in curved geometry. They analyzed the heat and mass transfer. Third grade fluid is the



differential type fluid. This model describes the shear thinning, shear thickening and normal stresses. Alsaedi et al. [80] addressed the Prandtl fluid to examine peristalsis. Convection transfer of heat has been also investigated. Hayat et al. [81] examined the Eyring Powell fluid with convection on the boundary. Chemical reaction has been also carried out. This model predicts the results accurately at high and low shear rates. Some studies reported by Hayat et al. [82, 83, 84, 85] on non-Newtonian fluids are also useful. Here the authors have utilized the Soret, Dufour, radial magnetic field, rotation effects. Sadaf and Noreen [86] carried out the investigation for Rabinowitch fluid. Rabinowitch model describes the viscous, shear thinning and shear thickening effects.

Amelioration of heat transfer capability is the need of time and required in every field. It is primary apprehensions for scientist nowadays. Peristalsis with heat transfer effects is necessary from the biomedical point of view. Whenever a process runs it involves heat loss. From the past era there is much more interest found in the field of nanotechnology. The reason behind this is the enhancement in heat transfer efficiency. Nanofluid are the new class of advanced heat transfer fluid that are homogeneous mixture of base fluid and suspended particles in it. These are not just prepared by mixing the nanoparticles in host fluids but involve the chemical processes. Utilizing the nanoparticles of millimeter or micro size caused eventual sedimentation and corrosion. Hence nano size particles (1-100 nm) are used. This will helps to minimize the gravitational effects and enhances the stability of mixture. For nanofluid the contact surface area is greater when compared with microparticles. This will cause quick thermal response and hence enhances the heat transfer. Size, material and shape of the particles are the main factor that effected the thermophysical properties of nanofluid. With same volume fraction of different nanoparticles, the efficiency of nanoliquids can be different. Different nanoparticles ceramics (Alumina, Silicon carbide etc.), metals (Aluminium, copper etc.) Carbon (Graphene etc.) are utilized in traditional liquids i.e. water, oils etc. Choi [87] gave the name “nanofluid” to this material. Nanoliquids are used for cooling purposes like cooling in automotive engine, solar energy, refrigeration, electronic cooling, drug delivery, aerospace, cooling and heating of buildings, oil recovery, desalination, lubrication, drilling, nuclear cooling, boiler etc. These new fluids have enhanced thermal properties when compared with traditional liquids. Due to its stability and little settling the nanofluids are found more proficient. Besides the industrial and

engineering applicability, the nanoliquids are also being used in biomedical field. Iron based nano materials are utilized as delivery vehicle up the blood stream to tumor. This will help to deliver the drugs in cancer patients. Nanoporous membranes with help of Ultraviolet source can kill the virus and bacteria from water. Due to such ample novelty the different models are used by the researchers. Maxwell [88] model for spherical shaped particles, Hamilton and Crosser [89] for different shapes of nanomaterial, Xue [90] for nanotubes particles are important to mention here. In these models the characteristics of fluid and particles are separately provided. Buongiorno [91] model was based on seven slip mechanisms for convective transport. He proposed that among these only Brownian motion and thermophoresis are prominent. Birkman [92] gave the model for viscosity of the nanofluids. Khanafer and Vafai [93] provided a critical synthesis for the nanoliquids characteristics. Sheikholeslami et al. [94-96] developed analyses in presence of MHD and radiation for different conditions. Shehzad et al. [97] addressed the peristaltic flow of nanofluid in presence of Joule heating. Abbasi et al. [98] reported the effect of spherical and cylindrical particles. Bhatti et al. [99] addressed the Sisko fluid treating it as blood and Titanium nanoparticles for endoscope application. Sayed et al. [100] examined the non-Newtonian nanofluid in an inclined asymmetric geometry. Some more attempts can be highlighted via refs. [101-110]. The utilization of hybrid nanofluid can be seen through refs. [111-115].

Magneto hydrodynamics is the study of dynamics of fluids when magnetic field is involved. It is the property of electrical conducting fluid that it become polarized and change the MHD itself. This property has significant importance and note worthy applications in the field of biomedical engineering. As blood behaves as the conducting fluid so this characteristic of blood has been considered in certain clinical applications. MHD is applied to reduce the bleeding in case of severe injuries. As magnetic field slows down the flow. This property is also accounted in surgical operation to drop blood flow. Magnetic resonance imaging (MRI) has been employing for diagnosis purposes. Further it is found for cancer treatment [116] method to guide the iron-based nanomaterials. Super paramagnetic iron oxide nanoparticles are found proficient for drug delivery. Trapping phenomenon may cause thrombus in blood vessels that can be disappeared with the help of MHD. Its applicability can also be seen in hyperthermia [117], intestinal disorders and magnetic endoscopy. Industrial processes may include solar power technique,

remote sensing to screen the non-proliferation, geothermal extractions, signal processing, power generation processes, MHDs sensors etc. In natural phenomenon like Earth magnetic field to solar wind, magnetic field of stars and planets this activity is also observed. During MHD another physical aspect has been also inspected named as Joule heating, which occurs as a result of implication of magnetohydrodynamic aspect. The result of current through conductor produces heating. Many common applications are working on this principle, like hair dryer, electric heater, iron to remove wrinkle etc. Different researches have been carried out on the concept of magnetohydrodynamics. Magnetic field during blood pumping has been studied by Stud et al. [118]. Shehawy and Husseny [119] presented a study of peristalsis by employing magneto fluid. Perturbation solution has been constructed in presence of porous boundaries. Mekheimer [120] studied the blood flow in non-uniform channel. Naby et al. [121] examined the trapping in presence of MHD. Eldabe et al. [122] analyzed bioviscosity fluid for MHD characteristics. Hayat and Ali [123] also investigated hydrodynamic flow. In another analysis Hayat et al. [124] covered the endoscope problem for Jeffrey fluid by employing magnetic field. Ebaid [125] carried out a numerical analysis for MHD peristalsis of biofluid with varying viscosity. Some more attempts here can be viewed (refs. [126-131]). It is also observed that Hall current cannot be ignored for situations associated with strong magnetic field (see refs. [132-139]).

In natural phenomenon chemical reactions also takes place. It may be of constructive or destructive type which depend on the nature of reactants that take part in chemical reaction. These reactions are homogeneous if the reactants are in same state otherwise named as heterogeneous reaction, which are of keen importance in medical field because of production of biodiversity. In peristalsis there are many processes where chemical reaction clearly involved, named as metabolism. During some reactions, the energy released is used by cell to proceed life e.g. during the breakdown of glucose, while for later energy is absorbed including the process of formation of protein. Catalytic reactions are also observed in living beings. Basically, catalyst is an agent that enhances the speed of reaction. In living organisms, enzymes play the role as catalyst. Without these enzymes the process of metabolisms is too slow that it will take even centuries to complete, hence there is no chance of survival. As temperature and concentration of the reactants is less to react itself. Enzymes helps to reduce the activation energy required.

There are different enzymes each worked with a particular substrate. Missing enzymes may lead to metabolic disorders. Beside these applicability catalysis converter has been utilized to produce Ammonia. Fog formation, batteries, production of polymer, electrolytic cells, hydrometallurgical industry witnessed some applicability of chemical reaction. Initial studies on homogeneous-heterogeneous reactions [140, 141] have been reported by Merkin and Chaudhary and Merkin respectively. Merkin investigated the first order heterogeneous and cubic autocatalytic homogeneous reaction. Further Hayat et al. [142, 143] put forward their analysis for chemical reaction, convective conditions and Hall effects. Awais et al. [144] commenced a study for chemical reactions in tapered channel by using two phase nanoliquids. They have utilized the silver and copper nanomaterial. More relevant studies in this direction can be seen via studies [145-149].

Porous material is characterized as having voids or pores in it. Many natural materials like soil rocks, zeolites, ceramics and cements, biological materials such as bones, cork, capillaries, filters etc. witnessed the examples of porous materials. This concept is utilized in different engineering branches such as petroleum engineering, construction engineering, geoscience, material science, biophysics, biology etc. Fluid flow via porous medium has gained a lot of interest and importance and it becomes a separate branch. Fluid flow from porous media is influenced by certain properties of media, tensile strength, permeability, porosity etc. Experimental work on flow via porous medium is experienced by Darcy [150]. Classical Darcy law works well for viscous flow. Simple relation between pressure gradient and flow rate is elucidated through this relation. These postulates are valid for the flow in tubes, capillaries and some other applications in earth sciences. For non-Newtonian fluids the modified Darcy law preserves the surface tension force. Johansen and Dunning [151] commenced a study for capillary system by focusing on wettability. Affifi and Gad [152] reported a study on porous medium for pulsatile fluid peristalsis. Rao and Mishra [153, 154] examined the porous medium for peristalsis. They [153] employed porous tube filled with power law fluid. In another study [154] porous peripheral layer for gastrointestinal tract has been investigated. Elshehawey et al. [155] canvassed the study for peristalsis in tapered pore by considering viscous fluid. They considered the compressible fluid. They deduced the fact that induced net flow is strongerly influenced by liquid compressibility. Tan and Masuoka [156, 157] reported their studies for porous medium by using second grade

and Oldroyd-B-fluid. They analyzed the Stoke's first problem. Vajravela et al. [158] attended peristalsis in porous annulus. By commencing the studies for porous medium Hayat et al. [159, 160] accounted the effects of Hall and rotation in peristalsis of Oldroyd-B-fluid and Stokes first problems for third grade fluid. Further studies [161-164] also gave a look on literature for highlighting the novelty of porous space.

For fluid flow problems there are two main boundary conditions namely no-slip and slip boundary conditions. No-slip condition has been validated through theory for viscous fluids according to which the fluid will adhere to wall and there in no relative velocity among them. Moreover, shear stress arises due to distortion of fluid particles. However, for certain conditions such as fluid flow in capillary vessels, polymer melts extrusion etc. where no-slip conditions are no more valid. In human body where flow also dissatisfied the no-slip conditions, slip conditions are adopted. This technique is significant to polish the artificial heart valve, polymer industry, paints etc. In slip there is direct relation between velocity and shear stress of the fluid. Depending upon the fluid's nature, slipping of fluid at the wall varies. Hayat et al. [165] presented the study for peristalsis in porous medium. They have chosen the partial slip conditions on boundary. Adomian decomposition technique has been used to find solution. Trapping and pumping have been also discussed. Ali et al. [166] also encountered the problem for peristalsis with slip conditions, MHD and variable viscosity. Series solution have been developed in this case. Ebaid [167] captured the effects for slip conditions in presence of MHD in an asymmetric geometry. Srinivas et al. [168] also reported the slip and magnetohydrodynamics in peristalsis. Johnson Segalman fluid model for slip conditions has been focused by Akbar et al. [169]. Mustafa et al. [170] attended slip effects for viscous nanofluid. Sayed et al. [171] explored the slip conditions for velocity. Tangent hyperbolic nanofluid model and copper water material has been investigated by Hayat et al. [172, 173]. Another type of boundary conditions has also been accounted during flow problems. These are collection of Fourier law and Newton law of cooling. Some literature is mentioned here for view. Ramesh [174] employed the convective conditions for couple stress fluid. He also accounted the porous media. Hayat et al. [175] adopted the convective boundary conditions in peristalsis through curved channel. Shahzadi and Nadeem [176] also employed these conditions for metallic nanoparticles.

Compliance as medical terminology is defined as the capability of vessel to bulged as a

result of pressure on it and persist its original position. On other side it is related to material's ability to deform elastically as a result of an applied force. It is the inherent property of capillaries, arteries, valves, veins and muscles in living organisms. This property of blood veins is responsible for blood pressure changing. This characteristics has been appealed by the researchers as compliant nature of surfaces cause reduction in drag force. As peristalsis is involved in physiology and clinical applications. Therefore this property has advantages to utilize. For mathematical modelling the compliant nature is describes in terms of elastance, rigidity and stiffness through mathematical expressions. This will help to treat these walls as membrane. Many studies have been conducted in this way. Mittra and Prasad [177] conducted an initial study by adopting flexible wall. Srivastava and Srivastava [178] presented the study by adopting the viscoelastic features of the wall geometry. Particulate phase effect has been investigated on qualitative and quantitative basis. Elnaby and Haroun [179] also pay attention to this effect. Javed et al. [180] addressed the study by using Burger fluid in flexible wall channel. Jyothi et al. [181] reported the investigation on MHD Johnson fluid in complaint wall channel. Hayat et al. [182] portrayed the study for endoscope analysis while adopting slip and flexible walls. The studies [183, 184] examined the wall properties effects under magnetic field and variable liquid characteristics. Javed and Naz [185] treated the realistic fluid in flow geometry having compliance characteristics.

Heat and mass transfer always occur during the process of flow. Heat transfer modes include conduction, convection and radiation. All these processes are involved during fluid flow. The conduction during fluid flow has been analyzed through Fourier's law. Convection is dominant mode in fluids for transfer of heat. Influence of gravity in different scenario also plays significant role. Sometimes these effects are so prominent and cannot be ignored. At horizontal surfaces these effects are not effective to study as compared to vertical and inclined geometry involved in laboratory and real-life situations. As a result of gravity natural convection occurs. Mixed convection is the combination of natural and forced convection. Mixed convection activity has been greatly carried out for heat transfer processes including process of nuclear impurities, MHD generators, chemical plants etc. Srinivas et al. [186, 187] modeled the mixed convection phenomenon. They have given the attention to heat and mass transfer effects and chemical reaction in their respective studies. Hayat et al. [188] commenced a study for mixed convective

flow with slip boundary conditions. Assumptions of Joule heating and Soret and Dufour effects have been modeled. Mustafa et al. [189] addressed mixed convective flow of fourth grade fluid with Soret and Dufour effects. Water based nanoliquids in presence of mixed convection has been studied by Hayat et al. [190]. Convective boundary conditions, Hall effects and Joule heating have been accounted. In another study [191] they accounted the mixed convection phenomenon in tapered asymmetric channel. Tanveer et al. [192] reported a study in view of mixed convection effect for Eyring Powell fluid in curved configuration. Radiation is also another mode of heat transfer nowadays applicable in many biomedical applications. All these modes maintained a healthy temperature and remove the extra heat from body if necessary. Sweating, vasoconstriction, vasodilation, through urine etc. are all different way of heat transfer. Heat and mass transfer effects have gained importance due to its existence and applicability. Srinivas and Kothandapani [193] talked about heat transfer aspect in asymmetric channel. Mekhemier and Elmaboud [194] elaborated the heat transfer in a vertical annulus. Nadeem and Akbar [195, 196] also worked for heat transfer aspects. Further studies about this aspect can be noticed from the refs. [197-200].

Natural activities are spontaneous, irreversible and complex. During fluid flow many processes involve fluid friction, Joule heating, chemical reactions etc. This caused change in system's thermodynamics. These kinds of activities caused disorderliness in the system. Study of disorderliness of the system is named as entropy. The concept of entropy goes back to Rudolf Clausius, who defined the entropy in the thermodynamic sense. Second law of thermodynamics is utilized for entropy. This law shows that entire actual processes are irreversible and this irreversibility can be assessed through entropy generation analysis. Heat transfer laws and fluid mechanics principles are combined to ascertained strategies for entropy generation optimization. Foremost target behind the designing of different devices and system is to provide the maximum output and to minimize the entropy. In thermodynamic sense this is related to enhance heat transportation rate and estimating the performance of a system. To obtain the sophisticated energy efficiency the researchers have moved to the thermodynamic approach EGM (entropy generation minimization) in thermal engineering system and devices. This approach is quite beneficial in designing the engineering devices. This great applicability and ample application can be seen through its utilization in reactors [201], chillers [202], microchannels [203], air sepa-

rators [204], fuel cells [205], helical coils [206], evaporative cooling [207], curved pipes [208], gas turbines [209] etc. Besides these with reference to peristalsis the study of entropy is very crucial, as physiological processes are complex and spontaneous. From the medical point of view, it is necessary to venture the factor that causes the greater irreversibility and find measures to control them.

Bejan [210] employed the thermodynamics second law to estimate the irreversibility in the processes of heat transfer. His paper comprises of two parts. Firstly he investigated the production of irreversibility. In other part he reviewed the second law for heat exchangers in classical engineering. He presented the analytic methods for irreversibility minimization. In another study [211] he gave the method for EMG in thermodynamics systems. Sheikholeslami and Ganji [212] scrutinized a study of entropy for nanofluids. Akbar [213] reported a study for irreversibility analysis in a tube. MHD characteristics have been also accounted. Akbar et al. [214] also paid attention to planar channel by employing water based nanoliquids. Abbass et al. [215] presented the study for irreversibility analysis in flexible wall channel. Hayat et al. [216, 217] studied entropy by employing single and multi-walled CNTs and Jeffrey fluid. More studies in this area can be highlighted through [218-225]. It is noticed that the literature on entropy analysis with reference to peristalsis is scarce yet. Researchers have started working in this field because of its utility and novelty.

## 1.2 Basic laws and fundamental equations

Real situations of fluid flow can be captured through mathematical modeling in terms of physical laws. These laws are:

### 1.2.1 Mass conservative law

This law witnessed the conservation of mass. For the case of no source/sink and compressible fluid, equation of continuity is

$$\operatorname{div}(\rho \mathbf{V}) + \frac{\partial \rho}{\partial t} = 0, \quad (1.1)$$

where  $\rho$ ,  $t$  and  $\mathbf{V} = (u, v, w)$  portrayed the respective density, time and velocity field.



For incompressible fluid it becomes

$$\frac{\partial u}{\partial x} + \frac{\partial v}{\partial y} + \frac{\partial w}{\partial z} = 0. \quad (1.2)$$

For Cylindrical coordinates

$$\frac{\partial u}{\partial r} + \frac{u}{r} + \frac{\partial w}{\partial z} = 0. \quad (1.3)$$

For curved geometry we have

$$\frac{\partial}{\partial r}[(r + R^*)v] + R^* \frac{\partial u}{\partial x} = 0. \quad (1.4)$$

### 1.2.2 Momentum conservative law

Equation of motion satisfies

$$\rho \frac{d\mathbf{V}}{dt} = \rho \mathbf{b} + \nabla \cdot \boldsymbol{\tau}, \quad (1.5)$$

here  $\mathbf{b}$ ,  $\boldsymbol{\tau}$  depicts the body force and Cauchy stress tensor.

$$\boldsymbol{\tau} = -p\mathbf{I} + \mathbf{S}, \quad (1.6)$$

where  $p$  the pressure and  $\mathbf{S}$  the extra stress tensor which varies for different fluid.

For two phase nanoliquids

$$\rho_{eff} \frac{d\mathbf{V}}{dt} = \rho_{eff} \mathbf{b} + \nabla \cdot \boldsymbol{\tau}, \quad (1.7)$$

where

$$\rho_{eff} = (1 - \phi^*)\rho_f + \phi^*\rho_p, \quad (1.8)$$

where  $\rho_p$  and  $\rho_f$  are densities of nanomaterial and base liquid.

### 1.2.3 Energy conservative law

It is expressed in the form

$$\rho C_p \frac{dT}{dt} = -\nabla \cdot \mathbf{q} + Q. \quad (1.9)$$

Here  $\mathbf{q}$ ,  $T$ ,  $C_p$  denote heat flux, temperature and specific heat.  $Q$  term describes heat characteristics, including viscous dissipation, radiation etc.

$$\mathbf{q} = -\kappa\nabla T, \quad (1.10)$$

where  $\kappa$  elucidate the thermal conductivity.

For two phase model for nanoliquids

$$(\rho C_p)_{eff} \frac{dT}{dt} = \kappa_{eff} \nabla^2 T + Q, \quad (1.11)$$

where

$$\begin{aligned} (\rho C_p)_{eff} &= (1 - \phi^*)(\rho C_p)_f + \phi^*(\rho C_p)_p, \\ \frac{\kappa_{eff}}{\kappa_f} &= \frac{\kappa_p + (n^* - 1)\kappa_f - (n^* - 1)\phi^*(\kappa_f - \kappa_p)}{\kappa_p + (n^* - 1)\kappa_f + \phi^*(\kappa_f - \kappa_p)}. \end{aligned} \quad (1.12)$$

Here subscript  $p$  and  $f$  represent the notation for nano solid material and base liquid and  $n^*$  is shape factor.

For Buongiorno model

$$(\rho C_p)_f \frac{dT}{dt} = -\nabla \cdot \mathbf{q} + \hat{h}_p \nabla \cdot \hat{j}_p, \quad (1.13)$$

where  $\hat{h}_p$  and  $\hat{j}_p$  highlight specific enthalpy and diffusion mass flux of nano materials. Here

$$\begin{aligned} \mathbf{q} &= -\kappa \nabla T + \hat{h}_p \hat{j}_p, \\ \hat{j}_p &= -\rho_p D_T \frac{\nabla T}{T_m} - \rho_p D_B \nabla C, \end{aligned} \quad (1.14)$$

where  $T_m$ ,  $D_T$ ,  $D_B$  are respective mean temperature, thermophoresis and Brownian coefficients.

Inserting for  $\mathbf{q}$  and simplifying, we get

$$(\rho C_p)_f \frac{dT}{dt} = \kappa \nabla^2 T - C_p \hat{j}_p \cdot \nabla T. \quad (1.15)$$

Finally utilizing  $\hat{j}_p$ , one arrives at

$$(\rho C_p)_f \frac{dT}{dt} = \kappa \nabla^2 T + (C_p \rho)_p D_T \frac{\nabla T \cdot \nabla T}{T_m} + (C_p \rho)_p D_B \nabla C \cdot \nabla T. \quad (1.16)$$

#### 1.2.4 Concentration law

Here one has

$$\frac{dC}{dt} = D \nabla^2 C + \varrho, \quad (1.17)$$

in which  $\varrho$  denotes the source term that may be in form of chemical reaction etc.

Concentration equation for nanoparticles is

$$\frac{dC}{dt} = -\frac{1}{\rho_p} \nabla \cdot \hat{j}_p. \quad (1.18)$$

Utilizing the expression for  $\hat{j}_p$ , we arrive at

$$\frac{dC}{dt} = D_T \frac{\nabla^2 T}{T_m} + D_B \nabla^2 C. \quad (1.19)$$

#### 1.2.5 Compliant walls

Compliance is linked to capability of an objects to bulged or recoil back to its original position. This property can be described in terms of elastance, rigidity and stiffness. Living organisms naturally include such muscular structure through which it is more feasible to exchange nutrient, water etc. The flexible walls is also known as Compliant walls. Mathematically we expressed as

$$L^* (\eta) = p - p_0, \quad (1.20)$$

where  $p_0$  is the pressure outside the wall due to muscles tension and  $L^*$  the characteristics of walls to consider them as membranes defined by

$$L^* = -\tau^* \frac{\partial^2}{\partial x^2} + m^* \frac{\partial^2}{\partial t^2} + d_1^* \frac{\partial}{\partial t}, \quad (1.21)$$

in which elastance ( $-\tau^*$ ), mass per unit area ( $m^*$ ) and damping ( $d_1^*$ ) characteristics are taken into consideration. Study of peristalsis with and without compliant characteristics are valid

where disturbance due to pressure is negligible. However the compliant characteristics are more suitable in case of deformable walls.

## Chapter 2

# Entropy generation in peristalsis with different shapes of nanomaterial

### 2.1 Introduction

This chapter analyzed the peristalsis in a vertical channel by using different shapes of nanomaterial. The nanomaterial utilized for this purpose is silver (*Ag*) with water as base fluid. The study is based on the comparison amongst different shapes of nanoparticles (bricks, cylinders and platelets). The walls of channel are of flexible nature. Study is done in the light of long wavelength and low Reynolds number approximations. Solution technique utilized here is perturbation with Grashof number as small parameter. Entropy generation analysis is also carried out with different shapes of nanoparticles. The graphs of Bejan number, entropy generation, velocity and temperature are drawn for the sake of comparison through considered nanoparticles. Streamlines are also studied. The results lead to the fact that an increase in nanomaterial volume fraction decays velocity and temperature of nanofluid. The Hall parameter and Hartman number show opposite behavior for velocity, temperature, entropy generation and Bejan number. Highest values of temperature, Bejan number and entropy generation have been seen for brick shaped particles and smallest for platelet shaped particles.

## 2.2 Flow configuration

Here a vertical channel of width  $2d$  is considered. The channel walls are considered flexible. The walls are at the positions  $y = \pm\eta$ . A wave travels with speed  $c$  along the walls which propel the fluid in motion. This wave has wavelength  $\lambda$  and amplitude  $a$  (see Fig. 2.1). The walls has temperature  $T_0$ . Moreover base fluid and nanoparticles are considered thermally consistent with respect to each other. A magnetic field of strength  $B_0$  is applied in a normal direction to flow. Induced magnetic field is ignored because of small magnetic Reynolds number.

The Lorentz force is defined as

$$\mathbf{F} = \mathbf{J} \times \mathbf{B}, \quad (2.1)$$

in which  $\mathbf{B} = [0, 0, B_0]$ , and  $\mathbf{J}$  are the applied magnetic field and current density respectively. When Hall effects are taken into account then current density satisfies

$$\mathbf{J} = \sigma_{eff} \left[ \mathbf{E} + \mathbf{V} \times \mathbf{B} - \frac{1}{en_e} [\mathbf{J} \times \mathbf{B}] \right]. \quad (2.2)$$

Here  $\sigma_{eff}$  elucidates the effective electric conductivity of nanofluid,  $\mathbf{E}$  is used for electric field, the velocity field  $\mathbf{V} = [u(x, y), v(x, y), 0]$ ,  $e$  represents the electron charge and  $n_e$  the number density of free electrons. Electric field is absent and thus

$$\mathbf{J} = \sigma_{eff} \left[ \mathbf{V} \times \mathbf{B} - \frac{1}{en_e} [\mathbf{J} \times \mathbf{B}] \right]. \quad (2.3)$$

The Lorentz force then takes the form as:

$$\mathbf{F} = \left[ \frac{\sigma_{eff} B_0^2}{1 + \left(\frac{\sigma_{eff} B_0}{en_e}\right)^2} \left( -u + \left(\frac{\sigma_{eff} B_0}{en_e}\right) v \right), \frac{-\sigma_{eff} B_0^2}{1 + \left(\frac{\sigma_{eff} B_0}{en_e}\right)^2} \left( v + \left(\frac{\sigma_{eff} B_0}{en_e}\right) u \right), 0 \right]. \quad (2.4)$$

The two-phase model of effective electric conductivity of nanofluid is represented below [135, 190]:

$$\frac{\sigma_{eff}}{\sigma_f} = 1 + \frac{3\left(\frac{\sigma_p}{\sigma_f} - 1\right)\phi^*}{\left(\frac{\sigma_p}{\sigma_f} + 2\right) - \left(\frac{\sigma_p}{\sigma_f} - 1\right)\phi^*}, \quad (2.5)$$

Here  $\sigma_p$  and  $\sigma_f$  are the electric conductivity of nanomaterial and base fluid respectively and  $\phi^*$

is used for nanoparticle volume fraction. Now we have

$$\mathbf{F} = \left[ \frac{A_1 \sigma_f B_o^2}{1 + (A_1 m)^2} (-u + A_1 m v), \frac{-A_1 \sigma_f B_o^2}{1 + (A_1 m)^2} (v + A_1 m u), 0 \right], \quad (2.6)$$

where  $A_1$  and the Hall parameter  $m$  are defined by:

$$m = \frac{\sigma_f B_o}{en_e}, \quad A_1 = 1 + \frac{3(\frac{\sigma_p}{\sigma_f} - 1)\phi^*}{(\frac{\sigma_p}{\sigma_f} + 2) - (\frac{\sigma_p}{\sigma_f} - 1)\phi^*}. \quad (2.7)$$

Shape of the peristaltic wall is

$$y = \pm \eta(x, t) = \pm \left[ d + a \sin \frac{2\pi}{\lambda} (x - ct) \right]. \quad (2.8)$$

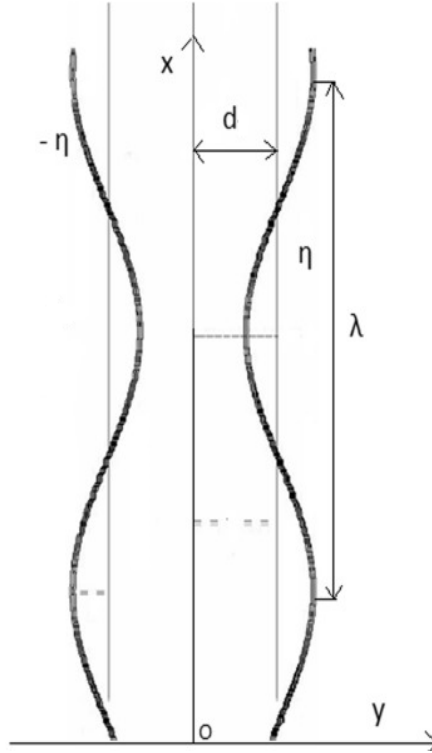


Fig. 2.1: Flow Configuration

The governing equations are:

$$\frac{\partial u}{\partial x} + \frac{\partial v}{\partial y} = 0, \quad (2.9)$$

$$\rho_{eff}\left(\frac{\partial}{\partial t}+u\frac{\partial}{\partial x}+v\frac{\partial}{\partial y}\right)u = -\frac{\partial p}{\partial x}+\mu_{eff}\left[\frac{\partial^2 u}{\partial x^2}+\frac{\partial^2 u}{\partial y^2}\right]+g(\rho\beta_T)_{eff}(T-T_0)-\frac{A_1\sigma_f B_o^2}{1+(A_1 m)^2}(u-A_1 m v), \quad (2.10)$$

$$\rho_{eff}\left(\frac{\partial}{\partial t}+u\frac{\partial}{\partial x}+v\frac{\partial}{\partial y}\right)v = -\frac{\partial p}{\partial y}+\mu_{eff}\left[\frac{\partial^2 v}{\partial x^2}+\frac{\partial^2 v}{\partial y^2}\right]-\frac{A_1\sigma_f B_o^2}{1+(A_1 m)^2}(v+A_1 m u), \quad (2.11)$$

$$\begin{aligned} (\rho C_p)_{eff}\left(\frac{\partial}{\partial t}+u\frac{\partial}{\partial x}+v\frac{\partial}{\partial y}\right)T &= \kappa_{eff}\left[\frac{\partial^2 T}{\partial x^2}+\frac{\partial^2 T}{\partial y^2}\right]+\mu_{eff}\left[2\left(\left(\frac{\partial u}{\partial x}\right)^2+\left(\frac{\partial v}{\partial y}\right)^2\right)\right. \\ &\quad \left.+\left(\frac{\partial u}{\partial y}+\frac{\partial v}{\partial x}\right)^2\right]-\frac{\partial q_r}{\partial y}. \end{aligned} \quad (2.12)$$

Here  $u$  and  $v$  are used to represent the velocity components in  $x$  and  $y$  directions,  $T$  the temperature,  $p$  the pressure,  $\rho_{eff}$  the effective density,  $\mu_{eff}$  the effective viscosity,  $(\rho\beta_T)_{eff}$  the effective thermal expansion,  $(\rho C_p)_{eff}$  the effective heat capacity,  $\kappa_{eff}$  the effective thermal conductivity of nanofluid and  $q_r$  ( $=\frac{-4\sigma^*}{3k^*}\frac{\partial T^4}{\partial y}$ ) the radiative heat flux.

The expressions for  $\rho_{eff}$ ,  $(\rho C_p)_{eff}$ ,  $(\rho\beta_T)_{eff}$ ,  $\mu_{eff}$  and  $\kappa_{eff}$  are:

$$\begin{aligned} \rho_{eff} &= (1-\phi^*)\rho_f+\phi^*\rho_p, & (\rho C_p)_{eff} &= (1-\phi^*)(\rho C_p)_f+\phi^*(\rho C_p)_p, \\ (\rho\beta_T)_{eff} &= (1-\phi^*)(\rho\beta_T)_f+\phi^*(\rho\beta_T)_p, & \mu_{eff} &= \frac{\mu_f}{(1-\phi^*)^{2.5}}, \\ \frac{\kappa_{eff}}{\kappa_f} &= \frac{\kappa_p+(n^*-1)\kappa_f-(n^*-1)\phi^*(\kappa_f-\kappa_p)}{\kappa_p+(n^*-1)\kappa_f+\phi^*(\kappa_f-\kappa_p)}. \end{aligned} \quad (2.13)$$

Table 1 given below represents the thermophysical properties of utilized base fluid and nanomaterial.

Table 1: Thermophysical parameters of water and nanoparticle [190]				
	$\rho$ (kg m <sup>-3</sup> )	$C_p$ (j kg <sup>-1</sup> K <sup>-1</sup> )	$\kappa$ (W m <sup>-1</sup> K <sup>-1</sup> )	$\beta_T$ (1/k) $\times 10^{-6}$
$H_2O$	997.1	4179	0.613	210
$Ag$	10500	235	429	18.9

Shape factor and sphericity of different shapes of nanomaterial are given in Table 2 below [106]



Nanomaterial shape	Sphericity	Shape factor
Brick	0.81	3.7
Cylinder	0.62	4.9
Platelet	0.52	5.7

The quantities in dimensionless form are given by

$$\begin{aligned}
x^* &= \frac{x}{\lambda}, & y^* &= \frac{y}{d}, & u^* &= \frac{u}{c}, & v^* &= \frac{v}{c}, & t^* &= \frac{ct}{\lambda}, & \eta^* &= \frac{\eta}{d}, \\
\xi_1^* &= \frac{\xi_1 \mu_f}{d}, & \xi_2^* &= \frac{\xi_2}{d}, & p^* &= \frac{d^2 p}{c \lambda \mu_f}, \\
Re &= \frac{\rho_f c d}{\mu_f}, & \theta &= \frac{T - T_0}{T_0}, & Pr &= \frac{(\mu C_p)_f}{\kappa_f}, \\
Ec &= \frac{c^2}{(C_p)_f T_0}, & Br &= Pr Ec, & Gr &= \frac{g (\rho \beta_T)_f T_0 d^2}{c \mu_f}, & M &= \sqrt{\frac{\sigma_f}{\mu_f}} B_o d \\
Rd &= \frac{16 \sigma^* T_0^3}{3 k^* \kappa_f}, & u &= \frac{\partial \psi}{\partial y}, & v &= -\delta \frac{\partial \psi}{\partial x}.
\end{aligned} \tag{2.14}$$

Here  $Re$ ,  $Pr$ ,  $Ec$ ,  $Br$ ,  $Gr$  and  $M$  are Reynolds, Prandtl, Eckert, Brinkman, Grashof and Hartman numbers respectively. Moreover  $Rd$  is the radiation parameter.

After invoking large wavelength and low Reynolds number assumptions [135, 190] the continuity equation is identically satisfied and others equations lead to

$$\frac{\partial p}{\partial x} = \frac{1}{(1 - \phi^*)^{2.5}} \frac{\partial^3 \psi}{\partial y^3} + Gr A_3 \theta - \frac{A_1 M^2}{1 + (A_1 m)^2} \frac{\partial \psi}{\partial y}, \tag{2.15}$$

$$\frac{\partial p}{\partial y} = 0, \tag{2.16}$$

$$K_1 \frac{\partial^2 \theta}{\partial y^2} + \frac{Br}{(1 - \phi^*)^{2.5}} \left( \frac{\partial^2 \psi}{\partial y^2} \right)^2 + Rd \frac{\partial^2 \theta}{\partial y^2} = 0, \tag{2.17}$$

$$\begin{aligned}
A_3 &= 1 - \phi^* + \phi^* \left( \frac{(\rho \beta_T)_p}{(\rho \beta_T)_f} \right), \\
K_1 &= \frac{\kappa_p + (n^* - 1) \kappa_f - (n^* - 1) \phi (\kappa_f - \kappa_p)}{\kappa_p + (n^* - 1) \kappa_f + \phi (\kappa_f - \kappa_p)}.
\end{aligned} \tag{2.18}$$

The velocity slip, compliant walls and thermal slip conditions are

$$u \pm \xi_1 S_{xy} = 0 \quad \text{at } y = \pm\eta, \quad (2.19)$$

$$\begin{aligned} \left[ -\tau^* \frac{\partial^3}{\partial x^3} + m^* \frac{\partial^3}{\partial x \partial t^2} + d_1^* \frac{\partial^2}{\partial t \partial x} \right] \eta &= \frac{\partial S_{xy}}{\partial y} + \frac{\partial S_{xx}}{\partial x} - \rho_f \left[ \frac{\partial u}{\partial t} + u \frac{\partial u}{\partial x} + v \frac{\partial u}{\partial y} \right] \\ &+ g(\rho\beta_T)_{eff} (T - T_0) - \frac{A_1 \sigma_f B_0^2}{1 + (A_1 m)^2} (u - A_1 m v) \end{aligned} \quad (2.20)$$

at  $y = \pm\eta$ ,

$$T \pm \xi_2 \frac{\partial T}{\partial y} = T_0 \quad \text{at } y = \pm\eta. \quad (2.21)$$

where  $\xi_1$  and  $\xi_2$  are dimensional slip parameters for velocity and temperature respectively.

The dimensionless forms of boundary conditions are

$$\frac{\partial \psi}{\partial y} \pm \frac{\xi_1}{(1 - \phi^*)^{2.5}} \frac{\partial^2 \psi}{\partial y^2} = 0, \quad \theta \pm \xi_2 \frac{\partial \theta}{\partial y} = 0, \quad \text{at } y = \pm\eta, \quad (2.22)$$

$$\left[ E_1 \frac{\partial^3}{\partial x^3} + E_2 \frac{\partial^3}{\partial x \partial t^2} + E_3 \frac{\partial^2}{\partial t \partial x} \right] \eta = \frac{1}{(1 - \phi^*)^{2.5}} \frac{\partial^3 \psi}{\partial y^3} + Gr A_3 \theta - \frac{A_1 M^2}{1 + (A_1 m)^2} \frac{\partial \psi}{\partial y}, \quad \text{at } y = \pm\eta. \quad (2.23)$$

Here  $E_1 (= -\tau^* d^3 / \lambda^3 c \mu_f)$ ,  $E_2 (= m^* c d^3 / \lambda^3 \mu_f)$  and  $E_3 (= d_1^* d^3 / \lambda^2 \mu_f)$  are the flexible walls parameters.

### 2.2.1 Entropy generation and viscous dissipation

Viscous dissipation effect is given by

$$\Phi = \mu_{eff} \left[ 2 \left( \left( \frac{\partial u}{\partial x} \right)^2 + \left( \frac{\partial v}{\partial y} \right)^2 \right) + \left( \frac{\partial u}{\partial y} + \frac{\partial v}{\partial x} \right)^2 \right]. \quad (2.24)$$

Dimensional form of volumetric entropy generation is defined as

$$S_{gen}''' = \frac{\kappa_{eff}}{T_m^2} \left( \left( \frac{\partial T}{\partial x} \right)^2 + \left( \frac{\partial T}{\partial y} \right)^2 \right) + \frac{1}{T_m^2} \frac{16\sigma^* T_0^3}{3k^*} \left( \frac{\partial T}{\partial y} \right)^2 + \frac{\Phi}{T_m}. \quad (2.25)$$

The entropy generation in dimensionless form becomes:

$$N_s = \frac{S'''_{gen}}{S'''_G} = (K_1 + Rd) \left( \frac{\partial \theta}{\partial y} \right)^2 + \frac{Br}{\Lambda(1-\phi)^{2.5}} \left( \frac{\partial^2 \psi}{\partial y^2} \right)^2, \quad (2.26)$$

$$S'''_G = \frac{\kappa_f T_0^2}{T_m^2 d^2}, \quad \Lambda = \frac{T_0}{T_m}. \quad (2.27)$$

Here  $T_m$  elucidates the mean temperature.

Bejan number is:

$$Be = \frac{N_{s_{cond}}}{N_{s_{cond}} + N_{s_{visc}}}. \quad (2.28)$$

Here Eq. (2. 25) can be split into two parts. One part comprises of entropy generation which is due to finite temperature difference ( $N_{s_{cond}}$ ) and the other part includes the entropy generation because of viscous dissipation effects ( $N_{s_{visc}}$ ).

## 2.3 Solution methodology

Perturbation technique is applied for small Grashof number. The equations and solutions for the cases of zeroth and first orders systems are:

### 2.3.1 Zeroth order systems and solutions

$$\frac{1}{(1-\phi^*)^{2.5}} \frac{\partial^4 \psi_0}{\partial y^4} - \frac{A_1 M^2}{1+(A_1 m)^2} \frac{\partial^2 \psi_0}{\partial y^2} = 0, \quad (2.29)$$

$$K_1 \frac{\partial^2 \theta_0}{\partial y^2} + \frac{Br}{(1-\phi^*)^{2.5}} \left( \frac{\partial^2 \psi_0}{\partial y^2} \right)^2 + Rd \frac{\partial^2 \theta_0}{\partial y^2} = 0, \quad (2.30)$$

$$\frac{\partial \psi_0}{\partial y} \pm \frac{\xi_1}{(1-\phi^*)^{2.5}} \frac{\partial^2 \psi_0}{\partial y^2} = 0, \quad \text{at } y = \pm \eta, \quad (2.31)$$

$$\left[ E_1 \frac{\partial^3}{\partial x^3} + E_2 \frac{\partial^3}{\partial x \partial t^2} + E_3 \frac{\partial^2}{\partial t \partial x} \right] \eta = \frac{1}{(1-\phi^*)^{2.5}} \frac{\partial^3 \psi_0}{\partial y^3} - \frac{A_1 M^2}{1+(A_1 m)^2} \frac{\partial \psi_0}{\partial y}, \quad \text{at } y = \pm \eta, \quad (2.32)$$

$$\theta_0 \pm \xi_2 \frac{\partial \theta_0}{\partial y} = 0, \quad \text{at } y = \pm \eta. \quad (2.33)$$

The solutions expressions are

$$\psi_0 = \frac{A_0 e^{\frac{\sqrt{A_1} M y}}{\sqrt{A_0 + A_0 A_1^2 m^2}} (1 + A_1^2 m^2) \left( e^{\frac{2\sqrt{A_1} M y}}{\sqrt{A_0 + A_0 A_1^2 m^2}} C_1 + C_2 \right)}{A_1 M^2} + C_3 + y C_4, \quad (2.34)$$

$$\theta_0 = -\frac{A_0 B r e^{\frac{-2\sqrt{A_1} M y}}{\sqrt{A_0 + A_0 A_1^2 m^2}} \left( C_2^2 + C_1^2 e^{\frac{4\sqrt{A_1} M y}}{\sqrt{A_0 + A_0 A_1^2 m^2}} \right) (1 + A_1^2 m^2)}{A_1 M^2} + 4C_1 C_2 y^2}{4K_2} + F_1 + y F_2. \quad (2.35)$$

### 2.3.2 First order systems and solutions

Here we have

$$\frac{1}{(1 - \phi^*)^{2.5}} \frac{\partial^4 \psi_1}{\partial y^4} + A_3 \frac{\partial \theta_0}{\partial y} - \frac{A_1 M^2}{1 + (A_1 m)^2} \frac{\partial^2 \psi_1}{\partial y^2} = 0, \quad (2.36)$$

$$K_1 \frac{\partial^2 \theta_1}{\partial y^2} + \frac{B r}{(1 - \phi)^{2.5}} \left( 2 \frac{\partial^2 \psi_0}{\partial y^2} \frac{\partial^2 \psi_1}{\partial y^2} \right) + R d \frac{\partial^2 \theta_1}{\partial y^2} = 0, \quad (2.37)$$

$$\frac{\partial \psi_1}{\partial y} \pm \frac{\xi_1}{(1 - \phi^*)^{2.5}} \frac{\partial^2 \psi_1}{\partial y^2} = 0, \quad \text{at } y = \pm \eta, \quad (2.38)$$

$$\frac{1}{(1 - \phi^*)^{2.5}} \frac{\partial^3 \psi_1}{\partial y^3} + A_3 \theta_0 - \frac{A_1 M^2}{1 + (A_1 m)^2} \frac{\partial \psi_1}{\partial y} = 0 \quad \text{at } y = \pm \eta, \quad (2.39)$$

$$\theta_1 \pm \xi_2 \frac{\partial \theta_1}{\partial y} = 0, \quad \text{at } y = \pm \eta. \quad (2.40)$$

The solution expressions are

$$\begin{aligned} \psi_1 = & \frac{1}{24 A_1^{5/2} K_2 M^5} (1 + A_1^2 m^2) (A_0^2 A_3 B r e^{\frac{-2\sqrt{A_1} M y}}{\sqrt{A_0 + A_0 A_1^2 m^2}} \left( -C_2^2 + C_1^2 e^{\frac{4\sqrt{A_1} M y}}{\sqrt{A_0 + A_0 A_1^2 m^2}} \right) \\ & (1 + A_1^2 m^2) \sqrt{A_0 + A_0 A_1^2 m^2} + 12 A_1^{3/2} A_3 F_2 K_2 M^3 y^2 + \\ & 8 A_0 A_1^{3/2} M^3 (-A_3 B r C_1 C_2 y^3 + 3 e^{\frac{-\sqrt{A_1} M y}}{\sqrt{A_0 + A_0 A_1^2 m^2}} \\ & K_2 (e^{\frac{2\sqrt{A_1} M y}}{\sqrt{A_0 + A_0 A_1^2 m^2}} B_1 + B_2))) + B_3 + y B_4, \end{aligned} \quad (2.41)$$

$$\begin{aligned}
\theta_1 = & \frac{1}{H} (H_1 - H_2 K_2 - H_3 K_2 + H_4 y^2 - 3A_0 A_3 C_2 e^{\frac{-\sqrt{A_1} M y}{\sqrt{A_0 + A_0 A_1^2 m^2}}} \\
& H_5 - 12A_0 Br C_1 C_2 \sqrt{A_0 + A_0 A_1^2 m^2 y}) + 3A_0 A_3 C_1 e^{\frac{\sqrt{A_1} M y}{\sqrt{A_0 + A_0 A_1^2 m^2}}} (1 + A_1^2 m^2)^2 \\
& (-\frac{H_6 + 6\sqrt{A_1} F_2 K_2 M}{\sqrt{A_1} M} + 12A_0 Br C_1 C_2 \sqrt{A_0 + A_0 A_1^2 m^2 y})) + G_1 + y G_2, \quad (2.42)
\end{aligned}$$

in which  $C_i$ 's,  $F_i$ 's,  $B_i$ 's,  $G_i$ 's and  $H_i$ 's are constants that can be evaluated through Mathematica. Here  $K_2 = K_1 + Rd$ .

## 2.4 Discussion

This section includes the graphs and related analyses for different embedded parameters. This section contains the graphs for velocity, temperature, streamlines, Bejan number and entropy generation. Each graph gives a comparison among different shapes of nanomaterial for the pertinent parameter. Fig. 2.2 is drawn for the comparative study of effective thermal conductivity of different shapes of nanomaterial when nanomaterial volume fraction varies. This Fig. clearly indicated that effective thermal conductivity for the case of platelet shaped particle is higher in all cases than brick and cylindrical shaped particles. The brick shaped particles have lowest effective thermal conductivity.

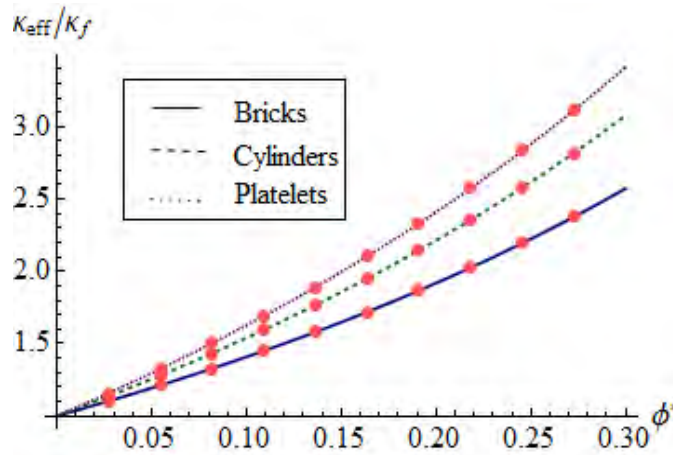


Fig. 2.2: Comparison of effective thermal conductivity for different shaped nanomaterials

Fig. 2.3 is sketched for the case of velocity when volume fraction of nanomaterial varies. As expected the velocity is decreased via nanoparticle volume fraction. As higher volume fraction enhance the shear rate, which provide resistance to flow so velocity decreases. Fig. 2.4 illustrates the Hartman number impact on velocity. Velocity is decreasing function of Hartman number. As Lorentz force provides obstruction to fluid flow. Hence the velocity reduces. Hall parameter influence on velocity can be seen through Fig. 2.5. It shows the increasing behavior of velocity for Hall parameter. Same impact is obtained for velocity slip parameter and Grashof number (see Fig. 2.6 and Fig. 2.7). Grashof number arises due to mixed convection which is also in the favor of velocity. In nuclear reactor cooling the mixed convection is utilized to dissipate energy when force convection not enough to do so. Wall properties behavior on velocity is increasing for elastance parameters while there is decreasing effect for damping parameter (see Fig. 2.8). In all the cases of velocity profile it is found through comparative study of different shaped nanoparticles that velocity remains lowest for case of bricks shaped particles and it is highest for cylindrical shaped particles.

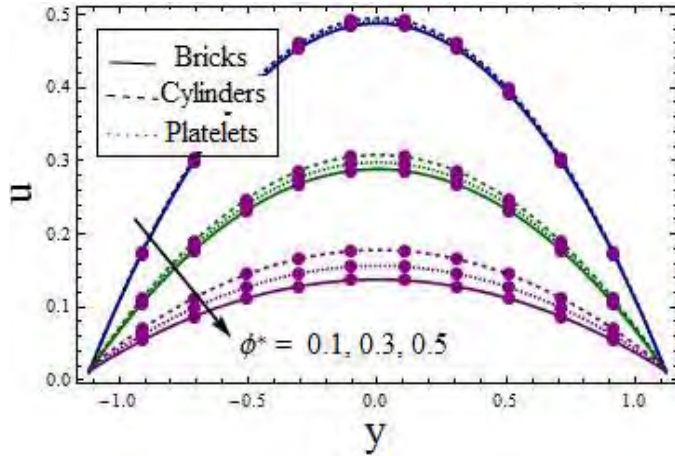


Fig. 2.3

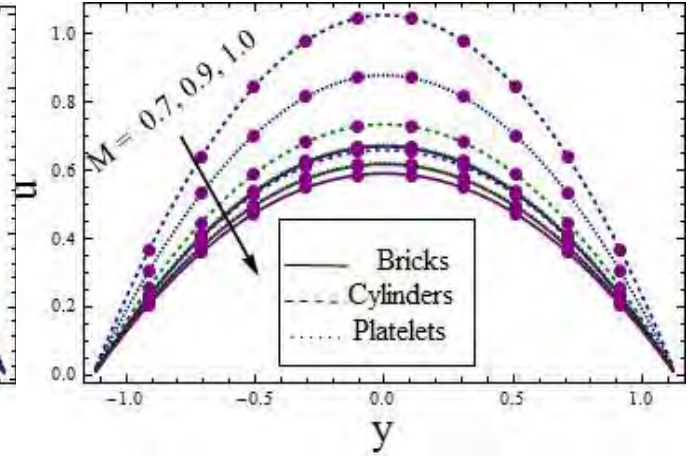


Fig. 2.4

Fig. 2.3.  $u$  versus  $\phi^*$  when  $E_1 = 0.02$ ,  $E_2 = 0.01$ ,  $E_3 = 0.01$ ,  $t = 0.1$ ,  $x = 0.2$ ,  $\varepsilon = 0.2$ ,

$M = 1.0$ ,  $m = 1.0$ ,  $Br = 5.0$ ,  $Gr = 0.1$ ,  $\xi_1 = 0.01$ ,  $\xi_2 = 0.01$ ,  $Rd = 0.5$ .

Fig. 2.4.  $u$  versus  $M$  when  $E_1 = 0.02$ ,  $E_2 = 0.01$ ,  $E_3 = 0.01$ ,  $t = 0.1$ ,  $x = 0.2$ ,  $\varepsilon = 0.2$ ,

$\phi^* = 0.1$ ,  $m = 1.0$ ,  $Br = 5.0$ ,  $Gr = 0.9$ ,  $\xi_1 = 0.01$ ,  $\xi_2 = 0.01$ ,  $Rd = 0.5$ .

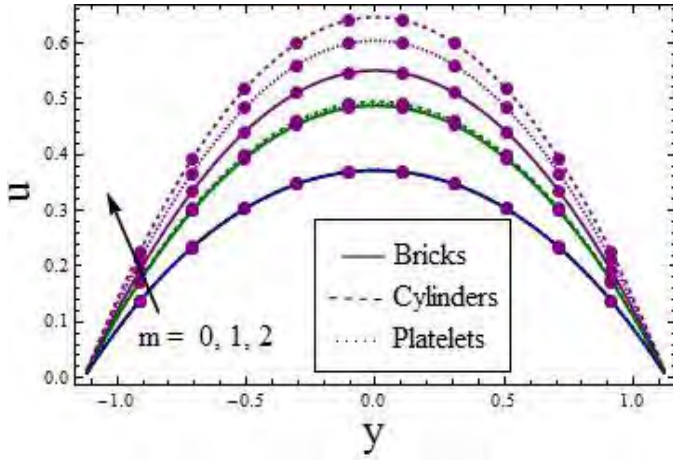


Fig. 2.5

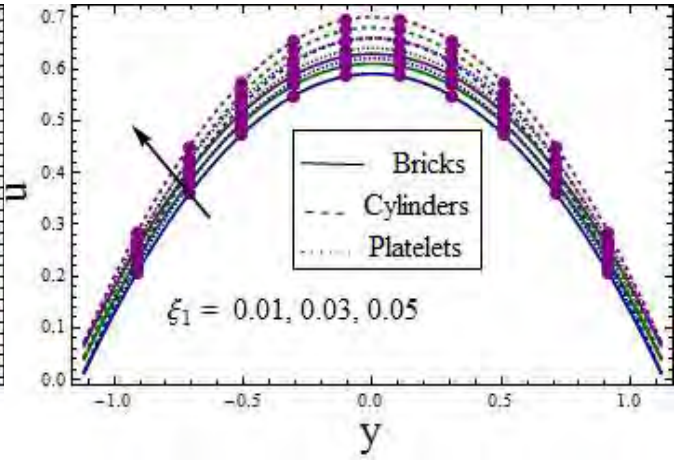


Fig. 2.6

Fig. 2.5.  $u$  versus  $m$  when  $E_1 = 0.02$ ,  $E_2 = 0.01$ ,  $E_3 = 0.01$ ,  $t = 0.1$ ,  $x = 0.2$ ,  $\varepsilon = 0.2$ ,  $\phi^* = 0.1$ ,  $M = 1.0$ ,  $Br = 5.0$ ,  $Gr = 0.1$ ,  $\xi_1 = 0.01$ ,  $\xi_2 = 0.01$ ,  $Rd = 0.5$ .

Fig. 2.6.  $u$  versus  $\xi_1$  when  $E_1 = 0.02$ ,  $E_2 = 0.01$ ,  $E_3 = 0.01$ ,  $t = 0.1$ ,  $x = 0.2$ ,  $\varepsilon = 0.2$ ,  $M = 1.0$ ,  $m = 1.0$ ,  $Br = 5.0$ ,  $Gr = 0.9$ ,  $\phi^* = 0.1$ ,  $\xi_2 = 0.01$ ,  $Rd = 0.5$ .

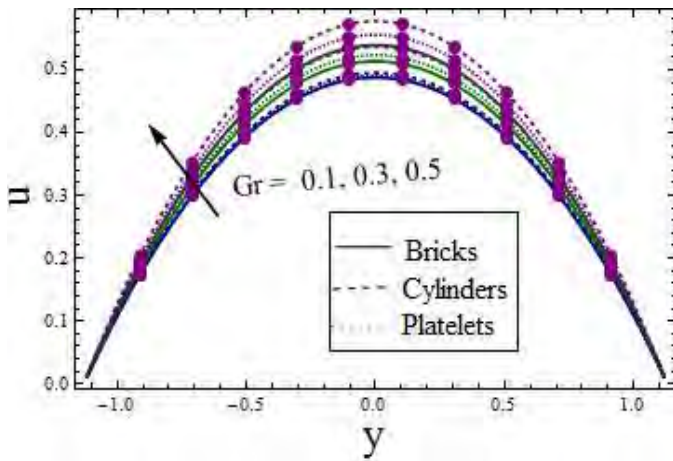


Fig. 2.7

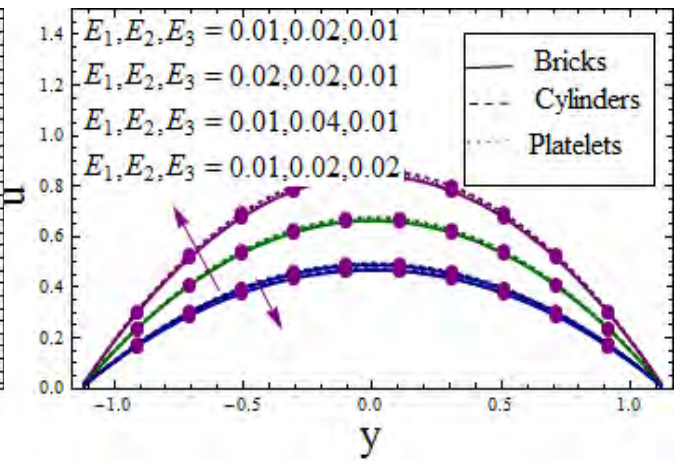


Fig. 2.8

Fig. 2.7.  $u$  versus  $Gr$  when  $E_1 = 0.02$ ,  $E_2 = 0.01$ ,  $E_3 = 0.01$ ,  $t = 0.1$ ,  $x = 0.2$ ,  $\varepsilon = 0.2$ ,  $M = 1.0$ ,  $m = 1.0$ ,  $Br = 5.0$ ,  $\phi^* = 0.1$ ,  $\xi_1 = 0.01$ ,  $\xi_2 = 0.01$ ,  $Rd = 0.5$ .

Fig. 2.8.  $u$  versus  $E_1, E_2, E_3$  when  $t = 0.1$ ,  $x = 0.2$ ,  $\varepsilon = 0.2$ ,  $M = 1.0$ ,  $m = 1.0$ ,  $Br = 5.0$ ,

$$Gr = 0.1, \phi^* = 0.1, \xi_1 = 0.01, \xi_2 = 0.01, Rd = 0.5.$$

Behavior of temperature is shown through Figs. 2.9-2.14. Fig. 2.9 explained influence of  $\phi^*$  on  $\theta$ . Temperature is decreasing function of volume fraction of nanomaterial. Due to similar reason the nanofluids are utilized for coolant purposes. As higher volume fraction of nanoparticles enhance the heat transfer capability, so temperature decreases. Through comparison it is concluded that temperature distribution remains highest for bricks shaped nanoparticles and lowest for platelets shaped nanomaterials. The results of Hall parameter and Hartman number on the temperature are opposite (see Figs. 2.10 and 2.11). Enhancement is seen for Hall parameter whereas decay is noticed for Hartman number. As Hall effect facilitate the flow, so flow with higher mean kinetic energy has greater heat loss and hence increase in temperature is noticed. Similarly regarding force the flow slows and hence less heat loss through fluid movement. Finally decay is noticed. The Grashof number and temperature slip parameter give increasing behavior for temperature (see Fig. 2.12 and 2.13). Radiation parameter effects on temperature is illustrated through Fig. 2.14. Decrease in temperature is noticed in this case.

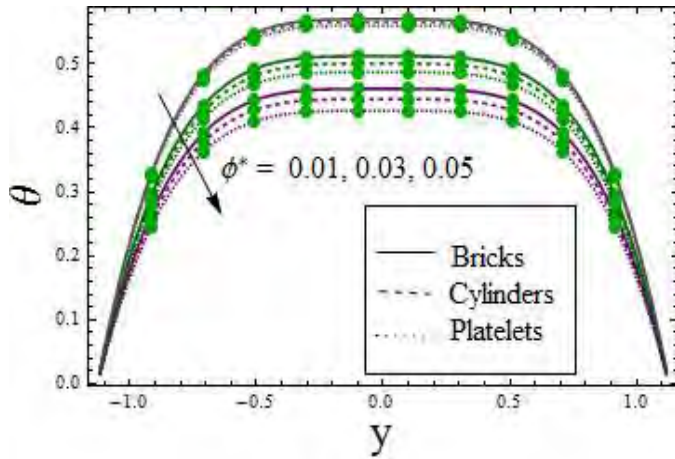


Fig. 2.9

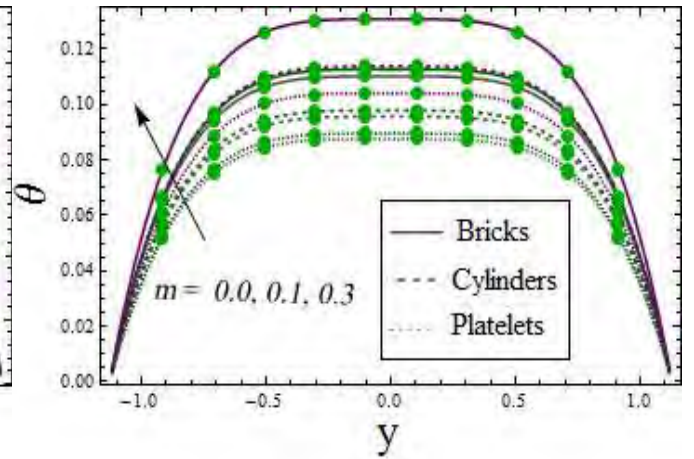


Fig. 2.10

Fig. 2.9.  $\theta$  versus  $\phi^*$  when  $E_1 = 0.02, E_2 = 0.01, E_3 = 0.01, t = 0.1, x = 0.2, \varepsilon = 0.2,$   
 $M = 1.0, m = 1.0, Br = 5.0, Gr = 0.1, \xi_1 = 0.01, \xi_2 = 0.01, Rd = 0.5.$

Fig. 2.10.  $\theta$  versus  $m$  when  $E_1 = 0.02, E_2 = 0.01, E_3 = 0.01, t = 0.1, x = 0.2, \varepsilon = 0.2,$   
 $M = 1.0, \phi^* = 0.2, Br = 5.0, Gr = 0.1, \xi_1 = 0.01, \xi_2 = 0.01, Rd = 0.5.$



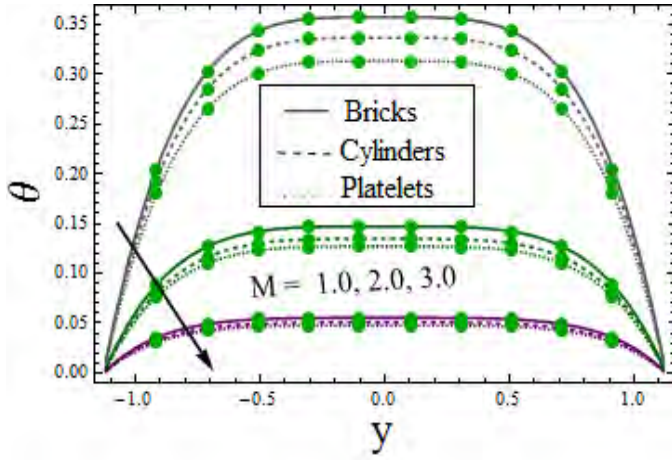


Fig. 2.11

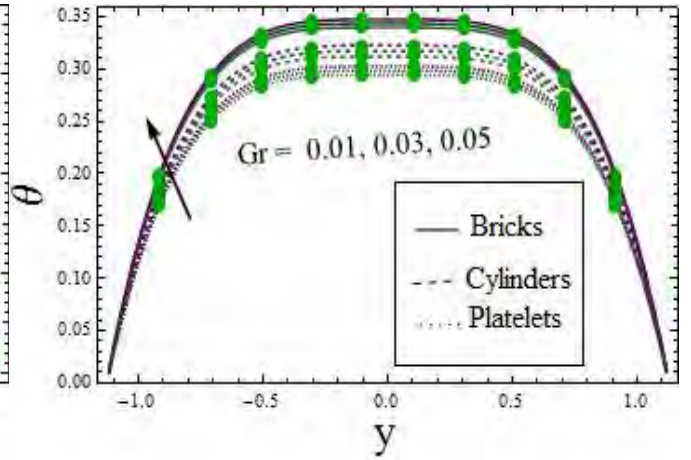


Fig. 2.12

Fig. 2.11.  $\theta$  versus  $M$  when  $E_1 = 0.02$ ,  $E_2 = 0.01$ ,  $E_3 = 0.01$ ,  $t = 0.1$ ,  $x = 0.2$ ,  $\varepsilon = 0.2$ ,  $\phi^* = 0.1$ ,  $m = 1.0$ ,  $Br = 5.0$ ,  $Gr = 0.1$ ,  $\xi_1 = 0.01$ ,  $\xi_2 = 0.01$ ,  $Rd = 0.5$ .

Fig. 2.12.  $\theta$  versus  $Gr$  when  $E_1 = 0.02$ ,  $E_2 = 0.01$ ,  $E_3 = 0.01$ ,  $t = 0.1$ ,  $x = 0.2$ ,  $\varepsilon = 0.2$ ,  $M = 1.0$ ,  $m = 1.0$ ,  $Br = 5.0$ ,  $\phi^* = 0.1$ ,  $\xi_1 = 0.01$ ,  $\xi_2 = 0.01$ ,  $Rd = 0.5$ .

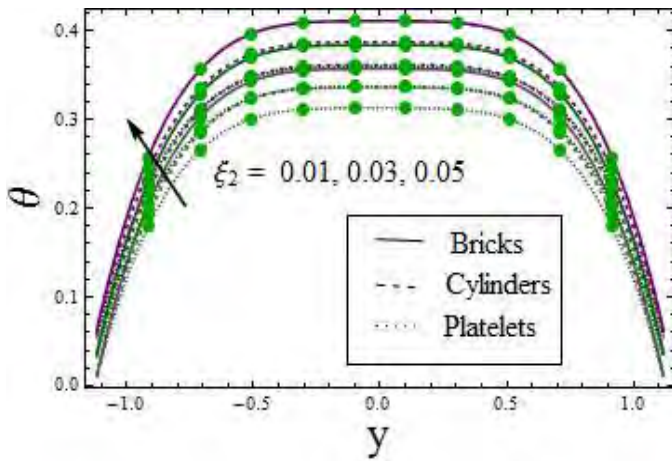


Fig. 2.13

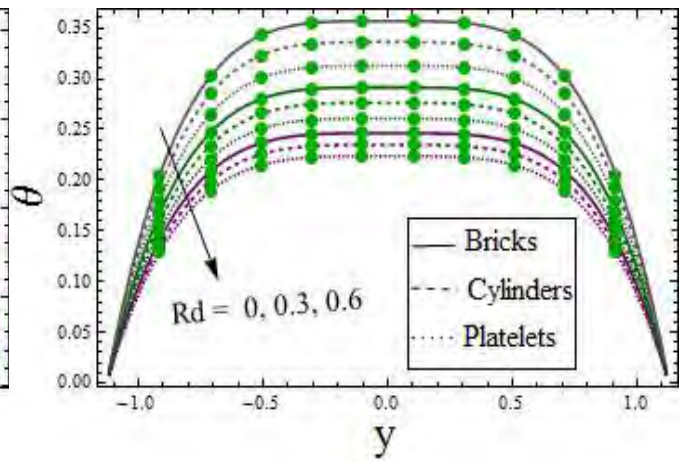


Fig. 2.14

Fig. 2.13.  $\theta$  versus  $\xi_2$  when  $E_1 = 0.02$ ,  $E_2 = 0.01$ ,  $E_3 = 0.01$ ,  $t = 0.1$ ,  $x = 0.2$ ,  $\varepsilon = 0.2$ ,  $M = 1.0$ ,  $m = 1.0$ ,  $Br = 5.0$ ,  $Gr = 0.1$ ,  $\xi_1 = 0.01$ ,  $\phi^* = 0.1$ ,  $Rd = 0.5$ .

Fig. 2.14.  $\theta$  versus  $Rd$  when  $E_1 = 0.02$ ,  $E_2 = 0.01$ ,  $E_3 = 0.01$ ,  $t = 0.1$ ,  $x = 0.2$ ,  $\varepsilon = 0.2$ ,

$$M = 1.0, m = 1.0, \phi^* = 0.1, Br = 5.0, Gr = 0.1, \xi_1 = 0.01, \xi_2 = 0.01.$$

The observation for entropy generation and Bejan number is covered here. Fig. 2.15 is prepared for entropy generation versus  $\phi^*$ . In view of this Fig. decrease in entropy generation is seen for volume fraction of the nanoparticle. As less disorderliness is noticed with small temperature effects. Fig. 2.16 is drawn for Hartman number variation on entropy generation and Fig. 2.17 for Hall parameter. Decay is seen for Hartman number while an enhancement is observed for larger Hall parameter. The reason can be directly related with temperature. Both  $Gr$  and the ratio of  $Br$  to  $\Lambda$  have displayed the increasing behavior for entropy generation (see Figs. 2.18 and 2.19). Fig. 2.20 is prepared for radiation parameter on entropy generation. Entropy generation decreases for radiation parameter ( $Rd$ ). Through all graphs it is found that brick shaped particles have higher values and platelet shaped particles have least entropy generation.

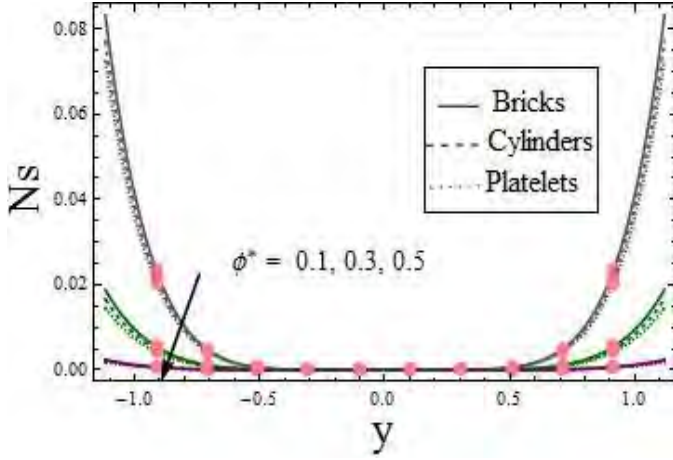


Fig. 2.15

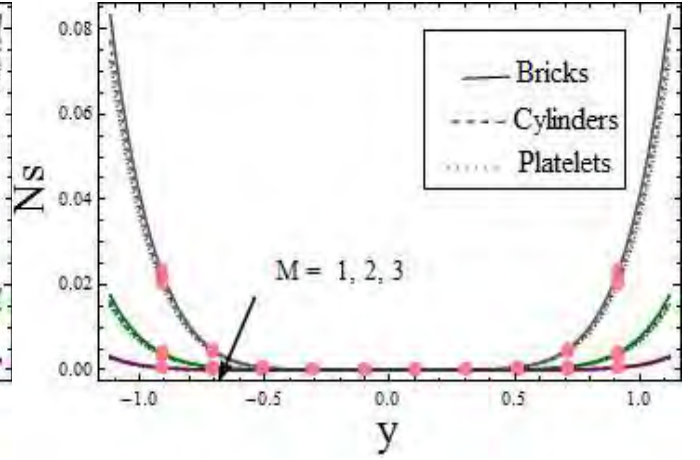


Fig. 2.16

Fig. 2.15.  $Ns$  versus  $\phi^*$  when  $E_1 = 0.02, E_2 = 0.01, E_3 = 0.01, t = 0.1, x = 0.2, \varepsilon = 0.2,$   
 $M = 1.0, m = 1.0, Br\Lambda^{-1} = 1.0, Gr = 0.1, \xi_1 = 0.01, \xi_2 = 0.01, Rd = 0.5.$

Fig. 2.16.  $Ns$  versus  $M$  when  $E_1 = 0.02, E_2 = 0.01, E_3 = 0.01, t = 0.1, x = 0.2, \varepsilon = 0.2,$   
 $\phi^* = 0.1, m = 1.0, Br\Lambda^{-1} = 1.0, Gr = 0.1, \xi_1 = 0.01, \xi_2 = 0.01, Rd = 0.5.$

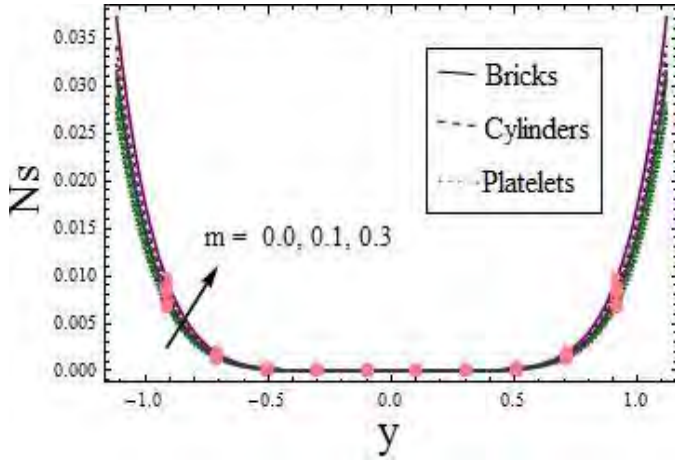


Fig. 2.17

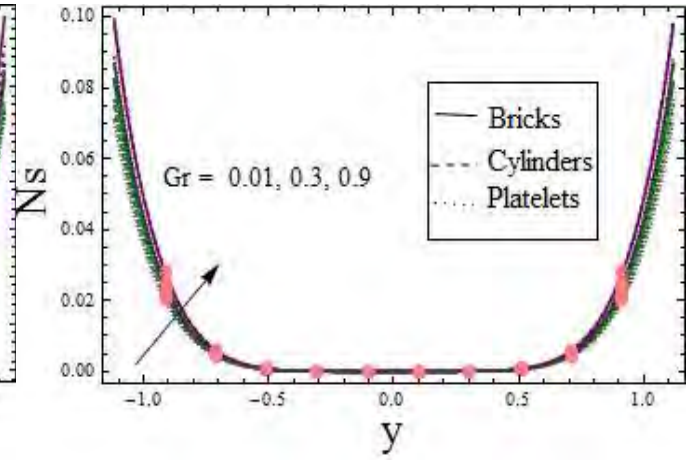


Fig. 2.18

Fig. 2.17.  $Ns$  versus  $m$  when  $E_1 = 0.02$ ,  $E_2 = 0.01$ ,  $E_3 = 0.01$ ,  $t = 0.1$ ,  $x = 0.2$ ,  $\varepsilon = 0.2$ ,  $M = 1.0$ ,  $\phi^* = 0.1$ ,  $Br\Lambda^{-1} = 1.0$ ,  $Gr = 0.1$ ,  $\xi_1 = 0.01$ ,  $\xi_2 = 0.01$ ,  $Rd = 0.5$ .

Fig. 2.18.  $Ns$  versus  $Gr$  when  $E_1 = 0.02$ ,  $E_2 = 0.01$ ,  $E_3 = 0.01$ ,  $t = 0.1$ ,  $x = 0.2$ ,  $\varepsilon = 0.2$ ,  $M = 1.0$ ,  $m = 1.0$ ,  $Br\Lambda^{-1} = 1.0$ ,  $\phi^* = 0.1$ ,  $\xi_1 = 0.01$ ,  $\xi_2 = 0.01$ ,  $Rd = 0.5$ .

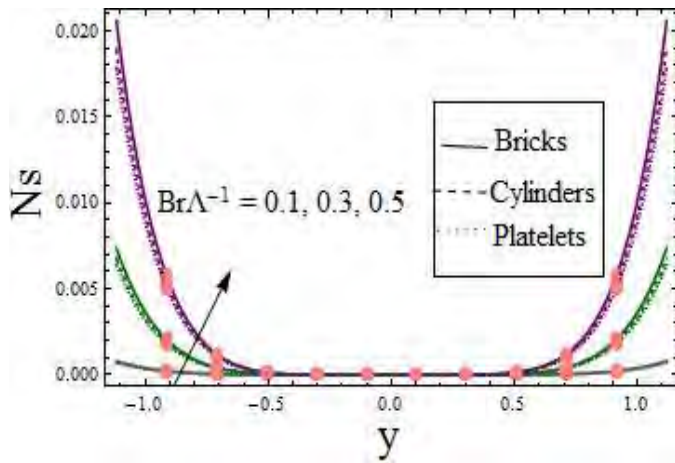


Fig. 2.19

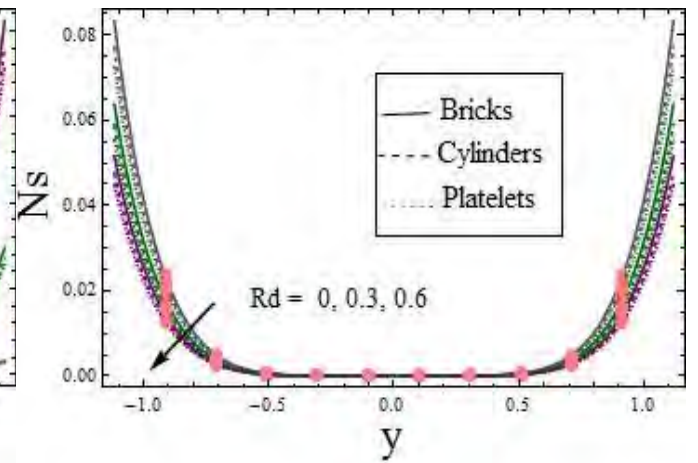


Fig. 2.20

Fig. 2.19.  $Ns$  versus  $Br\Lambda^{-1}$  when  $E_1 = 0.02$ ,  $E_2 = 0.01$ ,  $E_3 = 0.01$ ,  $t = 0.1$ ,  $x = 0.2$ ,  $\varepsilon = 0.2$ ,  $M = 1.0$ ,  $m = 1.0$ ,  $\phi^* = 0.1$ ,  $Gr = 0.1$ ,  $\xi_1 = 0.01$ ,  $\xi_2 = 0.01$ ,  $Rd = 0.5$ .

Fig. 2.20.  $Ns$  versus  $Rd$  when  $E_1 = 0.02$ ,  $E_2 = 0.01$ ,  $E_3 = 0.01$ ,  $\phi^* = 0.1$ ,  $t = 0.1$ ,  $x = 0.2$ ,

$$\varepsilon = 0.2, M = 1.0, m = 1.0, Br\Lambda^{-1} = 1.0, Gr = 0.1, \xi_1 = 0.01, \xi_2 = 0.01.$$

Bejan number observation is analyzed in this paragraph. In view of these graphical results we have seen that decay is seen via  $\phi^*$  (see Fig. 2.21). This result seems to be same here as in the case of temperature. The Bejan number result for change in Hartman number is observed via Fig. 2.22. This Fig. elucidates that Bejan number decreases with an enhancement of Hartman number. Fig. 2.23 shows that Hall parameter has increasing behavior for Bejan number. Moreover increasing impact of Bejan number is also observed for larger Grashof number and ratio of  $Br$  to  $\Lambda$  (see Figs. 2.24 and 2.25). Fig. 2.26 is prepared for impact of radiation parameter. The effects here are qualitatively similar to that of temperature. In all the above mentioned graphs for Bejan number we noticed that the values for nanoliquids with brick shape is larger than cylindrical and platelet shapes nanomaterials.

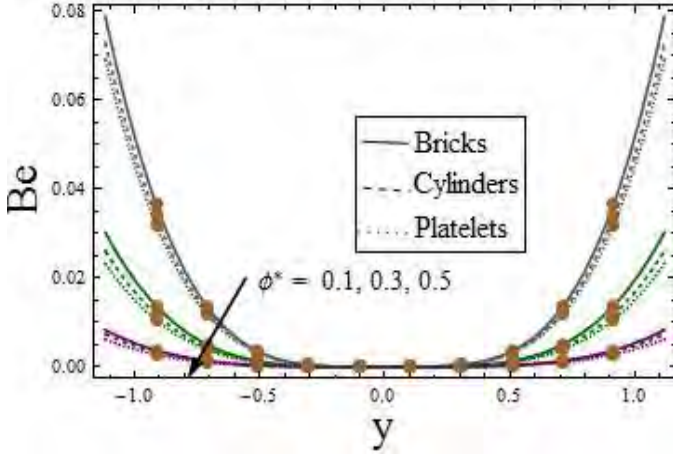


Fig. 2.21

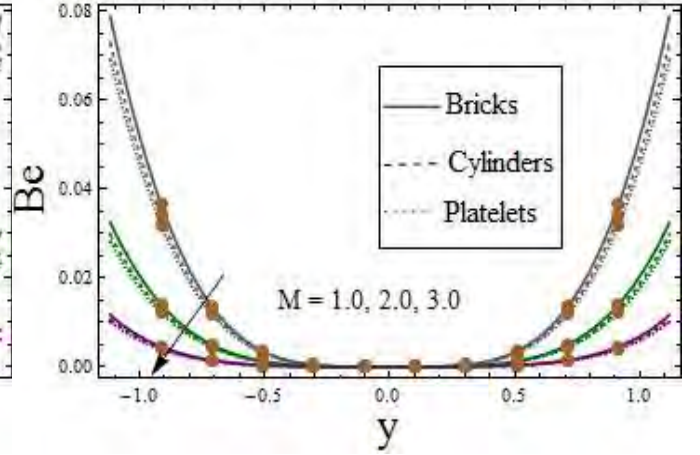


Fig. 2.22

Fig. 2.21.  $Be$  versus  $\phi^*$  when  $E_1 = 0.02, E_2 = 0.01, E_3 = 0.01, t = 0.1, x = 0.2, \varepsilon = 0.2,$   
 $M = 1.0, m = 1.0, Br\Lambda^{-1} = 1.0, Gr = 0.1, \xi_1 = 0.01, \xi_2 = 0.01, Rd = 0.5.$

Fig. 2.22.  $Be$  versus  $M$  when  $E_1 = 0.02, E_2 = 0.01, E_3 = 0.01, t = 0.1, x = 0.2, \varepsilon = 0.2,$   
 $\phi^* = 0.1, m = 1.0, Br\Lambda^{-1} = 1.0, Gr = 0.1, \xi_1 = 0.01, \xi_2 = 0.01, Rd = 0.5.$



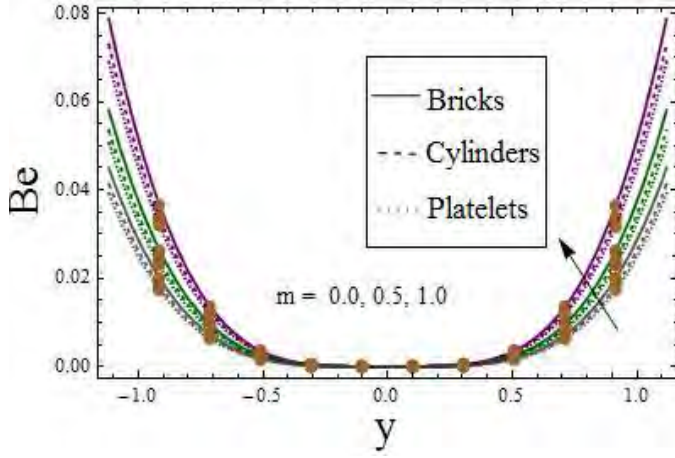


Fig. 2.23

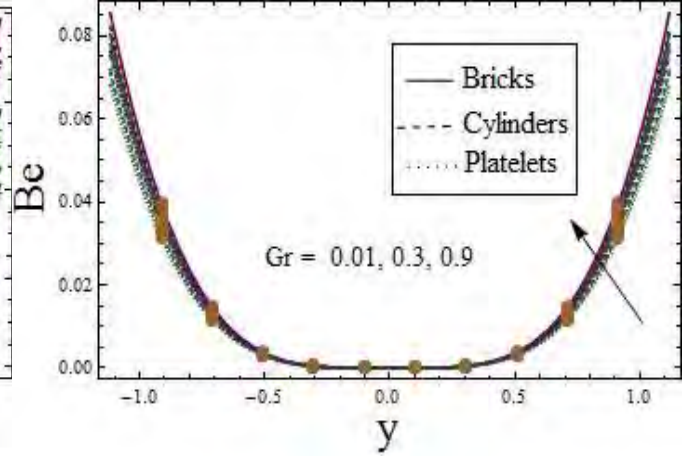


Fig. 2.24

Fig. 2.23.  $Be$  versus  $m$  when  $E_1 = 0.02$ ,  $E_2 = 0.01$ ,  $E_3 = 0.01$ ,  $t = 0.1$ ,  $x = 0.2$ ,  $\varepsilon = 0.2$ ,  $M = 1.0$ ,  $\phi^* = 0.1$ ,  $Br\Lambda^{-1} = 1.0$ ,  $Gr = 0.1$ ,  $\xi_1 = 0.01$ ,  $\xi_2 = 0.01$ ,  $Rd = 0.5$ .

Fig. 2.24.  $Be$  versus  $Gr$  when  $E_1 = 0.02$ ,  $E_2 = 0.01$ ,  $E_3 = 0.01$ ,  $t = 0.1$ ,  $x = 0.2$ ,  $\varepsilon = 0.2$ ,  $M = 1.0$ ,  $m = 1.0$ ,  $Br\Lambda^{-1} = 1.0$ ,  $\phi^* = 0.1$ ,  $\xi_1 = 0.01$ ,  $\xi_2 = 0.01$ ,  $Rd = 0.5$ .

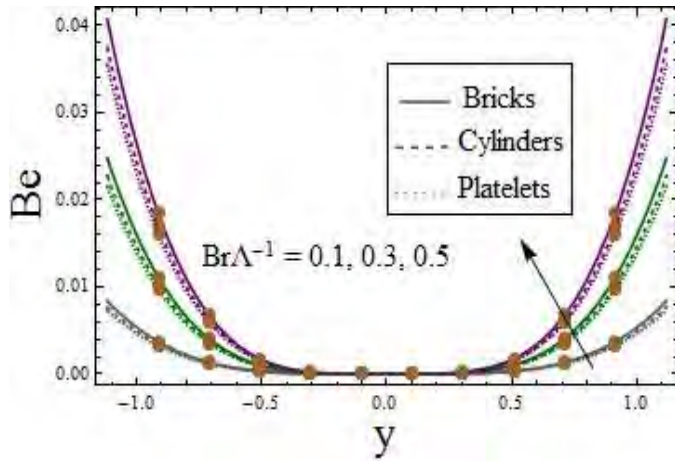


Fig. 2.25

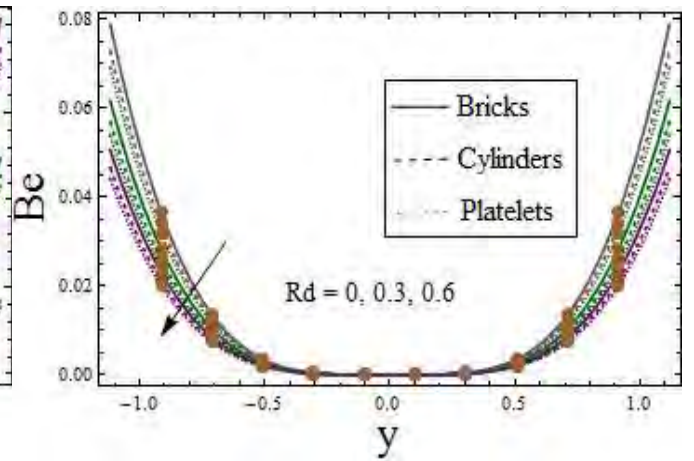


Fig. 2.26

Fig. 2.25.  $Be$  versus  $Br\Lambda^{-1}$  when  $E_1 = 0.02$ ,  $E_2 = 0.01$ ,  $E_3 = 0.01$ ,  $t = 0.1$ ,  $x = 0.2$ ,  $\varepsilon = 0.2$ ,  $M = 1.0$ ,  $m = 1.0$ ,  $\phi^* = 0.1$ ,  $Gr = 0.1$ ,  $\xi_1 = 0.01$ ,  $\xi_2 = 0.01$ ,  $Rd = 0.5$ .

Fig. 2.26.  $Be$  versus  $Rd$  when  $E_1 = 0.02$ ,  $E_2 = 0.01$ ,  $E_3 = 0.01$ ,  $\phi^* = 0.1$ ,  $t = 0.1$ ,  $x = 0.2$ ,

$$\varepsilon = 0.2, M = 1.0, m = 1.0, Br\Lambda^{-1} = 1.0, Gr = 0.1, \xi_1 = 0.01, \xi_2 = 0.01.$$

For the sake of trapping the streamlines are prepared. Figs. 2.27 (a-c) are drawn for the sake of shape factor . It is noted that the size of trapped bolus is lower for brick shaped than others. Figs. 2.28 (a and b) corresponding to brick shaped, Figs. 2.28 (c and d) are constructed to cylindrical shaped and Figs. 2.28 (e and f) to platelet shaped nanofluids for change in Hartman number. It is noted that increase in strength of magnetic field decreases trapped bolus size. This bolus size is smaller for the fluid containing brick shaped nanomaterials. Figs. 2.29 (a and b) are sketched to brick shaped, Figs. 2.29 (c and d) hold to cylindrical shaped and Figs. 2.29 (e and f) to platelet shaped nanofluids have been prepared for change in Hall parameter. It is noted that with higher Hall parameter caused decrease in the size of trapped bolus. This bolus size is smallest for brick shaped nanomaterials.

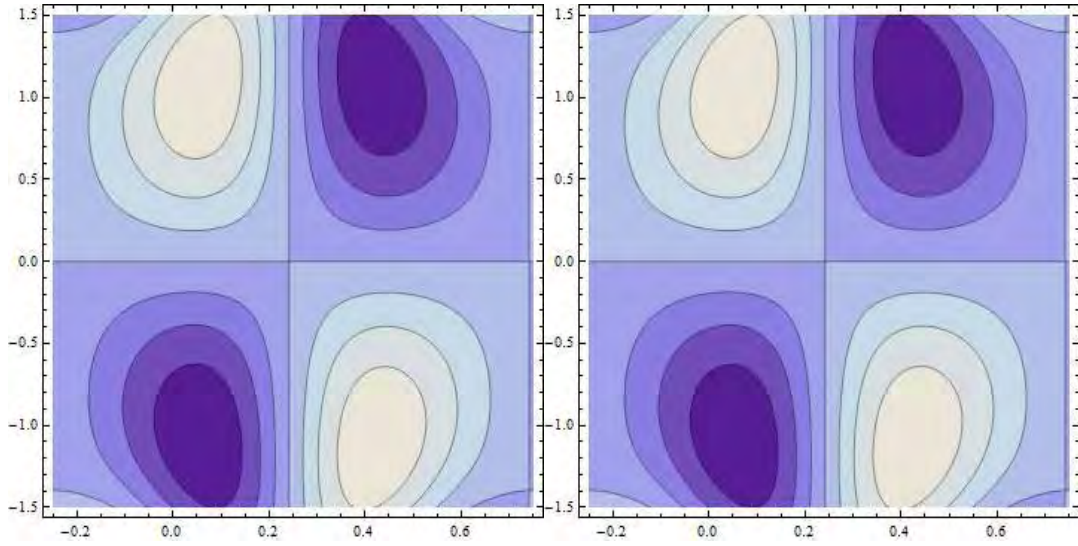
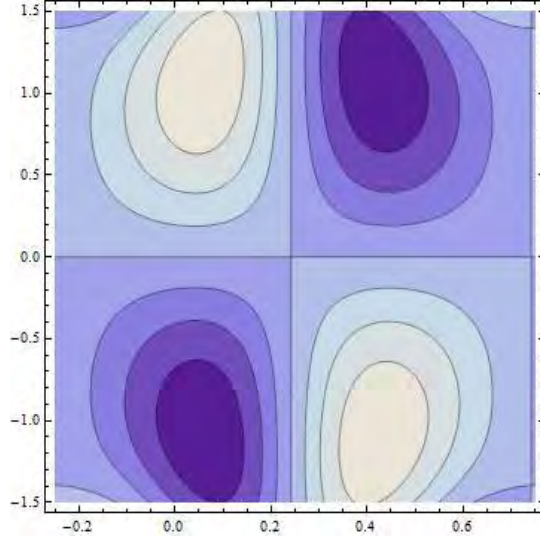


Fig. 2.27 (a)

(b)



(c)

Fig. 2.27.  $\psi$  versus  $n^*$  when  $E_1 = 0.02$ ,  $E_2 = 0.01$ ,  $E_3 = 0.01$ ,  $t = 0$ ,  $\varepsilon = 0.2$ ,  $\phi^* = 0.1$ ,  $M = 1.0$ ,  $m = 1.0$ ,  $Br = 5.0$ ,  $Gr = 0.1$ ,  $\beta = 0.01$ ,  $\gamma = 0.01$ .(a)  $n^* = 3.7$  (b)  $n^* = 4.9$  (c)  $n^* = 5.7$ .

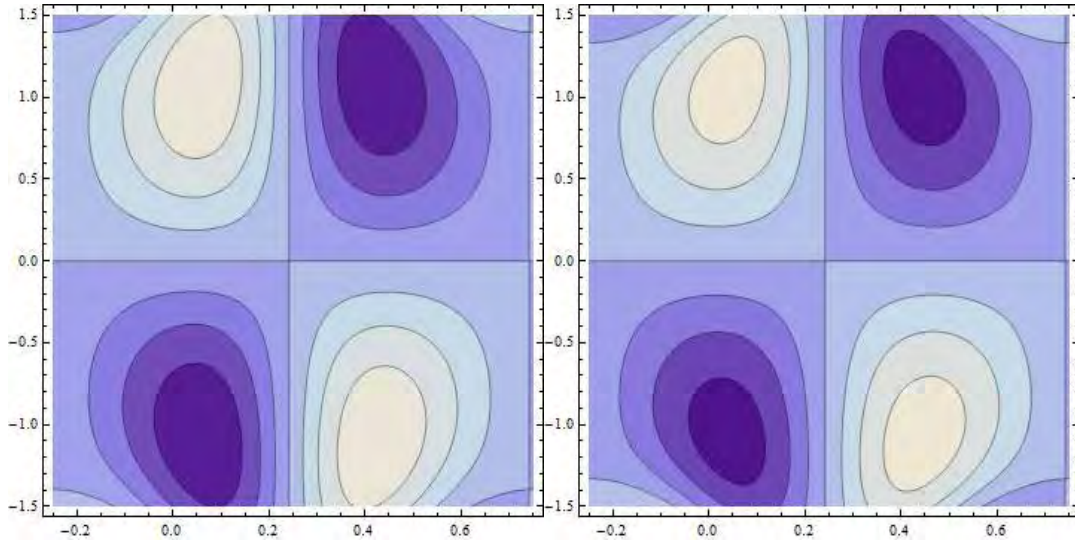


Fig. 2.28 (a)

(b)

Fig. 2.28.  $\psi$  versus  $M$  for nanofluid with brick shaped nanoparticles when  $E_1 = 0.02$ ,  $E_2 = 0.01$ ,  $E_3 = 0.01$ ,  $\phi^* = 0.1$ ,  $t = 0$ ,  $\varepsilon = 0.2$ ,  $m = 1.0$ ,  $Br = 5.0$ ,  $Gr = 0.1$ ,  $\xi_1 = 0.01$ ,

$\xi_2 = 0.01$ . (a)  $M = 1.0$  (b)  $M = 3.0$ .

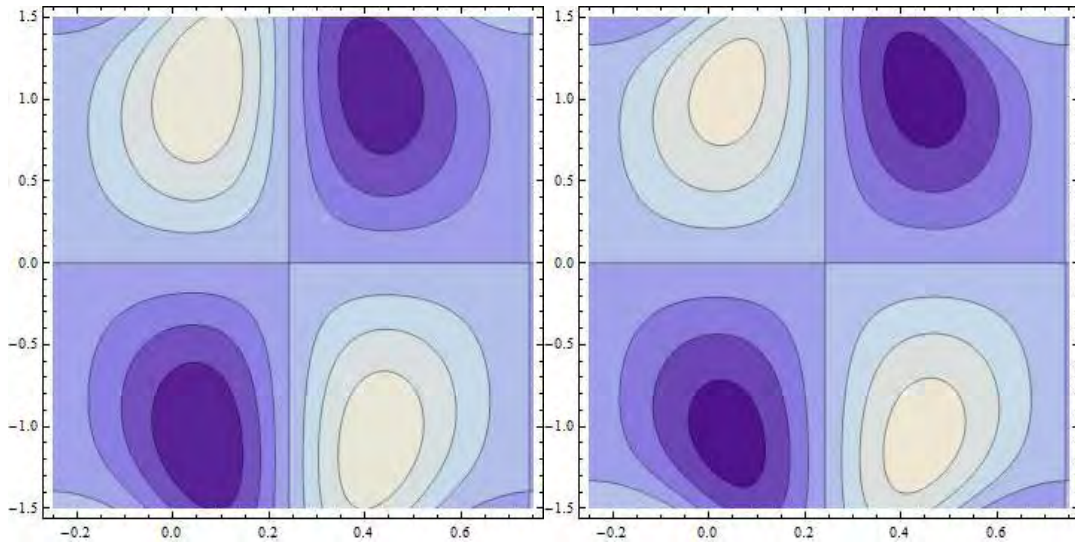


Fig. 2.28 (c)

(d)

Fig. 2.28.  $\psi$  versus  $M$  for nanofluid with cylindrical shaped nanoparticles when  $E_1 = 0.02$ ,  $E_2 = 0.01$ ,  $E_3 = 0.01$ ,  $\phi^* = 0.1$ ,  $t = 0$ ,  $\varepsilon = 0.2$ ,  $m = 1.0$ ,  $Br = 5.0$ ,  $Gr = 0.1$ ,  $\xi_1 = 0.01$ ,  $\xi_2 = 0.01$ . (c)  $M = 1.0$  (d)  $M = 3.0$ .

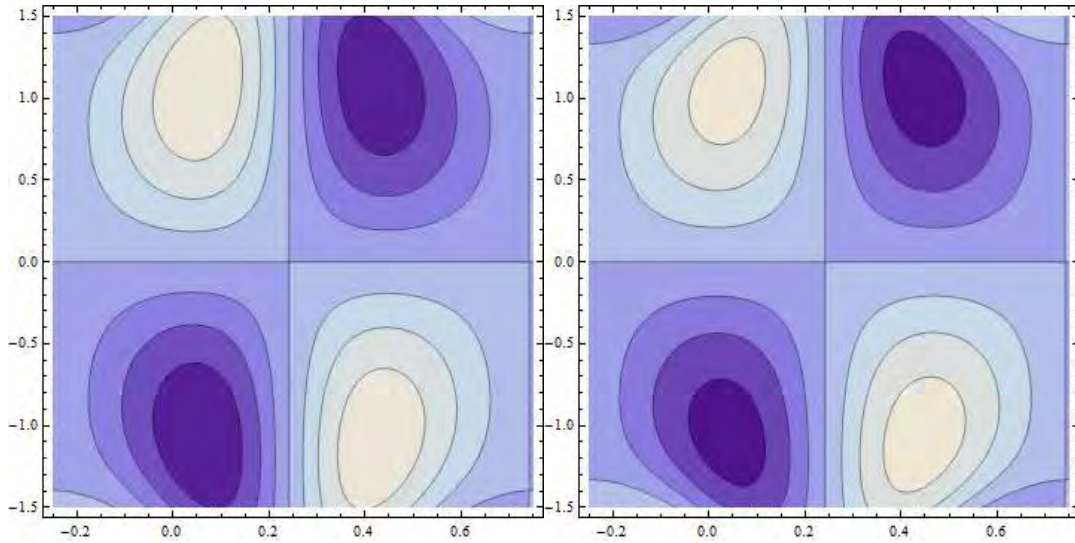


Fig. 2.28 (e)

(f)

Fig. 2.28.  $\psi$  versus  $M$  for nanofluid with platelet shaped nanoparticles when  $E_1 = 0.02$ ,



$E_2 = 0.01, E_3 = 0.01, \phi^* = 0.1, t = 0, \varepsilon = 0.2, m = 1.0, Br = 5.0, Gr = 0.1, \xi_1 = 0.01,$   
 $\xi_2 = 0.01.$  (e)  $M = 1.0$  (f)  $M = 3.0.$

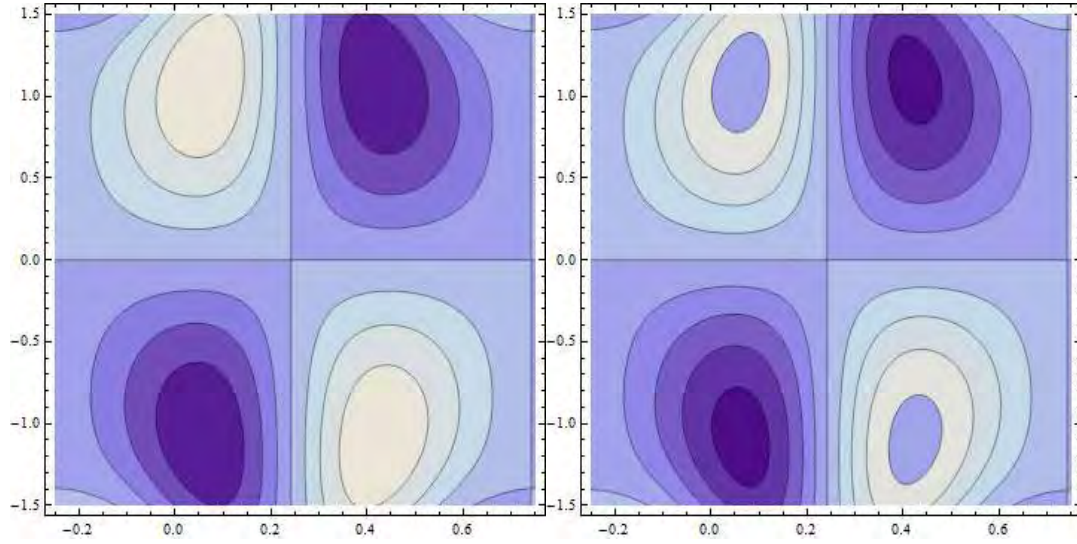
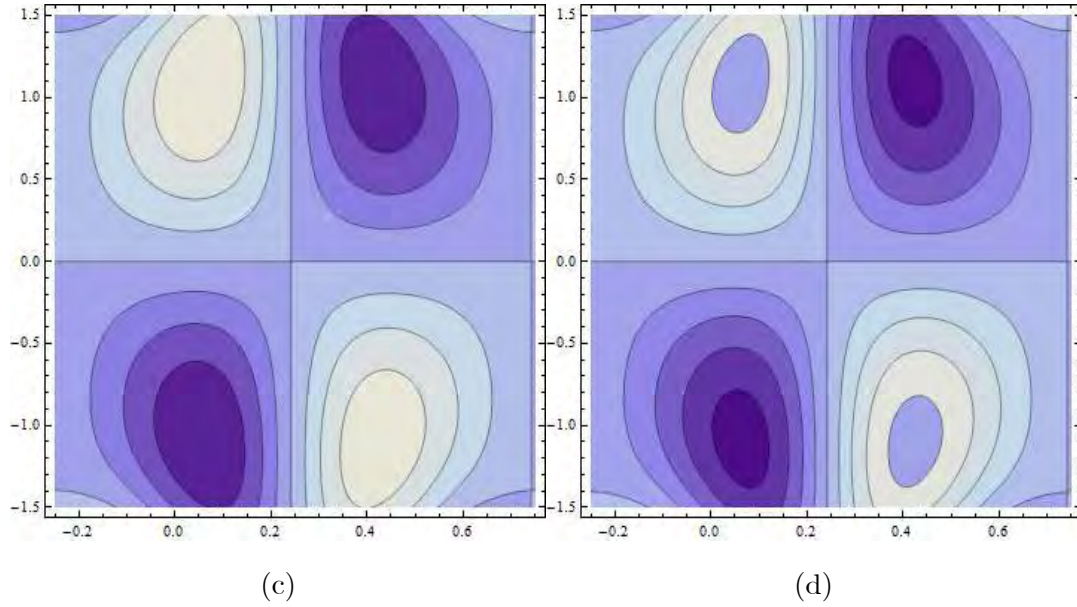


Fig. 2.29 (a)

(b)

*Fig. 2.29.*  $\psi$  versus  $m$  for nanofluid with brick shaped particles when  $E_1 = 0.02, E_2 = 0.01,$   
 $E_3 = 0.01, \phi^* = 0.1, t = 0, \varepsilon = 0.2, m = 1.0, Br = 5.0, Gr = 0.1, \xi_1 = 0.01, \xi_2 = 0.01.$  (a)  
 $m = 1.0$  (b)  $m = 3.0.$



*Fig. 2.29.*  $\psi$  versus  $m$  for nanofluid with cylindrical shaped nanoparticles when  $E_1 = 0.02$ ,  $E_2 = 0.01$ ,  $E_3 = 0.01$ ,  $\phi^* = 0.1$ ,  $t = 0$ ,  $\varepsilon = 0.2$ ,  $m = 1.0$ ,  $Br = 5.0$ ,  $Gr = 0.1$ ,  $\xi_1 = 0.01$ ,  $\xi_2 = 0.01$ . (c)  $m = 1.0$  (d)  $m = 3.0$ .

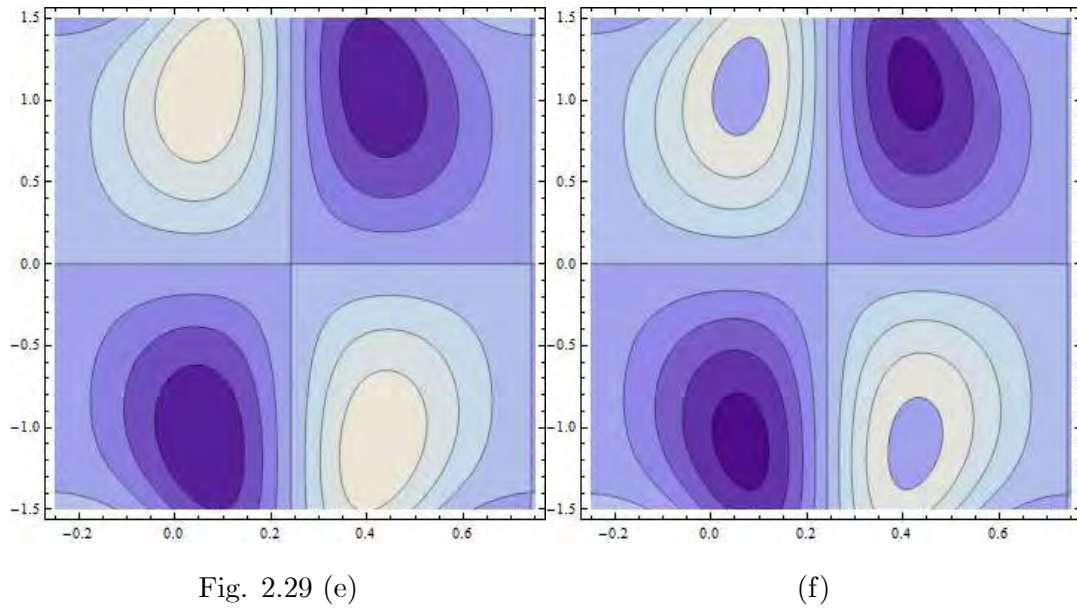


*Fig. 2.29.*  $\psi$  versus  $m$  for nanofluid with platelet shaped nanoparticles when  $E_1 = 0.02$ ,

$$E_2 = 0.01, E_3 = 0.01, \phi^* = 0.1, t = 0, \varepsilon = 0.2, M = 1.0, Br = 5.0, Gr = 0.1, \xi_1 = 0.01, \\ \xi_2 = 0.01. (e) m = 1.0 (f) m = 3.0.$$

## 2.5 Conclusions

Some key points of present study are:

- Enhancement in nanomaterial volume fraction leads to decay in velocity, temperature, entropy generation and Bejan number.
- Hall parameter and Hartman number have opposite behaviors in all cases.
- Grashof number has increasing impact in all cases.
- The behaviors for temperature, entropy generation and Bejan numbers are qualitatively similar.
- The temperature, Bejan number and entropy generation have highest values for brick shaped particles and smallest for platelet shaped particles.
- Size of bolus is smaller for brick shaped nanofluids than others particles.

## Chapter 3

# Investigation of entropy generation in peristalsis of magneto-nanofluid with second order slip conditions

### 3.1 Introduction

This chapter considers the peristalsis of magneto- nanoparticles suspended in water. Explicitly  $Fe_3O_4$ -water nanofluid is utilized for two-dimensional flow in a symmetric channel with compliant walls. Uniform magnetic field is applied. Temperature is arranged for viscous dissipation. Second order velocity and thermal slip conditions are utilized. Small Grashof number leads to perturbation solution. Examination of entropy generation is also made in this study. Maxwell and Hamilton-Crosser models are used. Analysis is based on the comparative study of these two models representing the cylindrical and spherical shaped particles. Graphs for velocity, temperature, entropy generation and Bejan numbers are plotted under the influence of sundry variables. Streamlines are plotted for the sake of trapping phenomenon.

### 3.2 Flow Configuration

Peristaltic flow of an incompressible nanofluid composing of  $Fe_3O_4$  and water is considered. The channel (with width  $2d$ ) is considered symmetric. Flexible walls channel placed at the positions

$y = \pm\eta$  where + and – denote the right and left walls respectively. The rectangular coordinates system is settled such as the  $x$ -axis lies along the channel length where the position of the  $y$ -axis is in the direction perpendicular to the  $x$ -axis. The temperature of the walls is maintained at  $T_0$ . Contribution due to constant applied magnetic field is taken into account. Induced magnetic and electric fields effects are omitted. Mixed convection and viscous dissipation are studied. Sinusoidal waves have wavelength  $\lambda$ , amplitude  $a$  and speed  $c$ . The shape of wave is defined by equation given below:

$$y = \pm\eta(x, t) = \pm \left[ d + a \sin \frac{2\pi}{\lambda} (x - ct) \right]. \quad (3.1)$$

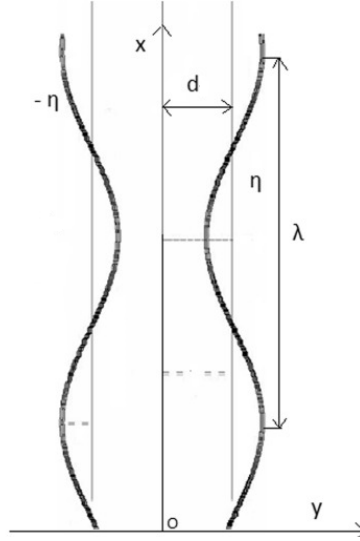


Fig. 3.1: Flow Geometry

Expressions for the considered flow configuration are:

$$\frac{\partial u}{\partial x} + \frac{\partial v}{\partial y} = 0, \quad (3.2)$$

$$\rho_{eff} \left( \frac{\partial}{\partial t} + u \frac{\partial}{\partial x} + v \frac{\partial}{\partial y} \right) u = -\frac{\partial p}{\partial x} + \mu_{eff} \left[ \frac{\partial^2 u}{\partial x^2} + \frac{\partial^2 u}{\partial y^2} \right] - \sigma_{eff} B_o^2 u + g(\rho\beta_T)_{eff} (T - T_0), \quad (3.3)$$

$$\rho_{eff} \left( \frac{\partial}{\partial t} + u \frac{\partial}{\partial x} + v \frac{\partial}{\partial y} \right) v = -\frac{\partial p}{\partial y} + \mu_{eff} \left[ \frac{\partial^2 v}{\partial x^2} + \frac{\partial^2 v}{\partial y^2} \right], \quad (3.4)$$

$$\begin{aligned}
(\rho C_p)_{eff} \left( \frac{\partial}{\partial t} + u \frac{\partial}{\partial x} + v \frac{\partial}{\partial y} \right) T &= \kappa_{eff} \left[ \frac{\partial^2 T}{\partial x^2} + \frac{\partial^2 T}{\partial y^2} \right] + \mu_{eff} \left[ 2 \left( \left( \frac{\partial u}{\partial x} \right)^2 + \left( \frac{\partial v}{\partial y} \right)^2 \right) \right. \\
&\quad \left. + \left( \frac{\partial u}{\partial y} + \frac{\partial v}{\partial x} \right)^2 \right]. \tag{3.5}
\end{aligned}$$

The quantities used in the above mentioned equations are defined as:  $u$  and  $v$  for components of velocity in the  $x$  and  $y$  directions,  $\rho_{eff}$  for effective density,  $p$  the pressure,  $\mu_{eff}$  the effective viscosity,  $\sigma_{eff}$  the effective thermal conductivity,  $g$  the acceleration due to gravity,  $(\rho\beta_T)_{eff}$ ,  $(\rho C_p)_{eff}$  and  $\kappa_{eff}$  for effective thermal expansion, the effective heat capacity and the effective thermal conductivity of nanofluids respectively. Here  $T$  is used to define temperature and  $t$  for time.

The expressions of  $\rho_{eff}$ ,  $(\rho C_p)_{eff}$ ,  $(\rho\beta_T)_{eff}$ ,  $\mu_{eff}$ ,  $\sigma_{eff}$  and  $\kappa_{eff}$  for the two phase models are:

$$\begin{aligned}
\rho_{eff} &= (1 - \phi^*)\rho_f + \phi^*\rho_p, & (\rho C_p)_{eff} &= (1 - \phi^*)(\rho C_p)_f + \phi^*(\rho C_p)_p, \\
(\rho\beta_T)_{eff} &= (1 - \phi^*)(\rho\beta_T)_f + \phi^*(\rho\beta_T)_p, & \mu_{eff} &= \frac{\mu_f}{(1 - \phi^*)^{2.5}}, \\
\frac{\sigma_{eff}}{\sigma_f} &= 1 + \frac{3(\frac{\sigma_p}{\sigma_f} - 1)\phi^*}{(\frac{\sigma_p}{\sigma_f} + 2) - (\frac{\sigma_p}{\sigma_f} - 1)\phi^*}, \\
\frac{\kappa_{eff}}{\kappa_f} &= \frac{\kappa_p + 2\kappa_f - 2\phi^*(\kappa_f - \kappa_p)}{\kappa + 2\kappa_f + \phi^*(\kappa_f - \kappa_p)} && \text{for Maxwell's model and} \\
\frac{\kappa_{eff}}{\kappa_f} &= \frac{\kappa_p + (n^* - 1)\kappa_f - (n^* - 1)\phi^*(\kappa_f - \kappa_p)}{\kappa_p + (n^* - 1)\kappa_f + \phi^*(\kappa_f - \kappa_p)} && \text{for Hamilton-Crosser's model,} \tag{3.6}
\end{aligned}$$

in which the symbols  $f$  and  $p$  in the subscript are used to represent the fluid and nanoparticles whereas  $\phi^*$  depicts volume fraction of nanoparticles. In this study two models of effective thermal conductivity are used in above equation. The Hamilton- Crosser model is used for the cylindrical shaped particles for  $n^* = 6$  whereas Maxwell model is used for spherical shaped particles. Here  $n^*$  represents the shape of nanoparticles. It is defined by  $3/\Psi$  where  $\Psi$  depicts the sphericity of nanoparticles. Value  $\Psi = 0.5$  is used for cylindrical shaped particles whereas  $\Psi = 1$  for spherical shaped particles.

Thermophysical properties of base fluid and nanoparticles are mentioned below in Table 1.

Table 1: Thermophysical parameters of water and nanoparticles

	$\rho$ (kg m <sup>-3</sup> )	$C_p$ (j kg <sup>-1</sup> K <sup>-1</sup> )	$\kappa$ (W m <sup>-1</sup> K <sup>-1</sup> )	$\beta_T$ (1/k) $\times 10^{-6}$	$\sigma$ ( $\Omega \cdot m$ ) <sup>-1</sup>
$H_2O$	997.1	4179	0.613	210	0.05
$Fe_3O_4$	5200	670	80.6	13	25000

The dimensionless quantities are introduced as:

$$\begin{aligned}
x^* &= \frac{x}{\lambda}, & y^* &= \frac{y}{d}, & u^* &= \frac{u}{c}, & v^* &= \frac{v}{c}, & t^* &= \frac{ct}{\lambda}, & \eta^* &= \frac{\eta}{d}, \\
\xi_1^* &= \frac{\xi_1 \mu_f}{d}, & \xi_2^* &= \frac{\xi_2}{d}, & \xi_4^* &= \frac{\xi_4 \mu_f}{d^2}, & \xi_5^* &= \frac{\xi_5}{d^2}, \\
p^* &= \frac{d^2 p}{c \lambda \mu_f}, & \text{Re} &= \frac{\rho_f c d}{\mu_f}, & \theta &= \frac{T - T_0}{T_0}, & \text{Pr} &= \frac{(\mu C_p)_f}{\kappa_f}, \\
Ec &= \frac{c^2}{(C_p)_f T_0}, & Br &= \text{Pr} Ec, & Gr &= \frac{g(\rho \beta_T)_f T_0 d^2}{c \mu_f}, & M &= \sqrt{\frac{\sigma_f}{\mu_f}} B_o d, \\
u &= \frac{\partial \psi}{\partial y}, & v &= -\delta \frac{\partial \psi}{\partial x}.
\end{aligned} \tag{3.7}$$

Here Re, Pr,  $Ec$ ,  $Br$ ,  $M$  and  $Gr$  denote the Reynolds, Prandtl, Eckert, Brinkman, Hartman and Grashof numbers respectively.

After long wavelength and small Reynolds number assumptions one has

$$\frac{\partial p}{\partial x} = \frac{1}{(1 - \phi^*)^{2.5}} \frac{\partial^3 \psi}{\partial y^3} + Gr A_3 \theta - M^2 A_1 \frac{\partial \psi}{\partial y}, \tag{3.8}$$

$$\frac{\partial p}{\partial y} = 0, \tag{3.9}$$

$$K_1 \frac{\partial^2 \theta}{\partial y^2} + \frac{Br}{(1 - \phi^*)^{2.5}} \left( \frac{\partial^2 \psi}{\partial y^2} \right)^2 = 0, \tag{3.10}$$

$$\begin{aligned}
A_1 &= 1 + \frac{3\left(\frac{\sigma_p}{\sigma_f} - 1\right)\phi^*}{\left(\frac{\sigma_p}{\sigma_f} + 2\right) - \left(\frac{\sigma_p}{\sigma_f} - 1\right)\phi^*}, & A_3 &= 1 - \phi^* + \phi^* \left( \frac{(\rho\beta)_p}{(\rho\beta)_f} \right), \\
K_1 &= \frac{\kappa_p + 2\kappa_f - 2\phi^*(\kappa_f - \kappa_p)}{\kappa_p + 2\kappa_f + \phi^*(\kappa_f - \kappa_p)} \text{ for Maxwell's model and} \\
K_1 &= \frac{\kappa_p + (n^* - 1)\kappa_f - (n^* - 1)\phi^*(\kappa_f - \kappa_p)}{\kappa_p + (n^* - 1)\kappa_f + \phi^*(\kappa_f - \kappa_p)} \text{ for Hamilton-Crosser's model.}
\end{aligned} \tag{3.11}$$

The dimensionless form of boundary conditions are:

$$\frac{\partial\psi}{\partial y} \pm \frac{\xi_1}{(1-\phi^*)^{2.5}} \frac{\partial^2\psi}{\partial y^2} \pm \frac{\xi_4}{(1-\phi^*)^{2.5}} \frac{\partial^3\psi}{\partial y^3} = 0, \quad \theta \pm \xi_2 \frac{\partial\theta}{\partial y} \pm \xi_5 \frac{\partial^2\theta}{\partial y^2} = 0, \quad \text{at } y = \pm\eta, \quad (3.12)$$

$$\left[ E_1 \frac{\partial^3}{\partial x^3} + E_2 \frac{\partial^3}{\partial x \partial t^2} + E_3 \frac{\partial^2}{\partial t \partial x} \right] \eta = \frac{1}{(1-\phi^*)^{2.5}} \frac{\partial^3\psi}{\partial y^3} + Gr A_3 \theta - M^2 A_1 \frac{\partial\psi}{\partial y}, \quad \text{at } y = \pm\eta. \quad (3.13)$$

Here  $E_1(= -\tau^* d^3 / \lambda^3 c \mu_f)$ ,  $E_2(= m^* c d^3 / \lambda^3 \mu_f)$  and  $E_3(= d_1^* d^3 / \lambda^2 \mu_f)$  are the walls parameters. Here velocity and temperature slip parameters in dimensionless form is denoted by  $\xi_1$ ,  $\xi_4$  and  $\xi_2$ ,  $\xi_5$  respectively.

### 3.2.1 Entropy generation and viscous dissipation

Viscous dissipation is represented by

$$\Phi = \mu_{eff} \left[ 2 \left( \left( \frac{\partial u}{\partial x} \right)^2 + \left( \frac{\partial v}{\partial y} \right)^2 \right) + \left( \frac{\partial u}{\partial y} + \frac{\partial v}{\partial x} \right)^2 \right]. \quad (3.14)$$

Dimensional form of volumetric entropy generation is

$$S'''_{gen} = \frac{\kappa_{eff}}{T_m^2} \left( \left( \frac{\partial T}{\partial x} \right)^2 + \left( \frac{\partial T}{\partial y} \right)^2 \right) + \frac{\Phi}{T_m}. \quad (3.15)$$

Entropy generation in dimensionless form becomes

$$N_s = \frac{S'''_{gen}}{S'''_G} = A_3 \left( \frac{\partial\theta}{\partial y} \right)^2 + \frac{Br}{\Lambda(1-\phi)^{2.5}} \left( \frac{\partial^2\psi}{\partial y^2} \right)^2, \quad (3.16)$$

$$S'''_G = \frac{\kappa_f T_0^2}{T_m^2 d^2}, \quad \Lambda = \frac{T_0}{T_m}. \quad (3.17)$$

Bejan number is:

$$Be = \frac{Ns_{cond}}{Ns_{cond} + Ns_{visc}}. \quad (3.18)$$

Here Eq. (3.15) can be split into two parts. One part comprises of entropy generation which is due to finite temperature difference ( $Ns_{cond}$ ) and the other part includes the entropy generation because of viscous dissipation effects ( $Ns_{visc}$ ).



### 3.3 Solution methodology

We adopted the perturbation technique for the solution. We choose the small Grashof number as perturbation parameter. The equations and solutions for the cases of zeroth and first orders are:

#### 3.3.1 Zeroth order systems and solutions

$$\frac{1}{(1-\phi^*)^{2.5}} \frac{\partial^4 \psi_0}{\partial y^4} - M^2 A_1 \frac{\partial^2 \psi_0}{\partial y^2} = 0, \quad (3.19)$$

$$K_1 \frac{\partial^2 \theta_0}{\partial y^2} + \frac{Br}{(1-\phi^*)^{2.5}} \left( \frac{\partial^2 \psi_0}{\partial y^2} \right)^2 = 0, \quad (3.20)$$

$$\frac{\partial \psi_0}{\partial y} \pm \frac{\xi_1}{(1-\phi^*)^{2.5}} \frac{\partial^2 \psi_0}{\partial y^2} \pm \frac{\xi_4}{(1-\phi^*)^{2.5}} \frac{\partial^3 \psi_0}{\partial y^3} = 0, \quad \text{at } y = \pm \eta, \quad (3.21)$$

$$\left[ E_1 \frac{\partial^3}{\partial x^3} + E_2 \frac{\partial^3}{\partial x \partial t^2} + E_3 \frac{\partial^2}{\partial t \partial x} \right] \eta = \frac{1}{(1-\phi^*)^{2.5}} \frac{\partial^3 \psi_0}{\partial y^3} - M^2 A_1 \frac{\partial \psi_0}{\partial y}, \quad \text{at } y = \pm \eta, \quad (3.22)$$

$$\theta_0 \pm \xi_2 \frac{\partial \theta_0}{\partial y} \pm \xi_5 \frac{\partial^2 \theta_0}{\partial y^2} = 0, \quad \text{at } y = \pm \eta. \quad (3.23)$$

The solutions of stream function and temperature are

$$\psi_0 = \frac{A_0 e^{\frac{-\sqrt{A_1} M y}{\sqrt{A_0}}} \left( e^{\frac{2\sqrt{A_1} M y}{\sqrt{A_0}}} C_1 + C_2 \right)}{A_1 M^2} + C_3 + y C_4, \quad (3.24)$$

$$\theta_0 = -\frac{1}{4A_1 K_1 M^2} A_0 Br \left( e^{\frac{-2\sqrt{A_1} M y}{\sqrt{A_0}}} (C_2^2 + C_1^2 e^{\frac{4\sqrt{A_1} M y}{\sqrt{A_0}}}) \right) + F_1 + y F_2. \quad (3.25)$$

#### 3.3.2 First order systems and solutions

Here we have

$$\frac{1}{(1-\phi^*)^{2.5}} \frac{\partial^4 \psi_1}{\partial y^4} + A_3 \frac{\partial \theta_0}{\partial y} - M^2 A_1 \frac{\partial^2 \psi_1}{\partial y^2} = 0, \quad (3.26)$$

$$K_1 \frac{\partial^2 \theta_1}{\partial y^2} + \frac{Br}{(1-\phi^*)^{2.5}} \left( 2 \frac{\partial^2 \psi_0}{\partial y^2} \frac{\partial^2 \psi_1}{\partial y^2} \right) = 0, \quad (3.27)$$

$$\frac{\partial \psi_1}{\partial y} \pm \frac{\xi_1}{(1-\phi^*)^{2.5}} \frac{\partial^2 \psi_1}{\partial y^2} \pm \frac{\xi_4}{(1-\phi^*)^{2.5}} \frac{\partial^3 \psi_1}{\partial y^3} = 0, \quad \text{at } y = \pm \eta, \quad (3.28)$$

$$\frac{1}{(1 - \phi^*)^{2.5}} \frac{\partial^3 \psi_1}{\partial y^3} + A_3 \theta_0 - M^2 A_1 \frac{\partial \psi_1}{\partial y} = 0 \quad \text{at } y = \pm \eta, \quad (3.29)$$

$$\theta_1 \pm \xi_2 \frac{\partial \theta_1}{\partial y} \pm \xi_5 \frac{\partial^2 \theta_1}{\partial y^2} = 0, \quad \text{at } y = \pm \eta. \quad (3.30)$$

The solution expressions are

$$\begin{aligned} \psi_1 = & -\frac{1}{24A_1^2 K_1 M^5} \left( \frac{A_0^{\frac{5}{2}} \frac{9}{8} A_3 Br e^{-\frac{\sqrt{A_1} M y}}{\sqrt{A_0}} \left( C_2^2 - C_1^2 e^{\frac{4\sqrt{A_1} M y}}{\sqrt{A_0}} \right)}{\sqrt{A_1}} - 12A_1 A_3 F_2 K_1 M^3 y^2 + 8A_0 A_1 M^3 \right. \\ & \left. (A_3 Br C_1 C_2 y^3 - 3e^{-\frac{\sqrt{A_1} M y}}{\sqrt{A_0}} K_1 (e^{\frac{2\sqrt{A_1} M y}}{\sqrt{A_0}} B_1 + B_2)) \right) + yB_4 + B_3, \end{aligned} \quad (3.31)$$

$$\begin{aligned} \theta_1 = & \frac{1}{9A_1^2 K_1 M^5} A_0 Br \left( \frac{A_0^{\frac{5}{2}} A_3 Br C_2^3 e^{-\frac{3\sqrt{A_1} M y}}{\sqrt{A_0}}}{3\sqrt{A_1} M} - \frac{A_0^{\frac{5}{2}} A_3 Br C_1^3 e^{\frac{3\sqrt{A_1} M y}}{\sqrt{A_0}}}{3\sqrt{A_1} M} - \right. \\ & \frac{9}{2} A_0 A_1 B_2 C_2 e^{-\frac{2\sqrt{A_1} M y}}{\sqrt{A_0}} K_1 M^2 - \frac{9}{2} A_0 A_1 B_1 C_1 e^{\frac{2\sqrt{A_1} M y}}{\sqrt{A_0}} K_1 M^2 - \\ & 9A_1^2 (B_2 C_1 + B_1 C_2) K_1 M^4 y^2 - 3\sqrt{A_0} A_3 C_2 e^{-\frac{\sqrt{A_1} M y}}{\sqrt{A_0}} \\ & \left. \left( \frac{\sqrt{A_0} (-25A_0^{\frac{3}{2}} Br C_1 C_2 + 6\sqrt{A_1} F_2 K_1 M)}{\sqrt{A_1} M} - 12A_0^{\frac{3}{2}} Br C_1 C_2 y \right) - \right. \\ & \left. 3\sqrt{A_0} A_3 C_1 e^{\frac{\sqrt{A_1} M y}}{\sqrt{A_0}} \right) \left( \frac{\sqrt{A_0} (25A_0^{\frac{3}{2}} Br C_1 C_2 + 6\sqrt{A_1} F_2 K_1 M)}{\sqrt{A_1} M} \right. \\ & \left. - 12A_0^{\frac{3}{2}} Br C_1 C_2 y \right) + G_1 + yG_2. \end{aligned} \quad (3.32)$$

Here  $Ci'$  s,  $Fi'$  s,  $Bi'$  s and  $Gi'$  s are constants that can be evaluated through Mathematica.

## 3.4 Discussion

This portion is devoted to the analysis of velocity, temperature, entropy generation, Bejan number and stream lines. Each quantity is analyzed in different subsections.

### 3.4.1 Analysis of velocity

In this subsection behavior of velocity is discussed under the influence of different important parameters. Fig. 3.2 represents impact of nanoparticle volume fraction for velocity profile.

This graphs shows the decreasing behavior which is related to the fact that by increasing the quantity of nanoparticles (as  $\phi^* = 0.01, 0.03, 0.05, 0.07$ ) resistance to the fluid increases so fluid velocity decays. Here the values for Hamilton-Crosser's model is greater than the Maxwell's model. Fig. 3.3 has been plotted against Hartman number. It elucidates that velocity has decreasing behavior for larger Hartman number ( $M = 2, 3, 4, 5$ ). Infact the Lorentz force acts as the resistive force. Grashof number behavior can be notified through Fig. 3.4. Here we see an increment in velocity profile by enhancing Grashof number ( $Gr = 0.1 - 0.7$ ). It is due to increase in buoyancy forces which facilitates the flow. Velocity profile for wall parameters can be observed through Fig. 3.5. The results illustrate that the velocity has the increasing behavior for elastance parameters ( $E_1 = 0.01, 0.02$ ) and ( $E_2 = 0.02, 0.04$ ) where as decreasing behavior for the damping parameter ( $E_3 = 0.01, 0.02$ ). Obviously elastance parameters provide less resistance so velocity increases whereas as damping resists the flow more. Slip parameters result is demonstrated through Figs. 3.6 and 3.7. Here we have observed that the velocity profile shows enhancement when we increase the slip parameters ( $\xi_1 = 0.1, 0.3, 0.5, 0.7$ ) and ( $\xi_4 = -0.1, -0.3, -0.5, -0.7$ ). We also noticed that this behavior is more prominent for second order slip parameter than the first order. Further the velocity profile is noted higher for case of Hamilton-Crosser's than the Maxwell's model.

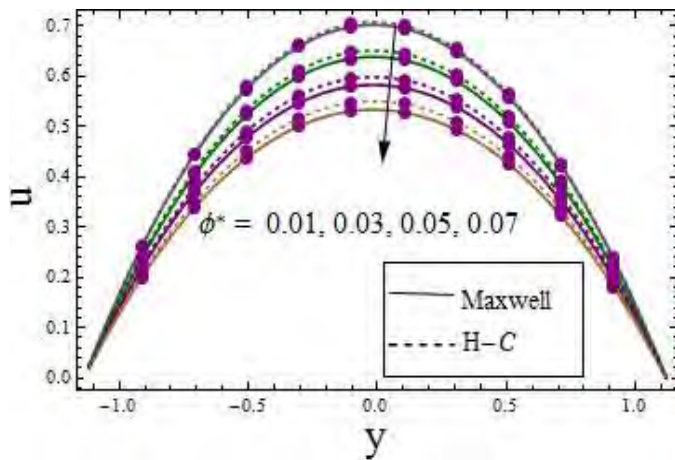


Fig. 3.2

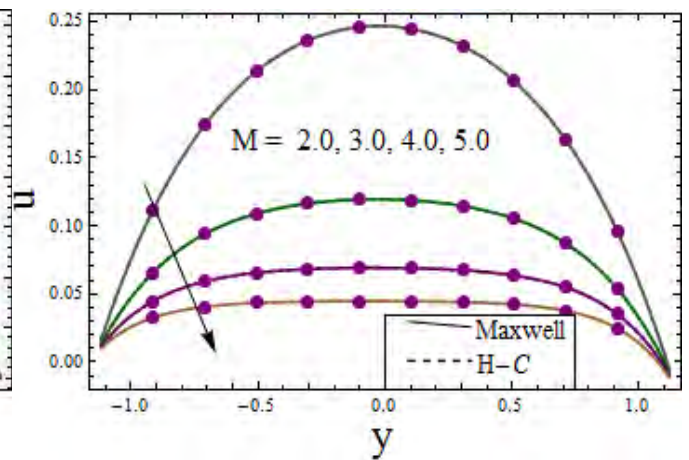


Fig. 3.3

Fig. 3.2.  $u$  via  $\phi^*$  when  $E_1 = 0.02, E_2 = 0.01, E_3 = 0.01, t = 0.1, x = 0.2, \varepsilon = 0.2, M = 1.0,$   
 $Br = 3.0, Gr = 0.03, \xi_1 = 0.01, \xi_4 = -0.01, \xi_2 = 0.01, \xi_5 = -0.01.$

Fig. 3.3.  $u$  via  $M$  when  $E_1 = 0.02, E_2 = 0.01, E_3 = 0.01, t = 0.1, x = 0.2, \varepsilon = 0.2, \phi^* = 0.01,$   
 $Br = 3.0, Gr = 0.03, \xi_1 = 0.01, \xi_4 = -0.01, \xi_2 = 0.01, \xi_5 = -0.01.$

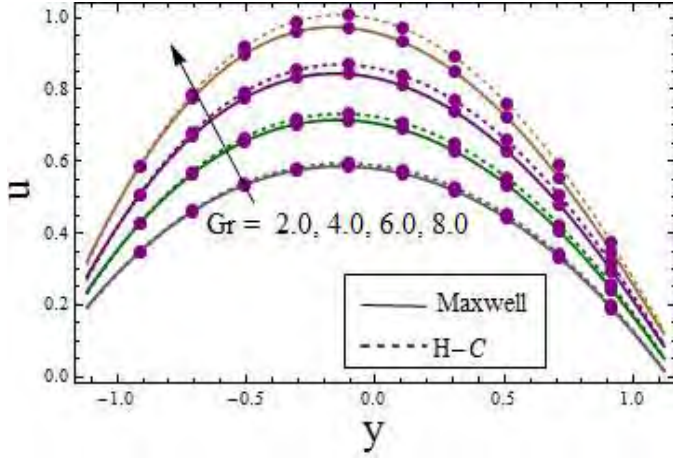


Fig. 3.4

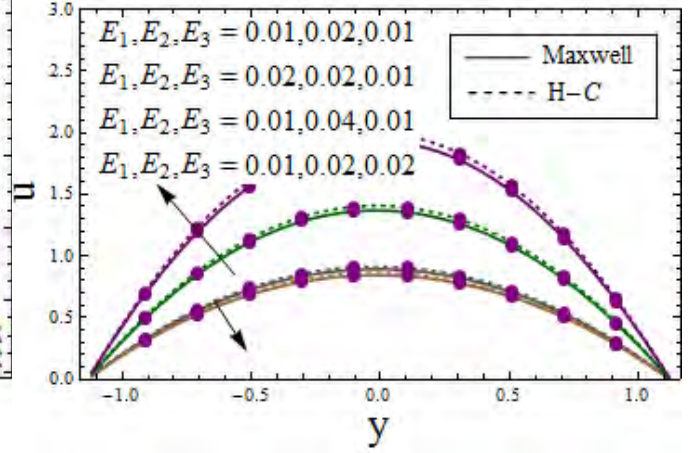


Fig. 3.5

Fig. 3.4.  $u$  via  $Gr$  when  $E_1 = 0.02, E_2 = 0.01, E_3 = 0.01, t = 0.1, x = 0.2, \varepsilon = 0.2, M = 1.0,$   
 $\phi^* = 0.1, Br = 3.0, \xi_1 = 0.01, \xi_4 = -0.01, \xi_2 = 0.01, \xi_5 = -0.01.$

Fig. 3.5.  $u$  via  $E_1, E_2, E_3$  when  $t = 0.1, x = 0.2, \varepsilon = 0.2, M = 1.0, \phi^* = 0.1, Br = 3.0,$   
 $Gr = 0.03, \xi_1 = 0.01, \xi_4 = -0.01, \xi_2 = 0.01, \xi_5 = -0.01.$

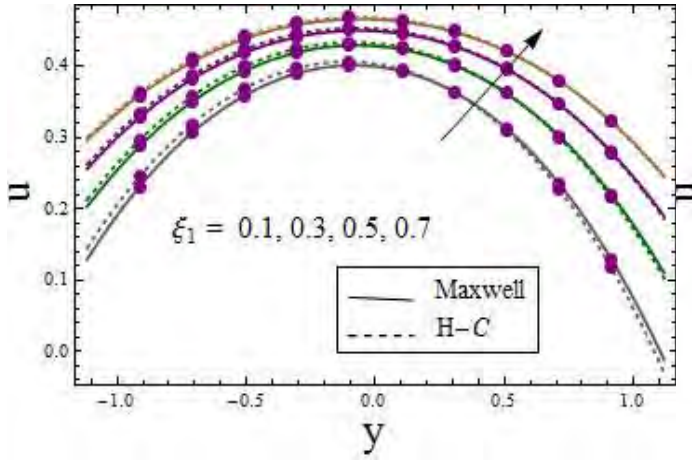


Fig. 3.6

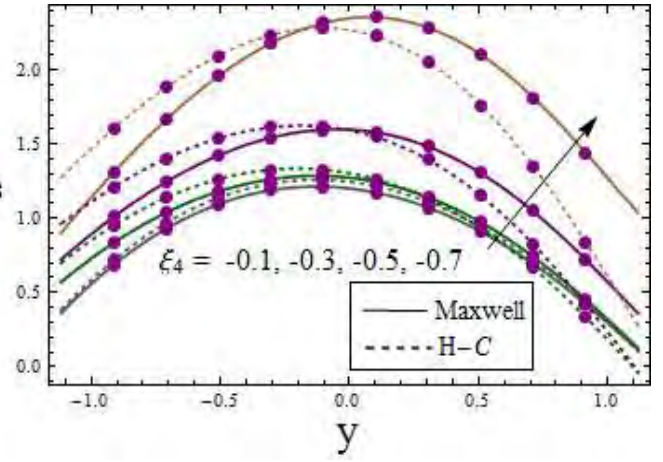


Fig. 3.7

Fig. 3.6.  $u$  via  $\xi_1$  when  $E_1 = 0.02$ ,  $E_2 = 0.01$ ,  $E_3 = 0.01$ ,  $t = 0.1$ ,  $x = 0.2$ ,  $\varepsilon = 0.2$ ,  $M = 1.0$ ,  $\phi^* = 0.1$ ,  $Br = 3.0$ ,  $Gr = 0.03$ ,  $\xi_4 = -0.01$ ,  $\xi_2 = 0.01$ ,  $\xi_5 = -0.01$ .

Fig. 3.7.  $u$  via  $\xi_4$  when  $E_1 = 0.02$ ,  $E_2 = 0.01$ ,  $E_3 = 0.01$ ,  $t = 0.1$ ,  $x = 0.2$ ,  $\varepsilon = 0.2$ ,  $M = 1.0$ ,  $\phi^* = 0.1$ ,  $Br = 3.0$ ,  $Gr = 0.03$ ,  $\xi_1 = 0.01$ ,  $\xi_2 = 0.01$ ,  $\xi_5 = -0.01$ .

### 3.4.2 Analysis of temperature

In this subsection the temperature profile for different pertinent parameters are displayed. Fig. 3.8 provides graphs for  $\phi^*$  ( $= 0.01, 0.03, 0.05, 0.07$ ) versus temperature distribution. This graph represents that the temperature profile is decreasing function of  $\phi^*$ . As increase in  $\phi^*$  enhances the thermal conductivity and cooling capabilities as well. Moreover the temperature is higher for Maxwell's model than Hamilton's-Crosser's expression. Fig. 3.9 plots the impact of Hartman number on  $\theta$ . This Fig. demonstrates decreasing behavior of temperature where Hartman number increases from (2–5). An increment is seen for temperature profile by varying Grashof number (as 0.1 – 0.7) (see Fig. 3.10). As  $Gr$  increases the velocity so the mean kinetic energy of the particles. Hence an increase in temperature. Wall parameters impact is elucidated through Fig. 3.11. It shows the similar behavior as in case of velocity profile when we varies the parameters as ( $E_1 = 0.01, 0.02$ ), ( $E_2 = 0.02, 0.04$ ) and ( $E_3 = 0.01, 0.02$ ). The reasons can be linked to velocity. First and second order thermal slip parameters outcomes are seen through

Figs. 3.12 and 3.13. For an increase of first order thermal slip ( $\xi_2 = 0.01, 0.03, 0.05, 0.07$ ) the temperature increases throughout the channel where as for second order thermal slip parameter ( $\xi_5 = -0.01$  to  $-0.07$ ) the temperature increases near the centre. A comparative study reveals that the temperature remains higher for spherical shaped particles than cylindrical shaped ones.

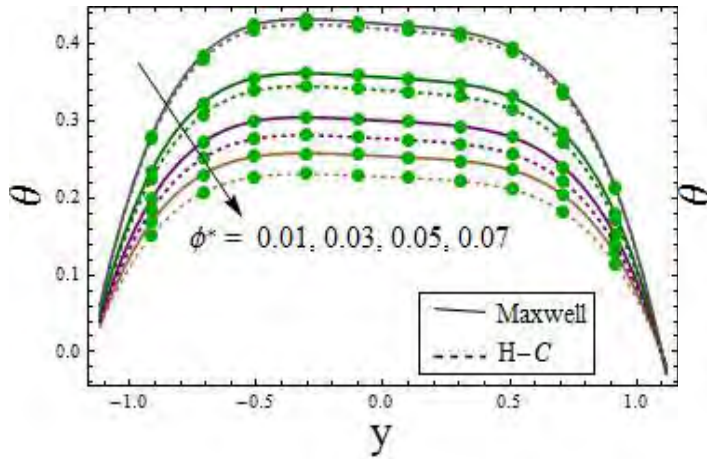


Fig. 3.8

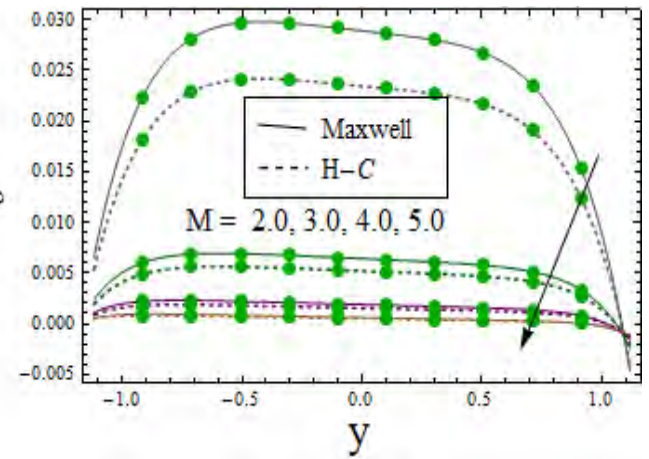


Fig. 3.9

Fig. 3.8.  $\theta$  via  $\phi^*$  when  $E_1 = 0.02$ ,  $E_2 = 0.01$ ,  $E_3 = 0.01$ ,  $t = 0.1$ ,  $x = 0.2$ ,  $\varepsilon = 0.2$ ,  $M = 1.0$ ,  
 $Gr = 0.03$ ,  $Br = 3.0$ ,  $\xi_1 = 0.01$ ,  $\xi_4 = -0.01$ ,  $\xi_2 = 0.01$ ,  $\xi_5 = -0.01$ .

Fig. 3.9.  $\theta$  via  $M$  when  $E_1 = 0.02$ ,  $E_2 = 0.01$ ,  $E_3 = 0.01$ ,  $t = 0.1$ ,  $x = 0.2$ ,  $\varepsilon = 0.2$ ,  $Gr = 0.03$ ,  
 $\phi^* = 0.1$ ,  $Br = 3.0$ ,  $\xi_1 = 0.01$ ,  $\xi_4 = -0.01$ ,  $\xi_2 = 0.01$ ,  $\xi_5 = -0.01$ .



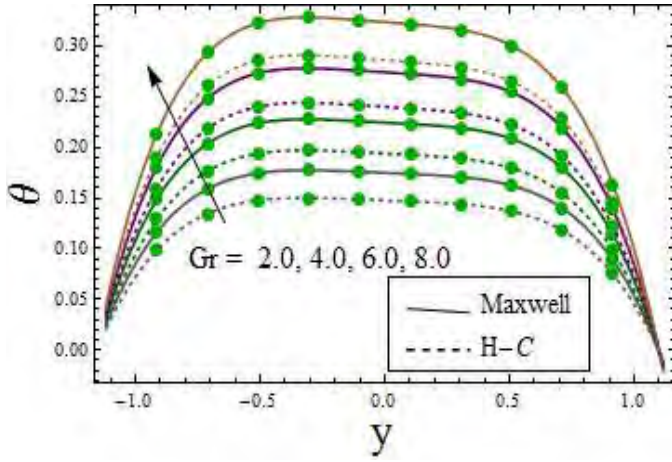


Fig. 3.10

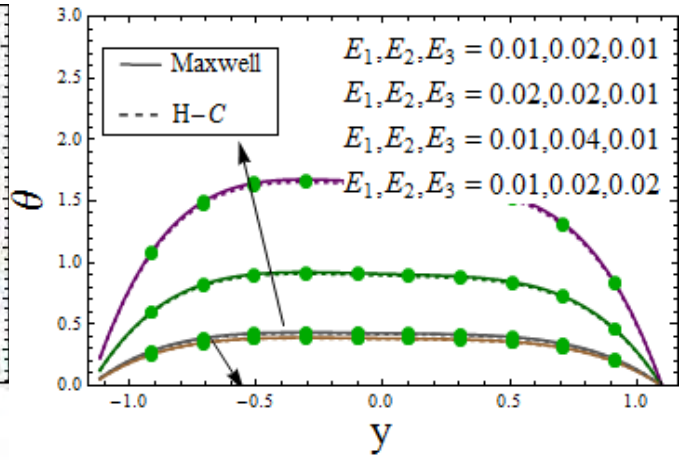


Fig. 3.11

Fig. 3.10.  $\theta$  via  $Gr$  when  $E_1 = 0.02$ ,  $E_2 = 0.01$ ,  $E_3 = 0.01$ ,  $t = 0.1$ ,  $x = 0.2$ ,  $\varepsilon = 0.2$ ,  $M = 1.0$ ,  $\phi^* = 0.1$ ,  $Br = 3.0$ ,  $\xi_1 = 0.01$ ,  $\xi_4 = -0.01$ ,  $\xi_2 = 0.01$ ,  $\xi_5 = -0.01$ .

Fig. 3.11.  $\theta$  via  $E_1, E_2, E_3$  when  $t = 0.1$ ,  $x = 0.2$ ,  $\varepsilon = 0.2$ ,  $M = 1.0$ ,  $\phi^* = 0.1$ ,  $Gr = 0.03$ ,  $Br = 3.0$ ,  $\xi_1 = 0.01$ ,  $\xi_4 = -0.01$ ,  $\xi_2 = 0.01$ ,  $\xi_5 = -0.01$ .

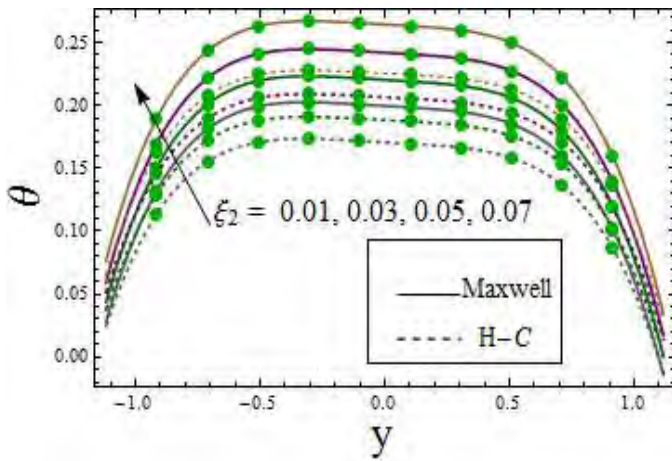


Fig. 3.12

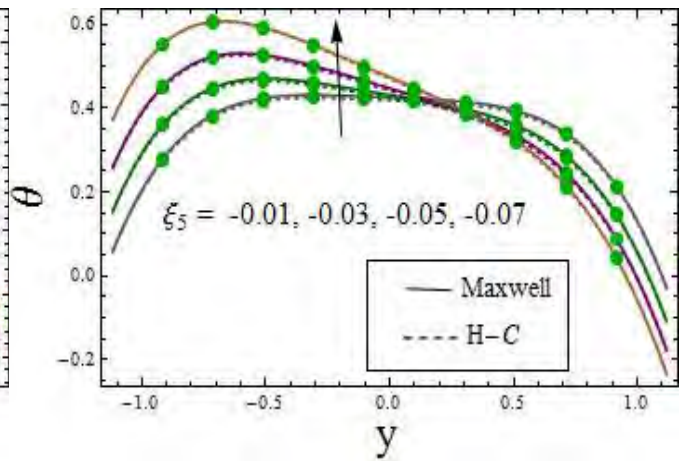


Fig. 3.13

Fig. 3.12.  $\theta$  via  $\xi_2$  when  $E_1 = 0.02$ ,  $E_2 = 0.01$ ,  $E_3 = 0.01$ ,  $t = 0.1$ ,  $x = 0.2$ ,  $\varepsilon = 0.2$ ,  $M = 1.0$ ,  $Gr = 0.03$ ,  $\phi^* = 0.1$ ,  $Br = 3.0$ ,  $\xi_1 = 0.01$ ,  $\xi_4 = -0.01$ ,  $\xi_5 = -0.01$ .

Fig. 3.13.  $\theta$  via  $\xi_5$  when  $E_1 = 0.02$ ,  $E_2 = 0.01$ ,  $E_3 = 0.01$ ,  $t = 0.1$ ,  $x = 0.2$ ,  $\varepsilon = 0.2$ ,  $M = 1.0$ ,

$$Gr = 0.03, \phi^* = 0.1, Br = 3.0, \xi_1 = 0.01, \xi_4 = -0.01, \xi_2 = 0.01.$$

### 3.4.3 Analysis of entropy generation and Bejan number

This subsection consists of entropy generation and Bejan number for different embedded parameters. To explain the impact of  $\phi^*$  on entropy generation the Fig. 3.14 is sketched. The results display that the entropy generation decreases with larger values of  $\phi^*$  i.e. 0.01, 0.03, 0.05, 0.07. It is due to decrease in temperature for larger nanoparticles volume fraction as entropy of system is directly linked with temperature. Fig. 3.15 portrayed the results for Hartman number. Through larger values of Hartman number (as 1.0, 1.5, 2.0, 2.5) the entropy generation decreases. Grashof number has increasing impact on  $Ns$  as  $Gr$  takes the values between (0.1 – 0.7) (see Fig. 3.16). Result in this case is qualitatively similar to temperature. Entropy generation enhances when the ratio of  $Br$  to  $\Lambda$  enlarges (0.1 – 0.7) (see Fig. 3.17). To notify the influence of wall parameters the Fig. 3.18 is sketched. Entropy generation is increasing function of  $E_1$  (= 0.01, 0.02) and  $E_2$  (= 0.02, 0.04) whereas it is decreasing function of  $E_3$  (= 0.01, 0.02). For all cases the values for Hamilton-Crosser's model is greater than Maxwell's model.

For the behavior of Bejan numbers on pertinent parameters the Figs. 3.19-3.23 are drawn. Fig. 3.19 displays the nanoparticle volume fraction impact on Bejan number. The inverse relation is seen between Bejan number and nanoparticle volume fraction i.e. increment in  $\phi^*$  (0.1 – 0.7) decreases Bejan number. For Hartman number as varied between 1.0 – 2.5 a decay is noticed (see Fig. 3.20). Fig. 3.21 is drawn for results of Grashof number (0.1 – 0.7) versus Bejan number. This Fig. portrayed that the direct relation is seen between Bejan and Grashof numbers. Bejan number enhances via enhancement in ratio of  $Br$  to  $\Lambda$  as 0.1 – 0.7 (see Fig. 3.22). The wall parameters results are revealed by Fig. 3.23. An enhancement is seen for larger elastance parameters  $E_1$  (= 0.01, 0.02) and  $E_2$  (= 0.02, 0.04) whereas decay is observed for the case of larger damping parameter  $E_3$  (= 0.01, 0.02). It can be seen that with an enhancement in pertinent parameter the increase in Bejan number demonstrates that heat transfer irreversibility is higher than the total irreversibility due to fluid friction and heat transfer. Moreover, in all cases the values of Hamilton-Crosser's model is less than Maxwell's relation.



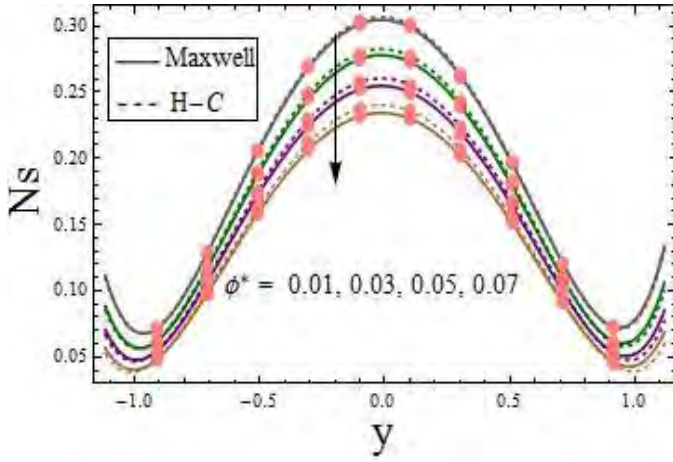


Fig. 3.14

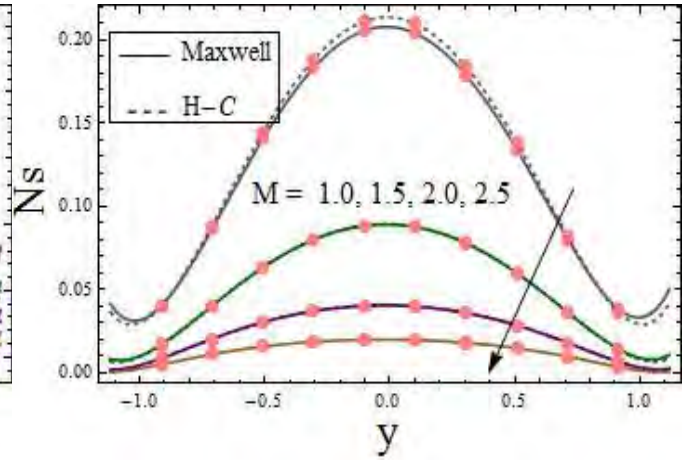


Fig. 3.15

Fig. 3.14.  $Ns$  via  $\phi^*$  when  $E_1 = 0.02$ ,  $E_2 = 0.01$ ,  $E_3 = 0.01$ ,  $t = 0.1$ ,  $x = 0.2$ ,  $\varepsilon = 0.2$ ,  $M = 1.0$ ,  $Br\Lambda^{-1} = 1.0$ ,  $Gr = 0.03$ ,  $Br = 3.0$ ,  $\xi_1 = 0.01$ ,  $\xi_4 = -0.01$ ,  $\xi_2 = 0.01$ ,  $\xi_5 = -0.01$ .

Fig. 3.15.  $Ns$  via  $M$  when  $E_1 = 0.02$ ,  $E_2 = 0.01$ ,  $E_3 = 0.01$ ,  $t = 0.1$ ,  $x = 0.2$ ,  $\varepsilon = 0.2$ ,  $\phi^* = 0.1$ ,  $Br\Lambda^{-1} = 1.0$ ,  $Gr = 0.03$ ,  $Br = 3.0$ ,  $\xi_1 = 0.01$ ,  $\xi_4 = -0.01$ ,  $\xi_2 = 0.01$ ,  $\xi_5 = -0.01$ .

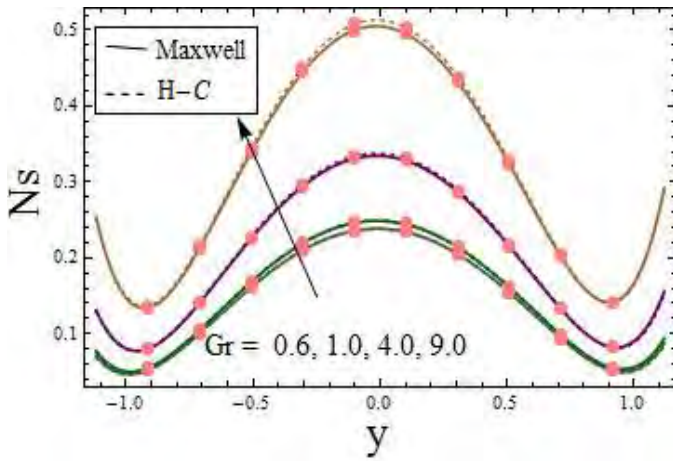


Fig. 3.16

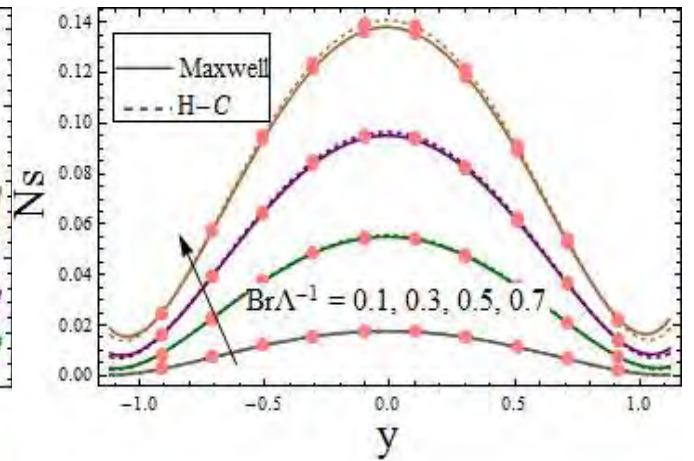


Fig. 3.17

Fig. 3.16.  $Ns$  via  $Gr$  when  $E_1 = 0.02$ ,  $E_2 = 0.01$ ,  $E_3 = 0.01$ ,  $t = 0.1$ ,  $x = 0.2$ ,  $\varepsilon = 0.2$ ,  $\phi^* = 0.1$ ,  $Br\Lambda^{-1} = 1.0$ ,  $M = 1.0$ ,  $Br = 3.0$ ,  $\xi_1 = 0.01$ ,  $\xi_4 = -0.01$ ,  $\xi_2 = 0.01$ ,  $\xi_5 = -0.01$ .

Fig. 3.17.  $Ns$  via  $Br\Lambda^{-1}$  when  $E_1 = 0.02$ ,  $E_2 = 0.01$ ,  $E_3 = 0.01$ ,  $t = 0.1$ ,  $x = 0.2$ ,  $\varepsilon = 0.2$ ,

$\phi^* = 0.1, M = 1.0, Gr = 0.03, Br = 3.0, \xi_1 = 0.01, \xi_4 = -0.01, \xi_2 = 0.01, \xi_5 = -0.01.$

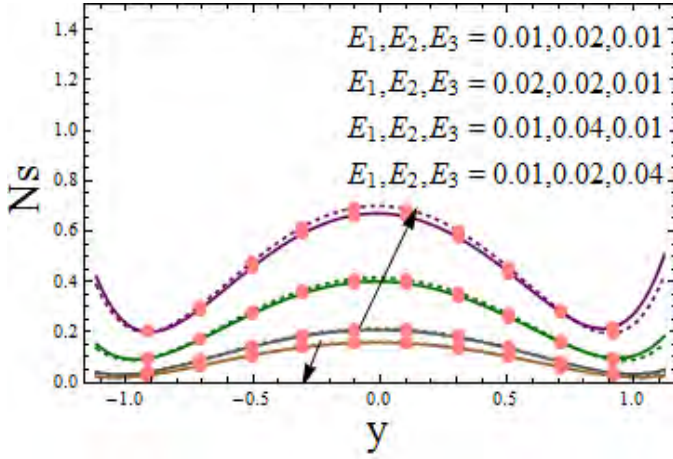


Fig. 3.18

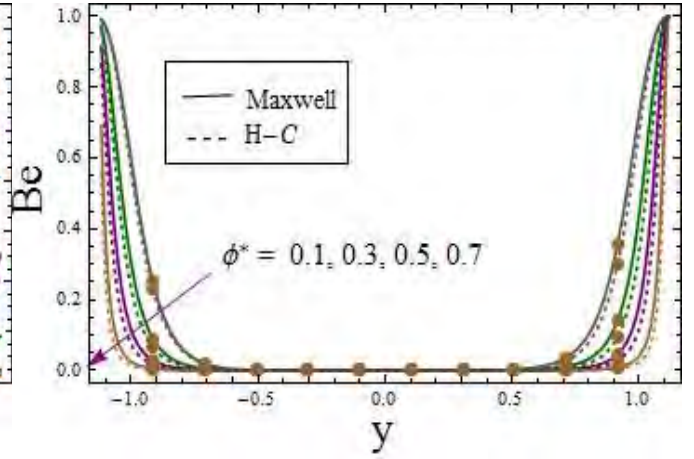


Fig. 3.19

Fig. 3.18.  $Ns$  via  $E_1, E_2, E_3$  when  $t = 0.1, x = 0.2, \varepsilon = 0.2, \phi^* = 0.1, Br\Lambda^{-1} = 1.0, M = 1.0, Gr = 0.03, Br = 3.0, \xi_1 = 0.01, \xi_4 = -0.01, \xi_2 = 0.01, \xi_5 = -0.01.$

Fig. 3.19.  $Be$  via  $\phi^*$  when  $E_1 = 0.02, E_2 = 0.01, E_3 = 0.01, t = 0.1, x = 0.2, \varepsilon = 0.2, M = 1.0, Br\Lambda^{-1} = 1.0, Gr = 0.03, Br = 3.0, \xi_1 = 0.01, \xi_4 = -0.01, \xi_2 = 0.01, \xi_5 = -0.01.$

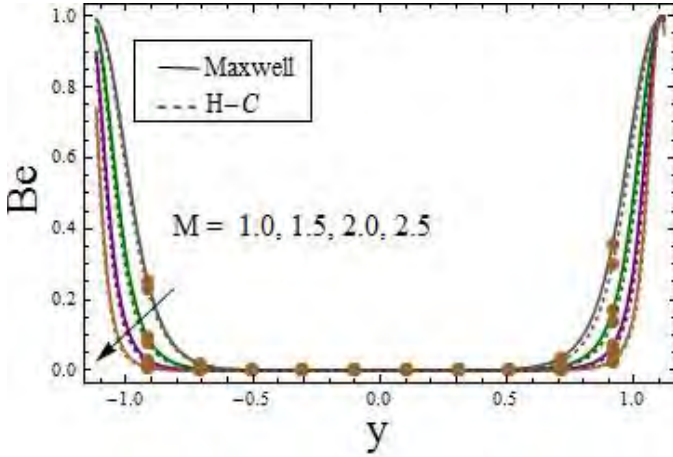


Fig. 3.20

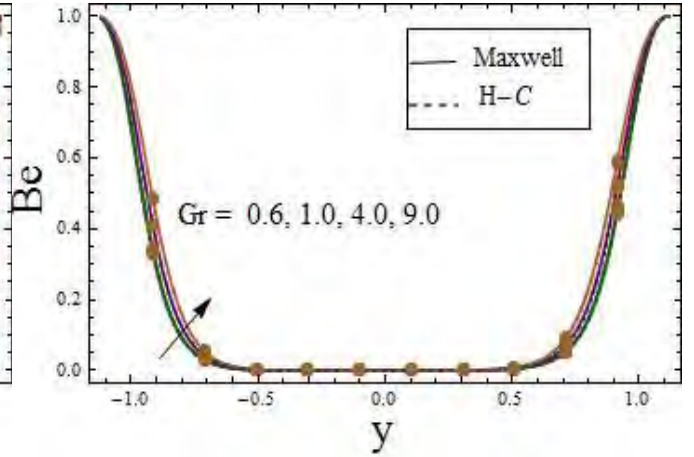


Fig. 3.21

Fig. 3.20.  $Be$  via  $M$  when  $E_1 = 0.02, E_2 = 0.01, E_3 = 0.01, t = 0.1, x = 0.2, \varepsilon = 0.2, \phi^* = 0.1, Br\Lambda^{-1} = 1.0, Gr = 0.03, Br = 3.0, \xi_1 = 0.01, \xi_4 = -0.01, \xi_2 = 0.01, \xi_5 = -0.01.$

Fig. 3.21.  $Be$  via  $Gr$  when  $E_1 = 0.02$ ,  $E_2 = 0.01$ ,  $E_3 = 0.01$ ,  $t = 0.1$ ,  $x = 0.2$ ,  $\varepsilon = 0.2$ ,  $\phi^* = 0.1$ ,  $Br\Lambda^{-1} = 1.0$ ,  $M = 1.0$ ,  $Br = 3.0$ ,  $\xi_1 = 0.01$ ,  $\xi_4 = -0.01$ ,  $\xi_2 = 0.01$ ,  $\xi_5 = -0.01$ .

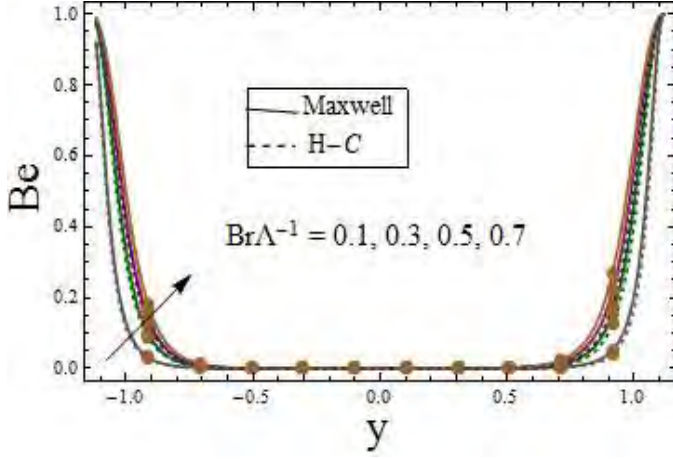


Fig. 3.22

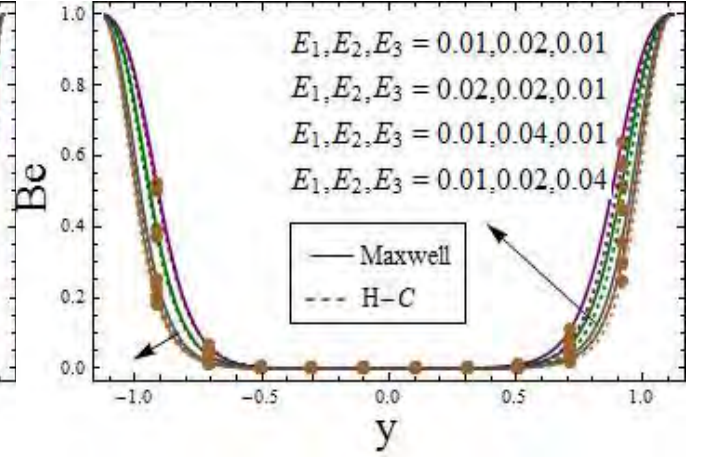


Fig. 3.23

Fig. 3.22.  $Be$  via  $Br\Lambda^{-1}$  when  $E_1 = 0.02$ ,  $E_2 = 0.01$ ,  $E_3 = 0.01$ ,  $t = 0.1$ ,  $x = 0.2$ ,  $\varepsilon = 0.2$ ,  $\phi^* = 0.1$ ,  $M = 1.0$ ,  $Gr = 0.03$ ,  $Br = 3.0$ ,  $\xi_1 = 0.01$ ,  $\xi_4 = -0.01$ ,  $\xi_2 = 0.01$ ,  $\xi_5 = -0.01$ .

Fig. 3.23.  $Be$  via  $E_1, E_2, E_3$  when  $t = 0.1$ ,  $x = 0.2$ ,  $\varepsilon = 0.2$ ,  $\phi^* = 0.1$ ,  $Br\Lambda^{-1} = 1.0$ ,  $Gr = 0.03$ ,  $Br = 3.0$ ,  $\xi_1 = 0.01$ ,  $\xi_4 = -0.01$ ,  $\xi_2 = 0.01$ ,  $\xi_5 = -0.01$ .

### 3.4.4 Streamlines

The streamlines are plotted for description of trapping. Fig. 3.24 (a) and (b) displayed the impact of Hartman number for Maxwell model whereas Fig. 3.24 (c) and (d) portrayed the influence for Hamilton Crosser model. For both cases the size of trapped bolus increases with higher values of Hartman number ( $M = 1.0, 2.0$ ). Figs. 3.25 and 3.26 (a) -(d) are sketched for behavior of first and second order slip parameters. These streamlines indicate that trapped bolus size enhances via increase in first order slip as (0.01, 0.03) and second order slip parameter as (-0.01, -0.03). Walls parameters impact for Maxwell model can be observed via Fig. 3.27 (a)-(d). However Figs. 3.27 (e)-(h) are for Hamilton-Crosser model. Both models show same behavior for these parameters i.e. trapped bolus size increases for  $E_1$  (= 0.7, 0.9) and  $E_2$  (= 0.4, 0.6) whereas decrease is noticed for  $E_3$  (= 0.2, 0.5).

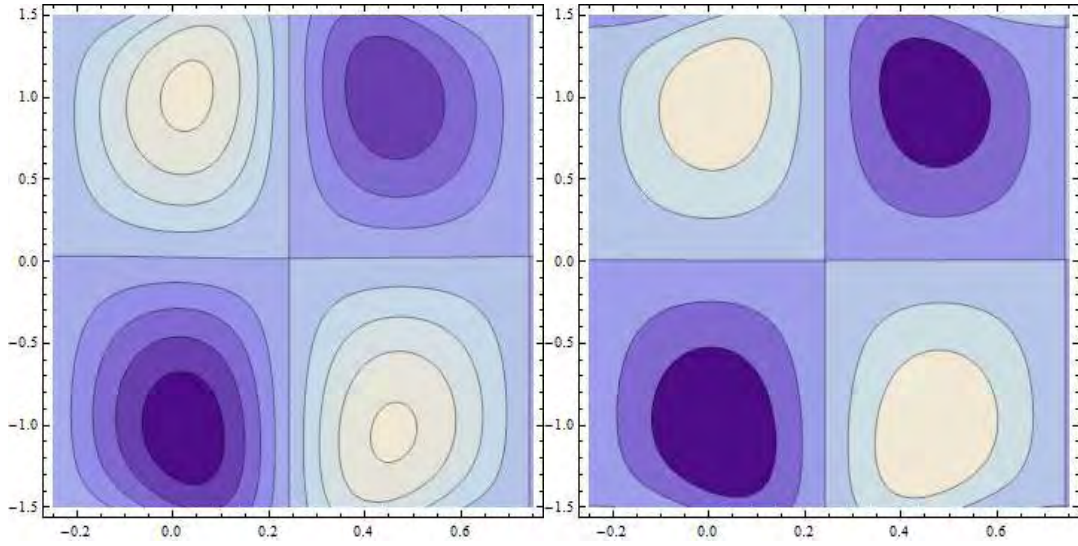
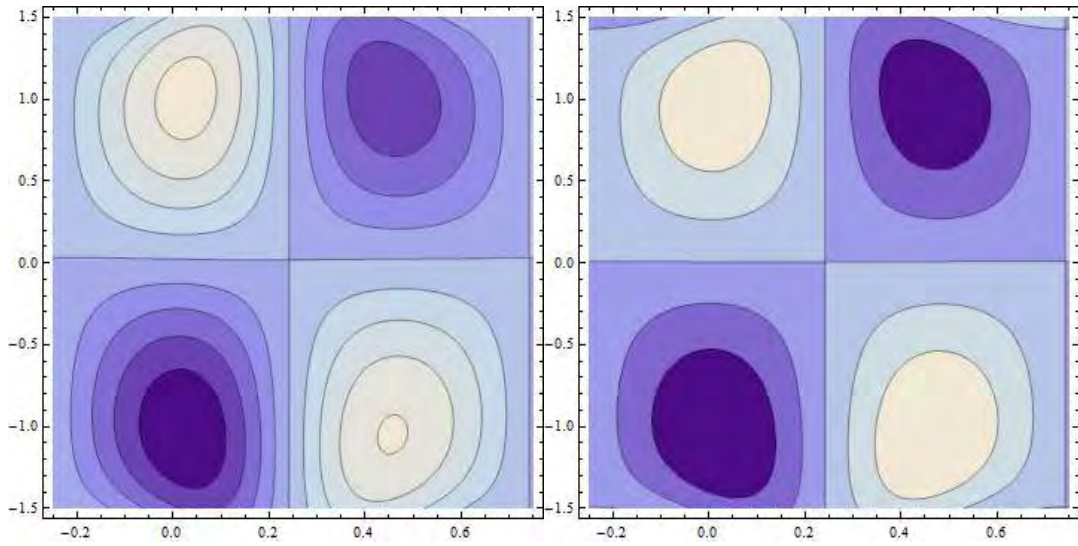


Fig. 3.24 (a)

(b)



(c)

(d)

Fig. 3.24.  $\psi$  via  $M$  for Maxwell model when  $E_1 = 0.02$ ,  $E_2 = 0.01$ ,  $E_3 = 0.01$ ,  $t = 0$ ,  $\varepsilon = 0.2$ ,  $\phi^* = 0.1$ ,  $Gr = 0.03$ ,  $Br = 3.0$ ,  $\xi_1 = 0.01$ ,  $\xi_4 = -0.01$ ,  $\xi_2 = 0.01$ ,  $\xi_5 = -0.01$ . (a)  $M = 1.0$ . (b)  $M = 2.0$ .

Fig. 3.24.  $\psi$  via  $M$  for Hamilton- Crosser model when  $E_1 = 0.02$ ,  $E_2 = 0.01$ ,  $E_3 = 0.01$ ,  $t = 0$ ,  $\varepsilon = 0.2$ ,  $\phi^* = 0.1$ ,  $Gr = 0.03$ ,  $Br = 3.0$ ,  $\xi_1 = 0.01$ ,  $\xi_4 = -0.01$ ,  $\xi_2 = 0.01$ ,  $\xi_5 = -0.01$ . (c)



$M = 1.0.$  (d)  $M = 2.0.$

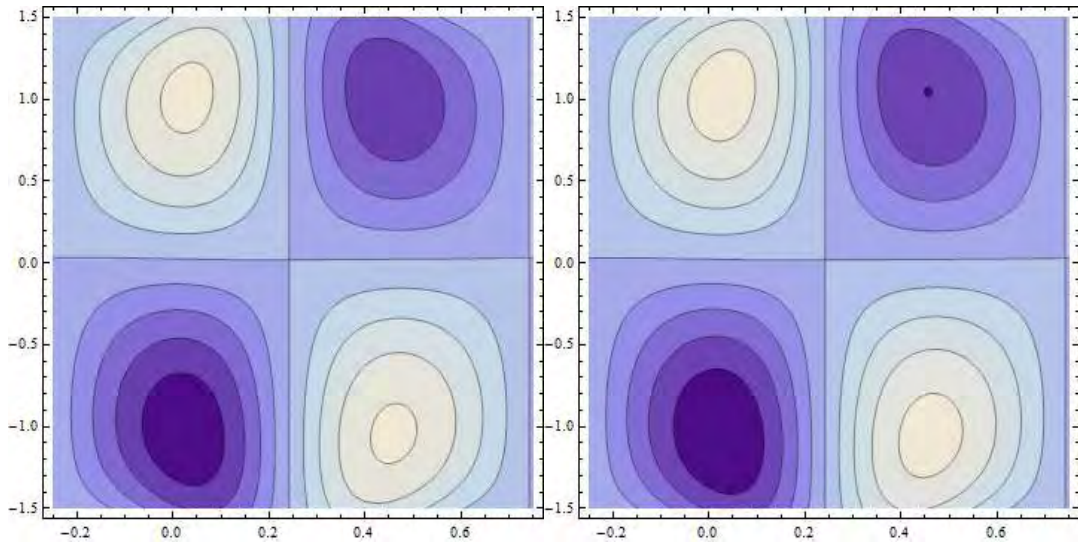
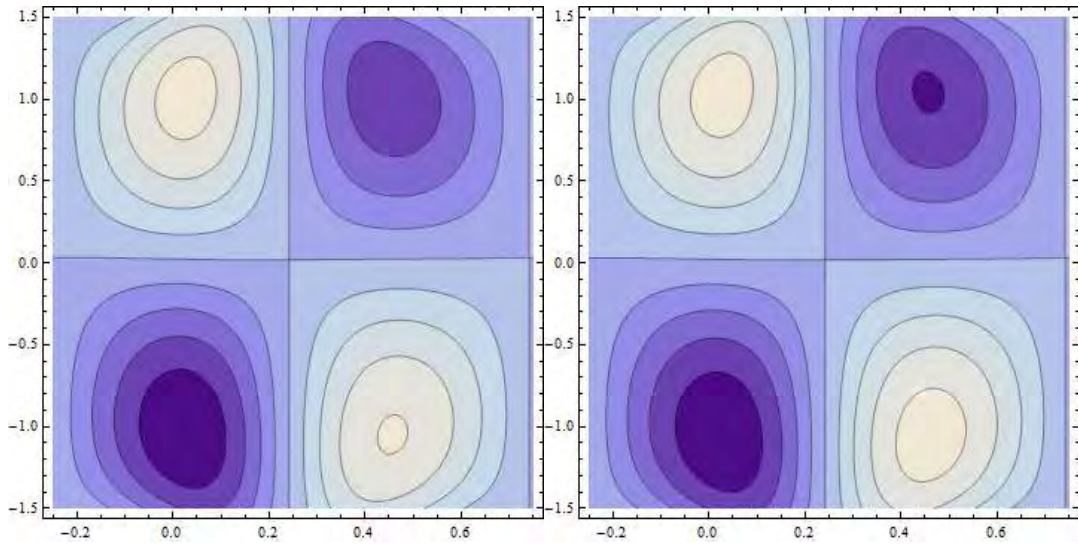


Fig. 3.25 (a)

(b)



(c)

(d)

Fig. 3.25.  $\psi$  via  $\xi_1$  for Maxwell model when  $E_1 = 0.02$ ,  $E_2 = 0.01$ ,  $E_3 = 0.01$ ,  $t = 0$ ,  $\varepsilon = 0.2$ ,  $\phi^* = 0.1$ ,  $M = 1.0$ ,  $Gr = 0.03$ ,  $Br = 3.0$ ,  $\xi_4 = -0.01$ ,  $\xi_2 = 0.01$ ,  $\xi_5 = -0.01$ . (a)  $\xi_1 = 0.01$ . (b)  $\xi_1 = 0.03$ .

Fig. 3.25.  $\psi$  via  $\xi_1$  for Hamilton- Crosser model when  $E_1 = 0.02$ ,  $E_2 = 0.01$ ,  $E_3 = 0.01$ ,  $t = 0$ ,  $\varepsilon = 0.2$ ,  $\phi^* = 0.1$ ,  $M = 1.0$ ,  $Gr = 0.03$ ,  $Br = 3.0$ ,  $\xi_4 = -0.01$ ,  $\xi_2 = 0.01$ ,  $\xi_5 = -0.01$ . (c)

$\xi_1 = 0.01$ . (d)  $\xi_1 = 0.03$ .

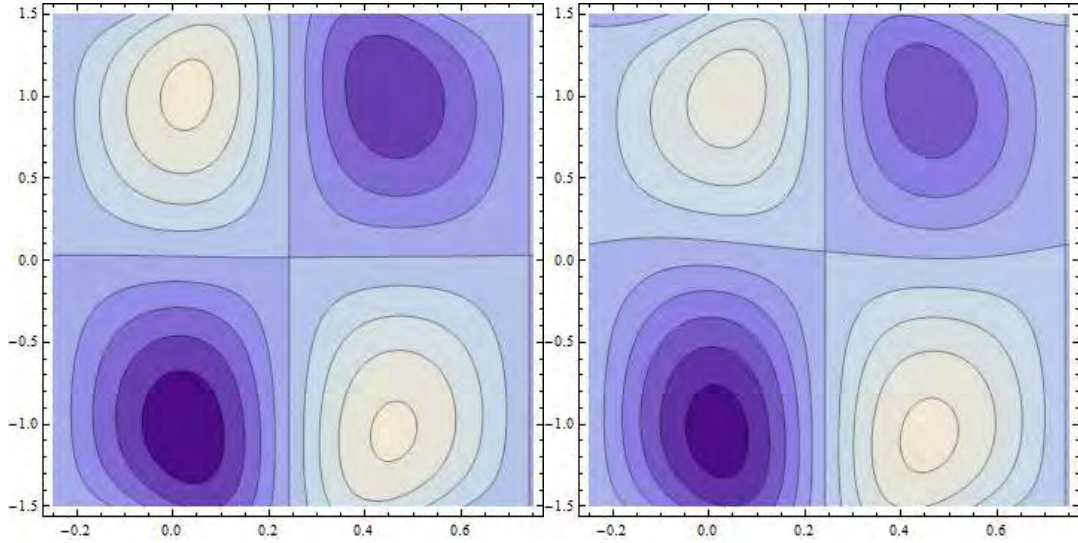
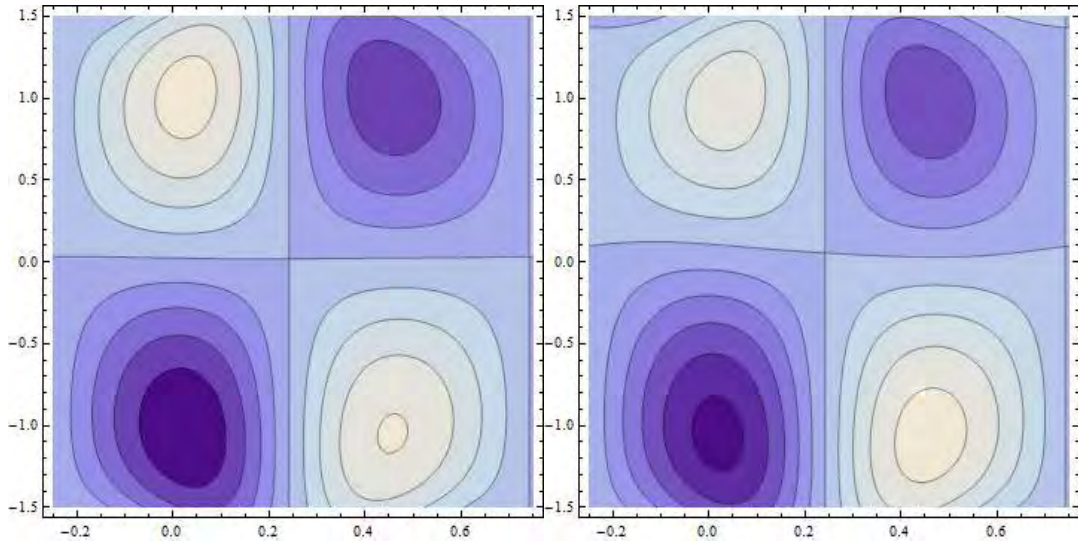


Fig. 3.26 (a)

(b)



(c)

(d)

Fig. 3.26.  $\psi$  via  $\xi_4$  for Maxwell model when  $E_1 = 0.02$ ,  $E_2 = 0.01$ ,  $E_3 = 0.01$ ,  $t = 0$ ,  $\varepsilon = 0.2$ ,  $\phi^* = 0.1$ ,  $M = 1.0$ ,  $Gr = 0.03$ ,  $Br = 3.0$ ,  $\xi_1 = 0.01$ ,  $\xi_2 = 0.01$ ,  $\xi_5 = -0.01$ . (a)  $\xi_4 = -0.01$ . (b)  $\xi_4 = -0.03$ .

Fig. 3.26.  $\psi$  via  $\xi_4$  for Hamilton- Crosser model when  $E_1 = 0.02$ ,  $E_2 = 0.01$ ,  $E_3 = 0.01$ ,  $t = 0$ ,

$\varepsilon = 0.2$ ,  $\phi^* = 0.1$ ,  $M = 1.0$ ,  $Gr = 0.03$ ,  $Br = 3.0$ ,  $\xi_1 = 0.01$ ,  $\xi_2 = 0.01$ ,  $\xi_5 = -0.01$ . (c)  
 $\xi_4 = -0.01$ . (d)  $\xi_4 = -0.03$ .

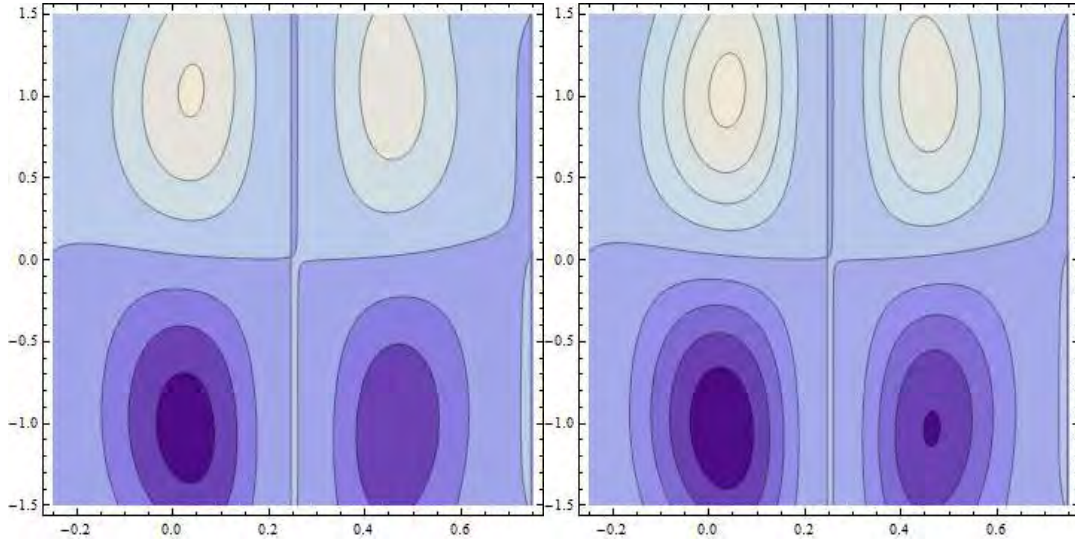
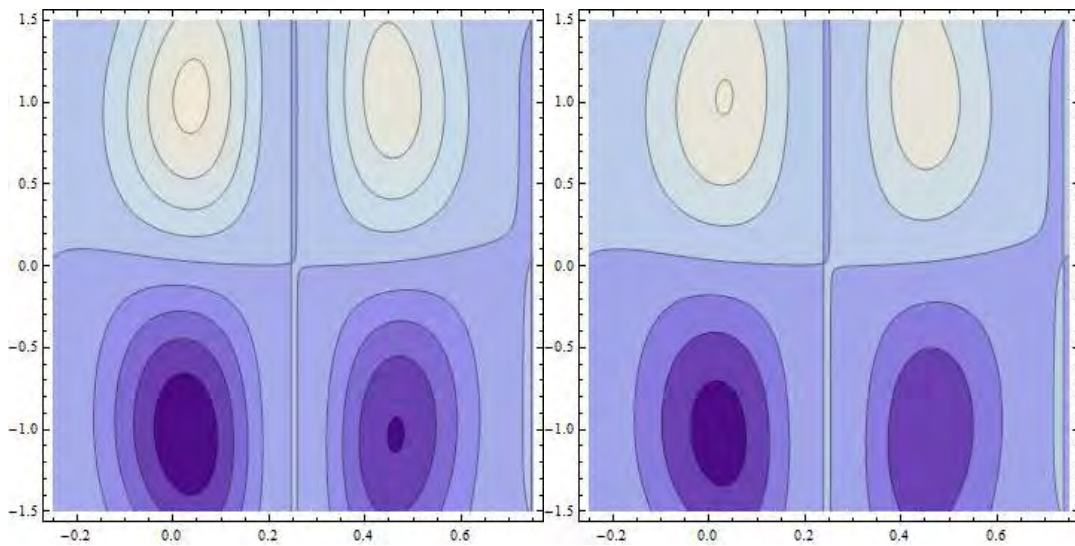


Fig. 3.27 (a)

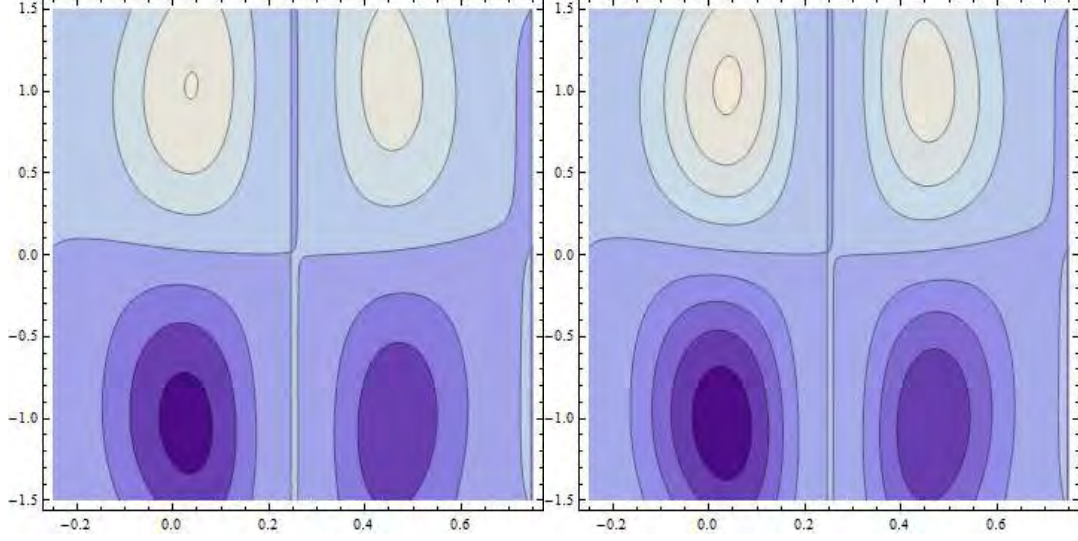
(b)



(c)

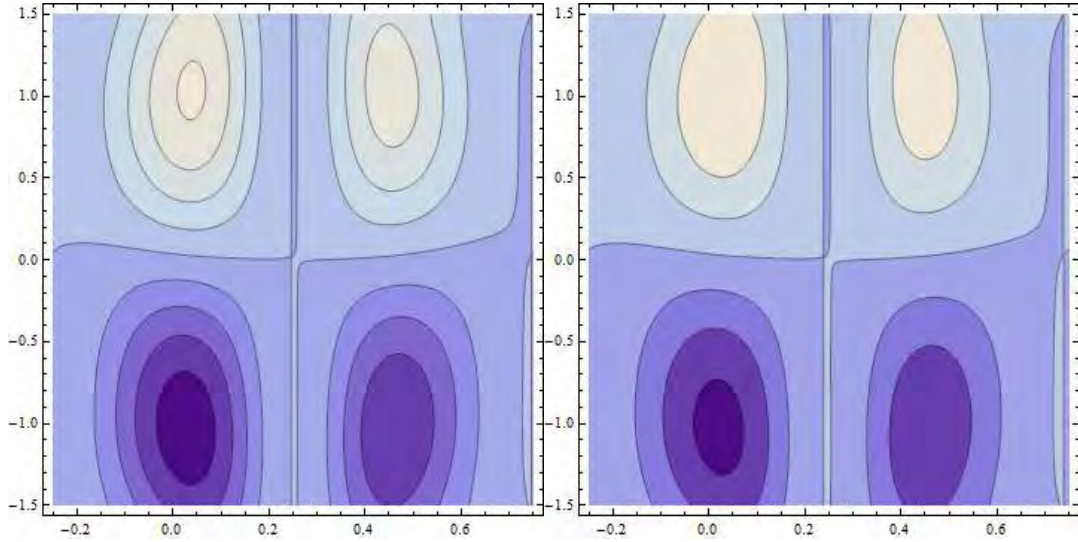
(d)





(e)

(f)



(g)

(h)

*Fig. 3.27.*  $\psi$  via  $E_1, E_2, E_3$  for Maxwell model when  $t = 0, \varepsilon = 0.2, \phi^* = 0.1, M = 1.0, Gr = 0.03, Br = 3.0, \xi_1 = 0.01, \xi_4 = -0.01, \xi_2 = 0.01, \xi_5 = -0.01$  (a)  $E_1 = 0.7, E_2 = 0.4, E_3 = 0.2$ . (b)  $E_1 = 0.9, E_2 = 0.4, E_3 = 0.2$ . (c)  $E_1 = 0.7, E_2 = 0.6, E_3 = 0.2$ . (d)  $E_1 = 0.7, E_2 = 0.4, E_3 = 0.5$ .

*Fig. 3.27.*  $\psi$  via  $E_1, E_2, E_3$  for Hamilton- Crosser model when  $t = 0, \varepsilon = 0.2, \phi^* = 0.1, M = 1.0, Gr = 0.03, Br = 3.0, \xi_1 = 0.01, \xi_4 = -0.01, \xi_2 = 0.01, \xi_5 = -0.01$  (e)  $E_1 = 0.7, E_2 = 0.4, E_3 = 0.2$ . (f)  $E_1 = 0.9, E_2 = 0.4, E_3 = 0.2$ . (g)  $E_1 = 0.7, E_2 = 0.6, E_3 = 0.2$ . (h)



$$E_1 = 0.7, E_2 = 0.4, E_3 = 0.5.$$

### 3.5 Conclusions

The key findings of this chapter are:

- Enhancement in velocity is seen for both first order and second order velocity slip in both models whereas reduction is observed for case of nanoparticle volume fraction.
- The values in Hamilton-Crosser model remain higher than Maxwell's model especially near the centre of channel for the case of velocity profile.
- Grashof and Hartman numbers for velocity have opposite effect.
- Results obtained indicate that temperature in Maxwell's model exceed than Hamilton-Crosser model.
- Enhancement is observed in entropy generation number for larger  $Br\Lambda^{-1}$  and Grashof number. Moreover inverse behavior of entropy generation number is obtained for the case of Hartman number and nanoparticle volume fraction.
- Bolus sizes increases in trapping phenomenon for the case of both first and second order velocity slip parameters.
- Bolus size reduces for  $E_3$  and it enhances for  $E_1$  and  $E_2$  in both models.

## Chapter 4

# Modeling and analysis of peristalsis of hybrid nanofluid with entropy generation

### 4.1 Introduction

This chapter intends to explore the peristaltic transport of rotating fluid in a channel. The channel is considered symmetric with flexible walls and porous medium. In this analysis hybrid nanofluids consisting of titanium oxides and copper particles. Water is used as the base fluid. MHD and Hall effects are employed in this problem. Formulation of energy equation is based on radiation and non uniform heat source or sink. Convective conditions are utilized. Thermodynamics second relation is employed for entropy generation. Maxwell-Garnetts model of thermal conductivity is employed. Numerical analysis is carried out using NDSolve of Mathematica. Graphs are plotted for the axial velocity, secondary velocity, temperature and entropy generation. Bar graphs are made for the analysis of heat transfer rate at the wall. Streamlines are displayed for trapping phenomenon. This study declares that enhancement in rotation parameter caused increase in secondary velocity. Moreover higher values of nanoparticle volume fraction caused decay in fluid velocity, temperature and entropy. This study further disclosed that heat transfer rate by higher volume fraction of nanoparticles enhances and more porous

structure lead to enhancement in fluid velocity, temperature and entropy.

## 4.2 Problem modeling

Here we consider the peristalsis of rotating fluid in a symmetric channel (see Fig. 4.1). The walls of channel have flexible characteristics. Porous medium is saturated by the fluid. MHD with Hall effects and Joule heating is accounted. Non-uniform heat source and sink parameter is present. The channel and fluid are in rigid body rotation. The hybrid nanofluid comprising of  $TiO_2$  and  $Cu$  nanoparticles with water as base liquid is utilized. The selection of the coordinates are considered in such a way that x-axis is taken along the flow direction whereas z-axis normal to it. The walls of channel are taken at temperature  $T_1$  and  $T_0$  respectively. Thermal radiation is also present. Rotation is about z-axis with the angular frequency  $\Omega$ . Peristaltic wave of involuntary contraction and expansion is responsible for the fluid flow. Wave shape is defined as follows:

$$z = \pm \eta(x, t) = \pm \left[ d + a \sin \frac{2\pi}{\lambda} (x - ct) \right], \quad (4.1)$$

where  $d$  represents the width of channel,  $a$  the wave amplitude,  $\lambda$  the wavelength and  $c$  wave speed.

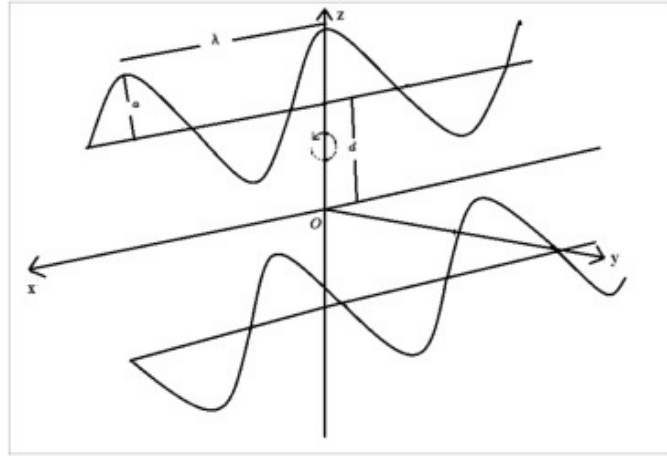


Fig. 4.1: Schematic Diagram

Related equations satisfy

$$\frac{\partial u}{\partial x} + \frac{\partial w}{\partial z} = 0. \quad (4.2)$$

$$\rho_{hnf} \left[ \frac{du}{dt} - 2\Omega v \right] = -\frac{\partial p}{\partial x} + \mu_{hnf} \left[ \frac{\partial^2 u}{\partial x^2} + \frac{\partial^2 u}{\partial z^2} \right] - \frac{\mu_{hnf} u}{k_1} + \frac{\sigma_{hnf} B_0^2}{1 + (K_4 m)^2} (-u + K_4 m v), \quad (4.3)$$

$$\rho_{hnf} \left[ \frac{dv}{dt} + 2\Omega u \right] = -\frac{\partial p}{\partial y} + \mu_{hnf} \left[ \frac{\partial^2 v}{\partial x^2} + \frac{\partial^2 v}{\partial z^2} \right] - \frac{\mu_{hnf} v}{k_1} - \frac{\sigma_{hnf} B_0^2}{1 + (K_4 m)^2} (v + K_4 m u), \quad (4.4)$$

$$\rho_{hnf} \left[ \frac{dw}{dt} \right] = -\frac{\partial p}{\partial z} + \mu_{hnf} \left[ \frac{\partial^2 w}{\partial x^2} + \frac{\partial^2 w}{\partial z^2} \right] - \frac{\mu_{hnf} w}{k_1}, \quad (4.5)$$

$$\begin{aligned} (\rho C_p)_{hnf} \left[ \frac{dT}{dt} \right] &= \kappa_{hnf} \left[ \frac{\partial^2 T}{\partial x^2} + \frac{\partial^2 T}{\partial z^2} \right] + \mu_{hnf} \left[ 2 \left( \left( \frac{\partial u}{\partial x} \right)^2 + \left( \frac{\partial w}{\partial z} \right)^2 \right) \right. \\ &\quad \left. + \left( \frac{\partial u}{\partial z} + \frac{\partial w}{\partial x} \right)^2 \right] + Q_0 (T - T_0) + \frac{\mu_{hnf} (u^2 + v^2 + w^2)}{k_1} \\ &\quad - \frac{\partial q_r}{\partial z} + \frac{\sigma_{hnf} B_0^2}{1 + (K_4 m)^2} (u^2 + v^2). \end{aligned} \quad (4.6)$$

The modified pressure is given by

$$p = \hat{p} - \frac{1}{2} \rho \Omega^2 (x^2 + y^2). \quad (4.7)$$

The velocity components in  $x$ ,  $y$  and  $z$  directions are given by  $[u(x, z, t), v(x, z, t), w(x, z, t)]$ .  $T$  denotes the temperature whereas  $q_r$  ( $= \frac{-4\sigma^*}{3k^*} \frac{\partial T^4}{\partial z}$ ) represents the radiative heat flux. The  $\rho_{hnf}$  for the density,  $\mu_{hnf}$  viscosity,  $(\rho C_p)_{hnf}$  the heat capacity and  $\kappa_{hnf}$  the thermal conductivity of hybrid nanofluid. These definitions are

$$\begin{aligned} \rho_{hnf} &= (1 - (\phi_{Cu} + \phi_{TiO_2})) \rho_f + \phi_{Cu} \rho_{Cu} + \phi_{TiO_2} \rho_{TiO_2}, \\ (\rho C_p)_{hnf} &= (1 - (\phi_{Cu} + \phi_{TiO_2})) (\rho C_p)_f + \phi_{Cu} (\rho C_p)_{Cu} + \phi_{TiO_2} (\rho C_p)_{TiO_2}, \\ \mu_{hnf} &= \frac{\mu_f}{(1 - (\phi_{Cu} + \phi_{TiO_2}))^{2.5}}, \\ \frac{\kappa_{hnf}}{\kappa_f} &= \frac{\frac{(\phi_{Cu} \kappa_{Cu} + \phi_{TiO_2} \kappa_{TiO_2})}{(\phi_{Cu} + \phi_{TiO_2})} + 2\kappa_f - 2(\phi_{Cu} + \phi_{TiO_2}) \kappa_f + 2(\phi_{Cu} \kappa_{Cu} + \phi_{TiO_2} \kappa_{TiO_2})}{\frac{(\phi_{Cu} \kappa_{Cu} + \phi_{TiO_2} \kappa_{TiO_2})}{(\phi_{Cu} + \phi_{TiO_2})} + 2\kappa_f + (\phi_{Cu} + \phi_{TiO_2}) \kappa_f - (\phi_{Cu} \kappa_{Cu} + \phi_{TiO_2} \kappa_{TiO_2})}, \\ \frac{\sigma_{hnf}}{\sigma_f} &= 1 + \frac{3 \left( \frac{\phi_{Cu} \sigma_{Cu} + \phi_{TiO_2} \sigma_{TiO_2}}{\sigma_f} - \phi_{Cu} - \phi_{TiO_2} \right)}{\left( \frac{\sigma_{Cu} + \sigma_{TiO_2}}{\sigma_f} + 2 \right) - \left( \frac{\phi_{Cu} \sigma_{Cu} + \phi_{TiO_2} \sigma_{TiO_2}}{\sigma_f} - \phi_{Cu} - \phi_{TiO_2} \right)}. \end{aligned} \quad (4.8)$$

Numerical values of hybrid nanofluid are given in Table 1.

Table 1: Thermophysical parameters of water and nanoparticles [190].

	$\rho$ (kg m <sup>-3</sup> )	$C_p$ (j kg <sup>-1</sup> K <sup>-1</sup> )	$\kappa$ (W m <sup>-1</sup> K <sup>-1</sup> )	$\sigma$ ( $\Omega.m$ ) <sup>-1</sup>
$H_2O$	997.1	4179	0.613	0.05
$Cu$	8933	765	401	$5.96 \times 10^7$
$TiO_2$	4250	686.2	8.9538	$1 \times 10^{-12}$

The boundary conditions for the considered flow are

$$u = 0 \quad \text{at } z = \pm\eta, \quad (4.9)$$

$$v = 0 \quad \text{at } z = \pm\eta, \quad (4.10)$$

$$\begin{aligned} \left[ -\tau^* \frac{\partial^3}{\partial x^3} + m^* \frac{\partial^3}{\partial x \partial t^2} + d_1^* \frac{\partial^2}{\partial t \partial x} \right] \eta &= \mu_{hnf} \left[ \frac{\partial^2 u}{\partial x^2} + \frac{\partial^2 u}{\partial z^2} \right] - \frac{\mu_{hnf} u}{k_1} + \frac{\sigma_{hnf} B_0^2}{1 + (K_4 m)^2} (-u + K_4 m v) \\ &\quad - \rho_{hnf} \left[ \frac{du}{dt} - 2\Omega v \right] \\ &\quad \text{at } z = \pm\eta, \end{aligned} \quad (4.11)$$

$$\kappa_{hnf} \frac{\partial T}{\partial z} = \begin{cases} -B_1(T - T_1) \\ -B_2(T_0 - T) \end{cases} \quad \text{at } z = \pm\eta. \quad (4.12)$$

in which  $B_i$  ( $i=1, 2$ ) are heat transfer coefficients,  $\tau^*$ ,  $m^*$  and  $d_1^*$  are the compliant walls coefficients.

The quantities in dimensionless form are given by

$$\begin{aligned} x^* &= \frac{x}{\lambda}, & y^* &= \frac{y}{\lambda}, & z^* &= \frac{z}{d}, & u^* &= \frac{u}{c}, & v^* &= \frac{v}{c}, & \delta &= \frac{d}{\lambda}, \\ w^* &= \frac{w}{c}, & t^* &= \frac{ct}{\lambda}, & \eta^* &= \frac{\eta}{d}, & k_1^* &= \frac{k_1}{d^2}, & p^* &= \frac{d^2 p}{c \lambda \mu_f}, \\ \theta &= \frac{T - T_0}{T_1 - T_0}, & u &= \frac{\partial \psi}{\partial z}, & w &= -\delta \frac{\partial \psi}{\partial x}. \end{aligned} \quad (4.13)$$

After using the non-dimensional parameters and utilizing stream function and lubrication approach we arrive at

$$\frac{\partial p}{\partial x} = 2T' K_3 v + K_2 \frac{\partial^3 \psi}{\partial z^3} - \frac{K_2}{k_1} \frac{\partial \psi}{\partial z} + \frac{K_4 M^2}{1 + (K_4 m)^2} \left( -\frac{\partial \psi}{\partial z} + K_4 m v \right), \quad (4.14)$$

$$\frac{\partial p}{\partial y} = -2T' K_3 \frac{\partial \psi}{\partial z} + K_2 \frac{\partial^2 v}{\partial z^2} - \frac{K_2}{k_1} v - \frac{K_4 M^2}{1 + (K_4 m)^2} (v + K_4 m u) \quad (4.15)$$

$$\frac{\partial p}{\partial z} = 0, \quad (4.16)$$

$$\begin{aligned} 0 = & K_1 \frac{\partial^2 \theta}{\partial z^2} + Br K_2 \left( \frac{\partial^2 \psi}{\partial z^2} \right)^2 + Rd \frac{\partial^2 \theta}{\partial z^2} + \\ & \frac{Br K_2}{k_1} \left( \left( \frac{\partial \psi}{\partial z} \right)^2 + v^2 \right) + \frac{Br K_4 M^2}{1 + (K_4 m)^2} \left( \left( \frac{\partial \psi}{\partial z} \right)^2 + v^2 \right) + S \theta, \end{aligned} \quad (4.17)$$

where

$$\begin{aligned} K_1 &= \frac{\frac{(\phi_{Cu} \kappa_{Cu} + \phi_{TiO_2} \kappa_{TiO_2})}{(\phi_{Cu} + \phi_{TiO_2})} + 2\kappa_f - 2(\phi_{Cu} + \phi_{TiO_2})\kappa_f + 2(\phi_{Cu} \kappa_{Cu} + \phi_{TiO_2} \kappa_{TiO_2})}{\frac{(\phi_{Cu} \kappa_{Cu} + \phi_{TiO_2} \kappa_{TiO_2})}{(\phi_{Cu} + \phi_{TiO_2})} + 2\kappa_f + (\phi_{Cu} + \phi_{TiO_2})\kappa_f - (\phi_{Cu} \kappa_{Cu} + \phi_{TiO_2} \kappa_{TiO_2})}, \\ K_2 &= \frac{1}{(1 - (\phi_{Cu} + \phi_{TiO_2}))^{2.5}}, \\ K_3 &= (1 - (\phi_{Cu} + \phi_{TiO_2})) + \frac{\phi_{Cu} \rho_{Cu} + \phi_{TiO_2} \rho_{TiO_2}}{\rho_f}, \\ K_4 &= 1 + \frac{3 \left( \frac{\phi_{Cu} \sigma_{Cu} + \phi_{TiO_2} \sigma_{TiO_2}}{\sigma_f} - \phi_{Cu} - \phi_{TiO_2} \right)}{\left( \frac{\sigma_{Cu} + \sigma_{TiO_2}}{\sigma_f} + 2 \right) - \left( \frac{\phi_{Cu} \sigma_{Cu} + \phi_{TiO_2} \sigma_{TiO_2}}{\sigma_f} - \phi_{Cu} - \phi_{TiO_2} \right)}, \end{aligned} \quad (4.18)$$

where the non-dimensional parameters are

$$\begin{aligned} T' &= \frac{Re \Omega d}{c}, \quad Rd = \frac{16\sigma^* T_0^3}{3k^* \kappa_f}, \quad M = \sqrt{\frac{\sigma_f}{\mu_f}} B_0 d, \quad m = \frac{\sigma_f B_0}{en_e}, \\ Pr &= \frac{(\mu C_p)_f}{\kappa_f}, \quad Ec = \frac{c^2}{(C_p)_f (T_1 - T_0)}, \quad Br = Pr Ec, \quad S = \frac{Q_0 d^2}{\kappa_f}. \end{aligned} \quad (4.19)$$

Here  $T'$  denotes the Taylor number,  $Rd$  the radiation parameter,  $M$  the Hartman number,  $m$  the Hall parameter,  $Pr$  the Prandtl number,  $Ec$  the Eckert number,  $Br$  the Brinkman number and  $S$  the heat source or sink parameter. Note that asterisks have been omitted for brevity.

The conditions now become

$$\begin{aligned}
\frac{\partial \psi}{\partial z} &= 0, & v &= 0, & \text{at } z &= \pm \eta, \\
\frac{\partial \theta}{\partial z} + \frac{Bi_1}{K_1}(\theta - 1) &= 0, & & & \text{at } z &= \eta, \\
\frac{\partial \theta}{\partial z} - \frac{Bi_2}{K_1}(\theta) &= 0, & & & \text{at } z &= -\eta,
\end{aligned} \tag{4.20}$$

$$\begin{aligned}
\left[ E_1 \frac{\partial^3}{\partial x^3} + E_2 \frac{\partial^3}{\partial x \partial t^2} + E_3 \frac{\partial^2}{\partial t \partial x} \right] \eta &= 2T' K_3 v + K_2 \frac{\partial^3 \psi}{\partial z^3} - \frac{K_2}{k_1} \frac{\partial \psi}{\partial z} \\
&+ \frac{K_4 M^2}{1 + (K_4 m)^2} \left( -\frac{\partial \psi}{\partial z} + K_4 m v \right), \\
&\text{at } z = \pm \eta.
\end{aligned} \tag{4.21}$$

in which  $Bi_1 (= B_1 d / \kappa_f)$  and  $Bi_2 (= B_2 d / \kappa_f)$  are the Biot numbers whereas the wall parameters  $E_1 (= -\tau^* d^3 / \lambda^3 c \mu_f)$ ,  $E_2 (= m^* c d^3 / \lambda^3 \mu_f)$  and  $E_3 (= d_1^* d^3 / \lambda^2 \mu_f)$  are respective elastance and damping coefficients.

#### 4.2.1 Entropy generation

Entropy generation is given by

$$\begin{aligned}
S_{gen}''' &= \frac{\kappa_{hnf}}{T_m^2} \left( \left( \frac{\partial T}{\partial x} \right)^2 + \left( \frac{\partial T}{\partial z} \right)^2 \right) + \frac{1}{T_m^2} \frac{16\sigma^* T_0^3}{3k^*} \left( \frac{\partial T}{\partial z} \right)^2 + \frac{\mu_{hnf}(u^2 + v^2 + w^2)}{T_m k_1} + \frac{\Phi}{T_m} \\
&+ \frac{1}{T_m} \left( \frac{\sigma_{hnf} B_0^2}{1 + (K_4 m)^2} (u^2 + v^2) \right) + \frac{1}{T_m} (Q_0(T - T_0)).
\end{aligned} \tag{4.22}$$

Expression for viscous dissipation is

$$\Phi = \mu_{hnf} \left[ 2 \left( \left( \frac{\partial u}{\partial x} \right)^2 + \left( \frac{\partial w}{\partial z} \right)^2 \right) + \left( \frac{\partial u}{\partial z} + \frac{\partial w}{\partial x} \right)^2 \right]. \tag{4.23}$$

In dimensionless form

$$\begin{aligned}
N_s &= \frac{S_{gen}'''}{S_G'''} = (K_1 + Rd) \left( \frac{\partial \theta}{\partial z} \right)^2 + \frac{BrK_2}{\Lambda} \left( \frac{\partial^2 \psi}{\partial z^2} \right)^2 + \frac{BrK_2}{\Lambda k_1} \left( \left( \frac{\partial \psi}{\partial z} \right)^2 + v^2 \right) \\
&+ \frac{K_4 M^2}{1 + (K_4 m)^2} \frac{Br}{\Lambda} \left( \left( \frac{\partial \psi}{\partial z} \right)^2 + v^2 \right) + \frac{S\theta}{\Lambda},
\end{aligned} \tag{4.24}$$

$$S_G''' = \frac{\kappa_f (T_1 - T_0)^2}{T_m^2 d^2}, \quad \Lambda = \frac{T_1 - T_0}{T_m}. \tag{4.25}$$

### 4.3 Analysis

Here we have adopted the NDSolve techniques of Mathematica 9.0 for the solutions. The computation has been carried out by varying the value in the following range: nanoparticle volume fraction (0.01-0.08), Taylor number (0.1-4.0), Hartman number (0.5-3.5), porosity parameter (1.0-4.0), Hall parameter (0.1-4.0), radiation parameter (0.1-3.5), Brinkman number (1.0-4.0) source parameter (0.1-1.0), Biot numbers (4.0-10.0) and wall parameters (0.01-0.3).

#### 4.3.1 Velocity

This subsection has been arranged for velocity. The subsections are arranged here to avoid complexity.

##### Axial velocity

This subsection contains information about the results of axial velocity via nanoparticle volume fraction, Taylor number, Hartman number, porosity parameter, Hall parameter and wall parameters. Increasing values of nanoparticle volume fraction enhance the resistance to flow. It is due to the fact that shear rate increases by enhancing the nanoparticle volume fraction. This may lead to decrease in axial velocity. Similar behavior is captured here for hybrid nanofluid through Fig. 4.2. Fig. 4.3 is made for the influence of Taylor number on axial velocity. As rotation caused the fluid motion in the secondary direction. It leads to decay the velocity in the axial direction. Hartman number effect can be seen via Fig. 4.4. Higher value of it caused decrease in the axial velocity as fluid offers more resistance because of Lorentz force. Fig. 4.5



portrayed the effect of porosity parameter on axial velocity. As more pores assist the velocity of fluid. So enhancement is observed. Fig. 4.6 presented the Hall parameter influence on velocity. It leads to enhancement in velocity profile. Moreover as elastance parameters provide less obstacles to fluid flow so axial velocity enhances for  $E_1$  and  $E_2$  whereas damping resists the motion of fluid so velocity decays against  $E_3$  (see Fig. 4.7)

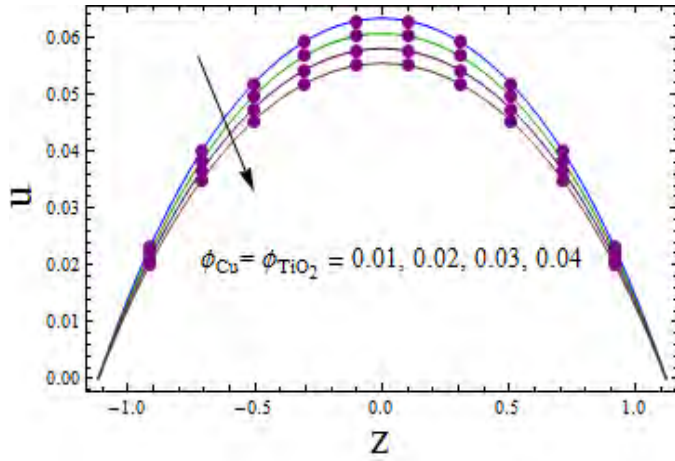


Fig. 4.2

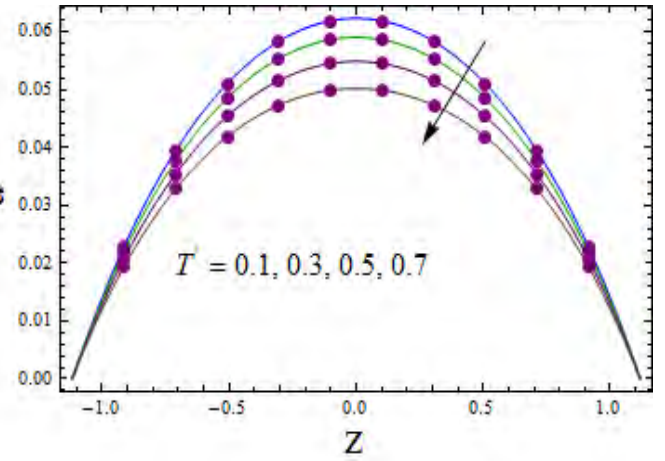


Fig. 4.3

Fig. 4.2. Axial velocity distribution for  $\phi_{Cu}$  and  $\phi_{TiO_2}$  when  $E_1 = 0.03$ ,  $E_2 = 0.03$ ,  $E_3 = 0.01$ ,  $T' = 0.1$ ,  $t = 0.1$ ,  $x = 0.2$ ,  $\varepsilon = 0.2$ ,  $M = 1.0$ ,  $m = 1.0$ ,  $S = 1.0$ ,  $Bi_1 = 4$ ,  $Bi_2 = 6$ ,  $Br = 3.0$ ,  $k_1 = 1$ ,  $Rd = 1$ .

Fig. 4.3. Axial velocity distribution for  $T'$  when  $E_1 = 0.03$ ,  $E_2 = 0.03$ ,  $E_3 = 0.01$ ,  $t = 0.1$ ,  $x = 0.2$ ,  $\varepsilon = 0.2$ ,  $\phi_{Cu} = \phi_{TiO_2} = 0.01$ ,  $M = 1.0$ ,  $m = 1.0$ ,  $S = 1.0$ ,  $Bi_1 = 4$ ,  $Bi_2 = 6$ ,  $Br = 3.0$ ,  $k_1 = 1$ ,  $Rd = 1$ .

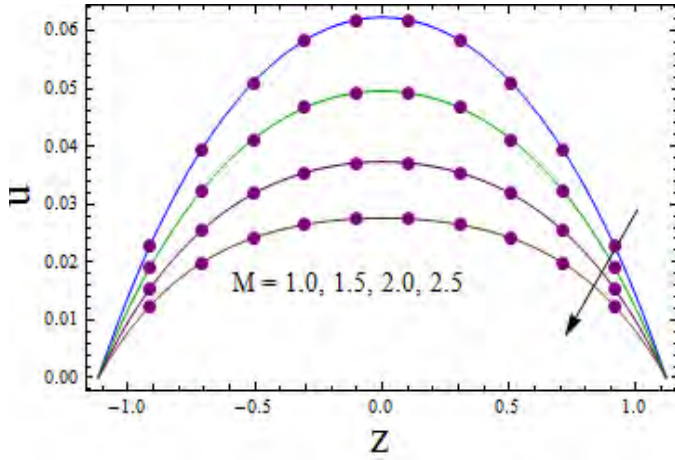


Fig. 4.4

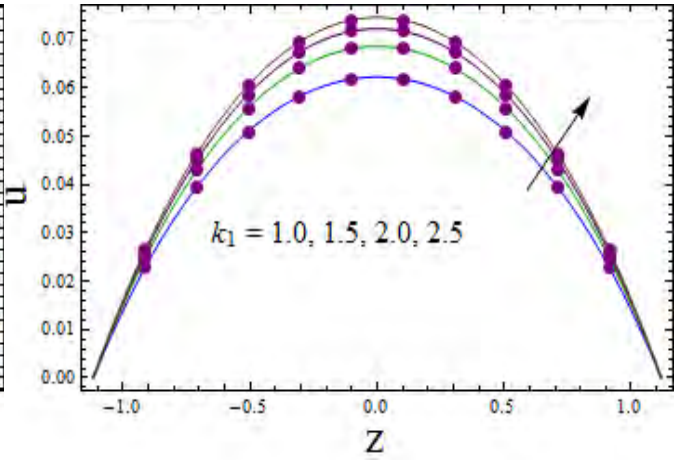


Fig. 4.5

Fig. 4.4. Axial velocity distribution for  $M$  when  $E_1 = 0.03$ ,  $E_2 = 0.03$ ,  $E_3 = 0.01$ ,  $T' = 0.1$ ,  $t = 0.1$ ,  $x = 0.2$ ,  $\varepsilon = 0.2$ ,  $\phi_{Cu} = \phi_{TiO_2} = 0.01$ ,  $m = 1.0$ ,  $S = 1.0$ ,  $Bi_1 = 4$ ,  $Bi_2 = 6$ ,  $Br = 3.0$ ,  $k_1 = 1$ ,  $Rd = 1$ .

Fig. 4.5. Axial velocity distribution for  $k_1$  when  $E_1 = 0.03$ ,  $E_2 = 0.03$ ,  $E_3 = 0.01$ ,  $T' = 0.1$ ,  $t = 0.1$ ,  $x = 0.2$ ,  $\varepsilon = 0.2$ ,  $\phi_{Cu} = \phi_{TiO_2} = 0.01$ ,  $M = 1.0$ ,  $m = 1.0$ ,  $S = 1.0$ ,  $Bi_1 = 4$ ,  $Bi_2 = 6$ ,  $Br = 3.0$ ,  $Rd = 1$ .

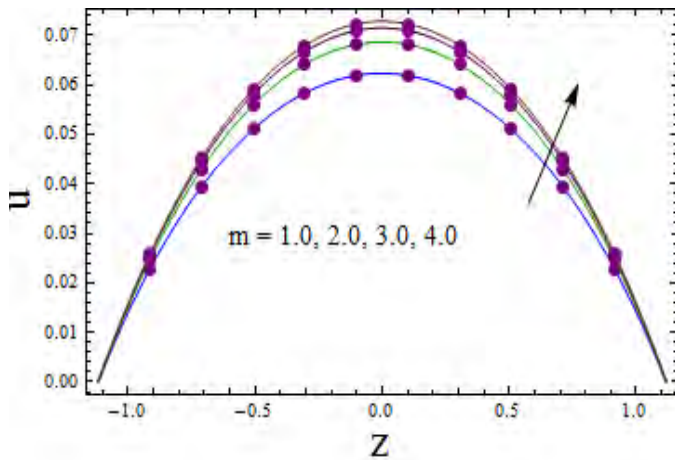


Fig. 4.6

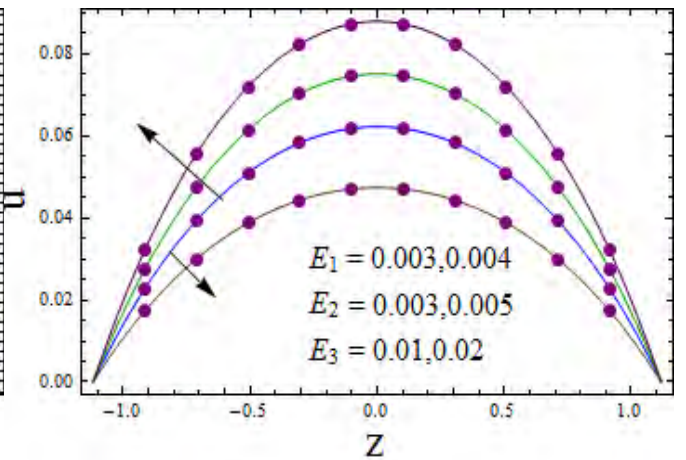


Fig. 4.7

Fig. 4.6. Axial velocity distribution for  $m$  when  $E_1 = 0.03$ ,  $E_2 = 0.03$ ,  $E_3 = 0.01$ ,  $T' = 0.1$ ,

$$t = 0.1, x = 0.2, \varepsilon = 0.2, \phi_{Cu} = \phi_{TiO_2} = 0.01, M = 1.0, S = 1.0, Bi_1 = 4, Bi_2 = 6, Br = 3.0, \\ k_1 = 1, Rd = 1.$$

Fig. 4.7. Axial velocity distribution for  $E_1$ ,  $E_2$  and  $E_3$  when  $T' = 0.1, t = 0.1, x = 0.2, \varepsilon = 0.2, \phi_{Cu} = \phi_{TiO_2} = 0.01, M = 1.0, m = 1.0, S = 1.0, Bi_1 = 4, Bi_2 = 6, Br = 3.0, k_1 = 3, Rd = 1.$

### Secondary velocity

This subsection includes the graphical interpretation of secondary velocity that has been induced by the rotation  $\Omega$ . Graphs are plotted for nanoparticle volume fraction, Taylor number, Hartman number, porosity parameter, Hall parameter and wall parameters on secondary velocity. Fig. 4.8 depicts influence of nanoparticle volume fraction on  $v$ . Qualitatively similar impact for secondary velocity is viewed as for axial velocity. Resistance produced by adding nanoparticles slows down the secondary velocity as well. As rotation is responsible to induce this secondary velocity therefore an increase in rotation enhances  $v$  (see Fig. 4.9). Hartman number effect for  $v$  is similar to  $u$  (see Fig. 4.10). Here fluid also slows down in view of Lorentz force. Fig. 4.11 displayed the results for  $k_1$  which is related to porosity parameter. Enhancement in  $k_1$  leads to increase of secondary velocity. Here pores also assist the secondary velocity. Fig. 4.12 presented the increasing influence of Hall parameter on secondary velocity. Fig. 4.13 is constructed for wall parameters. It is clearly seen that the elastance parameters decrease the secondary velocity whereas opposite holds for damping.

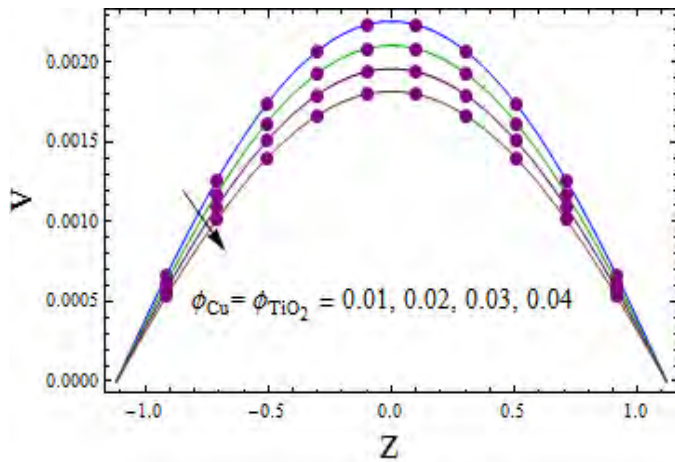


Fig. 4.8

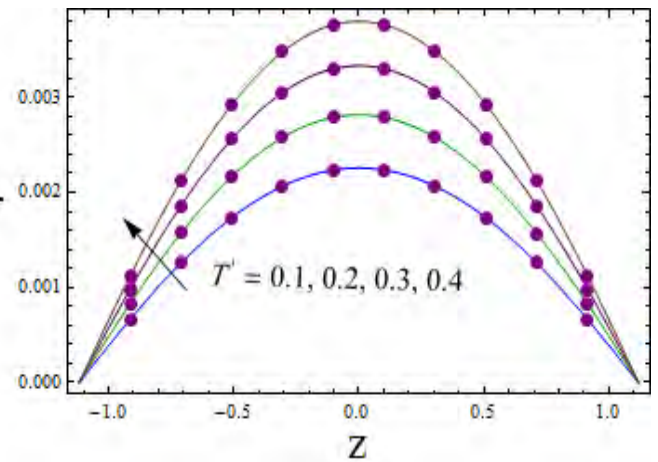


Fig. 4.9

Fig. 4.8. Secondary velocity distribution for  $\phi_{Cu}$  and  $\phi_{TiO_2}$  when  $E_1 = 0.0002$ ,  $E_2 = 0.0001$ ,  $E_3 = 0.01$ ,  $T' = 0.1$ ,  $t = 0.1$ ,  $x = 0.2$ ,  $\varepsilon = 0.2$ ,  $M = 1.0$ ,  $m = 1.0$ ,  $S = 1.0$ ,  $Bi_1 = 4$ ,  $Bi_2 = 6$ ,  $Br = 3.0$ ,  $k_1 = 1$ ,  $Rd = 1$ .

Fig. 4.9. Secondary velocity distribution for  $T'$  when  $E_1 = 0.0002$ ,  $E_2 = 0.0001$ ,  $E_3 = 0.01$ ,  $t = 0.1$ ,  $x = 0.2$ ,  $\varepsilon = 0.2$ ,  $\phi_{Cu} = \phi_{TiO_2} = 0.01$ ,  $M = 1.0$ ,  $m = 1.0$ ,  $S = 1.0$ ,  $Bi_1 = 4$ ,  $Bi_2 = 6$ ,  $Br = 3.0$ ,  $k_1 = 1$ ,  $Rd = 1$ .

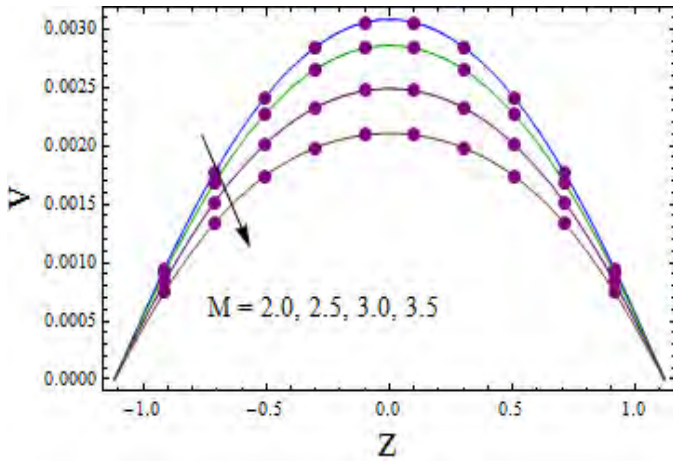


Fig. 4.10

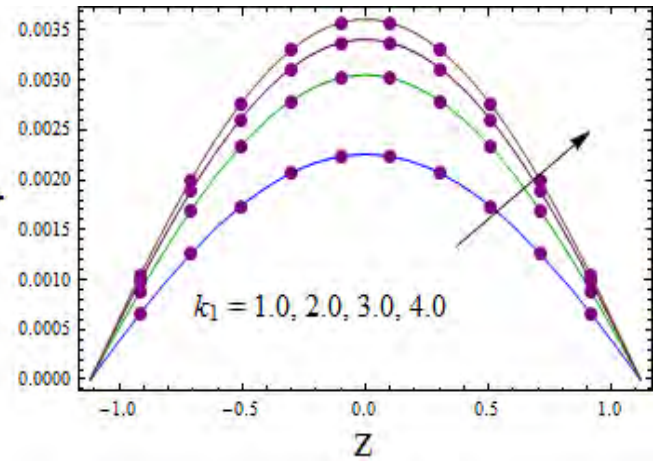


Fig. 4.11

Fig. 4.10. Secondary velocity distribution for  $M$  when  $E_1 = 0.0002$ ,  $E_2 = 0.0001$ ,  $E_3 = 0.01$ ,  $T' = 0.1$ ,  $t = 0.1$ ,  $x = 0.2$ ,  $\varepsilon = 0.2$ ,  $\phi_{Cu} = \phi_{TiO_2} = 0.01$ ,  $m = 1.0$ ,  $S = 1.0$ ,  $Bi_1 = 4$ ,  $Bi_2 = 6$ ,  $Br = 3.0$ ,  $k_1 = 1$ ,  $Rd = 1$ .

Fig. 4.11. Secondary velocity distribution for  $k_1$  when  $E_1 = 0.0002$ ,  $E_2 = 0.0001$ ,  $E_3 = 0.01$ ,  $T' = 0.1$ ,  $t = 0.1$ ,  $x = 0.2$ ,  $\varepsilon = 0.2$ ,  $\phi_{Cu} = \phi_{TiO_2} = 0.01$ ,  $M = 1.0$ ,  $m = 1.0$ ,  $S = 1.0$ ,  $Bi_1 = 4$ ,  $Bi_2 = 6$ ,  $Br = 3.0$ ,  $Rd = 1$ .

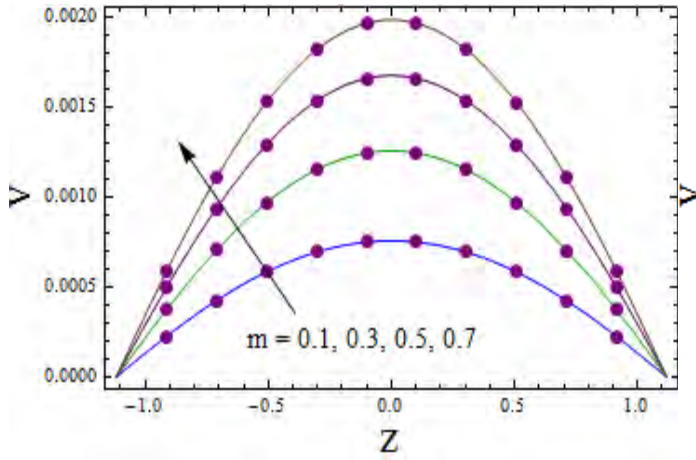


Fig. 4.12

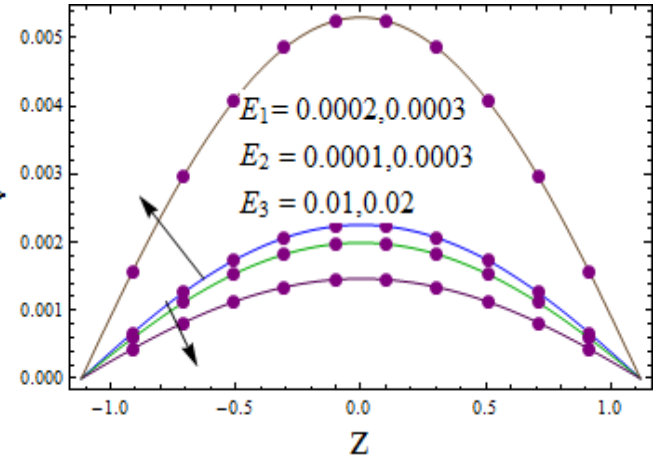


Fig. 4.13

Fig. 4.12. Secondary velocity distribution for  $m$  when  $E_1 = 0.0002$ ,  $E_2 = 0.0001$ ,  $E_3 = 0.01$ ,  $T' = 0.1$ ,  $t = 0.1$ ,  $x = 0.2$ ,  $\varepsilon = 0.2$ ,  $\phi_{Cu} = \phi_{TiO_2} = 0.01$ ,  $M = 1.0$ ,  $S = 1.0$ ,  $Bi_1 = 4$ ,  $Bi_2 = 6$ ,  $Br = 3.0$ ,  $k_1 = 1$ ,  $Rd = 1$ .

Fig. 4.13. Secondary velocity distribution for  $E_1$ ,  $E_2$  and  $E_3$  when  $T' = 0.1$ ,  $t = 0.1$ ,  $x = 0.2$ ,  $\varepsilon = 0.2$ ,  $\phi_{Cu} = \phi_{TiO_2} = 0.01$ ,  $M = 1.0$ ,  $m = 1.0$ ,  $S = 1.0$ ,  $Bi_1 = 4$ ,  $Bi_2 = 6$ ,  $Br = 3.0$ ,  $k_1 = 1$ ,  $Rd = 1$ .

### 4.3.2 Temperature

Temperature containing hybrid nanoparticles are studied in this subsection. Fig. 4.14 is prepared to observe the change in temperature via increasing values of volume fraction. Addition of nanoparticles in base fluid enhances the heat transfer ability of fluid. It leads to decay the temperature. Taylor number effect on  $\theta$  is checked through Fig. 4.15.  $T'$  leads to decrease the temperature. Fig. 4.16 witnessed the result for Hartman number  $M$ . Temperature enhancement is possible here. This is possible in view of Joule heating. Fig. 4.17 reveals the radiation parameter effect on temperature. Decay is observed clearly. Larger values of porosity parameter lead to enhance the temperature (see Fig. 4.18). Physical reasoning is directly related to velocity of fluid. Fig. 4.19 shows Brinkman number impact which is responsible for an enhancement of  $\theta$ . Brinkman number is directly related to viscous dissipation which results

in increase of temperature. Fig. 4.20 depicted the results for Hall parameter on temperature. Enhancement is observed here. The results can be related with velocity. Heat source parameter effect on temperature can be viewed via Fig. 4.21. Obviously heat source parameter leads to enhancement in  $\theta$ . Figs. 4.22 and 4.23 displayed the results for Biot numbers. In both cases the temperature profile decays. Fig. 4.24 elucidates the wall parameters influence on  $\theta$ . Damping coefficient leads to decrease the temperature whereas opposite is seen for elastance variable.

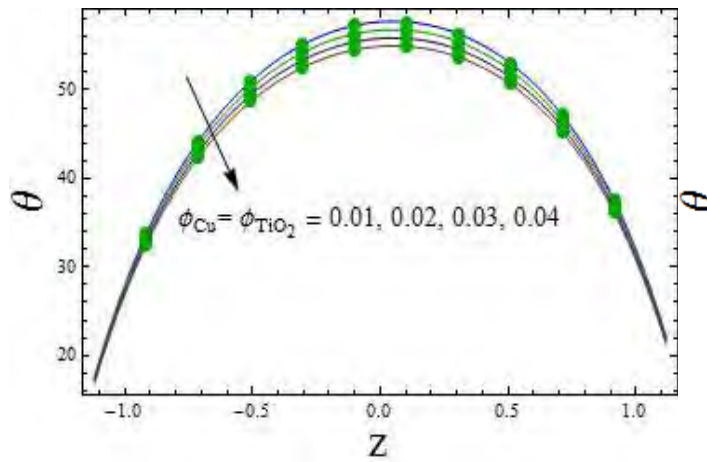


Fig. 4.14

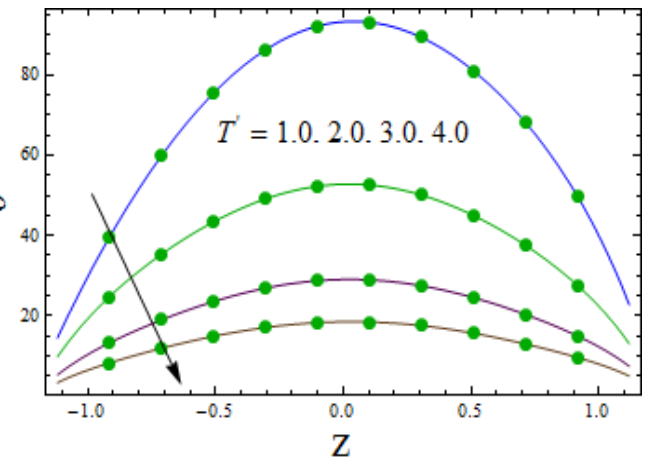


Fig. 4.15

*Fig. 4.14.* Temperature distribution for  $\phi_{Cu}$  and  $\phi_{TiO_2}$  when  $E_1 = 0.3$ ,  $E_2 = 0.3$ ,  $E_3 = 0.01$ ,  $T' = 1.0$ ,  $t = 0.1$ ,  $x = 0.2$ ,  $\varepsilon = 0.2$ ,  $M = 1.0$ ,  $m = 1.0$ ,  $S = 0.5$ ,  $Bi_1 = 8$ ,  $Bi_2 = 10$ ,  $Br = 3.0$ ,  $k_1 = 1$ ,  $Rd = 1$ .

*Fig. 4.15.* Temperature distribution for  $T'$  when  $E_1 = 0.3$ ,  $E_2 = 0.3$ ,  $E_3 = 0.01$ ,  $t = 0.1$ ,  $x = 0.2$ ,  $\varepsilon = 0.2$ ,  $\phi_{Cu} = \phi_{TiO_2} = 0.01$ ,  $M = 1.0$ ,  $m = 1.0$ ,  $S = 0.5$ ,  $Bi_1 = 8$ ,  $Bi_2 = 10$ ,  $Br = 3.0$ ,  $k_1 = 1$ ,  $Rd = 1$ .



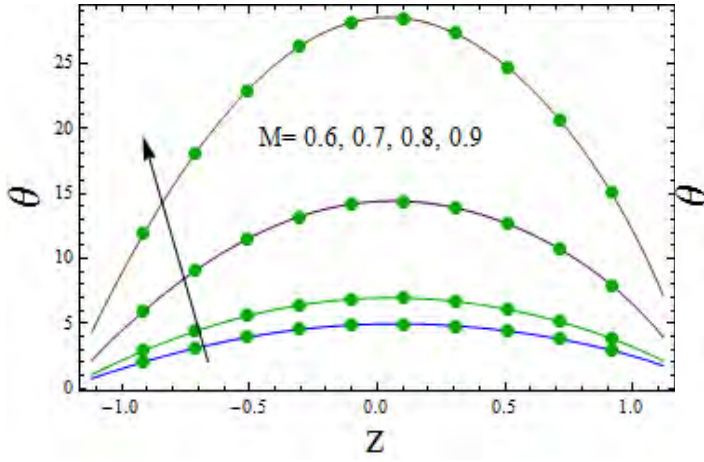


Fig. 4.16

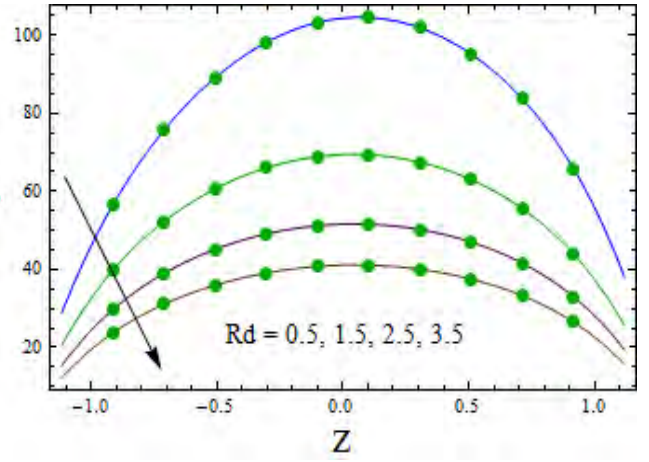


Fig. 4.17

Fig. 4.16. Temperature distribution for  $M$  when  $E_1 = 0.3$ ,  $E_2 = 0.3$ ,  $E_3 = 0.01$ ,  $T' = 1.0$ ,  $t = 0.1$ ,  $x = 0.2$ ,  $\varepsilon = 0.2$ ,  $\phi_{Cu} = \phi_{TiO_2} = 0.01$ ,  $m = 1.0$ ,  $S = 0.5$ ,  $Bi_1 = 8$ ,  $Bi_2 = 10$ ,  $Br = 3.0$ ,  $k_1 = 1$ ,  $Rd = 1$ .

Fig. 4.17. Temperature distribution for  $Rd$  when  $E_1 = 0.3$ ,  $E_2 = 0.3$ ,  $E_3 = 0.01$ ,  $T' = 1.0$ ,  $t = 0.1$ ,  $x = 0.2$ ,  $\varepsilon = 0.2$ ,  $\phi_{Cu} = \phi_{TiO_2} = 0.01$ ,  $M = 1.0$ ,  $m = 1.0$ ,  $S = 0.5$ ,  $Bi_1 = 8$ ,  $Bi_2 = 10$ ,  $Br = 3.0$ ,  $k_1 = 1$ .

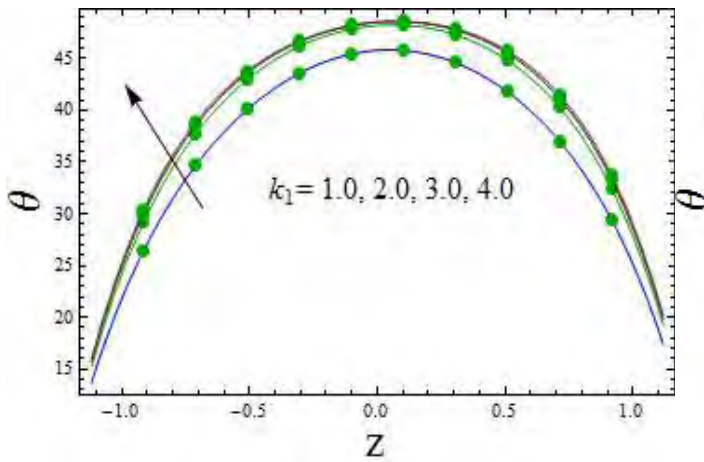


Fig. 4.18

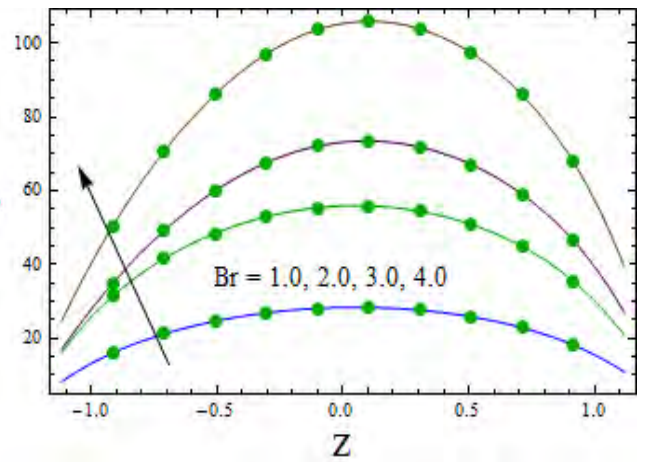


Fig. 4.19

Fig. 4.18. Temperature distribution for  $k_1$  when  $E_1 = 0.3$ ,  $E_2 = 0.3$ ,  $E_3 = 0.01$ ,  $T' = 1.0$ ,

$t = 0.1, x = 0.2, \varepsilon = 0.2, \phi_{Cu} = \phi_{TiO_2} = 0.01, M = 1.0, m = 1.0, S = 0.5, Bi_1 = 8, Bi_2 = 10,$   
 $Br = 3.0, Rd = 1.$

*Fig. 4.19.* Temperature distribution for  $Br$  when  $E_1 = 0.3, E_2 = 0.3, E_3 = 0.01, T' = 1.0,$   
 $t = 0.1, x = 0.2, \varepsilon = 0.2, \phi_{Cu} = \phi_{TiO_2} = 0.01, M = 1.0, m = 1.0, S = 0.5, Bi_1 = 8, Bi_2 = 10,$   
 $k_1 = 1, Rd = 1.$

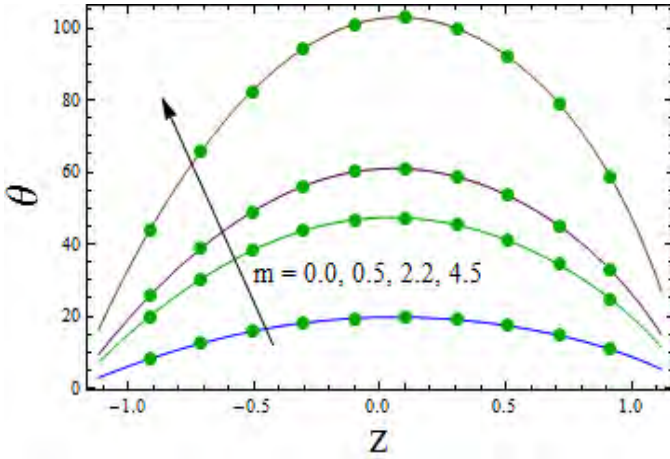


Fig. 4.20

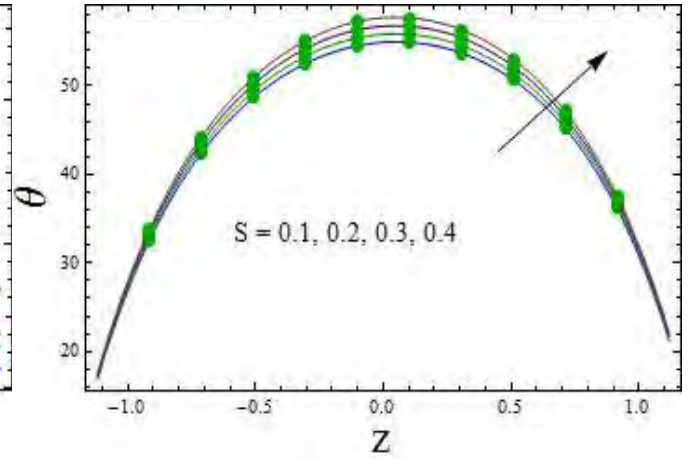


Fig. 4.21

*Fig. 4.20.* Temperature distribution for  $m$  when  $E_1 = 0.3, E_2 = 0.3, E_3 = 0.01, T' = 1.0,$   
 $t = 0.1, x = 0.2, \varepsilon = 0.2, \phi_{Cu} = \phi_{TiO_2} = 0.01, M = 1.0, S = 0.5, Bi_1 = 8, Bi_2 = 10, Br = 3.0,$   
 $k_1 = 1, Rd = 1.$

*Fig. 4.21.* Temperature distribution for  $S$  when  $E_1 = 0.3, E_2 = 0.3, E_3 = 0.01, T' = 1.0,$   
 $t = 0.1, x = 0.2, \varepsilon = 0.2, \phi_{Cu} = \phi_{TiO_2} = 0.01, M = 1.0, m = 1.0, Bi_1 = 8, Bi_2 = 10, Br = 3.0,$   
 $k_1 = 1, Rd = 1.$



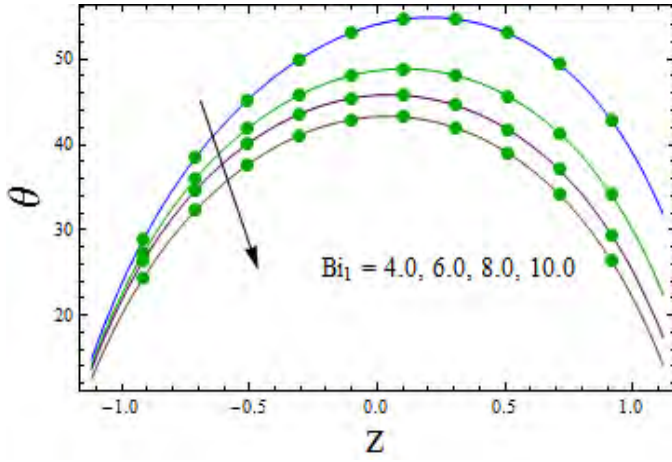


Fig. 4.22

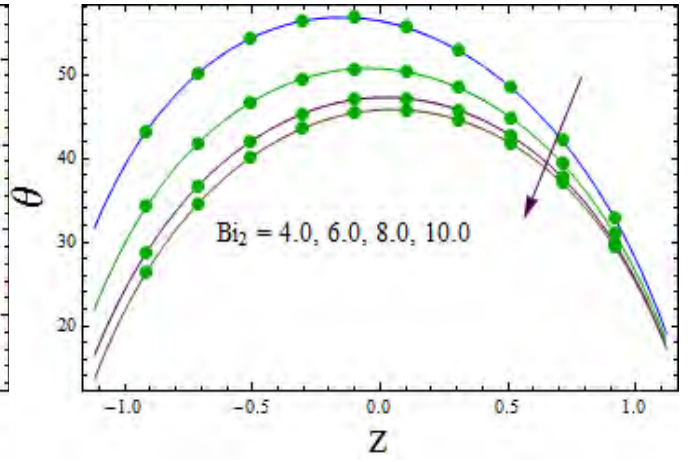


Fig. 4.23

Fig. 4.22. Temperature distribution for  $Bi_1$  when  $E_1 = 0.3$ ,  $E_2 = 0.3$ ,  $E_3 = 0.01$ ,  $T' = 1.0$ ,  $t = 0.1$ ,  $x = 0.2$ ,  $\varepsilon = 0.2$ ,  $\phi_{Cu} = \phi_{TiO_2} = 0.01$ ,  $M = 1.0$ ,  $m = 1.0$ ,  $S = 0.5$ ,  $Bi_2 = 10$ ,  $Br = 3.0$ ,  $k_1 = 1$ ,  $Rd = 1$ .

Fig. 4.23. Temperature distribution for  $Bi_2$  when  $E_1 = 0.3$ ,  $E_2 = 0.3$ ,  $E_3 = 0.01$ ,  $T' = 1.0$ ,  $t = 0.1$ ,  $x = 0.2$ ,  $\varepsilon = 0.2$ ,  $\phi_{Cu} = \phi_{TiO_2} = 0.01$ ,  $M = 1.0$ ,  $m = 1.0$ ,  $S = 0.5$ ,  $Bi_1 = 8$ ,  $Br = 3.0$ ,  $k_1 = 1$ ,  $Rd = 1$ .

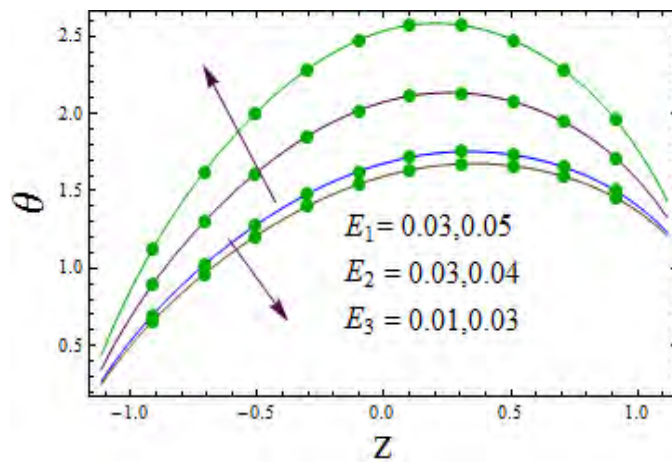


Fig. 4.24

Fig. 4.24. Temperature distribution for  $E_1$ ,  $E_2$  and  $E_3$  when  $T' = 1.0$ ,  $t = 0.1$ ,  $x = 0.2$ ,

$$\varepsilon = 0.2, \phi_{Cu} = \phi_{TiO_2} = 0.01, M = 1.0, m = 1.0, S = 0.5, Bi_1 = 8, Bi_2 = 10, Br = 3.0, k_1 = 1, \\ Rd = 1.$$

### 4.3.3 Entropy generation analysis

Figs. 4.25-4.32 are plotted in this subsection for the analysis of entropy of system. Fig. 4.25 is sketched for the nanoparticle volume fraction on  $Ns$ . An increase in nanoparticle volume fraction reduces the temperature and hence entropy. Similar reasoning is satisfied for the Taylor number (see Fig. 4.26). Fig. 4.27 provides the results of  $k_1$  on entropy. In this case the porosity is directed linked with temperature. Fig. 4.28 clearly indicates that viscous dissipation leads to an increase in  $\theta$  and  $Ns$ . Fig. 4.29 states that Hartman number increases the entropy due to Joule heating. Heat source parameter leads to increase in entropy (see Fig. 4.30). Fig. 4.31 presents the Hall parameter influence. Enhancement is noticed in this case. Fig. 4.32 displays that with  $E_i (i = 1, 2)$  the entropy enlarges whereas  $E_3$  leads to decrease the entropy.

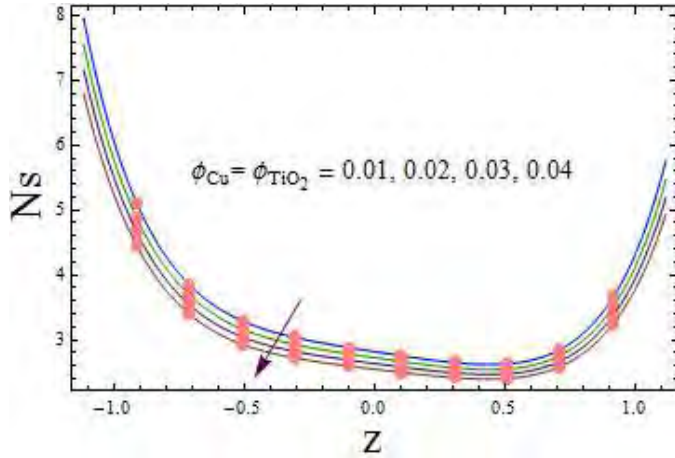


Fig. 4.25

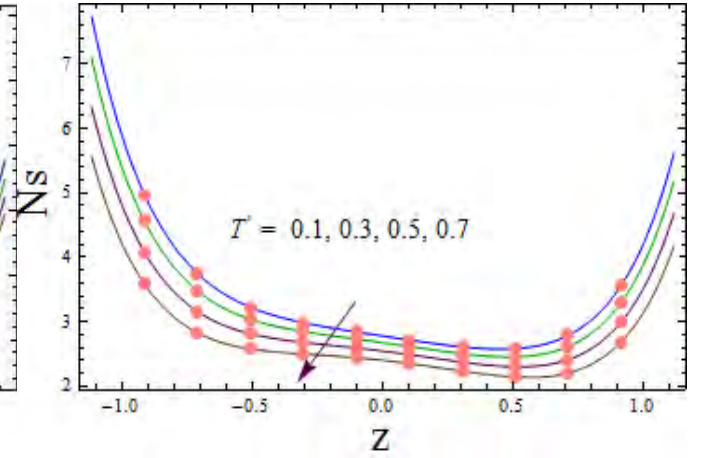


Fig. 4.26

*Fig. 4.25.* Entropy generation for  $\phi_{Cu}$  and  $\phi_{TiO_2}$  when  $E_1 = 0.02, E_2 = 0.01, E_3 = 0.01,$   
 $T' = 0.1, t = 0.1, x = 0.2, \varepsilon = 0.2, M = 1.0, m = 1.0, S = 0.5, Bi_1 = 8, Bi_2 = 10, Br = 3.0,$   
 $k_1 = 1, Rd = 1, \Lambda = 0.5.$

*Fig. 4.26.* Entropy generation for  $T'$  when  $E_1 = 0.02, E_2 = 0.01, E_3 = 0.01, t = 0.1, x = 0.2,$   
 $\varepsilon = 0.2, \phi_{Cu} = \phi_{TiO_2} = 0.01, M = 1.0, m = 1.0, S = 0.5, Bi_1 = 8, Bi_2 = 10, Br = 3.0, k_1 = 1,$

$$Rd = 1, \Lambda = 0.5.$$

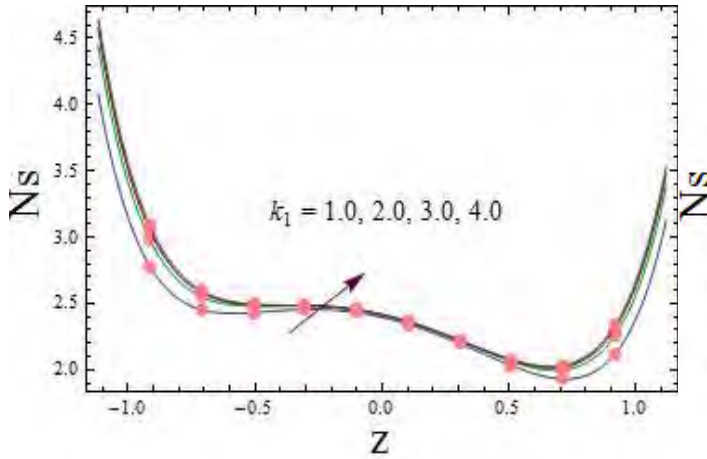


Fig. 4.27

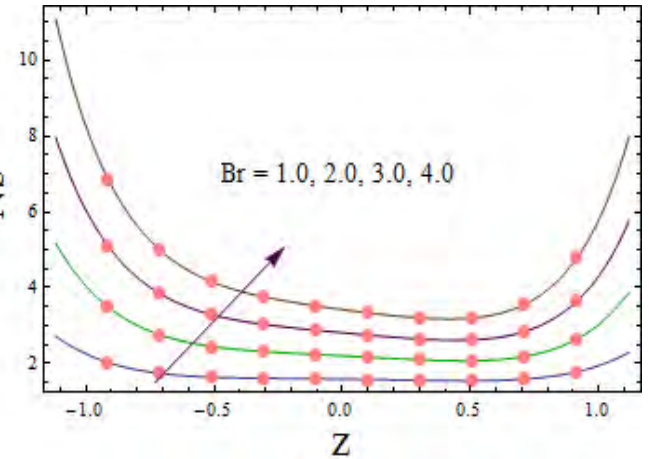


Fig. 4.28

Fig. 4.27. Entropy generation for  $k_1$  when  $E_1 = 0.02$ ,  $E_2 = 0.01$ ,  $E_3 = 0.01$ ,  $T' = 0.1$ ,  $t = 0.1$ ,  $x = 0.2$ ,  $\varepsilon = 0.2$ ,  $\phi_{Cu} = \phi_{TiO_2} = 0.01$ ,  $M = 1.0$ ,  $m = 1.0$ ,  $S = 0.5$ ,  $Bi_1 = 8$ ,  $Bi_2 = 10$ ,  $Br = 3.0$ ,  $Rd = 1$ ,  $\Lambda = 0.5$ .

Fig. 4.28. Entropy generation for  $Br$  when  $E_1 = 0.02$ ,  $E_2 = 0.01$ ,  $E_3 = 0.01$ ,  $T' = 0.1$ ,  $t = 0.1$ ,  $x = 0.2$ ,  $\varepsilon = 0.2$ ,  $\phi_{Cu} = \phi_{TiO_2} = 0.01$ ,  $M = 1.0$ ,  $m = 1.0$ ,  $S = 0.5$ ,  $Bi_1 = 8$ ,  $Bi_2 = 10$ ,  $k_1 = 1$ ,  $Rd = 1$ ,  $\Lambda = 0.5$ .

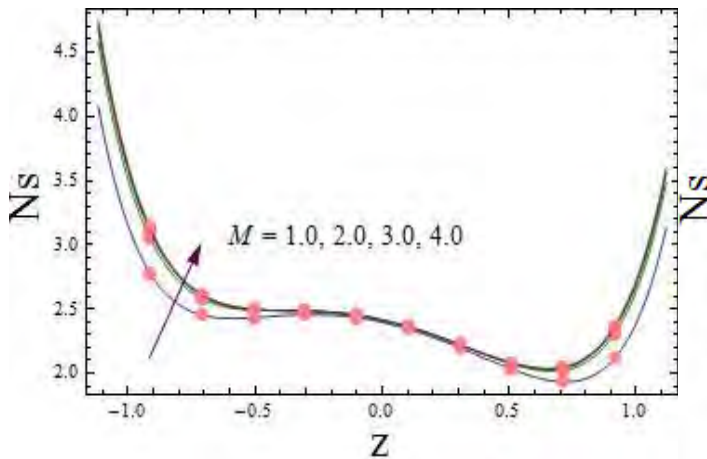


Fig. 4.29

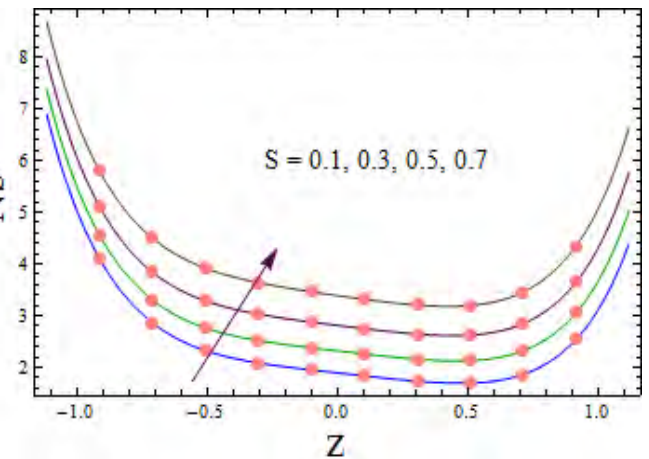


Fig. 4.30

Fig. 4.29. Entropy generation for  $M$  when  $E_1 = 0.02$ ,  $E_2 = 0.01$ ,  $E_3 = 0.01$ ,  $T' = 0.1$ ,  $t = 0.1$ ,  $x = 0.2$ ,  $\varepsilon = 0.2$ ,  $\phi_{Cu} = \phi_{TiO_2} = 0.01$ ,  $m = 1.0$ ,  $S = 0.5$ ,  $Bi_1 = 8$ ,  $Bi_2 = 10$ ,  $Br = 3.0$ ,  $k_1 = 1$ ,  $Rd = 1$ ,  $\Lambda = 0.5$ .

Fig. 4.30. Entropy generation for  $S$  when  $E_1 = 0.02$ ,  $E_2 = 0.01$ ,  $E_3 = 0.01$ ,  $T' = 0.1$ ,  $t = 0.1$ ,  $x = 0.2$ ,  $\varepsilon = 0.2$ ,  $\phi_{Cu} = \phi_{TiO_2} = 0.01$ ,  $M = 1.0$ ,  $m = 1.0$ ,  $Bi_1 = 8$ ,  $Bi_2 = 10$ ,  $Br = 3.0$ ,  $k_1 = 1$ ,  $Rd = 1$ ,  $\Lambda = 0.5$ .

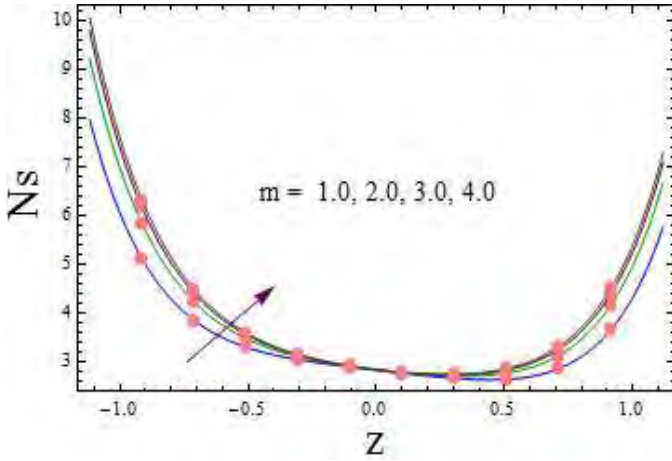


Fig. 4.31

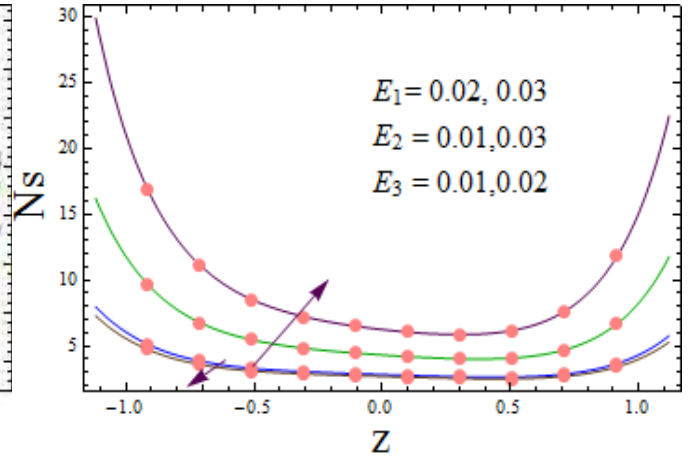


Fig. 4.32

Fig. 4.31. Entropy generation for  $m$  when  $E_1 = 0.02$ ,  $E_2 = 0.01$ ,  $E_3 = 0.01$ ,  $T' = 0.1$ ,  $t = 0.1$ ,  $x = 0.2$ ,  $\varepsilon = 0.2$ ,  $\phi_{Cu} = \phi_{TiO_2} = 0.01$ ,  $M = 1.0$ ,  $Br = 3.0$ ,  $S = 0.5$ ,  $Bi_1 = 8$ ,  $Bi_2 = 10$ ,  $k_1 = 1$ ,  $Rd = 1$ ,  $\Lambda = 0.5$ .

Fig. 4.32. Entropy generation for  $E_1$ ,  $E_2$  and  $E_3$  when  $T' = 0.1$ ,  $t = 0.1$ ,  $x = 0.2$ ,  $\varepsilon = 0.2$ ,  $\phi_{Cu} = \phi_{TiO_2} = 0.01$ ,  $M = 1.0$ ,  $m = 1.0$ ,  $S = 0.5$ ,  $Bi_1 = 8$ ,  $Bi_2 = 10$ ,  $Br = 3.0$ ,  $k_1 = 1$ ,  $Rd = 1$ ,  $\Lambda = 0.5$ .

#### 4.3.4 Heat transfer rate

In this subsection we have arranged the bar graphs to analyze the heat transfer rate at the wall. Fig. 4.33 shows that heat transfer rate at the wall has larger values as the volume fraction of nanoparticles enlarges. Since the enhancement in nanoparticles volume fraction increases the cooling capabilities so enhance the heat transfer rate higher. Fig. 4.34 is plotted against Taylor

number effect. Rotation leads to decrease the heat transfer rate. Hartman number increased the heat transfer rate at the wall (see Fig. 4.35). Fig. 4.36 portrayed the effect of porosity parameter on heat transfer rate. An increase in pores enhances the temperature. It means that there is less heat transfer rate at the wall. Fig. 4.37 demonstrated increasing value of heat transfer rate at the wall with higher values of Hall parameter. Fig. 4.38 depicted the heat transfer rate for Brinkman number. Heat transfer rate at wall increases for higher Brinkman number. Fig. 4.39 is constructed to see the influence of  $Rd$  on heat transfer rate. Heat transfer rate decreases with higher radiation parameter.

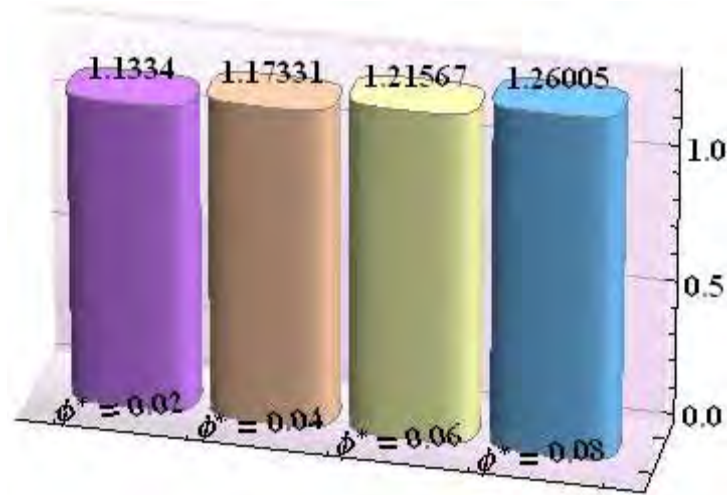


Fig. 4.33

*Fig. 4.33.* Heat transfer rate at the wall ( $-K_1\theta'(\eta)$ ) for  $\phi^*(=\phi_{Cu} + \phi_{TiO_2})$  when  $E_1 = 0.03$ ,  $E_2 = 0.03$ ,  $E_3 = 0.01$ ,  $T' = 2.0$ ,  $t = 0.1$ ,  $x = 0$ ,  $\varepsilon = 0.2$ ,  $M = 2.0$ ,  $m = 2.0$ ,  $S = 1.0$ ,  $Bi_1 = 8$ ,  $Bi_2 = 10$ ,  $Br = 3.0$ ,  $k_1 = 3$ ,  $Rd = 0.5$ .

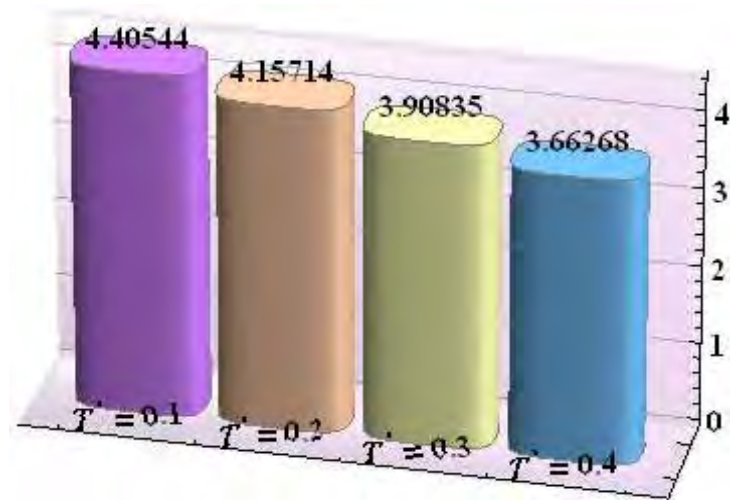


Fig. 4.34

Fig. 4.34. Heat transfer rate at the wall ( $-K_1\theta'(\eta)$ ) for  $T'$  when  $E_1 = 0.03$ ,  $E_2 = 0.03$ ,  $E_3 = 0.01$ ,  $t = 0.1$ ,  $x = 0$ ,  $\varepsilon = 0.2$ ,  $\phi_{Cu} = \phi_{TiO_2} = 0.01$ ,  $M = 2.0$ ,  $m = 2.0$ ,  $S = 1.0$ ,  $Bi_1 = 8$ ,  $Bi_2 = 10$ ,  $Br = 3.0$ ,  $k_1 = 3$ ,  $Rd = 0.5$ .

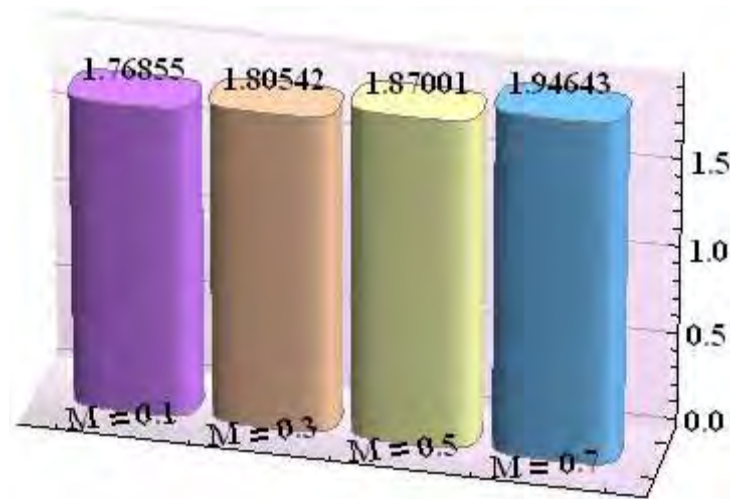


Fig. 4.35



Fig. 4.35. Heat transfer rate at the wall ( $-K_1\theta'(\eta)$ ) for  $M$  when  $E_1 = 0.03$ ,  $E_2 = 0.03$ ,  $E_3 = 0.01$ ,  $T' = 2.0$ ,  $t = 0.1$ ,  $x = 0$ ,  $\varepsilon = 0.2$ ,  $\phi_{Cu} = \phi_{TiO_2} = 0.01$ ,  $m = 0.1$ ,  $S = 1.0$ ,  $Bi_1 = 8$ ,  $Bi_2 = 10$ ,  $Br = 3.0$ ,  $k_1 = 3$ ,  $Rd = 0.5$ .

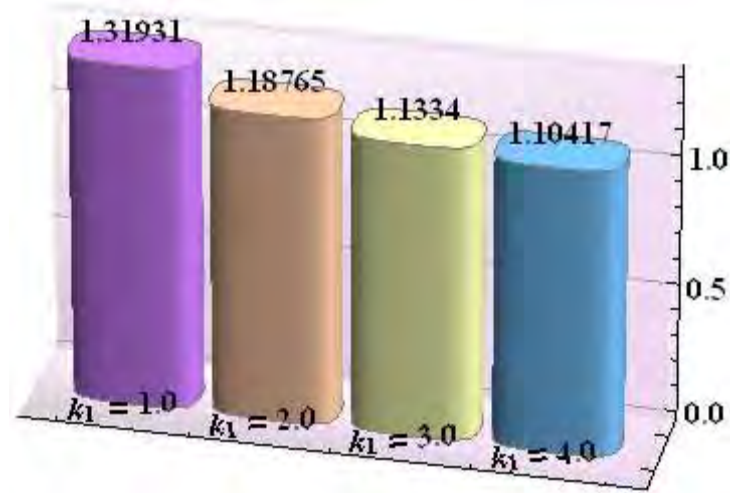


Fig. 4.36

Fig. 4.36. Heat transfer rate at the wall ( $-K_1\theta'(\eta)$ ) for  $k_1$  when  $E_1 = 0.03$ ,  $E_2 = 0.03$ ,  $E_3 = 0.01$ ,  $T' = 2.0$ ,  $t = 0.1$ ,  $x = 0$ ,  $\varepsilon = 0.2$ ,  $\phi_{Cu} = \phi_{TiO_2} = 0.01$ ,  $M = 2.0$ ,  $m = 2.0$ ,  $S = 1.0$ ,  $Bi_1 = 8$ ,  $Bi_2 = 10$ ,  $Br = 3.0$ ,  $Rd = 0.5$ .

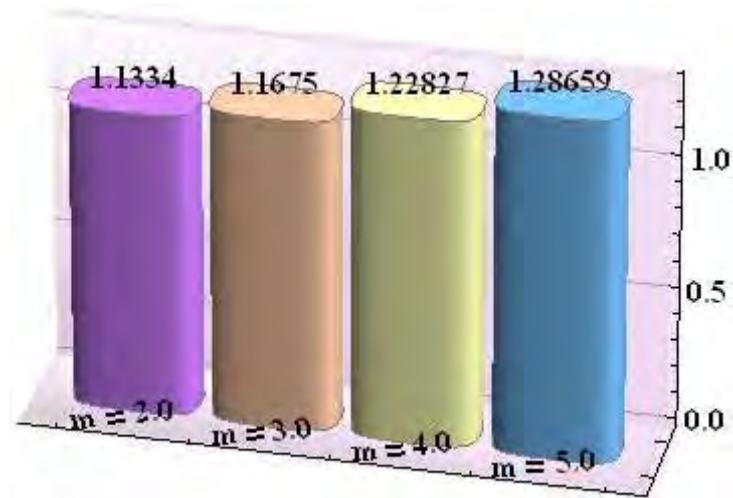


Fig. 4.37

Fig. 4.37. Heat transfer rate at the wall ( $-K_1\theta'(\eta)$ ) for  $m$  when  $E_1 = 0.03$ ,  $E_2 = 0.03$ ,  $E_3 = 0.01$ ,  $T' = 2.0$ ,  $t = 0.1$ ,  $x = 0$ ,  $\varepsilon = 0.2$ ,  $\phi_{Cu} = \phi_{TiO_2} = 0.01$ ,  $M = 2.0$ ,  $S = 1.0$ ,  $Bi_1 = 8$ ,  $Bi_2 = 10$ ,  $Br = 3.0$ ,  $k_1 = 3$ ,  $Rd = 0.5$ .

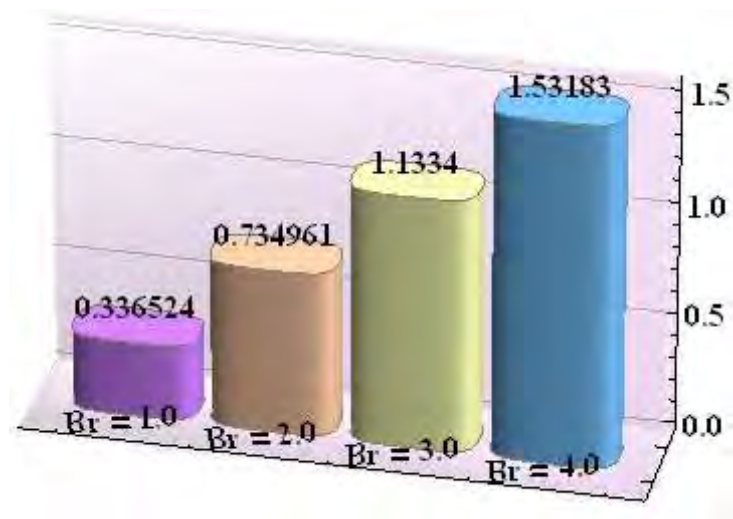


Fig. 4.38



Fig. 4.38. Heat transfer rate at the wall ( $-K_1\theta'(\eta)$ ) for  $Br$  when  $E_1 = 0.03$ ,  $E_2 = 0.03$ ,  $E_3 = 0.01$ ,  $T' = 2.0$ ,  $t = 0.1$ ,  $x = 0$ ,  $\varepsilon = 0.2$ ,  $\phi_{Cu} = \phi_{TiO_2} = 0.01$ ,  $M = 2.0$ ,  $m = 2.0$ ,  $S = 1.0$ ,  $Bi_1 = 8$ ,  $Bi_2 = 10$ ,  $k_1 = 3$ ,  $Rd = 0.5$ .

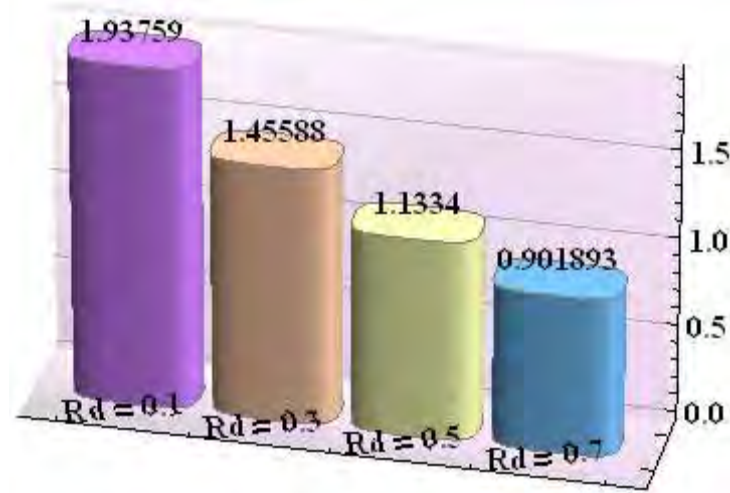


Fig. 4.39

Fig. 4.39. Heat transfer rate at the wall ( $-K_1\theta'(\eta)$ ) for  $Rd$  when  $E_1 = 0.03$ ,  $E_2 = 0.03$ ,  $E_3 = 0.01$ ,  $T' = 2.0$ ,  $t = 0.1$ ,  $x = 0$ ,  $\varepsilon = 0.2$ ,  $\phi_{Cu} = \phi_{TiO_2} = 0.01$ ,  $M = 2.0$ ,  $m = 2.0$ ,  $S = 1.0$ ,  $Bi_1 = 8$ ,  $Bi_2 = 10$ ,  $Br = 3.0$ ,  $k_1 = 3$ .

### 4.3.5 Streamlines

Trapping phenomenon has been analyzed in this subsection. Streamlines has been plotted for this purpose. Fig. 4.40 (a) and (b) describe the impact of volume fraction for hybrid nanofluid. In is seen that the size of trapped bolus increases as the volume fraction of nanoparticles enhances. Fig. 4.41 (a) and (b) show the bolus results for increasing values of Taylor number for hybrid nanofluid. In this case bolus sizes decrease for increasing values of Taylor number. Porosity parameter effect on streamlines can be seen via Fig. 4.42 (a) and (b) for hybrid nanofluid. Bolus sizes show a decrease for increasing values of  $k_1$ . Figs. 4.43, 4.44 (a) and (b) represent the impact of Hartman number and Hall parameter on bolus size. Decrease is noticed in both cases.

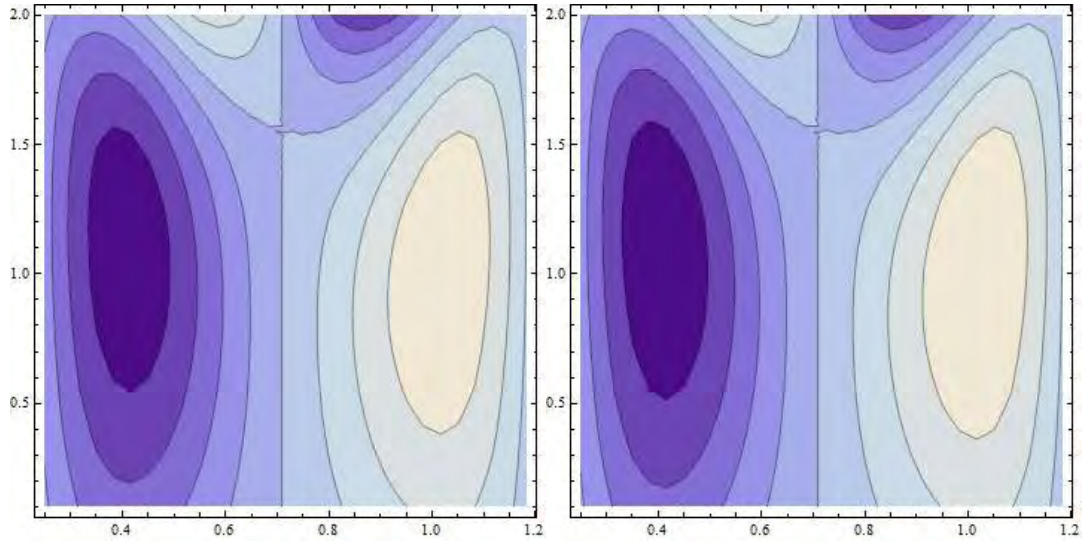


Fig. 4.40 (a)

(b)

Fig. 4.40.  $\psi$  via  $\phi^*$  for hybrid nanofluid when  $E_1 = 0.003$ ,  $E_2 = 0.003$ ,  $E_3 = 0.01$ ,  $T' = 0.01$ ,  $t = 0$ ,  $\varepsilon = 0.2$ ,  $M = 1.0$ ,  $m = 1.0$ ,  $S = 1.0$ ,  $Bi_1 = 4$ ,  $Bi_2 = 6$ ,  $Br = 3.0$ ,  $k_1 = 1$ ,  $Rd = 1$ . (a)

$\phi_{Cu} = \phi_{TiO_2} = 0.05$  (b)  $\phi_{Cu} = \phi_{TiO_2} = 0.09$ .

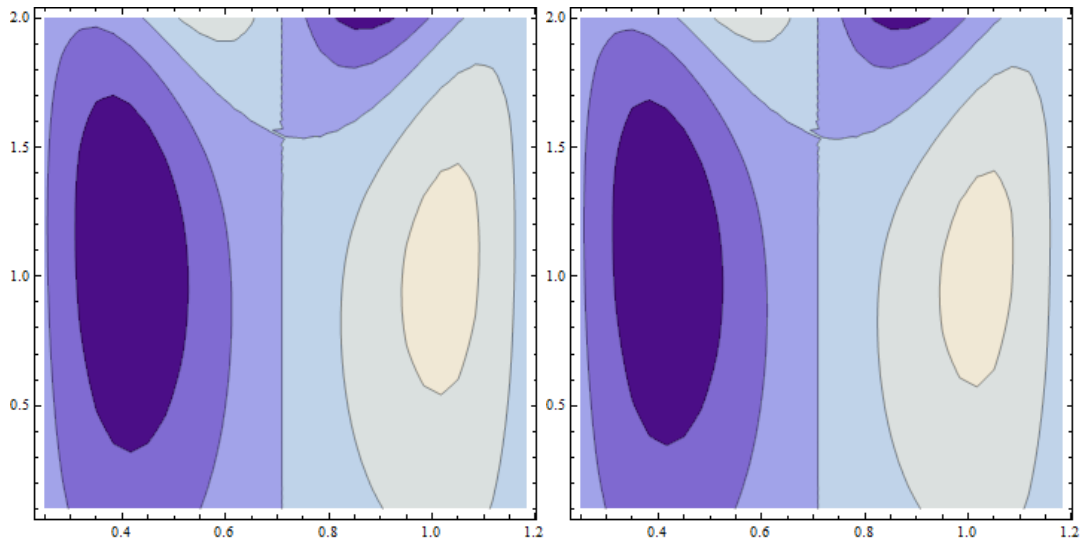


Fig. 4.41 (a)

(b)

*Fig. 4.41.*  $\psi$  via  $T'$  for hybrid nanofluid when  $E_1 = 0.003$ ,  $E_2 = 0.003$ ,  $E_3 = 0.01$ ,  $t = 0$ ,  $\varepsilon = 0.2$ ,  $M = 1.0$ ,  $m = 1.0$ ,  $S = 1.0$ ,  $\phi_{Cu} = \phi_{TiO_2} = 0.01$ ,  $Bi_1 = 4$ ,  $Bi_2 = 6$ ,  $Br = 3.0$ ,  $k_1 = 1$ ,  $Rd = 1$ . (a)  $T' = 0.1$  (b)  $T' = 0.2$ .

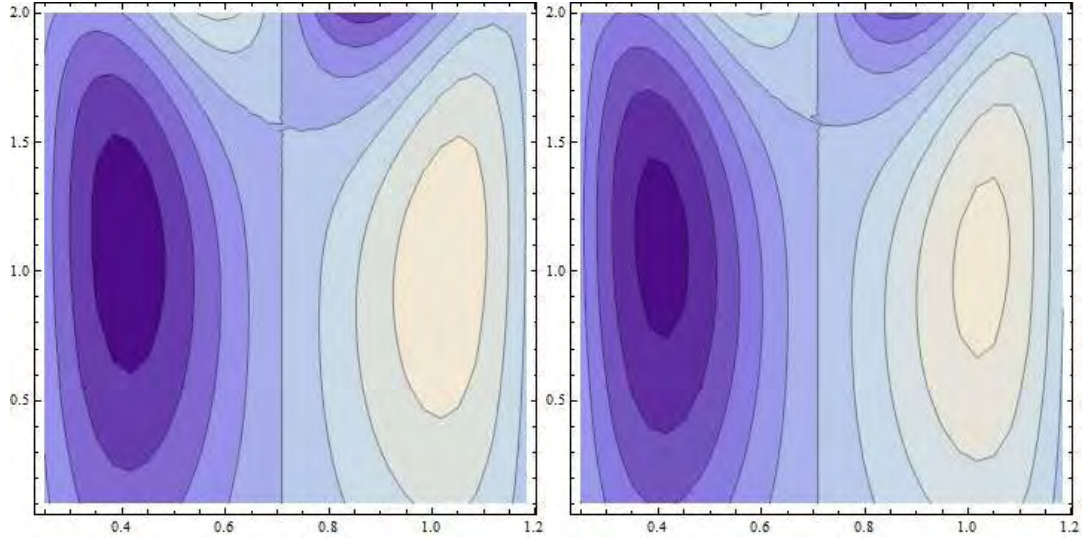


Fig. 4.42 (a)

(b)

*Fig. 4.42.*  $\psi$  via  $k_1$  for hybrid nanofluid when  $E_1 = 0.003$ ,  $E_2 = 0.003$ ,  $E_3 = 0.01$ ,  $T' = 0.1$ ,  $t = 0$ ,  $\varepsilon = 0.2$ ,  $M = 1.0$ ,  $m = 1.0$ ,  $S = 1.0$ ,  $\phi_{Cu} = \phi_{TiO_2} = 0.01$ ,  $Bi_1 = 4$ ,  $Bi_2 = 6$ ,  $Br = 3.0$ ,

$Rd = 1$ . (a)  $k_1 = 1$  (b)  $k_1 = 2$ .

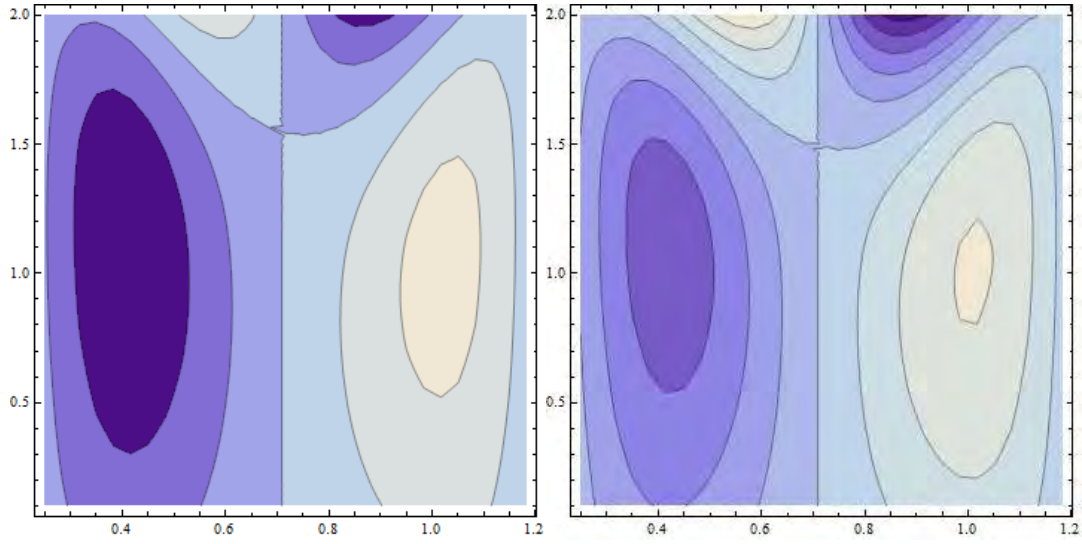


Fig. 4.43 (a)

(b)

Fig. 4.43.  $\psi$  via  $M$  for hybrid nanofluid when  $E_1 = 0.003$ ,  $E_2 = 0.003$ ,  $E_3 = 0.01$ ,  $T' = 0.1$ ,  $t = 0$ ,  $\varepsilon = 0.2$ ,  $m = 1.0$ ,  $S = 1.0$ ,  $\phi_{Cu} = \phi_{TiO_2} = 0.01$ ,  $Bi_1 = 4$ ,  $Bi_2 = 6$ ,  $Br = 3.0$ ,  $k_1 = 1$ ,

$Rd = 1$ . (a)  $M = 1$  (b)  $M = 2$ .

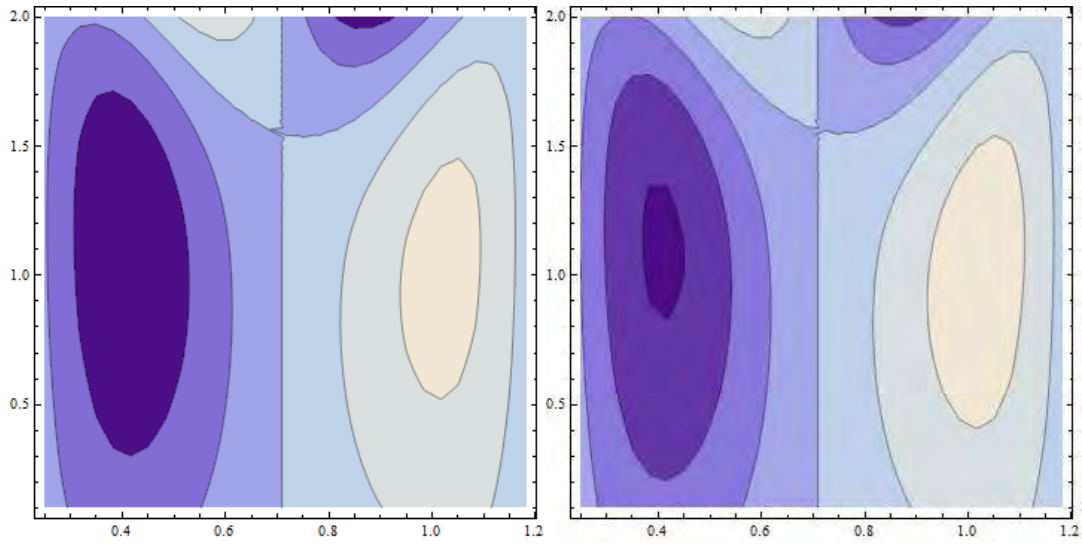


Fig. 4.44 (a)

(b)

*Fig. 4.44.*  $\psi$  via  $m$  for hybrid nanofluid when  $E_1 = 0.003$ ,  $E_2 = 0.003$ ,  $E_3 = 0.01$ ,  $T' = 0.1$ ,  $t = 0$ ,  $\varepsilon = 0.2$ ,  $M = 1.0$ ,  $S = 1.0$ ,  $\phi_{Cu} = \phi_{TiO_2} = 0.01$ ,  $Bi_1 = 4$ ,  $Bi_2 = 6$ ,  $Br = 3.0$ ,  $k_1 = 1$ ,  $Rd = 1$ . (a)  $m = 1$  (b)  $m = 2$ .

## 4.4 Conclusions

In this study we scrutinized the hybrid nanofluid in a rotating frame. MHD and Hall effects are incorporated in the momentum equation. Energy equation includes non-uniform heat source or sink parameter, radiation and Joule heating. Porous medium is considered in this problem. Main results of this analysis are concluded as follows.

- Non-Uniform heat source parameter leads to increase in temperature and entropy.
- Hall parameter and Hartman number effects on temperature and entropy are qualitatively similar.
- Nanoparticle volume fraction enhancement caused decay in temperature, axial and secondary velocities and entropy.
- Porosity parameters gives rise to axial and secondary velocities, temperature and entropy.
- Enhancement in the rotation caused increase in the secondary velocity whereas opposite behavior has been observed for axial velocity, temperature and entropy generation.
- Heat transfer rate enhances when we increase the nano particle volume fraction.
- Size of bolus increases for larger volume fraction of nanoparticles whereas it reduces for Taylor and porosity parameters.

## Chapter 5

# Entropy generation in peristaltic flow of Williamson nanofluid

### 5.1 Introduction

In this chapter the influences of an inclined magnetic field and Joule heating on peristalsis of Williamson nanofluid in a compliant walls channel are examined. Analysis is presented when no-slip conditions for velocity, temperature and concentration are no longer hold. Entropy generation is discussed. Formulated problem is numerically solved for large wavelength and small Reynolds number. Main emphasis is given to the outcomes of velocity, temperature, concentration, heat transfer coefficient and entropy generation. The results are discussed graphically.

### 5.2 Formulation

We examine flow of an electrically conducting Williamson nanofluid in a symmetric channel of width  $2d$ . The channel walls at  $y = \pm\eta$  are compliant in nature. Here  $y = \eta$  corresponds to the upper wall whereas the lower wall is taken at  $y = -\eta$  (see Fig. 5.1). Salient features of Brownian movement and thermophoresis are accounted. Here  $x$ -axis is taken along the channel whereas  $y$ -axis being normal to  $x$ . Temperature and concentration of the upper and lower walls are maintained  $T_1, T_0$  and  $C_1, C_0$  respectively. The sinusoidal waves traveling along the channel

walls are responsible for mechanism of peristalsis. Mathematical shape of such waves [172]:

$$y = \pm \eta(x, t) = \pm \left[ d + a \sin \frac{2\pi}{\lambda} (x - ct) \right]. \quad (5.1)$$

Here  $a$  is the amplitude of wave,  $\lambda$  the wavelength,  $c$  the speed of wave and  $t$  the time.

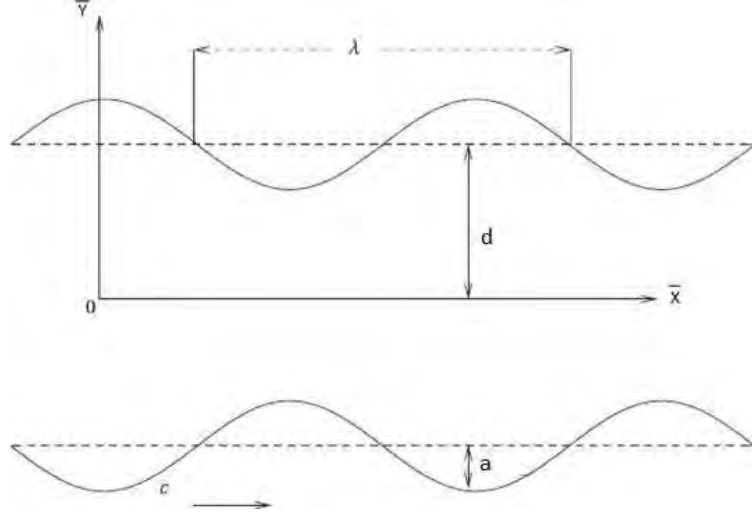


Fig. 5.1: Schematic diagram

An inclined magnetic field with inclination  $\chi$  is taken. Induced magnetic field for low magnetic Reynolds number is not accounted. Electric field is absent. Then [172]:

$$\mathbf{B} = [B_0 \sin \chi, B_0 \cos \chi, 0], \quad (5.2)$$

where  $B_0$  represents magnetic field strength. Lorentz force ( $\mathbf{F} = \mathbf{J} \times \mathbf{B}$ ) now yields [82]:

$$\mathbf{J} \times \mathbf{B} = [-\sigma B_0^2 \cos \chi (u \cos \chi - v \sin \chi), \sigma B_0^2 \sin \chi (u \cos \chi - v \sin \chi), 0]. \quad (5.3)$$

Here  $\sigma$ ,  $\mathbf{J}(=\sigma(\mathbf{V} \times \mathbf{B}))$  and  $\mathbf{V}(=[u, v, 0])$  are used to signify the electrical conductivity, current density and velocity of the fluid. The expressions which can govern the flow are [172]:

$$\frac{\partial u}{\partial x} + \frac{\partial v}{\partial y} = 0, \quad (5.4)$$

$$\frac{\partial u}{\partial t} + u \frac{\partial u}{\partial x} + v \frac{\partial u}{\partial y} = -\frac{1}{\rho_f} \frac{\partial p}{\partial x} + \frac{1}{\rho_f} \frac{\partial S_{xx}}{\partial x} + \frac{1}{\rho_f} \frac{\partial S_{xy}}{\partial y} - \frac{1}{\rho_f} \sigma B_0^2 \cos \chi (u \cos \chi - v \sin \chi), \quad (5.5)$$

$$\frac{\partial v}{\partial t} + u \frac{\partial v}{\partial x} + v \frac{\partial v}{\partial y} = -\frac{1}{\rho_f} \frac{\partial p}{\partial y} + \frac{1}{\rho_f} \frac{\partial S_{xy}}{\partial x} + \frac{1}{\rho_f} \frac{\partial S_{yy}}{\partial y} + \frac{1}{\rho_f} \sigma B_0^2 \sin \chi (u \cos \chi - v \sin \chi), \quad (5.6)$$

where  $p$  depicts the pressure,  $S_{ij}$  the component of extra stress tensor and  $\rho_f$  the fluid density.

Expressions of temperature and concentration satisfy [172]:

$$\begin{aligned} \frac{\partial T}{\partial t} + u \frac{\partial T}{\partial x} + v \frac{\partial T}{\partial y} &= \alpha^* \left[ \frac{\partial^2 T}{\partial x^2} + \frac{\partial^2 T}{\partial y^2} \right] + \frac{1}{(\rho C_p)_f} \left[ S_{xx} \frac{\partial u}{\partial x} + S_{xy} \left( \frac{\partial u}{\partial y} + \frac{\partial v}{\partial x} \right) + S_{yy} \frac{\partial v}{\partial y} \right] \\ &+ \tau \left[ D_B \left( \frac{\partial C}{\partial x} \frac{\partial T}{\partial x} + \frac{\partial C}{\partial y} \frac{\partial T}{\partial y} \right) + \frac{D_T}{T_m} \left( \left( \frac{\partial T}{\partial x} \right)^2 + \left( \frac{\partial T}{\partial y} \right)^2 \right) \right] \\ &+ \frac{1}{(\rho C_p)_f} \sigma B_0^2 (u \cos \chi - v \sin \chi)^2, \end{aligned} \quad (5.7)$$

$$\frac{\partial C}{\partial t} + u \frac{\partial C}{\partial x} + v \frac{\partial C}{\partial y} = D_B \left( \frac{\partial^2 C}{\partial x^2} + \frac{\partial^2 C}{\partial y^2} \right) + \frac{D_T}{T_m} \left( \frac{\partial^2 T}{\partial x^2} + \frac{\partial^2 T}{\partial y^2} \right). \quad (5.8)$$

Here  $\alpha^*$  denotes the thermal diffusivity and  $C_p$  the specific heat. Moreover  $D_B$ ,  $D_T$ , and  $T_m$  define the respective Brownian motion coefficient, thermophoretic diffusion coefficient and mean temperature of nanofluid.  $\tau = (\rho C_p)_p / (\rho C_p)_f$  is the ratio of specific heat capacity for nanomaterial and fluid. Symbols  $T$  and  $C$  are used for temperature and concentration of fluid.

For Williamson liquid, the extra stress tensor  $\mathbf{S}$  satisfies [82, 84]:

$$\mathbf{S} = [\mu_\infty + (\mu_0 + \mu_\infty)(1 - \Gamma \dot{\gamma})^{-1}] \mathbf{A}_1, \quad (5.9)$$

where  $\mu_0$  and  $\mu_\infty$  correspond to zero shear rate and infinite shear rate viscosities and  $\Gamma$  the time constant. Here  $\dot{\gamma}$  and  $\mathbf{A}_1$  are

$$\dot{\gamma} = \sqrt{\frac{1}{2} \Pi}, \quad (5.10)$$

$$\mathbf{A}_1 = \text{grad } \mathbf{V} + (\text{grad } \mathbf{V})^T, \quad (5.11)$$

$$\Pi = \text{tr}(\mathbf{A}_1^2). \quad (5.12)$$

Assuming that  $\mu_\infty = 0$  and  $\Gamma \dot{\gamma} < 1$  then expression of stress tensor for Williamson fluid becomes

$$\mathbf{S} = \mu_0 [(1 + \Gamma \dot{\gamma})] \mathbf{A}_1. \quad (5.13)$$

For  $\Gamma = 0$  the above expression reduces to incompressible viscous fluid. From Eq. (5.13) we



have

$$S_{xx} = 2\mu_0(1 + \Gamma\dot{\gamma})\frac{\partial u}{\partial x}, \quad (5.14)$$

$$S_{xy} = \mu_0(1 + \Gamma\dot{\gamma})\left(\frac{\partial u}{\partial y} + \frac{\partial v}{\partial x}\right), \quad (5.15)$$

$$S_{yy} = 2\mu_0(1 + \Gamma\dot{\gamma})\frac{\partial v}{\partial y}, \quad (5.16)$$

$$\dot{\gamma} = \sqrt{2\left(\frac{\partial v}{\partial y}\right)^2 + 2\left(\frac{\partial u}{\partial x}\right)^2 + \left(\frac{\partial v}{\partial x} + \frac{\partial u}{\partial y}\right)^2}. \quad (5.17)$$

The boundary conditions for problem are :

$$u \pm \xi_1 S_{xy} = 0 \quad \text{at } y = \pm\eta, \quad (5.18)$$

$$\left[ -\tau^* \frac{\partial^3}{\partial x^3} + m^* \frac{\partial^3}{\partial x \partial t^2} + d_1^* \frac{\partial^2}{\partial t \partial x} \right] \eta = \frac{\partial S_{xy}}{\partial y} + \frac{\partial S_{xx}}{\partial x} - \rho_f \left[ \frac{\partial u}{\partial t} + u \frac{\partial u}{\partial x} + v \frac{\partial u}{\partial y} \right] - \sigma B_0^2 \cos \chi (u \cos \chi - v \sin \chi), \quad \text{at } y = \pm\eta. \quad (5.19)$$

$$T \pm \xi_2 \frac{\partial T}{\partial y} = \begin{Bmatrix} T_1 \\ T_0 \end{Bmatrix} \quad \text{at } y = \pm\eta, \quad (5.20)$$

$$C \pm \xi_3 \frac{\partial C}{\partial y} = \begin{Bmatrix} C_1 \\ C_0 \end{Bmatrix} \quad \text{at } y = \pm\eta. \quad (5.21)$$

In above equations  $\tau^*$ ,  $m^*$ , and  $d_1^*$  represent the elastic tension, mass per unit area and the coefficient of viscous damping respectively. Extra stress tensor components are given by  $S_{xx}$ ,  $S_{xy}$  and  $S_{yy}$  whereas  $\xi_1$ ,  $\xi_2$  and  $\xi_3$  denote slip parameters for velocity, temperature and concentration respectively.

We set the dimensionless quantities as

$$\begin{aligned} x^* &= \frac{x}{\lambda}, & y^* &= \frac{y}{d}, & u^* &= \frac{u}{c}, & v^* &= \frac{v}{c}, & t^* &= \frac{ct}{\lambda}, & \eta^* &= \frac{\eta}{d}, \\ S_{ij}^* &= \frac{dS_{ij}}{c\mu_0}, & \dot{\gamma}^* &= \dot{\gamma} \frac{d}{c}, & p^* &= \frac{d^2 p}{c\lambda\mu_0}, & We &= \Gamma \frac{c}{d}, & \phi &= \frac{C - C_0}{C_1 - C_0}, \\ \theta &= \frac{T - T_0}{T_1 - T_0}, & u &= \frac{\partial \psi}{\partial y}, & v &= -\delta \frac{\partial \psi}{\partial x}. \end{aligned} \quad (5.22)$$

After utilizing the non-dimensional quantities we get the following equations and boundary conditions:

$$\text{Re} \left[ \delta \frac{\partial^2 \psi}{\partial t \partial y} + \delta \frac{\partial \psi}{\partial y} \frac{\partial^2 \psi}{\partial x \partial y} - \delta \frac{\partial \psi}{\partial x} \frac{\partial^2 \psi}{\partial y^2} \right] = -\frac{\partial p}{\partial x} + \delta \frac{\partial S_{xx}}{\partial x} + \frac{\partial S_{xy}}{\partial y} - M^2 \cos \chi \left( \cos \chi \frac{\partial \psi}{\partial y} + \delta \frac{\partial \psi}{\partial x} \sin \chi \right), \quad (5.23)$$

$$\text{Re} \delta \left[ -\delta^2 \frac{\partial^2 \psi}{\partial t \partial x} - \delta^2 \frac{\partial \psi}{\partial y} \frac{\partial^2 \psi}{\partial x^2} - \delta^2 \frac{\partial^2 \psi}{\partial x \partial y} \right] = -\frac{\partial p}{\partial y} + \delta^2 \frac{\partial S_{xy}}{\partial x} + \delta \frac{\partial S_{yy}}{\partial y} + \delta M^2 \sin \chi \left( \cos \chi \frac{\partial \psi}{\partial y} + \delta \frac{\partial \psi}{\partial x} \sin \chi \right), \quad (5.24)$$

$$\begin{aligned} \text{Re Pr} \left[ \delta \frac{\partial \theta}{\partial t} + \delta \frac{\partial \psi}{\partial y} \frac{\partial \theta}{\partial x} - \delta \frac{\partial \psi}{\partial x} \frac{\partial \theta}{\partial y} \right] &= \left[ \delta^2 \frac{\partial^2 \theta}{\partial x^2} + \frac{\partial^2 \theta}{\partial y^2} \right] \\ &+ Br \left[ \delta S_{xx} \frac{\partial^2 \psi}{\partial x \partial y} + S_{xy} \left( \frac{\partial^2 \psi}{\partial y^2} - \delta^2 \frac{\partial^2 \psi}{\partial x^2} \right) - \delta S_{yy} \frac{\partial^2 \psi}{\partial x \partial y} \right] \\ &+ Nb \text{Pr} \left( \delta^2 \frac{\partial \phi}{\partial x} \frac{\partial \theta}{\partial x} + \frac{\partial \phi}{\partial y} \frac{\partial \theta}{\partial y} \right) + Nt \text{Pr} \left( \delta^2 \left( \frac{\partial \theta}{\partial x} \right)^2 + \left( \frac{\partial \theta}{\partial y} \right)^2 \right) \\ &+ M^2 Br \left( \frac{\partial \psi}{\partial y} \cos \chi + \delta \frac{\partial \psi}{\partial x} \sin \chi \right)^2, \end{aligned} \quad (5.25)$$

$$\text{Re Sc} \left( \delta \frac{\partial \phi}{\partial t} + \frac{\partial \psi}{\partial y} \frac{\partial \phi}{\partial x} - \delta \frac{\partial \psi}{\partial x} \frac{\partial \phi}{\partial y} \right) = \left( \delta^2 \frac{\partial^2 \phi}{\partial x^2} + \frac{\partial^2 \phi}{\partial y^2} \right) + \frac{Nt}{Nb} \left( \delta^2 \frac{\partial^2 \theta}{\partial x^2} + \frac{\partial^2 \theta}{\partial y^2} \right), \quad (5.26)$$

$$S_{xx} = 2\delta(1 + We\dot{\gamma}) \frac{\partial^2 \psi}{\partial x \partial y}, \quad (5.27)$$

$$S_{xy} = (1 + We\dot{\gamma}) \frac{\partial^2 \psi}{\partial y^2}, \quad (5.28)$$

$$S_{yy} = -2\delta(1 + We\dot{\gamma}) \frac{\partial^2 \psi}{\partial x \partial y}, \quad (5.29)$$

with

$$\dot{\gamma} = \sqrt{2 \left( \delta \frac{\partial^2 \psi}{\partial x \partial y} \right)^2 + \left( -\delta^2 \frac{\partial^2 \psi}{\partial x^2} + \frac{\partial^2 \psi}{\partial y^2} \right)^2 + 2 \left( -\delta \frac{\partial^2 \psi}{\partial x \partial y} \right)^2}. \quad (5.30)$$

$$\frac{\partial \psi}{\partial y} \pm \xi_1 S_{xy} = 0, \quad \text{at } y = \pm \eta = \pm(1 + \varepsilon \sin 2\pi(x - t)), \quad (5.31)$$

$$\begin{aligned}
\left[ E_1 \frac{\partial^3}{\partial x^3} + E_2 \frac{\partial^3}{\partial x \partial t^2} + E_3 \frac{\partial^2}{\partial t \partial x} \right] \eta &= -\operatorname{Re} \left[ \delta \frac{\partial^2 \psi}{\partial t \partial y} + \delta \frac{\partial \psi}{\partial y} \frac{\partial^2 \psi}{\partial x \partial y} - \delta \frac{\partial \psi}{\partial x} \frac{\partial^2 \psi}{\partial y^2} \right] + \\
&\quad \delta \frac{\partial S_{xx}}{\partial x} + \frac{\partial S_{xy}}{\partial y} - M^2 \cos \chi \\
&\quad (\cos \chi \frac{\partial \psi}{\partial y} + \delta \frac{\partial \psi}{\partial x} \sin \chi), \quad \text{at } y = \pm \eta,
\end{aligned} \tag{5.32}$$

$$\theta \pm \xi_2 \frac{\partial \theta}{\partial y} = \begin{Bmatrix} 1 \\ 0 \end{Bmatrix} \quad \text{at } y = \pm \eta, \tag{5.33}$$

$$\phi \pm \xi_3 \frac{\partial \phi}{\partial y} = \begin{Bmatrix} 1 \\ 0 \end{Bmatrix} \quad \text{at } y = \pm \eta. \tag{5.34}$$

The quantities involved above include the amplitude ratio  $\varepsilon(= a/d)$ ,  $\delta(= d/\lambda)$  wave number,  $\operatorname{Re}(= \rho_f c d / \mu_0)$  Reynolds number,  $M = \sqrt{\sigma / \mu_0} B_0 d$  Hartman number and  $We$  Williamson fluid parameter known as Weissenberg number. The Brownian motion parameter, thermophoresis parameter, Schmidt number, Prandtl number and Brinkman number are  $Nb(= \tau \rho_f D_B (C_1 - C_0) / \mu_0)$ ,  $Nt(= \tau \rho_f D_T (T_1 - T_0) / \mu_0 T_m)$ ,  $Sc(= \mu_0 / \rho_f D_B)$ ,  $\operatorname{Pr}(= \mu_0 (C_p)_f / \kappa)$ , and  $Br(= c^2 \mu_0 / \kappa (T_1 - T_0))$  respectively. The dimensionless parameters representing the compliant nature of walls are  $E_1(= -\tau^* d^3 / \lambda^3 c \mu_0)$ ,  $E_2(= m^* c d^3 / \lambda^3 \mu_0)$  and  $E_3(= d_1^* d^3 / \lambda^2 \mu_0)$ . Furthermore the slip parameters for velocity, temperature and concentration are  $\xi_1^* = \xi_1 \mu_0 / d$ ,  $\xi_2^* = \xi_2 / d$  and  $\xi_3^* = \xi_3 / d$ .

The systems subject to large wavelength and low Reynolds number are reduced to the following set of equation whereas the continuity equation is satisfied identically.

$$\frac{\partial p}{\partial x} = \frac{\partial S_{xy}}{\partial y} - M^2 \cos^2 \chi \frac{\partial \psi}{\partial y}, \tag{5.35}$$

$$\frac{\partial p}{\partial y} = 0, \tag{5.36}$$

$$\frac{\partial^2 \theta}{\partial y^2} + Br S_{xy} \frac{\partial^2 \psi}{\partial y^2} + Nb \operatorname{Pr} \frac{\partial \phi}{\partial y} \frac{\partial \theta}{\partial y} + Nt \operatorname{Pr} \left( \frac{\partial \theta}{\partial y} \right)^2 + M^2 Br \left( \frac{\partial \psi}{\partial y} \cos \chi \right)^2 = 0, \tag{5.37}$$

$$\frac{\partial^2 \phi}{\partial y^2} + \frac{Nt}{Nb} \frac{\partial^2 \theta}{\partial y^2} = 0, \tag{5.38}$$

$$S_{xx} = 0 = S_{yy}, \tag{5.39}$$

$$S_{xy} = (1 + We \dot{\gamma}) \frac{\partial^2 \psi}{\partial y^2}, \tag{5.40}$$

$$\dot{\gamma} = \frac{\partial^2 \psi}{\partial y^2}. \quad (5.41)$$

$$\frac{\partial \psi}{\partial y} \pm \xi_1 S_{xy} = 0, \quad \text{at } y = \pm \eta = \pm(1 + \varepsilon \sin 2\pi(x - t)), \quad (5.42)$$

$$\left[ E_1 \frac{\partial^3}{\partial x^3} + E_2 \frac{\partial^3}{\partial x \partial t^2} + E_3 \frac{\partial^2}{\partial t \partial x} \right] \eta = \frac{\partial S_{xy}}{\partial y} - M^2 \cos^2 \chi \frac{\partial \psi}{\partial y}, \quad \text{at } y = \pm \eta, \quad (5.43)$$

$$\theta \pm \xi_2 \frac{\partial \theta}{\partial y} = \begin{Bmatrix} 1 \\ 0 \end{Bmatrix} \quad \text{at } y = \pm \eta, \quad (5.44)$$

$$\phi \pm \xi_3 \frac{\partial \phi}{\partial y} = \begin{Bmatrix} 1 \\ 0 \end{Bmatrix} \quad \text{at } y = \pm \eta. \quad (5.45)$$

From Eqs. (5.35) and (5.36) we get

$$\frac{\partial}{\partial y} \left[ \frac{\partial S_{xy}}{\partial y} - M^2 \cos^2 \chi \frac{\partial \psi}{\partial y} \right] = 0. \quad (5.46)$$

Now we numerically solve the Eqs. (5.37), (5.38) and (5.46) by utilizing the boundary conditions mentioned in Eqs. (5.42-5.45). NDSolve of Mathematica is utilized for this purpose. The results are analyzed numerically.

### 5.2.1 Determination of Entropy generation

Viscous dissipation expression is

$$\Phi = S_{xx} \frac{\partial u}{\partial x} + S_{yy} \frac{\partial v}{\partial y} + S_{xy} \left( \frac{\partial u}{\partial y} + \frac{\partial v}{\partial x} \right). \quad (5.47)$$

Dimensional volumetric entropy generation is

$$\begin{aligned} S_{gen}''' = & \underbrace{\frac{\kappa}{T_m^2} \left( \left( \frac{\partial T}{\partial x} \right)^2 + \left( \frac{\partial T}{\partial y} \right)^2 \right)}_{\text{Thermal irreversibility}} + \underbrace{\frac{\sigma B_0^2 (u \cos \chi - v \sin \chi)^2}{T_m}}_{\text{Joule friction irreversibility}} + \underbrace{\frac{\Phi}{T_m}}_{\text{Fluid friction irreversibility}} \\ & + \underbrace{\frac{RD}{C_m} \left( \left( \frac{\partial C}{\partial x} \right)^2 + \left( \frac{\partial C}{\partial y} \right)^2 \right) + \frac{RD}{T_m} \left( \frac{\partial C}{\partial x} \frac{\partial T}{\partial x} + \frac{\partial C}{\partial y} \frac{\partial T}{\partial y} \right)}_{\text{Diffusion irreversibility}} \end{aligned} \quad (5.48)$$

In dimensionless form one has

$$\begin{aligned}
N_s = \frac{S_{gen}'''}{S_G'''} &= \left(\frac{\partial\theta}{\partial y}\right)^2 + \frac{BrM^2}{\Lambda} \left(\frac{\partial\psi}{\partial y} \cos\chi\right)^2 + \frac{Br}{\Lambda} S_{xy} \left(\frac{\partial^2\psi}{\partial y^2}\right) \\
&+ \frac{L}{\Lambda} \left(\frac{\partial\theta}{\partial y}\right) \left(\frac{\partial\phi}{\partial y}\right) + \frac{L\zeta}{\Lambda^2} \left(\frac{\partial\phi}{\partial y}\right)^2,
\end{aligned} \tag{5.49}$$

with

$$S_G''' = \frac{\kappa(T_1 - T_0)^2}{T_m^2 d^2}, \quad \Lambda = \frac{T_1 - T_0}{T_m}, \quad L = \frac{RD(C_1 - C_0)}{\kappa}, \quad \zeta = \frac{(C_1 - C_0)}{C_m}. \tag{5.50}$$

### 5.3 Analysis

Here the velocity, temperature, concentration, heat transfer coefficient and entropy are examined via graphs for influence of different parameters. Problem is solved by using NDSolve of Mathematica. For detail analysis of the results we further divide this section into subsections.

#### 5.3.1 Velocity

This subsection intends to analyze the velocity. Fig. 5.2 (a) has been plotted for Hartman number ( $M$ ) effect. Here decreasing behavior of axial velocity by larger Hartman number is notified. Such behavior of velocity under the influence of Hartman number is because of resistive characteristic of Lorentz force. Fig. 5.2 (b) elucidated the influence of slip parameter on velocity. We have noticed that increasing behavior is seen for velocity against slip parameter. It is due to less resistance offered by fluid to flow. Fig. 5.2 (c) has been drawn to see the behavior of wall parameters. Enhancement in elastance parameters  $E_1$  and  $E_2$  give rise to velocity. It is because of decrease in resistance by increasing wall elastance parameters. An enhancement in wall damping coefficient  $E_3$  decreases velocity of fluid. Behavior of inclination of magnetic field  $\chi$  on velocity is observed through Fig. 5.2 (d). Increasing behavior has been noticed for velocity by larger  $\chi$ . Effect of Weissenberg number on axial velocity is analyzed in Fig. 5.2 (e). Weissenberg number for velocity has mixed behavior.

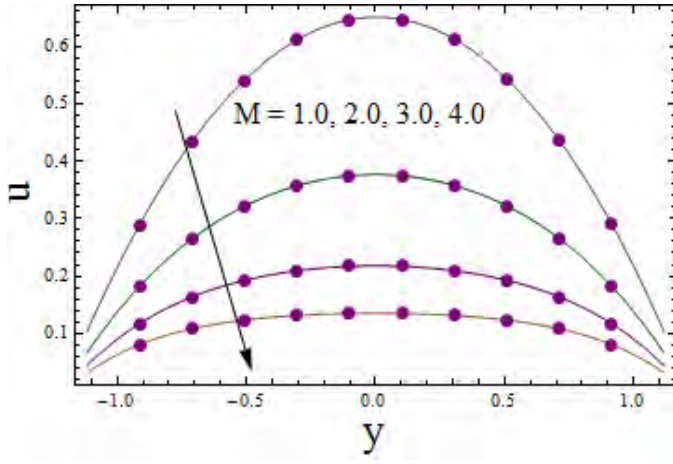


Fig. 5.2 (a)

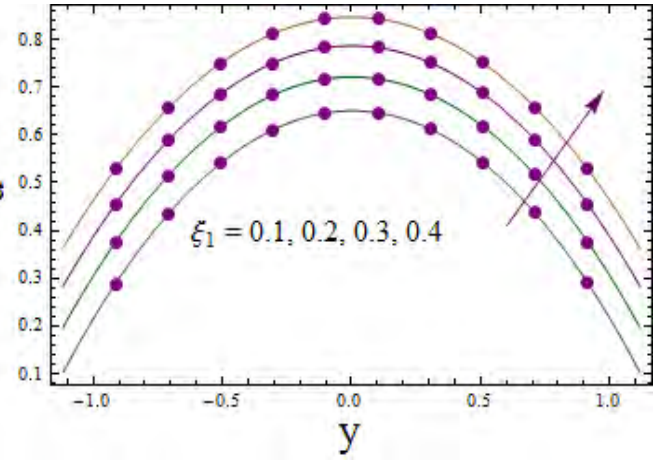


Fig. 5.2 (b)

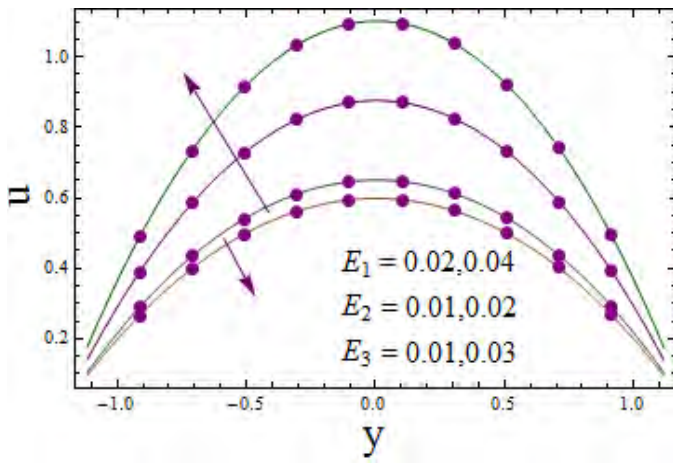


Fig. 5.2 (c)

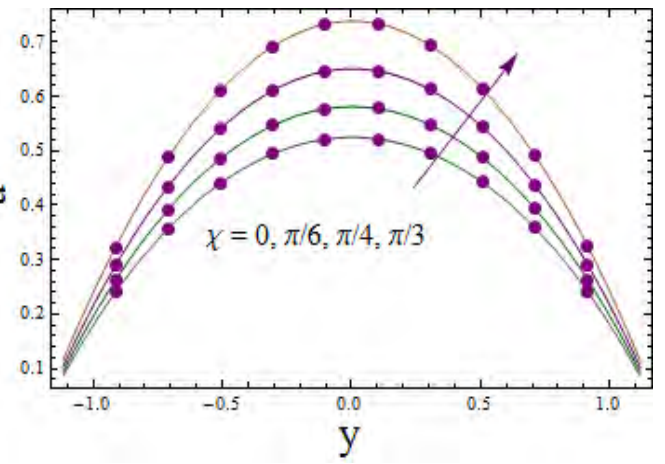


Fig. 5.2 (d)

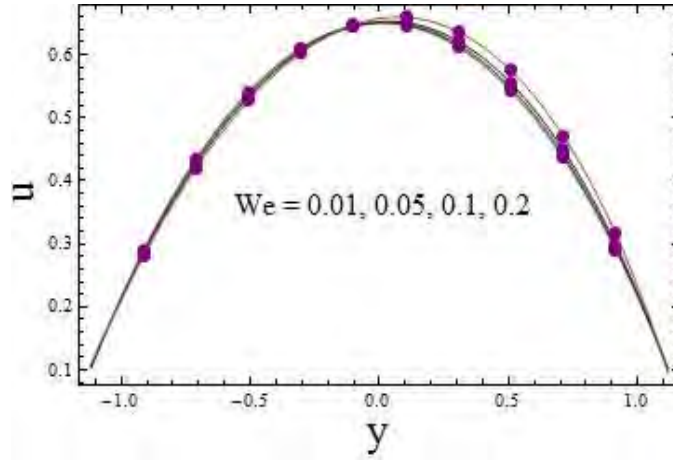


Fig. 5.2 (e)

*Fig. 5.2.* Graphs for  $u$  when  $E_1 = 0.02$ ,  $E_2 = 0.01$ ,  $E_3 = 0.01$ ,  $t = 0.1$ ,  $x = 0.2$ ,  $\varepsilon = 0.2$ ,  $We = 0.01$ ,  $\xi_1 = 0.1$ ,  $\xi_2 = 0.1$ ,  $\xi_3 = 0.1$ ,  $Nt = 0.1$ ,  $Nb = 0.1$ ,  $Pr = 1.5$ ,  $Br = 2.0$ ,  $M = 1.0$ ,  $\chi = \pi/4$ . (a)  $M$  impact on  $u$  (b)  $\xi_1$  impact on  $u$  (c)  $E_1, E_2, E_3$  impact on  $u$  (d)  $\chi$  impact on  $u$  (e)  $We$  impact on  $u$

### 5.3.2 Temperature

This subsection examined temperature for slip parameter ( $\xi_2$ ), Hartman number ( $M$ ), Brownian motion ( $Nb$ ), thermophoresis parameter ( $Nt$ ) and magnetic field inclination parameter ( $\chi$ ) on the temperature distribution. Fig. 5.3 (a) characterized temperature for Hartman number. An enhancement in temperature is observed at center of channel for larger Hartman number. An increase in temperature is caused by Joule heating phenomenon. Fig. 5.3 (b) has been prepared just to view the effect of thermal slip parameter on temperature. Enhancement is seen in temperature by larger slip parameter. The reason can be directly linked with velocity. Influences of Brownian motion and thermophoresis parameters have been studied through Figs. 5.3 (c) and (d). Temperature is an increasing function of both parameters. As increase in random motion of particles enhances the mean kinetic energy of the particles and consequently the temperature. Impact of magnetic field inclination angle  $\chi$  on temperature has been observed via Fig. 5.3 (e). Temperature is enhanced by  $\chi$ . Obviously magnetic field perpendicular to flow

is more effective and it caused more resistance to fluid, here increases the temperature.

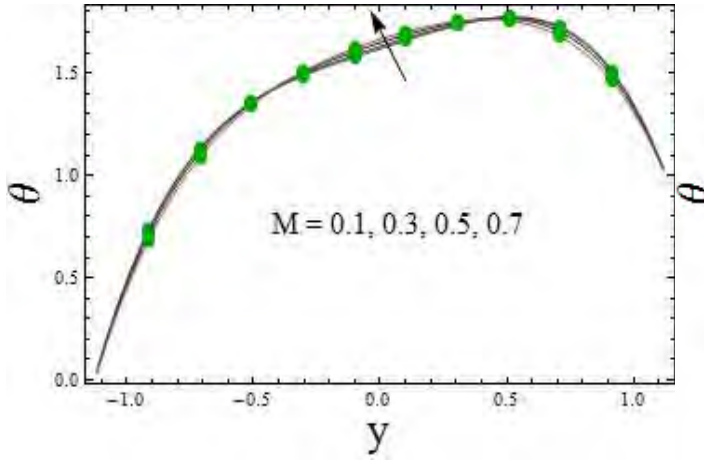


Fig. 5.3 (a)

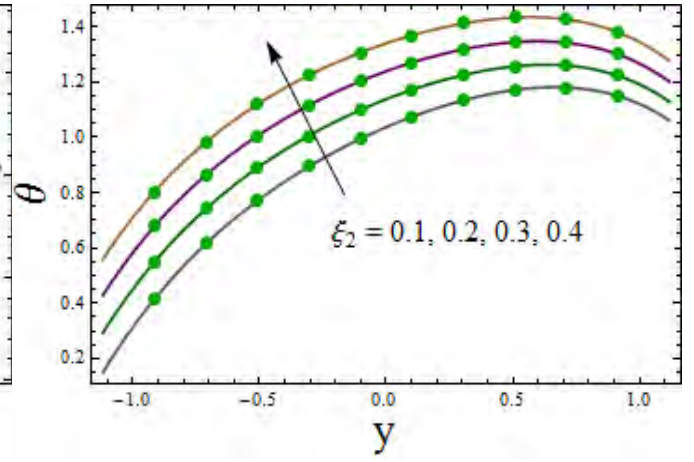


Fig. 5.3 (b)

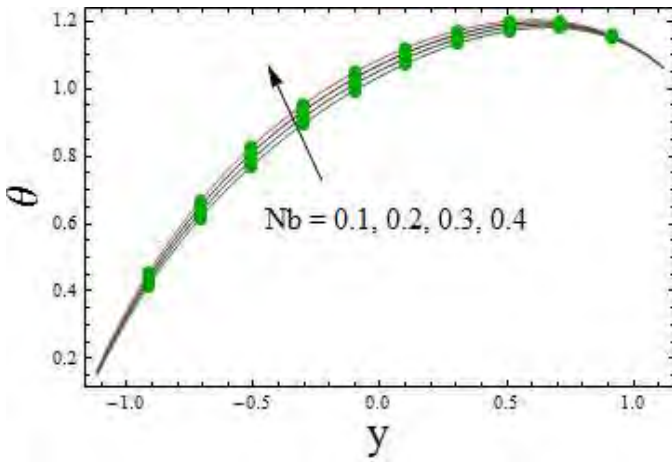


Fig. 5.3 (c)

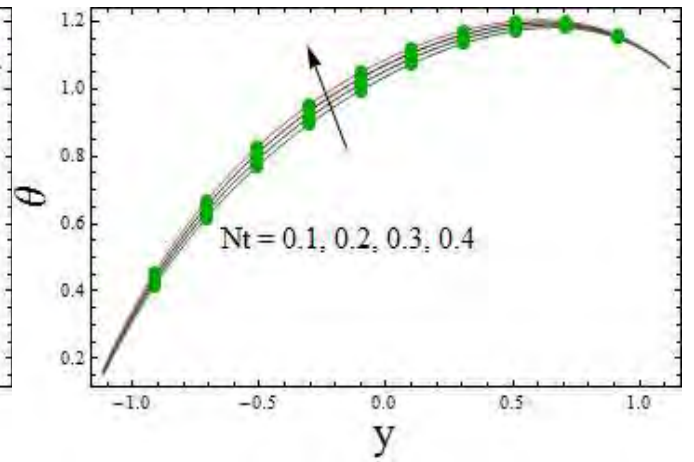


Fig. 5.3 (d)



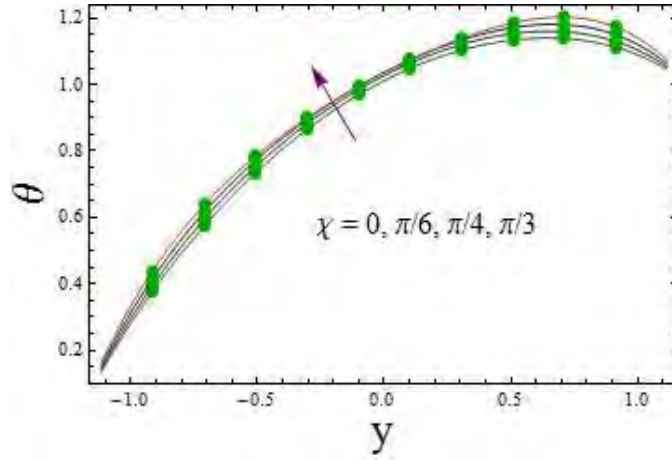


Fig. 5.3 (e)

*Fig. 5.3.* Graphs for  $\theta$  when  $E_1 = 0.02$ ,  $E_2 = 0.01$ ,  $E_3 = 0.01$ ,  $t = 0.1$ ,  $x = 0.2$ ,  $\varepsilon = 0.2$ ,  $We = 0.01$ ,  $\xi_1 = 0.1$ ,  $\xi_2 = 0.1$ ,  $\xi_3 = 0.1$ ,  $Nt = 0.1$ ,  $Nb = 0.1$ ,  $Pr = 1.5$ ,  $M = 1.0$ ,  $Br = 2.0$ ,  $\chi = \pi/4$ . (a)  $M$  impact on  $\theta$  (b)  $\xi_2$  impact on  $\theta$  (c)  $Nb$  impact on  $\theta$  (d)  $Nt$  impact on  $\theta$  (e)  $\chi$  impact on  $\theta$

### 5.3.3 Concentration

Here concentration is examined with respect to various influential parameters. Fig. 5.4 (a) displayed concentration for Hartman number. Clearly concentration is an increasing function of Hartman number. Increase in concentration slip parameter decreases concentration (see Fig. 5.4 (b)). Figs. 5.4 (c) and (d) elucidated effects of Brownian motion and thermophoresis on concentration. Concentration has opposite behavior for these both parameters. An inverse relation of these parameters has been observed in the concentration expression.

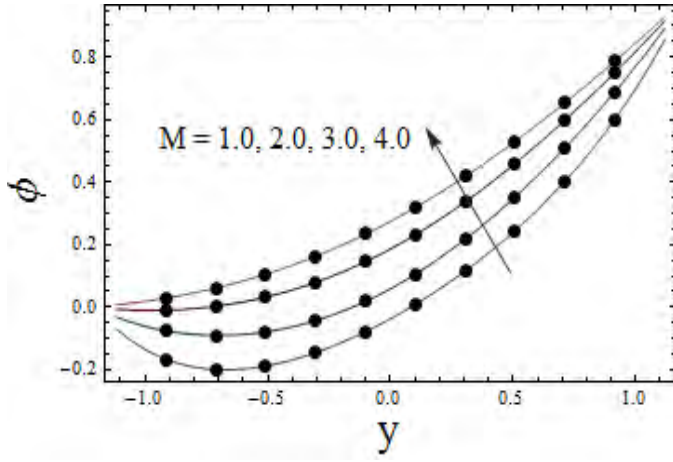


Fig. 5.4 (a)

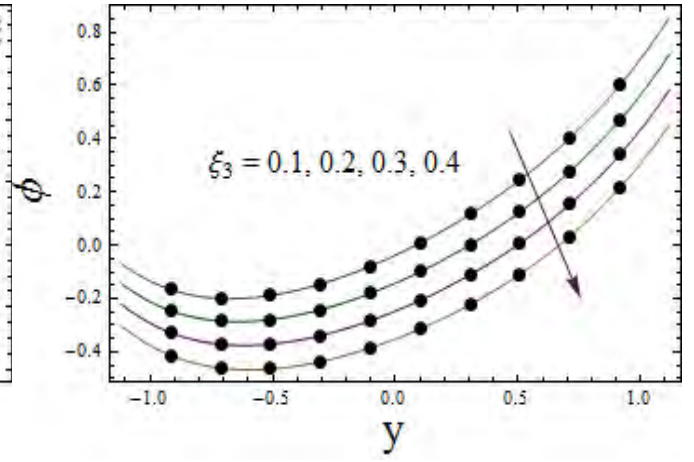


Fig. 5.4 (b)

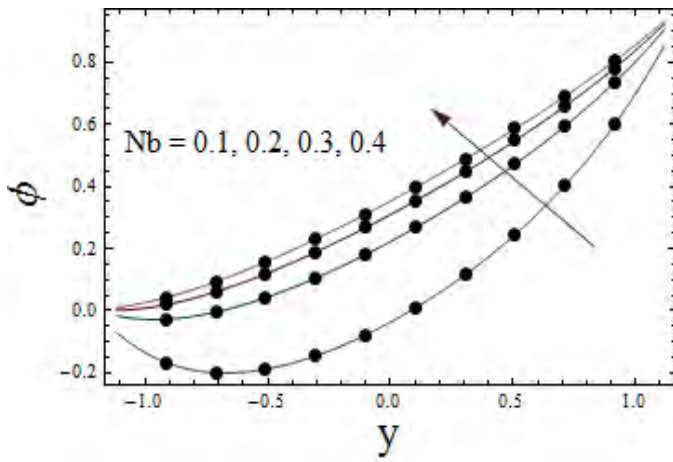


Fig. 5.4 (c)

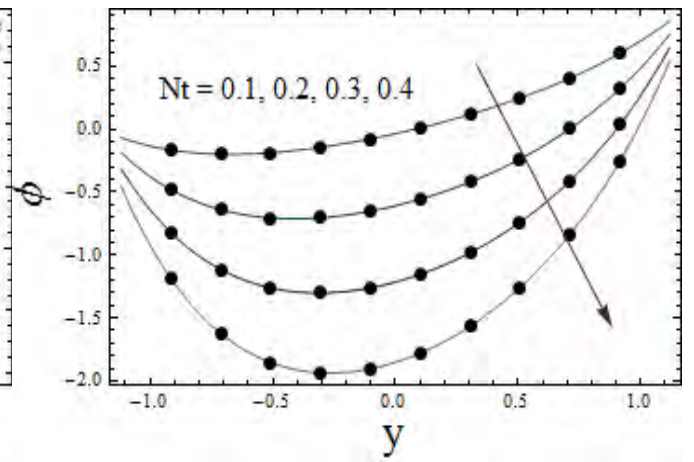


Fig. 5.4 (d)

Fig. 5.4. Graphs for  $\phi$  when  $E_1 = 0.02$ ,  $E_2 = 0.01$ ,  $E_3 = 0.01$ ,  $t = 0.1$ ,  $x = 0.2$ ,  $\varepsilon = 0.2$ ,  $We = 0.01$ ,  $\beta = 0.1$ ,  $\xi_1 = 0.1$ ,  $\xi_2 = 0.1$ ,  $\xi_3 = 0.1$ ,  $Nt = 0.1$ ,  $Nb = 0.1$ ,  $Pr = 1.5$ ,  $Br = 2.0$ ,  $M = 1.0$ ,  $\chi = \pi/4$ . (a)  $M$  impact on  $\phi$  (b)  $\xi_3$  impact on  $\phi$  (c)  $Nb$  impact on  $\phi$  (d)  $Nt$  impact on  $\phi$

### 5.3.4 Heat transfer coefficient

This subsection has been organized for the description of outcomes of various parameters on heat transfer coefficient ( $Z$ ). Impact of Hartman number on  $Z$  is shown in Fig. 5.5 (a). There is a decrease in  $Z$  for larger  $M$ . Further an increase in  $\chi$  leads to an enhancement of  $Z$ . (see Fig. 5.5 (b)). Furthermore through Figs. 5.5 (c) and (d) the heat transfer coefficient via change in  $Nb$  and  $Nt$  has been analyzed. Opposite behavior of heat transfer coefficient through these parameters is observed. These Figs. witness for an oscillatory behavior.

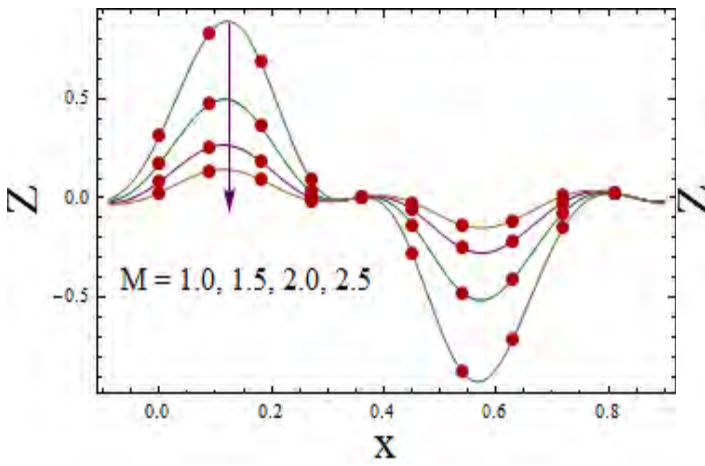


Fig. 5.5 (a)

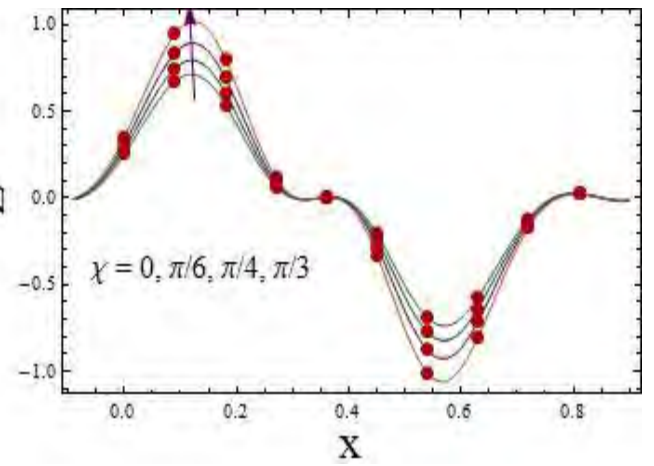


Fig. 5.5 (b)

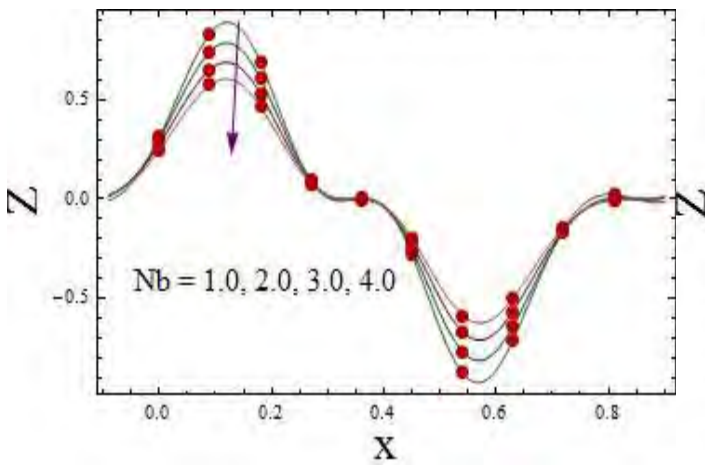


Fig. 5.5 (c)

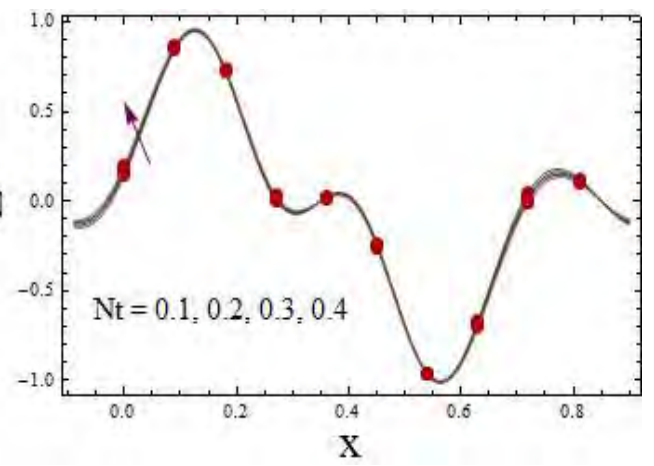


Fig. 5.5 (d)

Fig. 5.5. Graphs for  $Z$  when  $E_1 = 0.02$ ,  $E_2 = 0.01$ ,  $E_3 = 0.01$ ,  $t = 0.1$ ,  $\varepsilon = 0.2$ ,  $We = 0.01$ ,  $\xi_1 = 0.1$ ,  $\xi_2 = 0.1$ ,  $\xi_3 = 0.1$ ,  $Nt = 1.0$ ,  $Nb = 1.0$ ,  $Pr = 1.5$ ,  $Br = 2.0$ ,  $M = 1.0$ ,  $\chi = \pi/4$ . (a)  $M$  impact on  $Z$  (b)  $\chi$  impact on  $Z$  (c)  $Nb$  impact on  $Z$  (d)  $Nt$  impact on  $Z$

### 5.3.5 Entropy generation

This subsection has been prepared to analyze the entropy generation. Thus Figs. 5.6 (a-c) have been plotted for this purpose. Fig. 5.6 (a) described the influence of Hartman number ( $M$ ) on  $Ns$ . It is worth mentioning that  $Ns$  is an increasing function of  $M$ . It is in view of Joule heating aspect. Brownian motion ( $Nb$ ) and thermophoresis impacts have been seen via Figs. 5.6 (b) and (c). Increasing results are noticed for both variables. These results can be verified in view of directly linked with temperature.

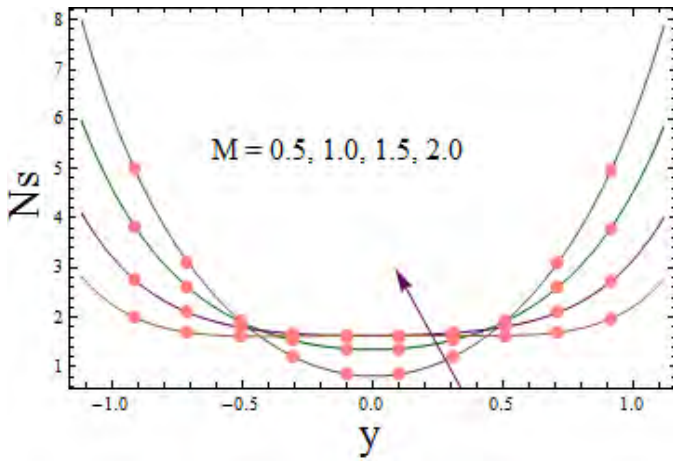


Fig. 5.6 (a)

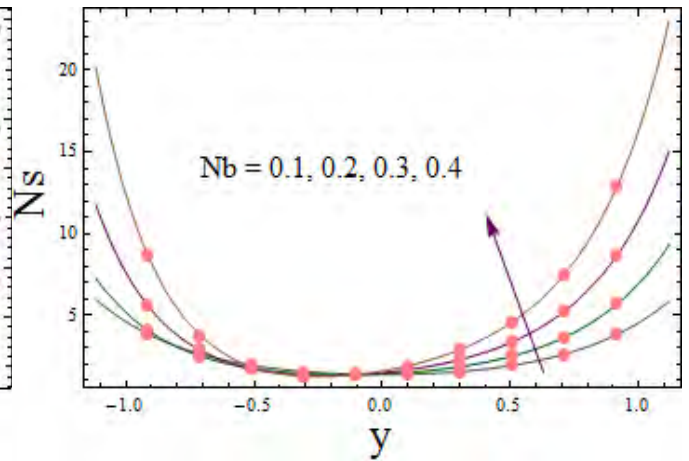


Fig. 5.6 (b)

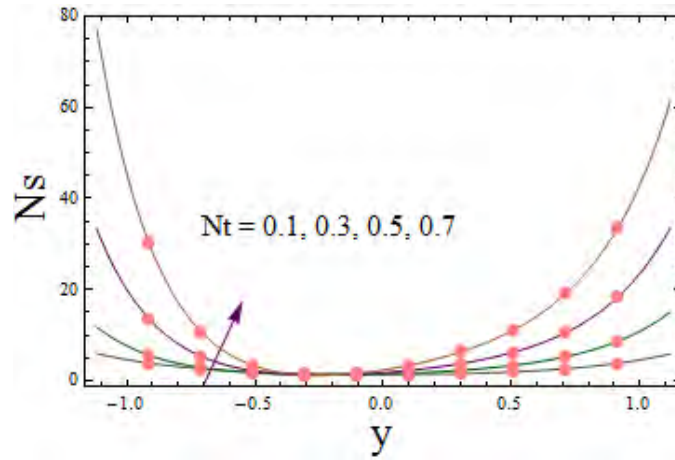


Fig. 5.6 (c)

Fig. 5.6. Graphs for  $Ns$  when  $E_1 = 0.02$ ,  $E_2 = 0.01$ ,  $E_3 = 0.01$ ,  $t = 0.1$ ,  $x = 0.2$ ,  $\varepsilon = 0.2$ ,  $We = 0.01$ ,  $\xi_1 = 0.1$ ,  $\xi_2 = 0.1$ ,  $\xi_3 = 0.1$ ,  $Nb = 0.1$ ,  $Nt = 0.1$ ,  $Br = 2.0$ ,  $L = 0.5$ ,  $\zeta = 0.5$ ,  $\Lambda = 0.5$ ,  $M = 1.0$ ,  $Pr = 1.5$ ,  $\chi = \pi/4$ . (a)  $M$  impact on  $Ns$  (b)  $Nb$  impact on  $Ns$  (c)  $Nt$  impact on  $Ns$

### 5.3.6 Validation of problem

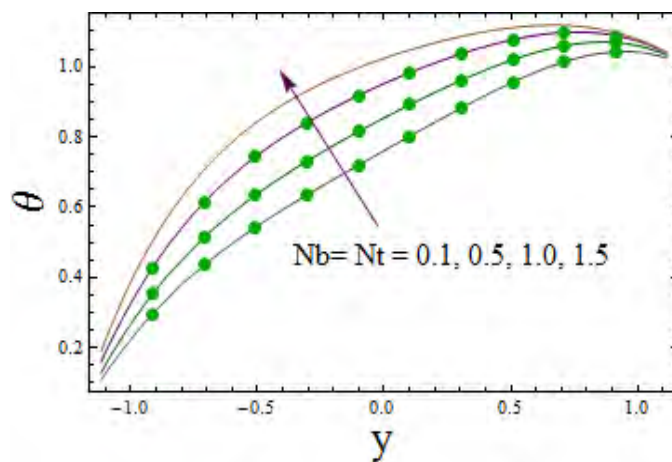


Fig. 5.7: Validation of the problem

*Fig. 5.7.*  $\theta$  via change in  $Nb$  and  $Nt$  when  $E_1 = 0.01$ ,  $E_2 = 0.02$ ,  $E_3 = 0.01$ ,  $t = 0.1$ ,  $x = 0.2$ ,  $\varepsilon = 0.2$ ,  $We = 0.0$ ,  $\xi_1 = 0.1$ ,  $\xi_2 = 0.1$ ,  $\xi_3 = 0.1$ ,  $Pr = 1.0$ ,  $Br = 1.0$ ,  $M = 0.0$ ,  $\chi = 0.0$ .

The purpose of Fig. 5.7 is to validate our results. Here we have chosen a study by Mustafa et al. [170]. The authors here have studied the nanofluid flow through Buongiorno model. They have utilized the homotopy analysis method to solve their proposed problem. In our problem if we exclude the inclined magnetic field and replace the Williamson fluid by viscous fluid we obtained the results of paper [170].

## 5.4 Conclusions

Major findings here include the following.

- Velocity is decreasing function of Hartman number and wall damping coefficient ( $E_3$ ) whereas it is increasing function of  $E_1$ ,  $E_2$  and velocity slip parameter.
- $Nb$  and  $Nt$  has same behavior on temperature.
- Temperature has same behavior for larger thermal slip parameter and Hartman number ( $M$ ).
- Concentration has opposite behavior for concentration slip parameter when compared with Hartman number ( $M$ ).
- Heat transfer coefficient for inclination angle for magnetic field has opposite response to that of Hartman number ( $M$ ).
- $Nb$  and  $Nt$  have opposite behavior on heat transfer coefficient.

## Chapter 6

# Effects of radial magnetic field and entropy on peristalsis of Williamson fluid in curved channel

### 6.1 Introduction

This chapter aims to analyze the peristaltic activity of Williamson fluid in curved configuration. Flow formulation is made by employing radial magnetic field and Soret and Dufour effects. Slip conditions for velocity, temperature and concentration are applied. Entropy analysis is also carried out. Modeling is given using lubrication approach. Stream function, velocity, temperature and concentration solutions have been derived. Effects of different parameters are analyzed on flow quantities of interest. Moreover streamlines are examined for different embedded parameters. Result reveals that Lorentz force tends to slow down the fluid velocity. The slip parameters for velocity and temperature lead to enhancement in corresponding profile whereas opposite behavior is noticed for concentration. Soret and Dufour effect lead to increase the temperature as well as entropy of the system. Compliant nature walls increase the fluid velocity for elastance parameters where as damping nature reduces the fluid velocity.

## 6.2 Modeling

Consider a curved configuration having channel width  $2d$ , which is coiled in a circle with centre at  $O$  and has radius  $R^*$  (see Fig. 6.1). An incompressible electrically conducting Williamson fluid in channel is taken. Walls of the channel are considered flexible. In radial direction a magnetic field is applied whose strength is taken  $B_0$ . Coordinate system has been taken such as that both  $x$ -axis and  $r$ -axis lie normal to each other.  $u(r, x, t)$  and  $v(r, x, t)$  are the respective axial and radial velocity components. The walls shape satisfies the following expression [50]

$$r = \pm \eta(x, t) = \pm \left[ d + a \sin \frac{2\pi}{\lambda} (x - ct) \right], \quad (6.1)$$

in which  $a$ ,  $\lambda$  and  $c$  elucidate the respective amplitude, wavelength and speed of the wave and  $t$  denotes the time.

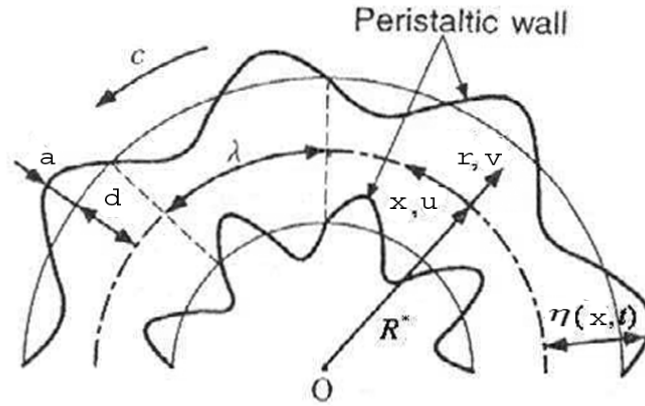


Fig. 6.1: Sketch of the geometry

The applied magnetic field can be expressed as follows [84]:

$$\mathbf{B} = \left[ \frac{R^* B_0}{r + R^*}, 0, 0 \right], \quad (6.2)$$



where  $B_0$  represents the magnetic field strength. The Lorentz force ( $\mathbf{F} = \mathbf{J} \times \mathbf{B}$ ) yields [50]

$$\mathbf{J} \times \mathbf{B} = \left[ 0, -\frac{\sigma(R^*)^2 B_0^2 u}{(r + R^*)^2}, 0 \right]. \quad (6.3)$$

Here  $\sigma$  and  $\mathbf{J}(=\sigma(\mathbf{V} \times \mathbf{B}))$  are used to describe the electrical conductivity and current density of the fluid. The continuity equation and components of velocity satisfy [50, 84]

$$\frac{\partial[(r + R^*)v]}{\partial r} + R^* \frac{\partial u}{\partial x} = 0, \quad (6.4)$$

$$\begin{aligned} \rho \left[ \frac{\partial v}{\partial t} + v \frac{\partial v}{\partial r} + \frac{uR^*}{r + R^*} \frac{\partial v}{\partial x} - \frac{u^2}{r + R^*} \right] &= -\frac{\partial p}{\partial r} + \frac{1}{r + R^*} \frac{\partial}{\partial r} \{(r + R^*)S_{rr}\} \\ &+ \frac{R^*}{r + R^*} \frac{\partial S_{xr}}{\partial x} - \frac{S_{xx}}{r + R^*}, \end{aligned} \quad (6.5)$$

$$\begin{aligned} \rho \left[ \frac{\partial u}{\partial t} + v \frac{\partial u}{\partial r} + \frac{uR^*}{r + R^*} \frac{\partial u}{\partial x} + \frac{uv}{r + R^*} \right] &= -\frac{R^*}{r + R^*} \frac{\partial p}{\partial x} + \frac{1}{(r + R^*)^2} \frac{\partial}{\partial r} \{(r + R^*)^2 S_{rx}\} \\ &+ \frac{R^*}{r + R^*} \frac{\partial S_{xx}}{\partial x} - \frac{\sigma(R^*)^2 B_0^2 u}{(r + R^*)^2}, \end{aligned} \quad (6.6)$$

where  $p$  is the pressure,  $S_{ij}$  are the component of extra stress tensor and  $\rho$  the fluid density.

The temperature and concentration equations with Soret and Dufour effects become [84, 189]:

$$\begin{aligned} \rho C_p \left[ \frac{\partial T}{\partial t} + v \frac{\partial T}{\partial r} + \frac{uR^*}{r + R^*} \frac{\partial T}{\partial x} \right] &= S_{xr} \left( \frac{\partial u}{\partial r} + \frac{R^*}{r + R^*} \frac{\partial v}{\partial x} - \frac{u}{r + R^*} \right) + \\ &(S_{rr} - S_{xx}) \frac{\partial v}{\partial r} + \left( \frac{R^*}{r + R^*} \right)^2 \sigma B_0^2 u^2 + \\ &\kappa \left[ \frac{\partial^2 T}{\partial r^2} + \frac{1}{r + R^*} \frac{\partial T}{\partial r} + \left( \frac{R^*}{r + R^*} \right)^2 \frac{\partial^2 T}{\partial x^2} \right] \\ &+ \frac{DK_T}{C_s} \left( \frac{\partial^2 C}{\partial r^2} + \frac{1}{r + R^*} \frac{\partial C}{\partial r} + \left( \frac{R^*}{r + R^*} \right)^2 \frac{\partial^2 C}{\partial x^2} \right) \end{aligned} \quad (6.7)$$

$$\frac{\partial C}{\partial t} + v \frac{\partial C}{\partial r} + \frac{uR^*}{r+R^*} \frac{\partial C}{\partial x} = D \left( \frac{\partial^2 C}{\partial r^2} + \frac{1}{r+R^*} \frac{\partial C}{\partial r} + \left( \frac{R^*}{r+R^*} \right)^2 \frac{\partial^2 C}{\partial x^2} \right) + \frac{DK_T}{T_m} \left( \frac{\partial^2 T}{\partial r^2} + \frac{1}{r+R^*} \frac{\partial T}{\partial r} + \left( \frac{R^*}{r+R^*} \right)^2 \frac{\partial^2 T}{\partial x^2} \right), \quad (6.8)$$

in which  $C_p$  is the specific heat,  $\kappa$  denotes the thermal conductivity and  $D$ ,  $K_T$ ,  $C_s$  and  $T_m$  represent the respective mass diffusivity, thermal diffusion ratio, concentration susceptibility and mean temperature of fluid. Here symbols  $T$  and  $C$  are used to define the temperature and concentration of the considered fluid respectively.

Williamson fluid extra stress tensor is [84]

$$\mathbf{S} = [\mu_\infty + (\mu_0 + \mu_\infty)(1 - \Gamma\dot{\gamma})^{-1}] \mathbf{A}_1, \quad (6.9)$$

where  $\mu_0$  and  $\mu_\infty$  are the zero shear rate and infinite shear rate viscosities and  $\Gamma$  denotes the time constant. Further  $\dot{\gamma}$  and  $\mathbf{A}_1$  are defined below [84]:

$$\dot{\gamma} = \sqrt{\frac{1}{2}\Pi}, \quad (6.10)$$

$$\mathbf{A}_1 = \text{grad } \mathbf{V} + (\text{grad } \mathbf{V})^T, \quad (6.11)$$

$$\Pi = \text{tr}(\mathbf{A}_1^2). \quad (6.12)$$

By taking  $\mu_\infty = 0$  and  $\Gamma\dot{\gamma} < 1$ , the extra stress tensor yields [84]

$$\mathbf{S} = \mu_0[(1 + \Gamma\dot{\gamma})] \mathbf{A}_1. \quad (6.13)$$

Notice that  $\Gamma = 0$  shows the case of viscous fluid. In component form the above expression gives [84]

$$S_{rx} = \mu_0(1 + \Gamma\dot{\gamma}) \left( \frac{R^*}{r+R^*} \frac{\partial v}{\partial x} - \frac{u}{r+R^*} + \frac{\partial u}{\partial r} \right), \quad (6.14)$$

$$S_{xx} = 2\mu_0(1 + \Gamma\dot{\gamma}) \left( \frac{v}{r+R^*} + \frac{R^*}{r+R^*} \frac{\partial u}{\partial x} \right), \quad (6.15)$$

$$S_{rr} = 2\mu_0(1 + \Gamma\dot{\gamma}) \frac{\partial v}{\partial r}, \quad (6.16)$$

$$\dot{\gamma} = \sqrt{2 \left( \frac{\partial v}{\partial r} \right)^2 + 2 \left( \frac{v}{r+R^*} + \frac{R^*}{r+R^*} \frac{\partial u}{\partial x} \right)^2 + \left( \frac{R^*}{r+R^*} \frac{\partial v}{\partial x} - \frac{u}{r+R^*} + \frac{\partial u}{\partial r} \right)^2}. \quad (6.17)$$

The boundary conditions for the analysis are [198]

$$u \pm \xi_1 S_{rx} = 0 \quad \text{at } r = \pm\eta, \quad (6.18)$$

$$\begin{aligned} R^* \left[ -\tau^* \frac{\partial^3}{\partial x^3} + m^* \frac{\partial^3}{\partial x \partial t^2} + d_1^* \frac{\partial^2}{\partial t \partial x} \right] \eta &= \frac{1}{r+R^*} \frac{\partial}{\partial r} \{ (r+R^*)^2 S_{rx} \} + R^* \frac{\partial S_{xx}}{\partial x} \\ &\quad - \rho(r+R^*) \left[ \frac{\partial u}{\partial t} + v \frac{\partial u}{\partial r} + \frac{uR^*}{r+R^*} \frac{\partial u}{\partial x} + \frac{uv}{r+R^*} \right] \\ &\quad - \frac{\sigma(R^*)^2 B_0^2 u}{(r+R^*)}, \quad r = \pm\eta, \end{aligned} \quad (6.19)$$

$$T \pm \xi_2 \frac{\partial T}{\partial r} = \begin{Bmatrix} T_1 \\ T_0 \end{Bmatrix} \quad \text{at } r = \pm\eta, \quad (6.20)$$

$$C \pm \xi_3 \frac{\partial C}{\partial r} = \begin{Bmatrix} C_1 \\ C_0 \end{Bmatrix} \quad \text{at } r = \pm\eta. \quad (6.21)$$

Here  $p$  is the pressure,  $R^*$  shows the curvature parameter,  $\tau^*$ ,  $d_1^*$ , and  $m^*$  describe the respective elastic tension, coefficient of viscous damping and mass per unit area whereas the extra stress tensor  $\mathbf{S}$  components are denoted by  $S_{rr}$ ,  $S_{rx}$  and  $S_{xx}$ . Moreover  $\xi_1$ ,  $\xi_2$ , and  $\xi_3$  are the slip parameters for velocity, temperature and concentration respectively. Temperature and concentration at the upper and lower walls of the channel are  $T_1$ ,  $T_0$  and  $C_1$ ,  $C_0$  respectively.

Dimensionless quantities are mentioned below:

$$\begin{aligned} x^* &= \frac{x}{\lambda}, \quad r^* = \frac{r}{d}, \quad u^* = \frac{u}{c}, \quad v^* = \frac{v}{c}, \quad t^* = \frac{ct}{\lambda}, \quad \eta^* = \frac{\eta}{d}, \\ S_{ij}^* &= \frac{dS_{ij}}{c\mu_0}, \quad k = \frac{R^*}{d}, \quad \dot{\gamma}^* = \dot{\gamma} \frac{d}{c}, \quad p^* = \frac{d^2 p}{c\lambda\mu_0}, \quad We = \Gamma \frac{c}{d}, \\ \theta &= \frac{T - T_0}{T_1 - T_0}, \quad \phi = \frac{C - C_0}{C_1 - C_0}. \end{aligned} \quad (6.22)$$

Using the dimensionless quantities Eqs. (6.5-6.8) and (6.14-6.21) take the forms

$$\text{Re } \delta \left[ \delta \frac{\partial v}{\partial t} + v \frac{\partial v}{\partial r} + \frac{\delta k u}{r+k} \frac{\partial v}{\partial x} - \frac{u^2}{r+k} \right] = -\frac{\partial p}{\partial r} + \delta \left[ \frac{1}{r+k} \frac{\partial}{\partial r} \{ (r+k) S_{rr} \} + \frac{k \delta}{r+k} \frac{\partial S_{xr}}{\partial x} - \frac{S_{xx}}{r+k} \right], \quad (6.23)$$

$$\begin{aligned} \text{Re} \left[ \delta \frac{\partial u}{\partial t} + v \frac{\partial u}{\partial r} + \frac{\delta k u}{r+k} \frac{\partial u}{\partial x} + \frac{uv}{r+k} \right] &= -\frac{k^2}{(r+k)^2} M^2 u - \frac{k}{r+k} \frac{\partial p}{\partial x} \\ + \frac{1}{(r+k)^2} \frac{\partial}{\partial r} \{ (r+k)^2 S_{rx} \} + \frac{k \delta}{r+k} \frac{\partial S_{xx}}{\partial x} &, \end{aligned} \quad (6.24)$$

$$\begin{aligned} \text{Re Pr} \left[ \delta \frac{\partial \theta}{\partial t} + v \frac{\partial \theta}{\partial r} + \frac{uk \delta}{r+k} \frac{\partial \theta}{\partial x} \right] &= \left( \frac{k}{r+k} \right)^2 M^2 Br u^2 + Br \left[ \begin{aligned} &(S_{rr} - S_{xx}) \frac{\partial v}{\partial r} + \\ &S_{xr} \left( \frac{\partial u}{\partial r} + \frac{k \delta}{r+k} \frac{\partial v}{\partial x} - \frac{u}{r+k} \right) \end{aligned} \right] + \\ &+ \left[ \frac{\partial^2 \theta}{\partial r^2} + \frac{1}{r+k} \frac{\partial \theta}{\partial r} + \delta^2 \left( \frac{k}{r+k} \right)^2 \frac{\partial^2 \theta}{\partial x^2} \right] \\ &+ Du \text{Pr} \left( \frac{\partial^2 \phi}{\partial r^2} + \frac{1}{r+k} \frac{\partial \phi}{\partial r} + \delta^2 \left( \frac{k}{r+k} \right)^2 \frac{\partial^2 \phi}{\partial x^2} \right), \end{aligned} \quad (6.25)$$

$$\begin{aligned} \text{Re} \left( \delta \frac{\partial \phi}{\partial t} + v \frac{\partial \phi}{\partial r} + \frac{uk \delta}{r+k} \frac{\partial \phi}{\partial x} \right) &= Sr \left( \frac{\partial^2 \theta}{\partial r^2} + \frac{1}{r+k} \frac{\partial \theta}{\partial r} + \delta^2 \left( \frac{k}{r+k} \right)^2 \frac{\partial^2 \theta}{\partial x^2} \right) + \\ &\frac{1}{Sc} \left( \frac{\partial^2 \phi}{\partial r^2} + \frac{1}{r+k} \frac{\partial \phi}{\partial r} + \delta^2 \left( \frac{k}{r+k} \right)^2 \frac{\partial^2 \phi}{\partial x^2} \right), \end{aligned} \quad (6.26)$$

$$S_{rx} = (1 + We \dot{\gamma}) \left( \delta \frac{\partial v}{\partial x} - \frac{u}{r+k} + \frac{\partial u}{\partial r} \right), \quad (6.27)$$

$$S_{rr} = 2(1 + We \dot{\gamma}) \frac{\partial v}{\partial r}, \quad (6.28)$$

$$S_{xx} = 2(1 + We \dot{\gamma}) \left( \frac{v}{r+k} + \frac{k}{r+k} \delta \frac{\partial u}{\partial x} \right), \quad (6.29)$$

where  $\dot{\gamma}$  in dimensionless form become

$$\dot{\gamma} = \sqrt{2 \left( \frac{\partial v}{\partial r} \right)^2 + 2 \left( \frac{v}{r+k} + \frac{k}{r+k} \delta \frac{\partial u}{\partial x} \right)^2 + \left( \frac{k}{r+k} \delta \frac{\partial v}{\partial x} - \frac{u}{r+k} + \frac{\partial u}{\partial r} \right)^2}. \quad (6.30)$$

The boundary conditions in non-dimensional form are

$$u \pm \xi_1 S_{rx} = 0, \quad \text{at } r = \pm\eta = \pm(1 + \varepsilon \sin 2\pi(x - t)), \quad (6.31)$$

$$\begin{aligned} k \left[ E_1 \frac{\partial^3}{\partial x^3} + E_2 \frac{\partial^3}{\partial x \partial t^2} + E_3 \frac{\partial^2}{\partial t \partial x} \right] \eta &= -\text{Re}(r + k) \left[ \delta \frac{\partial u}{\partial t} + v \frac{\partial u}{\partial r} + \frac{uk\delta}{r+k} \frac{\partial u}{\partial x} + \frac{uv}{r+k} \right] \\ &+ \frac{1}{r+k} \frac{\partial}{\partial r} \{ (r+k)^2 S_{rx} \} + \delta k \frac{\partial S_{xx}}{\partial x} \\ &- \frac{k^2}{r+k} M^2 u, \quad \text{at } r = \pm\eta, \end{aligned} \quad (6.32)$$

$$\theta \pm \xi_2 \frac{\partial \theta}{\partial r} = \begin{Bmatrix} 1 \\ 0 \end{Bmatrix} \quad \text{at } r = \pm\eta, \quad (6.33)$$

$$\phi \pm \xi_3 \frac{\partial \phi}{\partial r} = \begin{Bmatrix} 1 \\ 0 \end{Bmatrix} \quad \text{at } r = \pm\eta. \quad (6.34)$$

In above equations  $\varepsilon(= a/d)$  is the amplitude ratio,  $\text{Re}(= \rho cd/\mu_0)$  the Reynolds number,  $We$  the fluid parameter for Williamson fluid also named as Weissenberg number,  $\delta(= d/\lambda)$  the wave number,  $k$  the dimensionless curvature parameter,  $M = \sqrt{\sigma/\mu_0} B_0 d$  the Hartman number whereas expressions for Soret, Schmidt, Dufour, Brinkman and Prandtl numbers are given by  $Sr(= \rho DK_T(T_1 - T_0)/\mu_0 T_m(C_1 - C_0))$ ,  $Sc(= \mu_0/\rho D)$ ,  $Du(= DK_T(C_1 - C_0)/\mu_0 C_p C_s(T_1 - T_0))$ ,  $Br(= c^2 \mu_0/\kappa(T_1 - T_0))$ , and  $\text{Pr}(= \mu_0 C_p/\kappa)$  respectively. Moreover the non-dimensionalized form of elastance parameters are described by  $E_1(= -\tau^* d^3/\lambda^3 c \mu_0)$ ,  $E_2(= m^* c d^3/\lambda^3 \mu_0)$  and  $E_3(= d_1^* d^3/\lambda^2 \mu_0)$  respectively. The velocity, temperature and concentration slip parameters in dimensionless form are denoted by respective  $\xi_1$ ,  $\xi_2$  and  $\xi_3$  i.e.  $\xi_1^* = \xi_1 \mu_0/d$ ,  $\xi_2^* = \xi_2/d$ ,  $\xi_3^* = \xi_3/d$ , in which  $\xi_1$ ,  $\xi_2$ ,  $\xi_3$  are the dimensional slip parameters for the velocity, temperature and concentration. We have omitted the asterisks for brevity.

Using the expression given below:

$$u = -\frac{\partial \psi}{\partial r}, \quad v = \frac{\delta k}{r+k} \frac{\partial \psi}{\partial x}, \quad (6.35)$$

the continuity Eq. is identically satisfied and Eqs. (6.23-6.34) in view of lubrication approach

yields

$$\frac{\partial p}{\partial r} = 0, \quad (6.36)$$

$$-\frac{k}{r+k} \frac{\partial p}{\partial x} + \frac{1}{(r+k)^2} \frac{\partial}{\partial r} \{(r+k)^2 S_{rx}\} + \frac{k^2}{(r+k)^2} M^2 \frac{\partial \psi}{\partial r} = 0, \quad (6.37)$$

$$\frac{\partial^2 \theta}{\partial r^2} + \frac{1}{r+k} \frac{\partial \theta}{\partial r} + Br \left[ S_{xr} \left( -\psi_{rr} + \frac{\psi_r}{r+k} \right) \right] + \left( \frac{k}{r+k} \right)^2 M^2 Br \left( \frac{\partial \psi}{\partial r} \right)^2 + Du \text{Pr} \left( \frac{\partial^2 \phi}{\partial r^2} + \frac{1}{r+k} \frac{\partial \phi}{\partial r} \right) = 0, \quad (6.38)$$

$$\frac{\partial^2 \phi}{\partial r^2} + \frac{1}{r+k} \frac{\partial \phi}{\partial r} + SrSc \left( \frac{\partial^2 \theta}{\partial r^2} + \frac{1}{r+k} \frac{\partial \theta}{\partial r} \right) = 0, \quad (6.39)$$

$$\psi_r \pm \xi_1 S_{rx} = 0, \quad \text{at} \quad r = \pm \eta = \pm(1 + \varepsilon \sin 2\pi(x-t)), \quad (6.40)$$

$$k \left[ E_1 \frac{\partial^3}{\partial x^3} + E_2 \frac{\partial^3}{\partial x \partial t^2} + E_3 \frac{\partial^2}{\partial t \partial x} \right] \eta = \frac{1}{r+k} \frac{\partial}{\partial r} \{(r+k)^2 S_{rx}\} + \frac{k^2}{r+k} M^2 \frac{\partial \psi}{\partial r}, \quad \text{at} \quad r = \pm \eta, \quad (6.41)$$

$$\theta \pm \xi_2 \frac{\partial \theta}{\partial r} = \begin{Bmatrix} 1 \\ 0 \end{Bmatrix} \quad \text{at} \quad r = \pm \eta, \quad (6.42)$$

$$\phi \pm \xi_3 \frac{\partial \phi}{\partial r} = \begin{Bmatrix} 1 \\ 0 \end{Bmatrix} \quad \text{at} \quad r = \pm \eta, \quad (6.43)$$

$$S_{rr} = 0 = S_{xx}, \quad (6.44)$$

$$S_{rx} = (1 + We\dot{\gamma}) \left( \frac{1}{r+k} \frac{\partial \psi}{\partial r} - \frac{\partial^2 \psi}{\partial r^2} \right), \quad (6.45)$$

with

$$\dot{\gamma} = \frac{1}{r+k} \frac{\partial \psi}{\partial r} - \frac{\partial^2 \psi}{\partial r^2}. \quad (6.46)$$

### 6.3 Solution methodology

The system obtained is highly nonlinear. Therefore we find the series solution and use the perturbation technique about the small Weissenberg number. We expand the quantities as

$$\psi = \psi_0 + We\psi_1 + O(We^2), \quad (6.47)$$

$$S_{rx} = S_{0rx} + WeS_{1rx} + O(We^2), \quad (6.48)$$

$$\theta = \theta_0 + We\theta_1 + O(We^2), \quad (6.49)$$

$$\phi = \phi_0 + We\phi_1 + O(We^2). \quad (6.50)$$

The corresponding systems and their solutions are given as follows:

### 6.3.1 Zeroth order solutions

$$\frac{\partial}{\partial r} \left[ \frac{1}{k(r+k)} \frac{\partial}{\partial r} \{(r+k)^2 S_{0rx}\} + \frac{k}{r+k} M^2 \frac{\partial \psi_0}{\partial r} \right] = 0, \quad (6.51)$$

$$\begin{aligned} 0 = & \left[ \frac{\partial^2 \theta_0}{\partial r^2} + \frac{1}{r+k} \frac{\partial \theta_0}{\partial r} \right] + Br \left[ S_{0xr} \left( -\psi_{0rr} + \frac{\psi_{0r}}{r+k} \right) \right] \\ & + Du Pr \left( \frac{\partial^2 \phi_0}{\partial r^2} + \frac{1}{r+k} \frac{\partial \phi_0}{\partial r} \right) + \left( \frac{k}{r+k} \right)^2 M^2 Br \left( \frac{\partial \psi_0}{\partial r} \right)^2, \end{aligned} \quad (6.52)$$

$$\frac{\partial^2 \phi_0}{\partial r^2} + \frac{1}{r+k} \frac{\partial \phi_0}{\partial r} + SrSc \left( \frac{\partial^2 \theta_0}{\partial r^2} + \frac{1}{r+k} \frac{\partial \theta_0}{\partial r} \right) = 0, \quad (6.53)$$

$$\psi_{0r} \pm \xi_1 S_{0rx} = 0, \quad \text{at } r = \pm \eta, \quad (6.54)$$

$$k \left[ E_1 \frac{\partial^3}{\partial x^3} + E_2 \frac{\partial^3}{\partial x \partial t^2} + E_3 \frac{\partial^2}{\partial t \partial x} \right] \eta = \frac{1}{r+k} \frac{\partial}{\partial r} \{(r+k)^2 S_{0rx}\} + \frac{k^2}{r+k} M^2 \frac{\partial \psi_0}{\partial r}, \quad \text{at } r = \pm \eta, \quad (6.55)$$

$$\theta_0 \pm \xi_2 \frac{\partial \theta_0}{\partial r} = \begin{cases} 1 \\ 0 \end{cases} \quad \text{at } r = \pm \eta, \quad (6.56)$$

$$\phi_0 \pm \xi_3 \frac{\partial \phi_0}{\partial r} = \begin{cases} 1 \\ 0 \end{cases} \quad \text{at } r = \pm \eta, \quad (6.57)$$

$$S_{0rx} = \frac{1}{r+k} \frac{\partial \psi_0}{\partial r} - \frac{\partial^2 \psi_0}{\partial r^2}. \quad (6.58)$$

Solving the above systems one arrives at

$$\psi_0 = C_4 + C_3 kr + C_3 \frac{r^2}{2} + \frac{C_2 (k+r)^{1-\sqrt{1+k^2 M^2}}}{1-\sqrt{1+k^2 M^2}} + \frac{C_1 (k+r)^{1+\sqrt{1+k^2 M^2}}}{1+\sqrt{1+k^2 M^2}}. \quad (6.59)$$

$$\begin{aligned}\theta_0 &= -D_1(k+r)^{-2\sqrt{1+k^2M^2}} - D_2(k+r)^{2\sqrt{1+k^2M^2}} + F_2 + \\ &F_1 \log[k+r] + D_3 \log[k+r]^2,\end{aligned}\quad (6.60)$$

$$\begin{aligned}\phi_0 &= H_2 + H_1 \log[k+r] - ScSr(F_2 - D_1(k+r)^{-2\sqrt{1+k^2M^2}} \\ &- D_2(k+r)^{2\sqrt{1+k^2M^2}} + F_1 \log[k+r] + D_3 \log[k+r]^2).\end{aligned}\quad (6.61)$$

### 6.3.2 First order solutions

Here

$$\frac{\partial}{\partial r} \left[ \frac{1}{k(r+k)} \frac{\partial}{\partial r} \{(r+k)^2 S_{1rx}\} + \frac{k}{r+k} M^2 \frac{\partial \psi_1}{\partial r} \right] = 0, \quad (6.62)$$

$$\begin{aligned}\left[ \frac{\partial^2 \theta_1}{\partial r^2} + \frac{1}{r+k} \frac{\partial \theta_1}{\partial r} \right] + Br \left[ \begin{array}{l} S_{1xr} \left( -\psi_{0rr} + \frac{\psi_{0r}}{r+k} \right) + \\ S_{0xr} \left( -\psi_{1rr} + \frac{\psi_{1r}}{r+k} \right) \end{array} \right] + Du \text{Pr} \left( \frac{\partial^2 \phi_1}{\partial r^2} + \frac{1}{r+k} \frac{\partial \phi_1}{\partial r} \right) \\ + \left( \frac{k}{r+k} \right)^2 M^2 Br \left( 2 \frac{\partial \psi_0}{\partial r} \frac{\partial \psi_1}{\partial r} \right) = 0,\end{aligned}\quad (6.63)$$

$$\frac{\partial^2 \phi_1}{\partial r^2} + \frac{1}{r+k} \frac{\partial \phi_1}{\partial r} + SrSc \left( \frac{\partial^2 \theta_1}{\partial r^2} + \frac{1}{r+k} \frac{\partial \theta_1}{\partial r} \right) = 0, \quad (6.64)$$

$$\psi_{1r} \pm \xi_1 S_{1rx} = 0, \quad \text{at } r = \pm \eta, \quad (6.65)$$

$$\frac{1}{r+k} \frac{\partial}{\partial r} \{(r+k)^2 S_{1rx}\} + \frac{k^2}{r+k} M^2 \frac{\partial \psi_1}{\partial r} = 0, \quad \text{at } r = \pm \eta, \quad (6.66)$$

$$\theta_1 \pm \xi_2 \frac{\partial \theta_1}{\partial r} = \begin{Bmatrix} 1 \\ 0 \end{Bmatrix} \quad \text{at } r = \pm \eta, \quad (6.67)$$

$$\phi_1 \pm \xi_3 \frac{\partial \phi_1}{\partial r} = \begin{Bmatrix} 1 \\ 0 \end{Bmatrix} \quad \text{at } r = \pm \eta, \quad (6.68)$$

$$S_{1rx} = \frac{1}{r+k} \frac{\partial \psi_1}{\partial r} - \frac{\partial^2 \psi_1}{\partial r^2} + \left( \frac{1}{r+k} \frac{\partial \psi_0}{\partial r} - \frac{\partial^2 \psi_0}{\partial r^2} \right)^2, \quad (6.69)$$



and solution expressions are

$$\begin{aligned} \psi_1 = & C_5(k+r)^{-2\sqrt{1+k^2M^2}} + C_6(k+r)^{2\sqrt{1+k^2M^2}} \\ & + \frac{(k+r)^{1+\sqrt{1+k^2M^2}}B_1}{1+\sqrt{1+k^2M^2}} + \frac{(k+r)^{1-\sqrt{1+k^2M^2}}B_2}{1-\sqrt{1+k^2M^2}} + krB_3 + B_3\frac{r^2}{2} + B_4, \end{aligned} \quad (6.70)$$

$$\begin{aligned} \theta_1 = & -A_{11}(k+r)^{-2\sqrt{1+k^2M^2}} - A_{12}(k+r)^{2\sqrt{1+k^2M^2}} + A_{13}(k+r)^{-1-3\sqrt{1+k^2M^2}} \\ & + A_{14}(k+r)^{-1-\sqrt{1+k^2M^2}} + A_{15}(k+r)^{-1+\sqrt{1+k^2M^2}} + A_{16}(k+r)^{-1+3\sqrt{1+k^2M^2}} \\ & + G_2 + G_1 \log[k+r] + A_{17} \log[k+r]^2, \end{aligned} \quad (6.71)$$

$$\begin{aligned} \phi_1 = & O_2 + O_1 \log[k+r] - ScSr(G_2 - A_{11}(k+r)^{-2\sqrt{1+k^2M^2}} - A_{12}(k+r)^{2\sqrt{1+k^2M^2}} + \\ & A_{13}(k+r)^{-1-3\sqrt{1+k^2M^2}} + A_{14}(k+r)^{-1-\sqrt{1+k^2M^2}} + A_{15}(k+r)^{-1+\sqrt{1+k^2M^2}} \\ & + A_{16}(k+r)^{-1+3\sqrt{1+k^2M^2}} + G_1 \log[k+r] + A_{17} \log[k+r]^2). \end{aligned} \quad (6.72)$$

The heat transfer coefficient at the wall is

$$Z = \eta_x \left[ \begin{aligned} & \left( \frac{F_1}{k+\eta} + 2\sqrt{1+k^2M^2} \right) D_1(k+\eta)^{-1-2\sqrt{1+k^2M^2}} - 2\sqrt{1+k^2M^2} D_2(k+\eta)^{-1+2\sqrt{1+k^2M^2}} + \frac{2D_3 \log[k+\eta]}{(k+\eta)} \\ & + We \left( \frac{G_1}{k+\eta} + A_{13}(-1-3\sqrt{1+k^2M^2})(k+\eta)^{-2-3\sqrt{1+k^2M^2}} \right. \\ & + 2A_{11}\sqrt{1+k^2M^2}(k+\eta)^{-1-2\sqrt{1+k^2M^2}} + A_{14}(-1-\sqrt{1+k^2M^2})(k+\eta)^{-2-\sqrt{1+k^2M^2}} \\ & + A_{15}(-1+\sqrt{1+k^2M^2})(k+\eta)^{-2+\sqrt{1+k^2M^2}} + 2A_{12}\sqrt{1+k^2M^2}(k+\eta)^{-1+2\sqrt{1+k^2M^2}} \\ & \left. + A_{16}(-1+3\sqrt{1+k^2M^2})(k+\eta)^{-2+3\sqrt{1+k^2M^2}} + \frac{2A_{17} \log[k+\eta]}{(k+\eta)} \right) \end{aligned} \right] \quad (73)$$

where the constants  $C_i$ 's ( $i = 1 - 6$ ),  $B_i$ 's ( $i = 1 - 4$ ),  $G_i$ 's ( $i = 1 - 2$ ),  $F_i$ 's ( $i = 1 - 2$ ),  $H_i$ 's ( $i = 1 - 2$ ),  $A_i$ 's ( $i = 11 - 17$ ),  $D_i$ 's ( $i = 1 - 3$ ) and  $O_i$ 's ( $i = 1 - 2$ ) are obtained with the help of Mathematica.

### 6.3.3 Entropy analysis

Entropy generation satisfies

$$\begin{aligned}
S_{gen}''' = & \underbrace{\frac{\kappa}{T_m^2} \left( \frac{\partial T}{\partial r} + \frac{R^*}{r+R^*} \frac{\partial T}{\partial x} \right)^2}_{\text{Thermal irreversibility}} + \underbrace{\left( \frac{R^*}{r+R^*} \right)^2 \frac{\sigma B_0^2 u^2}{T_m}}_{\text{Joule friction irreversibility}} \\
& + \underbrace{\frac{1}{T_m} \left( (S_{rr} - S_{xx}) \frac{\partial v}{\partial r} + S_{xr} \left( \frac{\partial u}{\partial r} + \frac{R^*}{r+R^*} \frac{\partial v}{\partial x} - \frac{u}{r+R^*} \right) \right)}_{\text{Fluid friction irreversibility}} \\
& + \underbrace{\frac{RD}{C_m} \left( \frac{\partial C}{\partial r} + \frac{R^*}{r+R^*} \frac{\partial C}{\partial x} \right)^2 + \frac{RD}{T_m} \left( \frac{\partial C}{\partial r} \frac{\partial T}{\partial r} + \left( \frac{R^*}{r+R^*} \right)^2 \frac{\partial C}{\partial x} \frac{\partial T}{\partial x} \right)}_{\text{Diffusion irreversibility}} \quad (6.73)
\end{aligned}$$

In dimensionless form

$$\begin{aligned}
N_s = \frac{S_{gen}'''}{S_G'''} = & \left( \frac{\partial \theta}{\partial r} \right)^2 + \frac{BrM^2}{\Lambda} \left( \frac{k}{r+k} \right)^2 \left( \frac{\partial \psi}{\partial r} \right)^2 + \frac{Br}{\Lambda} S_{rx} \left( \frac{1}{r+k} \frac{\partial \psi}{\partial r} - \frac{\partial^2 \psi}{\partial r^2} \right) \\
& + \frac{L}{\Lambda} \left( \frac{\partial \theta}{\partial r} \right) \left( \frac{\partial \phi}{\partial r} \right) + \frac{L\zeta}{\Lambda^2} \left( \frac{\partial \phi}{\partial r} \right)^2, \quad (6.74)
\end{aligned}$$

with

$$S_G''' = \frac{\kappa (T_1 - T_0)^2}{T_m^2 d^2}, \quad \Lambda = \frac{T_1 - T_0}{T_m}, \quad L = \frac{RD(C_1 - C_0)}{\kappa}, \quad \zeta = \frac{(C_1 - C_0)}{C_m}. \quad (6.75)$$

## 6.4 Analysis

Here plots are displayed and discussed. Firstly we have examined the velocity profile under the influence of pertinent parameters involved in problem. Fig. 6.2 (a) depicts the impact via  $M$  on  $u$ . It is noted that the axial velocity is decreasing function of Hartman number ( $M$ ). The reason behind this act is the resistive nature of Lorentz force that caused decay in velocity for larger  $M$ . Fig. 6.2 (b) captured the curvature parameter ( $k$ ) influence on  $u$ . It can be seen that  $k$  shows dual behavior on the axial velocity. Moreover, the axial velocity is seen to be symmetric for larger curvature parameter ( $k$ ). Fig. 6.2 (c) has been displayed for impact of Weissenberg number ( $We$ ) on the velocity profile. Mixed behavior is also observed for  $We$  like curvature parameter.

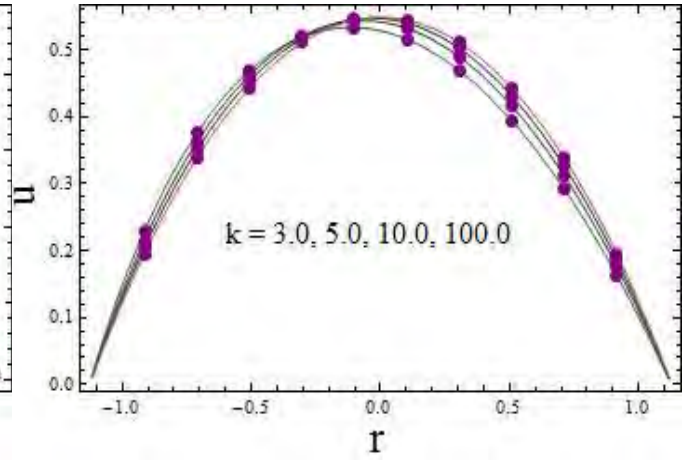
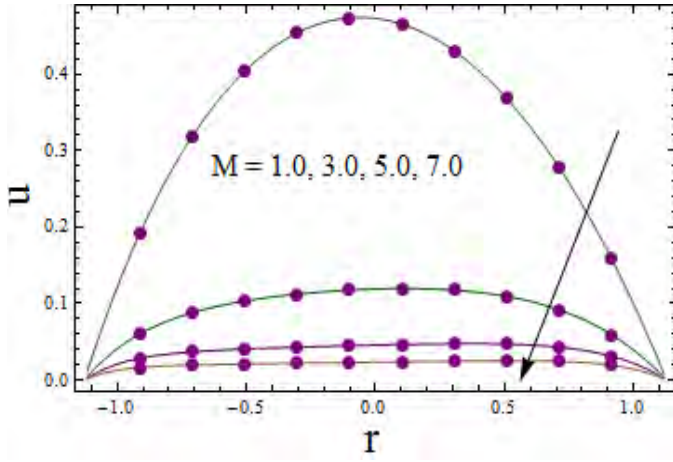
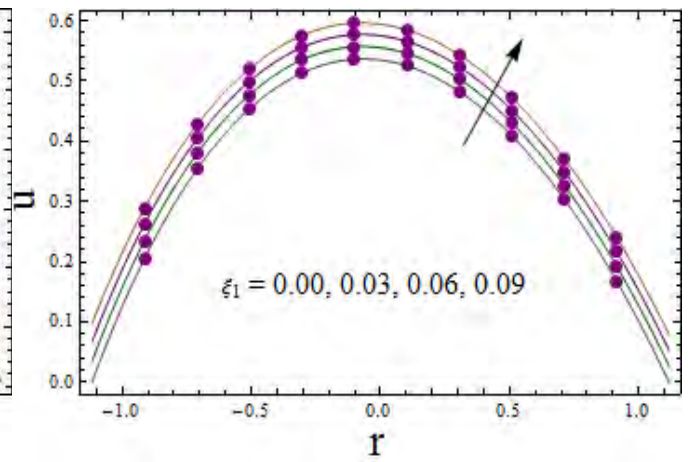
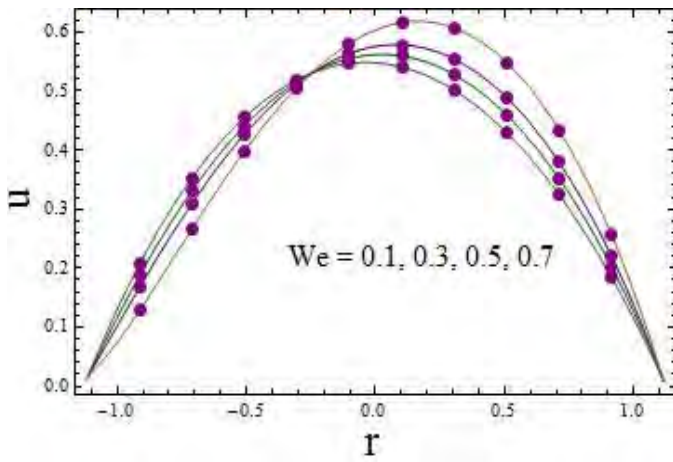


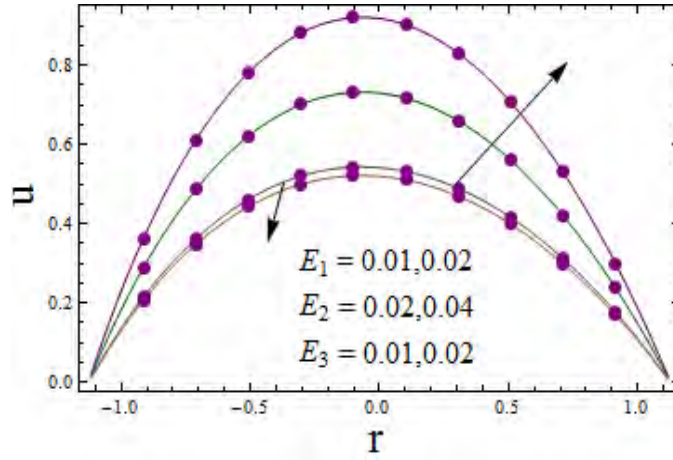
Fig. 6.2 (a)

(b)



(c)

(d)



(e)

Fig. 6.2. Velocity profile graphs when  $E_1 = 0.02$ ,  $E_2 = 0.01$ ,  $E_3 = 0.01$ ,  $t = 0.1$ ,  $x = 0.2$ ,  $\varepsilon = 0.2$ ,  $We = 0.01$ ,  $k = 5.0$ ,  $M = 0.8$ ,  $\xi_1 = 0.01$ . (a) Hartman number influence on  $u$  (b) Curvature parameter influence on  $u$  (c) Weissenberg number influence on  $u$  (d) Slip parameter influence on  $u$  (e) Compliant walls influence on  $u$

Through Fig. 6.2 (d) the influence of velocity slip parameter ( $\xi_1$ ) is examined. Velocity is seen an increasing function of ( $\xi_1$ ). Physically the slip between walls and the fluid decreases the resistance of the flow which causes increase in the axial velocity. Wall parameters behavior on  $u$  is analyzed through Fig. 6.2 (e). Enhancement in axial velocity is examined for  $E_1$  and  $E_2$  whereas decrease is noticed for  $E_3$ . Physically an increase in axial velocity for  $E_1$  and  $E_2$  is the less resistance offered during flow because of the increase in elastic nature of walls. However damping nature of the walls (wall damping coefficient  $E_3$ ) causes decay in fluid velocity.

To observe the impact of Hartman number, curvature parameter, Weissenberg number, Brinkman number, Soret number, Dufour number, Schmidt number and thermal slip parameter on temperature the Figs. 6.3 (a-h) are plotted. Fig. 6.3 (a) shows the influence of Hartman number ( $M$ ) on  $\theta$ . We noticed an enhancement in temperature for an increase in Hartman number. As resistance to the fluid produced heating that caused an enhancement in temperature. Fig. 6.3 (b) indicates impact of curvature parameter ( $k$ ) on temperature. Decay is observed for increase in curvature parameter ( $k$ ) on  $\theta$ . Increase is observed for Weissenberg

number ( $We$ ) on  $\theta$  (see Fig. 6.3 (c)). Fig. 6.3 (d) elucidates the Brinkman number effect on the temperature profile. Enhancing the value of  $Br$  causes rise in the temperature distribution. It is due to the increase in resistance offered by shear in flow and as a result of generation of heat produced because to viscous dissipation. Figs. 6.3 (e) and (f) represent the influence of  $Sr$  and  $Du$  on  $\theta$  respectively. Increase is seen in temperature by making increment in values of Soret and Dufour numbers. Basically enhancement in  $Sr$  produces the mass flux due to large difference in concentration which enlarges the temperature. Here  $Du$  causes the enhancement in concentration gradient which as a result increase the temperature. To examine the influence of Schmidt number ( $Sc$ ) the Fig. 6.3 (g) is plotted. Temperature distribution increases with larger Schmidt number. Fig. 6.3 (h) is prepared to see influence of slip parameter ( $\xi_2$ ) on  $\theta$ . It is found that the fluid temperature increases by enhancing the thermal slip parameter. As increase in slip caused increase in velocity that enhances the mean kinetic energy of the fluid. As a result heat is produced that enhances the fluid temperature.

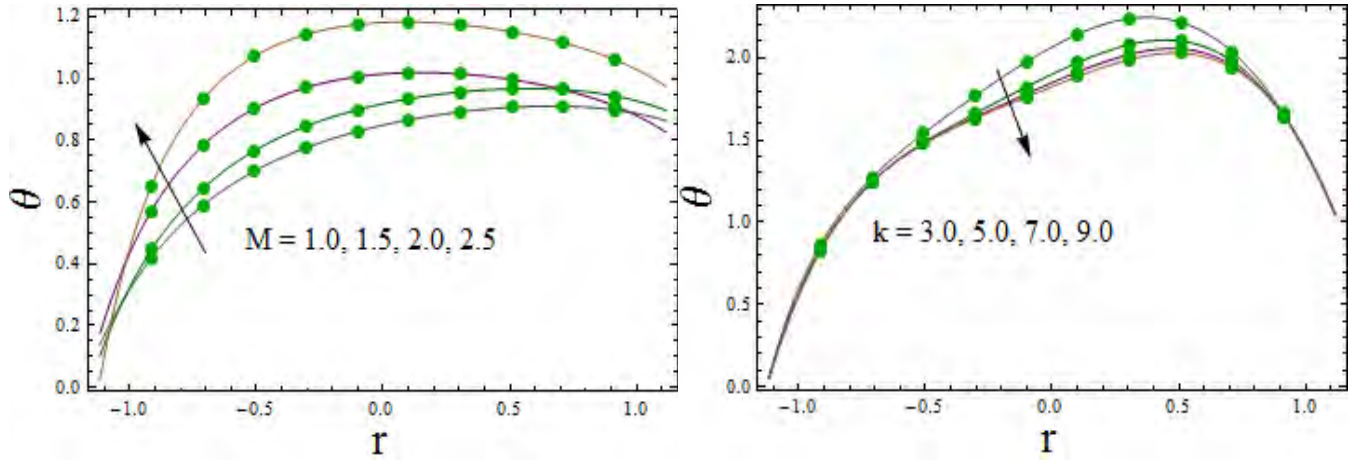
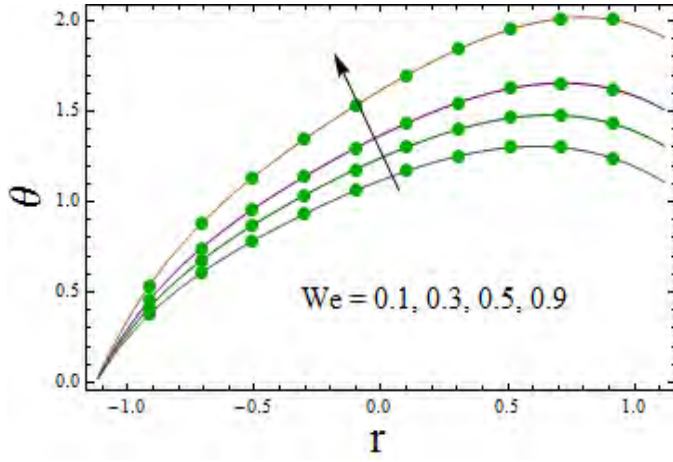
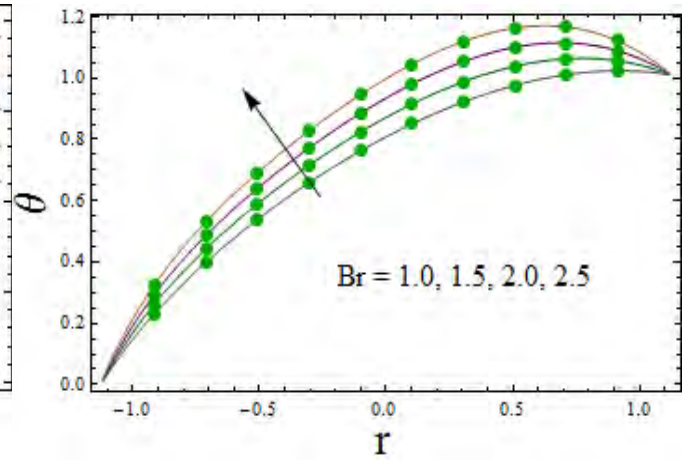


Fig. 6.3 (a)

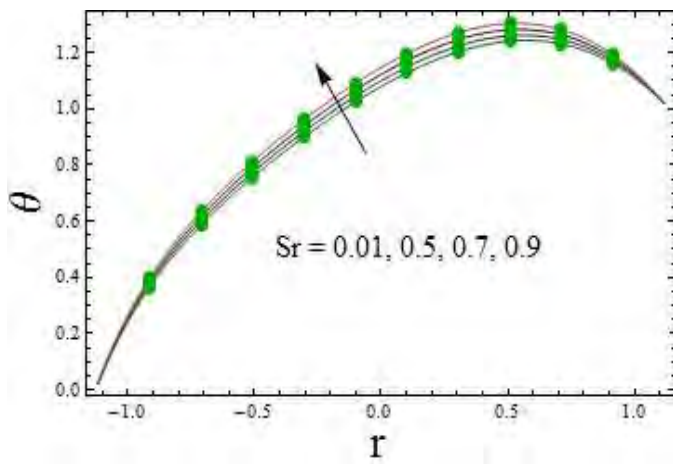
(b)



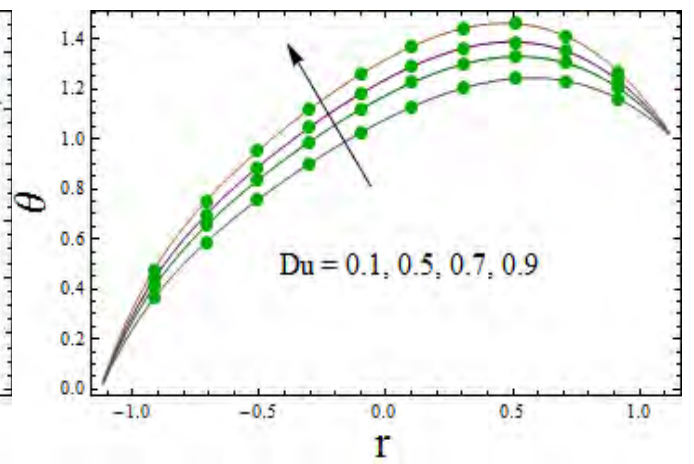
(c)



(d)



(e)



(f)

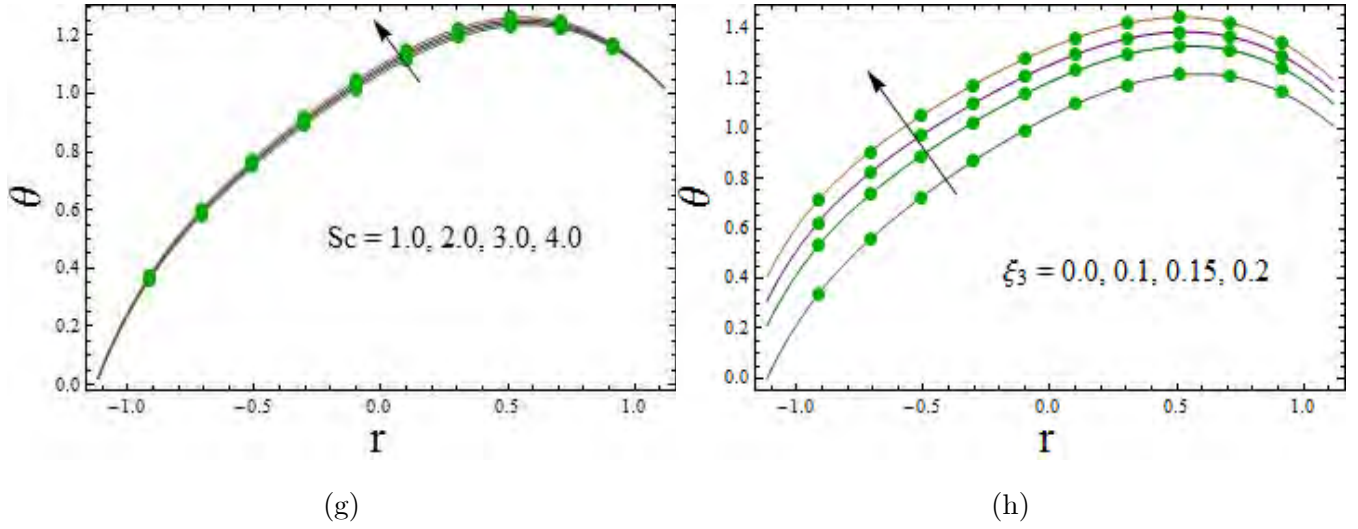


Fig. 6.3. Temperature profile graphs when  $E_1 = 0.02$ ,  $E_2 = 0.01$ ,  $E_3 = 0.01$ ,  $t = 0.1$ ,  $x = 0.2$ ,  $\varepsilon = 0.2$ ,  $We = 0.01$ ,  $k = 3.0$ ,  $Br = 3.0$ ,  $M = 0.7$ ,  $Pr = 2.0$ ,  $Du = 0.1$ ,  $Sc = 0.2$ ,  $Sr = 0.1$ ,  $\xi_1 = 0.01$ ,  $\xi_2 = 0.01$ ,  $\xi_3 = 0.01$ . (a) Hartman number influence on  $\theta$  (b) Curvature parameter influence on  $\theta$  (c) Weissenberg number influence on  $\theta$  (d) Brinkman number influence on  $\theta$  (e) Soret number influence on  $\theta$  (f) Dufour number influence on  $\theta$  (g) Schmidt number influence on  $\theta$  (h) Thermal slip parameter influence on  $\theta$

For influences regarding behavior of different embedded variables on concentration the Figs. 6.4 (a-f) are plotted. From Figs. 6.4 (a) and (b) inverse behavior is observed for curvature parameter ( $k$ ) and Weissenberg number ( $We$ ) on concentration. Figs. 6.4 (c) and (d) elucidate the influence of  $Sr$  and  $Du$ . Decay is noticed in both cases. Similar behavior is noticed for  $Sc$  (see Fig. 6.4 (e)). As increase in Schmidt number reduced the fluid density hence  $\phi$  decreases. From Fig. 6.4 (f) it is observed that by enhancing the concentration slip parameter the  $\phi$  decreases.



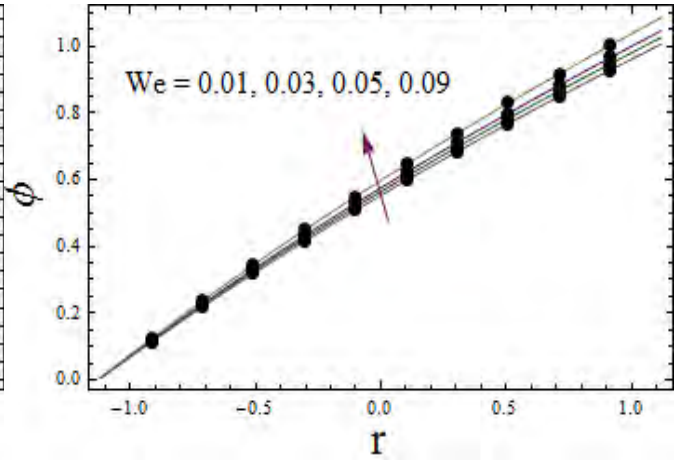
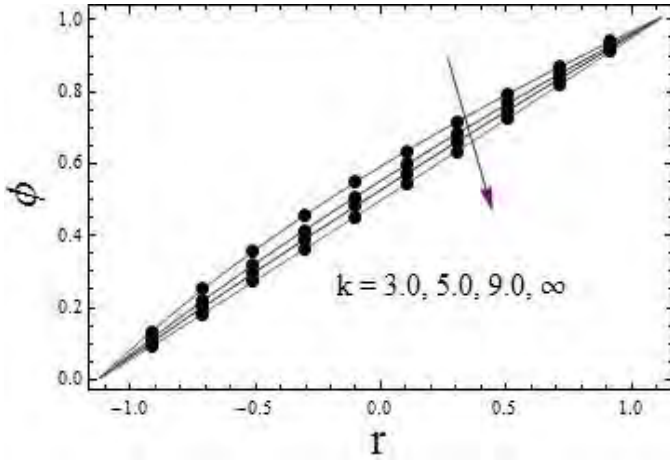
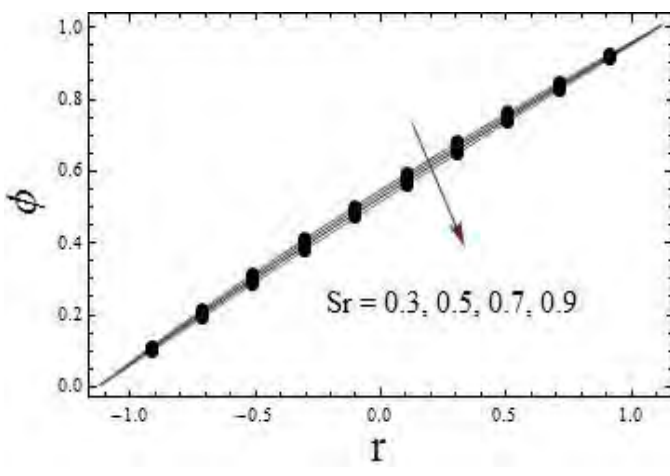
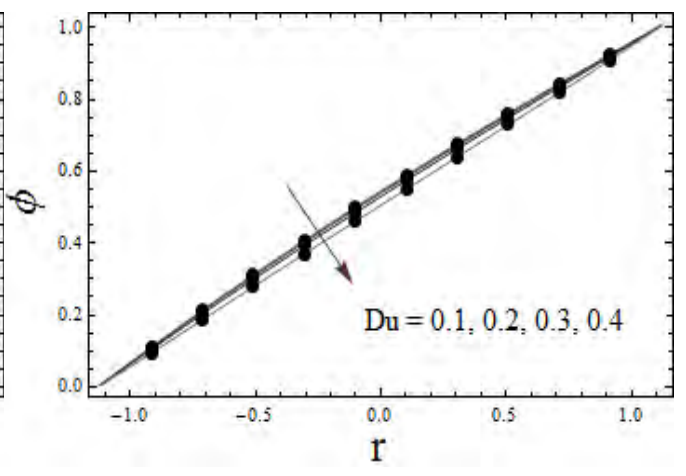


Fig. 6.4 (a)

(b)



(c)



(d)



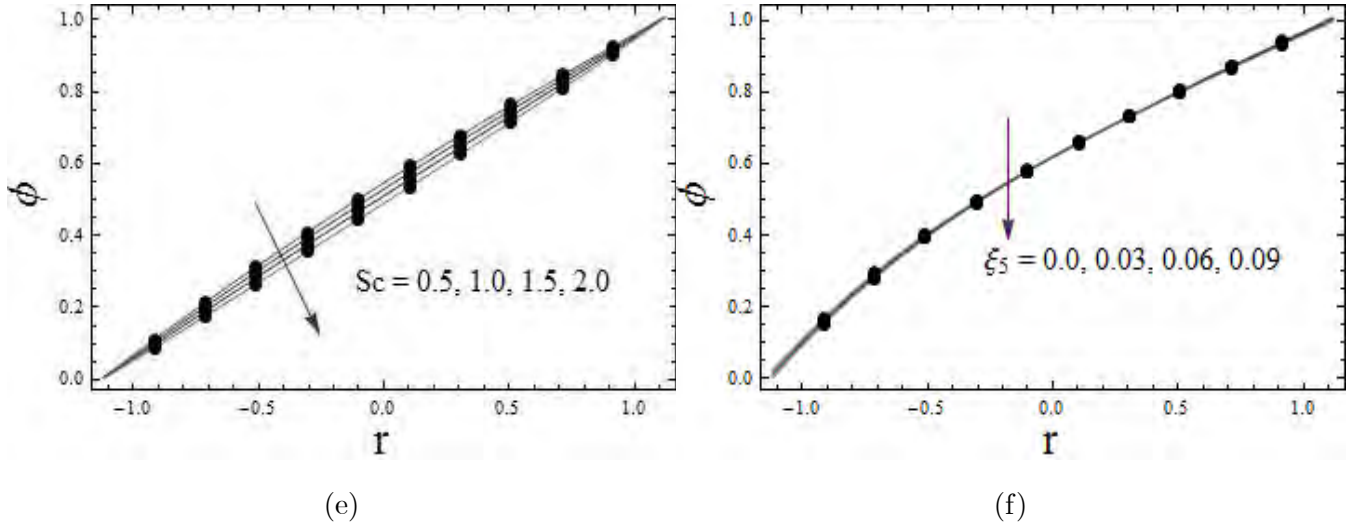


Fig. 6.4. Concentration profile graphs when  $E_1 = 0.02$ ,  $E_2 = 0.01$ ,  $E_3 = 0.01$ ,  $t = 0.1$ ,  $x = 0.2$ ,  $\varepsilon = 0.2$ ,  $We = 0.01$ ,  $M = 2.0$ ,  $k = 5.0$ ,  $Br = 3.0$ ,  $Pr = 2.0$ ,  $Du = 0.2$ ,  $Sc = 0.3$ ,  $Sr = 0.2$ ,  $\xi_1 = 0.01$ ,  $\xi_2 = 0.01$ ,  $\xi_3 = 0.01$ . (a) Curvature parameter influence on  $\phi$  (b) Weissenberg number influence on  $\phi$  (c) Soret number influence on  $\phi$  (d) Dufour number influence on  $\phi$  (e) Schmidt number influence on  $\phi$  (f) Concentration slip parameter influence on  $\phi$

Figs. 6.5 (a-f) are drawn to analyze the heat transfer rate for different parameters of interest. Fig. 6.5 (a) illustrates the impact of  $M$  on  $Z$ . Here  $Z$  decreases by enhancing Hartman number. It is seen that the curvature parameter ( $k$ ) caused increase in heat transfer coefficient (see Fig. 6.5 (b)). Fig. 6.5 (c) illustrates that heat transfer rate increases for  $Br$ . On the other hand, we can say that viscous dissipation influence is in favour of heat flux from the channel wall. Increase is seen in  $Z(x)$  when Soret, Dufour and Schmidt numbers attain the larger values (see Figs. 6.5 (d-f)). It is noticed from these Figs. that heat transfer coefficient shows oscillatory behavior.

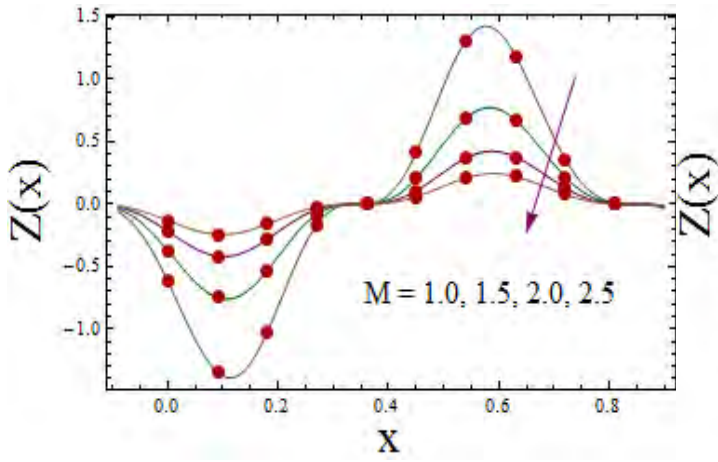
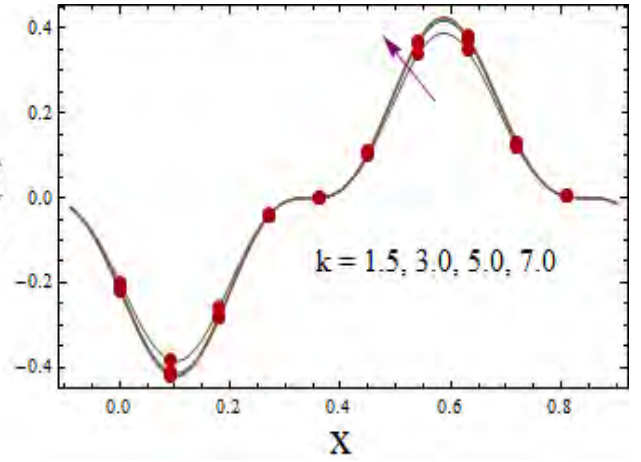
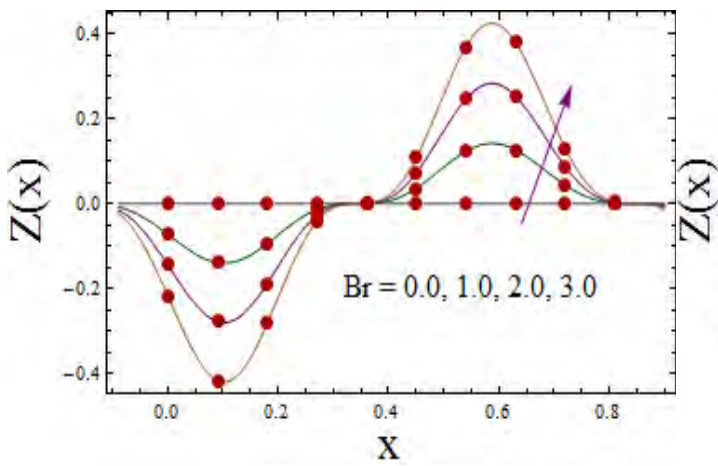


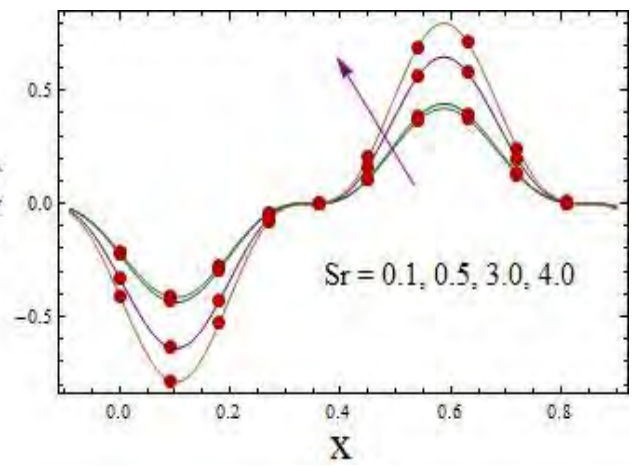
Fig. 6.5 (a)



(b)



(c)



(d)

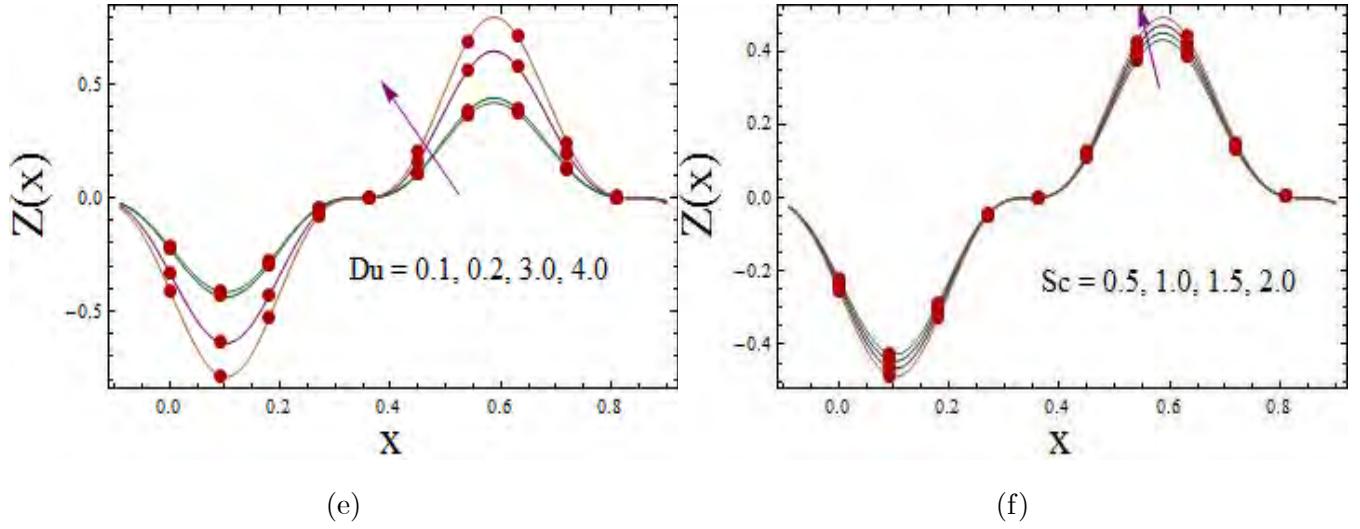


Fig. 6.5. Heat transfer coefficient graphs when  $E_1 = 0.02$ ,  $E_2 = 0.01$ ,  $E_3 = 0.01$ ,  $t = 0.1$ ,  $x = 0.2$ ,  $\varepsilon = 0.2$ ,  $We = 0.01$ ,  $k = 5.0$ ,  $M = 2.0$ ,  $Br = 3.0$ ,  $Pr = 2.0$ ,  $Du = 0.2$ ,  $Sc = 0.3$ ,  $Sr = 0.2$ ,  $\xi_1 = 0.01$ ,  $\xi_2 = 0.01$ ,  $\xi_3 = 0.01$ . (a) Hartman number influence on  $Z$  (b) Curvature parameter influence on  $Z$  (c) Brinkman number influence on  $Z$  (d) Soret number influence on  $Z$  (e) Dufour number influence on  $Z$  (f) Schmidt number influence on  $Z$

The bolus is formed because of splitting of streamlines under various circumstances. This phenomenon is known as trapping. Peristaltic wave completely enclosed this trapped bolus and moves with the same velocity as that of peristaltic wave. Increase is found in trapped bolus size when Hartman number becomes larger (see Figs. 6.6. (a),(b)). Curvature parameter ( $k$ ) and Weissenberg number ( $We$ ) show opposite behavior for stream function (see Figs. 6.7 and 6.8 (a),(b)). Fig. 6.9 (a) and (b) verify the increasing behavior of trapped bolus for higher slip parameter.

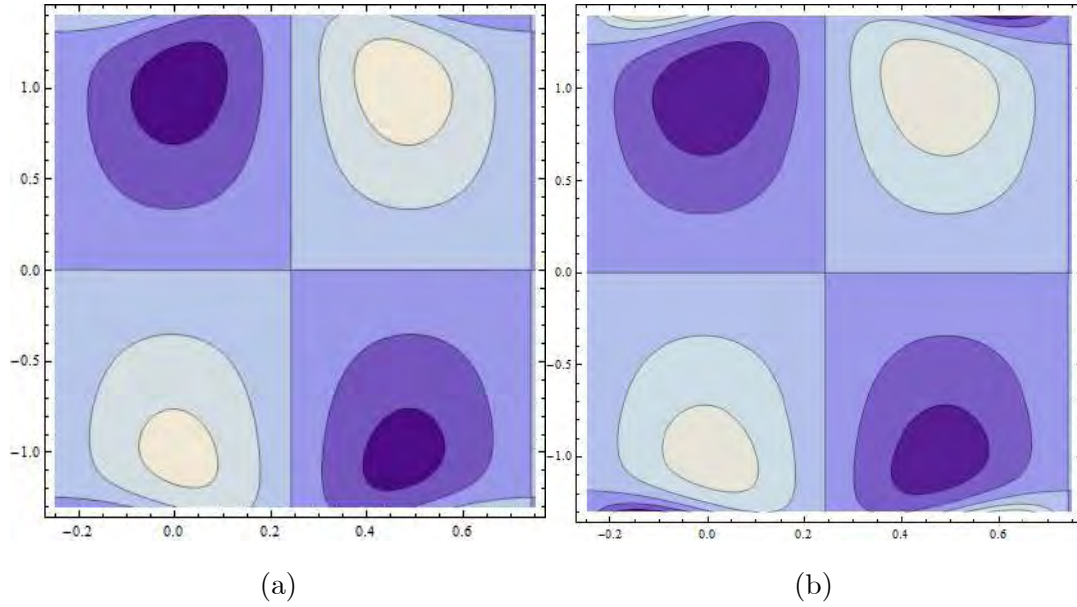


Fig. 6.6. Hartman number influence on  $\psi$  when  $E_1 = 0.02$ ,  $E_2 = 0.01$ ,  $E_3 = 0.01$ ,  $t = 0$ ,  $k = 5.0$ ,  $\varepsilon = 0.1$ ,  $We = 0.03$ ,  $\beta = 0.01$ . (a)  $M = 5.0$ . (b)  $M = 7.0$ .

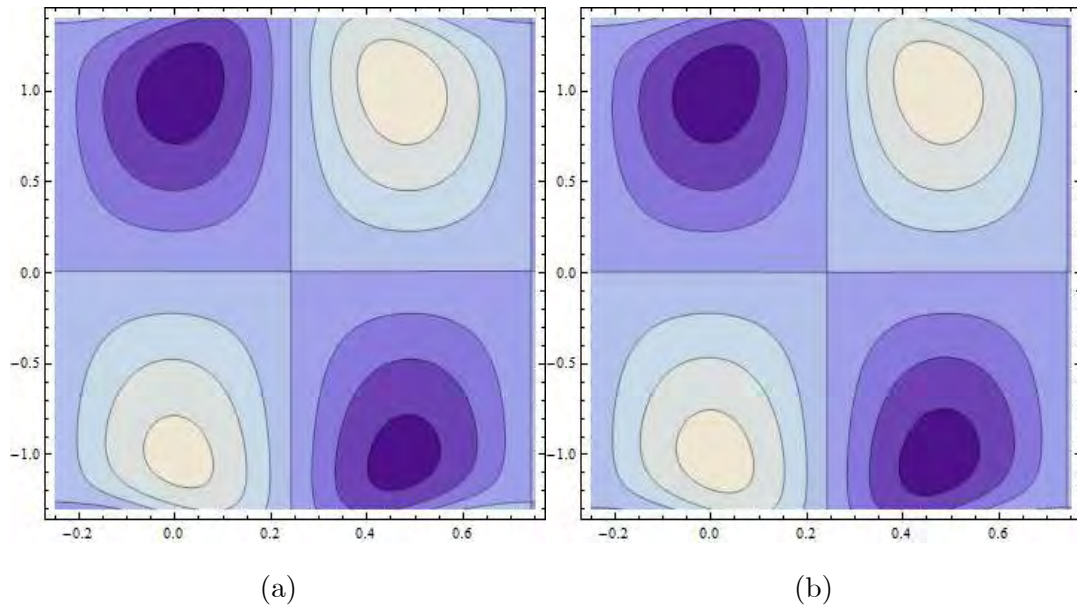
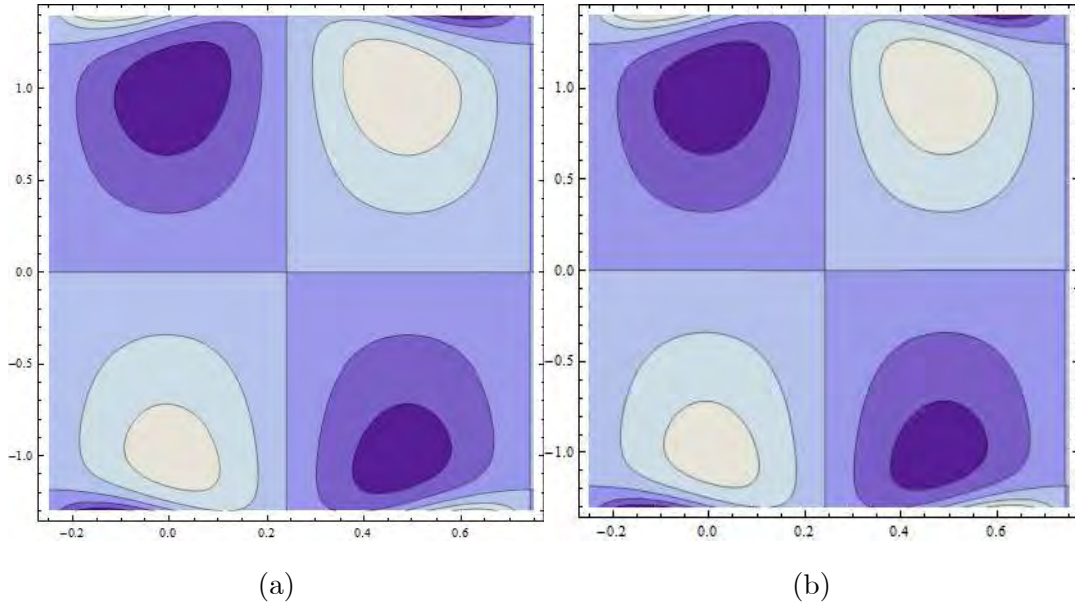
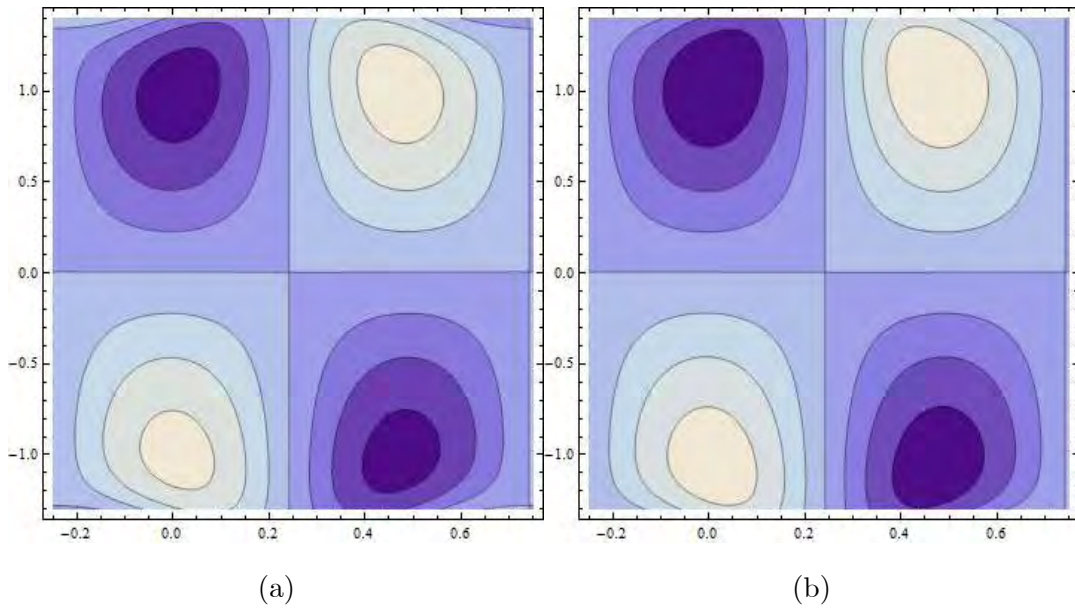


Fig. 6.7. Curvature parameter influence on  $\psi$  when  $E_1 = 0.02$ ,  $E_2 = 0.01$ ,  $E_3 = 0.01$ ,  $t = 0$ ,  $M = 4.0$ ,  $\varepsilon = 0.1$ ,  $We = 0.03$ ,  $\xi_1 = 0.01$ . (a)  $k = 3.0$ . (b)  $k = 5.0$ .



*Fig. 6.8.* Weissenberg number influence on  $\psi$  when  $E_1 = 0.02$ ,  $E_2 = 0.02$ ,  $E_3 = 0.01$ ,  $t = 0$ ,  $k = 5.0$ ,  $\varepsilon = 0.1$ ,  $M = 7.0$ ,  $\xi_1 = 0.01$ .. (a)  $We = 0.01$ . (b)  $We = 0.03$ .



*Fig. 6.9.* Slip parameter influence on  $\psi$  when  $E_1 = 0.02$ ,  $E_2 = 0.01$ ,  $E_3 = 0.01$ ,  $t = 0$ ,  $M = 4.0$ ,  $\varepsilon = 0.1$ ,  $We = 0.03$ ,  $k = 5$ . (a)  $\xi_1 = 0.0$ . (b)  $\xi_1 = 0.06$ .



Figs. 6.10 (a–e) are plotted for analysis of entropy of the system. Hartman number effect on  $Ns$  can be viewed through Fig. 6.10 (a). Increase is noticed at the center of channel. Fig. 6.10 (b) is sketched against Brinkman number. Entropy is increasing function of it. Figs. 6.10 (c–e) show the results for Dufour, Soret and Schmidt numbers on entropy. Increase has been viewed in all cases. These results can be directly linked with temperature profile. An increase in temperature caused more disorderedness hence enhancement in entropy.

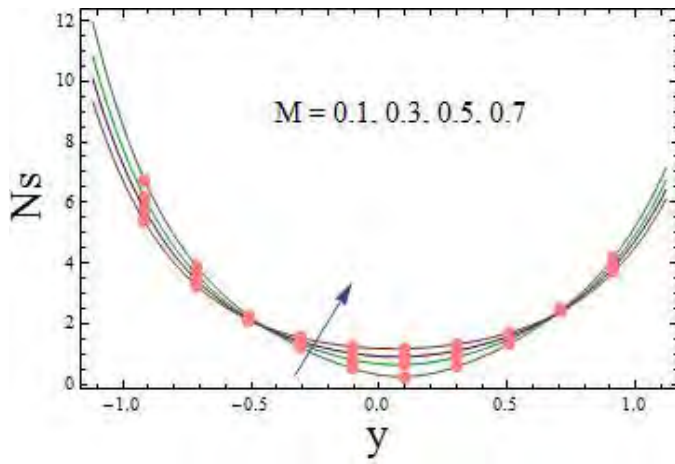
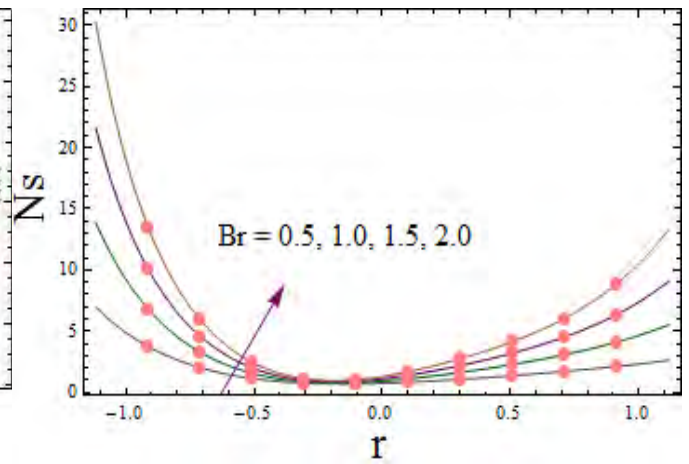
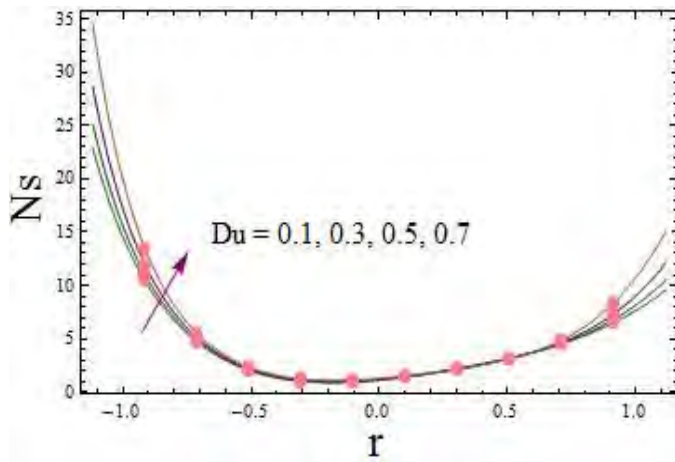


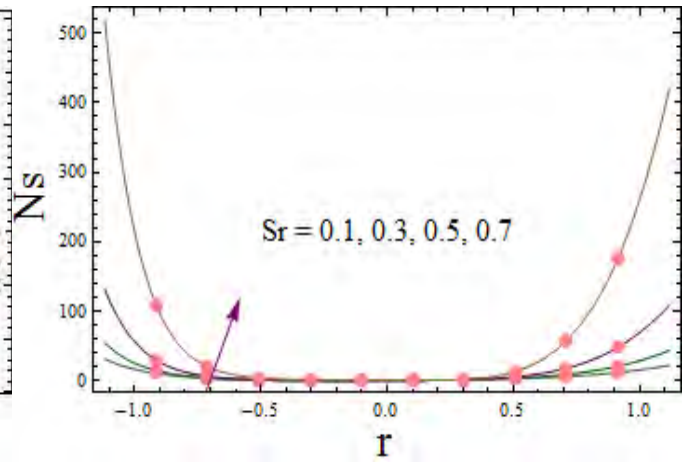
Fig. 6.10 (a)



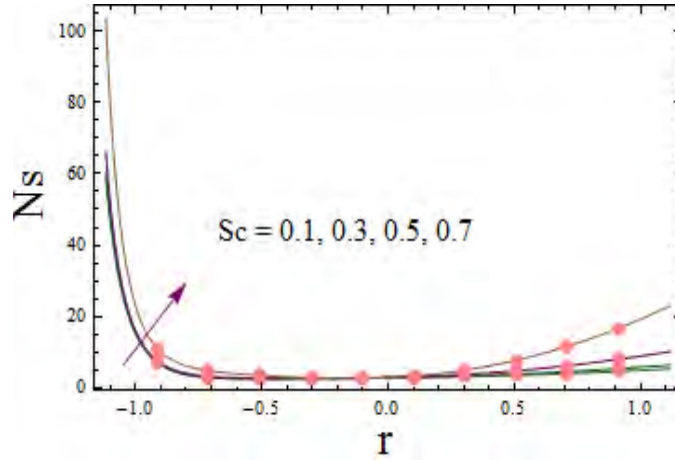
(b)



(c)



(d)



(e)

Fig. 6.10. Entropy generation graphs when  $E_1 = 0.02$ ,  $E_2 = 0.01$ ,  $E_3 = 0.01$ ,  $t = 0.1$ ,  $x = 0.2$ ,  $\varepsilon = 0.2$ ,  $We = 0.01$ ,  $k = 5.0$ ,  $M = 2.0$ ,  $Pr = 2.0$ ,  $Du = 0.2$ ,  $Br = 3.0$ ,  $Sc = 0.5$ ,  $Sr = 0.2$ ,  $\xi_1 = 0.01$ ,  $\xi_2 = 0.01$ ,  $\xi_3 = 0.01$ ,  $\Lambda = 0.5$ ,  $\zeta = 0.5$ ,  $L = 0.5$ . (a) Hartman number influence on  $Ns$  (b) Brinkman number influence on  $Ns$  (c) Dufour number influence on  $Ns$  (d) Soret number influence on  $Ns$  (g) Schmidt number influence on  $Ns$

#### 6.4.1 Validation of the Problem

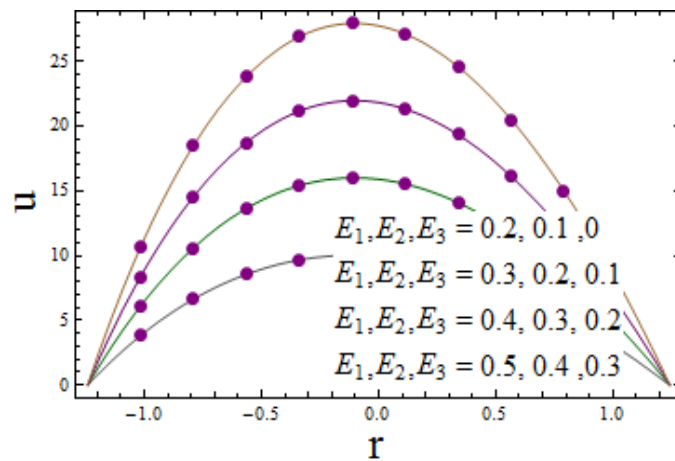


Fig. 6.11

*Fig. 6.11.* Velocity profile for influence of compliant walls when  $t = 0.05$ ,  $x = 0.2$ ,  $\varepsilon = 0.3$ ,  
 $k = 5.0$ ,  $We = 0$ ,  $M = 0$ ,  $\xi_1 = 0$ .

It can be clearly seen via this Fig. that our results are in good comparison with the article by Hayat et al. [50]. In this article the authors utilized the viscous fluid in the curved configuration. No slip conditions have been utilized. Closed form of solution has been found. In our problem if we put  $We = 0$ ,  $M = 0$  and  $\xi_1 = 0$ . then we obtained the same results in the study [50].

## 6.5 Conclusions

Here consideration is given to the peristaltic phenomenon in a curved channel. Effects of Soret and Dufour in Williamson fluid is studied. Main points of this study are given below.

- Axial velocity decreases by increasing the Hartman number and  $E_3$  whereas it is an increasing function for  $E_1$ ,  $E_2$  and velocity slip parameter.
- Weissenberg number and curvature parameter show dual effect on velocity.
- Increasing behavior of temperature is noticed for Soret, Dufour, Schmidt, Brinkman and Hartman number number.
- Opposite behaviors have been seen for concentration when compared with temperature through Soret, Dufour, Schmidt and slip parameters.
- Trapped bolus size enhances for large curvature parameter ( $k$ ), Hartman number ( $M$ ), slip parameter ( $\xi_1$ ) whereas it decreases with an increase in  $We$ .
- Entropy generation enhances for Dufour, Soret and Schmidt and Brinkman numbers.



## Chapter 7

# Numerical study for peristalsis of Sisko nanomaterials with entropy generation

### 7.1 Introduction

Present chapter aims to examine peristalsis in a symmetric channel having flexible walls. Sisko nanofluid is considered. Joule heating and non-linear thermal radiation are taken. Boundary conditions are subject to the slip conditions for velocity, temperature and concentration. Entropy generation analysis for viscous dissipation, Joule heating and non-linear thermal radiation is carried out. System is numerically computed through NDSolved of Mathematica. Graphical analysis is made for velocity, temperature, concentration, heat transfer coefficient and entropy generation. Conclusions are drawn through discussion. This study discloses that magnetic field leads to slow down the fluid velocity and caused decay in heat transfer coefficient. Further Brownian motion and thermophoresis parameter caused enhancement in temperature and entropy generation rate. Slip parameters for velocity and temperature lead to enhancement in the velocity and temperature whereas opposite impact is observed for concentration against concentration slip coefficient.

## 7.2 Problem formulation

Consider two-dimensional flow of Sisko nanofluid in a symmetric channel with flexible walls. The upper and the lower walls have temperatures  $T_1, T_0$  and concentration  $C_1, C_0$  respectively. Fluid is conducted subject to constant magnetic field of strength  $B_0$ . Brownian motion, thermophoresis and nonlinear radiation are discussed. Joule heating is present. Flow is induced by peristaltic waves which consists of contraction and expansion along channel walls. The wave speed is denoted by  $c$  and wavelength  $\lambda$ . The problem is formulated using the Cartesian coordinates system where  $x$ -axis is in the direction of flow and  $y$ -axis normal to  $x$ -axis (see Fig. 7.1). The wave geometry is given by:

$$y = \pm \eta(x, t) = \pm \left[ d + a \sin \frac{2\pi}{\lambda} (x - ct) \right], \quad (7.1)$$

where  $\eta$  and  $-\eta$  represent the upper and the lower walls respectively.  $d$  half channel width and symbol  $a$  the wave amplitude. Here  $t$  is used for time.

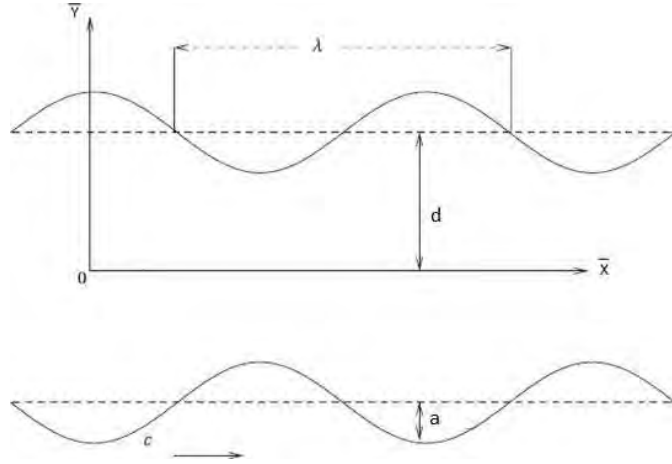


Fig. 7.1: Schematic diagram

Flow is governed by [172]:

$$\frac{\partial u}{\partial x} + \frac{\partial v}{\partial y} = 0. \quad (7.2)$$

$$\frac{\partial u}{\partial t} + u \frac{\partial u}{\partial x} + v \frac{\partial u}{\partial y} = -\frac{1}{\rho_f} \frac{\partial p}{\partial x} + \frac{1}{\rho_f} \frac{\partial S_{xx}}{\partial x} + \frac{1}{\rho_f} \frac{\partial S_{xy}}{\partial y} - \frac{1}{\rho_f} \sigma B_0^2 u, \quad (7.3)$$

$$\frac{\partial v}{\partial t} + u \frac{\partial v}{\partial x} + v \frac{\partial v}{\partial y} = -\frac{1}{\rho_f} \frac{\partial p}{\partial y} + \frac{1}{\rho_f} \frac{\partial S_{xy}}{\partial x} + \frac{1}{\rho_f} \frac{\partial S_{yy}}{\partial y}. \quad (7.4)$$

$$\begin{aligned}
\frac{\partial T}{\partial t} + u \frac{\partial T}{\partial x} + v \frac{\partial T}{\partial y} &= \alpha^* \left[ \frac{\partial^2 T}{\partial x^2} + \frac{\partial^2 T}{\partial y^2} \right] + \frac{1}{(\rho C_p)_f} \left[ S_{xx} \frac{\partial u}{\partial x} + S_{xy} \left( \frac{\partial u}{\partial y} + \frac{\partial v}{\partial x} \right) + S_{yy} \frac{\partial v}{\partial y} \right] \\
&+ \tau \left[ D_B \left( \frac{\partial C}{\partial x} \frac{\partial T}{\partial x} + \frac{\partial C}{\partial y} \frac{\partial T}{\partial y} \right) + \frac{D_T}{T_m} \left( \left( \frac{\partial T}{\partial x} \right)^2 + \left( \frac{\partial T}{\partial y} \right)^2 \right) \right] \\
&- \frac{1}{(\rho C_p)_f} \frac{\partial q_r}{\partial y} + \frac{1}{(\rho C_p)_f} \sigma B_0^2 u^2. \tag{7.5}
\end{aligned}$$

$$\frac{\partial C}{\partial t} + u \frac{\partial C}{\partial x} + v \frac{\partial C}{\partial y} = D_B \left( \frac{\partial^2 C}{\partial x^2} + \frac{\partial^2 C}{\partial y^2} \right) + \frac{D_T}{T_m} \left( \frac{\partial^2 T}{\partial x^2} + \frac{\partial^2 T}{\partial y^2} \right), \tag{7.6}$$

Here symbols  $D_B$  and  $D_T$  in Eqs. (7.5) and (7.6) are Brownian motion and thermophoretic diffusion coefficients,  $u$  and  $v$  the velocity components,  $\tau$  equals  $(\rho C_p)_p / (\rho C_p)_f$ ,  $T$  the temperature and  $C$  the concentration. Furthermore  $S_{ij}$ ,  $\rho_f$ ,  $p$ ,  $T_m$ ,  $\sigma$ ,  $\alpha^*$  elucidate the stress components, nanofluid density, pressure, nanofluid mean temperature, electric conductivity and thermal diffusivity respectively.

Extra stress tensor of Sisko fluid is [72]:

$$\mathbf{S} = \left( \alpha + \beta^* \sqrt{|\Pi|}^{n-1} \right) \mathbf{A}_1, \tag{7.7}$$

where  $\mathbf{A}_1$  and  $\Pi$  are

$$\mathbf{A}_1 = \text{grad } \mathbf{V} + (\text{grad } \mathbf{V})^T, \quad \Pi = \frac{1}{2} \text{tr} \mathbf{A}_1^2, \tag{7.8}$$

in which power law index is denoted by  $n$ , consistency index by  $\beta^*$  and shear rate viscosity by  $\alpha$ .

Further

$$S_{xx} = 2 \left[ \alpha + \beta \left( 2 \left( \frac{\partial u}{\partial x} \right)^2 + \left( \frac{\partial u}{\partial y} + \frac{\partial v}{\partial x} \right)^2 + 2 \left( \frac{\partial v}{\partial y} \right)^2 \right)^{(n-1)/2} \right] \frac{\partial u}{\partial x}, \tag{7.9}$$

$$S_{xy} = \left[ \alpha + \beta \left( 2 \left( \frac{\partial u}{\partial x} \right)^2 + \left( \frac{\partial u}{\partial y} + \frac{\partial v}{\partial x} \right)^2 + 2 \left( \frac{\partial v}{\partial y} \right)^2 \right)^{(n-1)/2} \right] \left( \frac{\partial u}{\partial y} + \frac{\partial v}{\partial x} \right), \tag{7.10}$$

$$S_{yy} = 2 \left[ \alpha + \beta \left( 2 \left( \frac{\partial u}{\partial x} \right)^2 + \left( \frac{\partial u}{\partial y} + \frac{\partial v}{\partial x} \right)^2 + 2 \left( \frac{\partial v}{\partial y} \right)^2 \right)^{(n-1)/2} \right] \frac{\partial v}{\partial y}, \tag{7.11}$$

Boundary conditions are [172]:

$$u \pm \xi_1 S_{xy} = 0 \quad \text{at } y = \pm\eta, \quad (7.12)$$

$$\left[ -\tau^* \frac{\partial^3}{\partial x^3} + m^* \frac{\partial^3}{\partial x \partial t^2} + d_1^* \frac{\partial^2}{\partial t \partial x} \right] \eta = \frac{\partial S_{xy}}{\partial y} + \frac{\partial S_{xx}}{\partial x} - \rho_f \left[ \frac{\partial u}{\partial t} + u \frac{\partial u}{\partial x} + v \frac{\partial u}{\partial y} \right] - \sigma B_0^2 u, \quad \text{at } y = \pm\eta, \quad (7.13)$$

$$T \pm \xi_2 \frac{\partial T}{\partial y} = \begin{Bmatrix} T_1 \\ T_0 \end{Bmatrix} \quad \text{at } y = \pm\eta, \quad (7.14)$$

$$C \pm \xi_3 \frac{\partial C}{\partial y} = \begin{Bmatrix} C_1 \\ C_0 \end{Bmatrix} \quad \text{at } y = \pm\eta. \quad (7.15)$$

Here  $\xi_1$ ,  $\xi_2$  and  $\xi_3$  are the slip parameters for velocity, temperature and concentration respectively and  $\tau^*$ ,  $m^*$ , and  $d_1^*$  represent the wall elastance and damping characteristics.

Non-dimensional parameters are represented as

$$\begin{aligned} x^* &= \frac{x}{\lambda}, & y^* &= \frac{y}{d}, & u^* &= \frac{u}{c}, & v^* &= \frac{v}{c}, & t^* &= \frac{ct}{\lambda}, \\ \xi_1^* &= \frac{\xi_1 \alpha}{d}, & \xi_2^* &= \frac{\xi_2}{d}, & \xi_3^* &= \frac{\xi_3}{d}, & \eta^* &= \frac{\eta}{d}, \\ S_{ij}^* &= \frac{d S_{ij}}{c \alpha}, & p^* &= \frac{d^2 p}{c \lambda \alpha}, & \phi &= \frac{C - C_0}{C_1 - C_0}, \\ \theta &= \frac{T - T_0}{T_1 - T_0}, & u &= \frac{\partial \psi}{\partial y}, & v &= -\delta \frac{\partial \psi}{\partial x}. \end{aligned} \quad (7.16)$$

After utilizing the non-dimensional quantities we get the following forms of equations:

$$\text{Re} \left[ \delta \frac{\partial^2 \psi}{\partial t \partial y} + \delta \frac{\partial \psi}{\partial y} \frac{\partial^2 \psi}{\partial x \partial y} - \delta \frac{\partial \psi}{\partial x} \frac{\partial^2 \psi}{\partial y^2} \right] = -\frac{\partial p}{\partial x} + \delta \frac{\partial S_{xx}}{\partial x} + \frac{\partial S_{xy}}{\partial y} - M^2 \frac{\partial \psi}{\partial y}, \quad (7.17)$$

$$\text{Re} \delta \left[ -\delta^2 \frac{\partial^2 \psi}{\partial t \partial x} - \delta^2 \frac{\partial \psi}{\partial y} \frac{\partial^2 \psi}{\partial x^2} + \delta^2 \frac{\partial \psi}{\partial x} \frac{\partial^2 \psi}{\partial x \partial y} \right] = -\frac{\partial p}{\partial y} + \delta^2 \frac{\partial S_{xy}}{\partial x} + \delta \frac{\partial S_{yy}}{\partial y}, \quad (7.18)$$

$$\begin{aligned}
\text{Re Pr} \left[ \delta \frac{\partial \theta}{\partial t} + \delta \frac{\partial \psi}{\partial y} \frac{\partial \theta}{\partial x} - \delta \frac{\partial \psi}{\partial x} \frac{\partial \theta}{\partial y} \right] &= \left[ \delta^2 \frac{\partial^2 \theta}{\partial x^2} + \frac{\partial^2 \theta}{\partial y^2} \right] \\
&+ Br \left[ \delta S_{xx} \frac{\partial^2 \psi}{\partial x \partial y} + S_{xy} \left( \frac{\partial^2 \psi}{\partial y^2} - \delta^2 \frac{\partial^2 \psi}{\partial x^2} \right) - \delta S_{yy} \frac{\partial^2 \psi}{\partial x \partial y} \right] \\
&+ Nb \text{Pr} \left( \delta^2 \frac{\partial \phi}{\partial x} \frac{\partial \theta}{\partial x} + \frac{\partial \phi}{\partial y} \frac{\partial \theta}{\partial y} \right) + Nt \text{Pr} \left( \delta^2 \left( \frac{\partial \theta}{\partial x} \right)^2 + \left( \frac{\partial \theta}{\partial y} \right)^2 \right) \\
&+ Rd \left[ 3 \left( (\theta_w - 1) \theta + 1 \right)^2 (\theta_w - 1) \left( \frac{\partial \theta}{\partial y} \right)^2 \right. \\
&\quad \left. + \left( (\theta_w - 1) \theta + 1 \right)^3 \frac{\partial^2 \theta}{\partial y^2} \right] \\
&+ M^2 Br \left( \frac{\partial \psi}{\partial y} \right)^2, \tag{7.19}
\end{aligned}$$

$$\text{Re Sc} \left( \delta \frac{\partial \phi}{\partial t} + \frac{\partial \psi}{\partial y} \frac{\partial \phi}{\partial x} - \delta \frac{\partial \psi}{\partial x} \frac{\partial \phi}{\partial y} \right) = \left( \delta^2 \frac{\partial^2 \phi}{\partial x^2} + \frac{\partial^2 \phi}{\partial y^2} \right) + \frac{Nt}{Nb} \left( \delta^2 \frac{\partial^2 \theta}{\partial x^2} + \frac{\partial^2 \theta}{\partial y^2} \right), \tag{7.20}$$

$$S_{xx} = 2\delta \left[ 1 + \beta_1 \left( 2\delta^2 \left( \frac{\partial^2 \psi}{\partial x \partial y} \right)^2 + \left( \frac{\partial^2 \psi}{\partial y^2} - 2\delta^2 \frac{\partial^2 \psi}{\partial x^2} \right)^2 + 2\delta^2 \left( \frac{\partial^2 \psi}{\partial x \partial y} \right)^2 \right)^{(n-1)/2} \right] \frac{\partial^2 \psi}{\partial x \partial y}, \tag{7.21}$$

$$S_{xy} = \left[ 1 + \beta_1 \left( 2\delta^2 \left( \frac{\partial^2 \psi}{\partial x \partial y} \right)^2 + \left( \frac{\partial^2 \psi}{\partial y^2} - 2\delta^2 \frac{\partial^2 \psi}{\partial x^2} \right)^2 + 2\delta^2 \left( \frac{\partial^2 \psi}{\partial x \partial y} \right)^2 \right)^{(n-1)/2} \right] \left( \frac{\partial^2 \psi}{\partial y^2} - \delta^2 \frac{\partial^2 \psi}{\partial x^2} \right), \tag{7.22}$$

$$S_{yy} = -2\delta \left[ 1 + \beta_1 \left( 2\delta^2 \left( \frac{\partial^2 \psi}{\partial x \partial y} \right)^2 + \left( \frac{\partial^2 \psi}{\partial y^2} - 2\delta^2 \frac{\partial^2 \psi}{\partial x^2} \right)^2 + 2\delta^2 \left( \frac{\partial^2 \psi}{\partial x \partial y} \right)^2 \right)^{(n-1)/2} \right] \frac{\partial^2 \psi}{\partial x \partial y}, \tag{7.23}$$

with boundary conditions

$$\frac{\partial \psi}{\partial y} \pm \xi_1 S_{xy} = 0, \quad \text{at } y = \pm \eta = \pm(1 + \varepsilon \sin 2\pi(x - t)), \tag{7.24}$$

$$\begin{aligned}
\left[ E_1 \frac{\partial^3}{\partial x^3} + E_2 \frac{\partial^3}{\partial x \partial t^2} + E_3 \frac{\partial^2}{\partial t \partial x} \right] \eta &= -\text{Re} \left[ \delta \frac{\partial^2 \psi}{\partial t \partial y} + \delta \frac{\partial \psi}{\partial y} \frac{\partial^2 \psi}{\partial x \partial y} - \delta \frac{\partial \psi}{\partial x} \frac{\partial^2 \psi}{\partial y^2} \right] + \\
&\delta \frac{\partial S_{xx}}{\partial x} + \frac{\partial S_{xy}}{\partial y} - M^2 \frac{\partial \psi}{\partial y}, \quad \text{at } y = \pm \eta, \tag{7.25}
\end{aligned}$$

$$\theta \pm \xi_2 \frac{\partial \theta}{\partial y} = \begin{Bmatrix} 1 \\ 0 \end{Bmatrix} \quad \text{at } y = \pm \eta, \tag{7.26}$$

$$\phi \pm \xi_3 \frac{\partial \phi}{\partial y} = \begin{Bmatrix} 1 \\ 0 \end{Bmatrix} \quad \text{at } y = \pm \eta. \quad (7.27)$$

The dimensionless parameters are

$$\begin{aligned} \varepsilon &= \frac{a}{d}, \quad \delta = \frac{d}{\lambda}, \quad \text{Re} = \frac{\rho_f c d}{\alpha}, \quad M = \sqrt{\frac{\sigma}{\alpha}} B_0 d, \quad \beta_1 = \frac{\beta^*}{\alpha} \left(\frac{c}{d}\right)^{n-1}, \\ Nb &= \frac{\tau \rho_f D_B (C_1 - C_0)}{\alpha}, \quad Nt = \frac{\tau \rho_f D_T (T_1 - T_0)}{\alpha T_m}, \quad Sc = \frac{\alpha}{\rho_f D_B}, \\ Pr &= \frac{\alpha C_f}{\kappa}, \quad Br = \frac{c^2 \alpha}{\kappa (T_1 - T_0)}, \quad Rd = \frac{16 \sigma^* T_0^3}{3 k^* \kappa}, \quad \theta_w = \frac{T_1}{T_0}, \\ E_1 &= -\frac{\tau^* d^3}{\lambda^3 \alpha}, \quad E_2 = \frac{m^* c d^3}{\lambda^3 \alpha}, \quad E_3 = \frac{d_1^* d^3}{\lambda^2 \alpha}. \end{aligned} \quad (7.28)$$

Here  $\varepsilon$  depicts amplitude ratio,  $\delta$  wave number,  $\text{Re}$  Reynolds number,  $M$  Hartman number,  $\beta_1$  Sisko fluid parameter,  $Nb$  Brownian motion parameter,  $Nt$  thermophoresis parameter,  $Sc$  Schmidt number,  $Pr$  Prandtl number,  $Br$  Brinkman number,  $Rd$  radiation parameter and  $E_1$ ,  $E_2$ ,  $E_3$  the compliant wall parameters.

Lubrication approach leads to

$$\frac{\partial p}{\partial x} = \frac{\partial S_{xy}}{\partial y} - M^2 \frac{\partial \psi}{\partial y}, \quad (7.29)$$

$$\frac{\partial p}{\partial y} = 0, \quad (7.30)$$

$$\begin{aligned} 0 &= \frac{\partial^2 \theta}{\partial y^2} + Br S_{xy} \frac{\partial^2 \psi}{\partial y^2} + Nb Pr \frac{\partial \phi}{\partial y} \frac{\partial \theta}{\partial y} + Nt Pr \left(\frac{\partial \theta}{\partial y}\right)^2 + M^2 Br \left(\frac{\partial \psi}{\partial y}\right)^2 \\ &+ Rd \left[ 3((\theta_w - 1)\theta + 1)^2 (\theta_w - 1) \left(\frac{\partial \theta}{\partial y}\right)^2 + ((\theta_w - 1)\theta + 1)^3 \frac{\partial^2 \theta}{\partial y^2} \right], \end{aligned} \quad (7.31)$$

$$\frac{\partial^2 \phi}{\partial y^2} + \frac{Nt}{Nb} \frac{\partial^2 \theta}{\partial y^2} = 0, \quad (7.32)$$

$$S_{xx} = 0 = S_{yy}, \quad (7.33)$$

$$S_{xy} = \left[ 1 + \beta_1 \left( \left( \frac{\partial^2 \psi}{\partial y^2} \right)^2 \right)^{(n-1)/2} \right] \left( \frac{\partial^2 \psi}{\partial y^2} \right), \quad (7.34)$$

with boundary conditions

$$\frac{\partial \psi}{\partial y} \pm \xi_1 S_{xy} = 0, \quad \text{at } y = \pm \eta = \pm(1 + \varepsilon \sin 2\pi(x - t)), \quad (7.35)$$

$$\left[ E_1 \frac{\partial^3}{\partial x^3} + E_2 \frac{\partial^3}{\partial x \partial t^2} + E_3 \frac{\partial^2}{\partial t \partial x} \right] \eta = \frac{\partial S_{xy}}{\partial y} - M^2 \frac{\partial \psi}{\partial y}, \quad \text{at } y = \pm \eta, \quad (7.36)$$

$$\theta \pm \xi_2 \frac{\partial \theta}{\partial y} = \begin{Bmatrix} 1 \\ 0 \end{Bmatrix} \quad \text{at } y = \pm \eta, \quad (7.37)$$

$$\phi \pm \xi_3 \frac{\partial \phi}{\partial y} = \begin{Bmatrix} 1 \\ 0 \end{Bmatrix} \quad \text{at } y = \pm \eta. \quad (7.38)$$

The above mentioned system via NDSolve of Mathematica 9.0 is computed.

### 7.2.1 Expression for entropy generation

Mathematical expressions for viscous dissipation is

$$\Phi = S_{xx} \frac{\partial u}{\partial x} + S_{yy} \frac{\partial v}{\partial y} + S_{xy} \left( \frac{\partial u}{\partial y} + \frac{\partial v}{\partial x} \right). \quad (7.39)$$

Volumetric entropy generation in dimensional form is given by

$$\begin{aligned} S_{gen}''' = & \underbrace{\frac{\kappa}{T_m^2} \left( \left( \frac{\partial T}{\partial x} \right)^2 + \left( \frac{\partial T}{\partial y} \right)^2 + \frac{16\sigma^*}{3k^*\kappa} \left( \frac{\partial T}{\partial y} \right)^2 \right)}_{\text{Thermal irreversibility}} + \underbrace{\frac{\sigma B_0^2 u^2}{T_m}}_{\text{Joule friction irreversibility}} + \underbrace{\frac{\Phi}{T_m}}_{\text{Fluid friction irreversibility}} \\ & + \underbrace{\frac{RD}{C_m} \left( \left( \frac{\partial C}{\partial x} \right)^2 + \left( \frac{\partial C}{\partial y} \right)^2 \right) + \frac{RD}{T_m} \left( \frac{\partial C}{\partial x} \frac{\partial T}{\partial x} + \frac{\partial C}{\partial y} \frac{\partial T}{\partial y} \right)}_{\text{Diffusion irreversibility}} \end{aligned} \quad (7.40)$$

In dimensionless form

$$\begin{aligned} N_s = \frac{S_{gen}'''}{S_G'''} = & \left( 1 + Rd((\theta_w - 1)\theta + 1)^3 \right) \left( \frac{\partial \theta}{\partial y} \right)^2 + \frac{BrM^2}{\Lambda} \left( \frac{\partial \psi}{\partial y} \right)^2 + \frac{Br}{\Lambda} S_{xy} \left( \frac{\partial^2 \psi}{\partial y^2} \right) \\ & + \frac{L}{\Lambda} \left( \frac{\partial \theta}{\partial y} \right) \left( \frac{\partial \phi}{\partial y} \right) + \frac{L\zeta}{\Lambda^2} \left( \frac{\partial \phi}{\partial y} \right)^2, \end{aligned} \quad (7.41)$$

$$S_G''' = \frac{\kappa(T_1 - T_0)^2}{T_m^2 d^2}, \quad \Lambda = \frac{T_1 - T_0}{T_m}, \quad L = \frac{RD(C_1 - C_0)}{\kappa}, \quad \zeta = \frac{(C_1 - C_0)}{C_m}. \quad (7.42)$$

### 7.3 Analysis

The involved problem comprises non-linear system. Thus exact solution of this problem is not possible. However an approximate solution can be found via any technique like numerical technique or perturbation technique. To solve this problem built in command NDSolve of Mathematica 9.0 is used. As this technique helps us to avoid the lengthy expressions and gave the best results in minimum CPU time (3-4 min). Therefore graphical analysis is done for velocity, temperature, concentration, heat transfer coefficient and entropy generation. For the sake of convenience we have made subsections for each physical quantity.

#### 7.3.1 Velocity

Velocity is discussed for the parameters of interest in this subsection. Fig. 7.2 manifested the behavior of Hartman number on velocity. Decreasing behavior for velocity is noticed. For enhancing the retarding force this acts as obstruction to flow. This investigation is employed to reduce the blood flow during operations and severe injuries. Fig. 7.3 is plotted against velocity slip parameter on velocity. Velocity enhances via increasing slip parameter. This happens due to reduction in frictional effects. Fig. 7.4 elucidates results of fluid parameter effect on velocity. Dual behavior is observed in this case. Compliant walls effect is seen via Fig. 7.5. Elastance nature of walls leads to an increase in velocity whereas damping resists the fluid flow. Elastance nature of walls allows the perfusion of blood in arteries and vein. These characteristics also allow the exchange of nutrient and oxygen.



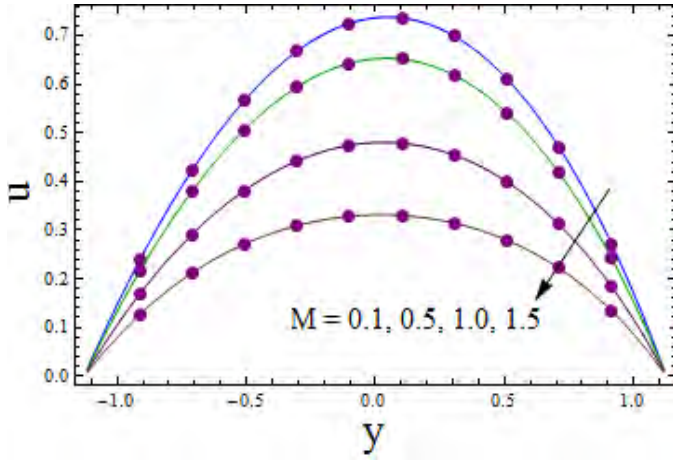


Fig. 7.2

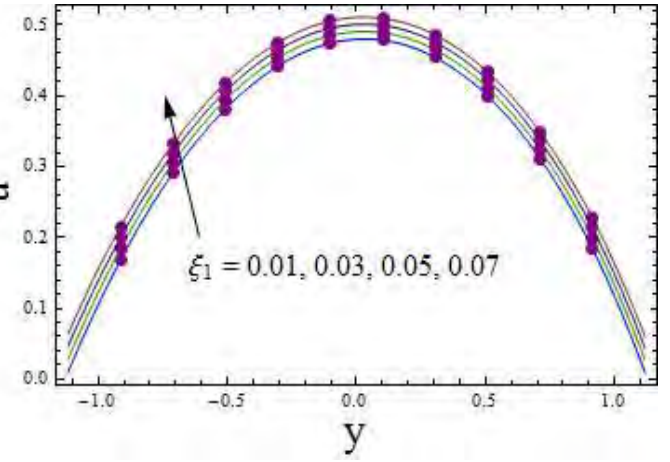


Fig. 7.3

Fig. 7.2.  $u$  via change in  $M$  when  $E_1 = 0.02$ ,  $E_2 = 0.01$ ,  $E_3 = 0.01$ ,  $t = 0.1$ ,  $x = 0.2$ ,  $\varepsilon = 0.2$ ,  $n = 1.5$ ,  $\xi_1 = 0.01$ ,  $\xi_2 = 0.01$ ,  $\xi_3 = 0.01$ ,  $Nt = 0.1$ ,  $Nb = 0.1$ ,  $\beta_1 = 0.2$ ,  $Pr = 1.5$ ,  $Br = 2.0$ ,  $Rd = 0.5$ ,  $\theta_w = 1.1$ .

Fig. 7.3.  $u$  via change in  $\xi_1$  when  $E_1 = 0.02$ ,  $E_2 = 0.01$ ,  $E_3 = 0.01$ ,  $t = 0.1$ ,  $x = 0.2$ ,  $\varepsilon = 0.2$ ,  $n = 1.5$ ,  $\xi_2 = 0.01$ ,  $\xi_3 = 0.01$ ,  $Nt = 0.1$ ,  $Nb = 0.1$ ,  $\beta_1 = 0.2$ ,  $Pr = 1.5$ ,  $Br = 2.0$ ,  $M = 0.1$ ,  $Rd = 0.5$ ,  $\theta_w = 1.1$ .

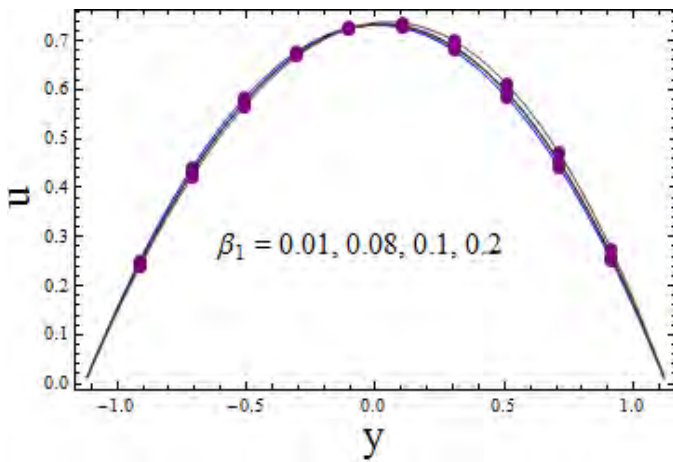


Fig. 7.4

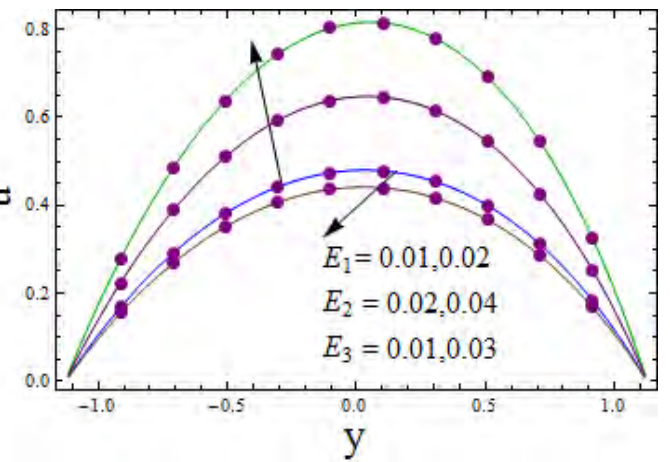


Fig. 7.5

Fig. 7.4.  $u$  via change in  $\beta_1$  when  $E_1 = 0.02$ ,  $E_2 = 0.01$ ,  $E_3 = 0.01$ ,  $t = 0.1$ ,  $x = 0.2$ ,  $\varepsilon = 0.2$ ,

$$n = 1.5, \xi_1 = 0.01, \xi_2 = 0.01, \xi_3 = 0.01, Nt = 0.1, Nb = 0.1, Pr = 1.5, Br = 2.0, M = 0.1, \\ Rd = 0.5, \theta_w = 1.1.$$

*Fig. 7.5.*  $u$  via change in  $E_1$ ,  $E_2$  and  $E_3$  when  $t = 0.1$ ,  $x = 0.2$ ,  $\varepsilon = 0.2$ ,  $n = 1.5$ ,  $\xi_1 = 0.01$ ,  $\xi_2 = 0.01$ ,  $\xi_3 = 0.01$ ,  $Nt = 0.1$ ,  $Nb = 0.1$ ,  $\beta_1 = 0.2$ ,  $Pr = 1.5$ ,  $Br = 2.0$ ,  $M = 0.1$ ,  $Rd = 0.5$ ,  $\theta_w = 1.1$ .

### 7.3.2 Temperature

Temperature behavior for pertinent parameters is discussed via Figs. 7.6-7.14. Fig. 7.6 indicated that for larger Hartman number,  $\theta$  tends to increase at center of channel in view of Joule heating effects. Fig. 7.7 is drawn for the sake of Brownian motion effects on temperature. Increasing Brownian motion parameter leads to higher temperature. Random motion of the particles elevated the kinetic energy and molecular vibrations. Hence rise in  $\theta$  is verified. Moreover thermophoresis ( $Nt$ ) on  $\theta$  shows the same behavior (see Fig. 7.8). Thermal slip result on  $\theta$  is notified through Fig. 7.9. It is clearly seen via this Fig. that thermal slip parameter leads to an enhancement in temperature. As slip reduces the friction and hence rise in velocity and in temperature. Fig. 7.10 demonstrates fluid parameter behavior. Here temperature is increasing. Figs. 7.11 and 7.12 display the radiation parameter and Brinkman number impacts on  $\theta$ . Reverse behavior is seen for both cases. Basically Brinkman number measures the heat loss due to viscous dissipation. This includes the conversion in internal energy results in heating up the fluid. So temperature rises for more heat loss. Fig. 7.13 portrayed the influence of  $\theta_w$  on temperature. Result show that decay is observed in this case. Fig. 7.14 is drawn for  $E'_i$ 's ( $i = 1 - 3$ ) influence on temperature. Here  $E_1$  and  $E_2$  tend to increase the temperature whereas  $E_3$  leads to decay of temperature. Reason can be linked with velocity in view of kinetic theory.

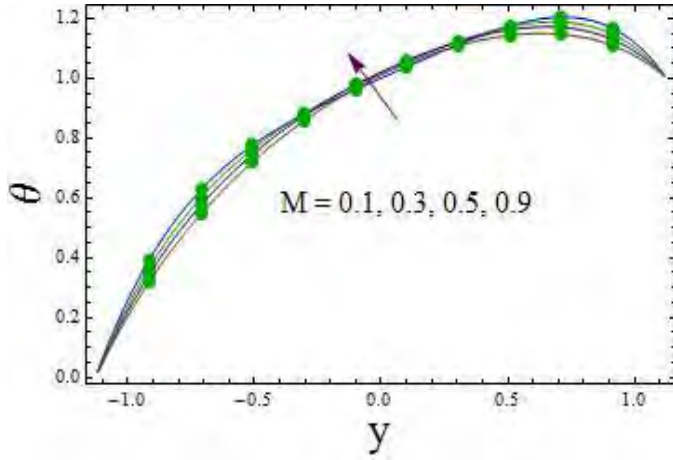


Fig. 7.6

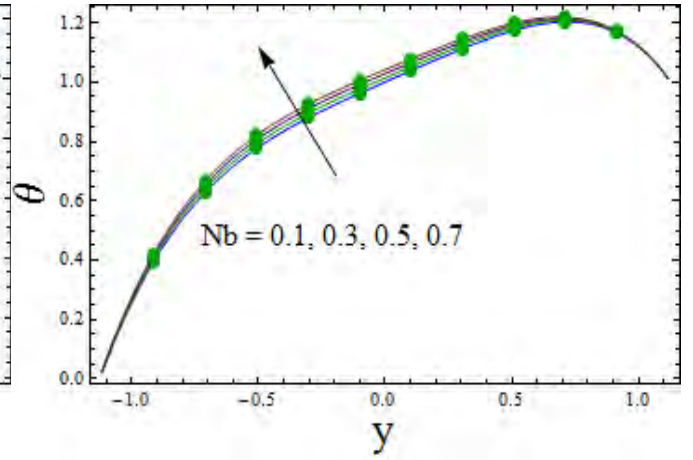


Fig. 7.7

Fig. 7.6.  $\theta$  via change in  $M$  when  $E_1 = 0.02$ ,  $E_2 = 0.01$ ,  $E_3 = 0.01$ ,  $t = 0.1$ ,  $x = 0.2$ ,  $\varepsilon = 0.2$ ,  $n = 1.5$ ,  $\xi_1 = 0.01$ ,  $\xi_2 = 0.01$ ,  $\xi_3 = 0.01$ ,  $Nt = 0.1$ ,  $Nb = 0.1$ ,  $\beta_1 = 0.2$ ,  $Pr = 1.5$ ,  $Br = 2.0$ ,  $Rd = 0.5$ ,  $\theta_w = 1.1$ .

Fig. 7.7.  $\theta$  via change in  $Nb$  when  $E_1 = 0.02$ ,  $E_2 = 0.01$ ,  $E_3 = 0.01$ ,  $t = 0.1$ ,  $x = 0.2$ ,  $\varepsilon = 0.2$ ,  $n = 1.5$ ,  $\xi_1 = 0.01$ ,  $\xi_2 = 0.01$ ,  $\xi_3 = 0.01$ ,  $Nt = 0.1$ ,  $\beta_1 = 0.2$ ,  $Pr = 1.5$ ,  $Br = 2.0$ ,  $M = 0.1$ ,  $Rd = 0.5$ ,  $\theta_w = 1.1$ .

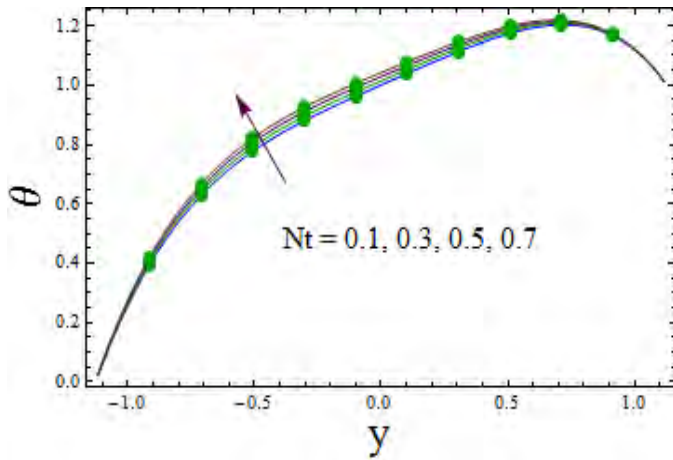


Fig. 7.8

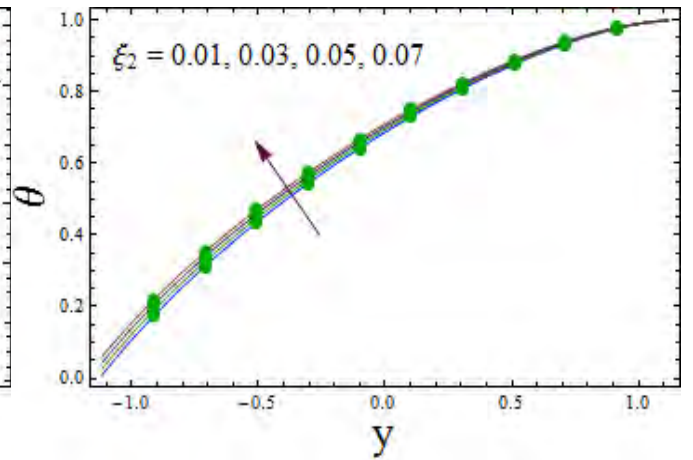


Fig. 7.9

Fig. 7.8.  $\theta$  via change in  $Nt$  when  $E_1 = 0.02$ ,  $E_2 = 0.01$ ,  $E_3 = 0.01$ ,  $t = 0.1$ ,  $x = 0.2$ ,  $\varepsilon = 0.2$ ,

$n = 1.5, \xi_1 = 0.01, \xi_2 = 0.01, \xi_3 = 0.01, Nb = 0.1, \beta_1 = 0.2, Pr = 1.5, Br = 2.0, M = 0.1,$   
 $Rd = 0.5, \theta_w = 1.1.$

*Fig. 7.9.*  $\theta$  via change in  $\xi_2$  when  $E_1 = 0.02, E_2 = 0.01, E_3 = 0.01, t = 0.1, x = 0.2, \varepsilon = 0.2,$   
 $n = 1.5, \xi_1 = 0.01, \xi_3 = 0.01, Nt = 0.1, Nb = 0.1, \beta_1 = 0.2, Pr = 1.5, Br = 2.0, M = 0.1,$   
 $Rd = 0.5, \theta_w = 1.1.$

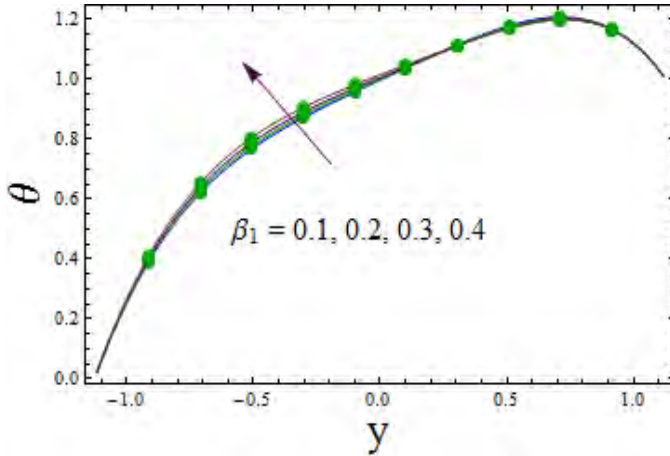


Fig. 7.10

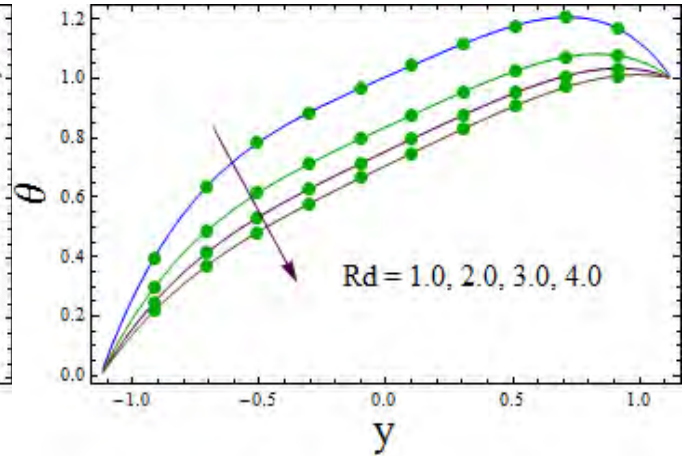


Fig. 7.11

*Fig. 7.10.*  $\theta$  via change in  $\beta_1$  when  $E_1 = 0.02, E_2 = 0.01, E_3 = 0.01, t = 0.1, x = 0.2, \varepsilon = 0.2,$   
 $n = 1.5, \xi_1 = 0.01, \xi_2 = 0.01, \xi_3 = 0.01, Nt = 0.1, Nb = 0.1, Pr = 1.5, Br = 2.0, M = 0.1,$   
 $Rd = 0.5, \theta_w = 1.1.$

*Fig. 7.11.*  $\theta$  via change in  $Rd$  when  $E_1 = 0.02, E_2 = 0.01, E_3 = 0.01, t = 0.1, x = 0.2, \varepsilon = 0.2,$   
 $n = 1.5, \xi_1 = 0.01, \xi_2 = 0.01, \xi_3 = 0.01, Nt = 0.1, Nb = 0.1, \beta_1 = 0.2, Pr = 1.5, Br = 2.0,$   
 $M = 0.1, \theta_w = 1.1.$

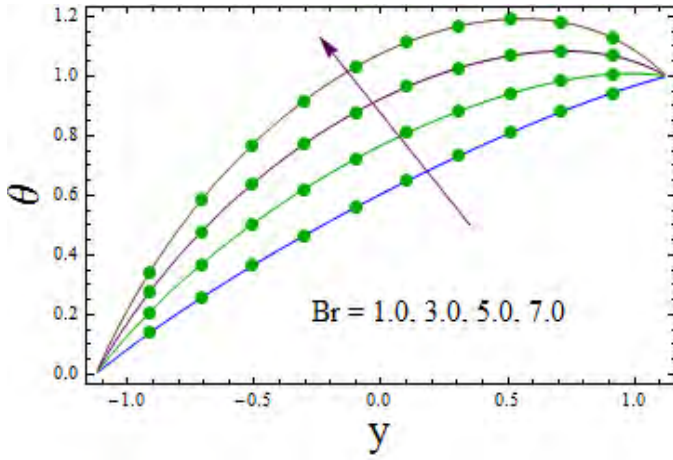


Fig. 7.12

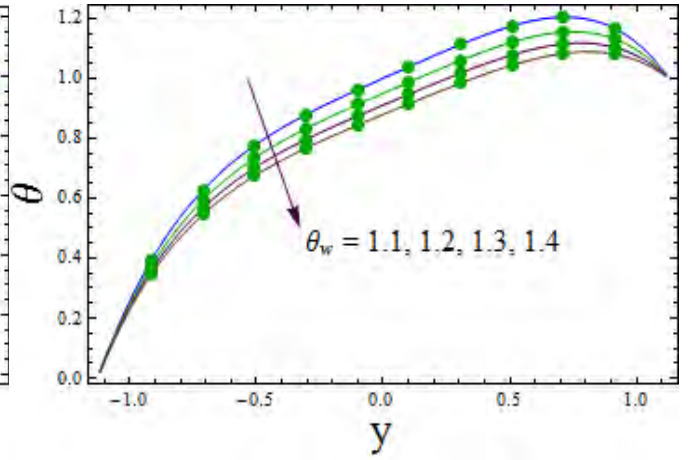


Fig. 7.13

Fig. 7.12.  $\theta$  via change in  $Br$  when  $E_1 = 0.02$ ,  $E_2 = 0.01$ ,  $E_3 = 0.01$ ,  $t = 0.1$ ,  $x = 0.2$ ,  $\varepsilon = 0.2$ ,  $n = 1.5$ ,  $\xi_1 = 0.01$ ,  $\xi_2 = 0.01$ ,  $\xi_3 = 0.01$ ,  $Nt = 0.1$ ,  $Nb = 0.1$ ,  $\beta_1 = 0.2$ ,  $Pr = 1.5$ ,  $M = 0.1$ ,  $Rd = 0.5$ ,  $\theta_w = 1.1$ .

Fig. 7.13.  $\theta$  via change in  $\theta_w$  when  $E_1 = 0.02$ ,  $E_2 = 0.01$ ,  $E_3 = 0.01$ ,  $t = 0.1$ ,  $x = 0.2$ ,  $\varepsilon = 0.2$ ,  $n = 1.5$ ,  $\xi_1 = 0.01$ ,  $\xi_2 = 0.01$ ,  $\xi_3 = 0.01$ ,  $Nt = 0.1$ ,  $Nb = 0.1$ ,  $\beta_1 = 0.2$ ,  $Pr = 1.5$ ,  $Br = 2.0$ ,  $M = 0.1$ ,  $Rd = 0.5$ .

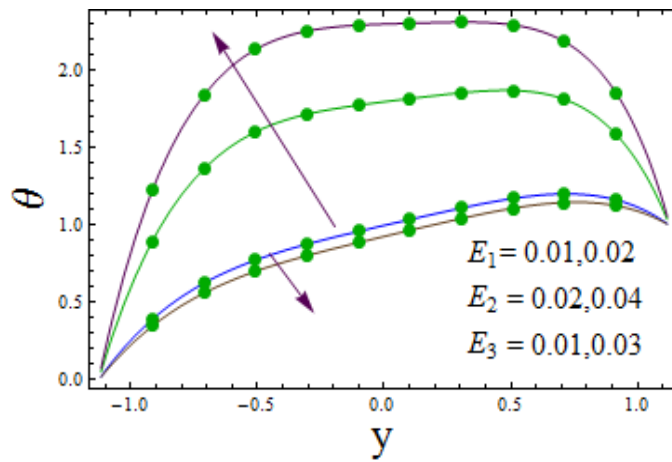


Fig. 7.14

Fig. 7.14.  $\theta$  via change in  $E_1$ ,  $E_2$  and  $E_3$  when  $t = 0.1$ ,  $x = 0.2$ ,  $\varepsilon = 0.2$ ,  $n = 1.5$ ,  $\xi_1 = 0.01$ ,

$$\xi_2 = 0.01, \xi_3 = 0.01, Nt = 0.1, Nb = 0.1, \beta_1 = 0.2, Pr = 1.5, Br = 2.0, M = 0.1, Rd = 0.5, \\ \theta_w = 1.1.$$

### 7.3.3 Nanoparticle concentration

This subsection contains the information about concentration under the influences of embedded parameters of interest. Fig. 7.15 is prepared for the sake of concentration slip parameter on  $\phi$ . It is seen that an enhancement in concentration slip parameter leads to decay in concentration. Fig. 7.16 reveals the result that enhancement in  $\theta_w$  give rise to  $\phi$ . Figs. 7.17 and 7.18 display decreasing behavior of radiation parameter ( $Rd$ ) and thermophoresis parameter ( $Nt$ ) respectively. Fig. 7.18 displayed opposite behavior when compared with temperature. Brownian motion parameter result on  $\phi$  is seen opposite than  $Nt$  (see Fig. 7.19). For increasing  $Nb$  the random motion of the particles enhances and rise in concentration is observed. Wall parameters display decay for elastance parameters whereas enhancement is observed for damping variable (see Fig. 7.20).

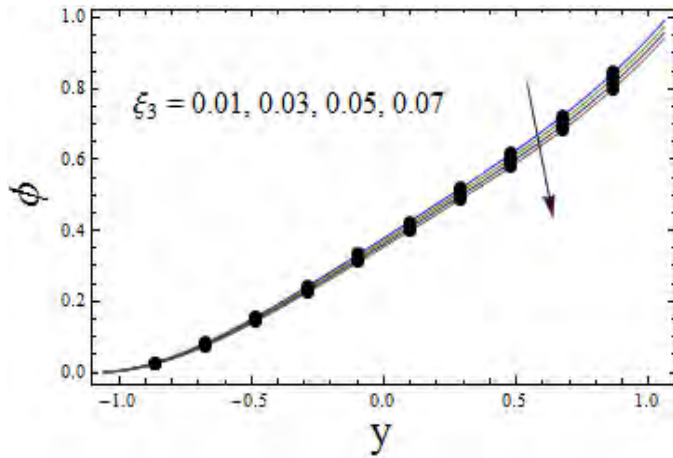


Fig. 7.15

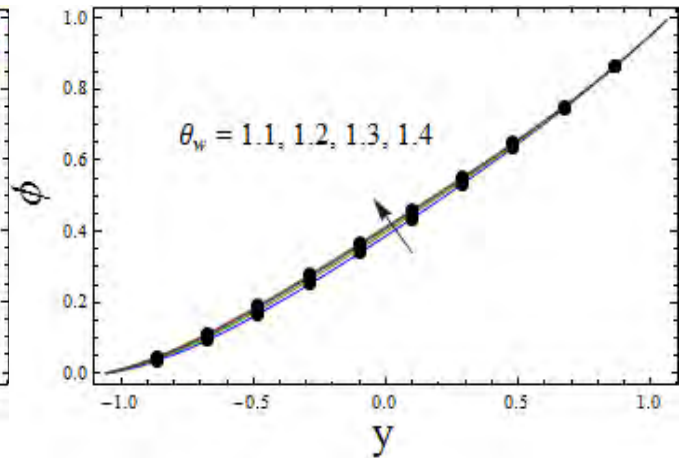


Fig. 7.16

Fig. 7.15.  $\phi$  via change in  $\xi_3$  when  $E_1 = 0.02, E_2 = 0.01, E_3 = 0.01, t = 0.1, x = 0.2, \varepsilon = 0.1, n = 1.5, \xi_1 = 0.01, \xi_2 = 0.01, Nt = 0.1, Nb = 0.1, \beta_1 = 0.2, Pr = 1.5, Br = 2.0, M = 0.1, Rd = 0.5, \theta_w = 1.1.$

Fig. 7.16.  $\phi$  via change in  $\theta_w$  when  $E_1 = 0.02, E_2 = 0.01, E_3 = 0.01, t = 0.1, x = 0.2, \varepsilon = 0.1,$

$n = 1.5, \xi_1 = 0.01, \xi_2 = 0.01, \xi_3 = 0.01, Nt = 0.1, Nb = 0.1, \beta_1 = 0.2, Pr = 1.5, Br = 2.0,$   
 $M = 0.1, Rd = 0.5.$

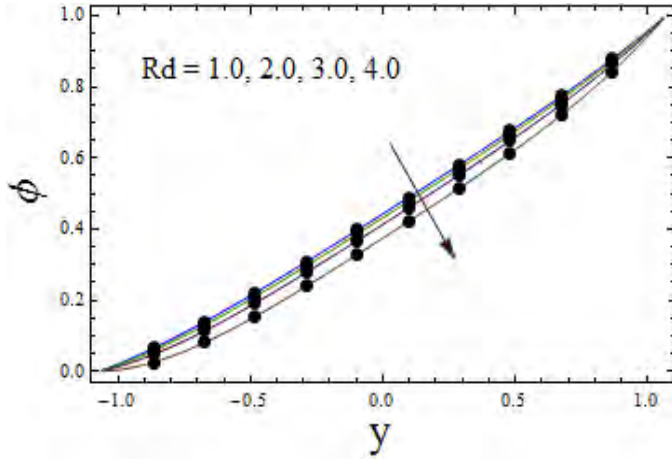


Fig. 7.17

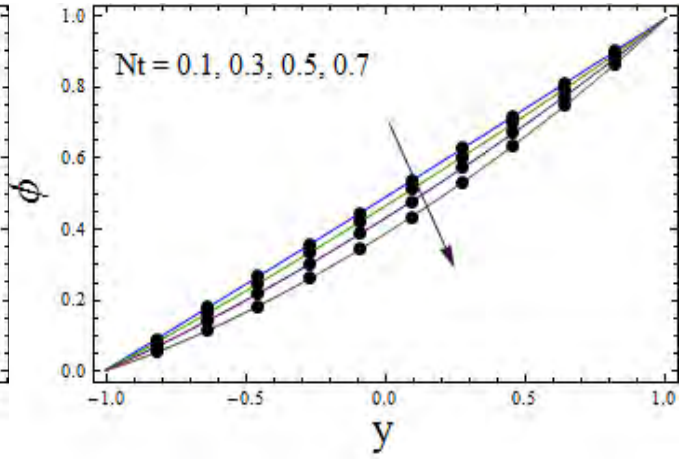


Fig. 7.18

*Fig. 7.17.*  $\phi$  via change in  $Rd$  when  $E_1 = 0.02, E_2 = 0.01, E_3 = 0.01, t = 0.1, x = 0.2, \varepsilon = 0.1,$   
 $n = 1.5, \xi_1 = 0.01, \xi_2 = 0.01, \xi_3 = 0.01, Nt = 0.1, Nb = 0.1, \beta_1 = 0.2, Pr = 1.5, Br = 2.0,$   
 $M = 0.1, \theta_w = 1.1.$

*Fig. 7.18.*  $\phi$  via change in  $Nt$  when  $E_1 = 0.02, E_2 = 0.01, E_3 = 0.01, t = 0.1, x = 0.2, \varepsilon = 0.1,$   
 $n = 1.5, \xi_1 = 0.01, \xi_2 = 0.01, \xi_3 = 0.01, Nb = 0.1, \beta_1 = 0.2, Pr = 1.5, Br = 2.0, M = 0.1,$   
 $Rd = 0.5, \theta_w = 1.1.$



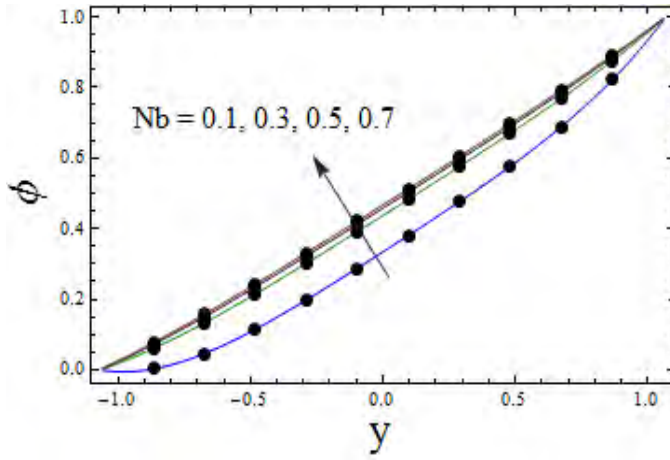


Fig. 7.19

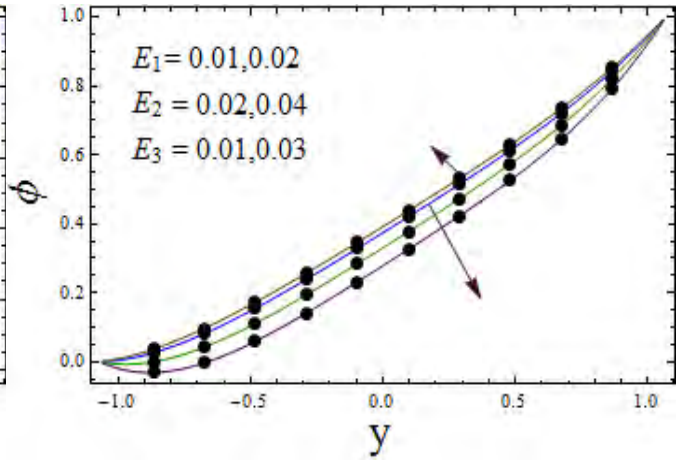


Fig. 7.20

Fig. 7.19.  $\phi$  via change in  $Nb$  when  $E_1 = 0.02$ ,  $E_2 = 0.01$ ,  $E_3 = 0.01$ ,  $t = 0.1$ ,  $x = 0.2$ ,  $\varepsilon = 0.1$ ,  $n = 1.5$ ,  $\xi_1 = 0.01$ ,  $\xi_2 = 0.01$ ,  $\xi_3 = 0.01$ ,  $Nt = 0.1$ ,  $\beta_1 = 0.2$ ,  $Pr = 1.5$ ,  $Br = 2.0$ ,  $M = 0.1$ ,  $Rd = 0.5$ ,  $\theta_w = 1.1$ .

Fig. 7.20.  $\phi$  via change in  $E_1$ ,  $E_2$  and  $E_3$  when  $E_1 = 0.02$ ,  $E_2 = 0.01$ ,  $E_3 = 0.01$ ,  $t = 0.1$ ,  $x = 0.2$ ,  $\varepsilon = 0.1$ ,  $n = 1.5$ ,  $\xi_1 = 0.01$ ,  $\xi_2 = 0.01$ ,  $\xi_3 = 0.01$ ,  $Nt = 0.1$ ,  $Nb = 0.1$ ,  $\beta_1 = 0.2$ ,  $Pr = 1.5$ ,  $Br = 2.0$ ,  $M = 0.1$ ,  $Rd = 0.5$ ,  $\theta_w = 1.1$ .

### 7.3.4 Entropy generation analysis

In this subsection the analysis of entropy generation is presented for pertinent parameters of interest. Fig. 7.21 is drawn for the analysis of entropy generation in view of Hartman number. Entropy increases near center of channel in view of Joule heating.  $Nt$  and  $Nb$  behaviors on entropy are observed via Figs. 7.22 and 7.23. Both cases show enhancement as in case of temperature. Enhancement in kinetic energy of the particles create more disorderliness. Fig. 7.24 elucidates radiation parameter results on entropy. Radiation caused enhancement in the disorderedness. Fig. 7.25 illustrates that larger values of  $\theta_w$  tend to decrease in entropy. For larger values of concentration difference parameter ( $\zeta$ ), Fig. 7.26 is plotted. Enhancement is observed in this case. Influence of diffusion coefficient parameter  $L$  on  $Ns$  is viewed via Fig. 7.27. Entropy is an increasing function of  $L$ . An increase in  $L$  causes decrease of thermal conductivity.



It shows an increase in temperature and entropy. Temperature difference parameter leads to decay in entropy (see Fig. 7.28). Thermal slip effect on entropy is plotted against Fig. 7.29. Results reveals decaying behavior here.

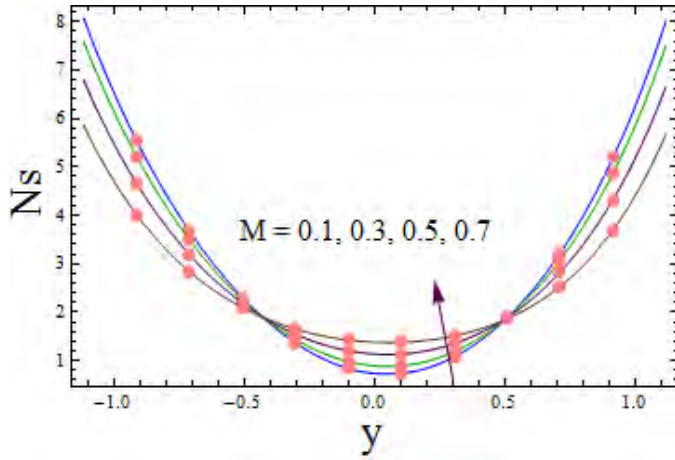


Fig. 7.21

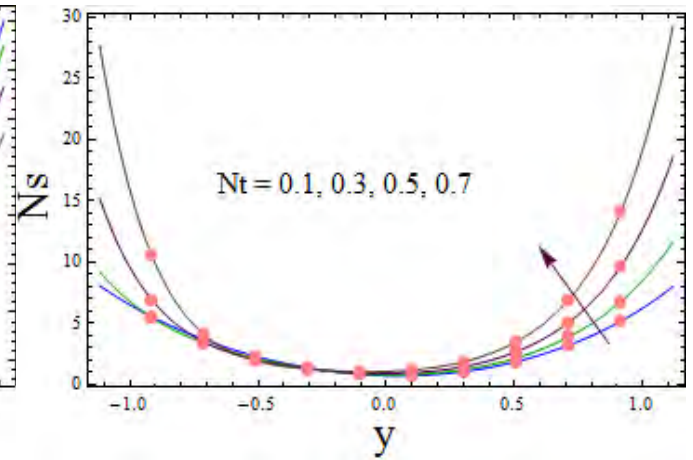


Fig. 7.22

*Fig. 7.21.*  $Ns$  via change in  $M$  when  $E_1 = 0.02$ ,  $E_2 = 0.01$ ,  $E_3 = 0.01$ ,  $t = 0.1$ ,  $x = 0.2$ ,  $\varepsilon = 0.2$ ,  $n = 1.5$ ,  $\xi_1 = 0.01$ ,  $\xi_2 = 0.01$ ,  $\xi_3 = 0.01$ ,  $Nt = 0.1$ ,  $Nb = 0.1$ ,  $\beta_1 = 0.2$ ,  $Pr = 1.5$ ,  $Br = 2.0$ ,  $Rd = 0.5$ ,  $\theta_w = 1.1$ ,  $\Lambda = 0.5$ ,  $\zeta = 0.5$ ,  $L = 0.5$ .

*Fig. 7.22.*  $Ns$  via change in  $Nt$  when  $E_1 = 0.02$ ,  $E_2 = 0.01$ ,  $E_3 = 0.01$ ,  $t = 0.1$ ,  $x = 0.2$ ,  $\varepsilon = 0.2$ ,  $n = 1.5$ ,  $\xi_1 = 0.01$ ,  $\xi_2 = 0.01$ ,  $\xi_3 = 0.01$ ,  $Nb = 0.1$ ,  $\beta_1 = 0.2$ ,  $Pr = 1.5$ ,  $Br = 2.0$ ,

$$M = 0.1, Rd = 0.5, \theta_w = 1.1, \Lambda = 0.5, \zeta = 0.5, L = 0.5.$$

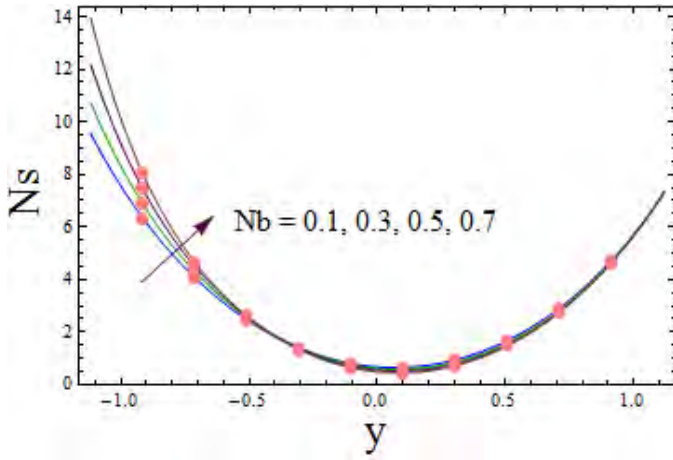


Fig. 7.23

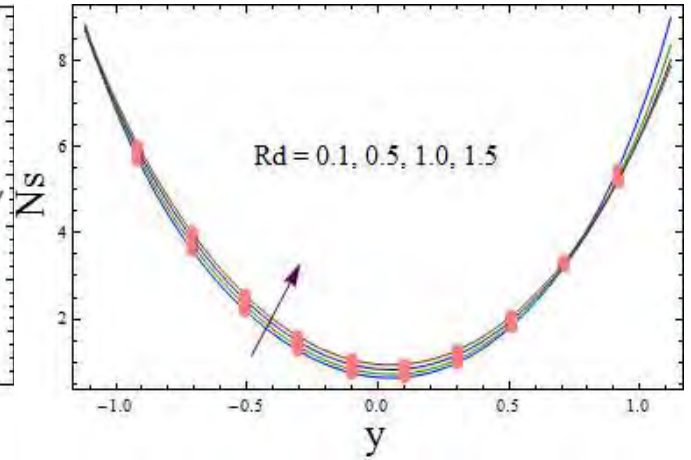


Fig. 7.24

Fig. 7.23.  $Ns$  via change in  $Nb$  when  $E_1 = 0.02$ ,  $E_2 = 0.01$ ,  $E_3 = 0.01$ ,  $t = 0.1$ ,  $x = 0.2$ ,  $\varepsilon = 0.2$ ,  $n = 1.5$ ,  $\xi_1 = 0.01$ ,  $\xi_2 = 0.01$ ,  $\xi_3 = 0.01$ ,  $Nt = 0.1$ ,  $\beta_1 = 0.2$ ,  $Pr = 1.5$ ,  $Br = 2.0$ ,  $M = 0.1$ ,  $Rd = 0.5$ ,  $\theta_w = 1.1$ ,  $\Lambda = 0.5$ ,  $\zeta = 0.5$ ,  $L = 0.5$ .

Fig. 7.24.  $Ns$  via change in  $Rd$  when  $E_1 = 0.02$ ,  $E_2 = 0.01$ ,  $E_3 = 0.01$ ,  $t = 0.1$ ,  $x = 0.2$ ,  $\varepsilon = 0.2$ ,  $n = 1.5$ ,  $\xi_1 = 0.01$ ,  $\xi_2 = 0.01$ ,  $\xi_3 = 0.01$ ,  $Nt = 0.1$ ,  $Nb = 0.1$ ,  $\beta_1 = 0.2$ ,  $Pr = 1.5$ ,  $Br = 2.0$ ,  $M = 0.1$ ,  $\theta_w = 1.1$ ,  $\Lambda = 0.5$ ,  $\zeta = 0.5$ ,  $L = 0.5$ .

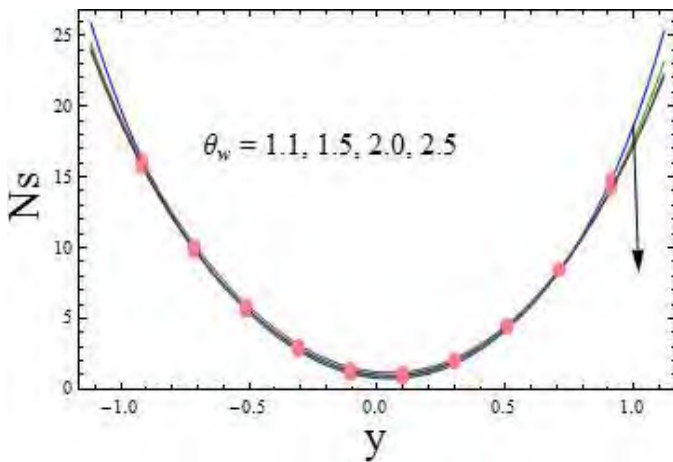


Fig. 7.25

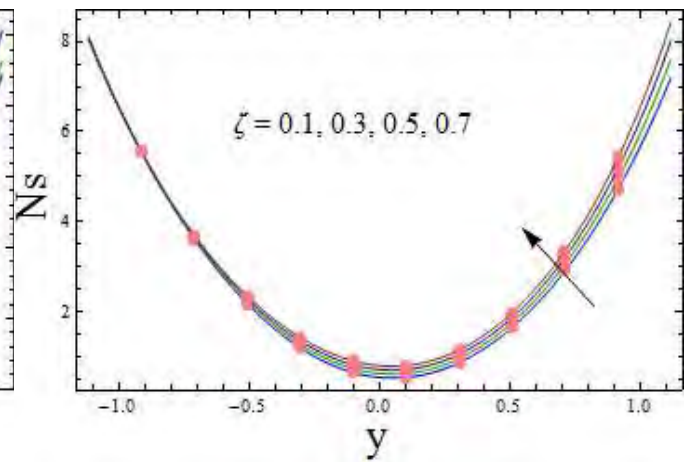


Fig. 7.26

Fig. 7.25.  $Ns$  via change in  $\theta_w$  when  $E_1 = 0.02$ ,  $E_2 = 0.01$ ,  $E_3 = 0.01$ ,  $t = 0.1$ ,  $x = 0.2$ ,

$$\varepsilon = 0.2, n = 1.5, \xi_1 = 0.01, \xi_2 = 0.01, \xi_3 = 0.01, Nt = 0.1, Nb = 0.1, \beta_1 = 0.2, Pr = 1.5,$$

$$Br = 2.0, M = 0.1, Rd = 0.5, \Lambda = 0.5, \zeta = 0.5, L = 0.5.$$

Fig. 7.26.  $Ns$  via change in  $\zeta$  when  $E_1 = 0.02, E_2 = 0.01, E_3 = 0.01, t = 0.1, x = 0.2, \varepsilon = 0.2,$   
 $n = 1.5, \xi_1 = 0.01, \xi_2 = 0.01, \xi_3 = 0.01, Nt = 0.1, Nb = 0.1, \beta_1 = 0.2, Pr = 1.5, Br = 2.0,$   
 $M = 0.1, Rd = 0.5, \theta_w = 1.1, \Lambda = 0.5, L = 0.5.$

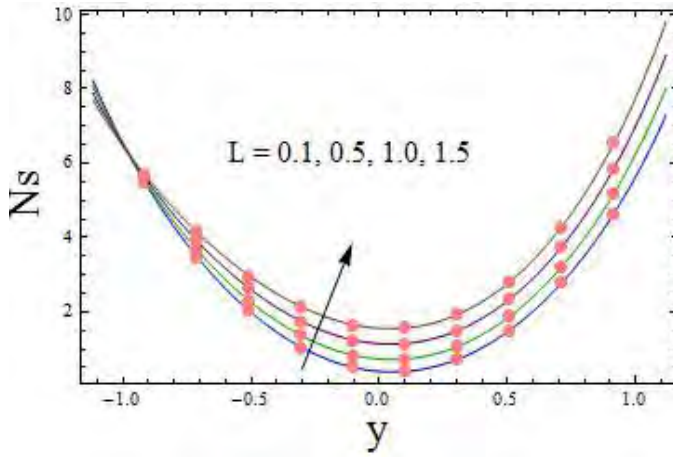


Fig. 7.27

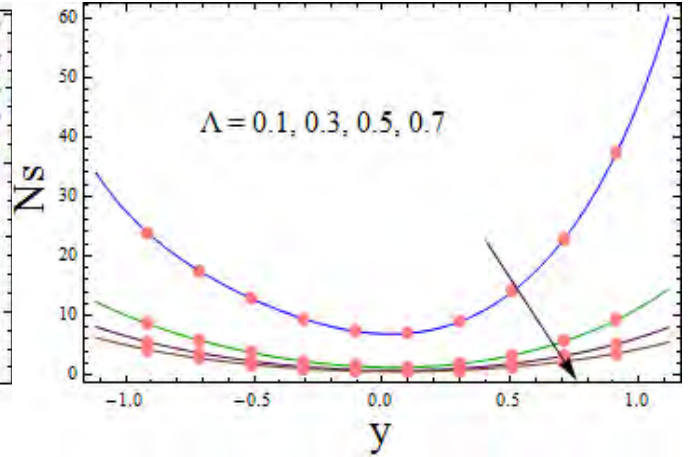


Fig. 7.28

Fig. 7.27.  $Ns$  via change in  $L$  when  $E_1 = 0.02, E_2 = 0.01, E_3 = 0.01, t = 0.1, x = 0.2,$   
 $\varepsilon = 0.2, n = 1.5, \xi_1 = 0.01, \xi_2 = 0.01, \xi_3 = 0.01, Nt = 0.1, Nb = 0.1, \beta_1 = 0.2, Pr = 1.5,$   
 $Br = 2.0, M = 0.1, Rd = 0.5, \theta_w = 1.1, \Lambda = 0.5, \zeta = 0.5.$

Fig. 7.28.  $Ns$  via change in  $\Lambda$  when  $E_1 = 0.02, E_2 = 0.01, E_3 = 0.01, t = 0.1, x = 0.2,$   
 $\varepsilon = 0.2, n = 1.5, \xi_1 = 0.01, \xi_2 = 0.01, \xi_3 = 0.01, Nt = 0.1, Nb = 0.1, \beta_1 = 0.2, Pr = 1.5,$   
 $Br = 2.0, M = 0.1, Rd = 0.5, \theta_w = 1.1, \zeta = 0.5, L = 0.5.$

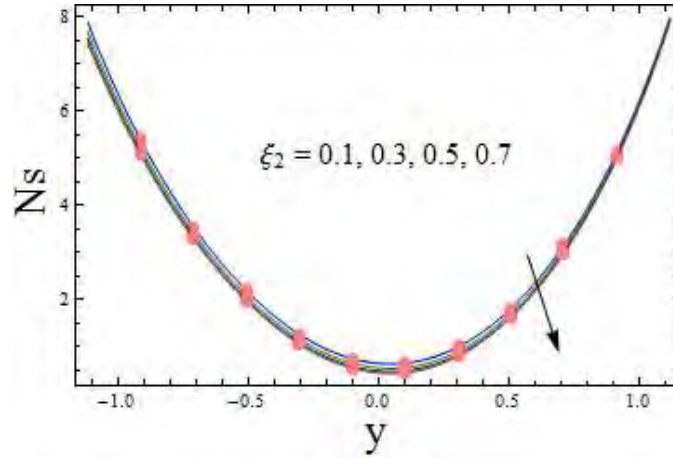


Fig. 7.29

*Fig. 7.29.*  $Ns$  via change in  $\xi_2$  when  $E_1 = 0.02$ ,  $E_2 = 0.01$ ,  $E_3 = 0.01$ ,  $t = 0.1$ ,  $x = 0.2$ ,  $\varepsilon = 0.2$ ,  $n = 1.5$ ,  $\xi_1 = 0.01$ ,  $\xi_3 = 0.01$ ,  $Nt = 0.1$ ,  $Nb = 0.1$ ,  $\beta_1 = 0.2$ ,  $Pr = 1.5$ ,  $Br = 2.0$ ,  $M = 0.1$ ,  $Rd = 0.5$ ,  $\theta_w = 1.1$ ,  $\Lambda = 0.5$ ,  $\zeta = 0.5$ ,  $L = 0.5$ .

### 7.3.5 Heat transfer coefficient

Plots for heat transfer coefficient are drawn through Figs. 7.30-7.35. Fig. 7.30 represents the  $M$  behavior. Heat transfer coefficient decreases via  $M$ . Results for  $Nb$  and  $\theta_w$  can be seen via Figs. 7.31 and 7.32. Decay in heat transfer coefficient are seen. Radiation parameter portrayed an enhancement in  $Z$  (see Fig. 7.33). Thermal slip parameter caused reduction in  $Z$  whereas walls parameters results are qualitatively similar to temperature (see Figs. 7.34 and 7.35).

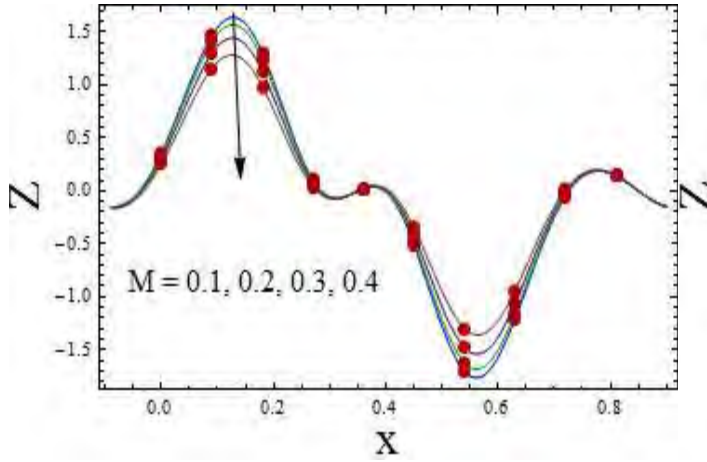


Fig. 7.30

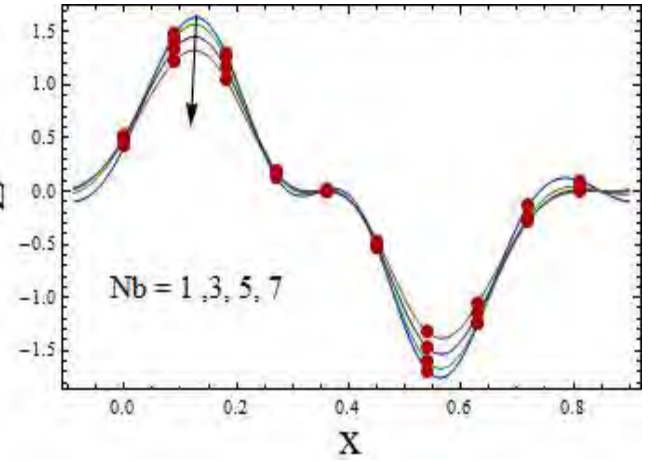


Fig. 7.31

Fig. 7.30.  $Z$  via change in  $M$  when  $E_1 = 0.02$ ,  $E_2 = 0.01$ ,  $E_3 = 0.01$ ,  $t = 0.1$ ,  $\varepsilon = 0.2$ ,  $n = 1.5$ ,  $\xi_1 = 0.01$ ,  $\xi_2 = 0.01$ ,  $\xi_3 = 0.01$ ,  $Nt = 0.1$ ,  $Nb = 0.1$ ,  $\beta_1 = 0.2$ ,  $Pr = 1.5$ ,  $Br = 2.0$ ,  $Rd = 0.5$ ,  $\theta_w = 1.1$ .

Fig. 7.31.  $Z$  via change in  $Nb$  when  $E_1 = 0.02$ ,  $E_2 = 0.01$ ,  $E_3 = 0.01$ ,  $t = 0.1$ ,  $\varepsilon = 0.2$ ,  $n = 1.5$ ,  $\xi_1 = 0.01$ ,  $\xi_2 = 0.01$ ,  $\xi_3 = 0.01$ ,  $Nt = 0.1$ ,  $\beta_1 = 0.2$ ,  $Pr = 1.5$ ,  $Br = 2.0$ ,  $M = 0.1$ ,  $Rd = 0.5$ ,  $\theta_w = 1.1$ .

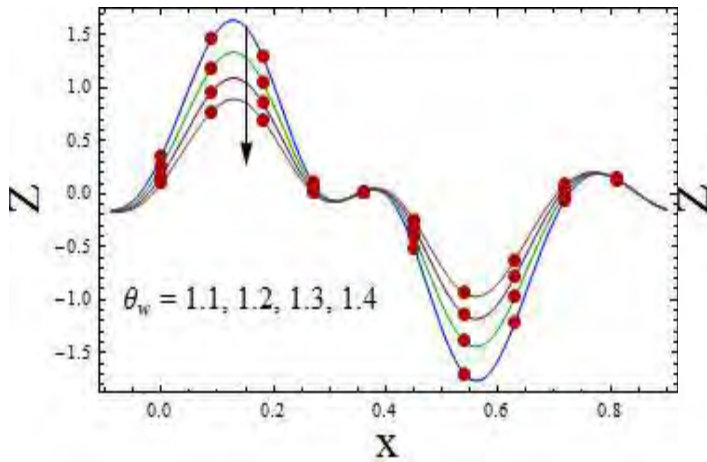


Fig. 7.32

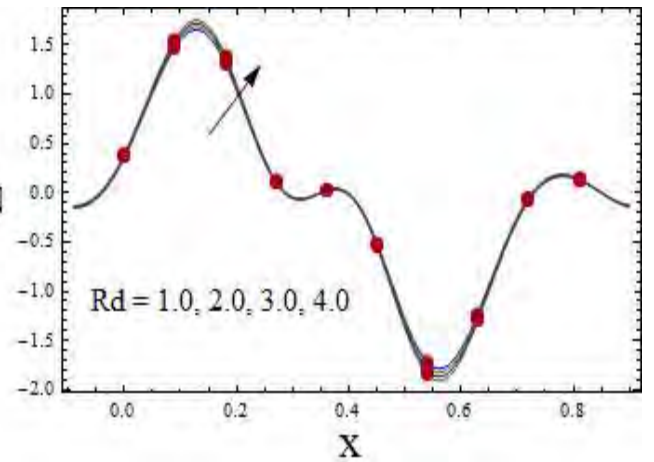


Fig. 7.33

Fig. 7.32.  $Z$  via change in  $\theta_w$  when  $E_1 = 0.02$ ,  $E_2 = 0.01$ ,  $E_3 = 0.01$ ,  $t = 0.1$ ,  $\varepsilon = 0.2$ ,  $n = 1.5$ ,

$$\xi_1 = 0.01, \xi_2 = 0.01, \xi_3 = 0.01, Nt = 0.1, Nb = 0.1, \beta_1 = 0.2, Pr = 1.5, Br = 2.0, M = 0.1, \\ Rd = 0.5.$$

*Fig. 7.33.*  $Z$  via change in  $Rd$  when  $E_1 = 0.02, E_2 = 0.01, E_3 = 0.01, t = 0.1, \varepsilon = 0.2,$   
 $n = 1.5, \xi_1 = 0.01, \xi_2 = 0.01, \xi_3 = 0.01, Nt = 0.1, Nb = 0.1, \beta_1 = 0.2, Pr = 1.5, Br = 2.0,$   
 $M = 0.1, \theta_w = 1.1.$

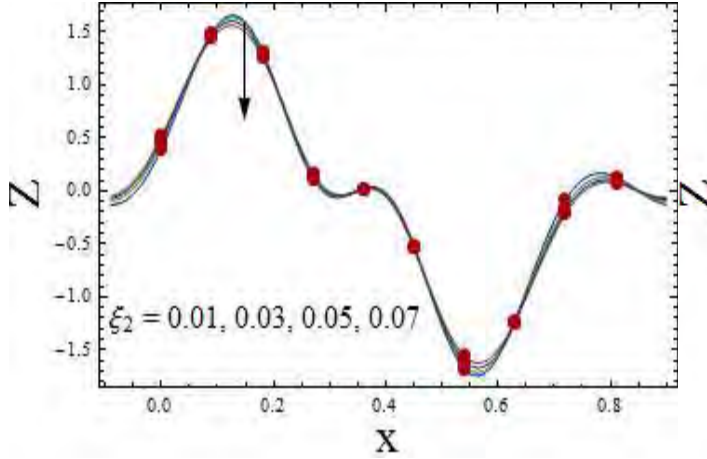


Fig. 7.34

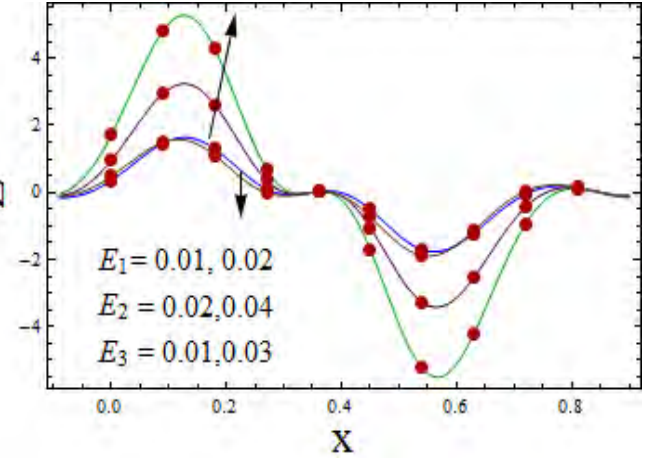


Fig. 7.35

*Fig. 7.34.*  $Z$  via change in  $\xi_2$  when  $E_1 = 0.02, E_2 = 0.01, E_3 = 0.01, t = 0.1, \varepsilon = 0.2, n = 1.5,$   
 $\xi_1 = 0.01, \xi_3 = 0.01, Nt = 0.1, Nb = 0.1, \beta_1 = 0.2, Pr = 1.5, Br = 2.0, M = 0.1, Rd = 0.5,$   
 $\theta_w = 1.1.$

*Fig. 7.35.*  $Z$  via change in  $E_1, E_2$  and  $E_3$  when  $t = 0.1, \varepsilon = 0.2, n = 1.5, \xi_1 = 0.01, \xi_2 = 0.01,$   
 $\xi_3 = 0.01, Nt = 0.1, Nb = 0.1, \beta_1 = 0.2, Pr = 1.5, Br = 2.0, M = 0.1, Rd = 0.5, \theta_w = 1.1.$

### 7.3.6 Trapping

In this subsection the results for trapping are arranged under different parameters. Figs. 7.36 (a) and (b) are plotted for slip parameters. Trapped bolus size increases in this case. Hartman number effects on bolus size are given through Figs. 7.37 (a) and (b). Bolus size decreases for larger  $M$ . Figs. 7.38 (a) and (b) are drawn for fluid parameter. Slight decrease is noticed for larger fluid parameter. Figs. 7.39 (a)-(d) are prepared for compliant walls parameters. Size of trapped bolus tend to decrease for damping coefficient whereas it increases for elastance

coefficients.

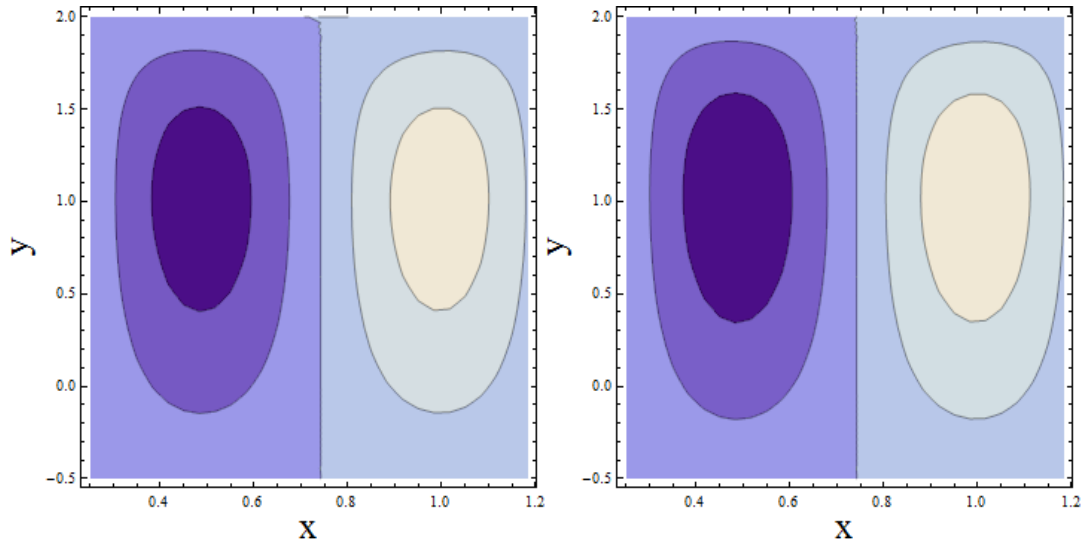


Fig. 7.36 (a).

(b)

Fig. 7.36.  $\psi$  via change in  $\xi_1$  when  $E_1 = 0.02$ ,  $E_2 = 0.01$ ,  $E_3 = 0.01$ ,  $t = 0.0$ ,  $\varepsilon = 0.2$ ,  $n = 1.5$ ,  $\xi_2 = 0.01$ ,  $\xi_3 = 0.01$ ,  $Nt = 0.1$ ,  $Nb = 0.1$ ,  $\beta_1 = 0.2$ ,  $Pr = 1.5$ ,  $Br = 2.0$ ,  $M = 0.1$ ,  $Rd = 0.5$ ,  $\theta_w = 1.1$ . (a)  $\xi_1 = 0.01$ . (b)  $\xi_1 = 0.03$ .

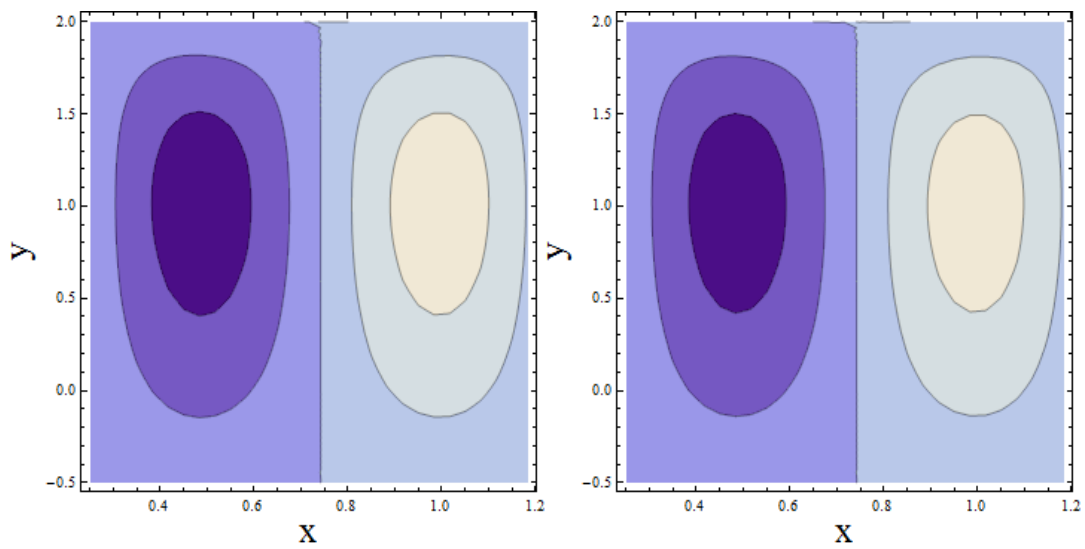


Fig. 7.37 (a)

(b)

Fig. 7.37.  $\psi$  via change in  $M$  when  $E_1 = 0.02$ ,  $E_2 = 0.01$ ,  $E_3 = 0.01$ ,  $t = 0.0$ ,  $\varepsilon = 0.2$ ,  $n = 1.5$ ,  $\xi_1 = 0.01$ ,  $\xi_2 = 0.01$ ,  $\xi_3 = 0.01$ ,  $Nt = 0.1$ ,  $Nb = 0.1$ ,  $\beta_1 = 0.2$ ,  $Pr = 1.5$ ,  $Br = 2.0$ ,  $Rd = 0.5$ ,  $\theta_w = 1.1$ . (a)  $M = 0.1$ . (b)  $M = 0.2$ .

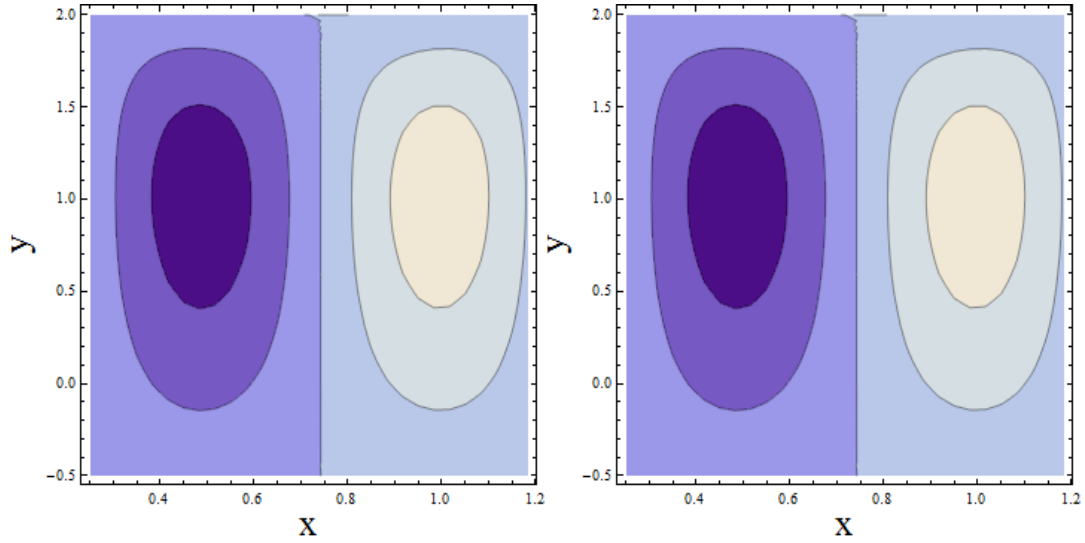


Fig. 7.38 (a)

(b)

Fig. 7.38.  $\psi$  via change in  $\beta_1$  when  $E_1 = 0.02$ ,  $E_2 = 0.01$ ,  $E_3 = 0.01$ ,  $t = 0.0$ ,  $\varepsilon = 0.2$ ,  $n = 1.5$ ,  $\xi_1 = 0.01$ ,  $\xi_2 = 0.01$ ,  $\xi_3 = 0.01$ ,  $Nt = 0.1$ ,  $Nb = 0.1$ ,  $Pr = 1.5$ ,  $Br = 2.0$ ,  $M = 0.1$ ,  $Rd = 0.5$ ,  $\theta_w = 1.1$ . (a)  $\beta_1 = 0.02$ . (b)  $\beta_1 = 0.04$ .



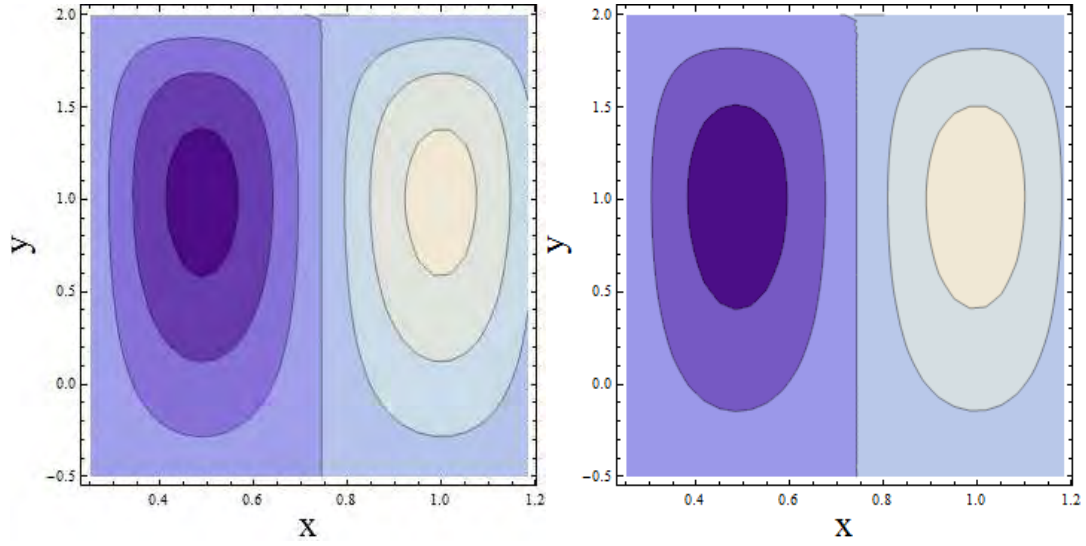
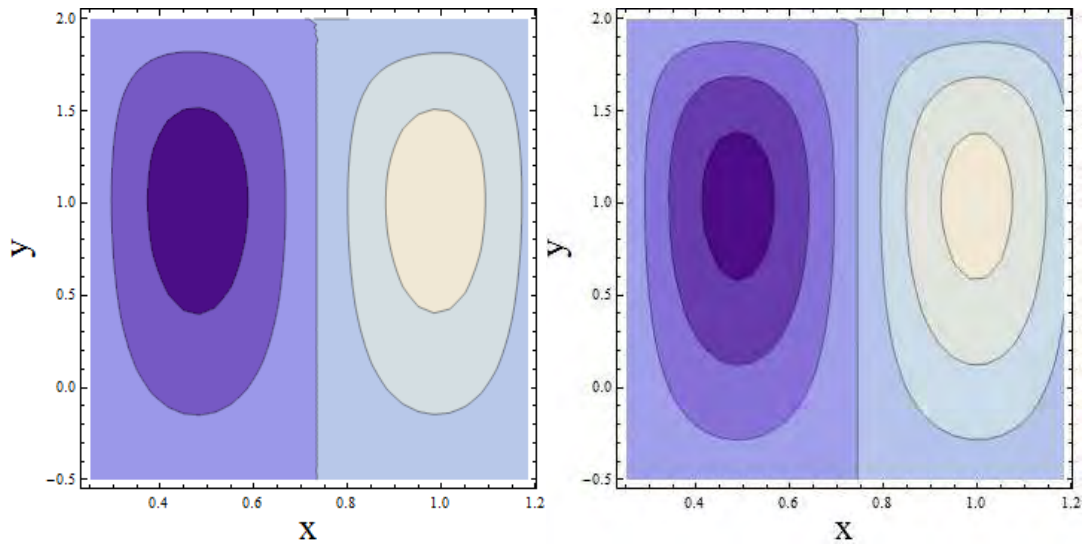


Fig. 7.39 (a)

(b)



(c)

(d)

Fig. 7.39.  $\psi$  via change in  $E_1, E_2, E_3$  when  $t = 0.0, \varepsilon = 0.2, n = 1.5, \xi_1 = 0.01, \xi_2 = 0.01, \xi_3 = 0.01, Nt = 0.1, Nb = 0.1, \beta_1 = 0.2, Pr = 1.5, Br = 2.0, M = 0.1, Rd = 0.5, \theta_w = 1.1$ .

(a)  $E_1 = 0.02, E_2 = 0.01, E_3 = 0.01$ . (b)  $E_1 = 0.03, E_2 = 0.01, E_3 = 0.01$ , (c)  $E_1 = 0.02, E_2 = 0.03, E_3 = 0.01$ . (d)  $E_1 = 0.02, E_2 = 0.01, E_3 = 0.02$ .

### 7.3.7 Validation of problem

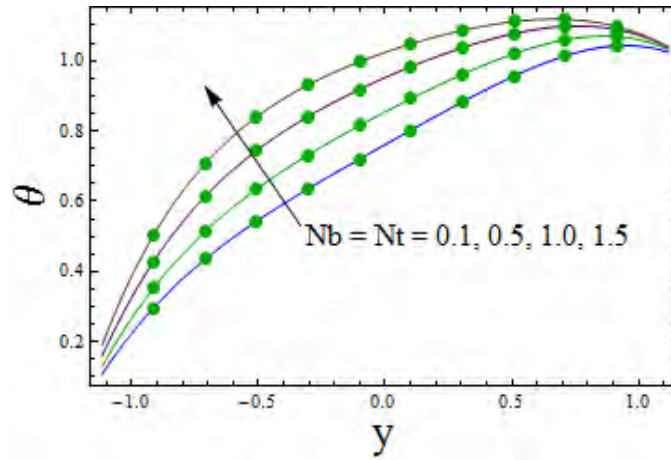


Fig. 7.40

*Fig. 7.40.*  $\theta$  via change in  $Nb$  and  $Nt$  when  $E_1 = 0.01$ ,  $E_2 = 0.02$ ,  $E_3 = 0.01$ ,  $t = 0.1$ ,  $x = 0.2$ ,  $\varepsilon = 0.2$ ,  $\xi_1 = 0.1$ ,  $\xi_2 = 0.1$ ,  $\xi_3 = 0.1$ ,  $\beta_1 = 0$ ,  $Pr = 1.0$ ,  $Br = 1.0$ ,  $M = 0$ ,  $Rd = 0$ .

This Fig. is sketched for the effect of Brownian motion and thermophoresis parameter on temperature which validates our results. In our problem we have taken  $\beta_1 = 0$ ,  $M = 0$ ,  $Rd = 0$  and get the result of study by Mustafa et. al. [170]. In this study the authors have taken the nanofluid, slip conditions and wall properties. They solved the problem by using homotopy analysis method (HAM). We observed that our results are in good agreement with limiting results of [170].

## 7.4 Conclusions

Key observations of present chapter are mentioned below.

- Velocity slip and Hartman number have opposite behaviors for velocity.
- Influences of  $Nb$  and  $Nt$  on temperature are similar.
- Radiation parameter and Brinkman number have opposite results on fluid temperature.
- Concentration slip parameter leads to decay in concentration.

- Entropy enhancement is noted for concentration difference and diffusion coefficient parameters.
- Radiation parameter and thermal slip parameter results on  $Z$  are opposite.
- Bolus size increases with larger slip parameter.

## Chapter 8

# Entropy generation and endoscopic effects on peristalsis with modified Darcy's law

### 8.1 Introduction

Present chapter highlights the outcomes of endoscopy and entropy generation in MHD peristaltic flow of Sisko fluid. Unlike the traditional approach, the flow modeling for porous medium is based upon modified Darcy's law. Salient features of Joule heating and viscous dissipation are investigated. Convective conditions for heat transfer are utilized. The problem after invoking long wavelength approximation is numerically solved. Graphical analysis provides physical insight. Graphs are plotted for velocity, temperature, entropy generation, Bejan number and heat transfer coefficient for the pertinent parameters of interest. Results disclose that the enhancement in Darcy number increases the fluid velocity and temperature. It also caused an enhancement in entropy generation and Bejan number. Magnetic field leads to enhance the temperature and entropy generation. Moreover the flexible wall parameters show increasing trend for elastance coefficients whereas damping coefficient decays the fluid velocity.

## 8.2 Modeling

Here magnetohydrodynamic flow of Sisko fluid between two coaxial uniform tubes is considered. Inner tube (at  $r = r_1$ ) is fixed while the outer tube (at  $r = r_2$ ) is subject to peristaltic wave [213]

$$r = r_1 = b, \quad (8.1)$$

$$r = r_2 = d + a \sin \frac{2\pi}{\lambda} (z - ct). \quad (8.2)$$

Here  $d$  and  $b$  are radii of outer and inner tubes. Further wavelength, wave amplitude, wave speed and time are symbolized as  $\lambda$ ,  $a$ ,  $c$  and  $t$  respectively (see Fig. 8.1). Cylindrical coordinate ( $r$ ,  $z$ ) are selected such that  $r$  along radial direction and  $z$  perpendicular to  $r$ . Viscous dissipation and Ohmic heating are present.

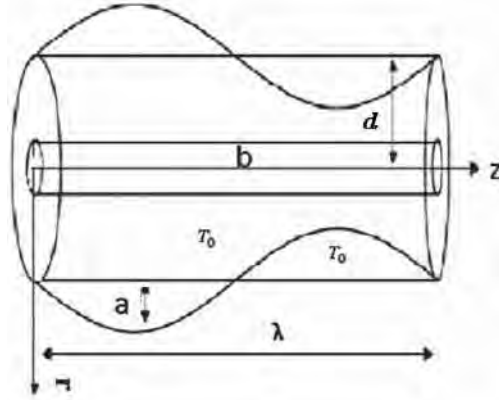


Fig. 8.1: Flow Configuration

Fluid is electrically conducting using constant magnetic field. Electric field consideration is not attended. Small magnetic Reynolds number leads to omission of induced magnetic field. In addition incompressible Sisko fluid fills the porous space. Thus by modified Darcy's law one has for pressure drop [217]:

$$\nabla p = -\frac{\mathcal{K}}{k_1} \left( \alpha + \beta^* \sqrt{|\Pi|}^{n-1} \right) \mathbf{V}, \quad (8.3)$$

in which porosity and permeability of medium are  $\varkappa$  and  $k_1$  respectively. Here  $\alpha$  and  $\beta^*$  are material constants. Keeping above expression in mind, the resistance satisfies [217]:

$$\mathbf{R} = -\frac{\varkappa}{k_1} \left( \alpha + \beta^* \sqrt{|\Pi|}^{n-1} \right) \mathbf{V}, \quad (8.4)$$

which in component form yields

$$R_r = -\frac{\varkappa}{k_1} \left( \alpha + \beta^* \sqrt{|\Pi|}^{n-1} \right) u, \quad (8.5)$$

$$R_z = -\frac{\varkappa}{k_1} \left( \alpha + \beta^* \sqrt{|\Pi|}^{n-1} \right) w, \quad (8.6)$$

where  $u$  and  $w$  are the velocities in  $r$  and  $z$ -directions. We have following expressions [124]:

$$\frac{\partial u}{\partial r} + \frac{u}{r} + \frac{\partial w}{\partial z} = 0, \quad (8.7)$$

$$\rho \left( \frac{du}{dt} \right) = -\frac{\partial p}{\partial r} + \frac{1}{r} \frac{\partial(rS_{rr})}{\partial r} + \frac{\partial(S_{rz})}{\partial z} - \frac{S_{\theta\theta}}{r} + R_r, \quad (8.8)$$

$$\rho \left( \frac{dw}{dt} \right) = -\frac{\partial p}{\partial z} + \frac{1}{r} \frac{\partial(rS_{rz})}{\partial r} + \frac{\partial(S_{zz})}{\partial z} - \sigma B_0^2 w + R_z, \quad (8.9)$$

$$\begin{aligned} \rho C_p \left( \frac{dT}{dt} \right) &= \kappa \left( \frac{\partial^2 T}{\partial r^2} + \frac{1}{r} \frac{\partial T}{\partial r} + \frac{\partial^2 T}{\partial z^2} \right) + S_{\theta\theta} \frac{u}{r} \\ &+ S_{rr} \frac{\partial u}{\partial r} + S_{zz} \frac{\partial w}{\partial z} + S_{rz} \left( \frac{\partial w}{\partial r} + \frac{\partial u}{\partial z} \right) \\ &+ \sigma B_0^2 w^2. \end{aligned} \quad (8.10)$$

In above equations  $T$  represents the temperature.  $\rho$  for density of fluid,  $S_{rr}$ ,  $S_{\theta\theta}$ ,  $S_{rz}$  and  $S_{zz}$  the extra stress components,  $p$  the pressure and  $\kappa$  the thermal conductivity.

Expression of  $S$  for Sisko material is [72]:

$$\mathbf{S} = \left( \alpha + \beta^* \sqrt{|\Pi|}^{n-1} \right) \mathbf{A}_1, \quad (8.11)$$

in which the first Rivlin-Ericksen tensor ( $\mathbf{A}_1$ ) is:

$$\mathbf{A}_1 = \nabla \mathbf{V} + (\nabla \mathbf{V})^T, \quad (8.12)$$

and

$$\Pi = \frac{1}{2} \text{tr} \mathbf{A}_1^2. \quad (8.13)$$

It should be noted that Sisko material contains two fluid models i.e. for  $\alpha = \mu$  and  $\beta^* = 0$  this model reduces to viscous fluid. On the other hand for  $\alpha = 0$  and  $\beta^* = \mu$  this model recovers power law model. Here power law index  $n$  describes shear thinning effect for  $0 < n < 1$  and shear thickening for  $n > 1$ .

The appropriate boundary conditions for present problem are:

$$w = 0 \quad \text{at} \quad r = r_1 = \xi, \quad w = 0 \quad \text{at} \quad r = r_2, \quad (8.14)$$

$$-\kappa \frac{\partial T}{\partial r} = h_1(T - T_0) \quad \text{at} \quad r = r_1 = \xi, \quad (8.15)$$

$$-\kappa \frac{\partial T}{\partial r} = h_2(T_0 - T) \quad \text{at} \quad r = r_2, \quad (8.16)$$

$$\left( -\tau^* \frac{\partial^3}{\partial z^3} + m^* \frac{\partial^3}{\partial z \partial t^2} + d_1^* \frac{\partial^2}{\partial t \partial z} \right) r_2 = \frac{\partial p}{\partial z}, \quad (8.17)$$

where Eq. (8.14) defines the no slip condition for velocity. Eqs. (8.15) and (8.16) are the convective boundary conditions. Here  $h_1$  and  $h_2$  are the heat transfer coefficients and compliance of walls are depicted through  $\tau^*$ ,  $m^*$  and  $d_1^*$ .

The non-dimensional quantities are

$$\begin{aligned} r^* &= \frac{r}{d}, \quad z^* = \frac{z}{\lambda}, \quad w^* = \frac{w}{c}, \quad u^* = \frac{u\lambda}{dc}, \\ p^* &= \frac{d^2 p}{c\lambda\alpha}, \quad r_1^* = \frac{r_1}{d} = \frac{b}{d} = \xi < 1, \quad r_2^* = \frac{r_2}{d}, \\ S_{ij}^* &= \frac{dS_{ij}}{\alpha c}, \quad t^* = \frac{ct}{\lambda}, \quad \theta = \frac{T - T_0}{T_0}. \end{aligned} \quad (8.18)$$

Non-dimensionlized form of system is

$$\text{Re } \delta^3 \left( \frac{\partial u}{\partial t} + u \frac{\partial u}{\partial r} + w \frac{\partial u}{\partial z} \right) = -\frac{\partial p}{\partial r} + \frac{\delta}{r} \frac{\partial(rS_{rr})}{\partial r} + \delta^2 \frac{\partial(S_{rz})}{\partial z} - \frac{\delta^2}{Da} \left( 1 + \beta_1 \sqrt{|\Pi|}^{n-1} \right) u - \delta \frac{S_{\theta\theta}}{r}, \quad (8.19)$$

$$\text{Re } \delta \left( \frac{\partial w}{\partial t} + u \frac{\partial w}{\partial r} + w \frac{\partial w}{\partial z} \right) = -\frac{\partial p}{\partial z} + \frac{1}{r} \frac{\partial(rS_{rz})}{\partial r} + \delta \frac{\partial(S_{zz})}{\partial z} - \frac{1}{Da} \left( 1 + \beta_1 \sqrt{|\Pi|}^{n-1} \right) w - M^2 w, \quad (8.20)$$

$$\begin{aligned} \text{Re Pr } \delta \left( \frac{\partial \theta}{\partial t} + u \frac{\partial \theta}{\partial r} + w \frac{\partial \theta}{\partial z} \right) &= \left( \frac{\partial^2 \theta}{\partial r^2} + \frac{1}{r} \frac{\partial \theta}{\partial r} + \delta^2 \frac{\partial^2 \theta}{\partial z^2} \right) + M^2 Br w^2 \\ &+ Br \delta S_{zz} \frac{\partial w}{\partial z} + Br \delta S_{rr} \frac{\partial u}{\partial r} + Br \delta S_{\theta\theta} \frac{u}{r} \\ &+ Br S_{rz} \left( \frac{\partial w}{\partial r} + \delta \frac{\partial u}{\partial z} \right), \end{aligned} \quad (8.21)$$

$$w = 0 \quad \text{at} \quad r = r_1 = \xi, \quad w = 0 \quad \text{at} \quad r = r_2, \quad (8.22)$$

$$\frac{\partial \theta}{\partial r} + Bi_1 \theta = 0 \quad \text{at} \quad r = r_1 = \xi, \quad (8.23)$$

$$\frac{\partial \theta}{\partial r} - Bi_2 \theta = 0 \quad \text{at} \quad r = r_2, \quad (8.24)$$

$$\begin{aligned} \left[ E_1 \frac{\partial^3}{\partial z^3} + E_2 \frac{\partial^3}{\partial z \partial t^2} + E_3 \frac{\partial^2}{\partial t \partial z} \right] r_2 &= \frac{1}{r} \frac{\partial(rS_{rz})}{\partial r} + \delta \frac{\partial(S_{zz})}{\partial z} - \text{Re } \delta \left( \frac{\partial w}{\partial t} + u \frac{\partial w}{\partial r} + w \frac{\partial w}{\partial z} \right) \\ &- \frac{1}{Da} \left( 1 + \beta_1 \sqrt{|\Pi|}^{n-1} \right) w \\ &- M^2 w, \quad \text{at } r = r_1 = \xi \quad \text{and} \quad r = r_2, \end{aligned} \quad (8.25)$$

with

$$\begin{aligned} \text{Re} &= \frac{\rho c d}{\alpha}, \quad M = \sqrt{\frac{\sigma}{\alpha}} B_0 d, \quad \text{Pr} = \frac{\alpha C_p}{\kappa}, \\ \text{Ec} &= \frac{c^2}{C_p T_0}, \quad Br = \text{Pr } \text{Ec}, \quad Da = \frac{k_1}{d^2 \mathcal{Z}}, \quad \delta = \frac{d}{\lambda}, \\ \beta_1 &= \frac{\beta^*}{\alpha} \left( \frac{c}{d} \right)^{n-1}, \quad Bi_1 = \frac{h_1 d}{\kappa}, \quad Bi_2 = \frac{h_2 d}{\kappa}, \\ E_1 &= -\frac{\tau^* d^3}{\lambda^3 c \alpha}, \quad E_2 = \frac{m^* c d^3}{\lambda^3 \alpha}, \quad E_3 = \frac{d_1^* d^3}{\lambda^2 \alpha}. \end{aligned} \quad (8.26)$$

Here Re depicts Reynolds number,  $M$  the Hartman number, Pr the Prandtl number,  $\text{Ec}$  the



Eckert number,  $Br$  (product of Eckert and Prandtl numbers) the Brinkman number,  $Da$  the Darcy number,  $\delta$  the wave number,  $\beta_1$  the fluid parameter,  $Bi$ 's ( $i = 1, 2$ ) the Biot numbers and  $E_i$ 's ( $i = 1 - 3$ ) the compliance wall parameter.

Definition of stream function is

$$u = -\frac{1}{r} \frac{\partial \psi}{\partial z}, \quad w = \frac{1}{r} \frac{\partial \psi}{\partial r}. \quad (8.27)$$

Employing above expression and lubrication approach we arrive at

$$\frac{\partial p}{\partial r} = 0, \quad (8.28)$$

$$\frac{\partial p}{\partial z} = \frac{1}{r} \frac{\partial(rS_{rz})}{\partial r} - \frac{M^2}{r} \frac{\partial \psi}{\partial r} - \frac{1}{Da} \left( 1 + \beta_1 \left( \frac{1}{r} \frac{\partial^2 \psi}{\partial r^2} - \frac{1}{r^2} \frac{\partial \psi}{\partial r} \right)^{n-1} \right) \left( \frac{1}{r} \frac{\partial \psi}{\partial r} \right), \quad (8.29)$$

$$\frac{\partial^2 \theta}{\partial r^2} + \frac{1}{r} \frac{\partial \theta}{\partial r} + BrS_{rz} \left( \frac{1}{r} \frac{\partial^2 \psi}{\partial r^2} - \frac{1}{r^2} \frac{\partial \psi}{\partial r} \right) + \frac{M^2 Br}{r^2} \left( \frac{\partial \psi}{\partial r} \right)^2 = 0, \quad (8.30)$$

$$S_{rz} = \left( 1 + \beta_1 \left( \frac{1}{r} \frac{\partial^2 \psi}{\partial r^2} - \frac{1}{r^2} \frac{\partial \psi}{\partial r} \right)^{n-1} \right) \left( \frac{1}{r} \frac{\partial^2 \psi}{\partial r^2} - \frac{1}{r^2} \frac{\partial \psi}{\partial r} \right), \quad (8.31)$$

$$\frac{\partial \psi}{\partial r} = 0 \quad \text{at} \quad r = r_1 = \xi, \quad \frac{\partial \psi}{\partial r} = 0 \quad \text{at} \quad r = r_2, \quad (8.32)$$

$$\frac{\partial \theta}{\partial r} + Bi_1 \theta = 0 \quad \text{at} \quad r = r_1 = \xi, \quad (8.33)$$

$$\frac{\partial \theta}{\partial r} - Bi_2 \theta = 0 \quad \text{at} \quad r = r_2, \quad (8.34)$$

$$\begin{aligned} & \frac{1}{r} \frac{\partial(rS_{rz})}{\partial r} - \frac{1}{Da} \left( 1 + \beta_1 \left( \frac{1}{r} \frac{\partial^2 \psi}{\partial r^2} - \frac{1}{r^2} \frac{\partial \psi}{\partial r} \right)^{n-1} \right) \left( \frac{1}{r} \frac{\partial \psi}{\partial r} \right) - \frac{M^2}{r} \frac{\partial \psi}{\partial r} \\ & = \left[ E_1 \frac{\partial^3}{\partial z^3} + E_2 \frac{\partial^3}{\partial z \partial t^2} + E_3 \frac{\partial^2}{\partial t \partial z} \right] r_2, \quad \text{at} \quad r = r_1 = \xi \quad \text{and} \quad r = r_2. \end{aligned} \quad (8.35)$$

where incompressibility condition is automatically justified. From Eqs. (8.28) and (8.29), one can write

$$\frac{\partial}{\partial r} \left[ \frac{1}{r} \frac{\partial(rS_{rz})}{\partial r} - \frac{M^2}{r} \frac{\partial \psi}{\partial r} - \frac{1}{Da} \left( 1 + \beta_1 \left( \frac{1}{r} \frac{\partial^2 \psi}{\partial r^2} - \frac{1}{r^2} \frac{\partial \psi}{\partial r} \right)^{n-1} \right) \left( \frac{1}{r} \frac{\partial \psi}{\partial r} \right) \right] = 0. \quad (8.36)$$

### 8.2.1 Entropy generation

Mathematical expressions for viscous dissipation is

$$\Phi = S_{rr} \frac{\partial u}{\partial r} + S_{\theta\theta} \frac{u}{r} + S_{zz} \frac{\partial w}{\partial z} + S_{rz} \left( \frac{\partial w}{\partial r} + \frac{\partial u}{\partial z} \right). \quad (8.37)$$

Volumetric entropy generation satisfies [213]:

$$S_{gen}''' = \underbrace{\frac{\kappa}{T_m^2} \left( \left( \frac{\partial T}{\partial r} \right)^2 + \left( \frac{\partial T}{\partial z} \right)^2 \right)}_{\text{Thermal irreversibility}} + \underbrace{\frac{\sigma B_0^2 w^2}{T_m}}_{\text{Joule friction irreversibility}} + \underbrace{\frac{\Phi}{T_m}}_{\text{Fluid friction irreversibility}}. \quad (8.38)$$

Dimensionless form of entropy generation is

$$N_s = \frac{S_{gen}'''}{S_G'''} = \left( \frac{\partial \theta}{\partial r} \right)^2 + \frac{BrM^2}{\Lambda} + \frac{Br}{\Lambda} S_{rz} \left( \frac{\partial w}{\partial r} \right), \quad (8.39)$$

$$S_G''' = \frac{\kappa T_0^2}{T_m^2 d^2}, \quad \Lambda = \frac{T_0}{T_m}. \quad (8.40)$$

Bejan number is given by [213]:

$$Be = \frac{\text{Entropy generation due to heat transfer}}{\text{Total entropy generation}} \quad (8.41)$$

or

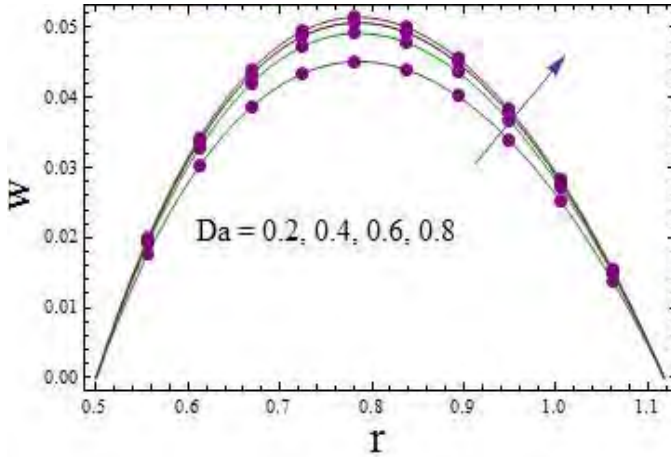
$$Be = \frac{\left( \frac{\partial \theta}{\partial r} \right)^2}{\left( \frac{\partial \theta}{\partial r} \right)^2 + \frac{BrM^2}{\Lambda} + \frac{Br}{\Lambda} S_{rz} \left( \frac{\partial w}{\partial r} \right)}. \quad (8.42)$$

### 8.3 Solution methodology

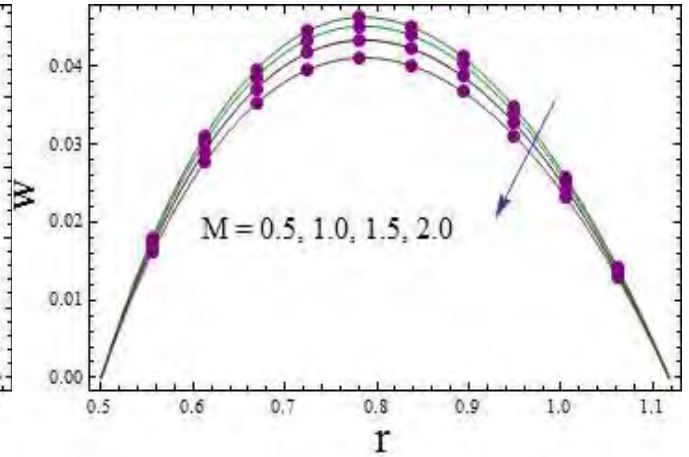
Arising system of equations is nonlinear. Hence it seems difficult to find the exact solution of considered problem. Thus an approximate solution can be evaluated via perturbation technique or numerical technique. To avoid lengthy solution expressions we have solved this problem numerically by NDSolve in Mathematica. This also saves time as it provides best computing results with minimum CPU time (3–4 min).

## 8.4 Analysis

This section contains information about graphical interpretation of the results. We firstly discuss the velocity function for Darcy number ( $Da$ ), Hartman number ( $M$ ), fluid parameter ( $\beta_1$ ) and compliant wall parameters ( $E_i = 1 - 3$ ). Fig. 8.2 (a) depicts  $Da$  influence on velocity. Velocity is an increasing function of  $Da$ . Obviously more pores aid the flow speed. Fig. 8.2 (b) is plotted for velocity against  $M$ . As expected the applied magnetic field provides a reduction in velocity. This is because of enhancement in resistive force offered to fluid. Fig. 8.2 (c) witnesses dual behavior of velocity for material parameter. Compliant nature is discussed via Fig. 8.2 (d). An enhancement in velocity is observed for  $E_1$  and  $E_2$  whereas damping force leads to decrease of velocity. This situation is quite useful in blood perfusion process in arteries and veins.



(a)



(b)

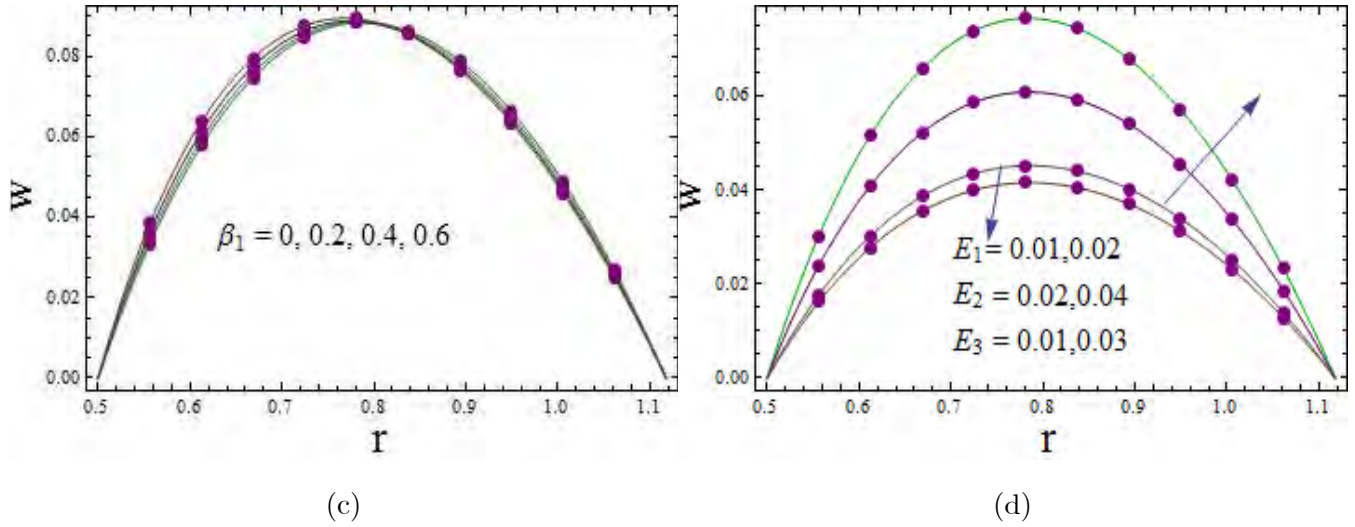
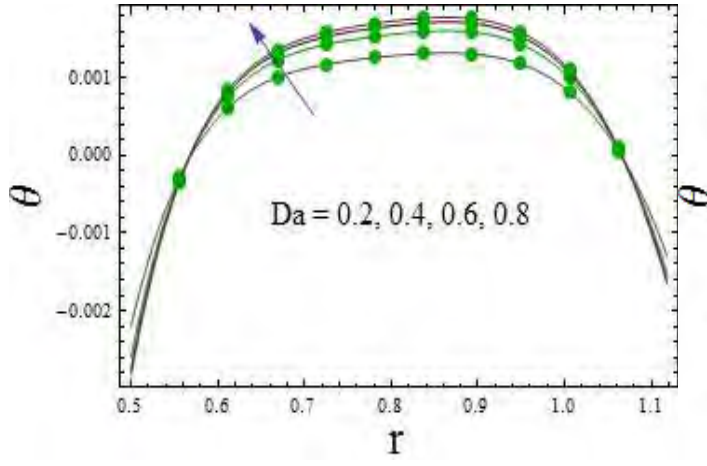
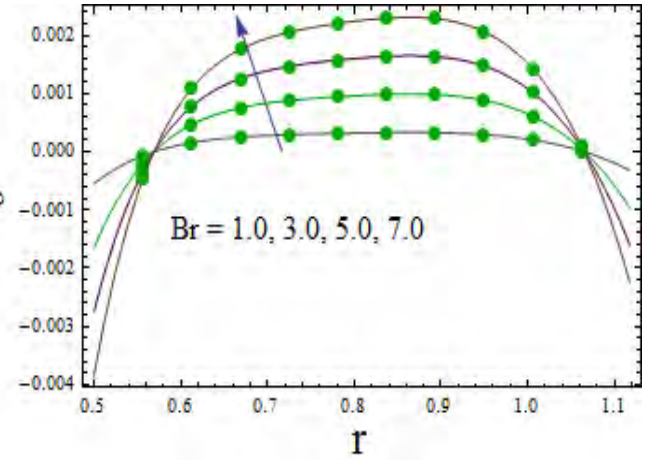


Fig. 8.2. Plots for velocity when  $E_1 = 0.02$ ,  $E_2 = 0.01$ ,  $E_3 = 0.01$ ,  $t = 0.1$ ,  $z = 0.2$ ,  $\varepsilon = 0.2$ ,  $n = 0.5$ ,  $M = 1.0$ ,  $Da = 0.2$ ,  $\beta_1 = 0.2$ ,  $Bi_1 = 8$ ,  $Bi_2 = 10$ ,  $Br = 4.0$ . (a)  $Da$  effect on  $w$  (b)  $M$  effect on  $w$  (c)  $\beta_1$  effect on  $w$  (d)  $E_1, E_2, E_3$  effects on  $w$

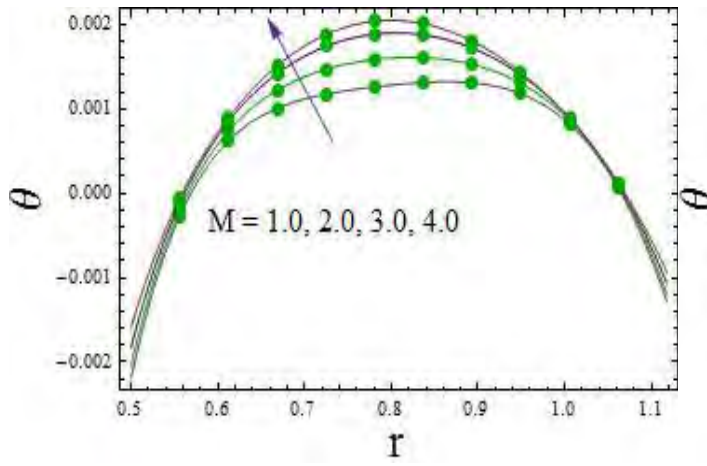
Temperature for different parameters is discussed via Figs. 3 (a-f). These Figs. include the influences of Darcy number ( $Da$ ), Brinkman number ( $Br$ ), Hartman number ( $M$ ), fluid parameter ( $\beta_1$ ) and Biot numbers ( $B_i$ 's). Fig. 8.3 (a) elucidates the results for increasing values of Darcy number. Temperature is enhanced for  $Da$ . As higher values of  $Da$  lead to more permeability which gave rise to the velocity of the fluid and as a result heat generation is possible. Hence the temperature of the fluid rises. Fig. 8.3 (b) depicts temperature variation for Brinkman number. Results reveal that temperature is an increasing function of  $Br$ . This happens in view of viscous dissipation effect. Hartman number ( $M$ ) shows an enhancement of temperature (see Fig. 8.3 (c)). Joule heating aspect is responsible for this act. Behavior of fluid parameter on thermal field is qualitatively similar to that of velocity (see Fig. 8.3 (d)). Biot numbers results on temperature are demonstrated through Figs. 8.3 (e) and (f). Temperature is enhanced for both Biot numbers.



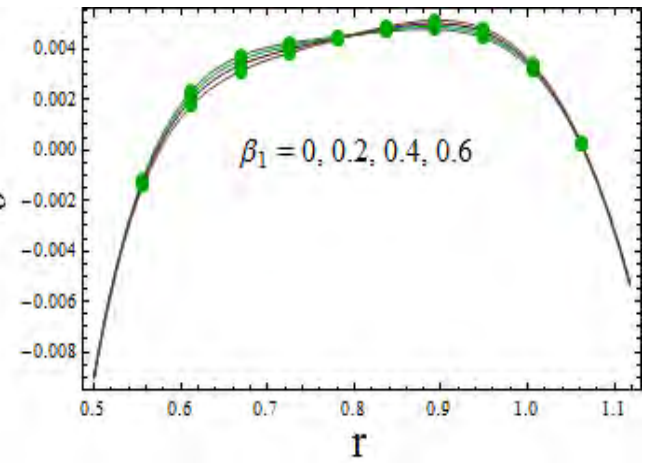
(a)



(b)



(c)



(d)

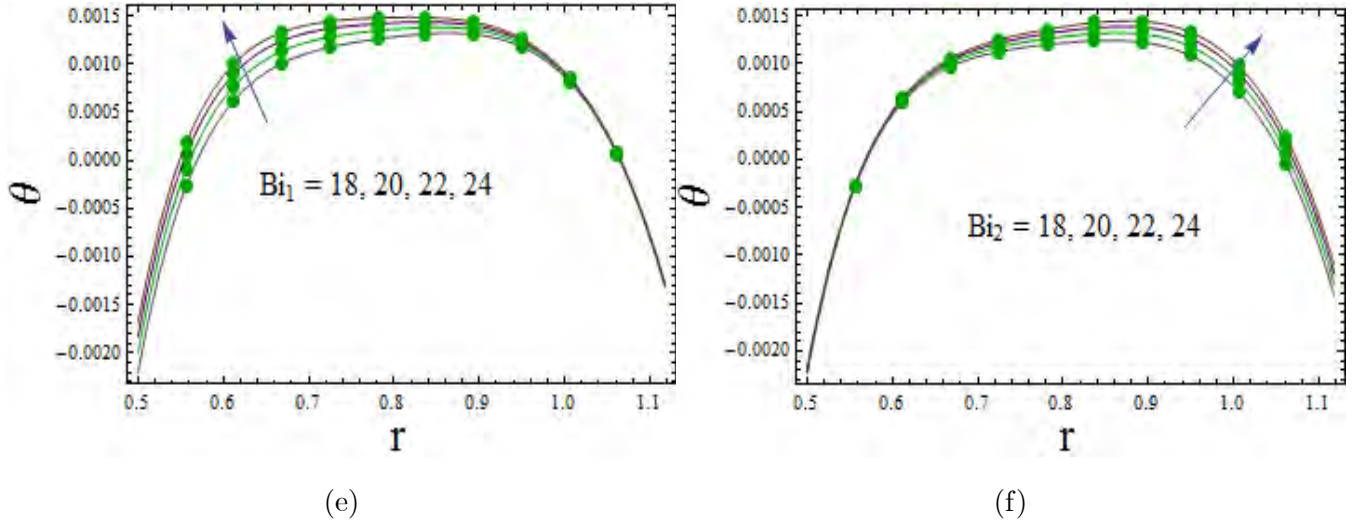


Fig. 8.3. Plots for temperature when  $E_1 = 0.02$ ,  $E_2 = 0.01$ ,  $E_3 = 0.01$ ,  $t = 0.1$ ,  $z = 0.2$ ,  $\varepsilon = 0.2$ ,  $n = 0.5$ ,  $M = 1.0$ ,  $Da = 0.2$ ,  $\beta_1 = 0.2$ ,  $Bi_1 = 8$ ,  $Bi_2 = 10$ ,  $Br = 4.0$ . (a)  $Da$  effect on  $\theta$  (b)  $Br$  effect on  $\theta$  (c)  $M$  effect on  $\theta$  (d)  $\beta_1$  effect on  $\theta$  (e)  $Bi_1$  effect on  $\theta$  (f)  $Bi_2$  effect on  $\theta$

Figs. 8.3 (a-d) have been prepared for examination of entropy generation. Fig. 8.4 (a) declared that Darcy number ( $Da$ ) leads to an enhancement in entropy generation. As more heat is produced with increase in permeability, that corresponds to more disorderliness. Fig. 8.4 (b) illustrated the results of Hartman number ( $M$ ). Here larger  $M$  give rise to entropy generation. It is because of the fact that temperature is directly related to  $Ns$ . Brinkman number influence on entropy generation is portrayed via Fig. 8.4 (c). Graphical analysis leads to the fact that enhancement in entropy generation is observed in presence of viscous dissipation. Fig. 8.4 (d) displayed the result of entropy generation through  $\Lambda$ . Reduction in  $Ns$  is noticed for larger  $\Lambda$ .

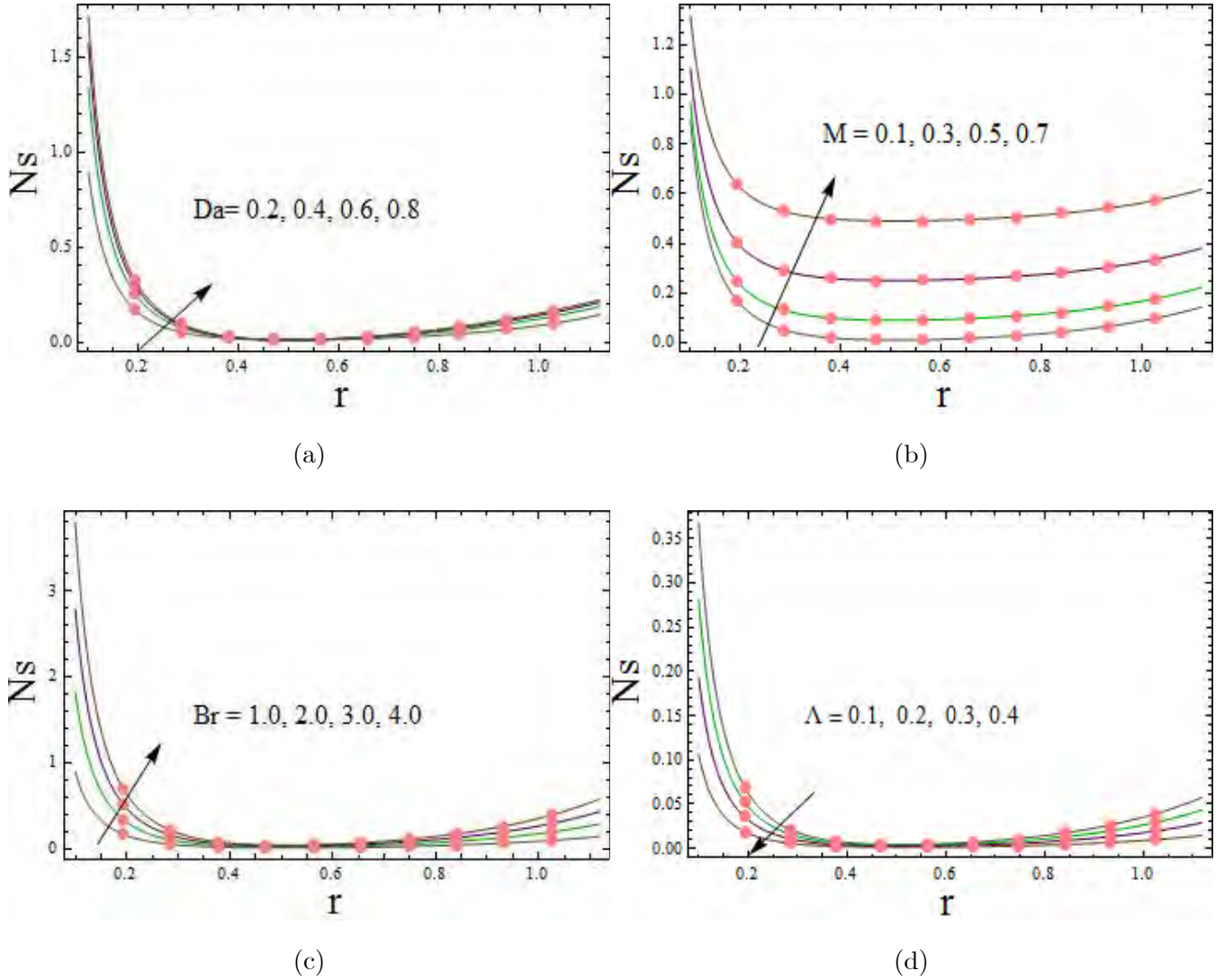


Fig. 8.4. Plots for entropy generation when  $E_1 = 0.02$ ,  $E_2 = 0.01$ ,  $E_3 = 0.01$ ,  $t = 0.1$ ,  $z = 0.2$ ,  $\varepsilon = 0.2$ ,  $n = 0.5$ ,  $M = 1.0$ ,  $Da = 0.2$ ,  $\beta_1 = 0.2$ ,  $Bi_1 = 8$ ,  $Bi_2 = 10$ ,  $\Lambda = 0.5$ ,  $Br = 1.0$ . (a)  $Da$  effect on  $Ns$  (b)  $M$  effect on  $Ns$  (c)  $Br$  effect on  $Ns$  (d)  $\Lambda$  effect on  $Ns$

Variation of Bejan number ( $Be$ ) for sundry variables is shown in the Figs. 8.5 (a-d). Fig. 8.5 (a) is prepared for impact of Darcy number on  $Be$ . Enhancement is seen for Bejan number for larger  $Da$ . Fig. 8.5 (b) is plotted for Brinkman number. It is noted that larger  $Br$  caused an enhancement in  $Be$ . Opposite results for  $M$  and  $\Lambda$  are seen for Bejan number (see Figs. 8.5 (c) and (d)). Here Bejan number enhancement in fact means that heat transfer irreversibility



is high when compared with total heat transfer irreversibility.

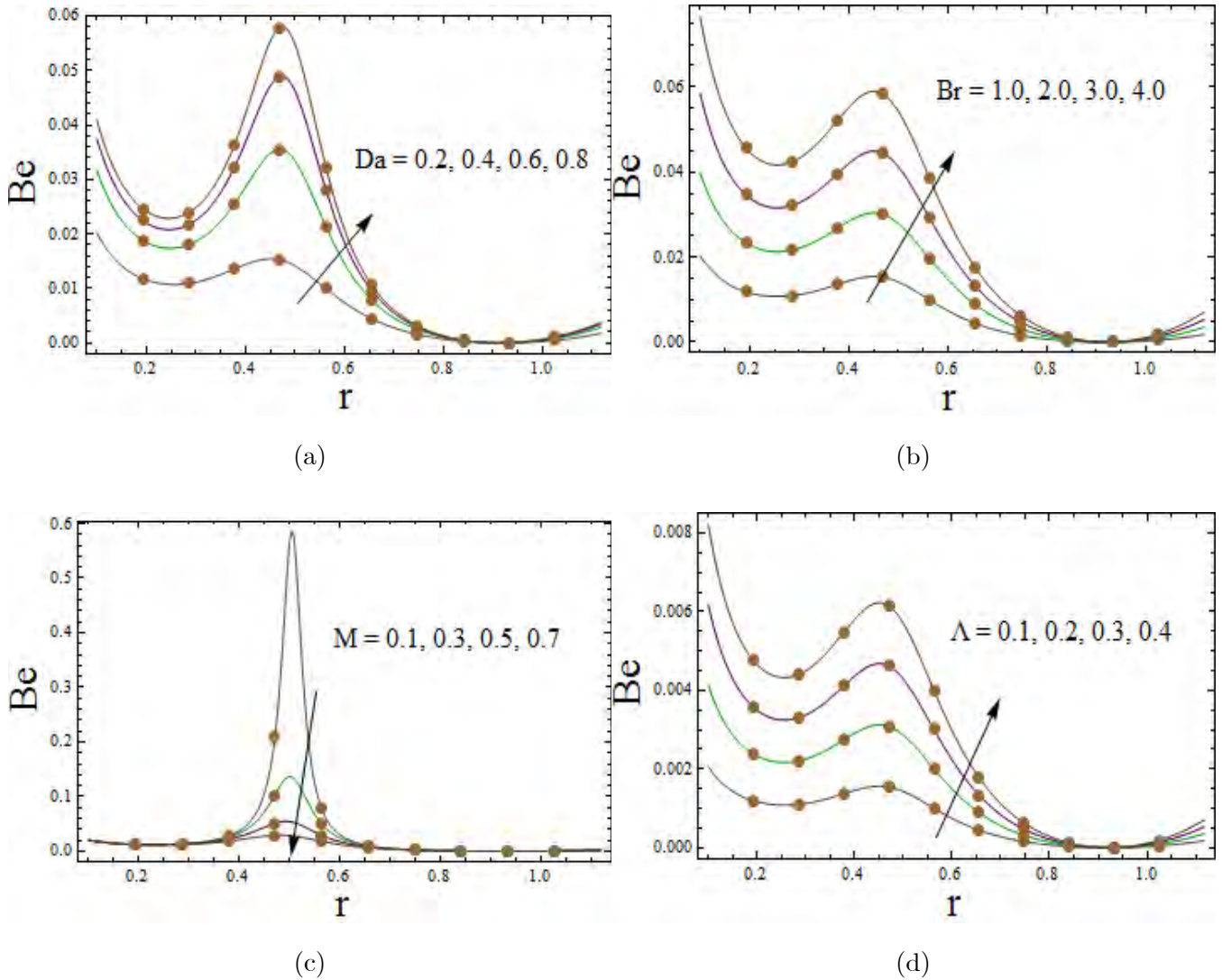
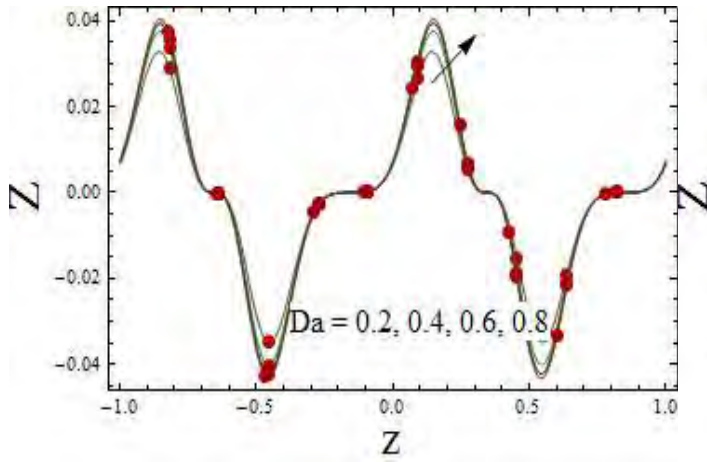


Fig. 8.5. Plots for Bejan number when  $E_1 = 0.02$ ,  $E_2 = 0.01$ ,  $E_3 = 0.01$ ,  $t = 0.1$ ,  $z = 0.2$ ,  $\varepsilon = 0.2$ ,  $n = 0.5$ ,  $M = 1.0$ ,  $Da = 0.2$ ,  $\beta_1 = 0.2$ ,  $Bi_1 = 8$ ,  $Bi_2 = 10$ ,  $\Lambda = 0.5$ ,  $Br = 1.0$ . (a)  $Da$  effect on  $Be$  (b)  $Br$  effect on  $Be$  (c)  $M$  effect on  $Be$  (d)  $\Lambda$  effect on  $Be$

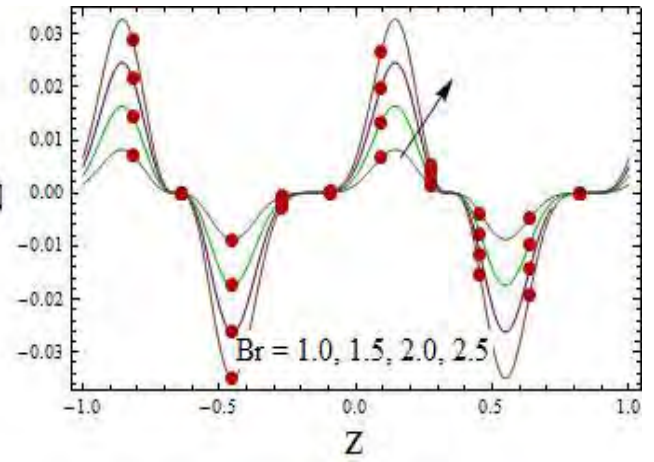
Figs. 8.6 (a–e) capture the results of heat transfer coefficient. Fig. 8.6 (a) is arranged for Darcy number. Here larger  $Da$  reveal an enhancement in heat transfer coefficient. Brinkman number outcome is seen through Fig. 8.6 (b). Clearly heat transfer coefficient is increased for Brinkman number. Heat transfer coefficient has decreasing impact for  $M$  (see Fig. 8.6 (c)).



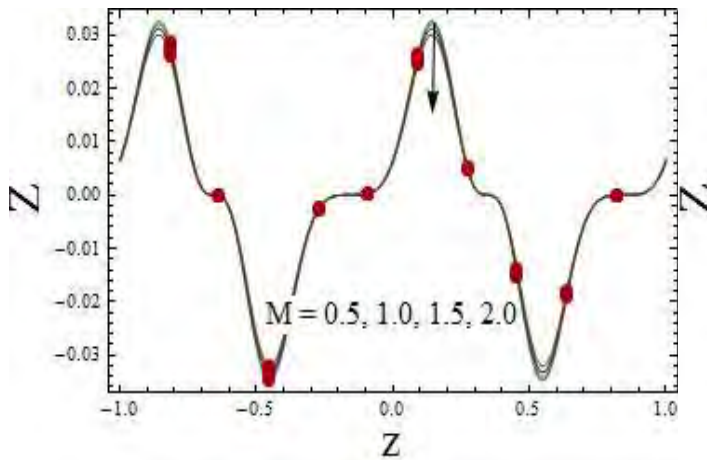
Biot numbers have opposite behavior for heat transfer coefficient (see Figs. 8.6 (d) and (e)).



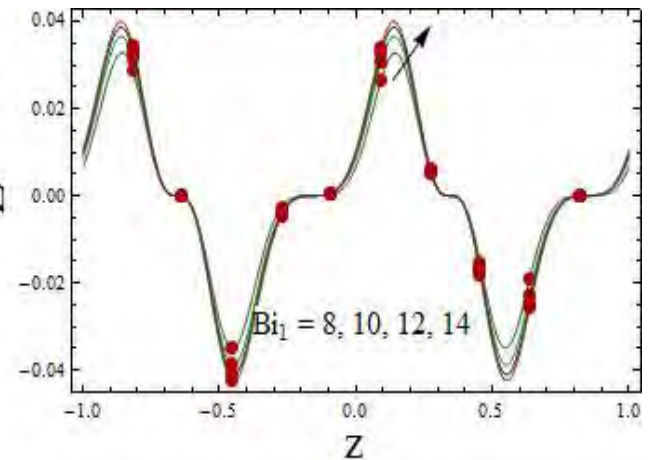
(a)



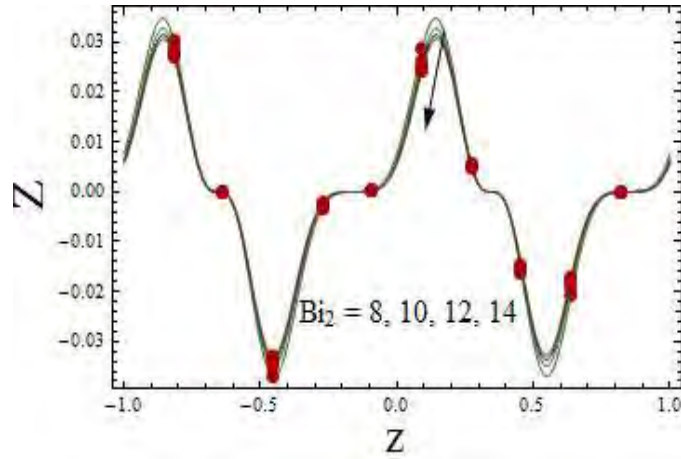
(b)



(c)



(d)



(e)

*Fig. 8.6.* Plots for heat transfer coefficient when  $E_1 = 0.02$ ,  $E_2 = 0.01$ ,  $E_3 = 0.01$ ,  $t = 0.1$ ,  $\varepsilon = 0.2$ ,  $n = 0.5$ ,  $M = 1.0$ ,  $Da = 0.2$ ,  $\beta_1 = 0.2$ ,  $Bi_1 = 8$ ,  $Bi_2 = 10$ ,  $Br = 1.0$ . (a)  $Da$  effect on  $Z$  (b)  $Br$  effect on  $Z$  (c)  $M$  effect on  $Z$  (c)  $Bi_1$  effect on  $Z$  (d)  $Bi_2$  effect on  $Z$

Now we display streamlines for trapping phenomenon. Figs. 8.7 (a , b) describe the Hartman number influence on bolus size. It is noted that size of trapped bolus reduces for larger strength of applied magnetic field. Figs. 8.8 (a , b) are plotted for impact of  $Da$  on size of trapped bolus. Bolus size shows an increase for larger  $Da$ . Figs. 8.9 (a , b) illustrate that bolus size is an increasing function of fluid parameter.

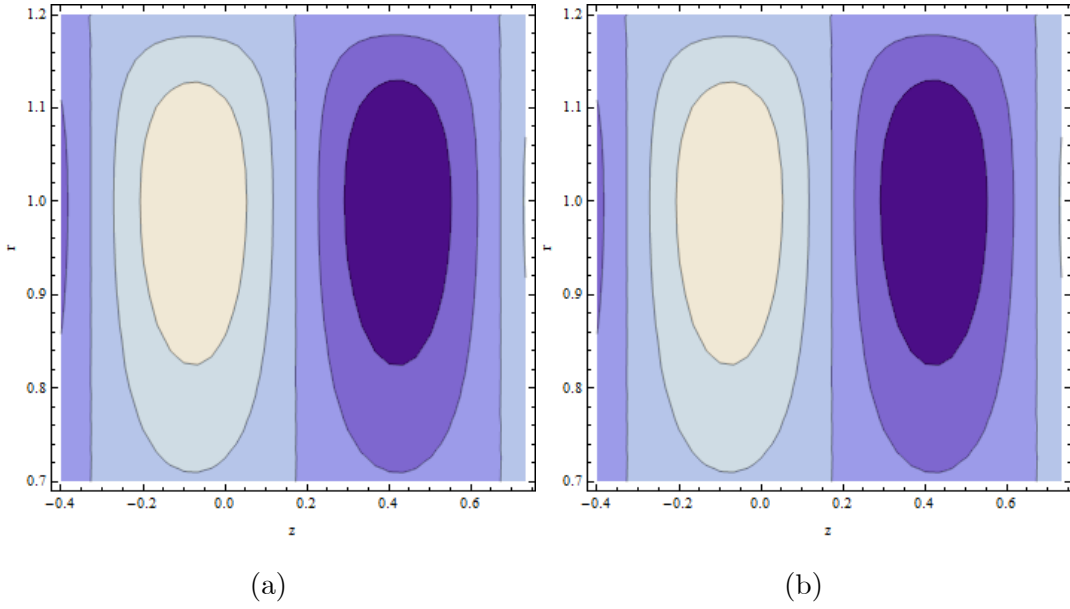


*Fig. 8.7.*  $M$  effect on  $\psi$  when  $E_1 = 0.002$ ,  $E_2 = 0.001$ ,  $E_3 = 0.01$ ,  $t = 0$ ,  $\varepsilon = 0.2$ ,  $Da = 0.2$ ,  $n = 0.5$ ,  $\beta_1 = 0.02$ ,  $Bi_1 = 2$ ,  $Bi_2 = 3$ ,  $Br = 1.0$ . (a)  $M = 1.0$ . (b)  $M = 3.0$ .

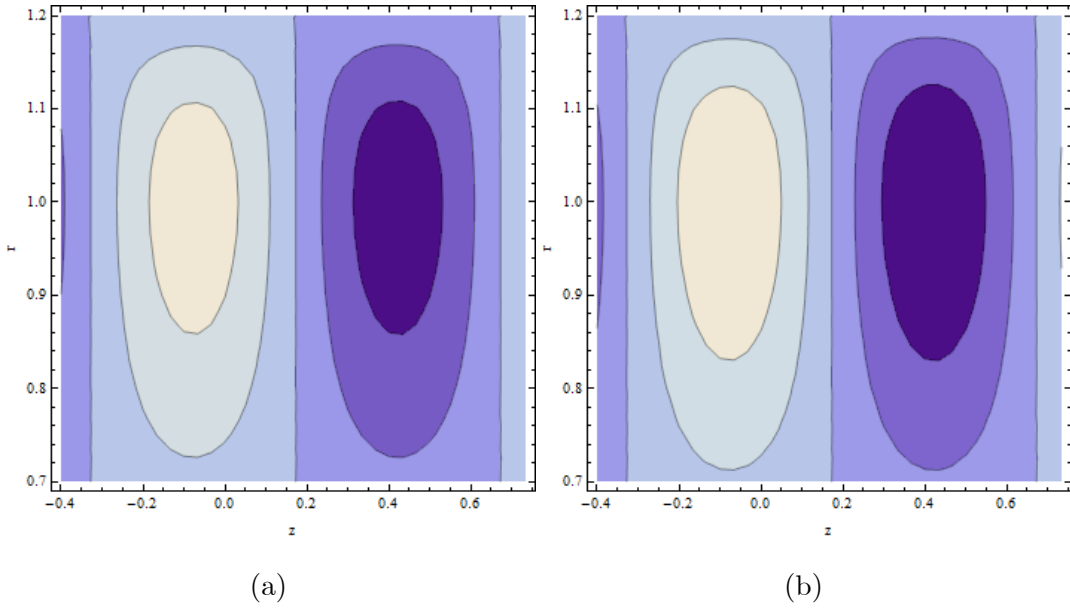


*Fig. 8.8.*  $Da$  effect on  $\psi$  when  $E_1 = 0.002$ ,  $E_2 = 0.001$ ,  $E_3 = 0.01$ ,  $t = 0$ ,  $\varepsilon = 0.2$ ,  $n = 0.5$ ,  $M = 1.0$ ,  $\beta_1 = 0.02$ ,  $Bi_1 = 2$ ,  $Bi_2 = 3$ ,  $Br = 1.0$ . (a)  $Da = 0.1$ . (b)  $Da = 0.2$ .

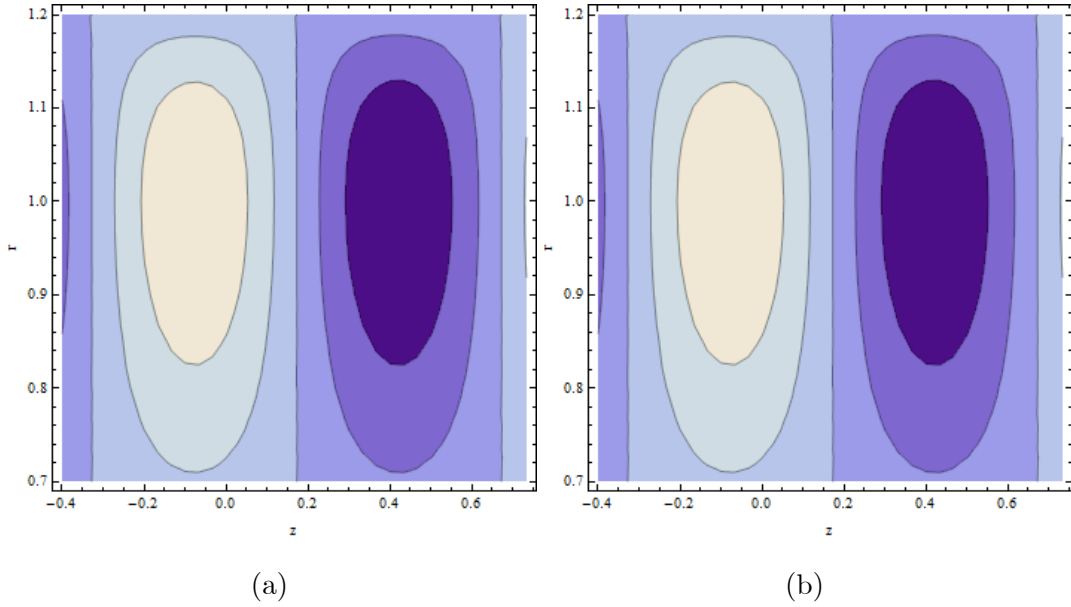


*Fig. 8.9.*  $\beta_1$  effect on  $\psi$  when  $E_1 = 0.002$ ,  $E_2 = 0.001$ ,  $E_3 = 0.01$ ,  $t = 0$ ,  $\varepsilon = 0.2$ ,  $Da = 0.2$ ,  $n = 0.5$ ,  $M = 1.0$ ,  $Bi_1 = 2$ ,  $Bi_2 = 3$ ,  $Br = 1.0$ . (a)  $\beta_1 = 0.02$ . (b)  $\beta_1 = 0.04$ .

## 8.5 Conclusions

We have following findings from the presented analysis.

- Darcy number has similar effects for entropy generation and Bejan number.
- Hartman number for temperature and velocity has opposite effects.
- Biot numbers have increasing impact for temperature.
- Increasing values of  $Br$  lead to enhancement of temperature, entropy generation and Bejan number.
- Heat transfer coefficient for  $Da$  increases.
- Bolus size for  $M$  tends to decrease.

## Chapter 9

# Entropy optimization for peristalsis of Rabinowitsch nanomaterial

### 9.1 Introduction

This chapter models peristaltic activity of Rabinowitsch material in a compliant walls channel. Energy equation is accounted in presence of viscous dissipation and heat source/sink. Chemical reaction is included in concentration expression. Nanomaterial characteristics are due to Brownian motion and thermophoresis. Slip condition are utilized for velocity, temperature and concentration. Exact solution is obtained for velocity. Further NDSolve is utilized for the graphical analysis of temperature, concentration, entropy and heat transfer coefficient at the wall. Results are also analyzed for viscous, shear thickening and shear thinning fluids. This study reveals that the shear thinning fluids move with higher velocity than the viscous and shear thickening fluids. Similarly temperature and entropy generation are also higher for shear thinning case when compared with others. Further heat source parameter enhances the temperature whereas sink parameter leads to decay. Slip parameter for velocity and temperature caused an increase in the respective velocity and temperature. Moreover chemical reaction parameter leads to enhancement in temperature and entropy generation for viscous, shear thickening and shear thinning fluids. However shear thinning fluids are found prominent.

## 9.2 Problem formulation

We have an interest to examine peristaltic flow of Rabinowitsch liquid in a symmetric channel with compliant boundaries. The walls are maintained at temperature  $T_0$ . Brownian motion and thermophoresis are discussed. Heat generation/absorption and chemical reaction are attended. The partial slip constraints for velocity, temperature and concentration are studied. Flow is due to travelling wave along the channel walls. Wall form is

$$y = \pm \eta(x, t) = \pm \left[ d + a \sin \frac{2\pi}{\lambda} (x - ct) \right], \quad (9.1)$$

where we take the channel width  $2d$ , wave amplitude  $a$ , speed  $c$ , wavelength  $\lambda$ . This phenomenon is shown via Fig. 9.1.

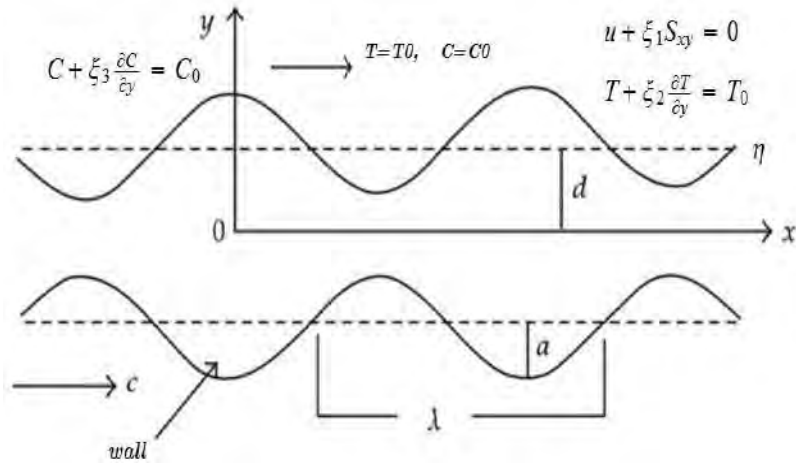


Fig. 9.1: Schematic Diagram

Flow problem is governed by the expressions [91, 108]

$$\frac{\partial u}{\partial x} + \frac{\partial v}{\partial y} = 0. \quad (9.2)$$

$$\frac{\partial u}{\partial t} + u \frac{\partial u}{\partial x} + v \frac{\partial u}{\partial y} = -\frac{1}{\rho_f} \frac{\partial p}{\partial x} + \frac{1}{\rho_f} \frac{\partial S_{xx}}{\partial x} + \frac{1}{\rho_f} \frac{\partial S_{xy}}{\partial y}, \quad (9.3)$$

$$\frac{\partial v}{\partial t} + u \frac{\partial v}{\partial x} + v \frac{\partial v}{\partial y} = -\frac{1}{\rho_f} \frac{\partial p}{\partial y} + \frac{1}{\rho_f} \frac{\partial S_{xy}}{\partial x} + \frac{1}{\rho_f} \frac{\partial S_{yy}}{\partial y}. \quad (9.4)$$

$$\begin{aligned}
\frac{\partial T}{\partial t} + u \frac{\partial T}{\partial x} + v \frac{\partial T}{\partial y} &= \alpha^* \left[ \frac{\partial^2 T}{\partial x^2} + \frac{\partial^2 T}{\partial y^2} \right] + \frac{1}{(\rho C_p)_f} \left[ S_{xx} \frac{\partial u}{\partial x} + S_{xy} \left( \frac{\partial u}{\partial y} + \frac{\partial v}{\partial x} \right) + S_{yy} \frac{\partial v}{\partial y} \right] \\
&+ \tau \left[ D_B \left( \frac{\partial C}{\partial x} \frac{\partial T}{\partial x} + \frac{\partial C}{\partial y} \frac{\partial T}{\partial y} \right) + \frac{D_T}{T_m} \left( \left( \frac{\partial T}{\partial x} \right)^2 + \left( \frac{\partial T}{\partial y} \right)^2 \right) \right] \\
&+ \frac{1}{(\rho C_p)_f} Q_0 (T - T_0). \tag{9.5}
\end{aligned}$$

$$\frac{\partial C}{\partial t} + u \frac{\partial C}{\partial x} + v \frac{\partial C}{\partial y} = D_B \left( \frac{\partial^2 C}{\partial x^2} + \frac{\partial^2 C}{\partial y^2} \right) + \frac{D_T}{T_m} \left( \frac{\partial^2 T}{\partial x^2} + \frac{\partial^2 T}{\partial y^2} \right) - k_1^* (C - C_0). \tag{9.6}$$

Here energy Eq. (9.5) is taken by including heat source/ sink parameter. Brownian motion and thermophoresis effects. These are represented by  $D_B$  and  $D_T$  respectively.  $(u, v)$  the velocity component,  $t$  the time,  $\tau$  is  $(\rho C_p)_p / (\rho C_p)_f$ ,  $T$  temperature,  $C$  the concentration,  $Q_0$  the heat generation/absorption coefficient,  $k_1^*$  the strength of chemical reaction and  $S_{xx}$ ,  $S_{xy}$ ,  $S_{yy}$  the stress components. Further  $\rho_f$ ,  $\alpha^*$ ,  $T_m$ ,  $p$  are the fluid density, thermal diffusivity, mean temperature of nanofluid and pressure respectively.

Boundary conditions are [81, 86]

$$\frac{\partial u}{\partial y} = 0, \quad \text{at } y = 0, \quad u + \xi_1 S_{xy} = 0 \quad \text{at } y = \eta, \tag{9.7}$$

$$\left[ -\tau^* \frac{\partial^3}{\partial x^3} + m^* \frac{\partial^3}{\partial x \partial t^2} + d_1^* \frac{\partial^2}{\partial t \partial x} \right] \eta = \frac{\partial S_{xy}}{\partial y} + \frac{\partial S_{xx}}{\partial x} - \rho_f \left[ \frac{\partial u}{\partial t} + u \frac{\partial u}{\partial x} + v \frac{\partial u}{\partial y} \right] \text{ at } y = \eta \tag{9.8}$$

$$\frac{\partial T}{\partial y} = 0, \quad \text{at } y = 0, \quad T + \xi_2 \frac{\partial T}{\partial y} = T_0 \quad \text{at } y = \eta, \tag{9.9}$$

$$\frac{\partial C}{\partial y} = 0, \quad \text{at } y = 0, \quad C + \xi_3 \frac{\partial C}{\partial y} = C_0 \quad \text{at } y = \eta, \tag{9.10}$$

in which  $\tau^*$ ,  $m^*$ , and  $d_1^*$  elucidate the wall characteristics in terms of elastic and damping coefficients while  $\xi_1$ ,  $\xi_2$  and  $\xi_3$  represent the velocity, temperature and concentration slip parameters.

Non-dimensional variables are

$$\begin{aligned}
x^* &= \frac{x}{\lambda}, & y^* &= \frac{y}{d}, & u^* &= \frac{u}{c}, & v^* &= \frac{v}{c}, & t^* &= \frac{ct}{\lambda}, \\
\xi_1^* &= \frac{\xi_1 \mu}{d}, & \xi_2^* &= \frac{\xi_2}{d}, & \xi_3^* &= \frac{\xi_3}{d}, & \eta^* &= \frac{\eta}{d}, \\
S_{ij}^* &= \frac{dS_{ij}}{c\mu}, & p^* &= \frac{d^2 p}{c\lambda\mu}, & \phi &= \frac{C - C_0}{C_0}, & \beta^* &= \frac{\beta\mu^3 c^3}{d^3}, \\
\theta &= \frac{T - T_0}{T_0}, & u &= \frac{\partial\psi}{\partial y}, & v &= -\delta \frac{\partial\psi}{\partial x}.
\end{aligned} \tag{9.11}$$

After invoking Eq. (9.11), our system of equations (9.3-9.6) reduce to

$$\text{Re} \left[ \delta \frac{\partial^2 \psi}{\partial t \partial y} + \delta \frac{\partial \psi}{\partial y} \frac{\partial^2 \psi}{\partial x \partial y} - \delta \frac{\partial \psi}{\partial x} \frac{\partial^2 \psi}{\partial y^2} \right] = -\frac{\partial p}{\partial x} + \delta \frac{\partial S_{xx}}{\partial x} + \frac{\partial S_{xy}}{\partial y}, \tag{9.12}$$

$$\text{Re} \delta \left[ -\delta^2 \frac{\partial^2 \psi}{\partial t \partial x} - \delta^2 \frac{\partial \psi}{\partial y} \frac{\partial^2 \psi}{\partial x^2} + \delta^2 \frac{\partial \psi}{\partial x} \frac{\partial^2 \psi}{\partial x \partial y} \right] = -\frac{\partial p}{\partial y} + \delta^2 \frac{\partial S_{xy}}{\partial x} + \delta \frac{\partial S_{yy}}{\partial y}, \tag{9.13}$$

$$\begin{aligned}
\text{Re Pr} \left[ \delta \frac{\partial \theta}{\partial t} + \delta \frac{\partial \psi}{\partial y} \frac{\partial \theta}{\partial x} - \delta \frac{\partial \psi}{\partial x} \frac{\partial \theta}{\partial y} \right] &= \left[ \delta^2 \frac{\partial^2 \theta}{\partial x^2} + \frac{\partial^2 \theta}{\partial y^2} \right] + Br \left[ \begin{aligned} &\delta S_{xx} \frac{\partial^2 \psi}{\partial x \partial y} \\ &+ S_{xy} \left( \frac{\partial^2 \psi}{\partial y^2} - \delta^2 \frac{\partial^2 \psi}{\partial x^2} \right) - \delta S_{yy} \frac{\partial^2 \psi}{\partial x \partial y} \end{aligned} \right] \\
&+ Nb \text{Pr} \left( \delta^2 \frac{\partial \phi}{\partial x} \frac{\partial \theta}{\partial x} + \frac{\partial \phi}{\partial y} \frac{\partial \theta}{\partial y} \right) + \\
&Nt \text{Pr} \left( \delta^2 \left( \frac{\partial \theta}{\partial x} \right)^2 + \left( \frac{\partial \theta}{\partial y} \right)^2 \right) + S\theta, \tag{9.14}
\end{aligned}$$

$$\text{Re Sc} \left( \delta \frac{\partial \phi}{\partial t} + \frac{\partial \psi}{\partial y} \frac{\partial \phi}{\partial x} - \delta \frac{\partial \psi}{\partial x} \frac{\partial \phi}{\partial y} \right) = \left( \delta^2 \frac{\partial^2 \phi}{\partial x^2} + \frac{\partial^2 \phi}{\partial y^2} \right) + \frac{Nt}{Nb} \left( \delta^2 \frac{\partial^2 \theta}{\partial x^2} + \frac{\partial^2 \theta}{\partial y^2} \right) - \gamma_1 Sc \phi, \tag{9.15}$$

with boundary conditions

$$\frac{\partial^2 \psi}{\partial y^2} = 0, \quad \text{at } y = 0, \quad \frac{\partial \psi}{\partial y} + \xi_1 S_{xy} = 0, \quad \text{at } y = \eta = (1 + \varepsilon \sin 2\pi(x - t)), \tag{9.16}$$

$$\begin{aligned}
\left[ E_1 \frac{\partial^3}{\partial x^3} + E_2 \frac{\partial^3}{\partial x \partial t^2} + E_3 \frac{\partial^2}{\partial t \partial x} \right] \eta &= -\text{Re} \left[ \delta \frac{\partial^2 \psi}{\partial t \partial y} + \delta \frac{\partial \psi}{\partial y} \frac{\partial^2 \psi}{\partial x \partial y} - \delta \frac{\partial \psi}{\partial x} \frac{\partial^2 \psi}{\partial y^2} \right] + \\
&\delta \frac{\partial S_{xx}}{\partial x} + \frac{\partial S_{xy}}{\partial y}, \quad \text{at } y = \eta, \tag{9.17}
\end{aligned}$$



$$\frac{\partial \theta}{\partial y} = 0, \quad \text{at } y = 0, \quad \theta + \xi_2 \frac{\partial \theta}{\partial y} = 0 \quad \text{at } y = \eta, \quad (9.18)$$

$$\frac{\partial \phi}{\partial y} = 0, \quad \text{at } y = 0, \quad \phi + \xi_3 \frac{\partial \phi}{\partial y} = 0 \quad \text{at } y = \eta. \quad (9.19)$$

with

$$\begin{aligned} \varepsilon &= \frac{a}{d}, \quad \delta = \frac{d}{\lambda}, \quad \text{Re} = \frac{\rho_f c d}{\mu}, \quad S = \frac{Q_0 d^2}{\kappa}, \\ Nb &= \frac{\tau \rho_f D_B C_0}{\mu}, \quad Nt = \frac{\tau \rho_f D_T T_0}{\mu T_m}, \quad \text{Pr} = \frac{\mu C_f}{\kappa}, \\ Sc &= \frac{\mu}{\rho_f D_B}, \quad Br = \frac{c^2 \mu}{\kappa (T_1 - T_0)}, \quad \gamma_1 = \frac{k_1^* d^2}{\nu}, \\ E_1 &= -\frac{\tau^* d^3}{\lambda^3 c \mu}, \quad E_2 = \frac{m^* c d^3}{\lambda^3 \mu}, \quad E_3 = \frac{d_1^* d^3}{\lambda^2 \mu}. \end{aligned} \quad (9.20)$$

Here  $\psi$  denotes the stream function,  $\theta$  the temperature,  $\phi$  the concentration,  $\varepsilon$  amplitude ratio,  $\delta$  wave number, Re Reynolds number,  $S$  heat source sink parameter,  $Nb$  and  $Nt$  the Brownian motion and thermophoresis parameters, Pr Prandtl number,  $Sc$  Schmidt number,  $Br$  Brinkman number,  $\gamma_1$  chemical reaction parameter and  $E_1, E_2, E_3$  the compliant wall parameters.

Invoking lubrication approach we obtain

$$\frac{\partial p}{\partial x} = \frac{\partial S_{xy}}{\partial y}, \quad (9.21)$$

$$\frac{\partial p}{\partial y} = 0, \quad (9.22)$$

$$0 = \frac{\partial^2 \theta}{\partial y^2} + Br S_{xy} \frac{\partial^2 \psi}{\partial y^2} + Nb \text{Pr} \frac{\partial \phi}{\partial y} \frac{\partial \theta}{\partial y} + Nt \text{Pr} \left( \frac{\partial \theta}{\partial y} \right)^2 + S \theta, \quad (9.23)$$

$$\frac{\partial^2 \phi}{\partial y^2} + \frac{Nt}{Nb} \frac{\partial^2 \theta}{\partial y^2} - \gamma_1 Sc \phi = 0, \quad (9.24)$$

with boundary conditions

$$\frac{\partial^2 \psi}{\partial y^2} = 0, \quad \text{at } y = 0, \quad \frac{\partial \psi}{\partial y} + \xi_1 S_{xy} = 0, \quad \text{at } y = \eta = (1 + \varepsilon \sin 2\pi(x - t)), \quad (9.25)$$

$$\left[ E_1 \frac{\partial^3}{\partial x^3} + E_2 \frac{\partial^3}{\partial x \partial t^2} + E_3 \frac{\partial^2}{\partial t \partial x} \right] \eta = \frac{\partial S_{xy}}{\partial y}, \quad \text{at } y = \eta, \quad (9.26)$$

$$\frac{\partial \theta}{\partial y} = 0, \quad \text{at } y = 0, \quad \theta + \xi_2 \frac{\partial \theta}{\partial y} = 0 \quad \text{at } y = \eta, \quad (9.27)$$

$$\frac{\partial \phi}{\partial y} = 0, \quad \text{at } y = 0, \quad \phi + \xi_3 \frac{\partial \phi}{\partial y} = 0 \quad \text{at } y = \eta. \quad (9.28)$$

where

$$S_{xy} + \beta(S_{xy})^3 = \frac{\partial u}{\partial y}. \quad (9.29)$$

### 9.2.1 Solution of the problem

As in eq. (9.29)  $S_{xy}$  is in implicit form. To obtain an explicit expression we will make use of eq. (9.21). By eq. (9.8) we can write:

$$\frac{\partial p}{\partial x} = \left[ -\tau^* \frac{\partial^3}{\partial x^3} + m^* \frac{\partial^3}{\partial x \partial t^2} + d_1^* \frac{\partial^2}{\partial t \partial x} \right] \eta. \quad (9.30)$$

This will be used to find  $S_{xy}$ .

We will now solve eq. (9.21) subject to slip condition of velocity. We arrive at

$$u(y) = \frac{\partial p}{\partial x} \left( \frac{y^2 - \eta^2}{2} \right) + \beta \left( \frac{\partial p}{\partial x} \right)^3 \left( \frac{y^4 - \eta^4}{2} \right) - \xi_1 \eta \left( \frac{\partial p}{\partial x} \right) \quad (9.31)$$

The energy and concentration equations for nanofluid involve of thermophoresis and Brownian motion effects. To tackle these equations we have utilized the NDSolve technique in Mathematica. This algorithm gives the solutions in less computation time and avoid the lengthy expressions.

### 9.2.2 Expression for entropy generation

Viscous dissipation here is

$$\Phi = S_{xx} \frac{\partial u}{\partial x} + S_{yy} \frac{\partial v}{\partial y} + S_{xy} \left( \frac{\partial u}{\partial y} + \frac{\partial v}{\partial x} \right). \quad (9.32)$$

Dimensional form is

$$\begin{aligned}
S_{gen}''' &= \frac{\kappa}{T_m^2} \left( \left( \frac{\partial T}{\partial x} \right)^2 + \left( \frac{\partial T}{\partial y} \right)^2 \right) + \frac{\Phi}{T_m} + \frac{1}{T_m} (Q_0(T - T_0)) \\
&+ \frac{RD}{C_m} \left( \left( \frac{\partial C}{\partial x} \right)^2 + \left( \frac{\partial C}{\partial y} \right)^2 \right) + \frac{RD}{T_m} \left( \frac{\partial C}{\partial x} \frac{\partial T}{\partial x} + \frac{\partial C}{\partial y} \frac{\partial T}{\partial y} \right)
\end{aligned} \tag{9.33}$$

In dimensionless form

$$\begin{aligned}
N_s &= \frac{S_{gen}'''}{S_G'''} = \left( \frac{\partial \theta}{\partial y} \right)^2 + \frac{Br}{\Lambda} S_{xy} \left( \frac{\partial^2 \psi}{\partial y^2} \right) + \frac{S}{\Lambda} \theta + \\
&+ \frac{L}{\Lambda} \left( \frac{\partial \theta}{\partial y} \right) \left( \frac{\partial \phi}{\partial y} \right) + \frac{L\zeta}{\Lambda^2} \left( \frac{\partial \phi}{\partial y} \right)^2,
\end{aligned} \tag{9.34}$$

$$S_G''' = \frac{\kappa T_0^2}{T_m^2 d^2}, \quad \Lambda = \frac{T_0}{T_m}, \quad L = \frac{RDC_0}{\kappa}, \quad \zeta = \frac{C_0}{C_m}. \tag{9.35}$$

## 9.3 Analysis

This section contains the graphical analysis of velocity, temperature, concentration, entropy and heat transfer coefficient. Separate subsections are organized for this purpose.

### 9.3.1 Velocity

This subsection is organized for the results of velocity profile. Slip parameter results can be viewed through Fig. 9.2. Higher slip parameter leads to velocity enhancement. It is due to less friction. Figs. 9.3 and 9.4 represent behavior for wall elastance parameters. Enhancement of velocity is seen in both cases. Result of damping parameter for wall behavior can be noticed via Fig. 9.5. As damping nature of wall resists the fluid to move that causes decay in velocity of fluid. It is also observed that for  $\beta > 0$  (shear thinning) cases the velocity is higher than viscous ( $\beta = 0$ ) and shear thickening ( $\beta < 0$ ) cases. This behavior is quite obvious as thick fluid flows slowly than thin material.

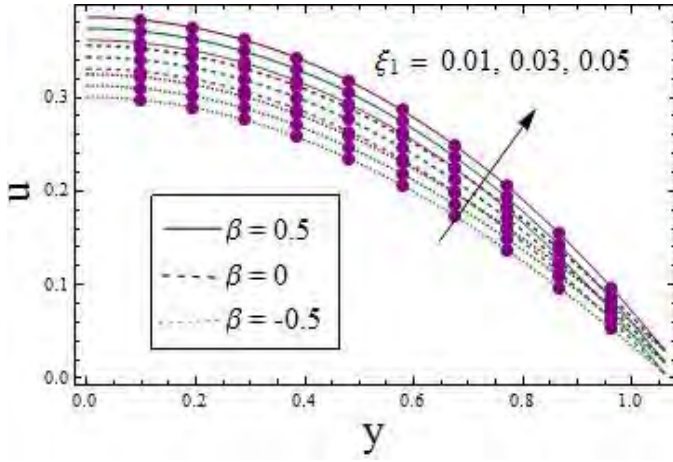


Fig. 9.2

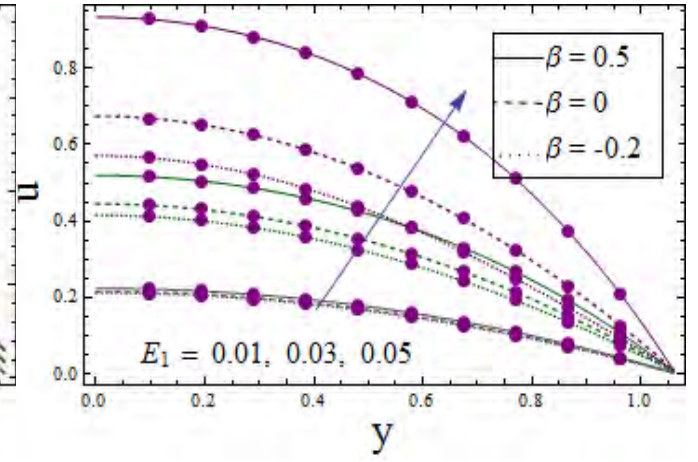


Fig. 9.3

Fig. 9.2.  $u$  via change in  $\xi_1$  when  $E_1 = 0.02$ ,  $E_2 = 0.01$ ,  $E_3 = 0.01$ ,  $t = 0.1$ ,  $x = 0.2$ ,  $\varepsilon = 0.1$ .

Fig. 9.3.  $u$  via change in  $E_1$  when  $E_2 = 0.01$ ,  $E_3 = 0.01$ ,  $t = 0.1$ ,  $x = 0.2$ ,  $\varepsilon = 0.1$ ,  $\xi_1 = 0.01$ .

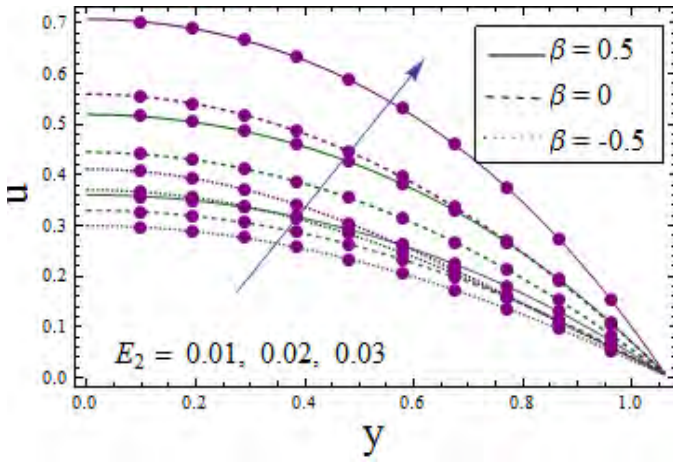


Fig. 9.4

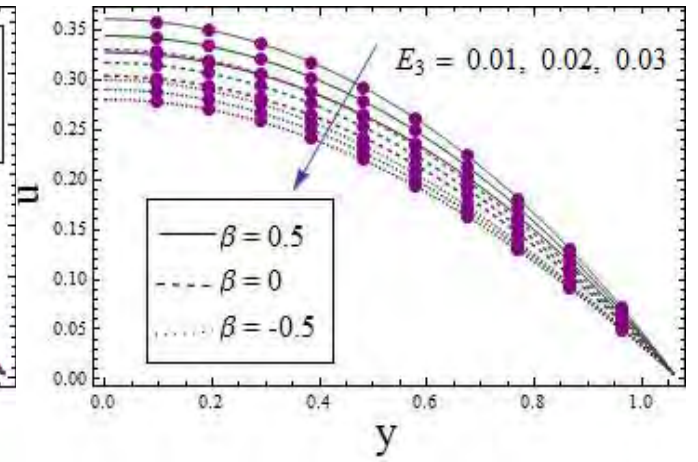


Fig. 9.5

Fig. 9.4.  $u$  via change in  $E_2$  when  $E_1 = 0.02$ ,  $E_3 = 0.01$ ,  $t = 0.1$ ,  $x = 0.2$ ,  $\varepsilon = 0.1$ ,  $\xi_1 = 0.01$ .

Fig. 9.5.  $u$  via change in  $E_3$  when  $E_1 = 0.02$ ,  $E_2 = 0.01$ ,  $t = 0.1$ ,  $x = 0.2$ ,  $\varepsilon = 0.1$ ,  $\xi_1 = 0.01$ .

### 9.3.2 Temperature

This subsection contains the information about temperature of considered system. Fig. 9.6 illustrates the result for heat source /sink parameter on temperature. It is clearly seen that for case of source parameter ( $S > 0$ ) temperature of fluid enhances whereas for case of sink ( $S < 0$ )  $\theta$  decreases. Moreover shear thinning fluid has higher temperature than viscous and shear thickening materials. Shear thinning fluid has higher velocity and so higher mean kinetic energy. Therefore higher temperature than shear thickening fluids. Similarly like velocity slip parameter caused enhancement in mean kinetic energy thermal slip parameter leads to increase in temperature (see Fig. 9.7).  $Br$  effect can be observed with Fig. 9.8. An increase in heat loss enhances the temperature. Fig. 9.9 demonstrates the impact of  $\varepsilon$ . Clearly wave with larger amplitude causes increase in velocity and temperature as well. Larger values of Prandtl number lead to increase of  $\theta$  (see Fig. 9.10). Viscous force also plays a vital role in enhancement of temperature. Infact viscous effects dominating the heat loss, signify the enhancement of temperature. Fig. 9.11 portrayed the impact of chemical reaction parameter. Clearly higher  $\gamma_1$  yields temperature enhancement. Physical aspects is linked with chemical reaction parameter and kinematic viscosity. Thermophoretic parameter caused an increase in  $\theta$  (see Fig. 9.12). Fig. 9.13 displays the  $Nb$  effect on  $\theta$ . In this case for higher values of  $Nb$  the temperature increases. However in this case the increment is not prominent. Elastance parameters caused enhancement of temperature (see Figs. 9.14, 9.15). Fig. 9.16 displays  $E_3$  effect on  $\theta$ . Decay is observed here. In all cases shear thinning fluid has higher values of temperature when compared with viscous and shear thickening materials.

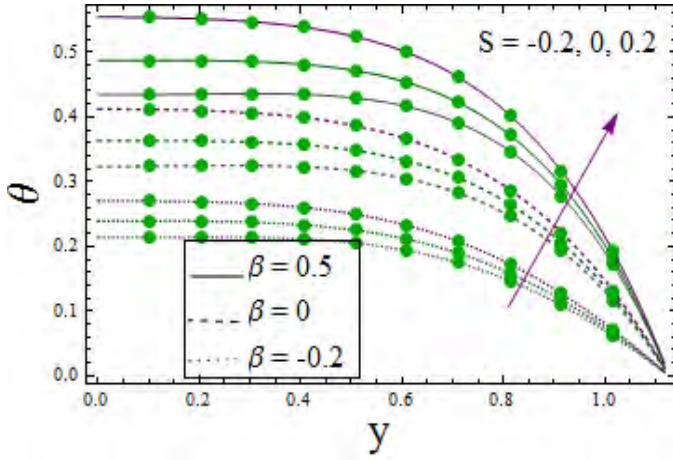


Fig. 9.6

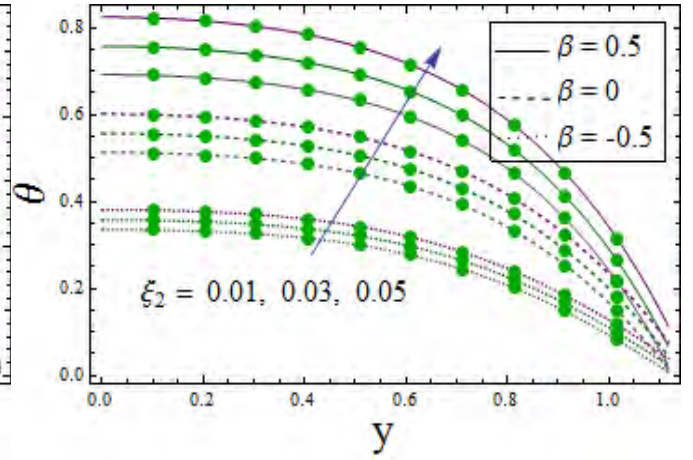


Fig. 9.7

Fig. 9.6.  $\theta$  via change in  $S$  when  $E_1 = 0.02$ ,  $E_2 = 0.01$ ,  $E_3 = 0.01$ ,  $t = 0.1$ ,  $x = 0.2$ ,  $\varepsilon = 0.2$ ,  $\xi_1 = 0.01$ ,  $\xi_2 = 0.01$ ,  $\xi_3 = 0.01$ ,  $Nt = 1.5$ ,  $\gamma_1 = 0.1$ ,  $Nb = 1.5$ ,  $Sc = 0.5$ ,  $Pr = 1.5$ ,  $Br = 2.0$ .

Fig. 9.7.  $\theta$  via change in  $\xi_2$  when  $E_1 = 0.02$ ,  $E_2 = 0.01$ ,  $E_3 = 0.01$ ,  $t = 0.1$ ,  $x = 0.2$ ,  $\varepsilon = 0.2$ ,  $S = 0.5$ ,  $\xi_1 = 0.01$ ,  $\xi_3 = 0.01$ ,  $Nt = 1.5$ ,  $\gamma_1 = 0.1$ ,  $Nb = 1.5$ ,  $Sc = 0.5$ ,  $Pr = 1.5$ ,  $Br = 2.0$ .

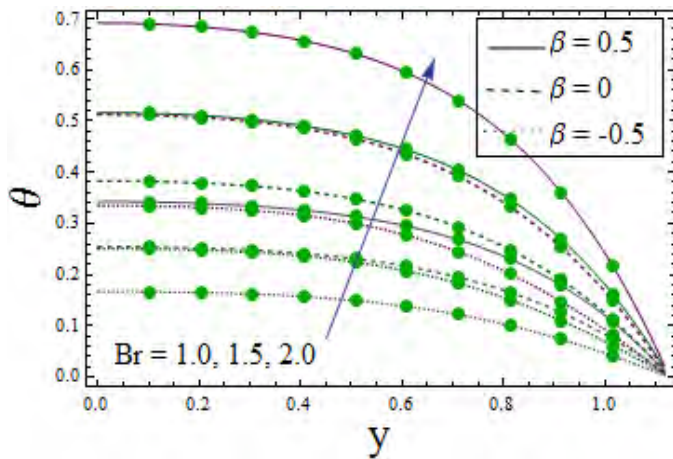


Fig. 9.8

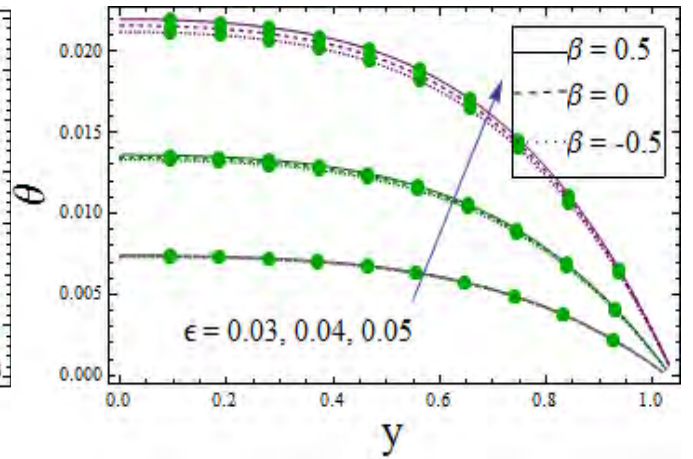


Fig. 9.9

Fig. 9.8.  $\theta$  via change in  $Br$  when  $E_1 = 0.02$ ,  $E_2 = 0.01$ ,  $E_3 = 0.01$ ,  $t = 0.1$ ,  $x = 0.2$ ,  $\varepsilon = 0.2$ ,  $S = 0.5$ ,  $\xi_1 = 0.01$ ,  $\xi_2 = 0.01$ ,  $\xi_3 = 0.01$ ,  $Nt = 1.5$ ,  $\gamma_1 = 0.1$ ,  $Nb = 1.5$ ,  $Sc = 0.5$ ,  $Pr = 1.5$ .

Fig. 9.9.  $\theta$  via change in  $\varepsilon$  when  $E_1 = 0.02$ ,  $E_2 = 0.01$ ,  $E_3 = 0.01$ ,  $t = 0.1$ ,  $x = 0.2$ ,  $S = 0.5$ ,

$\xi_1 = 0.01, \xi_2 = 0.01, \xi_3 = 0.01, Nt = 1.5, \gamma_1 = 0.1, Nb = 1.5, Sc = 0.5, Pr = 1.5, Br = 2.0.$

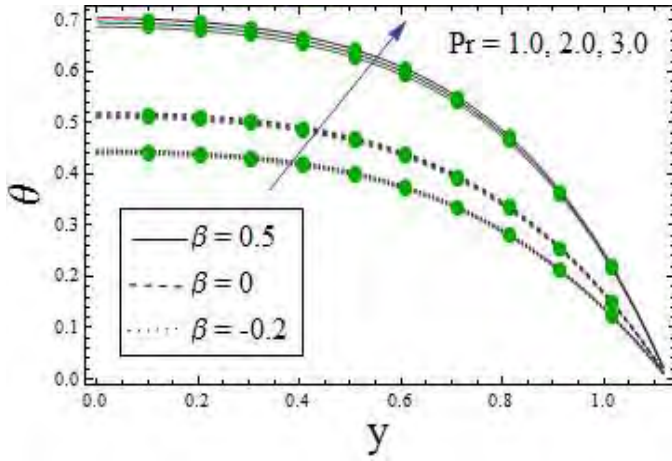


Fig. 9.10

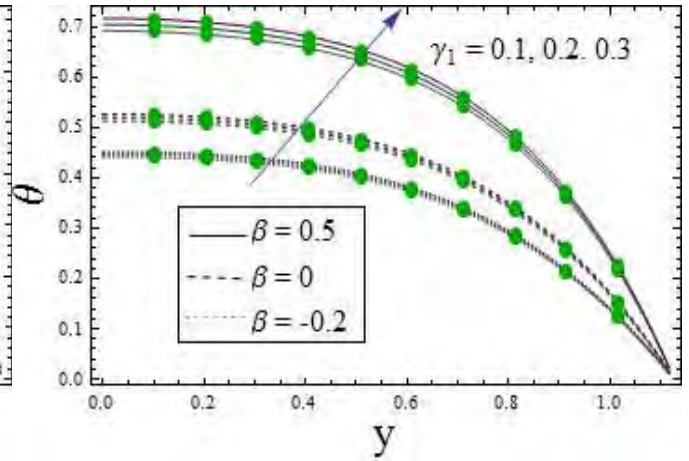


Fig. 9.11

Fig. 9.10.  $\theta$  via change in  $Pr$  when  $E_1 = 0.02, E_2 = 0.01, E_3 = 0.01, t = 0.1, x = 0.2, \varepsilon = 0.2,$

$S = 0.5, \xi_1 = 0.01, \xi_2 = 0.01, \xi_3 = 0.01, Nt = 1.5, \gamma_1 = 0.1, Nb = 1.5, Sc = 0.5, Br = 2.0.$

Fig. 9.11.  $\theta$  via change in  $\gamma_1$  when  $E_1 = 0.02, E_2 = 0.01, E_3 = 0.01, t = 0.1, x = 0.2, \varepsilon = 0.2,$

$S = 0.5, \xi_1 = 0.01, \xi_2 = 0.01, \xi_3 = 0.01, Nt = 1.5, Nb = 1.5, Sc = 0.5, Pr = 1.5, Br = 2.0.$

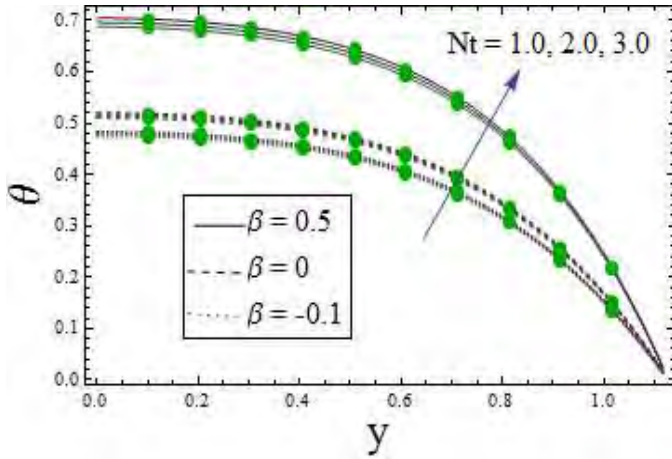


Fig. 9.12

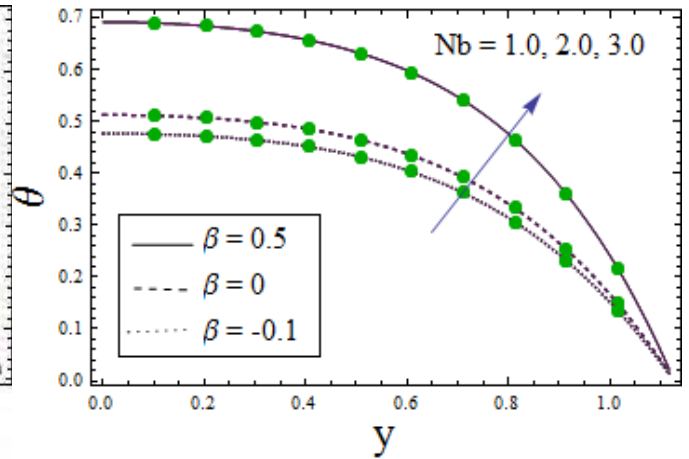


Fig. 9.13

Fig. 9.12.  $\theta$  via change in  $Nt$  when  $E_1 = 0.02, E_2 = 0.01, E_3 = 0.01, t = 0.1, x = 0.2, \varepsilon = 0.2,$

$S = 0.5, \xi_1 = 0.01, \xi_2 = 0.01, \xi_3 = 0.01, \gamma_1 = 0.1, Nb = 1.5, Sc = 0.5, Pr = 1.5, Br = 2.0.$



Fig. 9.13.  $\theta$  via change in  $Nb$  when  $E_1 = 0.02$ ,  $E_2 = 0.01$ ,  $E_3 = 0.01$ ,  $t = 0.1$ ,  $x = 0.2$ ,  $\varepsilon = 0.2$ ,  $S = 0.5$ ,  $\xi_1 = 0.01$ ,  $\xi_2 = 0.01$ ,  $\xi_3 = 0.01$ ,  $Nt = 1.5$ ,  $\gamma_1 = 0.1$ ,  $Sc = 0.5$ ,  $Pr = 1.5$ ,  $Br = 2.0$ .

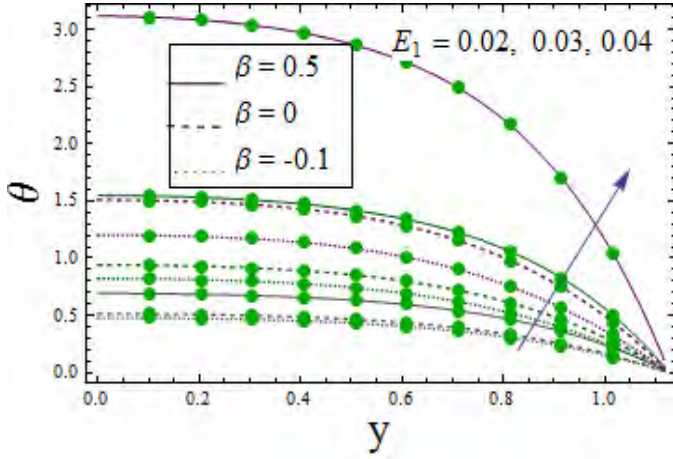


Fig. 9.14

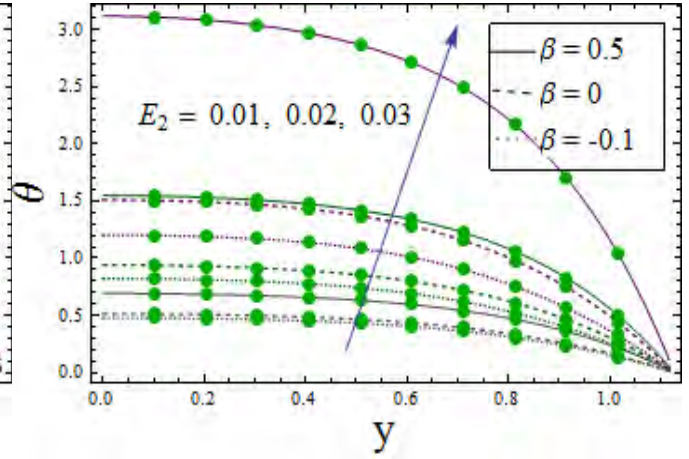


Fig. 9.15

Fig. 9.14.  $\theta$  via change in  $E_1$  when  $E_2 = 0.01$ ,  $E_3 = 0.01$ ,  $t = 0.1$ ,  $x = 0.2$ ,  $\varepsilon = 0.2$ ,  $S = 0.5$ ,  $\xi_1 = 0.01$ ,  $\xi_2 = 0.01$ ,  $\xi_3 = 0.01$ ,  $Nt = 1.5$ ,  $\gamma_1 = 0.1$ ,  $Nb = 1.5$ ,  $Sc = 0.5$ ,  $Pr = 1.5$ ,  $Br = 2.0$ .

Fig. 9.15.  $\theta$  via change in  $E_2$  when  $E_1 = 0.02$ ,  $E_3 = 0.01$ ,  $t = 0.1$ ,  $x = 0.2$ ,  $\varepsilon = 0.2$ ,  $S = 0.5$ ,  $\xi_1 = 0.01$ ,  $\xi_2 = 0.01$ ,  $\xi_3 = 0.01$ ,  $Nt = 1.5$ ,  $\gamma_1 = 0.1$ ,  $Nb = 1.5$ ,  $Sc = 0.5$ ,  $Pr = 1.5$ ,  $Br = 2.0$ .

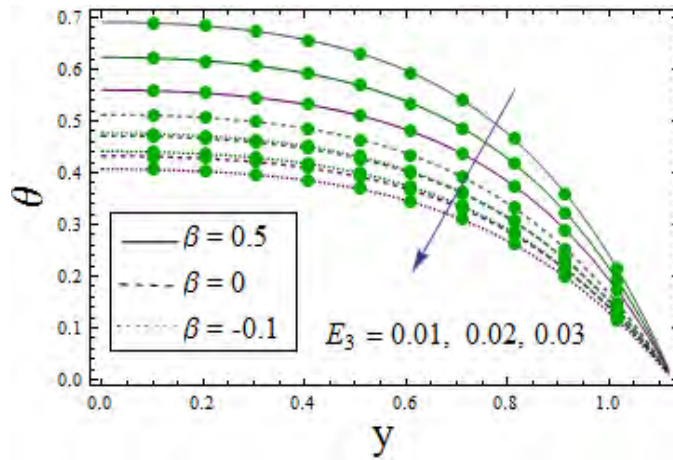


Fig. 9.16

Fig. 9.16.  $\theta$  via change in  $E_3$  when  $E_1 = 0.02$ ,  $E_2 = 0.01$ ,  $t = 0.1$ ,  $x = 0.2$ ,  $\varepsilon = 0.2$ ,  $S = 0.5$ ,



$$\xi_1 = 0.01, \xi_2 = 0.01, \xi_3 = 0.01, Nt = 1.5, \gamma_1 = 0.1, Nb = 1.5, Sc = 0.5, Pr = 1.5, Br = 2.0.$$

### 9.3.3 Concentration field

Graphical analysis of concentration is presented in this subsection. Slip effect on concentration can be viewed via Fig. 9.17. Decay is observed for larger slip parameter. Concentration is increasing function of Schmidt number (see Fig. 9.18). Viscous effects elevated the concentration. Similarly resemblance is observed here. By viewing Figs. 9.19 and 9.20 opposite impacts of  $Nb$  and  $Nt$  on  $\phi$  are observed. Larger values of  $Nb$  caused increase of  $\phi$ . Fig. 9.21 is prepared to see the result for chemical reaction parameter. Enhancement is also seen here. Reason is directly related to chemical reaction coefficient. Graphical illustration for amplitude ratio and heat source/sink parameter can be noticed through Figs. 9.22 and 9.23. Both show decaying trend for  $\phi$ . Elastance parameters for walls lead to decay in concentration. These observations can be noticed with Figs. 9.24 and 9.25. Damping coefficient result can be elucidated with Fig. 9.26.  $E_3$  caused increase in  $\phi$ . In all cases under discussion it can be clearly noticed that concentration for the shear thinning fluid is lower than the viscous and shear thickening materials.

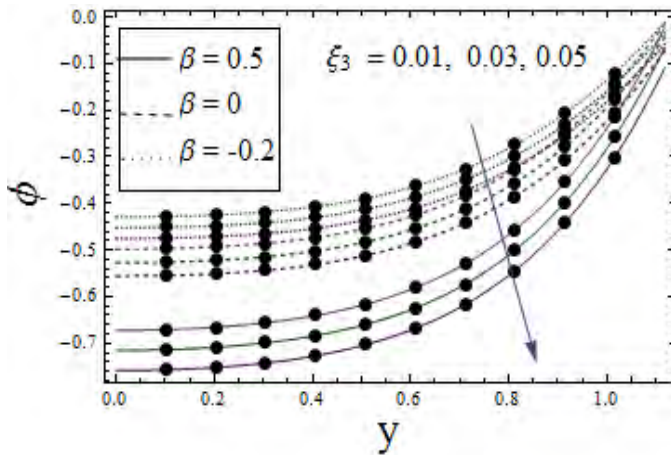


Fig. 9.17

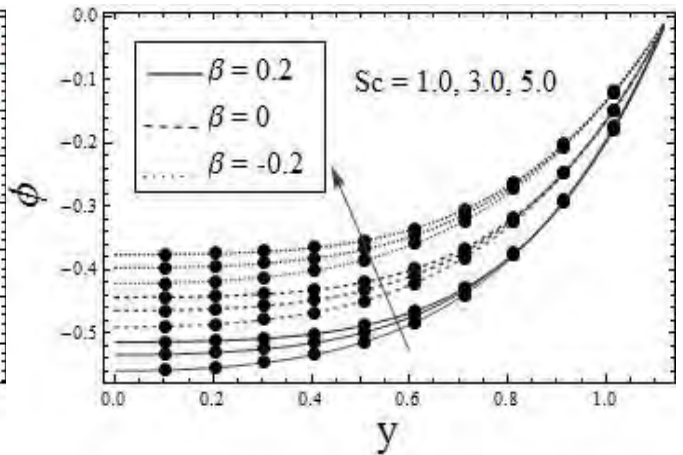


Fig. 9.18

Fig. 9.17.  $\phi$  via change in  $\xi_3$  when  $E_1 = 0.02, E_2 = 0.01, E_3 = 0.01, t = 0.1, x = 0.2, \varepsilon = 0.2, S = 0.5, \xi_1 = 0.01, \xi_2 = 0.01, Nt = 1.5, \gamma_1 = 0.1, Nb = 1.5, Sc = 0.5, Pr = 1.5, Br = 2.0.$

Fig. 9.18.  $\phi$  via change in  $Sc$  when  $E_1 = 0.02$ ,  $E_2 = 0.01$ ,  $E_3 = 0.01$ ,  $t = 0.1$ ,  $x = 0.2$ ,  $\varepsilon = 0.2$ ,  $S = 0.5$ ,  $\xi_1 = 0.01$ ,  $\xi_2 = 0.01$ ,  $\xi_3 = 0.01$ ,  $Nt = 1.5$ ,  $\gamma_1 = 0.1$ ,  $Nb = 1.5$ ,  $Pr = 1.5$ ,  $Br = 2.0$ .

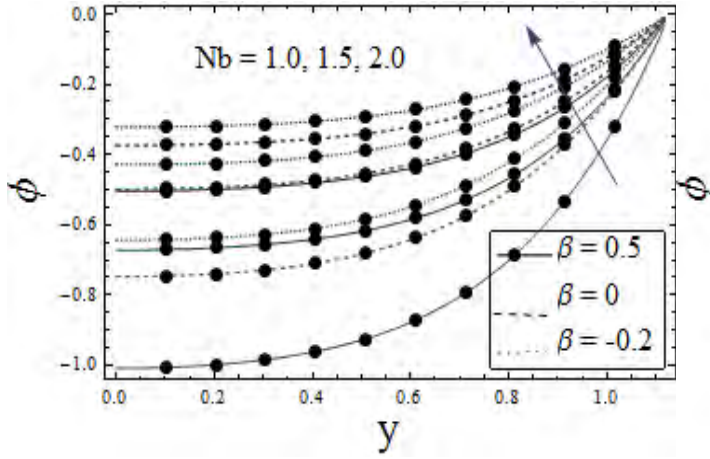


Fig. 9.19

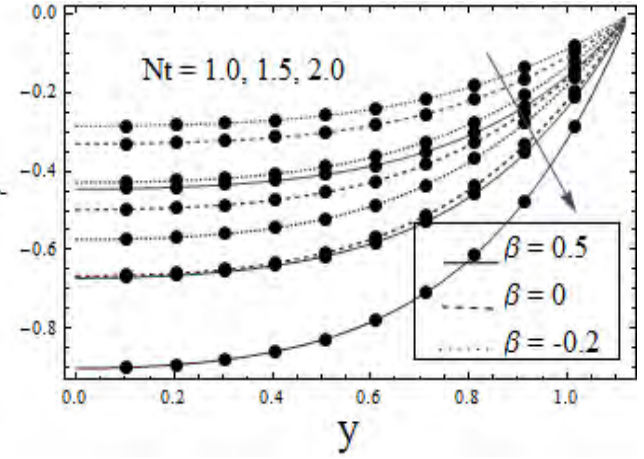


Fig. 9.20

Fig. 9.19.  $\phi$  via change in  $Nb$  when  $E_1 = 0.02$ ,  $E_2 = 0.01$ ,  $E_3 = 0.01$ ,  $t = 0.1$ ,  $x = 0.2$ ,  $\varepsilon = 0.2$ ,  $S = 0.5$ ,  $\xi_1 = 0.01$ ,  $\xi_2 = 0.01$ ,  $\xi_3 = 0.01$ ,  $Nt = 1.5$ ,  $\gamma_1 = 0.1$ ,  $Sc = 0.5$ ,  $Pr = 1.5$ ,  $Br = 2.0$ .

Fig. 9.20.  $\phi$  via change in  $Nt$  when  $E_1 = 0.02$ ,  $E_2 = 0.01$ ,  $E_3 = 0.01$ ,  $t = 0.1$ ,  $x = 0.2$ ,  $\varepsilon = 0.2$ ,  $S = 0.5$ ,  $\xi_1 = 0.01$ ,  $\xi_2 = 0.01$ ,  $\xi_3 = 0.01$ ,  $\gamma_1 = 0.1$ ,  $Nb = 1.5$ ,  $Sc = 0.5$ ,  $Pr = 1.5$ ,  $Br = 2.0$ .

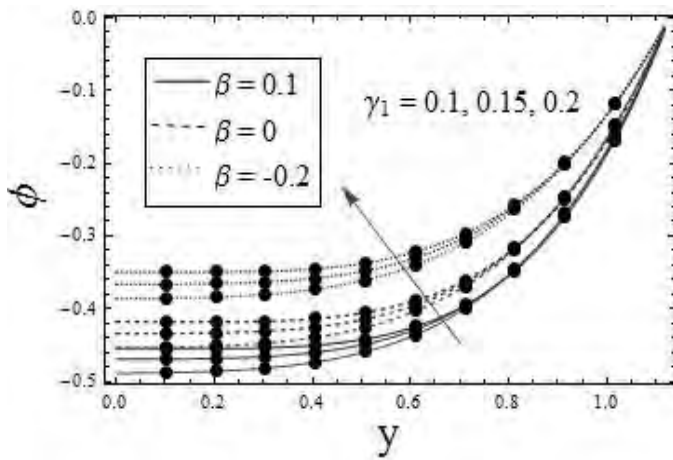


Fig. 9.21

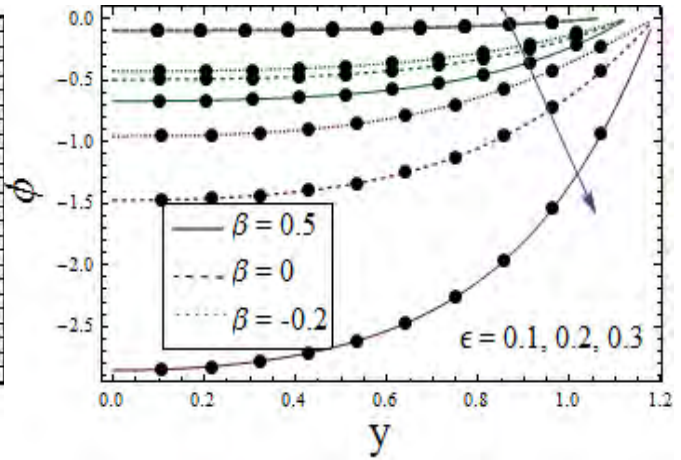


Fig. 9.22

Fig. 9.21.  $\phi$  via change in  $\gamma_1$  when  $E_1 = 0.02$ ,  $E_2 = 0.01$ ,  $E_3 = 0.01$ ,  $t = 0.1$ ,  $x = 0.2$ ,  $\varepsilon = 0.2$ ,

$S = 0.5, \xi_1 = 0.01, \xi_2 = 0.01, \xi_3 = 0.01, Nt = 1.5, Nb = 1.5, Sc = 4, Pr = 1.5, Br = 2.0.$

Fig. 9.22.  $\phi$  via change in  $\varepsilon$  when  $E_1 = 0.02, E_2 = 0.01, E_3 = 0.01, t = 0.1, x = 0.2, S = 0.5,$   
 $\xi_1 = 0.01, \xi_2 = 0.01, \xi_3 = 0.01, Nt = 1.5, \gamma_1 = 0.1, Nb = 1.5, Sc = 0.5, Pr = 1.5, Br = 2.0.$

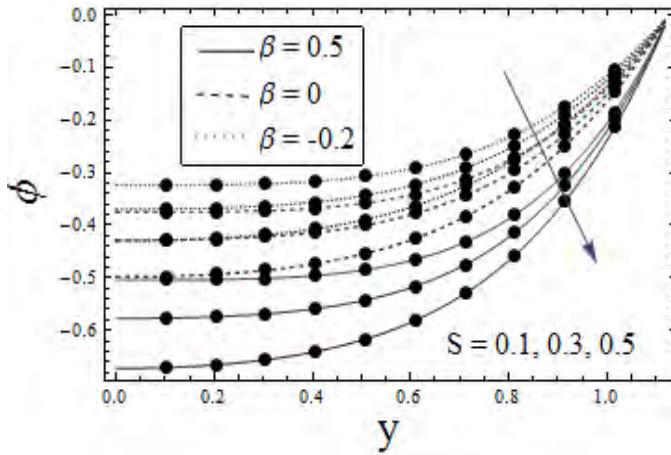


Fig. 9.23

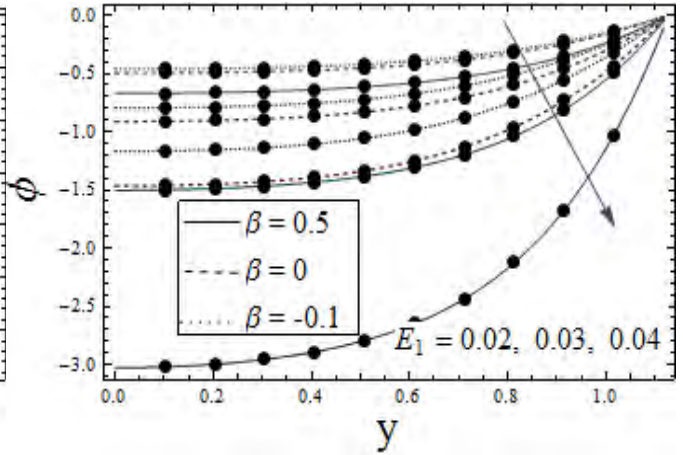


Fig. 9.24

Fig. 9.23.  $\phi$  via change in  $S$  when  $E_1 = 0.02, E_2 = 0.01, E_3 = 0.01, t = 0.1, x = 0.2, \varepsilon = 0.2,$   
 $\xi_1 = 0.01, \xi_2 = 0.01, \xi_3 = 0.01, Nt = 1.5, \gamma_1 = 0.1, Nb = 1.5, Sc = 0.5, Pr = 1.5, Br = 2.0.$

Fig. 9.24.  $\phi$  via change in  $E_1$  when  $E_2 = 0.01, E_3 = 0.01, t = 0.1, x = 0.2, \varepsilon = 0.2, S = 0.5,$   
 $\xi_1 = 0.01, \xi_2 = 0.01, \xi_3 = 0.01, Nt = 1.5, \gamma_1 = 0.1, Nb = 1.5, Sc = 0.5, Pr = 1.5, Br = 2.0.$

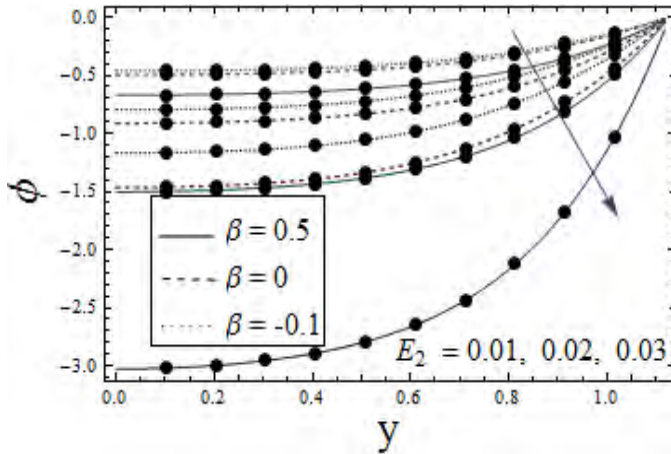


Fig. 9.25

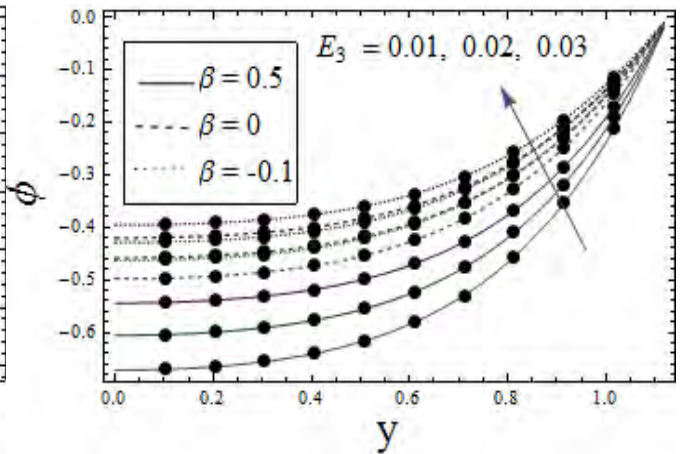


Fig. 9.26

Fig. 9.25.  $\phi$  via change in  $E_2$  when  $E_1 = 0.02$ ,  $E_3 = 0.01$ ,  $t = 0.1$ ,  $x = 0.2$ ,  $\varepsilon = 0.2$ ,  $S = 0.5$ ,  $\xi_1 = 0.01$ ,  $\xi_2 = 0.01$ ,  $\xi_3 = 0.01$ ,  $Nt = 1.5$ ,  $\gamma_1 = 0.1$ ,  $Nb = 1.5$ ,  $Sc = 0.5$ ,  $Pr = 1.5$ ,  $Br = 2.0$ .

Fig. 9.26.  $\phi$  via change in  $E_3$  when  $E_1 = 0.02$ ,  $E_2 = 0.01$ ,  $t = 0.1$ ,  $x = 0.2$ ,  $\varepsilon = 0.2$ ,  $S = 0.5$ ,  $\xi_1 = 0.01$ ,  $\xi_2 = 0.01$ ,  $\xi_3 = 0.01$ ,  $Nt = 1.5$ ,  $\gamma_1 = 0.1$ ,  $Nb = 1.5$ ,  $Sc = 0.5$ ,  $Pr = 1.5$ ,  $Br = 2.0$ .

### 9.3.4 Entropy generation analysis

This subsection contains information about entropy analysis of the considered system for prominent parameters of our study. Fig. 9.27 portrayed the effect of chemical reaction on  $Ns$ . For higher chemical reaction parameter the entropy enhances similar as in case of temperature. Brinkman number also enhances the entropy as this parameter occurs due to the effect of viscous dissipation which is responsible for enhancement of temperature and entropy (see Fig. 9.28). Fig. 9.29 witnessed increasing effect of heat source parameter. As expected the heat source parameter enhances temperature and hence entropy. Influences of  $Nt$  and  $\Lambda$  on  $Ns$  are opposite (see Figs. 9.30 and 9.31). Fig. 9.32 displays the impact of diffusion coefficient parameter  $L$ . Increasing trend of  $Ns$  is noticed in this case. In all graphs it can be observed that shear thinning fluids have higher entropy than the viscous and shear thickening materials. It is due to the fact that shear thinning fluid has higher mean kinetic energy than shear thickening materials which caused more disorderliness.

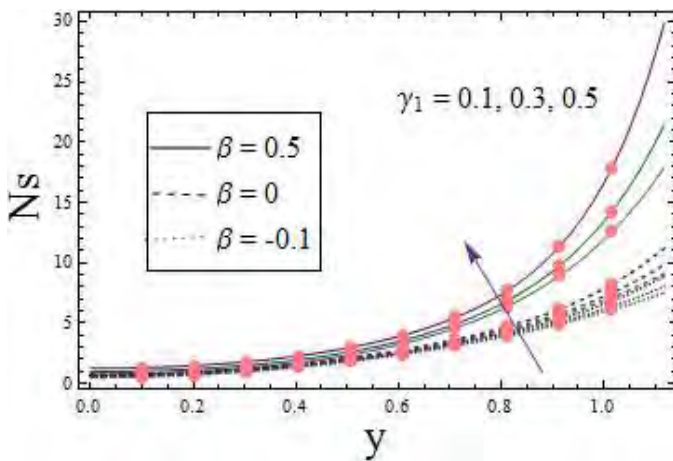


Fig. 9.27

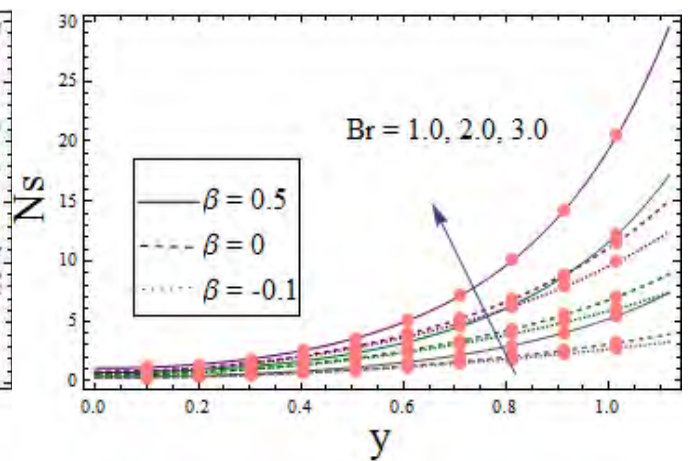


Fig. 9.28



Fig. 9.27.  $Ns$  via change in  $\gamma_1$  when  $E_1 = 0.02$ ,  $E_2 = 0.01$ ,  $E_3 = 0.01$ ,  $t = 0.1$ ,  $x = 0.2$ ,  $\varepsilon = 0.2$ ,  $S = 0.5$ ,  $\xi_1 = 0.01$ ,  $\xi_2 = 0.01$ ,  $\xi_3 = 0.01$ ,  $Nt = 1.5$ ,  $Nb = 1.5$ ,  $Sc = 3$ ,  $Pr = 1.5$ ,  $Br = 2.0$ ,  $L = 0.5$ ,  $\Lambda = 0.5$ ,  $\zeta = 0.5$ .

Fig. 9.28.  $Ns$  via change in  $Br$  when  $E_1 = 0.02$ ,  $E_2 = 0.01$ ,  $E_3 = 0.01$ ,  $t = 0.1$ ,  $x = 0.2$ ,  $\varepsilon = 0.2$ ,  $S = 0.5$ ,  $\xi_1 = 0.01$ ,  $\xi_2 = 0.01$ ,  $\xi_3 = 0.01$ ,  $Nt = 1.5$ ,  $\gamma_1 = 0.1$ ,  $Nb = 1.5$ ,  $Sc = 0.5$ ,  $Pr = 1.5$ ,  $L = 0.5$ ,  $\Lambda = 0.5$ ,  $\zeta = 0.5$ .

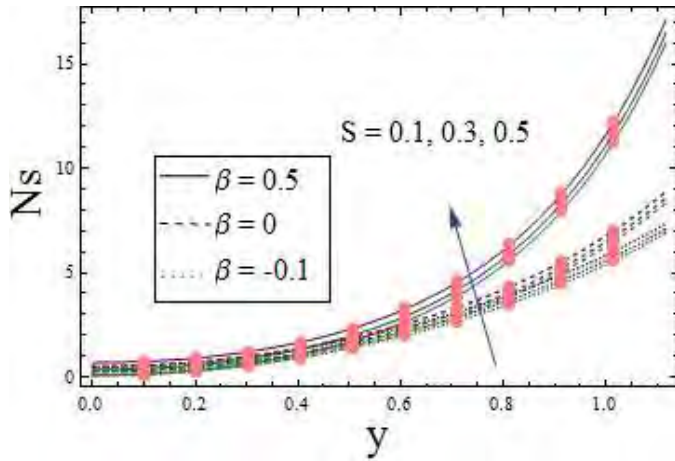


Fig. 9.29

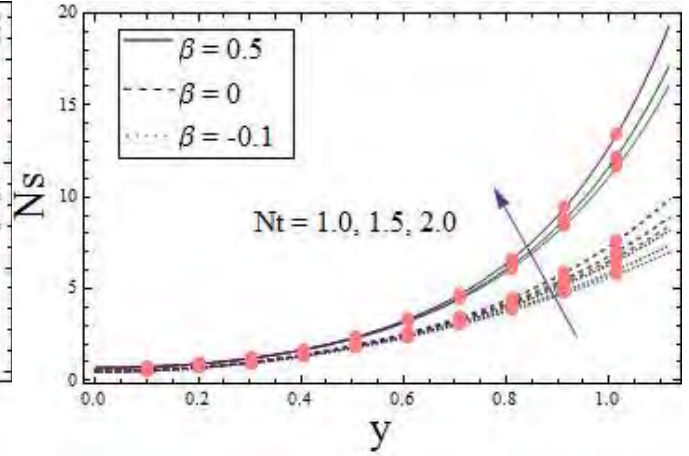


Fig. 9.30

Fig. 9.29.  $Ns$  via change in  $S$  when  $E_1 = 0.02$ ,  $E_2 = 0.01$ ,  $E_3 = 0.01$ ,  $t = 0.1$ ,  $x = 0.2$ ,  $\varepsilon = 0.2$ ,  $\xi_1 = 0.01$ ,  $\xi_2 = 0.01$ ,  $\xi_3 = 0.01$ ,  $Nt = 1.5$ ,  $\gamma_1 = 0.1$ ,  $Nb = 1.5$ ,  $Sc = 0.5$ ,  $Pr = 1.5$ ,  $Br = 2.0$ ,  $L = 0.5$ ,  $\Lambda = 0.5$ ,  $\zeta = 0.5$ .

Fig. 9.30.  $Ns$  via change in  $Nt$  when  $E_1 = 0.02$ ,  $E_2 = 0.01$ ,  $E_3 = 0.01$ ,  $t = 0.1$ ,  $x = 0.2$ ,  $\varepsilon = 0.2$ ,  $S = 0.5$ ,  $\xi_1 = 0.01$ ,  $\xi_2 = 0.01$ ,  $\xi_3 = 0.01$ ,  $\gamma_1 = 0.1$ ,  $Nb = 1.5$ ,  $Sc = 0.5$ ,  $Pr = 1.5$ ,  $Br = 2.0$ ,  $L = 0.5$ ,  $\Lambda = 0.5$ ,  $\zeta = 0.5$ .

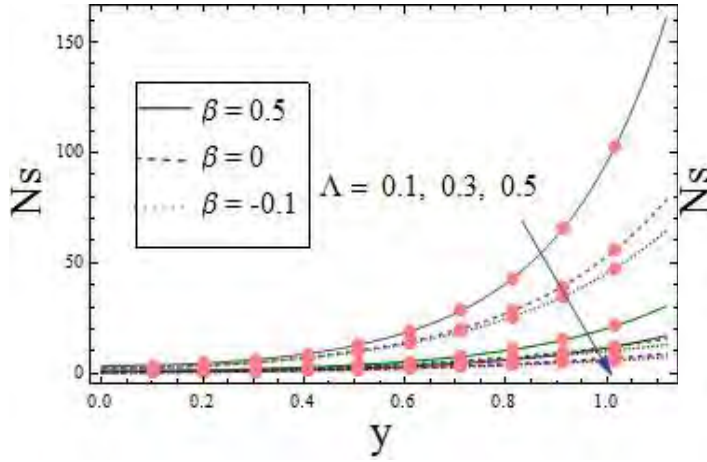


Fig. 9.31

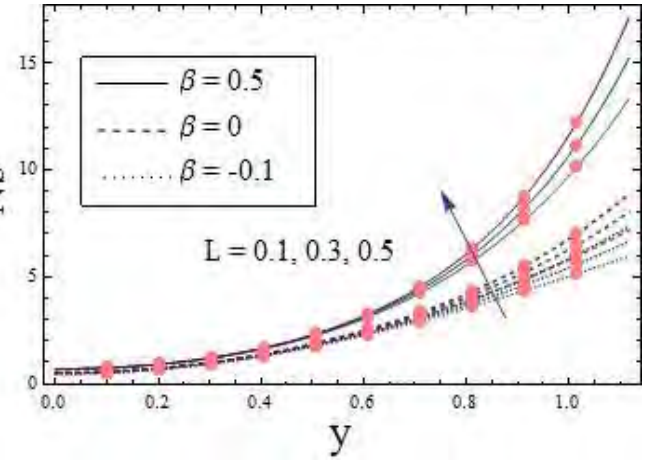


Fig. 9.32

Fig. 9.31.  $Ns$  via change in  $\Lambda$  when  $E_1 = 0.02$ ,  $E_2 = 0.01$ ,  $E_3 = 0.01$ ,  $t = 0.1$ ,  $x = 0.2$ ,  $\varepsilon = 0.2$ ,  $S = 0.5$ ,  $\xi_1 = 0.01$ ,  $\xi_2 = 0.01$ ,  $\xi_3 = 0.01$ ,  $Nt = 1.5$ ,  $\gamma_1 = 0.1$ ,  $Nb = 1.5$ ,  $Sc = 0.5$ ,  $Pr = 1.5$ ,  $Br = 2.0$ ,  $L = 0.5$ ,  $\zeta = 0.5$ .

Fig. 9.32.  $Ns$  via change in  $L$  when  $E_1 = 0.02$ ,  $E_2 = 0.01$ ,  $E_3 = 0.01$ ,  $t = 0.1$ ,  $x = 0.2$ ,  $\varepsilon = 0.2$ ,  $S = 0.5$ ,  $\xi_1 = 0.01$ ,  $\xi_2 = 0.01$ ,  $\xi_3 = 0.01$ ,  $Nt = 1.5$ ,  $\gamma_1 = 0.1$ ,  $Nb = 1.5$ ,  $Sc = 0.5$ ,  $Pr = 1.5$ ,  $Br = 2.0$ ,  $\Lambda = 0.5$ ,  $\zeta = 0.5$ .

### 9.3.5 Heat transfer coefficient

Graphs for heat transfer coefficient are displayed here for some influential parameters of our study. These graphs are plotted for the shear thinning, viscous and shear thickening cases. It can be seen that these graphs show oscillatory behavior which is due to peristaltic phenomenon. Fig. 9.32 is arranged to see effect of chemical reaction. An increase is noticed here. Result for  $Br$  on  $Z$  can be viewed from Fig. 9.33. Enhancement is observed. Fig. 9.34 displays the increasing trend of  $Z$  for heat source. In all cases it can be clearly noticed that shear thinning fluids have higher values for heat transfer coefficient than viscous and shear thickening materials.

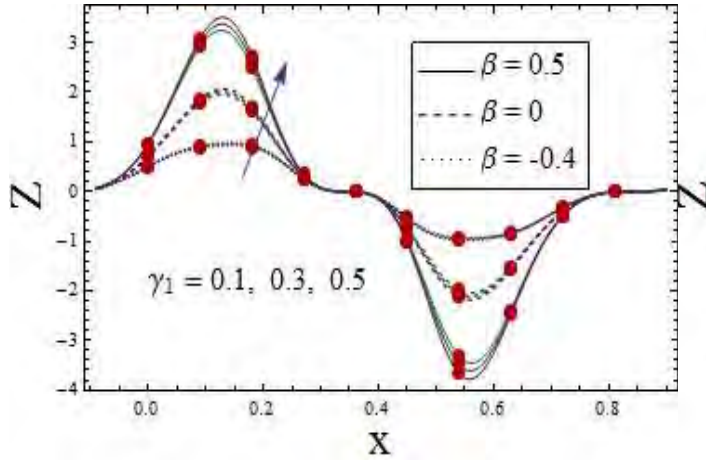


Fig. 9.33

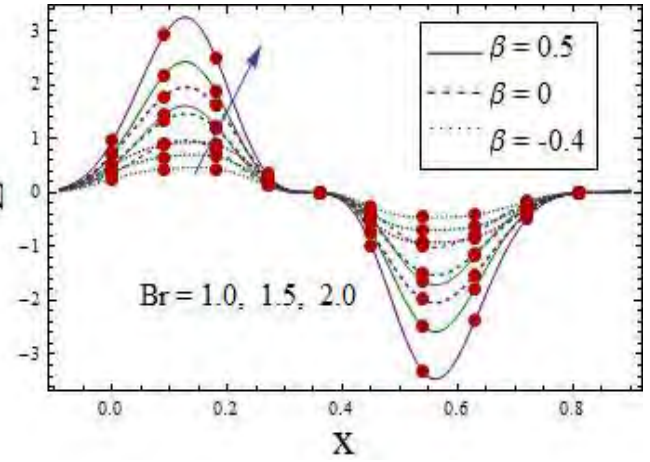


Fig. 9.34

Fig. 9.33.  $Z$  via change in  $\gamma_1$  when  $E_1 = 0.02$ ,  $E_2 = 0.01$ ,  $E_3 = 0.01$ ,  $t = 0.1$ ,  $\varepsilon = 0.2$ ,  $S = 0.5$ ,  $\xi_1 = 0.01$ ,  $\xi_2 = 0.01$ ,  $\xi_3 = 0.01$ ,  $Nt = 1.5$ ,  $Nb = 1.5$ ,  $Sc = 0.5$ ,  $Pr = 1.5$ ,  $Br = 2.0$ .

Fig. 9.34.  $Z$  via change in  $Br$  when  $E_1 = 0.02$ ,  $E_2 = 0.01$ ,  $E_3 = 0.01$ ,  $t = 0.1$ ,  $\varepsilon = 0.2$ ,  $S = 0.5$ ,  $\xi_1 = 0.01$ ,  $\xi_2 = 0.01$ ,  $\xi_3 = 0.01$ ,  $Nt = 1.5$ ,  $\gamma_1 = 0.1$ ,  $Nb = 1.5$ ,  $Sc = 0.5$ ,  $Pr = 1.5$ .

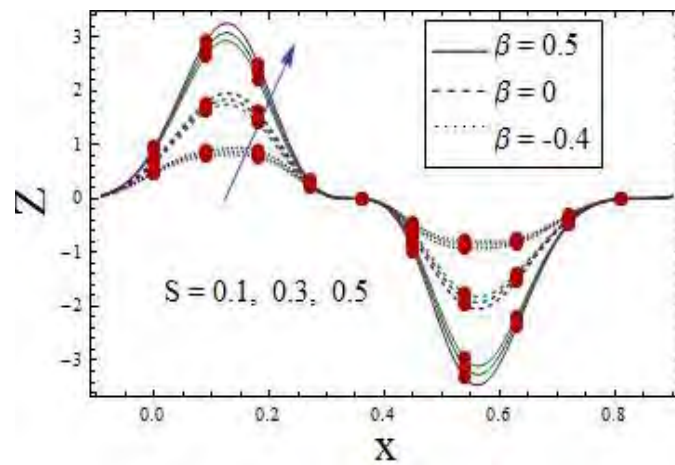


Fig. 9.35

Fig. 9.35.  $Z$  via change in  $S$  when  $E_1 = 0.02$ ,  $E_2 = 0.01$ ,  $E_3 = 0.01$ ,  $t = 0.1$ ,  $\varepsilon = 0.2$ ,  $\xi_1 = 0.01$ ,  $\xi_2 = 0.01$ ,  $\xi_3 = 0.01$ ,  $Nt = 1.5$ ,  $\gamma_1 = 0.1$ ,  $Nb = 1.5$ ,  $Sc = 0.5$ ,  $Pr = 1.5$ ,  $Br = 2.0$ .

## 9.4 Conclusions

Major findings are listed below.

- Velocity and thermal slip parameters lead to an increase in velocity and temperature.
- Velocity for shear thinning material is higher when compared with viscous and shear thickening fluids.
- Heat source parameter caused an increase in temperature and entropy.
- Temperature and entropy for shear thinning fluids are higher than viscous and shear thickening materials.
- Heat transfer coefficient enhances for chemical reaction parameter.
- Concentration for shear thickening fluids is higher than viscous and shear thinning materials.



## Chapter 10

# Entropy analysis in peristalsis with homogeneous-heterogeneous reaction

### 10.1 Introduction

Homogeneous-heterogeneous reactions in peristalsis of Prandtl fluid are examined. Magnetic field is applied in the perpendicular direction to the flow. Joule heating effect is also considered in this analysis. Buongiorno nanofluid model has been used which incorporates two prominent slip mechanisms i.e. Brownian motion and thermophoresis. Second law of thermodynamics has been utilized for entropy generation analysis. No slip boundary conditions are employed for the considered analysis. NDSolve command of Mathematica 9.0 is employed for the solution of problem. Graphs for pertinent parameters are plotted and analyzed. These graphs contain velocity, temperature, homogeneous-heterogeneous reaction, entropy and heat transfer coefficient. Key points are summarized in the conclusion.

### 10.2 Problem formulation

MHD peristaltic flow of the incompressible Prandtl nanofluid is considered. Peristaltic wave travel along the flexible walls of channel. Wall's temperature are maintained at  $T_1$  and  $T_0$  and concentration  $C_1$  and  $C_0$  respectively (see Fig. 10.1). Homogeneous- heterogeneous reaction is considered for the considered problem. Nanofluid slip mechanisms, Brownian motion and ther-

mophoresis are considered. Joule heating and viscous dissipation are also accounted. Peristaltic wave shape is

$$y = \pm\eta(x, t) = \pm \left[ d + a \sin \frac{2\pi}{\lambda} (x - ct) \right]. \quad (10.1)$$

Here wall shape is denoted by  $\pm\eta$  with  $d$ ,  $a$ ,  $t$  and  $c$  denote the half channel width, wave amplitude, time and wave speed.

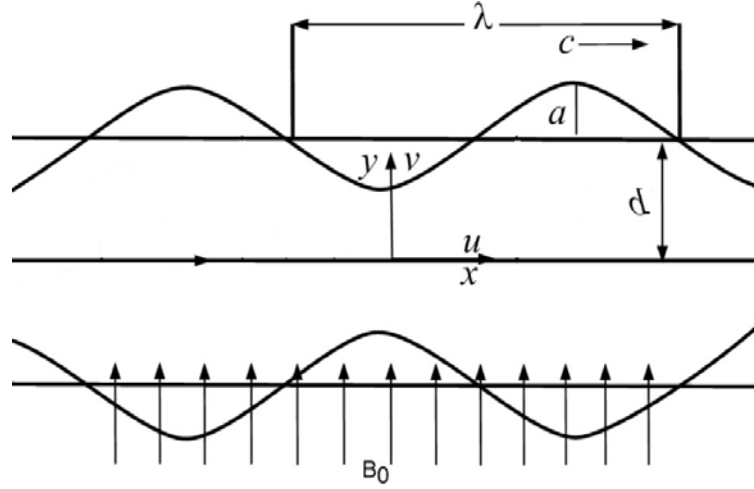
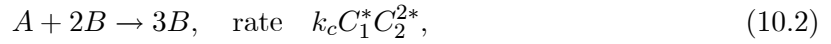
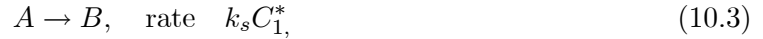


Fig. 10.1: Flow configuration

The model equations for homogeneous-heterogeneous equations are



in which  $k_c$  and  $k_s$  elucidate the rate constants. We consider the single first order isothermal reaction. On the surface of catalyst we have



where  $C_1^*$ ,  $C_2^*$  are the respective concentration of the species  $A$  and  $B$ . Flow expressions are

$$\frac{\partial u}{\partial x} + \frac{\partial v}{\partial y} = 0, \quad (10.4)$$

$$\frac{\partial u}{\partial t} + u \frac{\partial u}{\partial x} + v \frac{\partial u}{\partial y} = -\frac{1}{\rho_f} \frac{\partial p}{\partial x} + \frac{1}{\rho_f} \frac{\partial S_{xx}}{\partial x} + \frac{1}{\rho_f} \frac{\partial S_{xy}}{\partial y} - \frac{1}{\rho_f} \sigma B_0^2 u, \quad (10.5)$$

$$\frac{\partial v}{\partial t} + u \frac{\partial v}{\partial x} + v \frac{\partial v}{\partial y} = -\frac{1}{\rho_f} \frac{\partial p}{\partial y} + \frac{1}{\rho_f} \frac{\partial S_{xy}}{\partial x} + \frac{1}{\rho_f} \frac{\partial S_{yy}}{\partial y}, \quad (10.6)$$

$$\begin{aligned} \frac{\partial T}{\partial t} + u \frac{\partial T}{\partial x} + v \frac{\partial T}{\partial y} &= \alpha^* \left[ \frac{\partial^2 T}{\partial x^2} + \frac{\partial^2 T}{\partial y^2} \right] + \frac{1}{(\rho C_p)_f} \left[ S_{xx} \frac{\partial u}{\partial x} + S_{xy} \left( \frac{\partial u}{\partial y} + \frac{\partial v}{\partial x} \right) + S_{yy} \frac{\partial v}{\partial y} \right] \\ &+ \tau \left[ D_B \left( \frac{\partial C_1^*}{\partial x} \frac{\partial T}{\partial x} + \frac{\partial C_1^*}{\partial y} \frac{\partial T}{\partial y} + \frac{\partial C_2^*}{\partial x} \frac{\partial T}{\partial x} + \frac{\partial C_2^*}{\partial y} \frac{\partial T}{\partial y} \right) + \right. \\ &\quad \left. \frac{D_T}{T_m} \left( \left( \frac{\partial T}{\partial x} \right)^2 + \left( \frac{\partial T}{\partial y} \right)^2 \right) \right] \\ &+ \frac{1}{(\rho C_p)_f} \sigma B_0^2 u^2, \end{aligned} \quad (10.7)$$

$$\frac{\partial C_1^*}{\partial t} + u \frac{\partial C_1^*}{\partial x} + v \frac{\partial C_1^*}{\partial y} = \dot{D}_A \left( \frac{\partial^2 C_1^*}{\partial x^2} + \frac{\partial^2 C_1^*}{\partial y^2} \right) - k_c C_1^* C_2^{2*} + \frac{D_T}{T_m} \left[ \frac{\partial^2 T}{\partial x^2} + \frac{\partial^2 T}{\partial y^2} \right], \quad (10.8)$$

$$\frac{\partial C_2^*}{\partial t} + u \frac{\partial C_2^*}{\partial x} + v \frac{\partial C_2^*}{\partial y} = \dot{D}_B \left( \frac{\partial^2 C_2^*}{\partial x^2} + \frac{\partial^2 C_2^*}{\partial y^2} \right) + k_c C_1^* C_2^{2*} + \frac{D_T}{T_m} \left[ \frac{\partial^2 T}{\partial x^2} + \frac{\partial^2 T}{\partial y^2} \right]. \quad (10.9)$$

Here  $u$ ,  $v$ ,  $T$  describe respective velocity components and temperature.  $p$  the pressure,  $\rho_f$  density,  $S_{xx}$ ,  $S_{xy}$ ,  $S_{yy}$  the stress components of the considered Prandtl fluid.  $\alpha^*$  the thermal diffusivity,  $\tau (= (\rho C_p)_p / (\rho C_p)_f)$  the ratio of specific heat capacity of nanoparticles and base fluid,  $D_B$  the Brownian motion and  $D_T$  the thermophoretic diffusion coefficients,  $T_m$  the mean temperature of the fluid, and  $\dot{D}_A$  and  $\dot{D}_B$  the diffusion species coefficients for the species  $A$  and  $B$  respectively.

Prandtl fluid can be expressed by the following relation:

$$\boldsymbol{\tau} = -p\mathbf{I} + \mathbf{S}, \quad (10.10)$$

where the component  $S_{xy}$  is given by

$$S_{xy} = \frac{A^* \arcsin \left( \frac{1}{C^*} \left[ \left( \frac{\partial u}{\partial y} \right)^2 + \left( \frac{\partial v}{\partial x} \right)^2 \right]^{\frac{1}{2}} \right)}{\left[ \left( \frac{\partial u}{\partial y} \right)^2 + \left( \frac{\partial v}{\partial x} \right)^2 \right]^{\frac{1}{2}}} \frac{\partial u}{\partial y}, \quad (10.11)$$

With the boundary conditions

$$u = 0 \quad \text{at } y = \pm\eta, \quad (10.12)$$

$$T = \begin{Bmatrix} T_1 \\ T_0 \end{Bmatrix} \quad \text{at } y = \pm\eta, \quad (10.13)$$

$$\dot{D}_A \frac{\partial C_1^*}{\partial y} - k_s C_1^* = 0 \quad \text{at } y = \eta, \quad C_1^* \rightarrow C_0 \quad \text{at } y = -\eta, \quad (10.14)$$

$$\dot{D}_B \frac{\partial C_2^*}{\partial y} + k_s C_2^* = 0 \quad \text{at } y = \eta, \quad C_2^* \rightarrow 0 \quad \text{at } y = -\eta, \quad (10.15)$$

The equation mentioned below describe the decomposition of applied pressure in terms of compliant walls characteristics.

$$\left[ -\tau^* \frac{\partial^3}{\partial x^3} + m^* \frac{\partial^3}{\partial x \partial t^2} + d_1^* \frac{\partial^2}{\partial t \partial x} \right] \eta = \frac{\partial S_{xy}}{\partial y} + \frac{\partial S_{xx}}{\partial x} - \rho_f \left[ \frac{\partial u}{\partial t} + u \frac{\partial u}{\partial x} + v \frac{\partial u}{\partial y} \right] - \sigma B_0^2 u, \quad \text{at } y = \pm\eta, \quad (10.16)$$

Non-dimensional parameters are

$$\begin{aligned} x^* &= \frac{x}{\lambda}, & y^* &= \frac{y}{d}, & u^* &= \frac{u}{c}, & v^* &= \frac{v}{c}, & t^* &= \frac{ct}{\lambda}, \\ \eta^* &= \frac{\eta}{d}, & \theta &= \frac{T - T_0}{T_1 - T_0}, & S_{ij}^* &= \frac{dS_{ij}}{c\mu}, & f &= \frac{C_1^*}{C_0}, \\ h &= \frac{C_2^*}{C_0}, & p^* &= \frac{d^2 p}{c\lambda\mu}, & u &= \frac{\partial \psi}{\partial y}, & v &= -\delta \frac{\partial \psi}{\partial x}. \end{aligned} \quad (10.17)$$

After utilizing non-dimensional parameters, we obtained the following systems

$$\text{Re} \left[ \delta \frac{\partial^2 \psi}{\partial t \partial y} + \delta \frac{\partial \psi}{\partial y} \frac{\partial^2 \psi}{\partial x \partial y} - \delta \frac{\partial \psi}{\partial x} \frac{\partial^2 \psi}{\partial y^2} \right] = -\frac{\partial p}{\partial x} + \delta \frac{\partial S_{xx}}{\partial x} + \frac{\partial S_{xy}}{\partial y} - M^2 \frac{\partial \psi}{\partial y}, \quad (10.18)$$

$$\text{Re} \delta \left[ -\delta^2 \frac{\partial^2 \psi}{\partial t \partial x} - \delta^2 \frac{\partial \psi}{\partial y} \frac{\partial^2 \psi}{\partial x^2} + \delta^2 \frac{\partial \psi}{\partial x} \frac{\partial^2 \psi}{\partial x \partial y} \right] = -\frac{\partial p}{\partial y} + \delta^2 \frac{\partial S_{xy}}{\partial x} + \delta \frac{\partial S_{yy}}{\partial y}, \quad (10.19)$$

$$\begin{aligned}
\text{Re Pr} \left[ \delta \frac{\partial \theta}{\partial t} + \delta \frac{\partial \psi}{\partial y} \frac{\partial \theta}{\partial x} - \delta \frac{\partial \psi}{\partial x} \frac{\partial \theta}{\partial y} \right] &= \left[ \delta^2 \frac{\partial^2 \theta}{\partial x^2} + \frac{\partial^2 \theta}{\partial y^2} \right] \\
&+ Br \left[ \delta S_{xx} \frac{\partial^2 \psi}{\partial x \partial y} + S_{xy} \left( \frac{\partial^2 \psi}{\partial y^2} - \delta^2 \frac{\partial^2 \psi}{\partial x^2} \right) - \delta S_{yy} \frac{\partial^2 \psi}{\partial x \partial y} \right] \\
&+ Nb \text{Pr} \left( \delta^2 \frac{\partial f}{\partial x} \frac{\partial \theta}{\partial x} + \frac{\partial f}{\partial y} \frac{\partial \theta}{\partial y} + \delta^2 \frac{\partial h}{\partial x} \frac{\partial \theta}{\partial x} + \frac{\partial h}{\partial y} \frac{\partial \theta}{\partial y} \right) \\
&+ Nt \text{Pr} \left( \delta^2 \left( \frac{\partial \theta}{\partial x} \right)^2 + \left( \frac{\partial \theta}{\partial y} \right)^2 \right) + M^2 Br \left( \frac{\partial \psi}{\partial y} \right)^2 \quad (10.20)
\end{aligned}$$

$$\text{Re} \left[ \delta \frac{\partial f}{\partial t} + \delta \frac{\partial \psi}{\partial y} \frac{\partial f}{\partial x} - \delta \frac{\partial \psi}{\partial x} \frac{\partial f}{\partial y} \right] = \frac{1}{Sc_A} \left[ \delta^2 \frac{\partial^2 f}{\partial x^2} + \frac{\partial^2 f}{\partial y^2} \right] - Kfh^2 + \frac{1}{Sc Nb} \left[ \delta^2 \frac{\partial^2 \theta}{\partial x^2} + \frac{\partial^2 \theta}{\partial y^2} \right], \quad (10.21)$$

$$\text{Re} \left[ \delta \frac{\partial h}{\partial t} + \delta \frac{\partial \psi}{\partial y} \frac{\partial h}{\partial x} - \delta \frac{\partial \psi}{\partial x} \frac{\partial h}{\partial y} \right] = \frac{\xi^*}{Sc_A} \left[ \delta^2 \frac{\partial^2 h}{\partial x^2} + \frac{\partial^2 h}{\partial y^2} \right] + Kfh^2 + \frac{1}{Sc Nb} \left[ \delta^2 \frac{\partial^2 \theta}{\partial x^2} + \frac{\partial^2 \theta}{\partial y^2} \right], \quad (10.22)$$

$$S_{xy} = \alpha_1 \frac{\partial^2 \psi}{\partial y^2} + \frac{\beta}{6} \left[ \left( \frac{\partial^2 \psi}{\partial y^2} \right)^2 + \delta^4 \left( \frac{\partial^2 \psi}{\partial x^2} \right)^2 \right] \left( \frac{\partial^2 \psi}{\partial y^2} \right), \quad (10.23)$$

$$\frac{\partial \psi}{\partial y} = 0, \quad \text{at } y = \pm \eta = \pm(1 + \varepsilon \sin 2\pi(x - t)), \quad (10.24)$$

$$\begin{aligned}
\left[ E_1 \frac{\partial^3}{\partial x^3} + E_2 \frac{\partial^3}{\partial x \partial t^2} + E_3 \frac{\partial^2}{\partial t \partial x} \right] \eta &= -\text{Re} \left[ \delta \frac{\partial^2 \psi}{\partial t \partial y} + \delta \frac{\partial \psi}{\partial y} \frac{\partial^2 \psi}{\partial x \partial y} - \delta \frac{\partial \psi}{\partial x} \frac{\partial^2 \psi}{\partial y^2} \right] + \\
&\delta \frac{\partial S_{xx}}{\partial x} + \frac{\partial S_{xy}}{\partial y} - M^2 \frac{\partial \psi}{\partial y}, \quad \text{at } y = \pm \eta, \quad (10.25)
\end{aligned}$$

$$\theta = \left\{ \begin{array}{c} 1 \\ 0 \end{array} \right\} \quad \text{at } y = \pm \eta, \quad (10.26)$$

$$\frac{\partial f}{\partial y} - Hf = 0 \quad \text{at } y = \eta, \quad f = 1 \quad \text{at } y = -\eta, \quad (10.27)$$

$$\xi^* \frac{\partial h}{\partial y} + Hh = 0 \quad \text{at } y = \eta, \quad h = 0 \quad \text{at } y = -\eta, \quad (10.28)$$

with

$$\begin{aligned}
\text{Re} &= \frac{\rho_f c d}{\mu}, \quad \delta = \frac{d}{\lambda}, \quad M = \sqrt{\frac{\sigma}{\mu}} B_0 d, \quad \varepsilon = \frac{a}{d}, \\
Nt &= \frac{\tau \rho_f D_T (T_1 - T_0)}{\mu T_m}, \quad Nb = \frac{\tau \rho_f D_B C_0}{\mu}, \quad Sc = \frac{\mu}{\rho_f D_B}, \\
\text{Pr} &= \frac{\mu (C_p)_f}{\kappa}, \quad Br = \frac{c^2 \mu}{\kappa (T_1 - T_0)}, \quad \alpha_1 = \frac{A^*}{C^* \mu}, \\
\beta &= \frac{\alpha_1 c^2}{C^{*2} d^2}, \quad Sc_A = \frac{\mu}{\rho_f \dot{D}_A}, \quad H = \frac{k_s d}{\dot{D}_A}, \quad K = \frac{\rho k_c C_0^2 d^2}{\mu}, \\
E_1 &= -\frac{\tau^* d^3}{\lambda^3 c \mu}, \quad E_2 = \frac{m^* c d^3}{\lambda^3 \mu}, \quad E_3 = \frac{d_1^* d^3}{\lambda^2 \mu}.
\end{aligned} \tag{10.29}$$

where  $\text{Re}$  depicts Reynolds number,  $\delta$  wave number,  $M$  Hartman number,  $\varepsilon$  amplitude ratio,  $Nt$  thermophoresis parameter,  $Nb$  Brownian motion parameter,  $Sc$  Schmidt number,  $\text{Pr}$  Prandtl number,  $Br$  Brinkman number,  $\alpha_1$  and  $\beta$  are fluid parameters for Prandtl fluid,  $Sc_A$  Diffusion Schmidt number,  $H$  and  $K$  measures the strength of respective heterogeneous and homogeneous reactions and  $E_1, E_2, E_3$  the compliant walls coefficients. Here we have omitted the asterisks for simplicity.

After employing the theory of long wavelength and low Reynolds number assumptions we obtain

$$\frac{\partial p}{\partial x} = \frac{\partial S_{xy}}{\partial y} - M^2 \frac{\partial \psi}{\partial y}, \tag{10.30}$$

$$\frac{\partial p}{\partial y} = 0, \tag{10.31}$$

$$\begin{aligned}
&\frac{\partial^2 \theta}{\partial y^2} + Br \left[ S_{xy} \frac{\partial^2 \psi}{\partial y^2} \right] + Nb \text{Pr} \left( \frac{\partial f}{\partial y} \frac{\partial \theta}{\partial y} + \frac{\partial h}{\partial y} \frac{\partial \theta}{\partial y} \right) \\
&+ Nt \text{Pr} \left( \frac{\partial \theta}{\partial y} \right)^2 + M^2 Br \left( \frac{\partial \psi}{\partial y} \right)^2 = 0,
\end{aligned} \tag{10.32}$$

$$\frac{1}{Sc_A} \frac{\partial^2 f}{\partial y^2} - K f h^2 + \frac{1}{Sc Nb} \frac{Nt}{\partial y^2} \frac{\partial^2 \theta}{\partial y^2} = 0, \tag{10.33}$$

$$\frac{\xi^*}{Sc_A} \frac{\partial^2 h}{\partial y^2} + K f h^2 + \frac{1}{Sc Nb} \frac{Nt}{\partial y^2} \frac{\partial^2 \theta}{\partial y^2} = 0, \tag{10.34}$$

$$S_{xy} = \alpha_1 \frac{\partial^2 \psi}{\partial y^2} + \frac{\beta}{6} \left( \frac{\partial^2 \psi}{\partial y^2} \right)^3, \quad (10.35)$$

$$\frac{\partial \psi}{\partial y} = 0, \quad \text{at } y = \pm \eta = \pm(1 + \varepsilon \sin 2\pi(x - t)), \quad (10.36)$$

$$\left[ E_1 \frac{\partial^3}{\partial x^3} + E_2 \frac{\partial^3}{\partial x \partial t^2} + E_3 \frac{\partial^2}{\partial t \partial x} \right] \eta = \frac{\partial S_{xy}}{\partial y} - M^2 \frac{\partial \psi}{\partial y}, \quad \text{at } y = \pm \eta, \quad (10.37)$$

$$\theta = \left\{ \begin{array}{c} 1 \\ 0 \end{array} \right\} \quad \text{at } y = \pm \eta, \quad (10.38)$$

$$\frac{\partial f}{\partial y} - Hf = 0 \quad \text{at } y = \eta, \quad f = 1 \quad \text{at } y = -\eta, \quad (10.39)$$

$$\xi^* \frac{\partial h}{\partial y} + Hh = 0 \quad \text{at } y = \eta, \quad h = 0 \quad \text{at } y = -\eta. \quad (10.40)$$

In general the diffusion coefficient of the chemical species  $A$  and  $B$  are of comparable size. For application point of view this leads to the assumption that they are equal i.e.  $\dot{D}_A = \dot{D}_B$  and hence  $\xi^* = \frac{\dot{D}_B}{\dot{D}_A} = 1$ , and we have the relation  $f + h = 1$ . After utilizing this relation, We solved these equations via NDSolve of Mathematica.

### 10.2.1 Entropy generation

Entropy expression obeys

$$\begin{aligned} S_{gen}''' &= \frac{\kappa}{T_m^2} \left( \left( \frac{\partial T}{\partial x} \right)^2 + \left( \frac{\partial T}{\partial y} \right)^2 \right) + \frac{\sigma B_0^2 u^2}{T_m} + \frac{\Phi}{T_m} \\ &+ \frac{R\dot{D}_A}{C_m} \left( \left( \frac{\partial C_1^*}{\partial x} \right)^2 + \left( \frac{\partial C_1^*}{\partial y} \right)^2 \right) + \frac{R\dot{D}_A}{T_m} \left( \frac{\partial C_1^*}{\partial x} \frac{\partial T}{\partial x} + \frac{\partial C_1^*}{\partial y} \frac{\partial T}{\partial y} \right) + \\ &+ \frac{R\dot{D}_B}{C_m} \left( \left( \frac{\partial C_2^*}{\partial x} \right)^2 + \left( \frac{\partial C_2^*}{\partial y} \right)^2 \right) + \frac{R\dot{D}_B}{T_m} \left( \frac{\partial C_2^*}{\partial x} \frac{\partial T}{\partial x} + \frac{\partial C_2^*}{\partial y} \frac{\partial T}{\partial y} \right), \end{aligned} \quad (10.41)$$

where  $\Phi$  is given by

$$\Phi = S_{xx} \frac{\partial u}{\partial x} + S_{yy} \frac{\partial v}{\partial y} + S_{xy} \left( \frac{\partial u}{\partial y} + \frac{\partial v}{\partial x} \right). \quad (10.42)$$

Dimensionless form satisfies

$$\begin{aligned}
N_s = \frac{S_{gen}'''}{S_G'''} &= \left(\frac{\partial\theta}{\partial y}\right)^2 + \frac{BrM^2}{\Lambda} \left(\frac{\partial\psi}{\partial y}\right)^2 + \frac{Br}{\Lambda} S_{xy} \left(\frac{\partial^2\psi}{\partial y^2}\right) \\
&+ \frac{L_1}{\Lambda} \left(\frac{\partial\theta}{\partial y}\right) \left(\frac{\partial f}{\partial y}\right) + \frac{L_1\zeta}{\Lambda^2} \left(\frac{\partial f}{\partial y}\right)^2 + \\
&+ \frac{L_2}{\Lambda} \left(\frac{\partial\theta}{\partial y}\right) \left(\frac{\partial h}{\partial y}\right) + \frac{L_2\zeta}{\Lambda^2} \left(\frac{\partial h}{\partial y}\right)^2, \tag{10.43}
\end{aligned}$$

$$S_G''' = \frac{\kappa(T_1 - T_0)^2}{T_m^2 d^2}, \quad \Lambda = \frac{T_1 - T_0}{T_m}, \quad L_1 = \frac{RD_A C_0}{\kappa}, \quad L_2 = \frac{RD_B C_0}{\kappa}, \quad \zeta = \frac{C_0}{C_m}. \tag{10.44}$$

### 10.3 Analysis

Here we adopted the technique (NDSolve command of Mathematica) which gave the convergent solution in less computation time. Moreover this technique avoids the lengthy complicated expressions. Graphs are plotted directly for the physical analysis. These graphs include velocity, temperature, entropy and heat transfer coefficient. Figs. 10.2 and 10.3 displayed the results for fluid parameter on velocity. Decay in both cases is observed. Same results can be seen via studies [84, 85]. Magnetic field effect (utilized in ECG for synchronization purposes) can be observed via Fig. 10.4. As Lorentz force caused resistance in fluid flow. So decrease in fluid velocity has been observed. Fig. 10.5 manifested the effect of wall parameters. Decrease is noticed via damping nature of walls whereas an increase in velocity is observed for elastance characteristics of walls. These results have quite resemblance with the flow in blood vessels where the elastance nature enhances the blood velocity and damping nature reduced the blood velocity.



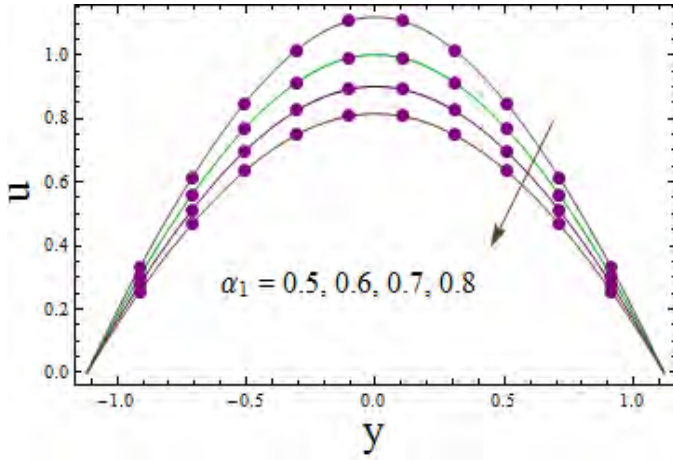


Fig. 10.2

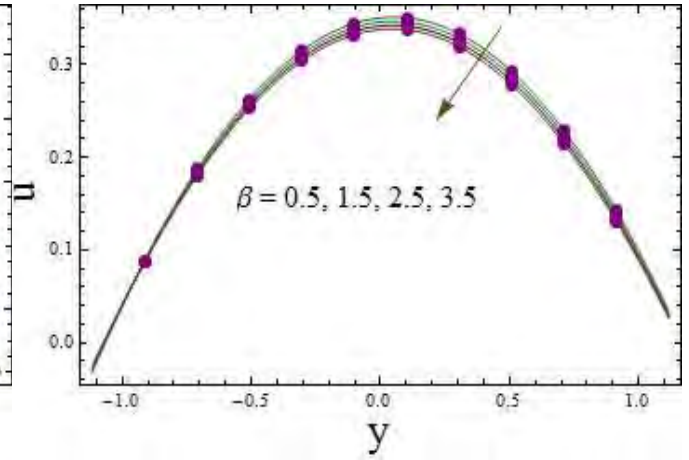


Fig. 10.3

Fig. 10.2.  $u$  for  $\alpha_1$  when  $E_1 = 0.02$ ,  $E_2 = 0.01$ ,  $E_3 = 0.01$ ,  $t = 0.1$ ,  $x = 0.2$ ,  $\varepsilon = 0.2$ ,  $\beta = 0.5$ ,  $M = 0.1$ ,  $H = 0.5$ ,  $K = 0.5$ ,  $Sc = Sc_A = 0.5$ ,  $Nt = 0.1$ ,  $Nb = 0.1$ ,  $Pr = 1.5$ ,  $Br = 2.0$ .

Fig. 10.3.  $u$  for  $\beta$  when  $E_1 = 0.02$ ,  $E_2 = 0.01$ ,  $E_3 = 0.01$ ,  $t = 0.1$ ,  $x = 0.2$ ,  $\varepsilon = 0.2$ ,  $\alpha_1 = 2.0$ ,  $M = 0.1$ ,  $H = 0.5$ ,  $K = 0.5$ ,  $Sc = Sc_A = 0.5$ ,  $Nt = 0.1$ ,  $Nb = 0.1$ ,  $Pr = 1.5$ ,  $Br = 2.0$ .

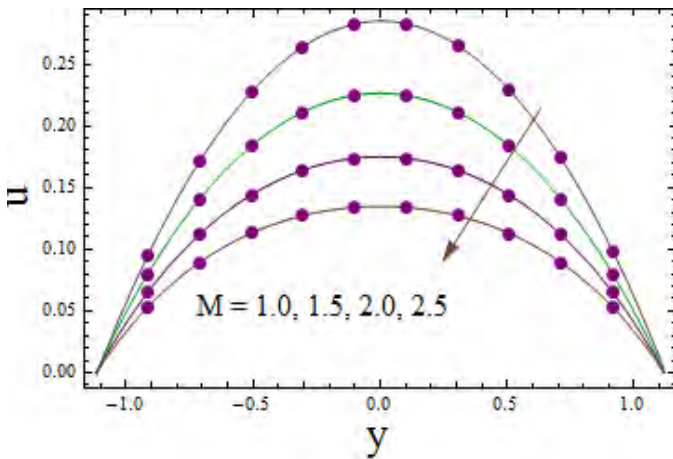


Fig. 10.4

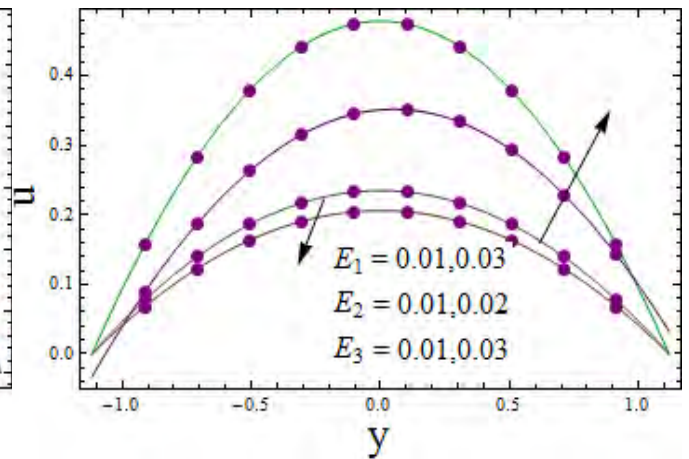


Fig. 10.5

Fig. 10.4.  $u$  for  $M$  when  $E_1 = 0.02$ ,  $E_2 = 0.01$ ,  $E_3 = 0.01$ ,  $t = 0.1$ ,  $x = 0.2$ ,  $\varepsilon = 0.2$ ,  $\alpha_1 = 2.0$ ,  $\beta = 0.5$ ,  $H = 0.5$ ,  $K = 0.5$ ,  $Sc = Sc_A = 0.5$ ,  $Nt = 0.1$ ,  $Nb = 0.1$ ,  $Pr = 1.5$ ,  $Br = 2.0$ .

Fig. 10.5.  $u$  for  $E_1$ ,  $E_2$  and  $E_3$  when  $t = 0.1$ ,  $x = 0.2$ ,  $\varepsilon = 0.2$ ,  $\alpha_1 = 2.0$ ,  $\beta = 0.5$ ,  $M = 0.1$ ,

$$H = 0.5, K = 0.5, Sc = Sc_A = 0.5, Nt = 0.1, Nb = 0.1, Pr = 1.5, Br = 2.0.$$

Temperature profile for effect of fluid parameters ( $\alpha, \beta$ ) can be viewed through Figs. 10.6 and 10.7. Decrease is noticed in these cases as can be seen through studies [84, 85]. As enhancement in mean kinetic energy of the particles leads to increase in temperature. Here higher values of fluid parameters slow down the fluid velocity so particles have less molecular vibrations and thus less temperature as well. Influence of Brinkman number on  $\theta$  is notified via Fig. 10.8. Note that resistance among fluid particle due to viscous effects produced heat. It results in enhancement of temperature of fluid. Fig. 10.9 elucidates the magnetic field influence on  $\theta$ . Applied magnetic field provide resistance to fluid which produce heating and caused an increase in temperature. Figs. 10.10 and 10.11 are manifested for the behaviors of  $Nb$  and  $Nt$  on temperature. Larger values for both parameters caused an increase in temperature of fluid.  $Nb$  is related to random motion of the particles. Larger values of it indicate more randomness and hence more heat loss which leads to increase in temperature. Fig. 10.12 displays the results for homogeneous reaction parameter on temperature. Decrease in seen in this case. As concentration decreases in this case so less concentrated fluid have less heat loss. Compliant wall characteristics are seen qualitatively similar with  $u$  (see Fig. 10.13). Compliant characteristics of walls are important as when wall are elastic it easily allows the exchange of water, oxygen and other nutrients.

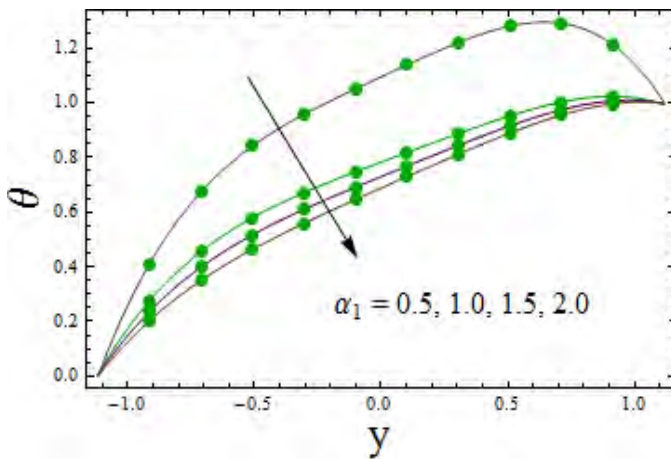


Fig. 10.6

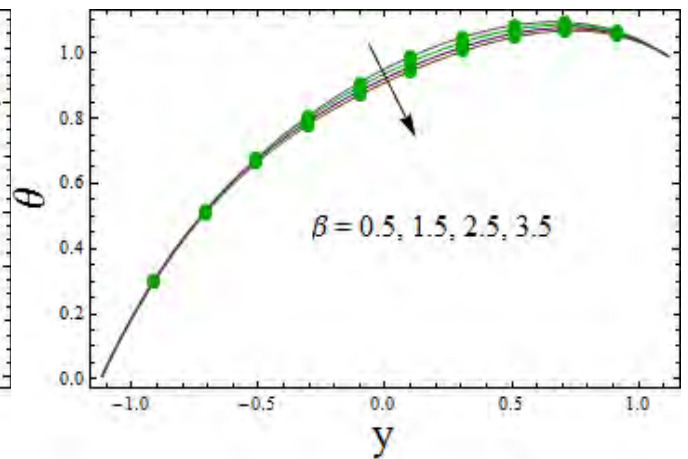


Fig. 10.7

Fig. 10.6.  $\theta$  for  $\alpha_1$  when  $E_1 = 0.02$ ,  $E_2 = 0.01$ ,  $E_3 = 0.01$ ,  $t = 0.1$ ,  $x = 0.2$ ,  $\varepsilon = 0.2$ ,  $\beta = 0.5$ ,

$M = 0.1$ ,  $H = 0.5$ ,  $K = 0.5$ ,  $Sc = Sc_A = 0.5$ ,  $Nt = 0.1$ ,  $Nb = 0.1$ ,  $Pr = 1.5$ ,  $Br = 2.0$ .

Fig. 10.7.  $\theta$  for  $\beta$  when  $E_1 = 0.02$ ,  $E_2 = 0.01$ ,  $E_3 = 0.01$ ,  $t = 0.1$ ,  $x = 0.2$ ,  $\varepsilon = 0.2$ ,  $\alpha_1 = 2.0$ ,

$M = 0.1$ ,  $H = 0.5$ ,  $K = 0.5$ ,  $Sc = Sc_A = 0.5$ ,  $Nt = 0.1$ ,  $Nb = 0.1$ ,  $Pr = 1.5$ ,  $Br = 2.0$ .

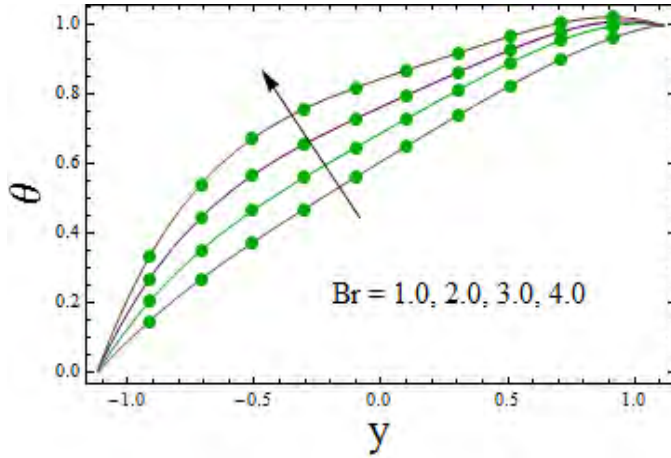


Fig. 10.8

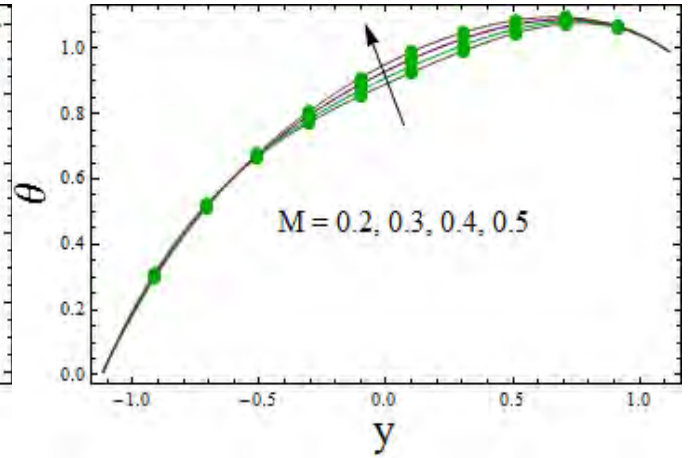


Fig. 10.9

Fig. 10.8.  $\theta$  for  $Br$  when  $E_1 = 0.02$ ,  $E_2 = 0.01$ ,  $E_3 = 0.01$ ,  $t = 0.1$ ,  $x = 0.2$ ,  $\varepsilon = 0.2$ ,  $\alpha_1 = 2.0$ ,

$\beta = 0.5$ ,  $M = 0.1$ ,  $H = 0.5$ ,  $K = 0.5$ ,  $Sc = Sc_A = 0.5$ ,  $Nt = 0.1$ ,  $Nb = 0.1$ ,  $Pr = 1.5$ .

Fig. 10.9.  $\theta$  for  $M$  when  $E_1 = 0.02$ ,  $E_2 = 0.01$ ,  $E_3 = 0.01$ ,  $t = 0.1$ ,  $x = 0.2$ ,  $\varepsilon = 0.2$ ,  $\alpha_1 = 2.0$ ,

$\beta = 0.5$ ,  $H = 0.5$ ,  $K = 0.5$ ,  $Sc = Sc_A = 0.5$ ,  $Nt = 0.1$ ,  $Nb = 0.1$ ,  $Pr = 1.5$ ,  $Br = 2.0$ .

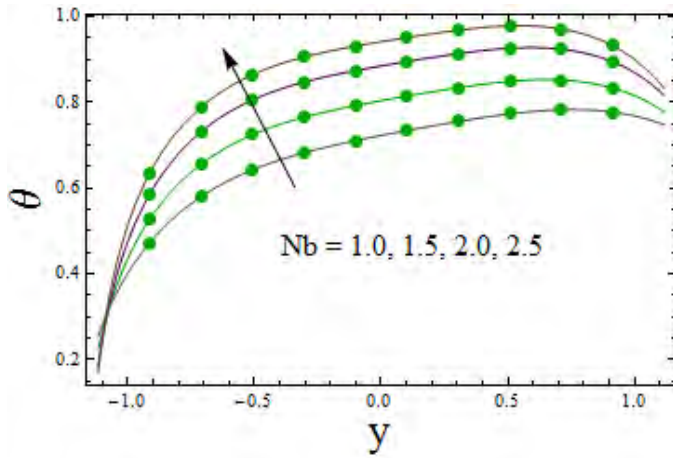


Fig. 10.10

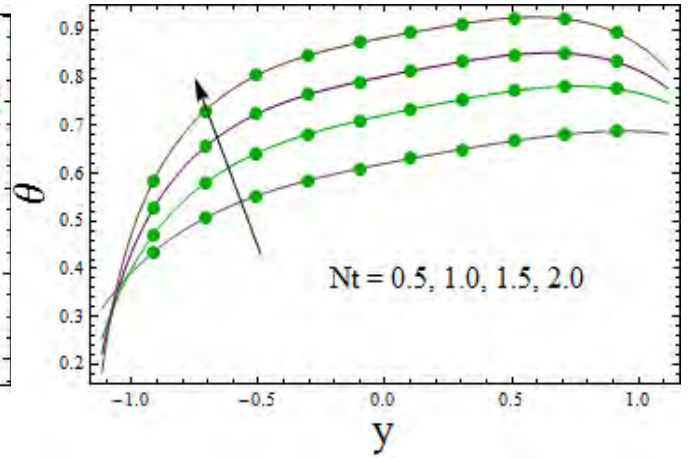


Fig. 10.11

Fig. 10.10.  $\theta$  for  $Nb$  when  $E_1 = 0.02$ ,  $E_2 = 0.01$ ,  $E_3 = 0.01$ ,  $t = 0.1$ ,  $x = 0.2$ ,  $\varepsilon = 0.2$ ,  $\alpha_1 = 2.0$ ,  $\beta = 0.5$ ,  $M = 0.1$ ,  $H = 0.5$ ,  $K = 0.5$ ,  $Sc = Sc_A = 0.5$ ,  $Nt = 0.1$ ,  $Pr = 1.5$ ,  $Br = 2.0$ .

Fig. 10.11.  $\theta$  for  $Nt$  when  $E_1 = 0.02$ ,  $E_2 = 0.01$ ,  $E_3 = 0.01$ ,  $t = 0.1$ ,  $x = 0.2$ ,  $\varepsilon = 0.2$ ,  $\alpha_1 = 2.0$ ,  $\beta = 0.5$ ,  $M = 0.1$ ,  $H = 0.5$ ,  $K = 0.5$ ,  $Sc = Sc_A = 0.5$ ,  $Nb = 0.1$ ,  $Pr = 1.5$ ,  $Br = 2.0$ .

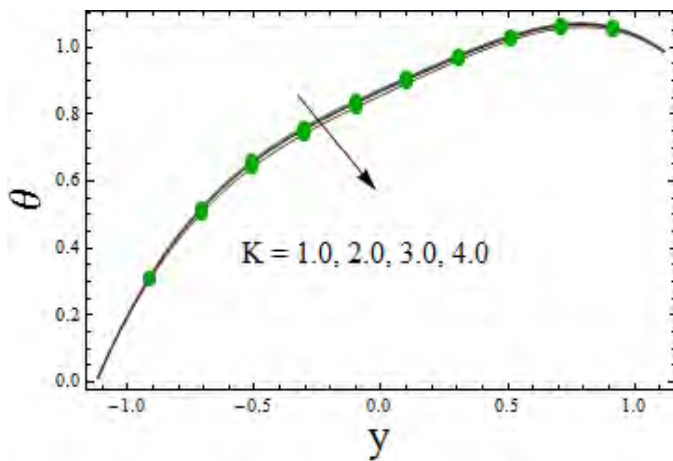


Fig. 10.12

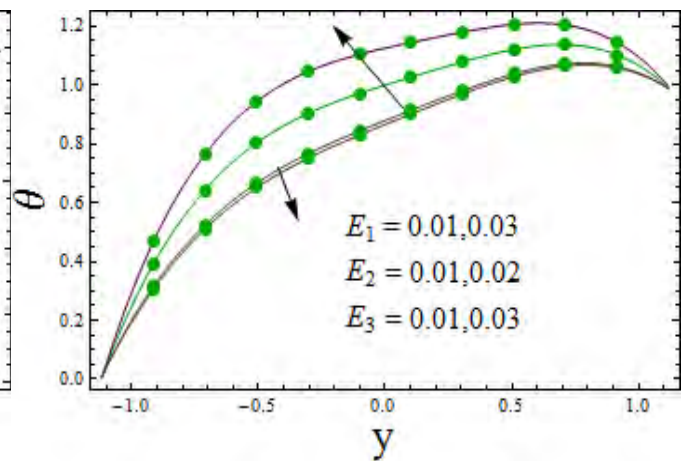


Fig. 10.13

Fig. 10.12.  $\theta$  for  $K$  when  $E_1 = 0.02$ ,  $E_2 = 0.01$ ,  $E_3 = 0.01$ ,  $t = 0.1$ ,  $x = 0.2$ ,  $\varepsilon = 0.2$ ,  $\alpha_1 = 2.0$ ,  $\beta = 0.5$ ,  $M = 0.1$ ,  $H = 0.5$ ,  $Nt = 0.1$ ,  $Sc = Sc_A = 0.5$ ,  $Nb = 0.1$ ,  $Pr = 1.5$ ,  $Br = 2.0$ .

Fig. 10.13.  $\theta$  for  $E_1$ ,  $E_2$ ,  $E_3$  when  $t = 0.1$ ,  $x = 0.2$ ,  $\varepsilon = 0.2$ ,  $\alpha_1 = 2.0$ ,  $\beta = 0.5$ ,  $M = 0.1$ ,

$$H = 0.5, K = 0.5, Sc = Sc_A = 0.5, Nt = 0.1, Nb = 0.1, Pr = 1.5, Br = 2.0.$$

Figs. 10.14 and 10.15 are plotted to observe the effect of heterogeneous and homogeneous reaction parameters on  $f$ . Decaying behavior of these parameters on concentration has been noticed. As increase in heterogeneous reaction parameter enhances the reaction rate which results in decrease of diffusion rate and hence concentration decreases whereas enhancement in homogeneous reaction parameter caused reduction in viscosity and hence in concentration. Fig. 10.16 is prepared for  $M$  (Hartman number) effect on concentration. Enhancement in concentration is seen here. Larger values of Schmidt number caused decay in concentration (see Fig. 10.17). As density of the fluid decreases. So less dense particles attained higher speed and it lessens the fluid concentration.

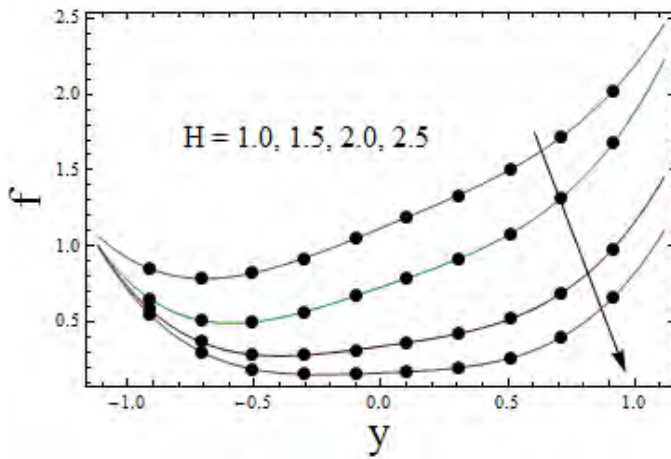


Fig. 10.14

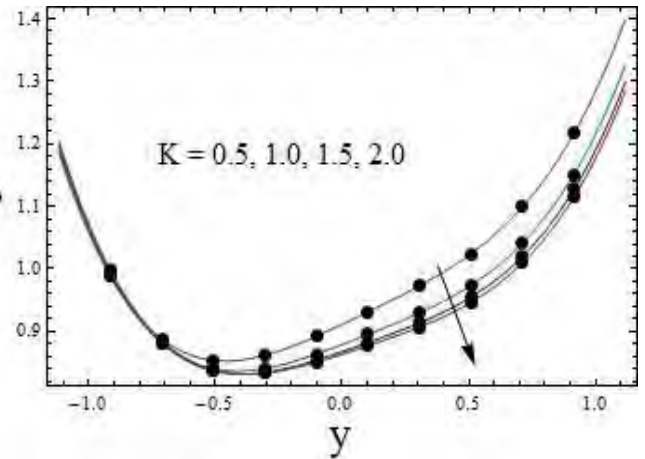


Fig. 10.15

Fig. 10.14.  $f$  for  $H$  when  $E_1 = 0.02, E_2 = 0.01, E_3 = 0.01, t = 0.1, x = 0.2, \varepsilon = 0.2, \alpha_1 = 2.0, \beta = 0.5, M = 0.1, K = 0.5, Sc = Sc_A = 0.5, Nt = 0.1, Nb = 0.1, Pr = 1.5, Br = 2.0$ .

Fig. 10.15.  $f$  for  $K$  when  $E_1 = 0.02, E_2 = 0.01, E_3 = 0.01, t = 0.1, x = 0.2, \varepsilon = 0.2, \alpha_1 = 2.0, \beta = 0.5, M = 0.1, H = 0.5, Sc = Sc_A = 0.5, Nt = 0.1, Nb = 0.1, Pr = 1.5, Br = 2.0$ .



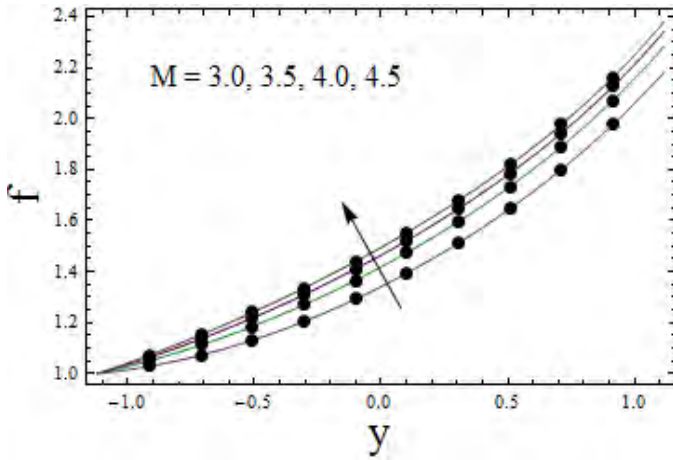


Fig. 10.16

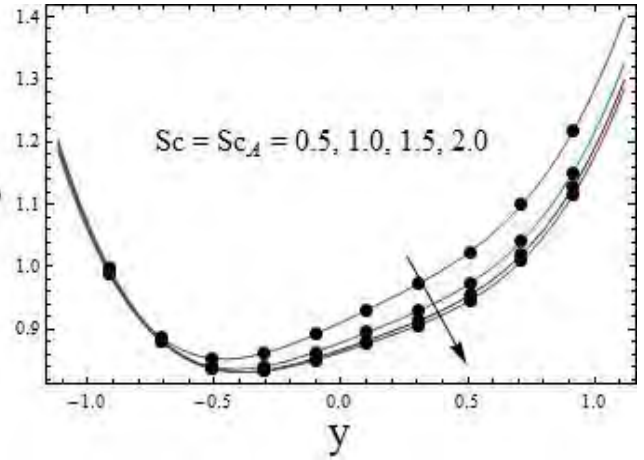


Fig. 10.17

Fig. 10.16.  $f$  for  $M$  when  $E_1 = 0.02$ ,  $E_2 = 0.01$ ,  $E_3 = 0.01$ ,  $t = 0.1$ ,  $x = 0.2$ ,  $\varepsilon = 0.2$ ,  $\alpha_1 = 2.0$ ,  $\beta = 0.5$ ,  $H = 0.5$ ,  $K = 0.5$ ,  $Sc = Sc_A = 0.5$ ,  $Nt = 0.1$ ,  $Nb = 0.1$ ,  $Pr = 1.5$ ,  $Br = 2.0$ .

Fig. 10.17.  $f$  for  $Sc$ ,  $Sc_A$  when  $E_1 = 0.02$ ,  $E_2 = 0.01$ ,  $E_3 = 0.01$ ,  $t = 0.1$ ,  $x = 0.2$ ,  $\varepsilon = 0.2$ ,  $\alpha_1 = 2.0$ ,  $\beta = 0.5$ ,  $M = 0.1$ ,  $H = 0.5$ ,  $K = 0.5$ ,  $Nt = 0.1$ ,  $Nb = 0.1$ ,  $Pr = 1.5$ ,  $Br = 2.0$ .

Entropy analysis for different embedded parameters has been carried out through Figs. 10.18–10.30. Hartman number impact can be observed via Fig. 10.18. As magnetic field provide resistance that produced heating so temperature enhances at the center of channel. Fig. 10.19 portrayed the results for  $Nb$  on  $Ns$ . Random motion of particles create more disorderedness hence entropy enhances for higher  $Nb$ . Similar behavior has been seen for  $Nt$  via Fig. 10.20. Entropy for Schmidt number is decreased (see Fig. 10.21). As less concentrated fluid has no more disorderedness. Fig. 10.22 demonstrated that increase in heterogeneous reaction caused enhancement in entropy generation.  $L_1$  and  $L_2$  results are displayed via Fig. 10.23. Enhancement is observed here. Fig. 10.24 is prepared for the study of Brinkman number impact on entropy. Obviously increase is noticed in this case. As increase in viscous dissipation produces more heating and thus increase in entropy. Opposite impacts for  $\zeta$  and  $\Lambda$  have been observed (see Figs. 10.25 and 10.26). Fluid parameters for Prandtl number results are illustrated via Figs. 10.27 and 10.28. Decrease is noticed like in the case of temperature. Entropy analysis for homogeneous reaction parameter can be observed through Fig. 10.29.

Decay is observed through reason directly linked to temperature. Compliant wall results are seen increasing for elastance coefficients whereas decreasing for damping coefficient (see Fig. 10.30).

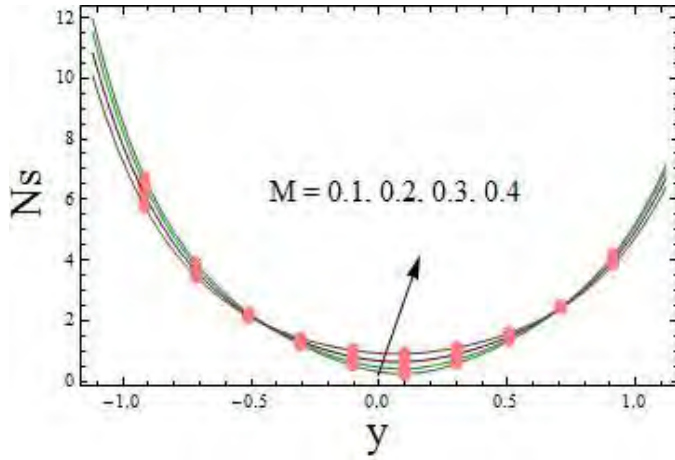


Fig. 10.18

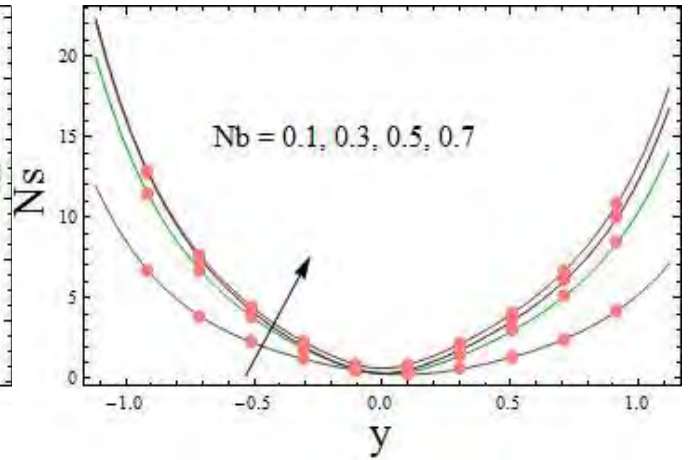


Fig. 10.19

*Fig. 10.18.*  $Ns$  for  $M$  when  $E_1 = 0.02$ ,  $E_2 = 0.01$ ,  $E_3 = 0.01$ ,  $t = 0.1$ ,  $x = 0.2$ ,  $\varepsilon = 0.2$ ,  
 $\alpha_1 = 0.2$ ,  $\beta = 0.5$ ,  $H = 0.5$ ,  $K = 0.5$ ,  $Sc = Sc_A = 0.1$ ,  $Nt = 0.1$ ,  $Nb = 0.1$ ,  $Pr = 1.5$ ,  
 $Br = 2.0$ ,  $\Lambda = 0.5$ ,  $\zeta = 0.5$ ,  $L_1 = L_2 = 0.5$ .

*Fig. 10.19.*  $Ns$  for  $Nb$  when  $E_1 = 0.02$ ,  $E_2 = 0.01$ ,  $E_3 = 0.01$ ,  $t = 0.1$ ,  $x = 0.2$ ,  $\varepsilon = 0.2$ ,  
 $\alpha_1 = 2.0$ ,  $\beta = 0.5$ ,  $M = 0.1$ ,  $H = 0.5$ ,  $K = 0.5$ ,  $Sc = Sc_A = 0.5$ ,  $Nt = 0.1$ ,  $Pr = 1.5$ ,  $Br = 2.0$ ,  
 $\Lambda = 0.5$ ,  $\zeta = 0.5$ ,  $L_1 = L_2 = 0.5$ .

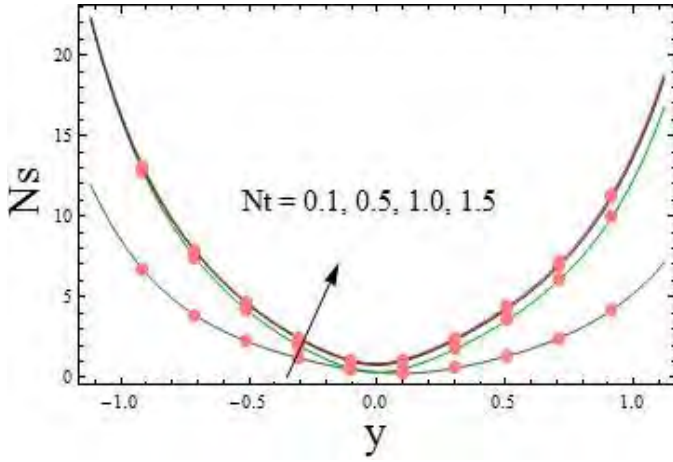


Fig. 10.20

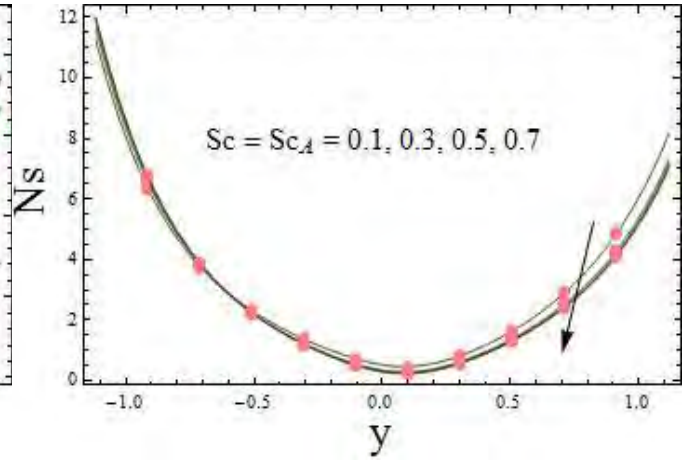


Fig. 10.21

Fig. 10.20.  $Ns$  for  $Nt$  when  $E_1 = 0.02$ ,  $E_2 = 0.01$ ,  $E_3 = 0.01$ ,  $t = 0.1$ ,  $x = 0.2$ ,  $\varepsilon = 0.2$ ,  $\alpha_1 = 2.0$ ,  $\beta = 0.5$ ,  $M = 0.1$ ,  $H = 0.5$ ,  $K = 0.5$ ,  $Sc = Sc_A = 0.5$ ,  $Nt = 0.1$ ,  $Nb = 0.1$ ,  $Pr = 1.5$ ,  $Br = 2.0$ ,  $\Lambda = 0.5$ ,  $\zeta = 0.5$ ,  $L_1 = L_2 = 0.5$ .

Fig. 10.21.  $Ns$  for  $Sc$ ,  $Sc_A$  when  $E_1 = 0.02$ ,  $E_2 = 0.01$ ,  $E_3 = 0.01$ ,  $t = 0.1$ ,  $x = 0.2$ ,  $\varepsilon = 0.2$ ,  $\alpha_1 = 2.0$ ,  $\beta = 0.5$ ,  $M = 0.1$ ,  $H = 0.5$ ,  $K = 0.5$ ,  $Nt = 0.1$ ,  $Nb = 0.1$ ,  $Pr = 1.5$ ,  $Br = 2.0$ ,  $\Lambda = 0.5$ ,  $\zeta = 0.5$ ,  $L_1 = L_2 = 0.5$ .

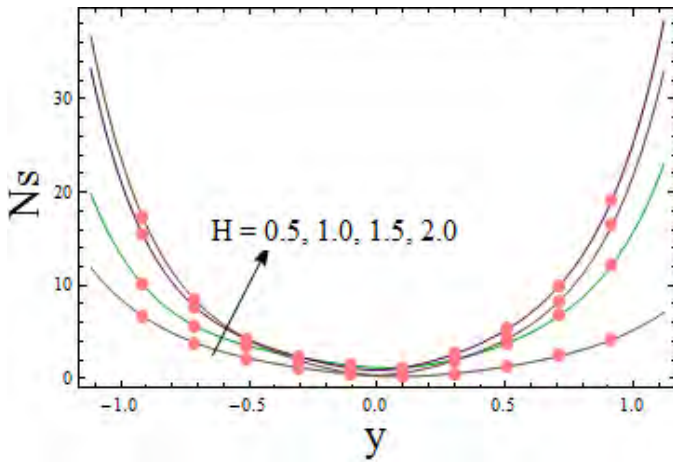


Fig. 10.22

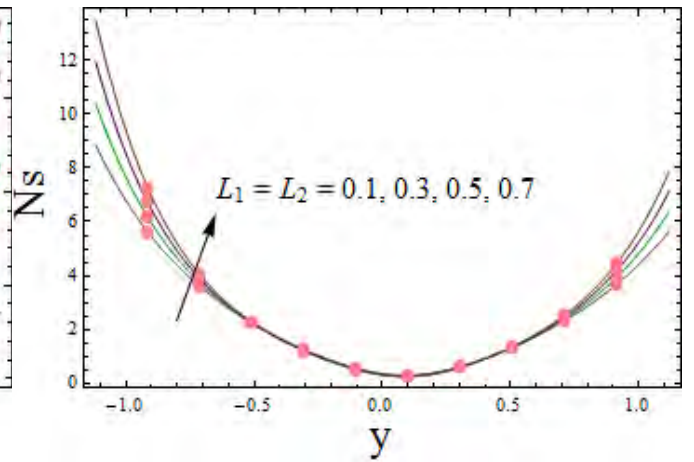


Fig. 10.23

Fig. 10.22.  $Ns$  for  $H$  when  $E_1 = 0.02$ ,  $E_2 = 0.01$ ,  $E_3 = 0.01$ ,  $t = 0.1$ ,  $x = 0.2$ ,  $\varepsilon = 0.2$ ,



$$\alpha_1 = 2.0, \beta = 0.5, M = 0.1, K = 0.5, Sc = Sc_A = 0.5, Nt = 0.1, Nb = 0.1, Pr = 1.5,$$

$$Br = 2.0, \Lambda = 0.5, \zeta = 0.5, L_1 = L_2 = 0.5.$$

*Fig. 10.23.*  $Ns$  for  $L_1, L_2$  when  $E_1 = 0.02, E_2 = 0.01, E_3 = 0.01, t = 0.1, x = 0.2, \varepsilon = 0.2,$   
 $\alpha_1 = 2.0, \beta = 0.5, M = 0.1, H = 0.5, K = 0.5, Sc = Sc_A = 0.5, Nt = 0.1, Nb = 0.1, Pr = 1.5,$   
 $Br = 2.0, \Lambda = 0.5, \zeta = 0.5.$

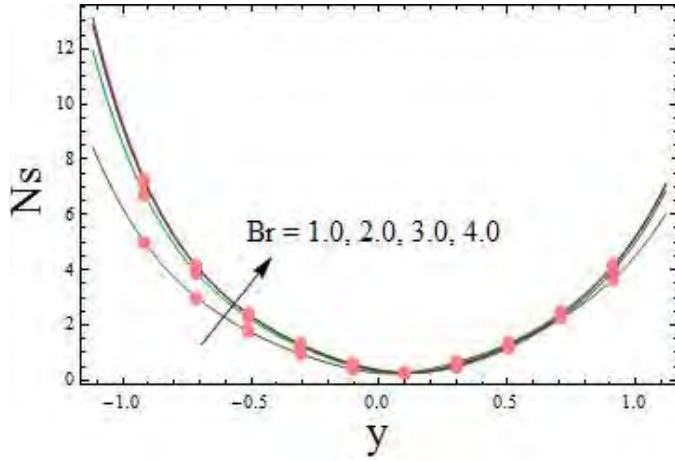


Fig. 10.24

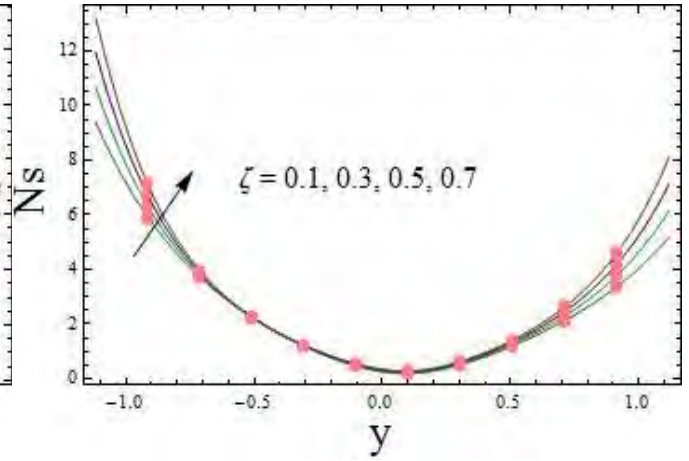


Fig. 10.25

*Fig. 10.24.*  $Ns$  for  $Br$  when  $E_1 = 0.02, E_2 = 0.01, E_3 = 0.01, t = 0.1, x = 0.2, \varepsilon = 0.2,$   
 $\alpha_1 = 2.0, \beta = 0.5, M = 0.1, H = 0.5, K = 0.5, Sc = Sc_A = 0.5, Nt = 0.1, Nb = 0.1, Pr = 1.5,$   
 $\Lambda = 0.5, \zeta = 0.5, L_1 = L_2 = 0.5.$

*Fig. 10.25.*  $Ns$  for  $\zeta$  when  $E_1 = 0.02, E_2 = 0.01, E_3 = 0.01, t = 0.1, x = 0.2, \varepsilon = 0.2,$   
 $\alpha_1 = 2.0, \beta = 0.5, M = 0.1, H = 0.5, K = 0.5, Sc = Sc_A = 0.5, Nt = 0.1, Nb = 0.1, Pr = 1.5,$

$$Br = 2.0, \Lambda = 0.5, L_1 = L_2 = 0.5.$$

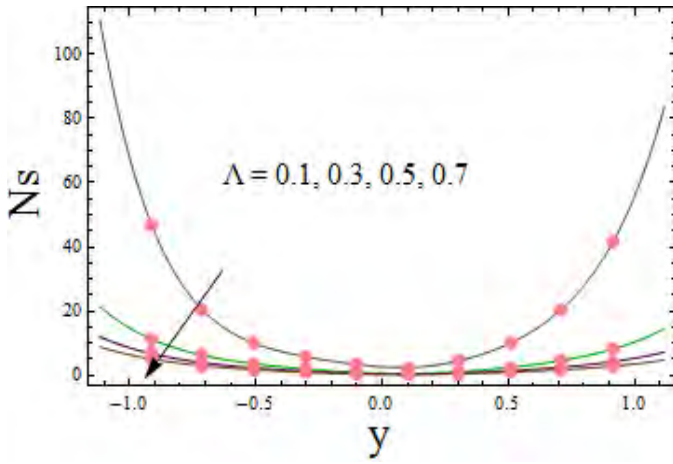


Fig. 10.26

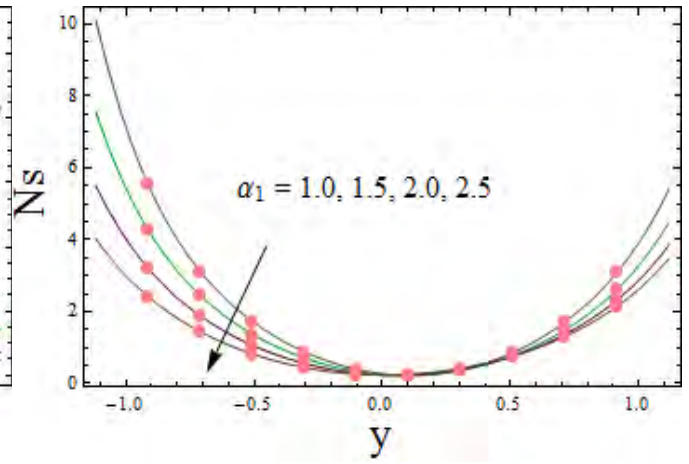


Fig. 10.27

Fig. 10.26.  $Ns$  for  $\Lambda$  when  $E_1 = 0.02$ ,  $E_2 = 0.01$ ,  $E_3 = 0.01$ ,  $t = 0.1$ ,  $x = 0.2$ ,  $\varepsilon = 0.2$ ,  $\alpha_1 = 2.0$ ,  $\beta = 0.5$ ,  $M = 0.1$ ,  $H = 0.5$ ,  $K = 0.5$ ,  $Sc = Sc_A = 0.5$ ,  $Nt = 0.1$ ,  $Nb = 0.1$ ,  $Pr = 1.5$ ,  $Br = 2.0$ ,  $\zeta = 0.5$ ,  $L_1 = L_2 = 0.5$ .

Fig. 10.27.  $Ns$  for  $\alpha_1$  when  $E_1 = 0.02$ ,  $E_2 = 0.01$ ,  $E_3 = 0.01$ ,  $t = 0.1$ ,  $x = 0.2$ ,  $\varepsilon = 0.2$ ,  $\beta = 0.5$ ,  $M = 0.1$ ,  $H = 0.5$ ,  $K = 0.5$ ,  $Sc = Sc_A = 0.5$ ,  $Nt = 0.1$ ,  $Nb = 0.1$ ,  $Pr = 1.5$ ,  $Br = 2.0$ ,  $\Lambda = 0.5$ ,  $\zeta = 0.5$ ,  $L_1 = L_2 = 0.5$ .

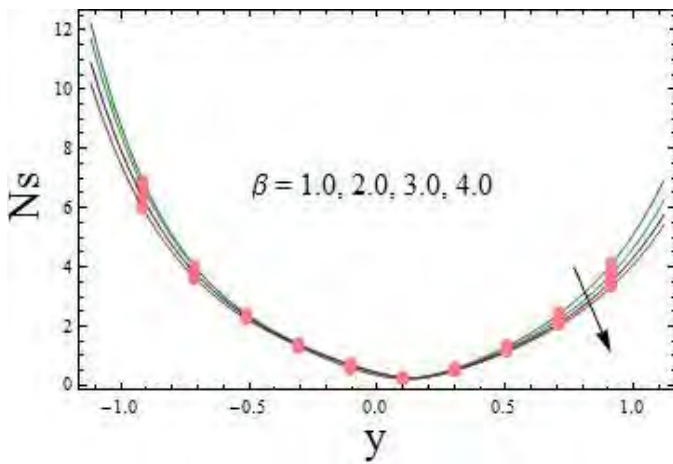


Fig. 10.28

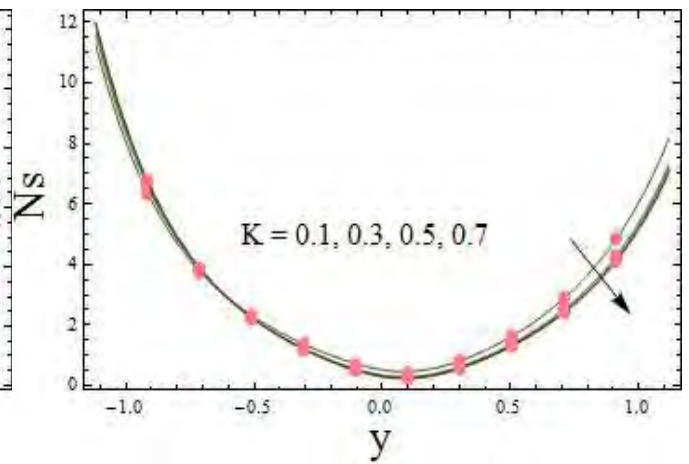


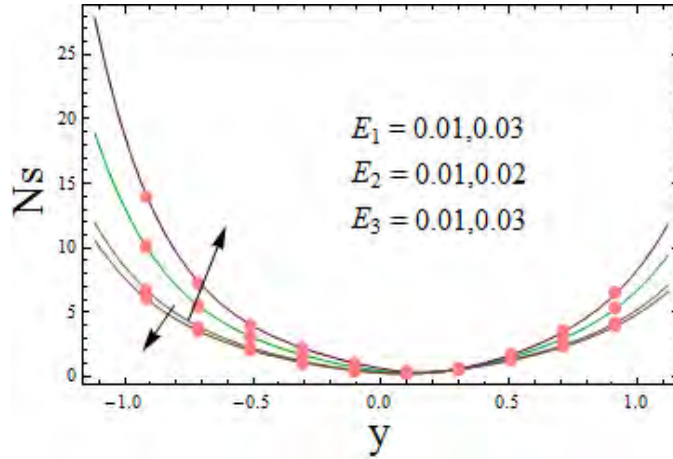
Fig. 10.29

Fig. 10.28.  $Ns$  for  $\beta$  when  $E_1 = 0.02$ ,  $E_2 = 0.01$ ,  $E_3 = 0.01$ ,  $t = 0.1$ ,  $x = 0.2$ ,  $\varepsilon = 0.2$ ,

$$\alpha_1 = 2.0, M = 0.1, H = 0.5, K = 0.5, Sc = Sc_A = 0.5, Nt = 0.1, Nb = 0.1, Pr = 1.5,$$

$$Br = 2.0, \Lambda = 0.5, \zeta = 0.5, L_1 = L_2 = 0.5.$$

*Fig. 10.29.*  $Ns$  for  $K$  when  $E_1 = 0.02, E_2 = 0.01, E_3 = 0.01, t = 0.1, x = 0.2, \varepsilon = 0.2,$   
 $\alpha_1 = 2.0, M = 0.1, H = 0.5, \beta = 0.5, Sc = Sc_A = 0.5, Nt = 0.1, Nb = 0.1, Pr = 1.5,$   
 $Br = 2.0, \Lambda = 0.5, \zeta = 0.5, L_1 = L_2 = 0.5.$



*Fig. 10.30*

*Fig. 10.30.*  $Ns$  for  $E_1, E_2, E_3$  when  $t = 0.1, x = 0.2, \varepsilon = 0.2, \alpha_1 = 2.0, \beta = 0.5, M = 0.1,$   
 $H = 0.5, K = 0.5, Sc = Sc_A = 0.5, Nt = 0.1, Nb = 0.1, Pr = 1.5, Br = 2.0, \Lambda = 0.5, \zeta = 0.5,$   
 $L_1 = L_2 = 0.5.$

Figs. 10.31-10.34 are plotted for investigation of heat transfer coefficient under influence of pertinent parameters. Fluid parameter for Prandtl fluid results can be discussed via Figs. 10.31 and 10.32. Increasing trend of  $Z$  is noticed for both parameters. Brinkman number effect can be seen through Fig. 10.33. Larger values of  $Br$  increases the heat transfer coefficient. Hartman number effect can be portrayed via Fig. 10.34. Decay in heat transfer coefficient is noticed for higher  $M$ .

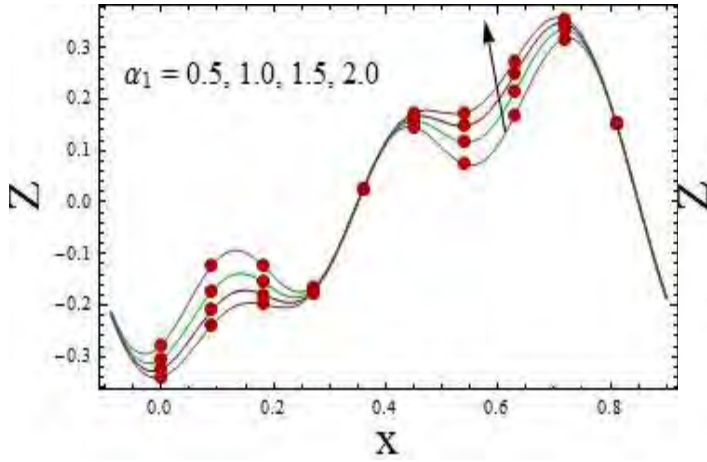


Fig. 10.31

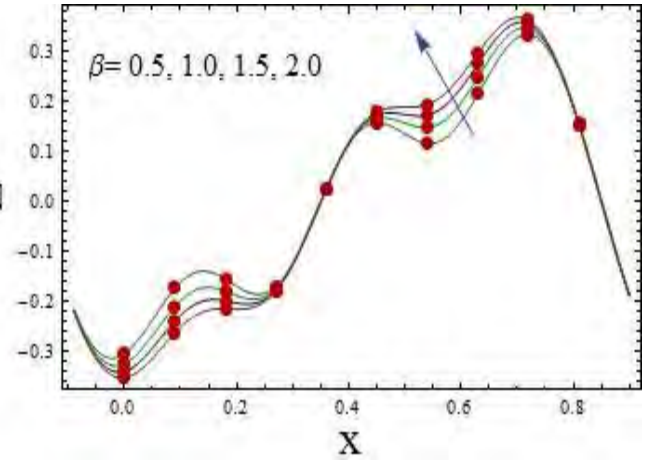


Fig. 10.32

Fig. 10.31.  $Z$  for  $\alpha_1$  when  $E_1 = 0.02$ ,  $E_2 = 0.01$ ,  $E_3 = 0.01$ ,  $t = 0.1$ ,  $\varepsilon = 0.2$ ,  $\beta = 0.5$ ,  $M = 3.0$ ,  $H = 0.5$ ,  $K = 0.5$ ,  $Sc = Sc_A = 0.5$ ,  $Nt = 0.1$ ,  $Nb = 0.1$ ,  $Pr = 1.5$ ,  $Br = 2.0$ .

Fig. 10.32.  $Z$  for  $\beta$  when  $E_1 = 0.02$ ,  $E_2 = 0.01$ ,  $E_3 = 0.01$ ,  $t = 0.1$ ,  $\varepsilon = 0.2$ ,  $\alpha_1 = 0.5$ ,  $M = 3.0$ ,  $H = 0.5$ ,  $K = 0.5$ ,  $Sc = Sc_A = 0.5$ ,  $Nt = 0.1$ ,  $Nb = 0.1$ ,  $Pr = 1.5$ ,  $Br = 2.0$ .

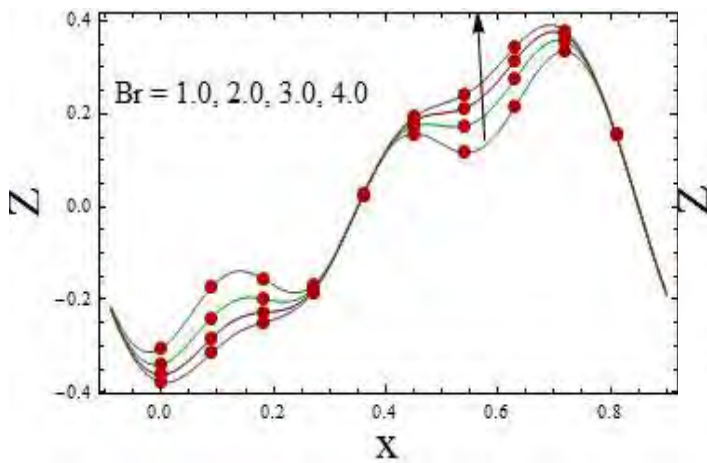


Fig. 10.33

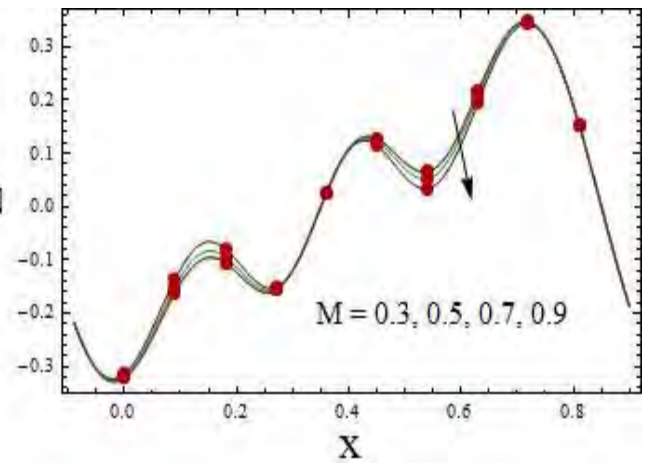


Fig. 10.34

Fig. 10.33.  $Z$  for  $Br$  when  $E_1 = 0.02$ ,  $E_2 = 0.01$ ,  $E_3 = 0.01$ ,  $t = 0.1$ ,  $\varepsilon = 0.2$ ,  $\alpha_1 = 0.5$ ,  $\beta = 0.5$ ,  $M = 3.0$ ,  $H = 0.5$ ,  $K = 0.5$ ,  $Sc = Sc_A = 0.5$ ,  $Nt = 0.1$ ,  $Nb = 0.1$ ,  $Pr = 1.5$ .

Fig. 10.34.  $Z$  for  $M$  when  $E_1 = 0.02$ ,  $E_2 = 0.01$ ,  $E_3 = 0.01$ ,  $t = 0.1$ ,  $\varepsilon = 0.2$ ,  $\alpha_1 = 0.5$ ,

$$\beta = 0.5, H = 0.5, K = 0.5, Sc = Sc_A = 0.5, Nt = 0.1, Nb = 0.1, Pr = 1.5, Br = 2.0.$$

### 10.3.1 Validation of problem:

To validate the results of our problem we have compared the results with study by Alsaedi et al [80]. They have utilized the perturbation method to solve their problem. We have made a comparison about velocity profile. In our problem if we exclude the nanofluid and homogeneous-heterogeneous reaction then our results are in good comparison with the study [80].

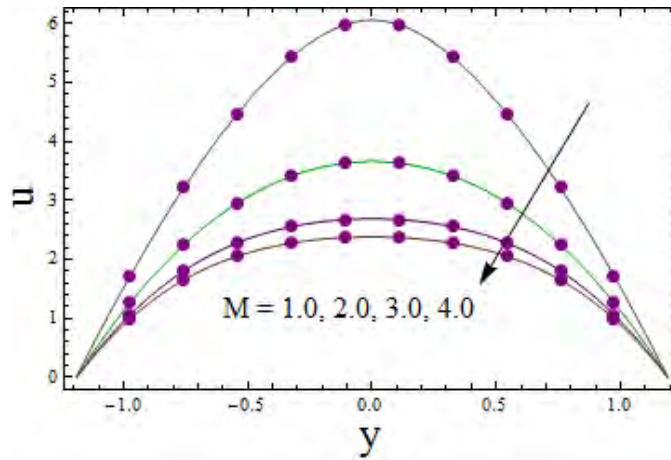


Fig. 10.35: Validation of the Problem

Fig. 10.35.  $u$  for  $M$  when  $E_1 = 1, E_2 = 0.5, E_3 = 0.5, t = 0.1, x = 0.3, \varepsilon = 0.2, \alpha_1 = 1.0,$   
 $\beta = 0.1, H = 0, K = 0, Nt = 0, Pr = 1.5, Br = 2.0.$

## 10.4 Conclusions

This study discloses the phenomenon of peristalsis with homogeneous-heterogeneous reaction. Entropy analysis has been carried out. Some important observations for the considered analysis can be summed up as follows:

- Prandtl number has decaying behavior for velocity, temperature and entropy generation.
- Magnetic field slows down the fluid velocity whereas it provides heating to the fluid and increase the system's entropy.

- Heterogeneous reaction parameter enhances the entropy.
- Temperature increases for  $Nt$ ,  $Nb$  and  $Br$ . Qualitatively similar behavior is observed for entropy.
- Homogeneous reaction parameter has same result on temperature and entropy.
- Concentration decreases for homogeneous and heterogeneous reaction parameters.
- Heat transfer coefficient rises for fluid parameter and Brinkman number whereas it decreases for Hartman number.

## Chapter 11

# Entropy analysis for the peristaltic flow of third grade fluid with variable thermal conductivity

### 11.1 Introduction

This chapter is based on the study of entropy analysis in fluid transport phenomenon by peristalsis. Mixed convective flow in compliant wall channel is considered. Here third grade fluid is considered. Effect of gravity is also encountered. Magnetohydrodynamics and Joule heating are part of flow modeling. Energy equation is addressed subject to viscous dissipation and variable thermal conductivity. Resulting system is solved with the help of NDSolve command in Mathematica. Proper attention is given to the study of velocity, temperature and entropy analysis. This analysis is carried out via graphical results for different embedded parameters. Graphs for heat transfer coefficient are also plotted and analyzed.

### 11.2 Modeling

Here we modeled the peristaltic phenomenon of an incompressible third grade fluid. The channel is considered vertical. Here x-axis lies along the flow direction and y-axis perpendicular to it (see Fig. 11.1). As the channel is vertical so effects of gravity cannot be ignored. Thus mixed

convection is also taken into account in this study. The channel walls are flexible. MHD and Joule heating phenomena are accounted. Here peristaltic waves are propagating in x-direction. Wave amplitude is  $a$  with speed  $c$ , wavelength  $\lambda$  and channel width  $2d$ . Temperature of the left wall is maintained at  $T_0$  and right wall by  $T_1$ . Shape of wall is given by:

$$y = \pm\eta(x, t) = \pm \left[ d + a \sin \frac{2\pi}{\lambda} (x - ct) \right]. \quad (11.1)$$

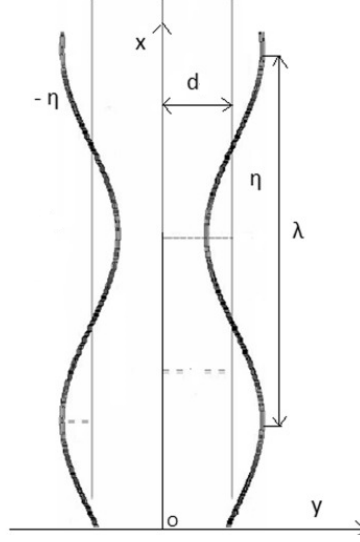


Fig. 11.1: Flow Diagram

An extra stress tensor for thermodynamic compatible third grade fluid is [79]

$$\mathbf{S} = \mu \mathbf{A}_1 + \alpha_1 \mathbf{A}_2 + \alpha_2 \mathbf{A}_1^2 + \beta \text{tr}(\mathbf{A}_1^2) \mathbf{A}_1, \quad (11.2)$$

in which material parameters satisfy the conditions

$$\alpha_1 \geq 0, \quad \beta \geq 0, \quad |\alpha_1 + \alpha_2| \leq \sqrt{24\mu\beta}, \quad (11.3)$$

The definitions of first and second Rivlin-Ericksen tensors are [79]

$$\mathbf{A}_1 = \nabla \mathbf{V} + (\nabla \mathbf{V})^T, \quad \mathbf{A}_2 = \frac{d\mathbf{A}_1}{dt} + \mathbf{A}_1(\nabla \mathbf{V}) + (\nabla \mathbf{V})^T \mathbf{A}_1, \quad (11.4)$$

where material derivative  $\frac{d}{dt}$  is given by  $(\frac{\partial}{\partial t} + u \frac{\partial}{\partial x} + v \frac{\partial}{\partial y})$ .



Flow configuration is described by the following set of equations [100, 181]

Continuity equation is:

$$\frac{\partial u}{\partial x} + \frac{\partial v}{\partial y} = 0, \quad (11.5)$$

Momentum equation in presence of MHD and mixed convection satisfies

$$\rho \left( \frac{\partial u}{\partial t} + u \frac{\partial u}{\partial x} + v \frac{\partial u}{\partial y} \right) = -\frac{\partial p}{\partial x} + \frac{\partial S_{xx}}{\partial x} + \frac{\partial S_{xy}}{\partial y} - \sigma B_0^2 u + g\rho\beta_T(T - T_0), \quad (11.6)$$

$$\rho \left( \frac{\partial v}{\partial t} + u \frac{\partial v}{\partial x} + v \frac{\partial v}{\partial y} \right) = -\frac{\partial p}{\partial y} + \frac{\partial S_{xy}}{\partial x} + \frac{\partial S_{yy}}{\partial y}, \quad (11.7)$$

Energy expression in presence of variable thermal conductivity, Joule heating and viscous dissipation leads to

$$\rho C_p \left( \frac{\partial T}{\partial t} + u \frac{\partial T}{\partial x} + v \frac{\partial T}{\partial y} \right) = \frac{\partial}{\partial x} \left( \kappa(T) \frac{\partial T}{\partial x} \right) + \frac{\partial}{\partial y} \left( \kappa(T) \frac{\partial T}{\partial y} \right) + S_{xx} \frac{\partial u}{\partial x} + S_{xy} \left( \frac{\partial u}{\partial y} + \frac{\partial v}{\partial x} \right) + S_{yy} \frac{\partial v}{\partial y} + \sigma B_0^2 u^2. \quad (11.8)$$

The boundary conditions are stated as follows

$$u = 0, \quad \text{at } y = \pm\eta, \quad (11.9)$$

$$T = \begin{cases} T_1 \\ T_0 \end{cases} \quad \text{at } y = \pm\eta, \quad (11.10)$$

$$\left[ -\tau^* \frac{\partial^3}{\partial x^3} + m^* \frac{\partial^3}{\partial x \partial t^2} + d_1^* \frac{\partial^2}{\partial t \partial x} \right] \eta = \frac{\partial S_{xy}}{\partial y} + \frac{\partial S_{xx}}{\partial x} - \rho \left[ \frac{\partial u}{\partial t} + u \frac{\partial u}{\partial x} + v \frac{\partial u}{\partial y} \right] - \sigma B_0^2 u + g\rho\beta_T(T - T_0), \quad \text{at } y = \pm\eta \quad (11.11)$$

Here  $u$  and  $v$  are the velocity components in the  $x$  and  $y$  directions,  $p$  the pressure,  $\kappa(T)$  the variable thermal conductivity,  $\rho$  the density,  $C_p$  the specific heat,  $B_0$  the strength of magnetic field,  $\sigma$  the electric conductivity,  $S_{ij}$  the components of third grade fluid,  $g$  the gravity,  $\beta_T$  the thermal expansion coefficient,  $T$  for temperature and  $\tau^*$ ,  $m^*$  and  $d_1^*$  the compliant walls coefficients that describes the elastic and damping characteristics of the walls.

Non-dimensional quantities are

$$\begin{aligned}
x^* &= \frac{x}{\lambda}, & y^* &= \frac{y}{d}, & u^* &= \frac{u}{c}, & v^* &= \frac{v}{c}, & t^* &= \frac{ct}{\lambda}, \\
\eta^* &= \frac{\eta}{d}, & \kappa(\theta) &= \frac{\kappa(T)}{\kappa_0}, & S_{ij}^* &= \frac{dS_{ij}}{c\mu}, & p^* &= \frac{d^2p}{c\lambda\mu}, \\
\beta^* &= \frac{\beta c^2}{\mu d^2}, & \theta &= \frac{T - T_0}{T_1 - T_0}, & u &= \frac{\partial\psi}{\partial y}, & v &= -\delta \frac{\partial\psi}{\partial x}.
\end{aligned} \tag{11.12}$$

Utilizing (11.12) one has in terms of stream function ( $\psi$ ) as

$$\text{Re} \left[ \delta \frac{\partial^2\psi}{\partial t\partial y} + \delta \frac{\partial\psi}{\partial y} \frac{\partial^2\psi}{\partial x\partial y} - \delta \frac{\partial\psi}{\partial x} \frac{\partial^2\psi}{\partial y^2} \right] = -\frac{\partial p}{\partial x} + \delta \frac{\partial S_{xx}}{\partial x} + \frac{\partial S_{xy}}{\partial y} - M^2 \frac{\partial\psi}{\partial y} + Gr\theta, \tag{11.13}$$

$$\text{Re} \delta \left[ -\delta^2 \frac{\partial^2\psi}{\partial t\partial x} - \delta^2 \frac{\partial\psi}{\partial y} \frac{\partial^2\psi}{\partial x^2} + \delta^2 \frac{\partial\psi}{\partial x} \frac{\partial^2\psi}{\partial x\partial y} \right] = -\frac{\partial p}{\partial y} + \delta^2 \frac{\partial S_{xy}}{\partial x} + \delta \frac{\partial S_{yy}}{\partial y}, \tag{11.14}$$

$$\begin{aligned}
\text{Re Pr} \left[ \delta \frac{\partial\theta}{\partial t} + \delta \frac{\partial\psi}{\partial y} \frac{\partial\theta}{\partial x} - \delta \frac{\partial\psi}{\partial x} \frac{\partial\theta}{\partial y} \right] &= \delta^2 \frac{\partial}{\partial x} \left( \kappa(\theta) \frac{\partial\theta}{\partial x} \right) + \frac{\partial}{\partial y} \left( \kappa(\theta) \frac{\partial\theta}{\partial y} \right) + \\
&+ Br \left[ \delta S_{xx} \frac{\partial^2\psi}{\partial x\partial y} + S_{xy} \left( \frac{\partial^2\psi}{\partial y^2} - \delta^2 \frac{\partial^2\psi}{\partial x^2} \right) - \delta S_{yy} \frac{\partial^2\psi}{\partial x\partial y} \right] \\
&+ M^2 Br \left( \frac{\partial\psi}{\partial y} \right)^2,
\end{aligned} \tag{11.15}$$

$$\frac{\partial\psi}{\partial y} = 0, \quad \text{at } y = \pm\eta = \pm(1 + \varepsilon \sin 2\pi(x - t)), \tag{11.16}$$

$$\begin{aligned}
\left[ E_1 \frac{\partial^3}{\partial x^3} + E_2 \frac{\partial^3}{\partial x\partial t^2} + E_3 \frac{\partial^2}{\partial t\partial x} \right] \eta &= -\text{Re} \left[ \delta \frac{\partial^2\psi}{\partial t\partial y} + \delta \frac{\partial\psi}{\partial y} \frac{\partial^2\psi}{\partial x\partial y} - \delta \frac{\partial\psi}{\partial x} \frac{\partial^2\psi}{\partial y^2} \right] + \\
&\delta \frac{\partial S_{xx}}{\partial x} + \frac{\partial S_{xy}}{\partial y} - M^2 \frac{\partial\psi}{\partial y} + Gr\theta, \quad \text{at } y = \pm\eta.
\end{aligned} \tag{11.17}$$

$$\theta = \left\{ \begin{array}{c} 1 \\ 0 \end{array} \right\} \quad \text{at } y = \pm\eta, \tag{11.18}$$

where

$$\begin{aligned}
\delta &= \frac{d}{\lambda}, \quad M = \sqrt{\frac{\sigma}{\mu}} B_0 d, \quad \varepsilon = \frac{a}{d}, \quad \text{Re} = \frac{\rho c d}{\mu}, \\
Br &= \frac{c^2 \mu}{\kappa_0 (T_1 - T_0)}, \quad \text{Pr} = \frac{\mu C_p}{\kappa_0}, \quad Gr = \frac{g \rho \beta_T (T_1 - T_0) d^2}{c \mu}, \\
E_1 &= -\frac{\tau^* d^3}{\lambda^3 c \mu}, \quad E_2 = \frac{m^* c d^3}{\lambda^3 \mu}, \quad E_3 = \frac{d_1^* d^3}{\lambda^2 \mu}.
\end{aligned} \tag{11.19}$$

Here  $\delta$  denotes wave number,  $M$  Hartman number,  $\varepsilon$  amplitude ratio,  $\text{Re}$  Reynolds number,  $Br$  Brinkman number,  $\text{Pr}$  Prandtl number,  $Gr$  Grashof number and  $E_1, E_2, E_3$  the compliant walls coefficients.

Employing long wavelength and low Reynolds number assumptions, one obtains

$$\frac{\partial p}{\partial x} = \frac{\partial S_{xy}}{\partial y} - M^2 \frac{\partial \psi}{\partial y} + Gr \theta, \tag{11.20}$$

$$\frac{\partial p}{\partial y} = 0, \tag{11.21}$$

$$0 = \frac{\partial}{\partial y} \left( \kappa(\theta) \frac{\partial^2 \theta}{\partial y^2} \right) + Br S_{xy} \frac{\partial^2 \psi}{\partial y^2} + M^2 Br \left( \frac{\partial \psi}{\partial y} \right)^2, \tag{11.22}$$

$$S_{xy} = \frac{\partial^2 \psi}{\partial y^2} + 6\beta \left( \frac{\partial^2 \psi}{\partial y^2} \right)^3, \tag{11.23}$$

$$\frac{\partial \psi}{\partial y} = 0, \quad \text{at } y = \pm \eta = \pm(1 + \varepsilon \sin 2\pi(x - t)), \tag{11.24}$$

$$\left[ E_1 \frac{\partial^3}{\partial x^3} + E_2 \frac{\partial^3}{\partial x \partial t^2} + E_3 \frac{\partial^2}{\partial t \partial x} \right] \eta = \frac{\partial S_{xy}}{\partial y} - M^2 \frac{\partial \psi}{\partial y} + Gr \theta, \quad \text{at } y = \pm \eta, \tag{11.25}$$

$$\theta = \left\{ \begin{array}{c} 1 \\ 0 \end{array} \right\} \quad \text{at } y = \pm \eta, \tag{11.26}$$

Here  $\kappa(\theta)$  is used for temperature dependent thermal conductivity i.e.  $\kappa(\theta) = 1 + \zeta \theta$ . Solution is obtained via Mathematica 9.0 with NDSolve technique.

### 11.2.1 Entropy generation

Mathematical expression for entropy analysis is [214]:

$$S_{gen}''' = \underbrace{\frac{\kappa(T)}{T_m^2} \left( \left( \frac{\partial T}{\partial x} \right)^2 + \left( \frac{\partial T}{\partial y} \right)^2 \right)}_{\text{Thermal irreversibility}} + \underbrace{\frac{\sigma B_0^2 u^2}{T_m}}_{\text{Joule friction irreversibility}} + \underbrace{\frac{\Phi}{T_m}}_{\text{Fluid friction irreversibility}}, \quad (11.27)$$

where  $\Phi$  is given by

$$\Phi = S_{xx} \frac{\partial u}{\partial x} + S_{yy} \frac{\partial v}{\partial y} + S_{xy} \left( \frac{\partial u}{\partial y} + \frac{\partial v}{\partial x} \right). \quad (11.28)$$

In dimensionless form

$$N_s = \frac{S_{gen}'''}{S_G'''} = \kappa(\theta) \left( \frac{\partial \theta}{\partial y} \right)^2 + \frac{BrM^2}{\Lambda} \left( \frac{\partial \psi}{\partial y} \right)^2 + \frac{Br}{\Lambda} S_{xy} \left( \frac{\partial^2 \psi}{\partial y^2} \right), \quad (11.29)$$

$$S_G''' = \frac{\kappa_0 (T_1 - T_0)^2}{T_m^2 d^2}, \quad \Lambda = \frac{T_1 - T_0}{T_m}. \quad (11.30)$$

## 11.3 Analysis

Here NDSolve of Mathematica is used for the solution of nonlinear system. Graphical results with physical interpretations are arranged in the separate subsections for simplicity.

### 11.3.1 Velocity

This subsection contains the information about velocity. Results of some physical parameters including  $Gr$ ,  $M$ ,  $\varsigma$ ,  $\beta$ ,  $\epsilon$  and  $E_1$ ,  $E_2$ ,  $E_3$  are examined. Grashof number behavior can be portrayed via Fig. 11.2. The buoyancy forces facilitate the flow. An increase is noticed clearly in this case. Opposite result for Hartman number is noticed via Fig. 11.3. As the resistive nature forces caused reduction in flow. Here Lorentz force plays this role. Applied magnetic field provides resistance to fluid particles. This fact is utilized for reduction of bleeding during surgeries and cancer tumor treatment. Influence of variable thermal conductivity parameter is seen via Fig. 11.4. Increase in  $\varsigma$  caused an enhancement of velocity. Fig. 11.5 is prepared for fluid parameter result. Fluid parameter leads to an increase of velocity. It is because of decrease in viscosity parameter. Here  $\epsilon$  leads to an enhancement in fluid velocity (see Fig. 11.6). Same

results can be seen through study [79] for the cases of  $\beta$  and  $\epsilon$ . Obviously as increase in wave amplitude caused an enhancement of fluid velocity. Flexible characteristics of walls impacts can be viewed via Fig. 11.7. Elastance parameters facilitate the flow whereas damping leads to slow down the fluid particles. These characteristics of walls have association with blood vessels.

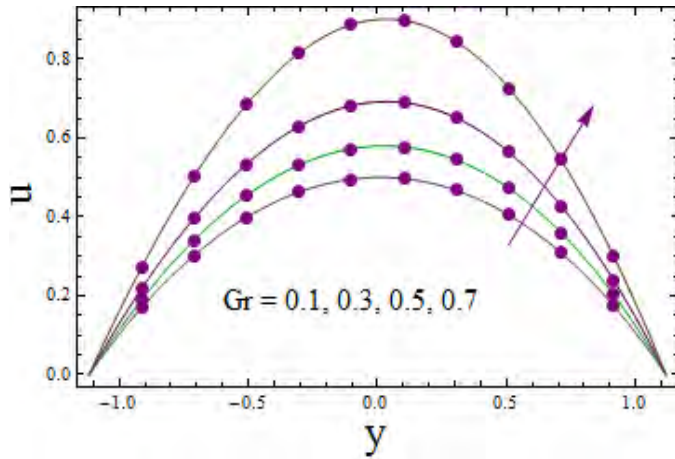


Fig. 11.2

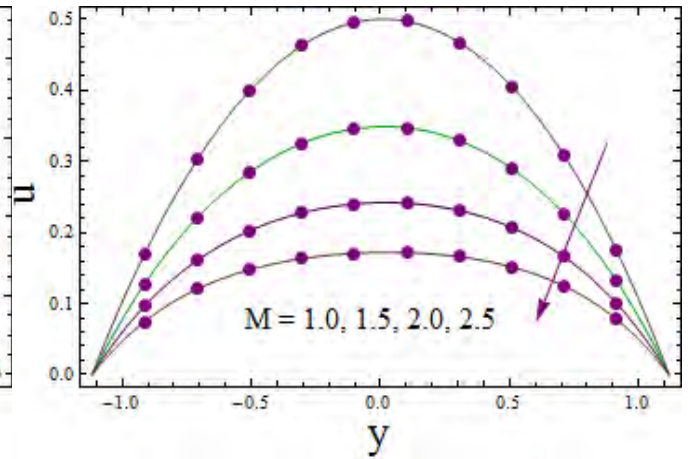


Fig. 11.3

*Fig. 11.2.*  $u$  versus  $Gr$  when  $E_1 = 0.02$ ,  $E_2 = 0.01$ ,  $E_3 = 0.01$ ,  $t = 0.1$ ,  $x = 0.2$ ,  $\epsilon = 0.2$ ,  
 $\zeta = 0.01$ ,  $\beta = 0.01$ ,  $M = 1.0$ ,  $Br = 2.0$ .

*Fig. 11.3.*  $u$  versus  $M$  when  $E_1 = 0.02$ ,  $E_2 = 0.01$ ,  $E_3 = 0.01$ ,  $t = 0.1$ ,  $x = 0.2$ ,  $\epsilon = 0.2$ ,  
 $\zeta = 0.01$ ,  $\beta = 0.01$ ,  $Gr = 0.1$ ,  $Br = 2.0$ .

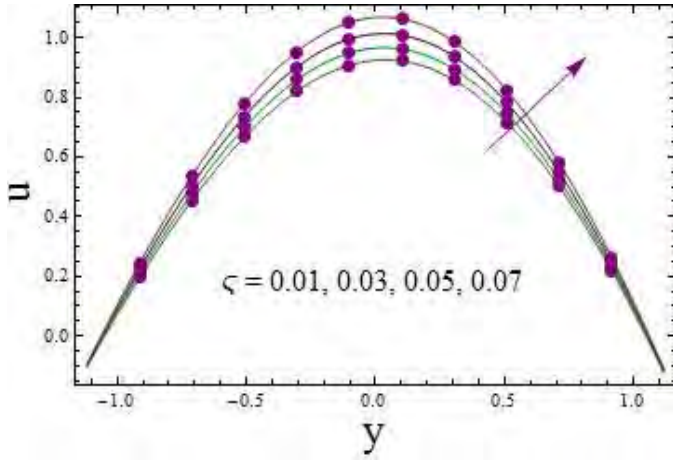


Fig. 11.4

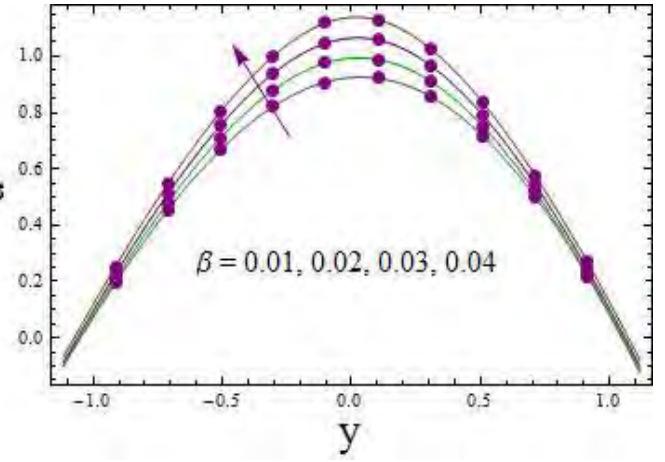


Fig. 11.5

Fig. 11.4.  $u$  versus  $\zeta$  when  $E_1 = 0.02$ ,  $E_2 = 0.01$ ,  $E_3 = 0.01$ ,  $t = 0.1$ ,  $x = 0.2$ ,  $\varepsilon = 0.2$ ,  $\beta = 0.01$ ,  $Gr = 0.1$ ,  $M = 1.0$ ,  $Br = 2.0$ .

Fig. 11.5.  $u$  versus  $\beta$  when  $E_1 = 0.02$ ,  $E_2 = 0.01$ ,  $E_3 = 0.01$ ,  $t = 0.1$ ,  $x = 0.2$ ,  $\varepsilon = 0.2$ ,  $\zeta = 0.01$ ,  $Gr = 0.1$ ,  $M = 1.0$ ,  $Br = 2.0$ .

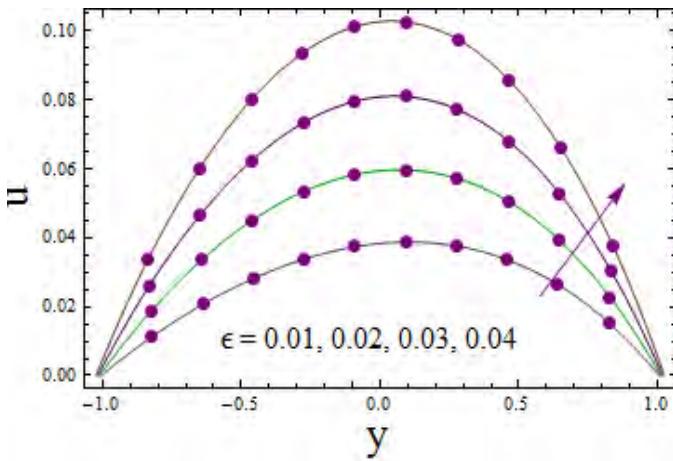


Fig. 11.6

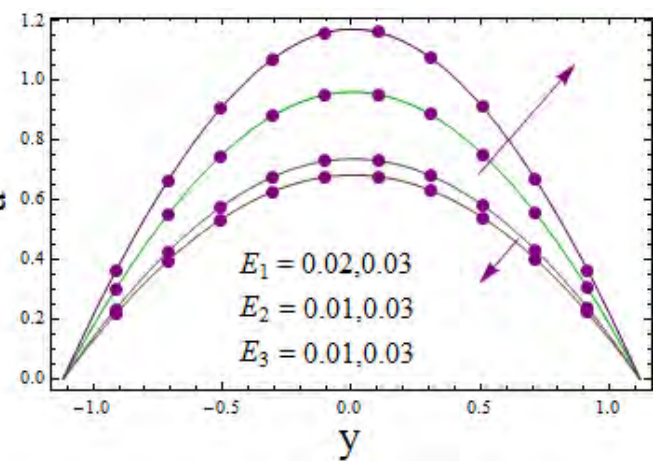


Fig. 11.7

Fig. 11.6.  $u$  versus  $\varepsilon$  when  $E_1 = 0.02$ ,  $E_2 = 0.01$ ,  $E_3 = 0.01$ ,  $t = 0.1$ ,  $x = 0.2$ ,  $\zeta = 0.01$ ,  $\beta = 0.01$ ,  $Gr = 0.1$ ,  $M = 1.0$ ,  $Br = 2.0$ .

Fig. 11.7.  $u$  versus  $E_1$ ,  $E_2$  and  $E_3$  when  $t = 0.1$ ,  $x = 0.2$ ,  $\varepsilon = 0.2$ ,  $\zeta = 0.01$ ,  $\beta = 0.01$ ,

$$Gr = 0.1, M = 1.0, Br = 2.0.$$

### 11.3.2 Temperature

This subsection contains information about temperature for different embedded parameters. Grashof number results can be seen via Fig. 11.8. Temperature is known as average kinetic energy. Thus an increase in the mean kinetic energy of the particles caused higher fluid temperature. Fluid parameter ( $\beta$ ) leads to decrease of temperature (see Fig. 11.9). As increase in fluid parameter decreases the viscosity. There is less heat loss and temperature decays. Study [79] reports the same observation. Hartman number caused an increase in temperature of fluid near the center of channel. It is due to Joule heating (see Fig. 11.10). Behavior for variable thermal conductivity parameter has been seen via Fig. 11.11. An increase in temperature is observed for this case. As increase in  $\zeta$  enhances the conductance property of fluid which increases temperature as well. Same result for variable thermal conductivity parameter has been examined in study [77]. Fig. 11.12 elucidated the behavior of  $\epsilon$  on  $\theta$ . Larger values of amplitude lead to an enhancement of temperature. This is also caused by an increase of mean kinetic energy of particles. Fig. 11.13 portrayed  $Br$  impact on  $\theta$ . Clearly an increase is viewed through view of viscous dissipation. Fig. 11.14 displays the results of flexible characteristics of walls. Here  $E_1, E_2$  results are opposite to that of  $E_3$ .

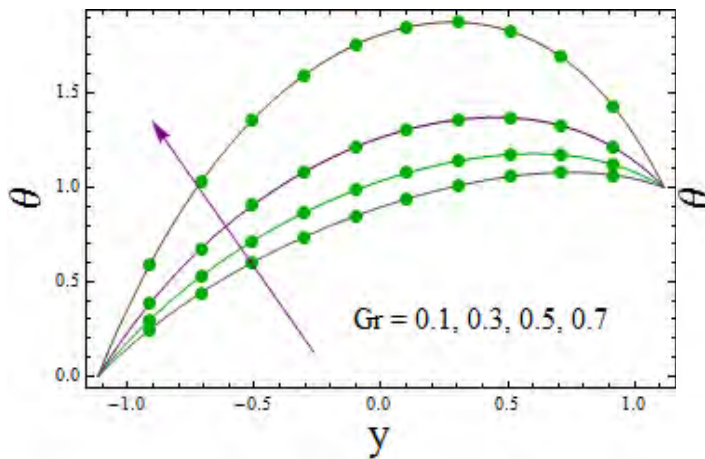


Fig. 11.8

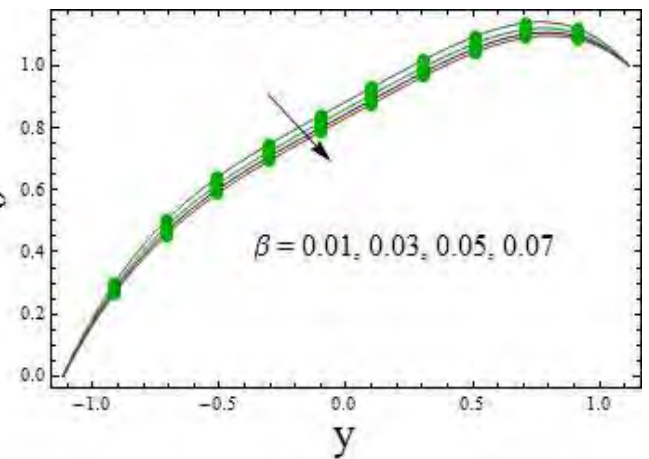


Fig. 11.9

Fig. 11.8.  $\theta$  versus  $Gr$  when  $E_1 = 0.02$ ,  $E_2 = 0.01$ ,  $E_3 = 0.01$ ,  $t = 0.1$ ,  $x = 0.2$ ,  $\varepsilon = 0.2$ ,  
 $\zeta = 0.01$ ,  $\beta = 0.01$ ,  $M = 1.0$ ,  $Br = 2.0$ .

Fig. 11.9.  $\theta$  versus  $\beta$  when  $E_1 = 0.02$ ,  $E_2 = 0.01$ ,  $E_3 = 0.01$ ,  $t = 0.1$ ,  $x = 0.2$ ,  $\varepsilon = 0.2$ ,  
 $\zeta = 0.01$ ,  $Gr = 0.1$ ,  $M = 1.0$ ,  $Br = 2.0$ .

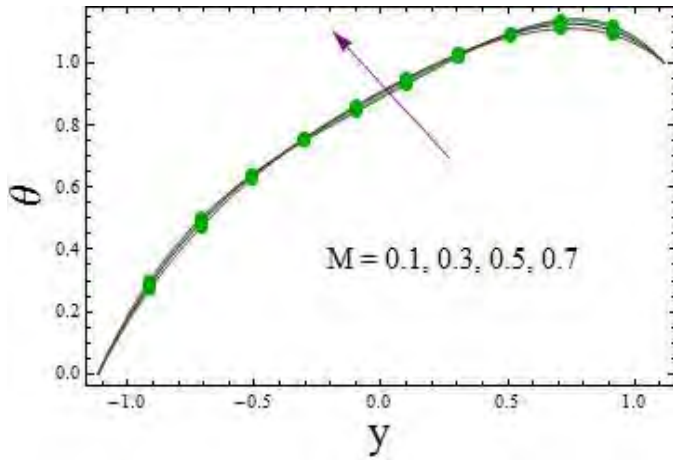


Fig. 11.10

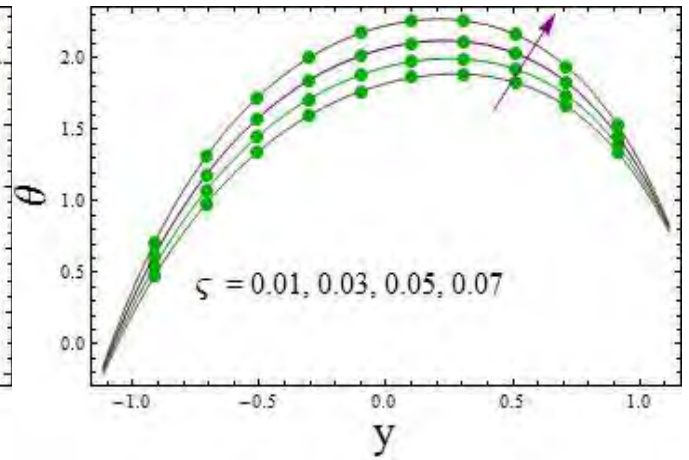


Fig. 11.11

Fig. 11.10.  $\theta$  versus  $M$  when  $E_1 = 0.02$ ,  $E_2 = 0.01$ ,  $E_3 = 0.01$ ,  $t = 0.1$ ,  $x = 0.2$ ,  $\varepsilon = 0.2$ ,  
 $\zeta = 0.01$ ,  $\beta = 0.01$ ,  $Gr = 0.1$ ,  $Br = 2.0$ .

Fig. 11.11.  $\theta$  versus  $\zeta$  when  $E_1 = 0.02$ ,  $E_2 = 0.01$ ,  $E_3 = 0.01$ ,  $t = 0.1$ ,  $x = 0.2$ ,  $\varepsilon = 0.2$ ,  
 $\beta = 0.01$ ,  $Gr = 0.1$ ,  $M = 1.0$ ,  $Br = 2.0$ .



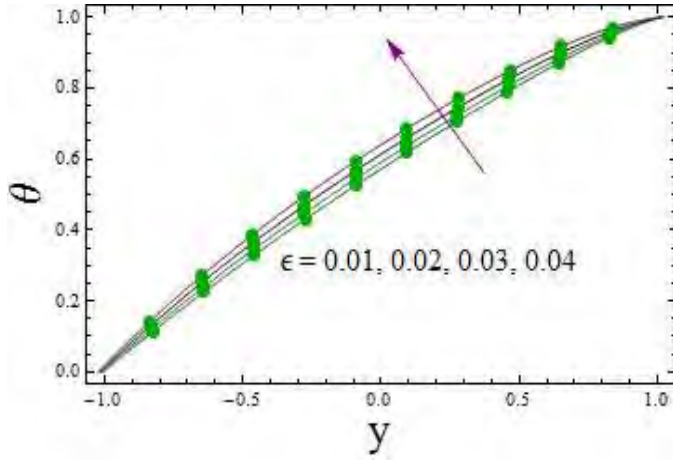


Fig. 11.12

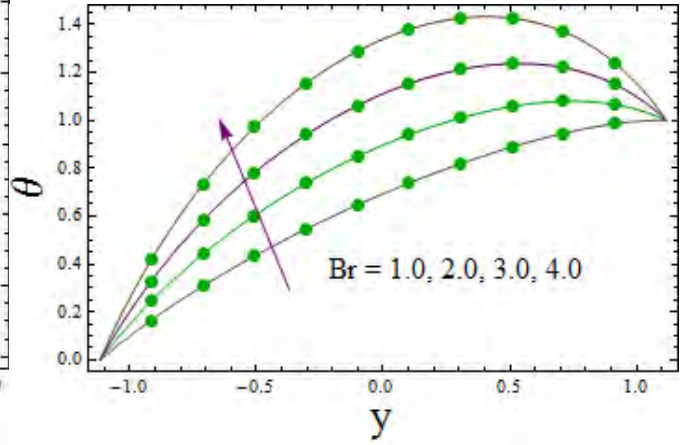


Fig. 11.13

Fig. 11.12.  $\theta$  versus  $\epsilon$  when  $E_1 = 0.02$ ,  $E_2 = 0.01$ ,  $E_3 = 0.01$ ,  $t = 0.1$ ,  $x = 0.2$ ,  $\varsigma = 0.01$ ,  $\beta = 0.01$ ,  $Gr = 0.1$ ,  $M = 1.0$ ,  $Br = 2.0$ .

Fig. 11.13.  $\theta$  versus  $Br$  when  $E_1 = 0.02$ ,  $E_2 = 0.01$ ,  $E_3 = 0.01$ ,  $t = 0.1$ ,  $x = 0.2$ ,  $\epsilon = 0.2$ ,  $\varsigma = 0.01$ ,  $\beta = 0.01$ ,  $Gr = 0.1$ ,  $M = 1.0$ .

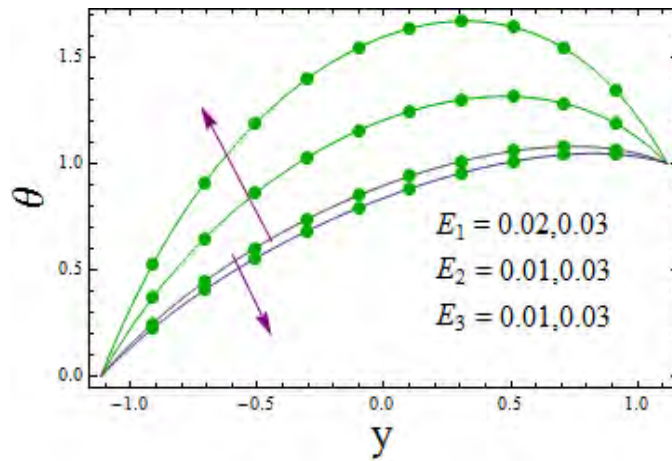


Fig. 11.14

Fig. 11.14.  $\theta$  versus  $E_1$ ,  $E_2$ ,  $E_3$  when  $t = 0.1$ ,  $x = 0.2$ ,  $\epsilon = 0.2$ ,  $\varsigma = 0.01$ ,  $\beta = 0.01$ ,  $Gr = 0.1$ ,  $M = 1.0$ ,  $Br = 2.0$ .

### 11.3.3 Entropy analysis

This subsection covers the entropy analysis for the considered system. Graphs for embedded parameters provide the information about entropy ( $Ns$ ) of the system. Figs. 11.15-11.22 are plotted for this purpose. Grashof number impact can be viewed via Fig. 11.15. It can be seen that high temperature also leads to an increase of system's entropy. Clearly Joule heating phenomenon rises the temperature of fluid and thus entropy enhances (see Fig. 11.16). Fig. 11.17 describes the effect of  $\Lambda$  on  $Ns$ . Larger values of  $\Lambda$  caused decay in  $Ns$ . Fluid parameter results can be observed with the help of Fig. 11.18. Clearly increasing values of  $\beta$  tend to decrease the entropy of system. Such fact can be verified by relating it with temperature. Fig. 11.19 is prepared to study effect of  $\epsilon$  on temperature. An enhancement in  $Ns$  is noticed clearly. Variable thermal conductivity parameter impact can be elucidated via Fig. 11.20. The results are seen qualitatively similar to that of temperature. Larger values of Brinkman number enhance the entropy of system (see Fig. 11.21). As more viscous dissipation lead to increase of temperature and hence more disorderliness. Walls parameters behavior has quite resemblance with temperature (see Fig. 11.22).

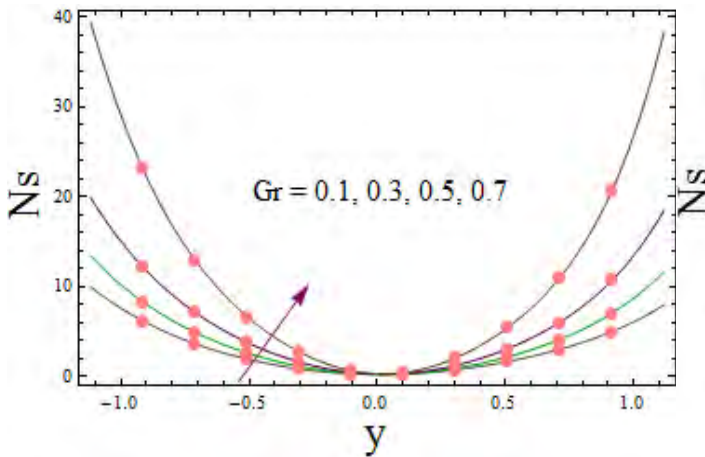


Fig. 11.15

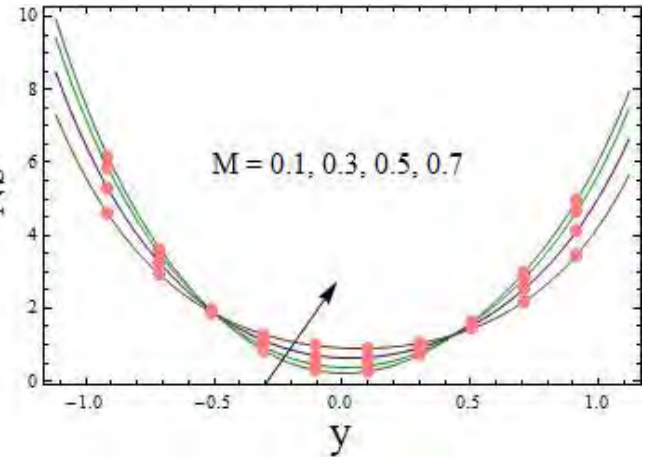


Fig. 11.16

Fig. 11.15.  $Ns$  versus  $Gr$  when  $E_1 = 0.02$ ,  $E_2 = 0.01$ ,  $E_3 = 0.01$ ,  $t = 0.1$ ,  $x = 0.2$ ,  $\epsilon = 0.2$ ,  $\varsigma = 0.01$ ,  $\beta = 0.01$ ,  $M = 1.0$ ,  $Br = 2.0$ ,  $\Lambda = 0.5$ .

Fig. 11.16.  $Ns$  versus  $M$  when  $E_1 = 0.02$ ,  $E_2 = 0.01$ ,  $E_3 = 0.01$ ,  $t = 0.1$ ,  $x = 0.2$ ,  $\epsilon = 0.2$ ,

$$\zeta = 0.01, \beta = 0.01, Gr = 0.1, Br = 2.0, \Lambda = 0.5.$$

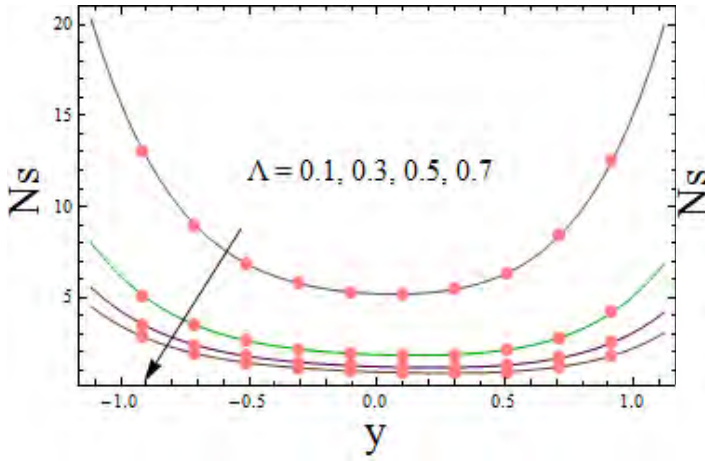


Fig. 11.17

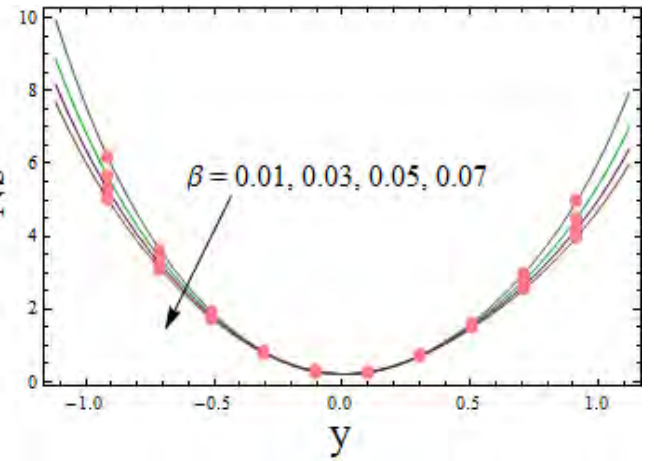


Fig. 11.18

Fig. 11.17.  $Ns$  versus  $\Lambda$  when  $E_1 = 0.02$ ,  $E_2 = 0.01$ ,  $E_3 = 0.01$ ,  $t = 0.1$ ,  $x = 0.2$ ,  $\varepsilon = 0.2$ ,

$$\zeta = 0.01, \beta = 0.01, Gr = 0.1, M = 1.0, Br = 2.0.$$

Fig. 11.18.  $Ns$  versus  $\beta$  when  $E_1 = 0.02$ ,  $E_2 = 0.01$ ,  $E_3 = 0.01$ ,  $t = 0.1$ ,  $x = 0.2$ ,  $\varepsilon = 0.2$ ,

$$\zeta = 0.01, Gr = 0.1, M = 1.0, Br = 2.0, \Lambda = 0.5.$$

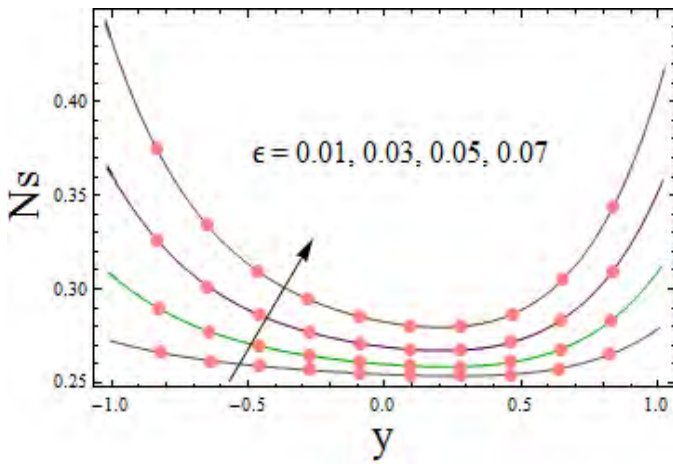


Fig. 11.19

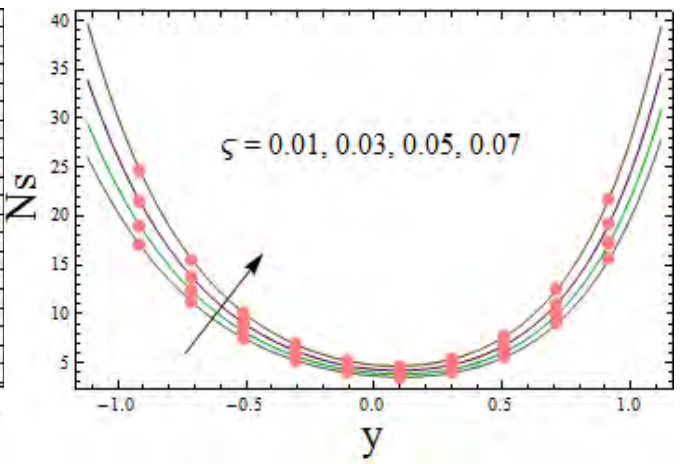


Fig. 11.20

Fig. 11.19.  $Ns$  versus  $\varepsilon$  when  $E_1 = 0.02$ ,  $E_2 = 0.01$ ,  $E_3 = 0.01$ ,  $t = 0.1$ ,  $x = 0.2$ ,  $\zeta = 0.01$ ,

$$\beta = 0.01, Gr = 0.1, M = 1.0, Br = 2.0, \Lambda = 0.5.$$

Fig. 11.20.  $Ns$  versus  $\zeta$  when  $E_1 = 0.02$ ,  $E_2 = 0.01$ ,  $E_3 = 0.01$ ,  $t = 0.1$ ,  $x = 0.2$ ,  $\varepsilon = 0.2$ ,  
 $\beta = 0.01$ ,  $Gr = 0.1$ ,  $M = 1.0$ ,  $Br = 2.0$ ,  $\Lambda = 0.5$ .

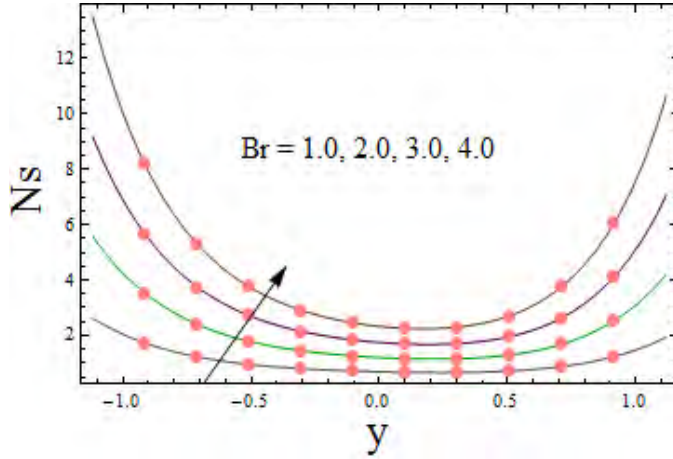


Fig. 11.21

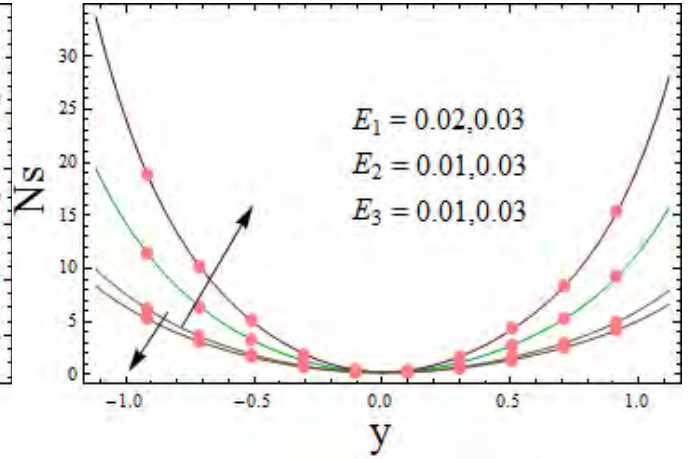


Fig. 11.22

Fig. 11.21.  $Ns$  versus  $Br$  when  $E_1 = 0.02$ ,  $E_2 = 0.01$ ,  $E_3 = 0.01$ ,  $t = 0.1$ ,  $x = 0.2$ ,  $\varepsilon = 0.2$ ,  
 $\zeta = 0.01$ ,  $\beta = 0.01$ ,  $Gr = 0.1$ ,  $M = 1.0$ ,  $\Lambda = 0.5$ .

Fig. 11.22.  $Ns$  versus  $E_1$ ,  $E_2$  and  $E_3$  when  $t = 0.1$ ,  $x = 0.2$ ,  $\varepsilon = 0.2$ ,  $\zeta = 0.01$ ,  $\beta = 0.01$ ,  
 $Gr = 0.1$ ,  $M = 1.0$ ,  $Br = 2.0$ ,  $\Lambda = 0.5$ .

### 11.3.4 Heat transfer coefficient

This subsection is devoted to the results for heat transfer coefficient. Fig. 11.23 portrayed the effect of  $Gr$  on  $Z$ . Grashof number is an increasing function of heat transfer coefficient. Opposite behavior of Hartman number on heat transfer coefficient is observed (see Fig. 11.24). Figs. 11.25 and 11.26 display the influences of  $\zeta$  and  $\beta$  on heat transfer coefficient ( $Z$ ). Both parameters depict similar impact on  $Z$ . Fig. 11.27 represents the  $Br$  influence on  $Z$ . Heat transfer coefficient increases for  $Br$ . These observations for  $\beta$  and  $Br$  are similar to that as in ref. [79].  $E_i$  ( $i = 1, 2$ ) show increasing trend and  $E_3$  illustrate decreasing effect of  $Z$  (see Fig. 11.28).

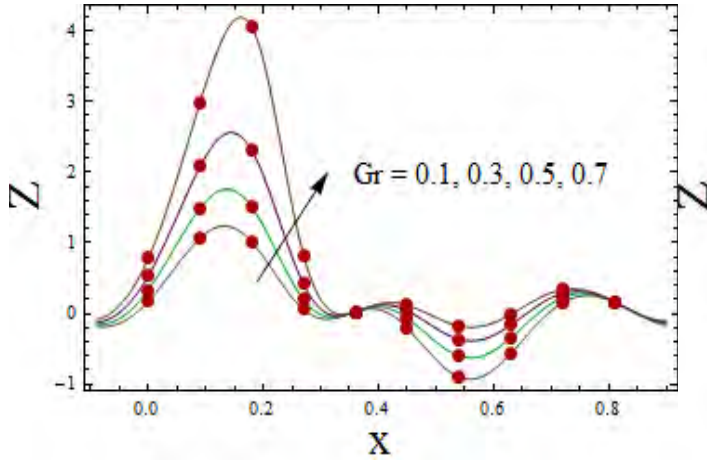


Fig. 11.23

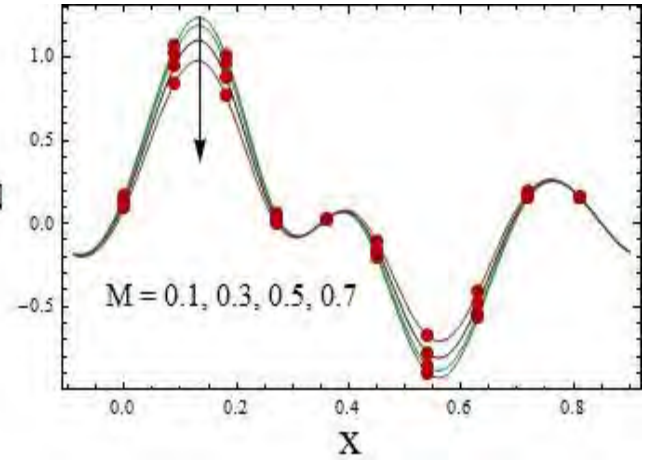


Fig. 11.24

Fig. 11.23.  $Z$  versus  $Gr$  when  $E_1 = 0.02$ ,  $E_2 = 0.01$ ,  $E_3 = 0.01$ ,  $t = 0.1$ ,  $\varepsilon = 0.2$ ,  $\zeta = 0.01$ ,  $\beta = 0.01$ ,  $Br = 2.0$ ,  $M = 1.0$ .

Fig. 11.24.  $Z$  versus  $M$  when  $E_1 = 0.02$ ,  $E_2 = 0.01$ ,  $E_3 = 0.01$ ,  $t = 0.1$ ,  $\varepsilon = 0.2$ ,  $\zeta = 0.01$ ,  $\beta = 0.01$ ,  $Gr = 0.1$ ,  $Br = 2.0$ .

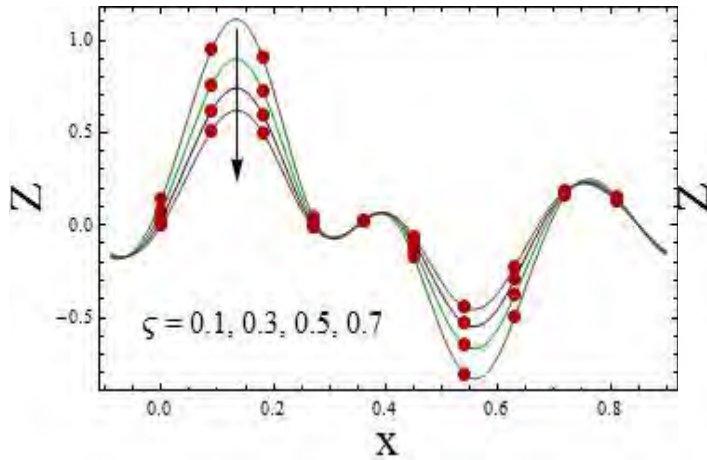


Fig. 11.25

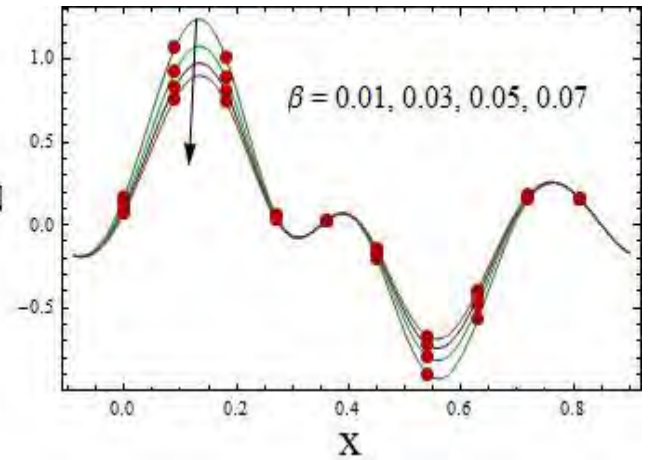


Fig. 11.26

Fig. 11.25.  $Z$  versus  $\zeta$  when  $E_1 = 0.02$ ,  $E_2 = 0.01$ ,  $E_3 = 0.01$ ,  $t = 0.1$ ,  $\varepsilon = 0.2$ ,  $\beta = 0.01$ ,  $Gr = 0.1$ ,  $M = 1.0$ ,  $Br = 2.0$ .

Fig. 11.26.  $Z$  versus  $\beta$  when  $E_1 = 0.02$ ,  $E_2 = 0.01$ ,  $E_3 = 0.01$ ,  $t = 0.1$ ,  $\varepsilon = 0.2$ ,  $\zeta = 0.01$ ,  $Gr = 0.1$ ,  $M = 1.0$ ,  $Br = 2.0$ .



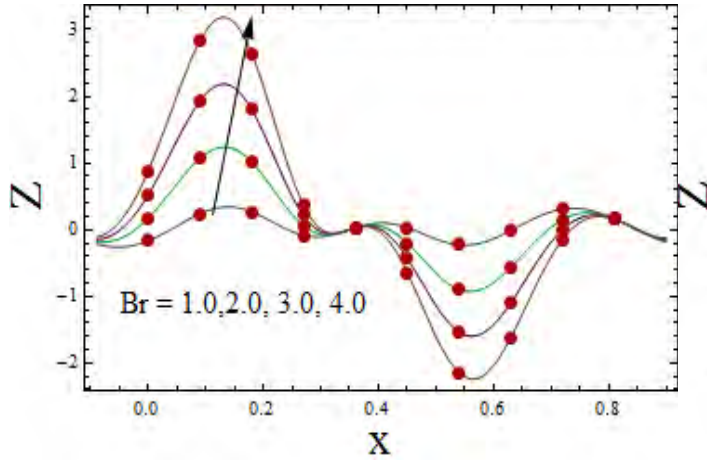


Fig. 11.27

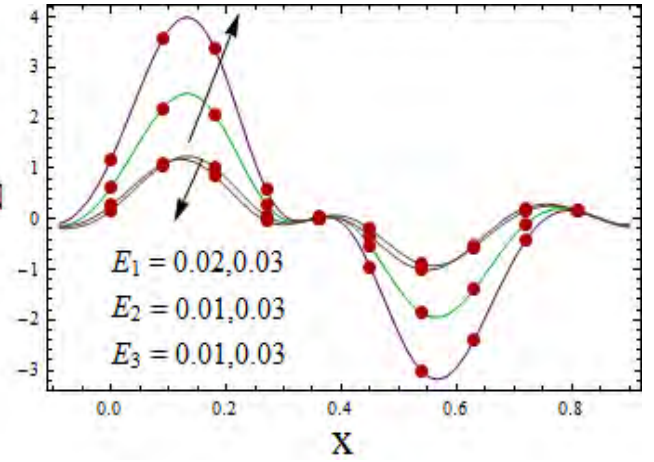


Fig. 11.28

Fig. 11.27.  $Z$  versus  $Br$  when  $E_1 = 0.02$ ,  $E_2 = 0.01$ ,  $E_3 = 0.01$ ,  $t = 0.1$ ,  $\varepsilon = 0.2$ ,  $\varsigma = 0.01$ ,  $\beta = 0.01$ ,  $Gr = 0.1$ ,  $M = 1.0$ .

Fig. 11.28.  $Z$  versus  $E_1$ ,  $E_2$ ,  $E_3$  when  $t = 0.1$ ,  $\varepsilon = 0.2$ ,  $\varsigma = 0.01$ ,  $\beta = 0.01$ ,  $Gr = 0.1$ ,  $M = 1.0$ ,  $Br = 2.0$ .

### 11.3.5 Trapping

Trapping is discussed in this subsection for some prominent parameters. Decrease is noticed for the size of trapped bolus for larger Hartman number (see Fig. 11.29 (a) and (b)).  $Gr$  impact on bolus size can be noticed via Fig. 11.30 (a) and (b). Bolus size increases in this case. Fig. 11.31 (a) and (b) displayed that bolus size decreases for the case of variable thermal conductivity parameter.

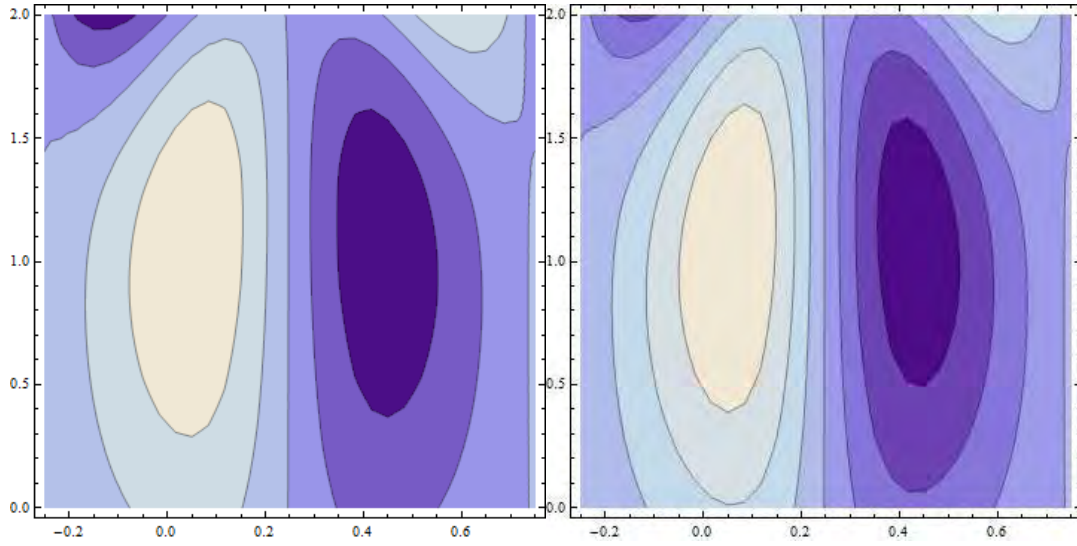


Fig. 11.29 (a)

(b)

Fig. 11.29.  $\psi$  versus  $M$  when  $E_1 = 0.02$ ,  $E_2 = 0.01$ ,  $E_3 = 0.01$ ,  $t = 0.0$ ,  $\varepsilon = 0.2$ ,  $\varsigma = 0.01$ ,  $\beta = 0.01$ ,  $Br = 2.0$ . (a)  $M = 1.0$ , (b)  $M = 1.5$ .

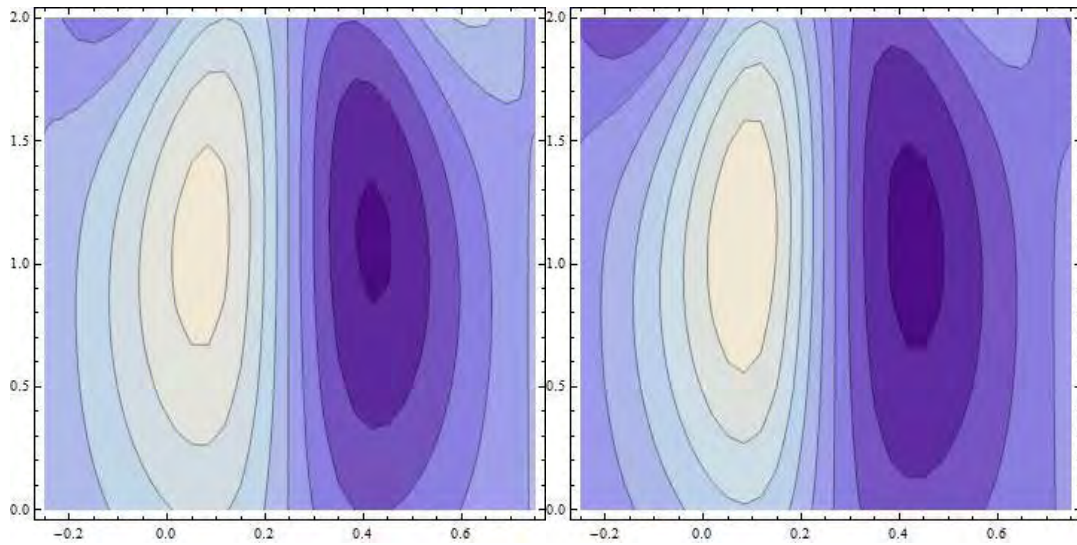


Fig. 11.30 (a)

(b)

Fig. 11.30.  $\psi$  versus  $Gr$  when  $E_1 = 0.02$ ,  $E_2 = 0.01$ ,  $E_3 = 0.01$ ,  $t = 0.0$ ,  $\varepsilon = 0.2$ ,  $\varsigma = 0.01$ ,  $\beta = 0.01$ ,  $M = 1.0$ ,  $Br = 2.0$ . (a)  $Gr = 0.1$ , (b)  $Gr = 0.5$ .

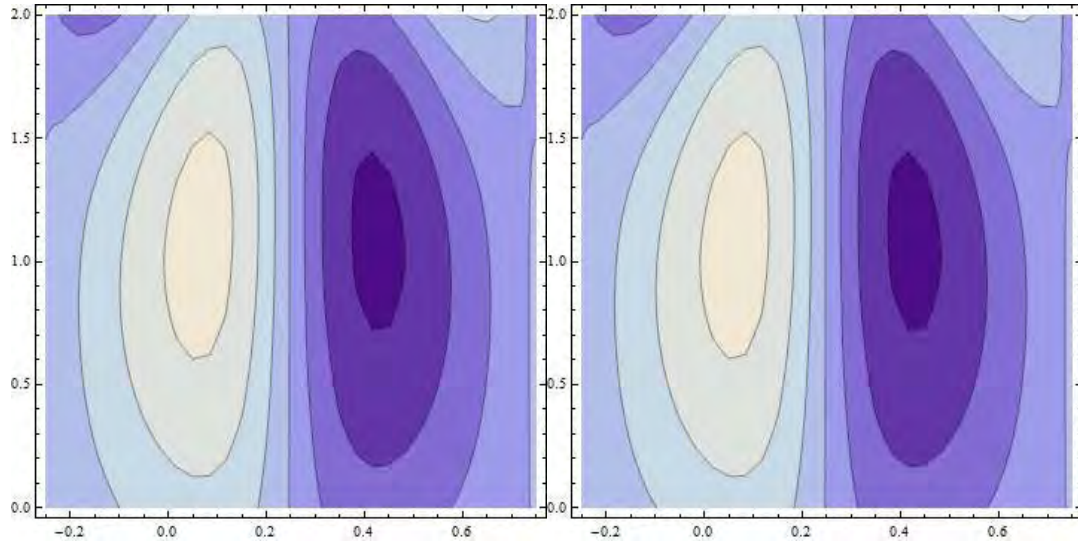


Fig. 11.31 (a)

(b)

Fig. 11.31.  $\psi$  versus  $\zeta$  when  $E_1 = 0.02$ ,  $E_2 = 0.01$ ,  $E_3 = 0.01$ ,  $t = 0.0$ ,  $\varepsilon = 0.2$ ,  $\beta = 0.01$ ,  $M = 1.0$ ,  $Br = 2.0$ . (a)  $\zeta = 0.1$ , (b)  $\zeta = 0.3$ .

## 11.4 Conclusions

Important points of present study can be summarized as follows:

- Variable thermal conductivity parameter increases the velocity, temperature and entropy of system.
- Hartman number caused decay in velocity but it increases the entropy and temperature near the center of channel.
- $Br$  effect on temperature, entropy and heat transfer coefficient are same.
- Bolus size decreases for  $M$ .



# Bibliography

- [1] W. M. Bayliss and E. H. Starling, The movement and innervation of the small intestine, *J. Physiol.*, 24 (1899) 99-143.
- [2] T. W. Engelmann, Zur Physiologie des Ureter, *Pflug. Arch. Ges. Physiol.*, 2 (1869) 243-293.
- [3] J. Lapidus, The physiology of the intact human ureter., *J. Urol.*, 59 (1948) 501-537.
- [4] S. Boyarsky, Surgical physiology of the renal pelvis and ureter, *Monogr. Sur. Sci.*, 1 (1964) 173-213.
- [5] T. W. Latham, Fluid motion in a peristaltic pump, M.S. Thesis, MIT., Cambridge, MA (1966).
- [6] A. H. Shapiro, M. Y. Jafrin and S. L. Weinberg, Peristaltic pumping with long wavelengths at low Reynolds number, *J. Fluid Mech.*, 37 (1969) 799-825.
- [7] J. C. Burns and T. Parkes, Peristaltic motion, *J. Fluid Mech.*, 29 (1967) 731-743.
- [8] C. Barton and S. Raynor, Peristaltic flow in tubes, *Bull. Math. Bio.*, 30 (1968) 663-680.
- [9] Y. C. Fung and C. S. Yih, Peristaltic transport, *J. Appl. Mech.*, 35 (1968) 669-675.
- [10] M. Hanin, The flow through a channel due to transversely oscillating walls, *Israel J. Technol.*, 6 (1968) 67-71.
- [11] C. C. Yin and Y. C. Fung, Peristaltic wave in circular cylindrical tubes, *J. Appl. Mech.*, 36 (1969) 579-587.

- [12] C. H. Li, Peristaltic transport in circular cylindrical tubes, *J. Biomech.*, 3 (1970) 513-523.
- [13] S. T. Chow, Peristaltic transport in a circular cylindrical pipe, *J. Appl. Mech.*, 37 (1970) 901-906.
- [14] J. R. Meginniss, An analytical investigation of flow and hemolysis in peristaltic type blood pumps, M. S. Thesis, Dep. Mech. Eng., MIT., Cambridge, MA (1970).
- [15] P. S. Lykoudis and R. Roos, The fluid mechanics of the ureter from a lubrication theory point of view, *J. Fluid Mech.*, 43 (1970) 661-674.
- [16] T. F. Zien and S. Ostrach, A long wave approximation to peristaltic motion, *J. Biomech.* 3 (1970) 63-75.
- [17] F. Yin, Theory and experiment in peristalsis, PhD. Thesis. University of California, San Diego, La Jolla, California. (1970).
- [18] E. C. Eckstein, Experimental and theoretical pressure studies of peristaltic pumping, M. S. Thesis, Dep. Mech. Eng., MIT., Cambridge MA, (1970).
- [19] S. L. Weinberg, A theoretical and experimental treatment of peristaltic pumping and its relation to ureteral function, PhD Thesis, Dep. Mech. Eng., MIT., Cambridge, MA (1970).
- [20] F. C. P. Yin and Y. C. Fung, Comparison of theory and experiment in peristaltic transport, *J. Fluid Mech.* 47 (1971) 93-112.
- [21] S. L. Weinberg, M. Y. Jaffrin and A. H. Shapiro, A hydrodynamical model of ureteral function. In "Proceedings Workshop Hydrodynam. Upper urinary tract"., Nat. Acad. Sci., Washington, D.C. (1971).
- [22] M. Y. Jaffrin and A. H. Shapiro, Peristaltic pumping, *Ann. Rev. Fluid Mech.*, 3 (1971) 13-36.
- [23] A. H. Shapiro and M. Y. Jaffrin, Reflux in peristaltic pumping: Is it determined by the Eulerian or Lagrangian mean velocity, *J. Appl. Mech.*, 38 (1971) 1060-1062.

- [24] H. S. Lew, Y. C. Fung and C. B. Lowenstein, Peristaltic carrying and mixing of chyme in the small intestine (An analysis of a mathematical model of peristalsis of the small intestine), *J. Biomech.*, 4 (1971) 297-315.
- [25] H. S. Lew and Y. C. Fung, A study on the low Reynolds number in a valved vessel, *J. Biomech.*, 4 (1971) 85-94.
- [26] Y. C. B. Fung, Peristaltic pumping: A bioengineering model, *Urodynamics*, (1971) 177-198 doi:10.1016/b978-0-12-121250-6.50022-8.
- [27] P. Tong and D. Vawter, An analysis of peristaltic pumping, *J. Appl. Mech.*, 39 (1972) 857-862.
- [28] M. Y. Jafrin, Inertia and streamline curvature effects on peristaltic pumping, *Int. J. Eng. Sci.*, 11 (1973) 681-699.
- [29] T. K. Mitra and S. N. Prasad, Interaction of peristaltic motion with Poiseuille flow, *Bull. Math. Biol.*, 36 (1974) 127-141.
- [30] M. P. Negrin, W. J. Shack and T. J. Lardner, A note on peristaltic pumping, *J. Appl. Mech.*, 96 (1974) 520-521.
- [31] M. J. Manton, Long-wavelength peristaltic pumping at low Reynolds number, *J. Fluid Mech.*, 68 (1975) 467-476.
- [32] B. B. Gupta and V. Seshadri, Peristaltic pumping in non-uniform tubes, *J. Biomech.*, 9 (1976) 105-109.
- [33] N. Liron, On peristaltic flow and its efficiency, *Bull. Math. Bio.*, 38 (1976) 573-596.
- [34] T. D. Brown and T. K. Hung, Computational and experimental investigations of two dimensional nonlinear peristaltic flows, *J. Fluid Mech.*, 83 (1977) 249-272.
- [35] T. K. Hung and T. D. Brown, An implicit finite-difference method for solving the Navier-Stokes equation using orthogonal curvilinear coordinates, *J. Comp. Phys.*, 23 (1977) 343-363.

- [36] M. R. Kaimal, Peristaltic pumping of a Newtonian fluid with particles suspended in it at low Reynolds number under long wavelength approximation, *J. Appl. Mech.*, 43 (1978) 31-36.
- [37] A. R. Bestman, Long wavelength peristaltic pumping in a heated tube at low Reynolds number, *Develop. Mech.*, 10 (1979) 195-199.
- [38] H. J. Rath, Peristaltic flow through a lobe-shaped tube, *Int. J. Mech. Sci.*, 24 (1982) 359-367.
- [39] L. M. Srivastava and V. P. Srivastava, Peristaltic transport of a two-layered model of physiological fluid, *J. Biomech.*, 15 (1982) 257-265.
- [40] S. Nakanishi and M. Kawaguti, Numerical study on peristaltic flow of viscous fluid, *J. Phys. Soc. Jpn.*, 52 (1983) 848-855.
- [41] L. M. Srivastava and V. P. Srivastava, Interaction of peristaltic flow with pulsatile flow in a circular cylindrical tube, *J. Biomech.*, 18 (1985) 247-253.
- [42] S. Takabatake, K. Ayukawa and A. Mori, Peristaltic pumping in circular cylindrical tubes: a numerical study of fluid transport and its efficiency, *J. Fluid Mech.*, 193 (1988) 267-283.
- [43] J. B. Shukla, P. Chandra, R. Sharma and G. Radhakrishnamacharya, Effects of peristaltic and longitudinal wave motion of the channel wall on movement of micro-organisms: Application to spermatozoa transport, *J. Biomech.*, 21 (1988) 947-954.
- [44] M. Li and J.G. Brasseur, Non-steady peristaltic transport in finite-length tubes, *J. Fluid Mech.* 248 (1993) 129-151.
- [45] B. V. R. Kumar and K. B. Naidu, A numerical study of peristaltic flows, *Comp. Fluids*, 24 (1995) 161-176.
- [46] L. K. Antanovskii and H. Ramkissoon, Long-wave peristaltic transport of a compressible viscous fluid in a finite pipe subject to a time-dependent pressure drop, *Fluid Dyn. Research*, 19 (1997) 115-123.

- [47] O. Eytan, A. J. Jaffa and D. Elad, Peristaltic flow in a tapered channel: application to embryo transport within the uterine cavity, *Med. Engr. Phys.*, 23 (2001) 475-484.
- [48] E. F. Elshehawey and Z. M. Gharsseidien, Peristaltic transport of three-layered flow with variable viscosity, *Appl. Math. Comp.*, 153 (2004) 417-432.
- [49] S. Srinivas and V. Pushparaj, Non-linear peristaltic transport in an inclined asymmetric channel, *Comm. Nonlinear Sci. Num. Simul.*, 13 (2008) 1782-1795.
- [50] T. Hayat, M. Javed and A. A. Hendi, Peristaltic transport of viscous fluid in a curved channel with compliant walls, *Inter. J. Heat Mass Trans.*, 54 (2011) 1615-1621.
- [51] M. M. Cross, Rheology of non-Newtonian fluids: a new flow equation for pseudoplastic systems, *J. Coll. Sci.*, 20 (1965) 417-437.
- [52] S. Wada and H. Hayashi, Hydrodynamic lubrication of journal bearings by pseudoplastic lubricants, *Bull. JSME*, 69 (1971) 268-278.
- [53] K. K. Raju and R. Devanathan, Peristaltic motion of a non-Newtonian fluid, *Rheo. Acta*, 11 (1972) 170-178.
- [54] E. Becker, Simple non-Newtonian fluid flows, *Adv. Appl. Mech.*, 20 (1980) 177-226.
- [55] J. A. Deiber and W. R. Schowalter, Modeling the flow of viscoelastic fluids through porous media, *AIChE J.*, 27 (1981) 912-920.
- [56] G. Bohme and R. Friedish, Peristaltic flow of viscoelastic liquids, *J. Fluid Mech.*, 128 (1983) 109-122.
- [57] G. Devi, and R. Devanathan, Peristaltic motion of a micropolar fluid, *Proc. Indian Acad. Sci.* 81A (1975) 149-163.
- [58] L. M. Srivastava and V. P. Srivastava, Peristaltic transport of blood: Casson model—II, *J. Biomechanics*, 17 (1984) 821-829.
- [59] A. M. Siddiqui and W. H. Schwarz, Peristaltic flow of a second-order fluid in tubes, *J. Non-Newtonian Fluid Mech.*, 53 (1994) 257-284.

- [60] J. C. Misra and S. K. Pandey, Peristaltic transport of a non-Newtonian fluid with a peripheral layer, *Int. J. Eng. Sci.*, 37 (1999) 1841-1858.
- [61] J. C. Misra and S. K. Pandey, A mathematical model for oesophageal swallowing of a food-bolus, *Mathe. Comp. Modell.*, 33 (2001) 997-1009.
- [62] A. V. Mernone, J. N. Mazumdar and S. K. Lucas, A mathematical study of peristaltic transport of Casson fluid, *Math. Comput. Model.*, 35 (2002) 894-912.
- [63] K. Vajravelu, S. Sreenadh and V. R. Babu, Peristaltic pumping of a Herschel-Bulkley fluid in a channel, *Appl. Math. Comput.*, 169 (2005) 726-735.
- [64] T. Hayat and N. Ali, Peristaltically induced motion of a MHD third grade fluid in a deformable tube, *Physica A*, 370 (2006) 225-239.
- [65] T. Hayat and N. Ali, On mechanism of peristaltic flows for power-law fluids. *Physica A*, 371 (2006) 188-194.
- [66] M. H. Haroun, Effect of Deborah number and phase difference on peristaltic transport of a third-order fluid in an asymmetric channel, *Comm. Nonlinear Sci. Numer. Simul.*, 12 (2007) 1464-1480.
- [67] M. H. Haroun, Non-linear peristaltic flow of a fourth grade fluid in an inclined asymmetric channel, *Comp. Mater. Sci.*, 39 (2007) 324-333.
- [68] M. V. S. Reddy, A. R. Rao and S. Sreenadh, Peristaltic motion of a power-law fluid in an asymmetric channel, *Int. J. Non-Linear Mech.*, 42 (2007) 1153-1161.
- [69] T. Hayat, N. Ali and S. Asghar, Peristaltic motion of a Burger's fluid in a planar channel, *Appl. Math. Comp.*, 186 (2007) 309-329.
- [70] T. Hayat, N. Ali and Z. Abbas, Peristaltic flow of a micropolar fluid in a channel with different wave forms, *Phy. Lett. A*, 370 (2007) 331-344.
- [71] N. Ali and T. Hayat, Peristaltic motion of a Carreau fluid in an asymmetric channel, *Appl. Math. Comp.*, 193 (2007) 535-552.

- [72] Y. Wang, T. Hayat, N. Ali and M. Oberlack, Magnetohydrodynamic peristaltic motion of a Sisko fluid in a symmetric or asymmetric channel, *Physica A*, 387 (2008) 347-362.
- [73] K. S. Mekheimer and Y. A. Elmaboud, Peristaltic flow of a couple stress fluid in an annulus: Application of an endoscope, *Physica A*, 387 (2008) 2403-2415.
- [74] P. Hariharana, V. Seshadri and R. K. Banerjee, Peristaltic transport of non-Newtonian fluid in a diverging tube with different wave forms, *Math. Comp. Model.*, 48 (2008) 998-1017.
- [75] P. Muthu, B. V. R. Kumar and P. Chandra, Peristaltic motion of micropolar fluid in circular cylindrical tubes: Effect of wall properties, *Appl. Math. Model.*, 32 (2008) 2019-2033.
- [76] T. Hayat, N. Alvi and N. Ali, Peristaltic mechanism of a Maxwell fluid in an asymmetric channel, *Nonlinear Analysis: Real World Appl.*, 9 (2008) 1474-1490.
- [77] T. Hayat, S. Farooq, B. Ahmad and A. Alsaedi, Consequences of variable thermal conductivity and activation energy on peristalsis in curved configuration, *J. Mol. Liqs.* 263 (2018) 258–267.
- [78] D. Tripathi, S. K. Pandey and S. Das, Peristaltic flow of viscoelastic fluid with fractional Maxwell model through a channel, *Appl. Math. Comp.*, 215 (2010) 3645-3654.
- [79] T. Hayat, S. Hina, A.A. Hendi and S. Asghar, Effect of wall properties on the peristaltic flow of a third grade fluid in a curved channel with heat and mass transfer, *Int. J. Heat Mass Transf.*, 54 (2011) 5126-5136.
- [80] A. Alsaedi, N. Batool, H. Yasmin and T. Hayat, Convective heat transfer analysis on Prandtl fluid model with peristalsis, *Appl. Bionics Biomech.*, 10 (2013) 197–208.
- [81] T. Hayat, A. Tanveer, H. Yasmin and A. Alsaedi, Effects of convective conditions and chemical reaction on peristaltic flow of Eyring-Powell fluid, *Appl. Bionics Biomech.*, 11 (2014) 221-233.

- [82] T. Hayat, S. Bibi, M. Rafiq, A. Alsaedi and F. M. Abbasi, Effect of inclined magnetic field on peristaltic flow of Williamson fluid in an inclined channel with convective conditions, *J. Magn. Mater.*, 401 (2016) 733-745.
- [83] T. Hayat, S. Nawaz, A. Alsaedi and M. Rafiq, Influence of radial magnetic field on the peristaltic flow of Williamson fluid in a curved compliant walls channel, *Results Phys.*, 7 (2017) 982–990.
- [84] T. Hayat, N. Aslam, A. Alsaedi and M. Rafiq, Numerical analysis for endoscope and Soret and Dufour effects on peristalsis of Prandtl fluid, *Results Physics*, 7 (2017) 2855–2864.
- [85] T. Hayat, H. Zahir, A. Tanveer and A. Alsaedi, Soret and Dufour effects on MHD peristaltic flow of Prandtl fluid in a rotating channel, *Results Phys.* 8 (2018) 1291–1300.
- [86] H. Sadaf and S. Noreen, Analysis of combined convective and viscous dissipation effects for peristaltic flow of Rabinowitsch fluid model, *J. Bionic Engr.*, 14 (2017) 182-190.
- [87] S. U. S. Choi, Enhancing thermal conductivity of the fluids with nanoparticles, *ASME Fluids Eng. Div.*, 231 99-105.
- [88] J. C. Maxwell, *A Treatise on Electricity and Magnetism*, 2nd Edition Oxford University Press, Cambridge, (1904) 435-441.
- [89] R. L. Hamilton and O. K. Crosser, Thermal conductivity of heterogeneous two component systems, *Ind. Eng. Chem. Fundam.*, 1 (1962) 187-191.
- [90] Q. Xue and X. Wen-Mei, A model of thermal conductivity of nanofluids with interfacial shells, *Mater. Chem. Phys.*, 90 (2005) 298-301.
- [91] J. Buongiorno, Convective transport in nanofluids, *ASME J. Heat Transf.*, 128 (2005) 240-250.
- [92] H. C. Birkman, The viscosity of concentrated suspensions and solution, *J. Chem. Phys.* 20 (1952) 571.
- [93] K. Khanafer and K. Vafai, A critical synthesis of thermophysical characteristics of nanofluids, *Int. J. Heat Mass Transf.*, 54 (2011) 4410-4428.



- [94] M. Sheikholeslami, D. D. Ganji, M. Y. Javed and R. Ellahi, Effect of thermal radiation on magnetohydrodynamics nanofluid flow and heat transfer by means of two phase model, *J. Magn. Magn. Mater.*, 374 (2015) 36-43.
- [95] M. Sheikholeslami, T. Hayat and A. Alsaedi, Numerical study for external magnetic source influence on water based nanofluid convective heat transfer, *Int. J. Heat Mass Transf.*, 106 (2017) 745-755.
- [96] M. Sheikholeslami, M. Jafaryar and Z. Li, Nanofluid turbulent convective flow in a circular duct with helical turbulators considering CuO nanoparticles, *Int. J. Heat Mass Transf.*, 124 (2018) 980-989.
- [97] S. A. Shehzad, F. M. Abbasi, T. Hayat, and F. Alsaadi, MHD mixed convective peristaltic motion of nanofluid with Joule heating and thermophoresis effects, *Plos One*, 9 (2014) e111417.
- [98] F. M. Abbasi, T. Hayat, F. Alsaadi, A. M. Dobai and H. Gao, MHD peristaltic transport of spherical and cylindrical magneto-nanoparticles suspended in water, *AIP Advances*, 5 (2015) 077104.
- [99] M. M. Bhatti, A. Zeeshan and R. Ellahi, Endoscope analysis on peristaltic blood flow of Sisko fluid with Titanium magneto-nanoparticles, *Comp. Bio Med.*, 78 (2016) 29-41.
- [100] H. M. Sayed, E. H. Aly and K. Vajravelu, Influence of slip and convective boundary conditions on peristaltic transport of non-Newtonian nanofluids in an inclined asymmetric channel, *Alex. Eng. J.*, 55 (2016) 2209-2220.
- [101] T. Hayat, S. Nawaz, F. Alsaadi, M. Rafiq and M. Mustafa, A model for an application to biomedical engineering through nanoparticles, *Int. J. Heat Mass Transf.*, 101 (2016) 112-120.
- [102] T. Hayat, S. Nawaz, A. Alsaadi and M. Rafiq, Impact of second-order velocity and thermal slips in the mixed convective peristalsis with carbon nanotubes and porous medium, *J. Mol. Liq.*, 221 (2016) 434-442.

- [103] S. Nadeem and I. Shahzadi, Single wall carbon nanotube (SWCNT) analysis on peristaltic flow in an inclined tube with permeable walls, *Int. J. Heat Mass Transf.*, 97 (2016) 794-802.
- [104] M. M. Bhatti, A. Zeeshan and R. Ellahi, Simultaneous effects of coagulation and variable magnetic field on peristaltically induced motion of Jeffrey nanofluid containing gyrotactic microorganism, *Microvas. Research*, 110 (2017) 32-42.
- [105] S. Ayub, T. Hayat, S. Asghar and B. Ahmad, Thermal radiation impact in mixed convective peristaltic flow of third grade nanofluid, *Results Phys.*, 7 (2017) 3687-3695.
- [106] N. Ahmed, Adnan, U. Khan and S. T. Mohyud-Din, Influence of shape factor on flow of magneto nanofluid squeezed between parallel disks, *Alex. Eng. J.*, 57 (2018) 1893-1903.
- [107] S. Mosayebidorcheh and M. Hatami, Analytical investigation of peristaltic nanofluid flow and heat transfer in an asymmetric wavy wall channel, *Int. J. Heat Mass Transf.*, 126 (2018) 790-799.
- [108] A. Tanveer, M. Khan, T. Salahuddin and M. Y. Malik, Numerical simulation of electroosmosis regulated peristaltic transport of Bingham nanofluid, *Com. Meth. Prog. Biomed.*, 180 (2019) 105005.
- [109] J. Prakash, D. Tripathi, A. K. Tiwari, S. M. Sait and R. Ellahi, Peristaltic pumping of nanofluids through tapered channel in porous environment: Applications in blood flow, *Symmetry*, 11 (2019) 868.
- [110] A. Riaz, A. Zeeshan, M. M. Bhatti and R. Ellahi, Peristaltic propulsion of Jeffrey nanofluid and heat transfer through a symmetrical duct with moving walls in a porous medium, *Physica A*, 545 (2020) 123788.
- [111] M. N. Rostami, S. Dinarvand and I. Pop, Dual solutions for mixed convective stagnation-point flow of an aqueous silica–alumina hybrid nanofluid, *Chin. J. Phys.*, 56 (2018) 2465-2478.

- [112] A. M. Rashad, A. J. Chamkha, M. A. Ismael and T. Salah, MHD natural convection in a triangular cavity filled with a Cu-Al<sub>2</sub>O<sub>3</sub>/water hybrid nanofluid with localized heating from below and internal heat generation, *J. Heat Transf.*, (2018) doi:10.1115/1.4039213.
- [113] M. Usman, M. Hamid, T. Zubair, R. Haq and W. Wang, Cu-Al<sub>2</sub>O<sub>3</sub>/Water hybrid nanofluid through a permeable surface in the presence of nonlinear radiation and variable thermal conductivity via LSM, *Int. J. Heat Mass Transf.*, 126 (2018) 1347-1356.
- [114] G. Huminic and A. Huminic, The influence of hybrid nanofluids on the performances of elliptical tube: Recent research and numerical study, *Int. J. Heat Mass Trans.*, 129 (2019) 132-143.
- [115] S. M. Mousavi, F. Esmailzadeh and X. P. Wang, A detailed investigation on the thermo-physical and rheological behavior of MgO/TiO<sub>2</sub> aqueous dual hybrid nanofluid, *J. Mol. Liq.*, 282 (2019) 323-329.
- [116] C. Alexiou, W. Arnold, R. J. Klein, F. G. Parak, P. Hulin, C. Bergemann, W. Erhardt, S. Wagenpfeil and A.S. Lübke, Locoregional cancer treatment with magnetic drug targeting, *Cancer Res.*, 60 (2000) 6641-6648.
- [117] J. R. Oleson, Hyperthermia by magnetic induction: I. Physical characteristics of the technique, *Int. J. Radiation Oncology (Biology and Physics)*, 8 (2001) 1747-1756.
- [118] V. K. Stud, G. S. Sephon and R. K. Mishra, Pumping action on blood flow by a magnetic field, *Bull. Math. Bio.*, 39 (1977) 385-390.
- [119] E. F. El-Shehawey and S. Z. A. Husseny, Peristaltic transport of a magneto-fluid with porous boundaries, *Appl. Math. Comp.*, 129 (2002) 421-440.
- [120] K. S. Mekheimer, Peristaltic flow of blood under effect of a magnetic field in a non-uniform channels, *Appl. Math. Comp.*, 153 (2004) 763-777.
- [121] A. E. H. A. El Naby, A. E. M. El Misery and M. F. A. El Kareem, Effects of a magnetic field on trapping through peristaltic motion for generalized Newtonian fluid in channel, *Physica A*, 367 (2006) 79-92.

- [122] N. T. M. Eldabe, M. F. El-Sayed, A. Y. Ghaly and H. M. Sayed, Peristaltically induced transport of a MHD biviscosity fluid in a non-uniform tube, *Physica A*, 383 (2007) 253-266.
- [123] T. Hayat and N. Ali, A mathematical description of peristaltic hydromagnetic flow in a tube, *Appl. Math. Comp.*, 188 (2007) 1491-1502.
- [124] T. Hayat, N. Ahmad and N. Ali, Effects of an endoscope and magnetic field on the peristalsis involving Jeffrey fluid, *Commu. Nonlinear Sci. Numer. Simul.*, 13 (2008) 1581-1591.
- [125] A. Ebaid, A new numerical solution for the MHD peristaltic flow of a bio-fluid with variable viscosity in a circular cylindrical tube via Adomian decomposition method, *Phy. Lett. A*, 372 (2008) 5321-5328.
- [126] R. Ellahi and F. Hussain, Simultaneous effects of MHD and partial slip on peristaltic flow of Jeffrey fluid in a rectangular duct, *J. Magn. Magn. Mater.*, 393 (2015) 284-292.
- [127] A. M. Abd-Alla, S. M. Abo-Dahab and A. Kilicman, Peristaltic flow of a Jeffrey fluid under the effect of radially varying magnetic field in a tube with an endoscope, *J Magn Magn Mater.*, 384 (2015) 79-86.
- [128] F. M. Abbasi, T. Hayat and B. Ahmad, Impact of magnetic field on mixed convective peristaltic flow of water based nanofluids with Joule heating, *Z. Naturforsch.*, 70a (2015) 125-132.
- [129] K. V. V. Satyanarayana, S. Sreenadh, P. Lakshminarayana and G. Sucharitha, MHD peristaltic transport of a micropolar fluid in an asymmetric channel with porous medium, *Adv. Appl. Sci. Res.*, 7 (2016) 105-114.
- [130] M. M. Bhatti, A. Zeeshan, N. Ijaz, O. A. Bég and A. Kadir, Mathematical modelling of nonlinear thermal radiation effects on EMHD peristaltic pumping of viscoelastic dusty fluid through a porous medium duct, *Eng. Sci. Technol. Int. J.*, 20 (2017) 1129-1139.

- [131] A. Tanveer, M. Khan, T. Salahuddin, M. Y. Malik and F. Khan, Theoretical investigation of peristaltic activity in MHD based blood flow of non-Newtonian material, *Computer Methods Programs Biomedicine*, 187 (2020) 105225.
- [132] T. Hayat, N. Ali and S. Asghar, Hall effects on peristaltic flow of a Maxwell fluid in a porous medium, *Phys. Lett. A*, 363 (2007) 397-403.
- [133] N. S. Gad, Effect of Hall currents on interaction of pulsatile and peristaltic transport induced flows of a particle–fluid suspension, *Appl. Math. Comp.*, 217 (2011) 4313-4320.
- [134] F. M. Abbasi, T. Hayat and A. Alsaedi, Numerical analysis for MHD peristaltic transport of Carreau–Yasuda fluid in a curved channel with Hall effects, *J. Magn. Magn. Mater.*, 382 (2015) 104-110.
- [135] F. M. Abbasi, T. Hayat and B. Ahmad, Peristalsis of silver-water nanofluid in the presence of Hall and Ohmic heating effects: Applications in drug delivery, *J. Mol. Liq.*, 207 (2015) 248-255.
- [136] F. M. Abbasi, M. Gul and S. A. Shehzad, Hall effects on peristalsis of boron nitride-ethylene glycol nanofluid with temperature dependent thermal conductivity, *Physica E*, 99 (2018) 275-284.
- [137] M. Rafiq, H. Yasmin, T. Hayat and F. Alsaadi, Effect of Hall and ion-slip on the peristaltic transport of nanofluid: A biomedical application, *Chinese J. Phy.*, 60 (2019) 208-227.
- [138] S. Noreen and T. Kousar, Hall, ion slip and Ohmic heating effects in thermally active sinusoidal channel, *Propulsion Power Resear.*, 8 (2019) 263-273.
- [139] S. K. Asha and G. Sunitha, Thermal radiation and Hall effects on peristaltic blood flow with double diffusion in the presence of nanoparticles, *Case Studies Ther. Engr.*, 17 (2020) 100560.
- [140] M. A. Chaudhary and J. H. Merkin, A simple isothermal model for homogeneous-heterogeneous reactions in boundary-layer flow. II Different diffusivities for reactant and autocatalyst, *Fluid Dyn. Research*, 16 (1995) 335-359.

- [141] J. H. Merkin, A model for isothermal homogeneous-heterogeneous reactions in boundary layer flow, *Math. Comput. Model.*, 24 (1996) 125-136.
- [142] T. Hayat, A. Tanveer, H. Yasmin and A. Alsaedi, Homogeneous-heterogeneous reactions in peristaltic flow with convective conditions, *Plos One*, (2014) DOI:10.1371/journal.pone.0113851.
- [143] T. Hayat, A. Bibi, H. Yasmin and B. Ahmad, Simultaneous effects of Hall current and homogeneous/heterogeneous reactions on peristalsis, *J. Taiwan Inst. Chem. Eng.*, 58 (2016) 28-38.
- [144] M. Awais, S. Farooq, T. Hayat and B. Ahmad, Comparative study of silver and copper water magneto nanoparticles with homogeneous-heterogeneous reactions in a tapered channel, *Int. J. Heat Mass Transf.*, 115 (2017) 108-114.
- [145] A. Tanveer, T. Hayat, A. Alsaedi and B. Ahmad, Mixed convective peristaltic flow of Sisko fluid in curved channel with homogeneous-heterogeneous reaction effects, *J. Mol. Liq.*, 233 (2017) 131-138.
- [146] N. L. Xu, H. Xu and A. Raees, Homogeneous-heterogeneous reactions in flow of nanofluids near the stagnation region of a plane surface: The Buongiorno's model, *Int. J. Heat Mass Transf.*, 125 (2018) 604-609.
- [147] T. Hayat, J. Akram, A. Alsaedi and H. Zahir, Endoscopy and homogeneous-heterogeneous reactions in MHD radiative peristaltic activity of Ree-Eyring fluid, *Results Phys.*, 8 (2018) 481-488.
- [148] M. I. Khan, T. Hayat, A. Alsaedi, S. Qayyum and M. Tamoor, Entropy optimization and quartic autocatalysis in MHD chemically reactive stagnation point flow of Sisko nanomaterial, *Int. J. Heat Mass Transf.*, 127 (2018) 829-837.
- [149] T. Hayat, S. Ayub and A. Alsaedi, Homogeneous-heterogeneous reactions in curved channel with porous medium, *Results Phys.*, 9 (2018) 1455-1461.
- [150] H. Darcy, *Les Fontaines Publiques de la Ville de Dijon*, Dalmont, Paris, (1856) 647.

- [151] R. T. Johansen and H. N. Dunning, Homogeneous fluid flow through consolidated porous media, *J. Colloid Scien.*, 12 (1957) 68-79.
- [152] N. A. S. Afifi and N. S. Gad, Interaction of peristaltic flow with pulsatile fluid through a porous medium. *Appl. Math. Comp.*, 142 (2003) 167–176.
- [153] A. R. Rao and M. Mishra, Peristaltic transport of a power-law fluid in a porous tube, *J. Non-Newtonian Fluid Mech.*, 121 (2004) 163–174.
- [154] M. Mishra and A. R. Rao, Peristaltic transport in a channel with a porous peripheral layer: model of a flow in gastrointestinal tract, *J. Biomech.*, 38 (2005) 779–789.
- [155] E. F. Elshehawey, A. E. R. El-Saman, M. El-Shahed and M. Dagher, Peristaltic transport of a compressible viscous liquid through a tapered pore, *Appl. Math. Comp.*, 169 (2005) 526–543.
- [156] W. C. Tan and T. Masuoka, Stokes' first problem for a second grade fluid in a porous half-space with heated boundary, *Int. J. Nonlinear Mech.*, 40 (2005) 515–522.
- [157] W. C. Tan and T. Masuoka, Stokes' first problem for an Oldroyd-B fluid in a porous half-space, *Phys. Fluids*, 17 (2005) 3101–3107.
- [158] K. Vajravelu, G. Radhakrishnamacharya, G and V. Radhakrishnamurty, Peristaltic flow and heat transfer in a vertical porous annulus, with long wave approximation, *Int. J. Non-Linear Mech.*, 42 (2007) 754–759.
- [159] T. Hayat, S. B. Khan and M. Khan, The influence of Hall current on the rotating oscillating flows of an Oldroyd-B fluid in a porous medium, *Nonlinear Dyn.*, 47 (2007) 353–362.
- [160] T. Hayat, F. Shahzad, M. Ayub and S. Asghar, Stokes' first problem for a third grade fluid in a porous half space, *Comm. Nonlinear Sci. Numer. Simul.*, 13 (2008) 1801–1807.
- [161] K. S. Mekheimer, A. M. Salem and A. Z. Zaher, Peristaltically induced MHD slip flow in a porous medium due to a surface acoustic wavy wall, *J. Egypt. Math. Soc.*, 22 (2014) 143-151.

- [162] F. M. Abbasi, T. Hayat and B. Ahmad, Peristaltic transport of copper-water nanofluid saturating porous medium, *Physica E*, 67 (2015) 47-53.
- [163] M. M. Bhatti and M. A. Abbas, Simultaneous effects of slip and MHD on peristaltic blood flow of Jeffrey fluid model through a porous medium, *Alex. Eng. J.*, 55 (2016) 1017–1023.
- [164] T. Hayat, A. Tanveer and A. Alsaedi, Numerical analysis of partial slip on peristalsis of MHD Jeffrey nanofluid in curved channel with porous space, *J. Mol. Liq.*, 224 (2016) 944–953.
- [165] T. Hayat, Q. Hussain and N. Ali, Influence of partial slip on the peristaltic flow in a porous medium, *Physica A*, 387 (2008) 3399-3409.
- [166] N. Ali, Q. Hussain, T. Hayat and S. Asghar, Slip effects on the peristaltic transport of MHD fluid with variable viscosity, *Phys. Lett. A*, 372 (2008) 1477-1489.
- [167] A. Ebaid, Effects of magnetic field and wall slip conditions on the peristaltic transport of a Newtonian fluid in an asymmetric channel, *Phy. Lett. A*, 372 (2008) 4493-4499.
- [168] S. Srinivas, R. Gayathri and M. Kothandapani, The influence of slip conditions, wall properties and heat transfer on MHD peristaltic transport, *Comp. Phys. Comm.*, 180 (2009) 2115-2122.
- [169] N. S. Akbar, S. Nadeem and T. Hayat, Simulation of thermal and velocity slip on the peristaltic flow of a Johnson–Segalman fluid in an inclined asymmetric channel, *Inter. J. Heat Mass Transf.*, 55 (2012) 5495-5502.
- [170] M. Mustafa, S. Hina, T. Hayat and A. Alsaedi, Slip effects on the peristaltic motion of nanofluid in a channel with wall properties. *J. Heat Transf.*, 135 (2013) 041701-1.
- [171] H. M. Sayed, E. H. Aly and K. Vajravelu, Influence of slip and convective boundary conditions on peristaltic transport of non-Newtonian nanofluids in an inclined asymmetric channel, *Alex. Eng. J.*, 55 (2016) 2209-2220.
- [172] T. Hayat, M. Shafique, A. Tanveer and A. Alsaedi, Slip and Joule heating effects on radiative peristaltic flow of hyperbolic tangent nanofluid, *Int. J. Heat Mass Transf.*, 112 (2017) 559-567.



- [173] T. Hayat, S. Farooq and A. Alsaedi, Mixed convection peristaltic motion of copper-water nanomaterial with velocity slip effects in a curved channel, *Comp. Meth. Prog. Biomed.*, 142 (2017) 117-128.
- [174] K. Ramesh, Effects of slip and convective conditions on the peristaltic flow of couple stress fluid in an asymmetric channel through porous medium, *Comp. Meth. Prog. Biomed.*, 135 (2016) 1-14.
- [175] T. Hayat, A. Tanveer, F. Alsaadi and G. Mousa, Impact of radial magnetic field on peristalsis in curved channel with convective boundary conditions, *J. Magn. Magn. Mater.*, 403 (2016) 47-59.
- [176] I. Shahzadi and S. Nadeem, Inclined magnetic field analysis for metallic nanoparticles submerged in blood with convective boundary condition, *J. Mol. Liq.*, 230 (2017) 61-73.
- [177] T. K. Mitra and S. N. Prasad, On the influence of wall properties and Poiseuille flow in peristalsis, *J. Biomech.*, 6 (1973) 681-693.
- [178] V. P. Srivastava and L. M. Srivastava, Influence of wall elasticity and poiseuille flow on peristaltic induced flow of a particle-fluid mixture, *Int. J. Engr. Sci.*, 35 (1997) 1359-1386.
- [179] M. A. A. Elnaby, M. H. Haroun, A new model for study the effect of wall properties on peristaltic transport of a viscous fluid, *Comm. Nonlinear Sci. Num. Simul.*, 13 (2008) 752-762.
- [180] M. Javed, T. Hayat and A. Alsaedi, Peristaltic flow of Burgers' fluid with compliant walls and heat transfer, *Appl. Mathe. Comp.*, 244 (2014) 654-671.
- [181] N. N. Jyothi, P. Devaki and S. Sreenadh, Analysis of magnetic field on the peristaltic transport of Johnson fluid in an inclined channel bounded by flexible walls, *Int. J. Curr. Res.*, 8 (2016) 26617-26634.
- [182] T. Hayat, A. Saleem, A. Tanveer and F. Alsaadi, Numerical study for MHD peristaltic flow of Williamson nanofluid in an endoscope with partial slip and wall properties, *Int. J. Heat Mass Transf.*, 114 (2017) 1181-1187.


- [183] G. Manjunatha, C. Rajashekhar, H. Vaidya, K. V. Prasad and O. D. Makinde, Effects of wall properties on peristaltic transport of Rabinowitsch fluid through an inclined non-uniform slippery tube, *Defect Diffusion Forum*, 392 (2019) 138-157.
- [184] H. Vaidya, C. Rajashekhar, G. Manjunatha and K. V. Prasad, Peristaltic mechanism of a Rabinowitsch fluid in an inclined channel with compliant wall and variable liquid properties, *J. Braz. Soc. Mech. Sci. Engr.*, 41 (2019) 52.
- [185] M. Javed and R. Naz, Peristaltic flow of a realistic fluid in a compliant channel, *Physica A*, 551 (2020) 12389.
- [186] S. Srinivas, R. Gayathri and M. Kothandapani, Mixed convective heat and mass transfer in an asymmetric channel with peristalsis, *Comm. Nonlinear Sci. Num. Simul.* 16 (2011) 1845-1862.
- [187] S. Srinivas and R. Muthuraj, Effects of chemical reaction and space porosity on MHD mixed convective flow in a vertical asymmetric channel with peristalsis, *Math. Comp. Model.*, 54 (2011) 1213-1227.
- [188] T. Hayat, F. M. Abbasi, M. Al-Yami and S. Monaquel, Slip and Joule heating effects in mixed convection peristaltic transport of nanofluid with Soret and Dufour effects, *J. Mol. Liq.*, 194 (2014) 93-99.
- [189] M. Mustafa, S. Abbasbandy, S. Hina and T. Hayat, Numerical investigation on mixed convective peristaltic flow of fourth grade fluid with Dufour and Soret effects, *J. Taiwan Inst. Chem. Engr.*, 45 (2014) 308-316.
- [190] T. Hayat, S. Nawaz, A. Alsaadi and M. Rafiq, Mixed convective peristaltic flow of water based nanofluids with Joule heating and convective boundary conditions, *Plos One*, 11 (2016) e0153537.
- [191] T. Hayat, R. Iqbal, A. Tanveer and A. Alsaadi, Mixed convective peristaltic transport of Carreau-Yasuda nanofluid in a tapered asymmetric channel, *J. Mol. Liq.*, 223 (2016) 1100-1113.

- [192] A. Tanveer, T. Hayat, F. Alsaadi and A. Alsaedi, Mixed convection peristaltic flow of Eyring-Powell nanofluid in a curved channel with compliant walls, *Comp. Bio. Med.*, 82 (2017) 71-79.
- [193] S. Srinivas and M. Kothandapani, Peristaltic transport in an asymmetric channel with heat transfer - A note, *Int. Comm. Heat Mass Trans.*, 35 (2008) 514-522.
- [194] K. S. Mekheimer and Y. A. Elmagboud, The influence of heat transfer and magnetic field on peristaltic transport of a Newtonian fluid in a vertical annulus: Application of an endoscope, *Phy. Lett. A*, 372 (2008) 1657-1665.
- [195] S. Nadeem and N. S. Akbar, Influence of heat transfer on a peristaltic transport of Herschel-Bulkley fluid in a non-uniform inclined tube, *Comm. Nonlinear Sci. Num. Simul.*, 14 (2009) 4100-4113.
- [196] S. Nadeem and N. S. Akbar, Effects of heat transfer on the peristaltic transport of MHD Newtonian fluid with variable viscosity: Application of Adomian decomposition method, *Comm. Nonlinear Sci. Num. Simul.*, 14 (2009) 3844-3855
- [197] S. Srinivas and R. Gayathri, Peristaltic transport of a Newtonian fluid in a vertical asymmetric channel with heat transfer and porous medium, *Appl. Math. Comp.*, 215 (2009) 185-196.
- [198] S. Hina, M. Mustafa, T. Hayat and A. Alsaedi, Peristaltic flow of Powell-Eyring fluid in curved channel with heat transfer: A useful application in biomedicine, *Comp. Meth. Prog. Biomed.*, 135 (2016) 89-100.
- [199] T. Hayat and S. Hina, The influence of wall properties on the MHD peristaltic flow of a Maxwell fluid with heat and mass transfer, *Nonlinear Analy.: Real World Appl.*, 11 (2010) 3155-3169.
- [200] M. M. Bhatti, A. Zeeshan, R. Ellahi and G. C. Shit, Mathematical modeling of heat and mass transfer effects on MHD peristaltic propulsion of two-phase flow through a Darcy-Brinkman-Forchheimer porous medium, *Adv. Powder Technol.*, 29 (2018) 1189-1197.

- [201] L. V. Van der Ham, J. Gross and S. Kjelstrup, Two performance indicators for the characterization of the entropy production in a process unit, *Energy*, 36 (2011) 3727-3732.
- [202] N. Chekir and A. Bellagi, Performance improvement of a butane/octane absorption chiller, *Energy*, 36 (2011) 6278-6284.
- [203] J. Guo, M. Xu, J. Cai and X. Huai, Viscous dissipation effect on entropy generation in curved square microchannels, *Energy*, 36 (2011) 5416-5423.
- [204] C. Fu and T. Gundersen, Using exergy analysis to reduce power consumption in air separation units for oxycombustion processes, *Energy*, 44 (2012) 60-68.
- [205] X. Li and A. Faghri, Local entropy generation analysis on passive highconcentration DMFCs (direct methanol fuel cell) with different cell structures, *Energy*, 36 (2011) 403-414.
- [206] F. Bahiraei, R. K. Saray and A. Salehzadeh, Investigation of potential of improvement of helical coils based on avoidable and unavoidable exergy destruction concepts, *Energy*, 36 (2011) 3113-3119.
- [207] M. F. Farahani, S. Delfani and J. Esmaeliani, Exergy analysis of evaporative cooling to select the optimum system in diverse climates, *Energy*, 40 (2012) 250-257.
- [208] E. Amani and M. R. H. Nobari, A numerical investigation of entropy generation in the entrance region of curved pipes at constant wall temperature, *Energy*, 36 (2011) 4909-4918.
- [209] M. A. Ehyaei, A. Mozafari and M. H. Alibiglou, Exergy, economic and environmental (3E) analysis of inlet fogging for gas turbine power plant, *Energy*, 36 (2011) 6851-6861.
- [210] A. Bejan, Second law analysis in heat transfer, *Energy*, 5 (1980) 720-732.
- [211] A. Bejan, Entropy Generation Minimization: The method of thermodynamic optimization of finite-time systems and finite-time processes, CRC Press, New York, NY, USA, (1996).


- [212] M. Sheikholeslami and D. D. Ganji, Entropy generation of nanofluid in presence of magnetic field using Lattice Boltzmann Method, *Physica A*, 417 273-286.
- [213] N. S. Akbar, Entropy generation and energy conversion rate for the peristaltic flow in a tube with magnetic field, *Energy*, 82 (2015) 23–30.
- [214] N. S. Akbar, M. Raza and R. Ellahi, Peristaltic flow with thermal conductivity of  $H_2O + Cu$  nanofluid and entropy generation, *Results Phys.*, 5 (2015) 115-124.
- [215] M. A. Abbas, Y. Bai, M. M. Rashidi and M. M. Bhatti, Analysis of entropy generation in the flow of peristaltic nanofluids in channels with compliant walls, *Entropy*, 18 (2016) 90.
- [216] T. Hayat, S. Nawaz, A. Alsaadi and M. Rafiq, Analysis of entropy generation in mixed convective peristaltic flow of nanofluid, *Entropy*, 18 (2016) 355.
- [217] T. Hayat, S. Farooq and B. Ahmed, Effectiveness of entropy generation and energy transfer on peristaltic flow of Jeffrey material with Darcy resistance, *Int. J. Heat Mass Transf.*, 106 (2017) 244-250.
- [218] J. A. Esfahani, M. Akbarzadeh, S. Rashidi, M. A. Rosen and R. Ellahi, Influences of wavy wall and nanoparticles on entropy generation over heat exchanger plat, *Int. J. Heat Mass Transf.*, 109 (2017) 1162–1171.
- [219] S. Rashidi, S. Akbar, M. Bovand and R. Ellahi, Volume of fluid model to simulate the nanofluid flow and entropy generation in a single slope solar still, *Renewable Energy*, 115 (2018) 400-410.
- [220] M. Jafaryar, A. Shafee and Z. Li, Nanofluid heat transfer and entropy generation through a heat exchanger considering a new turbulator and CuO nanoparticles, *J. Therm Anal Calorim.*, 134 (2018) 2295-2303.
- [221] S. Farooq, T. Hayat, A. Alsaedi and S. Asghar, Mixed convection peristalsis of carbon nanotubes with thermal radiation and entropy generation, *J. Mol. Liq.*, 250 (2018) 451-467.

- [222] F. M. Abbasi, I. Shanakhat and S. A. Shehzad, Entropy generation analysis for peristalsis of nanofluid with temperature dependent viscosity and Hall effects, *J. Magn. Magn. Mater.*, 474 (2019) 434-441.
- [223] S. K. Asha and C. K. Deepa, Entropy generation for peristaltic blood flow of a magnetomicropolar fluid with thermal radiation in a tapered asymmetric channel, *Resul. Eng.*, 3 (2019) 100024.
- [224] N. K. Ranjit, G. C. Shit and D. Tripathi, Entropy generation and Joule heating of two layered electroosmotic flow in the peristaltically induced micro-channel, *Int. J. Mech. Sci.*, 153-154 (2019) 430-444.
- [225] V. K. Narla, D. Tripathi and O. A. Bég, Analysis of entropy generation in biomimetic electroosmotic nanofluid pumping through a curved channel with Joule dissipation, *Ther. Sci. Eng. Prog.*, 151 (2020) 100424.

 Turnitin Originality Report

Peristalsis subject to Entropy Generation by Sadaf Nawaz .

From DRSM (DRSM L)

  
Focal Person (Turnitin)  
Quaid-i-Azam University  
Islamabad

- Processed on 03-Jun-2021 09:12 PKT
- ID: 1599433282
- Word Count: 40010

Similarity Index  
6%  
Similarity by Source

Internet Sources:  
2%  
Publications:  
5%  
Student Papers:  
1%

3/6/2021  
PROFESSOR  
Department of Mathematics  
Quaid-i-Azam University  
Islamabad

sources:

1

1% match (Internet from 15-Dec-2019)

<https://journals.plos.org/plosone/article?id=10.1371/journal.pone.0153537>

2

< 1% match (student papers from 03-Sep-2013)

[Submitted to Higher Education Commission Pakistan on 2013-09-03](#)

3

< 1% match (student papers from 09-Apr-2018)

[Submitted to Higher Education Commission Pakistan on 2018-04-09](#)

4

< 1% match (student papers from 12-Jan-2018)

[Submitted to Higher Education Commission Pakistan on 2018-01-12](#)

5

< 1% match (student papers from 02-Dec-2009)

[Submitted to Higher Education Commission Pakistan on 2009-12-02](#)

6

< 1% match (student papers from 14-May-2018)

[Submitted to Higher Education Commission Pakistan on 2018-05-14](#)

7